IntechOpen

Powder Metallurgy
Fundamentals and Case Studies

Edited by Leszek A. Dobrzanski

POWDER METALLURGY - FUNDAMENTALS AND CASE STUDIES

Edited by **Leszek A. Dobrzanski**

Powder Metallurgy - Fundamentals and Case Studies
http://dx.doi.org/10.5772/61469
Edited by Leszek A. Dobrzanski

Contributors

Ping Huang, Dong Chen, Zhongning Guo, Glenn Kwabena Gyimah, Silvio Francisco Brunatto, Antonín Kříž, David Bricín, Leszek A. Dobrzański, mario rosso, Ildiko Peter, Mykhaylo Pashechko, Joanna Szulżyk-Cieplak, Aneta Duda, Klaudiusz Lenik, Jan Dzugan, Boguslaw Onderka, Joanna Karwan-Baczewska

Notice

First published in Croatia, 2017 by INTECH d.o.o.
eBook (PDF) Published by IN TECH d.o.o.
Place and year of publication of eBook (PDF): Rijeka, 2019.
IntechOpen is the global imprint of IN TECH d.o.o.
Printed in Croatia

Legal deposit, Croatia: National and University Library in Zagreb

Additional hard and PDF copies can be obtained from orders@intechopen.com

Powder Metallurgy - Fundamentals and Case Studies
Edited by Leszek A. Dobrzanski

p. cm.

Print ISBN 978-953-51-3053-6

Online ISBN 978-953-51-3054-3

eBook (PDF) ISBN 978-953-51-4892-0

Meet the editor

Professor Leszek A. Dobrzański DSc, PhD, MSc, Eng, M. Dr. h.c. (born in 1947) is one of the 55 most frequently cited contemporary Polish scientists of all disciplines. He is a full professor of the Silesian University of Technology in Gliwice, Poland, and doctor honoris causa of the universities in Ruse, Bulgaria; Khmelnitsky, Ukraine; and Miskolc, Hungary. He was the vice rector, dean of the faculty, director of the institute, head of Doctoral Studies and visiting professor in ca. 100 universities and an invited lecturer at ca. 100 international scientific conferences around the world. He is a founding fellow and the president of the World Academy of Materials and Manufacturing Engineering and editor-in-chief of *Archives of Materials Science and Engineering*, the *Journal of Achievements in Mechanical and Materials Engineering* and Open Access Library. He organised ca. 50 international conferences in Poland and was the member of the scientific committees of the next 100 conferences abroad. He advised ca. 60 finished PhD theses and ca. 1000 BSc and MSc theses and is the author of ca. 2400 papers, more than 50 books, 40 chapters and 50 patents. He is awarded with a lot awards, among others, William Jonson, Albert Schweitzer, Ferdinand Martinengo, Tadeusz Sendzimir, Rudolf Clausius, Wieslaw Chladek and Commander's Crosses of the Orders of Rebirth of Poland and "Merite de l'Invention" by Kingdom of Belgium, and ca. 80 awards on International Innovation Fairs around the world.

Contents

Preface

Powder metallurgy is one of the important technologies in forming the products' shape and geometrical characteristics and also their structure and the physical and chemical properties. Powder metallurgy plays an important role in technologies of material processes and in the formation of product and properties of engineering materials. Powder metallurgy methods have found applications in the mass production of numerous elements produced from iron, carbide steels and alloy steels. Powder metallurgy can be competitive in relation to other production processes, for example casting, plastic working and machining, by complementing or replacing such techniques.

The book presents in the first part the fundamentals and the role of powder metallurgy in contemporary technologies and the state of the art of classical powder metallurgy technologies and a general description of new variants and special and hybrid technologies used in powder metallurgy. The next part of the book includes over a dozen case studies provided in the following chapters, comprehensively describing authors' accomplishments of numerous teams from different countries across the world in advanced research areas relating to powder metallurgy and to special and hybrid technologies.

This book on *Powder Metallurgy - Fundamentals and Case Studies* is my 50th successive book published in my personal academic career in the year 2017, which is the year of my 70th birthday anniversary. In this sense, it is a solemn edition. I have a great honour to thank all my co-authors and co-operators from InTech Publishing House for their personal efforts in preparing this book.

I hope that the detailed information collected in the book, largely deriving from own and original research and R&D works pursued by the authors, will be beneficial for the readers to develop their knowledge and harmonise specific information concerning these topics and will convince the manufacturers about the advantages of using the powder metallurgy technology in many branches of industry, which—on one hand—makes it possible to gain improvements in economical manufacturing and on the other hand will enhance the functional properties of multiple products in their service conditions. The book will be useful for the scientists and students and PhD students also.

I wish that the readers enjoy reading this book and that it may serve them in solving real engineering problems.

Prof. Leszek A. Dobrzański
Silesian University of Technology
Gliwice, Poland

Medical and Dental Engineering Centre
For Research, Design and Production ASKLEPIOS Ltd
Gliwice, Poland

Chapter 1

Goals and Contemporary Position of Powder Metallurgy in Products Manufacturing

Leszek A. Dobrzański

Additional information is available at the end of the chapter

http://dx.doi.org/10.5772/65378

Abstract

This chapter is an introduction to the book on powder metallurgy (PM). It presents the basis of the selection of powder metallurgy technologies for manufacturing of products, including such applied in medicine and dentistry, and the state of the art concerning the general characteristic of powder metallurgy. The materials and products manufactured with the classical powder metallurgy methods are generally described. The last section presents the general contents of the book based on the above general information.

Keywords: products manufacturing, materials engineering, engineering design, powder metallurgy, sintered materials and products

1. The basis of the selection of powder metallurgy technologies for manufacturing of products, especially products used in medicine and dentistry

Products and other consumer goods available at the market and supplied by manufacturers dictate the standard and quality of life, exchange of information, educational standards, the quality and capabilities of medical care and other aspects of the environment we live in. Engineering designs constitute a basis for the initiated and conducted production [1]. The quality of manufacturing is closely connected with the standard of life's quality understood as how requirements are satisfied determining the level of the material and spiritual welfare of particular persons and the whole society. The needs addressed by the medical sector are higher and higher. In this sector, implants, implant-scaffolds and other devices and appropriate instruments and

apparatuses have to be used in many cases in post-operative losses of natural tissues, especially bone or dental tissues due to disease-related lesions, inflammatory conditions or injuries, especially traffic and sports injuries, and also as a result of natural ageing processes. In terms of product design, all engineering materials able to provide the required product properties are on an equal footing, and multicriteria optimisation is essential for selecting materials with the best functional and technological properties and lowest possible costs of material and product production, processing and operation. The aspects related to materials play an important role in fulfilling the tasks of the engineering environment, as a paradigm of materials engineering requires to select an engineering material which, in an appropriately selected technological process of forming a product's geometrical form and structure and engineering material properties, will ensure the suitable, required and expected usable product properties. Therefore, the issues involving materials science and materials engineering are complex and encompass the following general topics:

- an atomic and molecular structure of materials;
- dependence between the structure and properties of materials;
- formation of the structure and properties of materials;
- technologies of materials processes;
- investigations into a structure and properties of materials;
- examination of properties of products fabricated from materials in operating conditions; and
- predicting the properties of products, also in operating conditions.

This chapter concerns the detailed and selected aspects of synthesis and technologies of materials processing as an important part of manufacturing, understood as the making of products using raw materials in various processes, with various machines and in operations managed in line with a well-elaborated plan. Product designing—after the phase of industrial design, where product functions are generally described and a product concept is generally developed, including its external form, colour and potential general ideas as to how to assemble the key components—is composed of engineering design and subsequent production preparation. Engineering designing, in which product shape and product components are defined, materials are selected from which they are to be made and appropriate technological processes are selected, enables to design and produce products meeting their expected usable functions, as well as requirements concerning the shape, economic and reliability aspects. Material properties can be changed by changing a technological process, and some combinations of the product shape and material may be infeasible using certain technological processes. Materials design provides a material with the most advantageous set of functional properties ensured by appropriate chemical composition and the material's technological process. Engineering design combines, therefore, the three equally important and inseparable components:

http://dx.doi.org/10.5772/65378

- materials design to guarantee the required durability of a product or product components made of engineering materials with the required physiochemical and technological properties;
- structural design whose purpose is to develop a shape and geometrical features of a product satisfying human needs; and
- technological process design enabling to achieve the required geometrical features and properties for particular product elements and also their correct interaction after assembly considering the volume of production, level of automation and computer aid, while ensuring also the lowest possible product costs.

An engineering design process is influenced by the selected technological process and by a possibility of using certain technologies. Such factors dictate material selection and a sequence of technological operations, as well as dimensions, dimensional tolerances, the joining of elements and other constructional aspects. Numerous factors linked to a technological process have to be taken into account in a design process by designing in consideration of:

- production and assembly;
- casting;
- plastic working;
- powder metallurgy (PM);
- machining;
- joining;
- heat and surface treatment;
- processes applied for ceramic materials;
- processes applied for polymer materials; and
- manufacture of composite materials.

Producibility should also be considered in a design process.

2. General characteristic of powder metallurgy

Powder metallurgy (PM) plays an important role in technologies of materials processes and in the formation of product forms and properties of engineering materials. PM is a field of technology covering the manufacturing methods of powders of materials and metallic materials or their mixtures with non-metallic powders and the manufacturing of semi-products and products from such powders without having to melt the main component [1–7]. At present, in about 80% the parts fabricated by powder metallurgy methods are employed in the automotive industry, mainly for economic reasons. Moreover, powder metallurgy methods

are utilised in other industries, among others in aviation, energy and household sector, and for producing certain complex parts applied in medicine and dentistry, especially for bone and dental implants and implant-scaffolds and epitheses. The history of powder metallurgy dates back 3000 years before Christ, because ancient Egyptians were making parts with this technology, and ancient Incas were making valuable items of gold and noble metals, although mass production began at the end of the twentieth century. Initially, small particles were extracted from sponge iron, which were then melted or sintered. Metal powders were started to be produced later, and then they were initially formed and sintered. Generally speaking, the following operations can be distinguished in a classical technological process of products fabricated by the powder metallurgy method:

- metal powder or a mixture of different metals is produced;
- powder is prepared and mixed with lubricating and slipping agents;
- cold-powder moulding and compactions;
- sintering; and
- finishing.

Figure 1 shows a sequence of technological operations suitable for the powder metallurgy process.

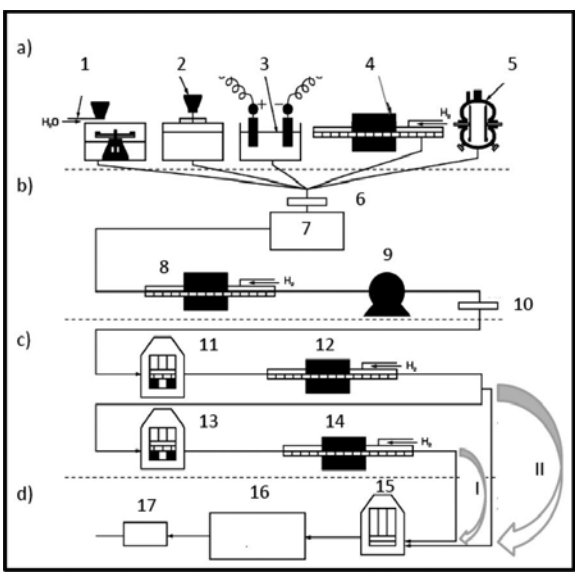

Figure 1. Simplified diagram of mass production of powders from iron and steel powders: (a) powder production, (b) powder preparation, (c) preliminary moulding and sintering, (d) finishing; 1, DPG sputtering; 2, sputtering; 3, electrolysis; 4, reduction; 5, crushing in Hametag mill; 6, screen; 7, tank; 8, preliminary reduction; 9, mill; 10, screen; 11, I pressing; 12, I sintering; 13, II pressing; 14, II sintering; 15, calibration; 16, heat treatment (hardening, quenching and tempering, surface treatment); 17, final control; I, double cycle; II, single cycle.

http://dx.doi.org/10.5772/65378

The phenomena taking place during preliminary moulding and then sintering are the essence of powder metallurgy. Cold compaction of material can take place only to a certain limit value of space filling, which, in the case of typical actual systems of powders, according to the percolation theory, is 0.6. This is related to the fact that although the grains of metallic raw materials may be subject to plastic deformation, and the grains of raw materials used in ceramics are rigid, at room temperature they cannot be deformed plastically under the influence of mechanical forces. Further compaction of the system is connected with increasing the level of space filling, that is, consolidation can take place only in sintering as a result of thermal activation. Grain regrouping takes place subsequently, the driving force of which is excessive energy collected on their grain surface, and then the number of inter-grain contacts is rising. The process is thermodynamically advantageous as the unit surface energy of the separation boundary solid body/solid body is lower than the unit energy of the separation boundary solid body/gas, thus the formation processes of the solid body/solid body boundary can take place by themselves. Activisation energy connected with temperature rise is needed to initiate such processes. Under the influence of the energy supplied, atomic (ionic) vibrations are activated, particularly on the surface of grains. This has an effect on an increased number of bonds and durable inter-grain necks are created. Their surface is increasing, preventing the relative movement of grains and is leading to the transport of the mass in the grain area. Consequently, it leads to changes in the shape of grains and higher and higher elimination of pores.

Sintering usually takes place below a melting point of the main component. It can also occur in the solid phase. In the first phase of sintering in the solid phase, powder grains are bonding due to adhesion caused mainly by moulding. The diffusion of atoms occurs on the surface after heating, taking place in the entire volume of powder as time passes. Grains are joined permanently as a result of such phenomena and sinter porosity is lowered. Excess surface energy of the system of powder grains is the basic driving force in sintering in the solid phase. The system being sintered, while striving for energy minimisation, is reducing the area of free surfaces by creating inter-grain necks, by smoothing the surface, by spheroidisation and by elimination of pores. Sintering in the solid phase occurs at a temperature lower than a material melting point, as a result of which the liquid phase is not being formed even temporarily, and the sinter reaches its high properties owing to various mechanisms of matter transportation, including slipping at the grain boundaries, diffusion and evaporation and condensation. In the case where sintering is done together with moulding, the external forces cause additional plastic deformation of metal powder grains, which—due to high temperature—is usually accompanied by recovery and recrystallisation processes—either static or dynamic.

Material sintering with the liquid phase takes place when at least two components are present in a mixture of powders, and sintering occurs above a melting point of the lowest melting component. An important characteristic of the liquid phase present in sintering is the ability of wetting the solid insoluble particles. The wetting ability of the liquid phase, depending on surface energy, may be modified by using alloy additives with high surface activity and by the growth of system temperature, thus increasing the intensity of sintering. Sintering with the liquid phase is usually suitable for multicomponent powders, and low-melting eutectics

created by particular components are melted. A liquid filling the pores between powder grains is created in the first stage of sintering with the liquid phase, facilitating the regrouping and compact arrangement of grains. The liquids of certain small grains are being solved and crystals with large grains are precipitated from the liquid. The solid particles finally adhere to each other and are sintered. The excessive content of the liquid phase may, however, lead to losing the shape of the element being sintered, when maximum wetting takes place, and the liquid phase completely separates solid particles. Solid particles are being regrouped due to the presence of the liquid phase with high wetting ability, penetrating boundaries between the solid particles, and the element being sintered shrinks. The sinters achieved by sintering with the liquid phase are characterised by a structure composed of evenly arranged solid-phase particles in the solidified liquid.

Apart from sintering in the solid phase or with participation of the liquid phase, the third type of supersolidus sintering is distinguished, which is a variant of sintering in the liquid phase and is distinct for high-carbon steels, high-speed steels and nickel-based superalloys. Supersolidus sintering is accompanied by preformed shrinkage and increased physical and mechanical properties. In some cases, when double-component mixtures of powders A and B are sintered, and where a diffusion rate of components A to B is many times higher than diffusion from B to A, the sinters are swelling, and their high porosity, called diffusive porosity, can be useful in a production process of porous preforms.

Process / Characteristic	Dimension	Shape complexity	Density	Dimensional tolerances	Production yield	Cost
Conventional	◑	◑	◕	○	○	○
Powder Injection Moulding	◕	○	◔	◑	◑	◑
Hot Isostatic Pressing	○	◔	○	●	●	●
Powder Forging	◑	◑	○	◔	○	◔
Symbols: ○ very high, ◔ high, ◑ medium, ◕ small, ● very small.						

Table 1. Comparison of powder metallurgy processes.

At present, parts with a complicated shape, tight-dimensional tolerances, controlled density and properties can be manufactured by powder metallurgy methods. A technological process of powder metallurgy ensures high flexibility in the selection of physiochemical properties and other requirements, including:

- production of structural parts with complex shapes;

http://dx.doi.org/10.5772/65378

- controlled porosity;
- controlled properties;
- high mechanical strength and resistance to vibrations;
- high hardness and wear resistance;
- high manufacturing precision and good surface quality; and
- large number of production series while ensuring tight-dimensional tolerances.

Table 1 compares the basic characteristics of different powder metallurgy processes.

Powder metallurgy is becoming an unrivalled manufacturing process in the following cases:

- product porosity is the desired property, for example, in special filters;
- a porous structure is required to store lubricants as for self-lubricating bearings; and
- a structure is obtained composed by infiltration of the sintered porous skeleton from one metal with another liquid metal with a lower melting point, as in the case of tungsten-silver electric contacts or steel contact infiltered with copper to improve conductivity and strength.

Elements made of some materials, for example, had melting metals and sintered carbides, may only be fabricated with powder metallurgy methods.

The following usually conditions the application of powder metallurgy for product manufacturing:

- costs reduction versus other manufacturing processes and
- unique properties provided only by powder metallurgy.

Powder metallurgy process	Range of density, g/cm^3	Relative selling price in agreed, units/kg
Pressing and sintering	6–7.1	5.4–6
Pressing, sintering, dimensional moulding	6–7.1	6.4–7.1
Saturation with copper	7.3–7.5	7.8–7.9
Hot moulding	7.2–7.4	6.9–7.3
Double pressing and sintering	7.2–7.4	8.9–9.1
Powder injection moulding	7.5–7.6	100–155.6
Hot powder forging	7.8	11.1–12.2
Double pressing and sintering + Hot isostatic pressing	7.87	13.3–15.6

The values given are averaged; small parts are more costly than large parts.

Table 2. Comparison of indicative prices of elements fabricated by different powder metallurgy methods from iron or steel powders.

Powder metallurgy can be competitive in relation to other production processes, for example, casting, plastic working and machining, by complementing or replacing such techniques. It is usually substantiated for a large scale of production, not smaller than 1000–10,000 pieces, when investment expenses are depreciated for tooling and accessories. **Table 2** presents indicative prices of parts manufactured by various powder metallurgy methods.

The following benefits of powder metallurgy can be quantified: maximum usage of charge materials (over 95%), minimised proper energy required for producing 1 kg of ready elements and some of them cannot be fabricated by other methods (approx. 43%), reduced number of technological operations vis-à-vis plastic working or machining and lower temperatures than in conventional metallurgy. The cons of the powder metallurgy method are associated with the production of materials with high porosity and hence with relatively low strength, and with difficulties in obtaining products with a complex shape due to uneven distribution of pressure in the powder volume in pressing. Product porosity can be used, for example, in filters and porous (self-lubricating) bearings. Powder metallurgy and ceramic materials technologies are often similar, and hence the selected sintered materials and ceramic materials are sometimes discussed together.

3. General presentation of materials and products manufactured with the classical powder metallurgy methods

Powder metallurgy methods have found applications in the mass production of numerous elements produced from iron, carbide steels and alloy steels. Work intensity can be significantly reduced with them, machines can be relieved, raw materials saved and wastes reduced. Sintered elements of machines are used in the machine and car industry. Toothed gears, rollers, washers, nuts, pawls, parts of shock absorbers, valve seats, bearings, building joinery, parts of reinforcement, office machines and sewing machines are fabricated from sintered powders.

Products sintered from low-carbon steel have the tensile strength of approx. 220 MPa, hardness of 50 HBW and elongation of up to 20%. Strength as well as corrosion and abrasion resistance can be enhanced by applying products from steel powders, in particular with the chemical composition corresponding to special steels. Such products can be achieved by various methods, namely by:

- sintering steel powders with chemical composition corresponding to a ready sinter;
- mixing, at a suitably chosen ratio, iron powders with powdered carbon and powders of other alloy components and then sintering;
- mixing iron powders with cast iron powders or ferroalloys and then sintering; and
- carburising the products achieved by iron powder sintering.

Products sintered from copper and copper alloys are widely used. They are fabricated from a mixture of Cu, Sn or Zn powders or alloy powders, for example, Cu-Pb or Cu-Zn. Copper and

http://dx.doi.org/10.5772/65378

bronze or brass are used for the manufacture of sintered parts of equipment and machinery, building joinery and in production of medals.

Powder metallurgy methods allow producing products which cannot be manufactured by other methods. Such products include, among others,

- solid bearings;
- porous bearings; and
- sintered filters.

Sintered slide bearings possess good mechanical properties. They are usually made by hot pressing or skeleton infiltration from the skeleton of hard-melting metals having a lower melting point. They are used at an elevated and reduced temperature and with high loads and such conditions exclude lubrication with oils.

Sintered solid bearings with the appropriate fraction of graphite or soft low-melting metals are self-lubricating. They are usually produced from ferrographite or copper graphite. Iron can be partially replaced by Cu, Pb, Sn or Zn, and copper by Sn, Zn or Pb. Lead bronze with a concentration of 10–40% Pb can also be used. Depending on working conditions, slide bearings may also contain 0–60% of Cu, 0–70% of Ni, 0–70% of Co, 0–30% of Cr, 0–10% of Al, 0–10% of Mo, up to 50% of graphite and 0–40% of carbides and metal borides.

Self-lubricating bearings are produced as porous from metal powders, usually from iron or copper alloys, in particular from copper alloys with tin, to which non-metal powders, for example, graphite, may be added. The pores existing in the material can be joined, forming capillary channels. The volume of pores reaches up to 50% of the total volume of bearings. Such bearings are generally produced as thin-walled sleeves with jackets, and also as barrels. Porous tapes are also made, which are placed onto steel washers and rolled into half-sleeves. Porous bearings are saturated with special oil lubricating a shaft or an axle in work. Sintered porous bearings are used in systems where additional lubrication cannot be provided.

Sintered products with a porosity of up to 50% include filters having good mechanical properties, including tensile strength, bending strength, and also high resistance to impact loads and high temperature. They are used in arms, aviation, automotive, chemical and lathe machinery industry. Depending on working conditions, mainly temperature, they are made of powders of tin bronze, chromium or austenite steels resistant to corrosion or nickel brass, and also powders of other metals. Metal fibres can also be sintered. Porous sintered filters allow to clean particles with the diameter of 10^{-3}–10^{-4} mm. Gases are cleaned of mechanical contaminants, and also to some extent dried. Gas pressure can also be regulated to some extent with porous filters. Liquids are cleaned from mechanical contaminants mainly.

Stainless steels fabricated by powder metallurgy methods, for example, **ASEA-STORA process (ASP)** method or by sintering Fe, Cr and Ni powders, have enjoyed technical importance considering sintered materials. Such methods allow producing steels with a very small concentration of carbon, which are hard to achieve by a conventional method.

Powder metallurgy methods allow producing pristine hard-melting metals, for example, Ta, Nb, Ti, resistant to corrosion, or W or Mo used at high temperatures, especially in electrical and electronic engineering. Hard-melting sintered metals are subjected to hot plastic working, for example, peening, wire drawing, forging or rolling.

Ceramic-metallic composites represent a large group of heat-resistant and high-temperature creep-resisting sinters, as one of important groups of composite materials manufactured by this technology. Oxides, carbides, silicides or borides are the ceramic materials in cermet composites. They increase resistance to high temperature and the insensitivity of strength properties to temperature changes, heat resistance, high hardness and abrasion resistance at high temperature. Sintered carbides and sintered oxides can be used as heat-resistant materials.

The discussed group of materials also includes metals reinforced through dispersion by an external hard and heat-resistant phase, for example, tungsten sintered with a small additive of sodium oxide, calcium or aluminium, silicon dioxide or thorium dioxide, preventing excess growth of grains and tungsten creepage. This is similar to sintered chromium with added yttrium oxide. The **sintering aluminium powder (SAP)** method is employed in the production of Al + Al_2O_3 sinters. The fraction of oxides in such sinters is up to 15%, usually 5–11%. Today, apart from aluminium, especially U + UO_2, Fe + Al_2O_3, Fe–Cr + Al_2O_3, Fe + Fe_2O_3 and Ni + Al_2O_3 sinters are manufactured by this method.

It should be stressed that conventional and especially special powder metallurgy methods allow, in many cases, to fabricate implants, implant-scaffolds, scaffolds, very often made of titanium and its alloys, as well as parts of instruments, for example, surgical instruments or other parts of devices applied directly or indirectly in medicine or dentistry, which are also manufactured from stainless steels or other special alloys.

Powder metallurgy has found broad applications in the production of sintered tool materials such as sintered metal carbides, carbide steels, high-speed steels with a high concentration of carbon and alloy elements, and also cermetals and ceramic sinters, which cannot be produced otherwise. Powder metallurgy enables to achieve such materials as, for example, high-speed steels with better technological properties than those of materials fabricated by traditional metallurgical methods. Carbide segregation and banding were managed to be eliminated almost completely in such steels, even in products with larger section. Tools can be made from high-speed steels or carbide steels directly by pressing and sintering or large blocks can be made with dimensions similar to conventional ingots (not used these days usually as continuous casting processes are common), which can then be subjected to plastic working, as in ASP process or its latest variants, for example, STAMP or MICROCLEAN. Advanced sintered tool materials are witnessing constant advancements connected with fast progress in materials engineering. The properties and intended use of the finished products made of sintered tool materials are diverse depending on the phase composition, the content of hard-phase particles in sintered tool materials (whether they are present or not), the chemical composition of a binding material, as well as on the material's thermal workability. In general—in the group of sintered tool materials—one can distinguish the following:

http://dx.doi.org/10.5772/65378

- steels and cermetals based on carbides of transition metals and cermetals based on nitrides or mixtures of nitrides and carbides of transition metals;
- ceramic materials containing mostly α-Al_2O_3 and/or Si_3N_4, possibly with the addition of oxides of other elements;
- mixed materials—ceramic-carbide materials—containing α-Al_2O_3 and (or) Si_3N_4, as well as carbides of transition metals with potential addition of oxides or nitrides of other elements; and
- super hard-sintered materials—including polycrystalline synthetic diamond and boron nitride (BN) with a regular special network, called borazon—deposited on sinter carbide plates.

A group of sintered tool materials based on carbides of transition metals, due to a volume fraction of carbides in the structure, can be split into:

- sintered high-speed steels;
- sintered carbide steels; and
- sintered carbides.

Powder metallurgy allows fabricating sintered **tool-gradient materials (TGMs)** with a continuous or discrete-graded structure within the entire volume.

4. Overview of the selected research problems

The second chapter—on the basis of general information concerning the fundamentals of selection of the powder metallurgy technology and the general description of the technology, supplemented by a general review of materials and products fabricated by this technology covered in the first chapter—presents the state of the art of classical powder metallurgy technologies and a general description of new variants and special and hybrid technologies used in powder metallurgy, also for fabrication of products finding their applications in medicine and dentistry. Such descriptions, prepared according to a thorough review of extensive literature in this field, set a basis, especially for students, PhD students and engineering staff less experienced in this technical field, for scrutinising over a dozen case studies provided in the following chapters, comprehensively describing author's accomplishments of numerous teams from different countries across the world in advanced research areas relating to powder metallurgy and to special and hybrid technologies.

The first of the chapters is devoted to the sintering of prealloyed Fe-Ni-Cu-Mo powders modified by boron based on thermodynamic investigations. Prealloyed diffusion powder of such a type is applied for structural parts in the automotive industry. One of the methods to reduce porosity and increase mechanical properties of sintered materials is to apply activated sintering by introducing boron powder. The sintering process elaborated was very detailed, based on a thermodynamic analysis and microstructure investigations. It was stated that the

sintering process is impacting changes in the morphology of porosity and the increase of density, as well as the mechanical properties of the sintered alloys.

On the other hand, the direct current-assisted sintering of metal parts was presented as a promising and relatively new research and development field of powder metallurgy. Attention was then drawn to the physicochemical aspects of the plasma environment, basic knowledge of plasma heating and surface-related phenomena during the direct current plasma sintering of parts. All these aspects are approached considering the main techniques of the direct current plasma-assisted-sintering process applied to powder metallurgy. Finally, some results on direct current plasma heating and surface modification are presented.

The next chapter presents the outcomes of own investigations into four alternative manufacturing technologies of sintered porous skeletons by powder metallurgy methods, being the reinforcement of aluminium alloy matrix composite materials fabricated by infiltration. Porous skeletons were manufactured from Al_2O_3 aluminium powders by reactive sintering using blowing agents or by ceramic injection moulding, from mullite $3Al_2O_3$ $2SiO_2$ by sintering a mixture of halloysite nanotubes with agents forming an open structure of pores and from titanium by selective laser sintering. The structure and basic mechanical properties were also presented of such composite materials with small density ensured by an aluminium alloys matrix, and their broad application possibilities, in particular for medical and dental purposes.

The next chapter describes the structure, as well as mechanical properties of aluminium alloy matrix nanocomposites reinforced with multiwalled carbon nanotubes and halloysite nanotubes fabricated using powder metallurgy techniques, including mechanical alloying and hot extrusion. The powder of aluminium alloy AlMg1SiCu was used as a nanocomposite matrix. The investigation's results show that the technology of nanocomposite materials manufacturing can find the practical application in the production of new light-metal-matrix nanocomposites.

An important part of the book is devoted to the potential applications of powder metallurgy technologies for medical and dental uses. One of the chapters discusses how porous scaffolds are produced with the method of selective laser melting from Ti/Ti6Al4V powders in line with the make-to-order concept according to individual needs of each patient. The material is additionally subjected to surface treatment consisting of the deposition of atomic layers of titanium dioxide with nanometric thickness. The clinical data acquired from a patient during computer tomography, nuclear magnetic resonance or using traditional plaster casts are converted by a computer into a virtual solid model of a patient's loss.

The numerous technological applications of powders of different materials, also metals and their alloys, include additive manufacturing processes of metallic parts. Another chapter presents the latest overview of developments in the field of additive manufacturing of metallic components. Input materials and specific requirements for input materials are briefly mentioned. An overview of the technological process is described and the selective laser-melting technology as well as beam-melting technologies. Some examples of applications for this technology and its influence on the properties of the so-manufactured materials are described.

http://dx.doi.org/10.5772/65378

Another example is the use of powder metallurgy methods for the fabrication of vacuum-sintered duplex stainless steels. The structure of sintered stainless steels in terms of sintering atmospheres, including vacuum sintering, the influence of sintering parameters on microstructural changes of the single phase and duplex microstructure, was described. A relationship between sintering and corrosion resistance was presented by focusing on the effect of sintering density on corrosion resistance. The mechanical, magnetic and physical properties of sintered stainless steel were also discussed. The main sectors, and examples of applications of sintered stainless components, were presented.

An important part of the book, covering a few chapters, is devoted to tool materials manufactured by powder metallurgy methods and to the potential extension of service life of the so-manufactured tools through integrated surface treatment. First of the chapters presents essential information concerning sintered tool materials containing carbides and characterises graded materials whose properties change gradually according to their volume. The results of investigations are presented into the structure and properties of newly developed sintered-graded tool materials produced by the conventional metallurgy method from a mixture of high-speed HS6-5-2 steel powder and WC carbides. Manufacturing, composition, properties and applications of sintered hard metals are also presented. The general idea when using hard metals is to exploit their excellent properties in terms of hardness, toughness, wear resistance and chemical stability. Due to such characteristics, hard metals are excellent for cutting tools and this is the main field of their applications. An overview of the actual scenario concerning different tool materials is presented, including a short history and description of state-of-the-art techniques as regards their composition, manufacturing routes and key properties. This part will present some results of the authors' own research in this field, carried out over the recent years. Such research is continued in the next chapter devoted to the properties and testing of cemented carbides. The chapter comprises three main parts concerning degradation processes associated with the grinding of cemented carbides, the origin of residual stresses and their impact on cemented carbide properties and finally on the corrosion of cemented carbides in various environments. Nevertheless, little attention continues to be attached to the damages of cemented carbide cutting tools and such a phenomenon tends to be ascribed to various other factors such as the coatings applied, cutting process conditions, and the work-piece material. This part ends with a chapter providing a general description of the selected sintered tool materials, including injection-moulded ceramic-metallic tool materials and treatment technologies of their surface, especially physical and chemical vapour deposition (PVD) and (CVD) in view of the results of own investigations with technology foresight methods. The outcomes of multifaceted research, carried out with advanced materials engineering methods, into the structure and properties of multicomponent, graded and multilayer coatings on the investigated materials, are also presented.

Another chapter depicts coatings having an effect on the increased abrasive wear using powder eutectic materials of Fe-Mn-C-B system. The structural state and physical-mechanical properties of eutectic powder alloys and coatings correspond to composite dispersion-strengthened materials. The formation of a hardened layer with the eutectic structure on metal surface corresponds to the creation of a new material with certain mechanical properties.

The last one chapter of the book presents the production of a novel Cu-based composite frictional train-brake material by powder metallurgy methods. The tribological behaviour of these materials is analysed by pad-on-disk tests without lubrication, and the coefficient of friction, wear rate and wear value were studied in order to identify the effects of the sintering temperature on the base materials composition. Generally, the material obtained demonstrated excellent brake performance and wear resistance.

The editor, publisher and the whole team of authors, by making this book available to the readers, deeply believe that the detailed information collected in the book, largely deriving from own and original research and R&D works pursued by the authors, will be beneficial for the readers to develop their knowledge and harmonise specific information concerning these topics, and will convince the manufacturers about the advantages of using the powder metallurgy technology in many branches of industry, which—on one hand—makes it possible to gain improvements in economical manufacturing, on the other hand will enhance the functional properties of multiple products in their service conditions.

5. Additional information

The investigations were made mainly in the framework of the Project 'BIOLASIN—Investigations of structure and properties of newly created porous biomimetic materials fabricated by selective laser sintering' funded by the DEC-2013/08/M/ST8/00818 of the Polish National Science Centre in the framework of the 'Harmony 4' competitions, headed by Prof. Leszek A. Dobrzański.

Author details

Leszek A. Dobrzański

Address all correspondence to: leszek.adam@gmail.com

Faculty of Mechanical Engineering, Silesian University of Technology, Gliwice, Poland

References

[1] Dobrzański LA. Engineering materials and materials design; Fundamentals of materials science and physical metallurgy. Warszawa: WNT; 2006.: p. 1–1600 (in Polish). 1–1600 p. ISBN 83-204-3249-9.

[2] Jones W. Fundamental Principles of Powder Metallurgy. London: Edward Arnold Publishers Ltd.; 1960. 1032 p.

http://dx.doi.org/10.5772/65378

[3] German RM. Powder metallurgy and particulate materials processing. Metal Powder Industries Federation; 2005. p. 1–528.

[4] Ruys A, Gingu O, Sima G, Maleksaeedi S. Powder processing of bulk components in manufacturing. In: Nee AYC, editor. Handbook of Manufacturing Engineering and Technology. London: Springer-Verlag; 2015. p. 487–566. DOI: 10.1007/978-1-4471-4670-4_48.

[5] Dobrzański LA, Matula G. Powder metallurgy fundamentals and sintered materials. Open Access Library. 2012;8: p. 1–156 (in Polish).

[6] Samal PK, Newkirk JW, editors. ASM Handbook: Volume 7: Powder Metallurgy. ASM International; 2015. p. 1–907.

[7] Chang I, Zhao Y, editors. Advances in Powder Metallurgy: Properties, Processing and Applications. Woodhead Publishing Limited; 2013. p. 1–604.

Chapter 2

Fabrication Technologies of the Sintered Materials Including Materials for Medical and Dental Application

Leszek A. Dobrzański ,
Anna D. Dobrzańska-Danikiewicz,
Anna Achtelik-Franczak, Lech B. Dobrzański,
Eugeniusz Hajduczek and Grzegorz Matula

Additional information is available at the end of the chapter

http://dx.doi.org/10.5772/65376

Abstract

This chapter of the book presents the basis of classical powder metallurgy technologies and discusses powder fabrication, preparation, preliminary moulding, sintering and finish treatment operations. A general description of the materials and products manufactured with the classical powder metallurgy methods is presented. New variants are characterised along with special and hybrid technologies finding their applications in powder metallurgy. Special attention was drawn to microporous titanium and to TiAl6V4 alloy fabricated using hybrid rapid manufacturing technologies with selective laser sintering/selective laser melting (SLS/SLM) used for innovative implant scaffolds in medicine and regenerative dentistry. Laser deposition, thermal spraying and detonation spraying of powders are also discussed as special methods in which powders of metals and other materials are used as raw materials.

Keywords: powder metallurgy, moulding, sintering, special power metallurgy methods, additive manufacturing, near net shape, implant scaffolds, laser deposition of powders, thermal spraying and detonation spraying of powders

1. General description of the classical technological process of powder metallurgy for product manufacturing, especially products used in medicine and dentistry

Powder metallurgy (PM) is an important area of the technology of material processes which is still being intensively developed. In general, powder fabrication, preparation, preliminary moulding, sintering and finish treatment operations can be distinguished in a classical technological process of products fabricated by the powder metallurgy method [1–8]. Deviations from a typical technological process often occur in industrial or research practice. For example—preliminary moulding and sintering can often be combined into a single operation or, in so-called sinter-hardening, fast controlled cooling is used from a sintering temperature to harden or appropriately supersaturate the sintered element. Sometimes, the sinter achieved, having high porosity, is next saturated with melted metal with its melting point lower than this of the main component by infiltration. Other deviations can also exist from the said typical technological process, but it is distinctive that an input material in the form of powder is always produced and its sintering takes place at a temperature lower than the melting point of the main component [1, 3].

Metal powders are produced as a result of mechanical or physiochemical disintegration of the input solid material or as a result of chemical or physiochemical reactions—from other materials or chemical compounds, by reducing oxides, decomposition in high temperature, electrolytically, in hydrometallurgy processes or by sputtering a metallic liquid [1, 9]. Powder fabrication methods are split into five basic groups preconditioning the powder size, thus the properties in the subsequent pressing and sintering processes:

- mechanical from the solid phase (stripping, milling, grinding, breaking, grinding, crushing, shattering);
- physiochemical from the liquid phase (sputtering, granulation, sputtering and mechanical granulation);
- physical (evaporation and condensation);
- physicochemical (solidification, decomposition of carbonyls, reduction of oxides and other compounds, dissociation of oxides and other compounds, self-decomposition)
- chemical (sol-gel, electrolysis of melted salts or aqueous salt solutions, thermally from chemical compounds).

Disc-shaped, multiwalled-shaped or fraction-shaped powders are obtained by mechanical methods by crushing in ball, vibration or centrifugal-impact mills (Hametag powder in **Figure 1a**) [3, 10]. Mechanical methods are those having small efficiency and can be used basically for crushing metals and non-metals cleaned with the mill lining and ball materials, which then requires mechanical cleaning. A Hametag centrifugal and impact mill is a device most often used for powder crushing. Two steel propellers rotating in opposite directions at high speed in the mill drum create air whirls which capture the particles of the

http://dx.doi.org/10.5772/65376

metallic charge such as cut wires, chippings and other residues. The particles are crushed as a result of being hit by propellers and drum walls and by colliding against each other. The gas blown into the drum by a fan is lifting the powder and directs the powder via a segregator into a settler. Powder is periodically collected to air-tight magazines.

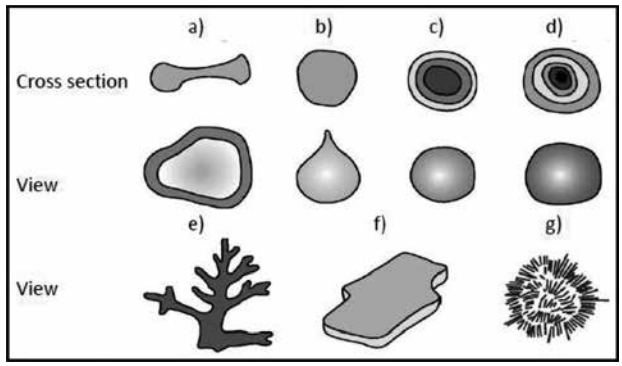

Figure 1. Examples of shapes of metal powders produced with different methods: (a) crushed mechanically in Hametag mill; (b) sputtered and reduced; (c) reduced; (d) carbonyl; (e) electrolytic; (f) flaky; and (g) reduced.

Sputtering is carried out by breaking up a stream of liquid (**Figure 2a**) into fine droplets by a sputtering agent working under high pressure. The agent is usually water, water vapour, air or inert gases. The liquid droplets solidify (**Figure 1b**) before falling onto the tank bottom. In addition, in a method known as DPG, mechanical disintegration takes place of a stream of liquid metal with blades—wedges mounted on a rotating disc (**Figure 2b**). In a method known as RZ (**Figure 1c**), a sputtering process is combined with chemical reactions of oxidisation, carbon burning or reduction taking place during the process or used later [3, 9, 10].

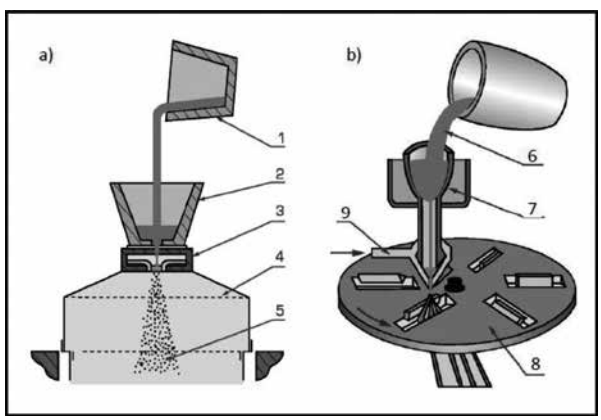

Figure 2. Diagram of device (a) for metal sputtering; 1—ladle, 2—melting pot, 3—nozzle, 4—sputtering chamber, 5—powder and (b) for production of metallic powders by DPG sputtering; 6—liquid metal, 7—funnel with nozzle, 8—water, 9—rotating disc with blades-wedges.

The electrolytic method consists of metal precipitation on a cathode, most often in the form of sponge, which is crushed into powder after drying (**Figure 1e**). Metal powders with a low boiling point, for example Zn, can be produced with the metal evaporation method and condensation of its vapours in a tank called condenser [1, 3, 9].

The aim of powder preparation is to produce an appropriate charge for further technological operations. Charge preparation processes include powder segregation into different grain fractions, mixing in the right proportions, adding slipping and pore-forming agents, as well as powder granulation [3, 4, 10].

In cold moulding, the powder is pressed in a closed space as a result of which compression occurs. A relevant cold-moulding method is selected depending on the die shape and powder properties, especially on powder plasticity, compactibility and mouldability, [3, 4, 10] namely:

- cold pressing in different types of presses in closed dies (**Figure 3a**),
- isostatic pressing in high-pressure chambers,
- vibration compaction of powders,
- circumferential pressing (**Figure 3b**),
- rolling pressing (**Figure 3c**),
- rolling of powders (**Figure 4a**),
- cold extrusion of powders (**Figure 4b**),
- impact moulding,
- cold forging
- casting and sputtering of slip, that is, a strongly compressed suspension of the powder of basic material in liquid with addition of agents preventing agglomeration of grains.

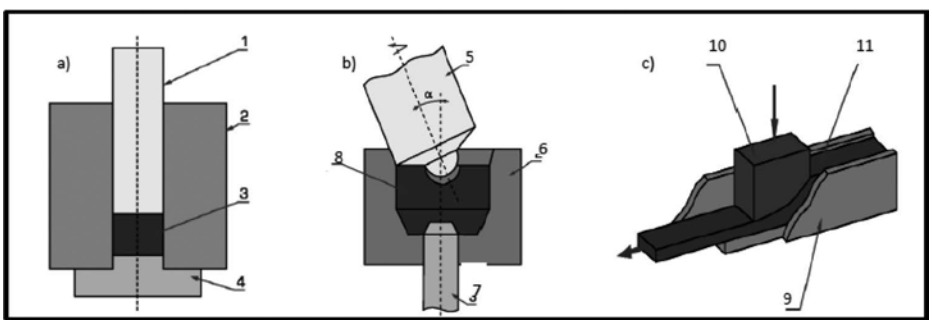

Figure 3. Compaction diagram (a) one-sided compaction of powders; 1—top punch, 2—die, 3—powder, 4—bottom punch; (b) circumferential compaction of powders; 5—rotating punch, 6—die, 7—pusher, 8—powder; and (c) rolling compaction of powders; 9—longitudinal die, 10—transferring metal piston, 11—powder.

http://dx.doi.org/10.5772/65376

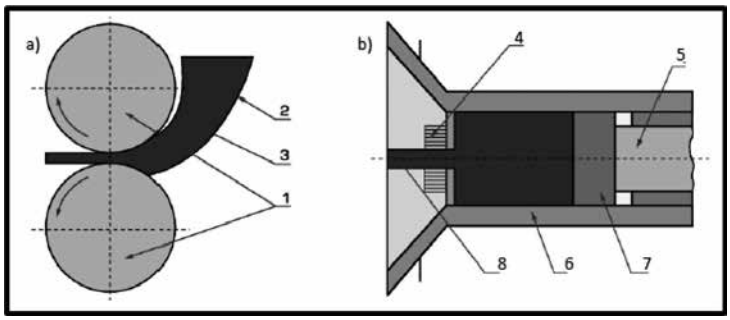

Figure 4. Diagram of (a) powder rolling; 1—roll, 2—fill funnel, 3—powder and (b) powder extrusion without shield; 4—die, 5—steel pipe, 6—powder pusher, 7—punch, 8—formed powder.

Matrices are created as a result of moulding, for example mouldings, forgings, wire rods.

Powder sintering refers to a technological operation (applied to a moulded element or loosely poured powder grains) whereby particular powder grains are bonded under the influence of heat and form a composite with specific mechanical and physiochemical properties [1, 3, 4, 6, 10–12]. Metal sinters or ceramic-metallic sinters called cermetals are produced as a result of sintering. Sintering can be carried out:

- freely,
- under the influence of force, that is, combined with moulding ensuring a specific shape, for example, by hot pressing of powders, hot rolling or hot forging.

A compact material is achieved due to sintering, which is usually however porous to a certain degree, with a single- or multi-phase structure. A homogenous or heterogeneous structure can be achieved by sintering with the solid phase and liquid phase.

Sinters have the following characteristics:

- particular grain powders are bonded,
- new grain boundaries are created,
- properties different than properties of matrices,
- volume usually smaller than matrices
- density higher than matrices.

Volume may be increase sometimes, however, due to sintering. Volume change caused by sintering should be taken into account in designing by using appropriate additives for matrices [1, 3].

The finish treatment of sinters includes:

- cold re-pressing or hot re-pressing, including hot isostatic pressing;

- plastic working, including forging;
- calibrating;
- machining;
- infiltration with metals with lower melting point;
- impregnation with organic materials, for example, oil;
- heat treatment and thermochemical treatment;
- plating;
- coatings deposition
- de-burring and burnishing.

In order to improve mechanical and physical properties, metal sinters can be subjected to re-pressing with various methods (cold re-pressing, hot re-pressing, hot isostatic pressing) as well as normal heat treatment which—depending on the chemical composition of the sinter—consists of hardening and tempering, supersaturation and aging, surface hardening, as well as thermochemical treatment, mainly carburising, carbonitriding or nitriding and passivation (steam treatment and blueing) [13]. Due to lower thermal conductivity, the heating and cooling rates of sinters are smaller than for conventional materials and their annealing time is longer [3, 4, 6, 10].

Finished products are calibrated under loads much lower than during a cold-moulding operation to achieve high dimensional accuracy and to achieve the required geometrical characteristics and properties, semi-products made of sintered metals shaped as blocks undergo plastic working, for example, forging or rolling.

Sinters with high porosity can be saturated with metals with a melting point lower than that of the ready sinter in the process of infiltration [1–3]. This can take place by immerging the sintered and porous skeleton in the melted saturating metal or by heating the skeleton with the powder of saturating metal in a furnace with a controlled atmosphere. Various liquid metal infiltration methods are utilised for a porous matrix of a product, among others a vacuum method and low- and high-pressure method, ensuring the thorough filling of the moulding pores with a metal matrix. Porous sinters can be soaked with organic materials, for example, oils in impregnation processes.

Machining, for example, grinding, allows to achieve the final shape and the required surface smoothness. Various surface treatment operations are also applied, including the deposition of coatings, for example, by physical and chemical vapour deposition PVD/CVD, plating with, for example, copper or stainless steel to enhance surface resistance to corrosion or for decoration purposes and also de-burring and burnishing [3, 4, 6, 10, 13].

Some of the mentioned technologies are considered special powder metallurgy methods and are presented in detail in one of the following sub-chapters.

http://dx.doi.org/10.5772/65376

2. Special powder metallurgy methods

Apart from classical powder metallurgy methods, many new special and hybrid variants and technologies have been developed and implemented, where the fabrication and application of metal powders and their alloys are of basic importance. Further works are taking place to improve the methods established so far and new ones are also being developed, for example, shock consolidation which uses high-pressure shock waves [4, 14–16]. The selected unconventional methods applied in powder metallurgy are characterised further in the sub-chapter.

Continuous powder processing (**CPP**) may relate to, for example, hot production of sheets made of powders where the powdered material is rolled at a rate of 0.5 m/s to decrease thickness twofold and to produce a strip which is next sintered and rolled again and finally sintered. Such a technology is commonly used for producing sheets and electrotechnical and electronic parts, as well as for coins [2, 3]. Extrusion processes are usually continuous both in case of mixing powder with a binder or plasticiser at room temperature and in case of extrusion at an elevated temperature without reinforcement. Continuous powder extrusion with binders is widely used for producing tool cermetals and also pipes and shaped products and sections and also spiral drills with a small diameter, for example, 0.5 mm and hard metal wires with the diameter of 0.1 mm. The Authors' own experience concerns the fabrication of rods made of aluminium alloys reinforced with halloysite and carbon nanotubes using this method [17–19]. The processes can also be employed for various metals and alloys and the length of extrusion can be 3–30 m and the diameter from several to several dozens of mm. It is also possible to sputter the powder continuously on a moving strip and then sinter it although the removal of the cold-formed materials in a cold manner from the moving strip may cause technological problems.

Powder forging (P/F) is a technology which is an extension of the traditional press and sinter method used in powder metallurgy [20, 21]. Porous preforms, obtained in a way similar to the conventional method, are then compressed by hot forging with a single blow (**Figure 5**) by one of the following methods:

- hot upsetting in which a preform is subject to considerable lateral flow of material;
- hot re-pressing, also called re-striking or hot coining, where the flow of material takes place mainly towards deformation.

This technology, known already before, was developed about 20 years ago mainly in connection with production of connecting rods in diesel engines in the car industry due to positive influence on the level of noise, reduced vibrations, improved surface roughness and lower production costs. This technology allows to reduce the number of technological operations from 17 to 8, to lower investment and operational costs of technological machines and decreases production costs by approx. 10% compared to a connecting rod forged from a solid material. It also became possible to reduce an active section and the mass of connecting rods made by P/F using an Fe-1.8Cu-0.4C powder blend as compared to those forged from a solid material made of microalloy steel despite decreasing fatigue strength by nearly 15% in relation

to forged products [20, 21]. Pistons were also manufactured by this method, made of an aluminium alloy produced from the mixture of Al-4.5Cu-0.5Mg-0.7Si powders.

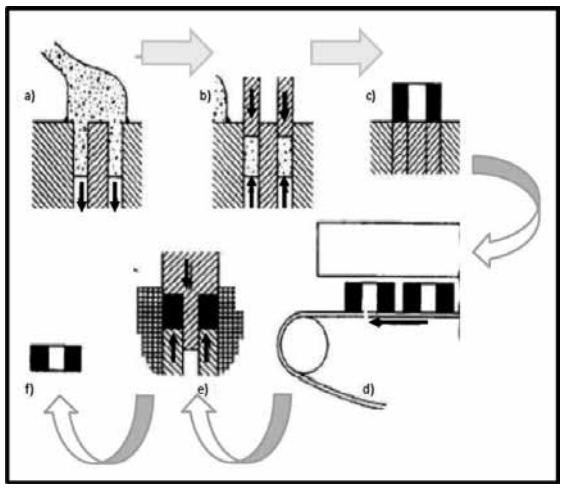

Figure 5. Operating scheme of powder forging (P/F) process; (a) powder full; (b) press preform; (c) eject from die; (d) preheat furnace with controlled atmosphere; (e) hot forge; and (f) eject fully dense part.

Hot pressing (HP) is a widely spread technology and thus can be classified as a conventional powder metallurgy method. Powders are formed or re-pressed at the temperature sufficiently high to induce sintering and creepage processes as a result of the aggregated activity of thermal energy and high pressure at a small rate of deformation [4, 5, 7]. Loosely charged or pre-compressed powder is in most of the cases placed in a mould made of graphite or steel which is ensuring electrical induction or resistance heating to the temperature of usually 2400°C in order to perform the process under the pressure of up to 50 MPa. Re-pressing takes place as a result of powder grain regrouping and plastic flow on grain interfaces. Three heating methods can be employed as induction heating or indirect resistance heating.

For conventional hot isostatic heating, heat is created inside the mould and a charge is subjected to the activity of a high-frequency electromagnetic field generated with an induction coil coupled with an electronic generator and with pressure applied to the punch by one or two cylinders. The mould is positioned inside the induction coil. Powders undergo this process even in the liquid phase and low pressure is possible, as well. An advantage of this method and the equipment used is that pressure and induction supply act independently. In case of indirect resistance heating, the mould is placed in a heating chamber (**Figure 6a**). The chamber is heated electrically with graphite heating elements and heat is transferred by convection. Regardless of mould conductivity, temperature and pressure, a high treatment temperature can be achieved which is an advantage of this method, while long heating time is the method's obvious disadvantage. The method is mainly used for producing hard and brittle materials, in particular for consolidating composite diamond-metal cutting tools and technical ceramics [1, 2].

http://dx.doi.org/10.5772/65376

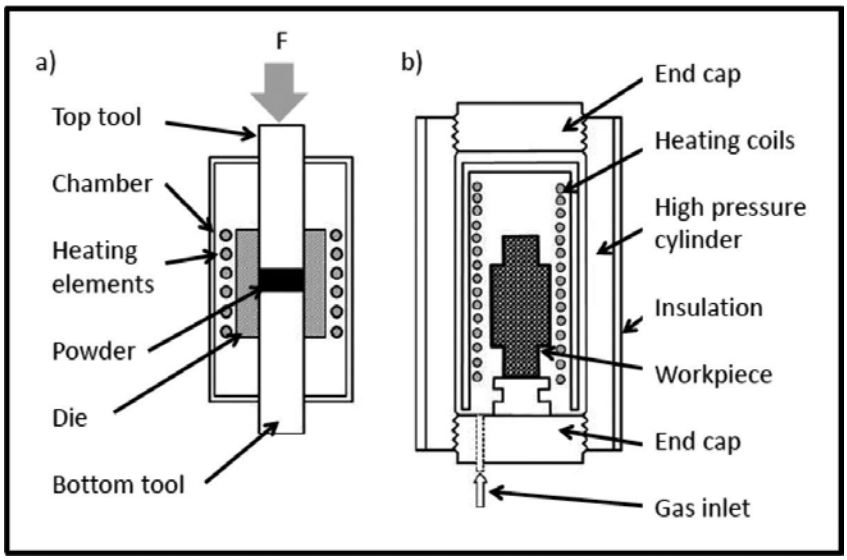

Figure 6. Comparison of the methods: (a) hot pressing (HP) and (b) hot isostatic pressing (HIP).

Hot isostatic pressing (**HIP**) is carried out in a high-pressure chamber (**Figure 6b**) at an elevated temperature, approx. 0.8 of the solidus temperature and under the isostatic pressure of gas, usually argon, although other gases or gas mixtures are used in special applications. The chamber is being heated, hence pressure in the tank rises and most often the device is equipped with a gas pumping system to ensure the pressure of 50–300 MPa [22]. Internal voids and microporosities are eliminated at the same time during the process and density is increased by combining plastic deformation, creepage and diffusion welding, as a result of which consolidation and re-pressing of sinters take place, in particular with a metallic matrix [4, 7, 22–24], notably nickel, cobalt, wolfram, molybdenum, titanium, aluminium, copper and iron and their alloys, as well as oxide and nitride ceramics, glass, intermetallic phases and composite materials. The process conditions are dependent on the type of sintered materials. The process is carried out by filling, closing and venting the tank, heating and increasing gas pressure in the tank, soaking under constant pressure and fast cooling with dropping pressure with a control rate of up to 100°C/min.

Spark plasma sintering (**SPS**) is a technology having different names in literature, notably electric-current-assisted sintering (ECAS); current-activated, pressure-assisted densification (CAPAD); pulsed electric current sintering (PECS); field-assisted sintering technique (FAST); direct hot pressing (DHP); electro sinter forging (ESF), although no differences exist between them essentially, apart from generally small construction differences in the devices used [2, 7, 25–30]. The methods can be indeed considered as the extension of the hot-pressing (HP) method. A direct method of heating is used in this method for rapid powder consolidation, ensuring high heating and cooling rates through pulsed electric current under atmospheric pressure and with uniaxial deformation. Initially, the devices introduced enabled to sinter powders conducting electric current only in **electric discharge compaction (EDC)** or **electric**

discharge sintering (EDS) processes. Non-conductive materials can be sintered in **plasma activated sintering (PAS)** and **spark plasma sintering (SPS)** processes apart from conductive powders. A single pulse cycle process is used in the PAS process, in which pulsed constant current is used at room temperature for short time and constant current is then used in the remaining part of the process. Pulse heating with electric current is used repeatedly during the whole progress of sintering in a multiple pulse cycle process corresponding to the SPS technology. An SPS sintering device is shown with a vertical uniaxial pressuriser with an incorporated water-cooled energising mechanism, a water-cooled vacuum chamber, accessories for controlling the vacuum atmosphere and exhaustion system, DC current pulse generator and a control system (**Figure 7**).

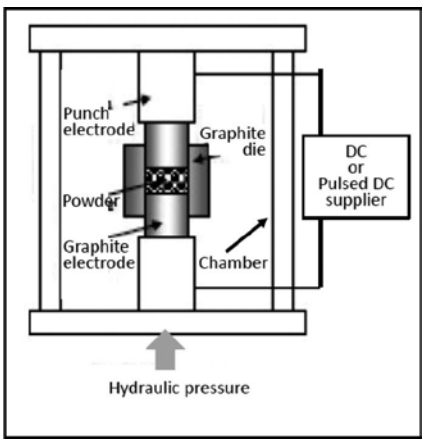

Figure 7. Principle of spark plasma sintering (SPS).

Powder materials are placed between a punch and a die between electrodes, which ensures rapid temperature growth to 1000–2500°C. As compared to hot press sintering (HP) and hot isostatic pressing (HIP) methods or atmospheric furnaces, the SPS method ensures easy operation and high reliability and accurate control of sintering energy at a high heating rate of 1000°C/min to the sintering temperature within several minutes, depending on the material type, dimensions and shape of the treated element, as well as device power and type (**Figure 7**). This distinguishes this method positively from conventional methods where sintering lasts more than ten and even several dozens of hours; hence, the SPS is finding more and more applications [30–32]. A temperature gradient inside the element being produced must be reduced to achieve sintering homogeneity, the decomposition of which is dependent upon electrical conductivity of powder, thickness of the die wall and presence of graphite insulation preventing direct contact with the element being treated and also ensuring electric contact between all the elements. The SPS is more and more widely used [2, 4, 7, 30–33] with the reservation that it enables to solid sinters only. The use of metal powders and die conductivity ensures fast heating of the treated part, especially when moulds have large diameter and relatively small height. This process is especially suitable for applications requiring high heating rates. This refers to materials which can

http://dx.doi.org/10.5772/65376

stay shortly at high temperature or in processes requiring high heating rates to achieve high temperature. Such materials can be sintered to obtain final density with near-net-shape accuracy; thus, it is not necessary to perform their final mechanical treatment, especially that they cause major difficulties when mechanical treatment is applied. The SPS technology has been recently employed for, among others, fabrication of sputtering discs and high-performance ceramic parts such as boron carbide, titanium diboron and sialon. This technology is becoming more and more important in the sector of friction materials, for production of sintered brake shoes used in fast trains and different cars and also in wind energy devices and even in quads and mountain bikes. Sintered clutch plates manufactured by this technology are used mainly for heavy trucks, ships, tractors and other farming machinery.

Powder injection moulding (PIM), with an important variant of **metal injection moulding (MIM)**, is a dynamically developing technology of manufacturing small-sized parts with an expanded surface [1, 2, 4, 34–36]. The PIM method has developed more broadly by advancements in the processing of polymers and by applying polymers as a binder and by establishing binder removal methods. This technology is applied for the mass manufacturing of small near-net-shape parts, which are additionally characterised by the fact they are highly complex and hard to produce with other techniques. Despite high costs, the PIM method has been developing exceptionally fast. Metallic powder moulding with metal injection moulding (MIM) is especially significant [37–39]. The sinters manufactured this method mainly have a homogenous structure, although the method also enables to attain a multi-layer or graded structure, for example, a material with a growing fraction of hard ceramic particles towards the tool surface, on the substrate material produced in the same technological process with the PIM method or on another material.

Several powder moulding techniques which employ binders exist, which can be generally classified into one of the pressure-free moulding techniques [1]:

- immersion method in which binder content is about 50%;
- casting of a polymer-powder slip into rubber moulds, in which a paraffin-based binder is used;
- pouring where the surface is covered with a binder and then powder is poured, which binds to the plasticised binder;
- electrophoresis;
- strip casting;
- surface lamination with thin coatings produced by strip casting;
- stream printing on part surface;
- stereolithography using a laser;
- pressing a slip through capillary nozzles arranged as x–y

- surface spraying.

Regardless of the methods of pressure-free moulding, extrusion and injection moulding, the entire process consists of mixing the powder and a binder, moulding, removal of binder and sintering [1, 4, 6, 7]. Classical injection moulding in moulders does not differ from the moulding of thermoplastic polymers, while the injected preforms should be subjected to binder removal and sintering to achieve the expected functional properties (**Figure 8**).

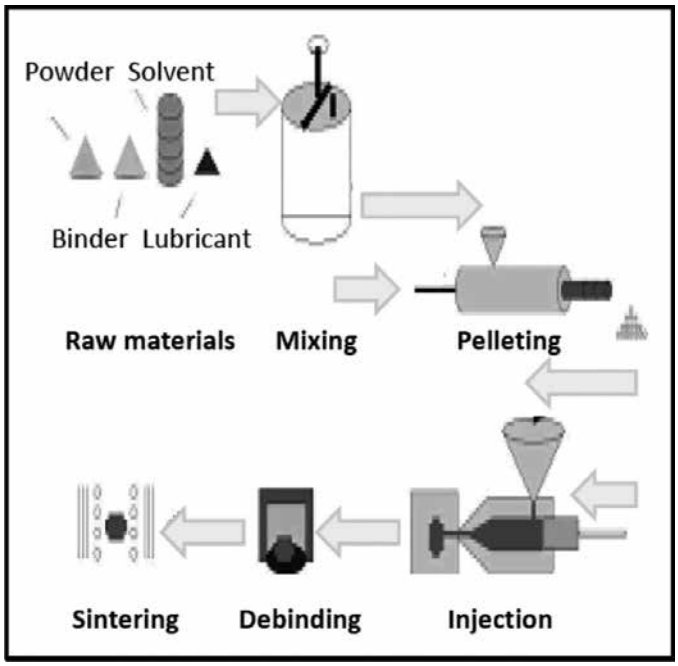

Figure 8. Principle of powder injection molding method.

The use of thermoplastic polymers as a binder which is binding metallic or ceramic powder also enables to transport it and mould it in an injector socket. Two types of binders based on, respectively, paraffin or polymers and an aqueous methylcellulose solution are used most often. Owing to the key advantage of this method where ready parts are produced without additional treatment necessary, it is used more and more extensively for producing hard materials, including tool materials which are exceptionally difficult and costly to machine. The formability of metal and ceramic powders and their mixtures allows to fabricate, in particular, metal tools with relatively high ductility, ceramic tools with high hardness or composites with a metal matrix composites (MMC) and ceramic matrix composites (CMC) matrix combining high properties characteristic for metals and ceramics [1, 40]. A powder-to-binder ratio is closely linked to the shape, the size of powder particles, powder wettability by a binder and the properties of the binder itself as well as is linked to mixture production conditions. Despite numerous advantages, an injection moulding process is not suitable for fabrication of large parts with dimensions exceeding 100 mm.

http://dx.doi.org/10.5772/65376

Binder removal is costly, which affects the final price of the materials so produced and removal can be either [1]:

- thermal,
- hydrolytic,
- mechanical,
- environmental,
- by biodegradation or
- by photodegradation.

Thermal and solvent degradation is utilised predominantly for removing polymers serving as binders in the PIM method. The mixing method is linked to combined degradation techniques, for example, solvent and thermal technique.

At present, for exceptionally small preforms, binder degradation is associated with heating to a sintering temperature [1]. At least two binder components are required for fast binder removal so that one of them, that is, skeleton polymer, maintains the composite shape to high temperature in which sintering occurs. A temperature of this polymer's thermal degradation should be as high as possible. The second binder component should be removed in low temperature or during solvent or catalytic degradation. Paraffin can be an example of this. The component which is degraded first should account for 30–98% of the binder content. Oils and wax have low melting points. Oil or wax can be removed by filtering off, that is, can be sucked away by porous pads.

A binder is often removed with a solvent and thermally [1]. A solvent removes one of binder components by opening pores in the whole volume of the preform, which allows for the quick thermal removal of the next binder component. In all binder degradation types, higher velocity is possible using a higher temperature, which, however, increases the probability of preform damages or deformations. An atmosphere of flowing gas, which evacuates degradation products and is constantly replenished, also assists in higher degradation velocity.

Solvent degradation is relatively fast, but necessitates solvents which are frequently aggressive and unfriendly for the environment [1, 34–36]. Water-thinnable binders are recommended for this purpose. Another solution is to use water as a binding substance, together with starch, salt or sugar. Once a preform is formed, it is dried or frozen and water is removed by freeze drying. Catalytic degradation combines thermal and solvent degradation, where the rate is determined by the temperature and a catalyst concentration. Skeleton polymer, on which a catalyst has no influence, maintains the element's shape until sintering temperature. As degradation takes place at the interface between polymer and a catalytic atmosphere, a nearly flat degradation front moves through the whole moulding. The final decomposition of the binding substance occurs due to thermal degradation and requires slow heating which is preventing damages.

Solvent and catalytic methods cause a smaller deformation as compared to thermal degradation made at the same time, but they require two operations. Sintering is initiated by growth

in the concentration of carbon resulting from binder degradation; however, in case of some materials such as stainless or high-speed steels, a carbon concentration must be closely monitored due to their properties or influence on heat treatment [35, 36, 38]. This type of the binder used influences the final carbon concentration.

Preform density depends on injection pressure, powder particle size and binder content and it is about 60% of theoretical density when the binder is completely removed. Binder content is 30–55% depending on the powder shape and wettability. Irrespective of the preform density, it is subjected to densification and shrinkage due to sintering, which is higher for high porosity. Sintering is usually the last stage of the technological process decisive for density and properties of the ready product and is irreversible. If the ready element should have high mechanical properties, final heat treatment and often machining are used to ensure accurate dimensions of the produced sinters. The sintering of injection moulded or pressure-free moulded powders does not differ largely from the sintering of powders formed by other methods. High-speed steels are subject to supersolidus sintering. Sintering activators in the form of boron, copper, phosphorous copper, carbon, molybdenum, tantalum, titanium, vanadium and tungsten powder are added to iron powders and iron alloys, while the process itself is called activated sintering with the forming liquid phase. In case of graphite, if it has not been used as a reducer of the oxides situated on the surface of powder particles, it leads to a reduction in solidus temperature, as in the sintered high-speed steels. In general, the growing content of carbon is, however, reducing sintering temperature, broadening the range of sintering temperature and lowering the content of pores and allows to produce a homogenous structure with small carbide precipitates [1, 35, 36, 38]. Fine-grained powders are remelted faster and the size of a powder particle is also decisive for surface roughness.

An atmosphere inside the furnace chamber is an important factor conditioning sintering [1]. It is not suitable to choose inert gas, for example, argon, for high-speed steels, as this gas is not soluble in steel and gaseous bubbles may form. An atmosphere during sintering should also be selected in terms of costs generated by the selected gases. Vacuum sintering is a costly alternative, but nevertheless, vacuum is often used for sintering high-speed steels. The sintering of injection moulded high-speed steels in high vacuum is quite difficult due to gas products being released, coming from the thermal degradation of skeleton polymer residues; hence, a better solution is an atmosphere of flowing gas or a gas mixture, most often N_2-5%H_2 or N_2-10%H_2 with the right dew point temperature.

In **mechanical alloying (MA)**, also called **mechanical powder press (MPP)**, alloys are produced from powders of pristine metals as a result of milling in high-power mills [7, 41–45]. The procedure begins by placing a mixture of powders with the right proportions in a tightly closed mill container together with crushing parts made of abrasion resistant materials, for example, hardened steel, sintered carbides or ceramics from other abrasion resistant materials. Then milling, as long as necessary, is carried out with strong vibrations and with the activity of centrifugal forces, which are inducing a high collision energy and the temperature is growing itself to approx. 200°C. It lasts as long as the predefined state is reached, when the chemical composition of each powder grain corresponds to the initial proportions of the charge materials (**Figure 9**).

http://dx.doi.org/10.5772/65376

Several types of mills are used, in particular vibration and planetary ones, atritors and others [4, 9]. In high-power milling, welding takes place repeatedly along with crushing (breaking) and re-welding of powder grains. It is accompanied by the crushing of the powder structure and many defects are formed. The structure becomes metastable and can be either a solid solution, an intermetallic phase and a mixture of components or have the amorphous form. The mechanical alloying method produces a nanocrystalline structure in metals. This is a result of dislocations being generated successively in powder grains. Their density is constantly increasing and annihilation takes place during recovery and polygonisation and then static recrystallisation occurs. Recovery in metals with a low melting point takes place easier and the substantial refinement of structure grains usually is not taking place. The crushed powder is next consolidated with different methods to achieve the desired shape. In some cases, it is required to apply a hot isostatic pressing (HIP) process for uniform powder compaction and sintering [1]. Ready products are heat treated to ensure the required structure and properties.

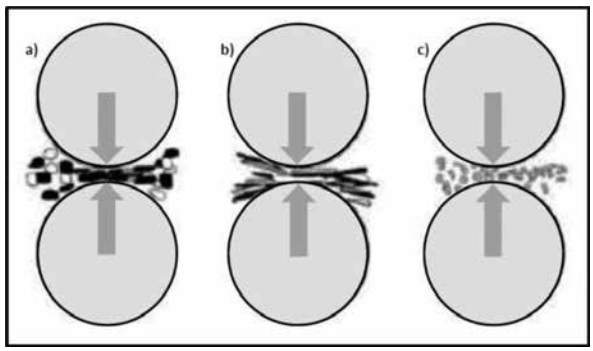

Figure 9. Principle of mechanical alloying (MA); (a) mixture of input powders: (b) elongated composite particles; and (c) homogenous equiaxial powder grains.

The advantages of the mechanical alloying method include crossing the solubility limit in the solid state, the synthesis of new crystalline and quasi-crystalline phases. Amorphous phases as well as ordered and unordered intermetallic phases are produced. Certain elements can be used in an unrivalled way as alloy additives and chemical reactions can be triggered, which are usually occurring at a low temperature. Process scalability is also achievable; besides, it is possible to dispergate, as described below, the particles of the second phase (usually oxides) in a matrix of the material produced. The strength and physiochemical properties of products of mechanical synthesis depend on the type of mill, temperature and milling atmosphere. High-melting nitrides, carbides, borides and oxides can also be achieved with mechanical alloying methods [1, 43].

The mechanical alloying (MA) method, describing a process in which a mixture of powders is milled at the same time—usually different metals or alloys and phases—thus leading to the fabrication of homogenous alloys, can also be otherwise called in literature mechanical milling (MM). In this method, the powder with the uniform composition of, for example, pristine metal, intermetallic phase or metal alloy is subjected to the process. Even the name of me-

chanical disordering (MD) can be met when, as a result of long-lasting milling of intermetallic phase powder, its disorder takes place or an amorphous phase is created. Moreover, the term of mechanical grinding (MG) can be found in some works [44–46], which is normally used, however, for abrasive machining processes, inherent to the formation of chippings, which is not appropriate for the process discussed.

Mechanical alloying and oxides dispersion strengthened (MA/ODS) encompass metallurgy methods utilised until the 2nd half of the twentieth century to fabricate materials with a nickel, iron and aluminium matrix [2, 4]. The materials were used for the first time as parts of gas turbines for aviation engines, later for industrial turbines, including blades, nozzles and combustion chambers. At present, the materials fabricated with powder metallurgy methods by mechanical alloying and dispersion hardening with MA ODS oxides are used for numerous parts in various branches of industry, including diesel engine heater plugs, parts of heat treatment furnaces such as shields, baskets, pallets, slide tracks for steel pallets, combustion chambers of coal and oil furnaces, guards of thermoelements, parts for liquid glass processing. Metal powders with an appropriately selected chemical composition and structure are manufactured by the mechanical alloying method in mills with horizontal balls or between vertical disc-type grinding wheels. Powder particles with varied composition, that is, Ni, Ti and Al, are joined in cold conditions and at the same time, other particles are cracking. This stabilises the powder size and chemical composition. Subsequently, the powder manufactured by the mechanical alloying method is mixed as a matrix with the average size of 150 μm (fraction of approx. 15%) with nickel powder with the size of 4–7 μm (with the fraction of approx. 64%), chromium powder with the size of 150 μm (with the fraction of approx. 20%) and also approx. 2% of Y_2O_3 with the size of approx. 25 nm. The mechanical alloying and oxides dispersion strengthened (MA/ODS) method can be used for manufacturing various materials, in particular MA 754, MA 758, MA 760, MA 6000, MA 956 superalloys according to ASTM, containing nickel and in case of MA 956—iron and 15–30% of Cr, 0.3–6% of Al, up to 2.5% of Ti, up to 4% of W, up to 2% of Mo, up to 2% of Ta, 0.5–1.1% of Y_2O_3 and possibly microadditives as rods, sheets, panels, tubes, wires, sections and forgings [47–50]. Their properties depend on the structure of grains and also the presence of fine-grained oxide precipitates. Annealing is usually applied after fabrication, for example, at 1315°C. The grains have an elongated structure connected with the pressing or deformation technology and ensure high mechanical properties at elevated temperatures. If an equiaxial structure of grains in the sheet plane is ensured by applying the technology with due care, nearly isotropic properties are existing in the sheet plane. Materials may be welded with a tungsten electrode in the shield of inert gases, with an electron beam or by a laser and also welded in a vacuum or brazed by diffusion.

Selective laser sintering (SLS), otherwise called direct metal laser sintering (DMLS) or high temperature laser sintering (HTLS), is currently one of the most popular additive manufacturing technologies of laser additive manufacturing (LAM), which can be considered one of the most advanced powders metallurgy methods in which sequentially acts of local sintering are taking place with or without a liquid phase of two or several powder grains with a preconsolidated part of an element manufactured by this method [4, 51, 52]. It is possible to remelt powder with a laser beam and in such case, the material is transiting from the solid

http://dx.doi.org/10.5772/65376

state, in form of powder, through the liquid state, to the solid state, in the form of the item being produced. The method known as selective laser melting (SLM) is indeed very similar to the discussed SLS method. In such technologies, an infrared laser radiation beam is used, a source of which is a CO_2 or Nd:YAG laser, in order to melt or remelt metal or metal alloy powder grains, or even a mixture of one or several metals or alloys, ceramics, glass or polymer materials powders and a powder layer is bonded initially with the working base plate and then with the systematically constituted successive layers of the element produced with a designed #D shape. A beam of laser radiation is selectively bonding the powdered material on the powder bed surface by scanning the successive sections of a 3-D model of the designed element in a special software environment of computer-aided design (CAD) based on scanning data for reverse engineering (RE). A double and even a multiple system of lasers can also be applied. No additional supporting elements have to be used here, as the material subjected to sintering is supporting the projecting and inclined parts or the closing surfaces of the element being produced. The process is controlled by a computer, after designing and modelling the manufactured product using a special CAD programme [53–55]. In order to execute an entire manufacturing cycle of any part by one of the technologies mentioned, the subsequent thin layers of powder or a mixture of powders have to be spread automatically across the working table surface with appropriate roughness and temperature, placed on a working table with automatic position adjustment and then on the surface of the layers bonded in advance (**Figure 10**).

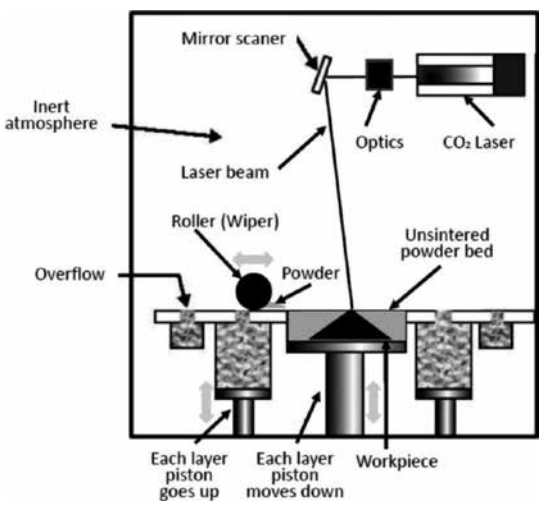

Figure 10. Principles of selective laser sintering.

Each layer of powder is levelled each time with a scraper. A computer-controlled laser beam is guided across the powder surface with a CAD programme in successive layers (corresponding to the cross section of a virtual special model of an item recorded using CAD 3-D digital recording), causing the sintering of the powder particles in a strictly defined manner and in the selectively chosen places on the powder surface. A table with another layer of powder is

lowered to the set height corresponding to one thickness of a layer resulting from the automatic virtual division of the spatial item model into layers with the set thickness, after each cycle corresponding to one scanning section of the powder bed and another, new layer of material is applied on the top [51, 52, 54, 56, 57]. The powder particle size range is between 20 and 70 μm, while the thickness of a single layer corresponds to approx. 0.1 mm. The process of powder distribution and laser sintering cycle is repeated until a fully bonded item is achieved in line with the model designed, which can be put into use after cooling down and cleaning off the excess powder. This is critical for increasing or decreasing dimensional accuracy and surface roughness of the parts produced. If the unsintered powder surrounding such an element during the process cannot be removed mechanically with a scraper, it can be removed through small windows or drain openings specially designed in a given element, which prevents any small volume of powder from being seized in its closed sections. This distinguishes such technologies positively from other technologies, by ensuring design freedom unavailable in other traditional technologies. The system ensures temperature monitoring of the item produced and laser sintering conditions of the item with mechanical properties reproducible in the whole volume. Depending on the powder material, after laser sintering, it is possible to achieve up to 100% of the density and properties of the materials with the identical chemical composition, but which were produced with conventional methods.

The quality of elements fabricated by SLS may be influenced by powder quality and laser power having an effect on the density of the item produced. As density depends on the peak laser power, hence the impact time of a laser is not very important, a pulsed laser is used most often. An SLS device is heating a loose powder material in a bed just below its melting point to facilitate the local growth of temperature with a laser beam. The quality of the fabricated elements depends on the maintenance level of the device, an operator's design and operational experience and even the manufacturer's business practices. It is important to align the element being produced relative to the working table, for example, the best accuracy of element diameter in different directions can be achieved by aligning a wheel in the XY plane level and then approx. 0.5 mm thick layers can be best produced by aligning them in the Z axis, while some parts can be achieved most advantageously in a plane oriented at the angle of 45° [54, 58].

Additive manufacturing methods are used for sintering a broad array of metallic powders, including, among others, light metal alloys, titanium alloys, steel, cobalt and chromium alloys and superalloys and their mixtures and also polymer materials, such as nylon (pure, with glass filling or with other fillings), polystyrene, polyamide or ceramics and composite materials [51, 54, 57–59]. Single-component powder, usually produced in a ball mill, has to be used for some SLS devices and double-component powders are, however, used in majority of cases, usually in the form of coated powders or a powder mixture. A laser in single-component powders is melting the external surface of powder grains only, as a result of which unmelted solid cores of such grains are bonded with the previously sintered layer [57, 59, 60].

SLS technologies are commonly used across the world as it is easy to fabricate parts with highly complex shapes directly from digital data in CAD systems, without having to produce any tools. The applications of SLS technologies in arts and industrial design and even

http://dx.doi.org/10.5772/65376

in jewellery and for decoration, were initially less expected but are witnessing sharp growth. SLS technologies enable to fabricate single elements or elements in small series, according to individual market demands, ensuring hollows, cuts and internal channels which are difficult or even impossible to achieve conventionally [51–60]. As several or multiple, even small, elements can be manufactured at the same time on a single working table and after loading once to a device's working chamber, very high process performance can be attained. All the quantified types of SLS/SLM belong to advanced additive manufacturing methods, among others to **rapid prototyping (RP)** and **low-volume production (LVP)**, for example, for machine parts and to **rapid tooling (RT)** used in particular for producing steel moulds for injection moulding or pressure casting, for metal stamp dies and also for machine parts. The methods are also employed for producing metal prototypes and final products as a result of laser sintering of metallic powders and also for applications in medicine, implantology, regenerative medicine and regenerative dentistry, for example, for an artificial lower jaw made of titanium and ceramic and for fabrication of highly specialised medical tools [55, 56]. For this, the expected biocompatibility of the applied powder material must be ensured and it must be possible to sterilise the ready product. Another example are own investigations [54, 58] pertaining to the development of metallic microporous materials with the average size of micropores of 100–600 nm, microporous composite materials and microskeleton composite materials fabricated using hybrid rapid manufacturing technologies with selective laser sintering/selective laser melting (SLS/SLM) of titanium and TiAl6V4 alloys combined with chemical treatment, by etching the surface of porous skeletons and then covering the internal surface of micropores with biocompatible materials by **atomic layer deposition (ALD)** or by methods of immersion, pressing, sol-gel method and by infiltration [56].

Innovative implant scaffolds used for implantation to replace the bone pieces removed surgically due to cancerous disorders or inflammatory conditions were developed (**Figure 11**). An implant scaffold is comprised of a solid zone and a porous zone with pores sized 100–600 μm, fulfilling the functions of scaffolds. It is possible to cover the internal surface of micropores with a thin layer of a bioactive material up to 500 μm thick and to integrate the implant scaffold with joint implants. The porous zone ensures appropriate osteosynthesis with bone elements remaining after the removal of joints and enables the living tissue to outgrow across the porous zone after implantation. For this method of manufacturing a bone implant scaffold, individual patient data have to be acquired with medical imaging methods, for example, computer tomography. A virtual model prepared in, for example, STL format, created by means of software, for example, AutoFab, enables to design a virtual technological model of an implant scaffold with a method of repeatable unit cells. Such a model enables to manufacture a ready real bone implant scaffold by selective laser sintering with the shape adjusted to the patient's bone loss. A manufacturing method of personalised dental implant scaffolds used in the treatment of teeth and bone losses situated in the dental system and in a craniofacial bone is identical. Individually fabricated tooth implant scaffolds with geometrical features reflecting the shape of a post-extraction alveolar bone with integrated abutments will ensure a single-operation surgical procedure of tooth extraction and implantation without having to bore the perio-

dontal tissue bone of the upper or lower jaw, guaranteeing a substantial improvement of osseointegration compared to classical implants [55, 56, 61–63].

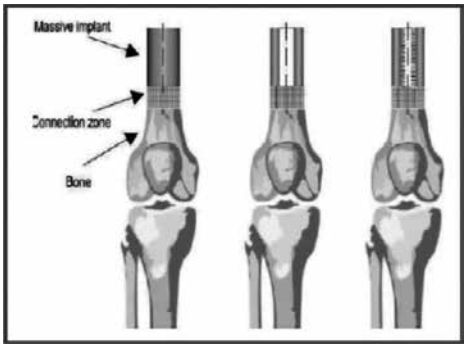

Figure 11. Schematic of combination of implants and scaffolds produced by SLS with natural bone stumps.

Electron beam melting (EBM) is an additive technology similar to SLS, but a beam of electrons is used for metal powder melting instead of a laser beam (**Figure 12**) [57, 64, 65]. In this technology, the element produced is constituted a layer after layer, so that after alloying and solidification of one powder layer, the process is repeated for the subsequent layers until a ready part is created. The EBM process takes place in vacuum; hence, elements can be produced with reactive metals with high affinity to oxygen with high energy efficiency, even 5–10 times higher than for open processes in laser technology. Parts made of titanium and its alloys can be produced this way, including TiAl6V4 commonly used in, for example, aviation industry and for implants, for example, bone and dental implants. The elements made with this technology from titanium alloys exhibit mechanical properties corresponding to forged materials but are much better than cast materials.

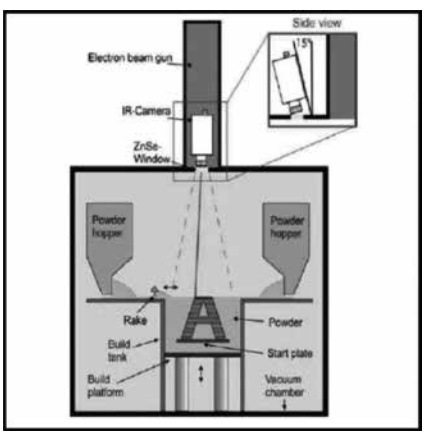

Figure 12. Principles of electron beam melting (EBM).

http://dx.doi.org/10.5772/65376

A beam of accelerated electrons emitted by an electron tungsten gun after passing through a beam concentrating electrode and obtaining a beam size with the required diameter is specially deflected and directed as designed in a CAD system in the right place on the powder bed surface and as a result of impacting the metal powder, its kinetic energy is converted into thermal energy [65]. If the temperature rises above the powder melting temperature, it can be melted and sintered with the previously constituted layer of the fabricated element. A scanning rate of the beam reaches 1000 m/s, which allows to constitute a newly created element with the efficiency rate of up to 60 cm^3/h and ranks this technology among the most efficient additive manufacturing technologies.

3. Laser deposition, thermal spraying and detonation spraying of powders

Apart from the classical powder metallurgy methods and new special and hybrid variants and technologies already discussed in this chapter, numerous derivative methods have been established requiring the use of powders, manufactured with classical methods, serving to improve the properties of different products produced with other technologies. Selected laser deposition, thermal spraying and detonation spraying of powders methods are characterised further in the sub-chapter.

Laser treatment including alloying, laser cladding and hardfacing and laser treatment of biomaterials has been enjoying increased popularity over the recent several decades and rising importance in forming the structure and surface properties of engineering materials [13, 40, 66, 67]. In laser surface treatment, a laser beam is interacting with the surface of the treated material and thermal energy is absorbed and as a result, the surface layer is remelted and some absorbed thermal energy is penetrating the material as a result of which a high temperature gradient exists between the remelted material layer and an unmelted substrate. Convection occurs in the melted material layer due to the differential temperature between the remelted surface and the bottom of the remelted area and by the supply of shield gas and the material is mixed. A high temperature gradient contributes to the fast solidification of the remelted and mixed material of the surface layer and surface layers are achieved with their thickness of decimals of millimetres to several millimetres and with enhanced functional properties on a substrate made of a relatively cheap material [13]. The following laser technologies can be distinguished, which use material powders to ensure the required properties of materials' surface, depending on the density of laser beam power and the duration of beam interaction on the material:

- alloying,
- cladding
- melting (hardfacing).

In laser alloying, an alloying material and a substrate are melted at the same time by a laser beam by mixing them intensively in a liquid pool. Remelting and cladding are differentiated between depending on the method of introducing an alloying additive to the pool. The alloying

process consists of depositing an alloying material onto the substrate and then remelting it together with the surface layer of the material substrate [13, 66, 67]. An alloying material is being applied onto the substrate material by painting methods, by covering with the glued pastes or by powders (with powdered ferroalloys of saturating metals, boron, wolfram and titanium carbides) or by thermal spraying (plasma, flame, detonation spraying). As heat is conducted from the pool, a thin layer of material in the solid state contiguous to the pool is also melted, as a result of which a very thin 10-μm-thick diffusion zone exists on a boundary of the solid and liquid phase after cooling although in some cases, alloying elements diffuse even to the depth of 200–300 μm. Alloying is carried out with a laser beam passing once or several times [13]. The material in the alloyed layer solidifies once the laser beam ceases to operate and the substrate material in its adjacency is hardened. The structure of this layer, its chemical composition and physiochemical properties differ from the substrate and from the alloying material. The thickness of the layers attained by remelting alloying is 0.3–0.4 mm with impulse heating or 0.3–1.0 mm with continuous heating.

Laser alloying may also be used to introduce non-metals, carbon, nitride, silicon and boron into the surface layer. Laser remelting usually consists of enriching a surface layer of materials with such metals as Co, Cr, Sn, Mn, Nb, Ni, Mo, W, Ta, V or with some of their alloys, for example, Cr-Mo-W, Ni-Nb. Machine steels are employed most often by remelting with powdered carbides WC, TiC or mixtures of WC-Co and tool steels—with different mixtures of carbides, tungsten, tungsten carbide and titanium carbide, chromium or vanadium borides, vanadium carbides, boride carbides or their mixtures with chromium and mixtures of Mo-Cr-B-Si-Ni [68–71].

Laser remelting is carried out the same as laser alloying, except that the cladded powder particles are not remelted in the liquid surface layer but are mixed by convective movements in a liquid matrix and after cooling and solidification, the dispersion hardening of the surface layer matrix takes place [13].

In **laser cladding**, also called plating or hardfacing, a thick layer of the cladded material is melted and a very thin layer of the substrate material is remelted together with melting the deposited coating material, remelted to obtain a coating more resistant to erosion, corrosion or abrasion than the substrate. The cladded layers may be several millimetres thick and are thicker than the alloyed layers [66, 72]. The cladded material may be either soluble or insoluble in the substrate material. A transient layer produced between the substrate and the cladded layer is strongly connected with the substrate. Remelting from the top is disadvantageous as it promotes the formation of bubbles and unmelted spots near the substrate, which is also supported by the binder of the cladded layer powders. In an injection cladding process, powder can be poured either by inertia or by vibration or delivered in a stream of insert gas (e.g. nitride, helium, argon) or also air. If active gas is used for powder feeding, an exothermic reaction takes place intensifying the process. As in such cases, the powder or a powder mixture is blown into a laser beam zone; therefore, they are subject to remelting and in such a condition, they fall on the substrate and form a solidifying remelted layer on its surface from the bottom. A laser beam is coupled to a powder feeding nozzle as per the motion of the worked item. Laser remelt-

http://dx.doi.org/10.5772/65376

ing causes structure refinement and dissolution of carbide phases, as a result of which a solution supersaturated with alloy elements is created after cooling. This ameliorates operating properties and enhances wear resistance and properties at an elevated temperature, which make them suitable for use with corrosion-resistant materials, tool materials, materials resistant to wear and heat-resistant materials and those resistant to wear at high temperature. Steel is cladded with aluminium, cobalt and titanium alloys, the mixtures of C-Cr-Mn, C-Cr-W, Cr-B-Ni, Cr-Ni, Cr-Ni-B-Fe with an admixture of C and Si, Fe-Cr-Mn-C, Mo-Cr-CrC-Ni-Si, Mo-Ni, TiC-Al_2O_3-Al, TiC- Al_2O_3-B_4C-Al, stellites, carbides WC, TiC, B_4C, SiC, nitrides, including BN, chromium oxides and SiO_2. Nickel alloys are used for the cladding of alloys and the mixtures of ZrO_2-CaO or ZrO_2-Y_2O_3 are used for cladding aluminium and copper [13].

Laser alloying, cladding and hardfacing ensure the highest quality of surface layers with the thickness of 0.1–1.5 mm although the main difficulty is a cracking tendency in the area of surface layers and in the heat-affected zone of the substrate [13, 66, 67, 71, 73–80]. A cracking tendency can be limited or totally eliminated by applying a graded fraction of hard ceramic phases or a gradient concentration of an alloying component in the surface layer, as well as by applying an indirect layer between a top layer and a substrate [68–70, 81].

Powders of different materials can also be used in traditional hardfacing technologies, which were not described in this chapter. The binder material may then be fed through a magazine or powder feeder. In plasma cladding, an additional material, in particular in the form of powder with the grain size of 0.06–0.3 mm with a slightly remelted substrate, is melted in a plasma arc with the temperature of 18,000–24,000°C. The powder is entered into a plasma burner from a feeder by means of transporting gas, normally argon, ensuring thorough protection against the access of air, so that after melting in a plasma arc exiting the nozzle, it is transported by gases under pressure to the substrate, creating a padding weld with the minimum fraction of the substrate material and thickness of 0.25–6 mm in one pass. An additional material is powder on a matrix of cobalt, nickel, iron, chromium, copper and zinc. Plasma cladding is applied to parts of combustion engines, cutting tools, cutting blades of tools for earthworks, valves, valve sockets, steel roll necks, connectors of drilling lines made of non-alloy steels, stainless steels, cast steel and some type of cast iron [13, 82].

Thermal spraying (TS) is a method to produce coatings in which the melted or doughy substrate material is applied onto the surface of a pre-prepared substrate. Pristine metals, metal alloys, ceramics (oxides, carbides, nitrides, borides and some glasses), metallic compounds (sulphides, silicides, cermetals, intermetallic compounds) and some polymer materials (epoxides, nylon, Teflon and others) are used for coatings. The coatings of such materials are applied onto a substrate made of much less costly materials or such having better availability than a substrate, including metals, ceramics, glass, as well as on some polymer materials, wood and paper, which is not the topic of this chapter, similar as the use of solid or powder wires as charge materials [13, 83–88]. Thermal spraying methods are often used for the deposition of materials onto non-metallic materials; for this reason, this method is called 'metallisation'.

The following thermal spraying technologies are distinguished:

- arc spraying,
- plasma spraying
- classical or ultrasound flaming.

The cover material powder is situated in an electric or plasma arc or in a gas flame where it is melted and scattered by a stream of gas such as argon, nitride or compressed air or in a gas flame. The stream of gas is covering liquid particles with the diameter of 0.01–0.05 mm directs them onto the surface of the covered element with the velocity presented for each method in **Table 1**. Those particles have an impact on the surface, are cooled on and joined with it. Little heat is delivered onto the substrate, as a result of which its temperature is rising only to 100–250°C. Thermal spraying is therefore not causing any structural changes or plastic deformation of the substrate and this type of coverings can be used, among others, in thin and precise parts and for materials susceptible to the activity of heat. The substrate being sprayed has a layered structure with a varied concentration of pores, which can reach up to 20%. Coatings are usually between 0.05 and 2.5 mm thick although may be even 12 mm thick. The coatings attained can also be thinner than for other methods [3, 13, 82, 89–91]. A spraying operation can be carried out by a structure fabricator, on an assembly area or in the place where the structure is to be operated. This allows to reduce transport and assembly costs.

Method	Source of heat	Process temperature (°C)	Deposited material	Velocity of impacting particles (m/s)	Adhesivity	Efficiency (kg/h)
Arc method	Electric arc	5000–6000	Metals	250	◔	30
Plasma spraying		8000–20,000	All	250–1200	◔	1–25
Flame spraying with powder	Flame	3000	Metals, ceramics, polymer materials	30	◕	7
High-velocity oxygen fuel (HVOF) spraying		3000	Metals, carbides	600–1200	○	14

Symbol: ○ very high; ◔ high; ◑ average; ◕ low.

Table 1. Comparison of basic methods of thermal spraying with powders [3].

The application of thermally sprayed coatings has been growing year by year and thermally sprayed coatings have gained numerous practical applications, including those ensuring [13]:

- anticorrosion resistance—Zn or Al on cast irons or steels, notably on structural parts of steel bridges, in petroleum industry, car industry, shipbuilding industry, road sector, railway, electrical engineering, construction and infrastructure components;

http://dx.doi.org/10.5772/65376

- heightened heat resistance and corrosion resistance—high-chromium alloys on internal surfaces of boilers, Al or modified on the Al matrix, such as Al-Si, Al-Cr, Al-Pt, Pt-Al-Cr, Ni alloys crystallised directionally and monocrystals on parts of gas turbines;
- heightened heat resistance and fatigue strength—coatings as MeCrAlY, where Me is Co, Ni, NiCo and also CoNiCrAlYHfSi and CoCrAlYSi and thermal barrier coatings TBC providing thermal insulation against high temperature, ZrO_2-Y_2O_3 or Al_2O_3, Al_2O_3+5% Ni coatings and Me-CrAl coatings on a nickel alloy substrate as interlayers, sometimes with other coatings;
- surface hardening—when smaller thickness is required, this is achievable by cladding, for example, in car engine cylinders, piston rings, parts of textile machines, pump and bearing parts;
- electrical conductivity—Cu, Al or Ag on surfaces of weak conductors or materials not conducting electric current;
- insulating performance—for example, Al_2O_3 on glass or polymer materials;
- surface porosity—Co or Ti and ceramic materials on medical implants to ensure adhesion and growth of living cells;
- light reflection—Al on glass forming mirrors;
- decorative effects—precious metals or such with high costs in return for conventional plating and decorative materials on different products and parts of architectural structures;
- repair of surface recesses—technological or service surface defects of, for example, parts of aviation engines
- regeneration of worn parts—porous coatings enabling the penetration of lubricating substances into pores and improving bearing operation, on rollers in the bearing location of usually steel or made of copper alloys.

The negative characteristics of a thermal spraying process include losses of the material used for producing coatings, which are largely influencing costs, connected with the use of different coating materials and guns with a different construction, including an open or closed system for sputtering the melted material ensuring small particle size and lower porosity.

High-velocity oxy-fuel (HVOF), as a special thermal flame spraying method, allows to increase the density of coatings and improves their adhesivity to the substrate as the droplets being sprayed are carried by an ultrasonic stream of hot gas, to impact the substrate with high kinetic energy [92–95]. Material is fed to the burner in the form of powder. A high pressure is produced as a result of burning a mixture of gases (or oxide with aviation petrol) inside a special chamber and then, a stream of gases with ultrasound speed is produced with a special expansion nozzle, which allows to deposit particles of the selected material onto a coating with high kinetic energy.

Warm spraying (WS) as a new type of HVOF provides high speed of oxygen and fuel spraying where the fume gas temperature is reduced by mixing combustion gases with independently supplied nitrogen, which considerably lowers the process temperature. Coating efficiency is

indeed higher; however, a level of contaminants is rising due to high content of water vapour, unreacted hydrocarbons and oxygen. On the other hand, a reduction in temperature is limiting a disadvantageous effect on reactivity, especially the oxidisation of input powder; therefore, it is especially beneficial to apply the WS process to obtain all Ti coatings, plastics and metallic glasses [96–98].

Detonation gun spraying (DGS) is one of the technologies for forming the structure and properties of engineering materials broadly employed in practice, although it is a subject of numerous tests performed in different research institutes worldwide [99, 100]. The essence of the detonation coating deposition method is the use of energy of explosive combustion of a gas mixture for heating and for providing the particles of the powdered material coatings with the necessary kinetic energy. The appropriately matched flow of an explosive mixture and transporting gas and spraying distance secure favourable spraying conditions by ensuring the required level of the detonation energy essential for the quality of the coatings produced. A constant rate of detonation depends here also on the geometry and roughness of the internal surface of a barrel of the detonating device and on the type, granulation and morphology of the coating powder material being sprayed. This method produces layers with an amorphous structure of the matrix with fine crystalline inclusions of supersaturated solid solutions and hard melting phases [99]. It also allows to produce coatings with a structure of intermetallic phases with the content of aluminium, in particular FeAl and Fe_3Al for applications in the car and energy industry. The detonation application of coatings is one of the possible technological variants of detonation hardening as the hardening of metal by a shock wave created as a result of sudden evaporation of the substrate material under the activity of the energy of an external factor (stream of electrons, stream of photons or detonative explosive material), where electron, laser and explosive hardening are distinguished. For the detonation method (unlike for the others), the most advantageous conditions for creating a coating occur when the particles of the powder being applied are in a slightly softened condition when in contact with the substrate surface. The slightly softened powder particles making up the coating material are deposited by detonation onto the substrate surface and are deformed in contact with the surface, causing its indentation deformation, thus hardening. A coating is constituted with very good usable properties as a result of very high kinetic energy of powder particles carried by a detonation wave despite relatively small thermal impact on the substrate. A surface with low roughness and very good substrate adhesion is created as a result of a single working cycle being repeated multiple times with its frequency resulting from the explosive mixture being used and the powder material. The coating structure consists of successive layers with strong anisotropy with flattened, parallely oriented grains with high cohesion and small porosity. The substrate temperature usually does not exceed 100°C [101] and additional cooling allows to maintain the room temperature of the substrate. Polymer and even textile materials can form a substrate for this reason. Detonation coatings on metallic materials exhibit strength higher by approx. 20% as compared to the core and the depth of the hardened layer depends in particular on the type of the substrate material and powder. Detonation coatings show very high wear resistance, hardness, static and fatigue strength, corrosion resistance and good thermal insulation properties [100, 101]. The method of detonative deposition of coatings is competitive versus the HVOF method due to a relatively lower cost of producing coatings,

durability of devices and low operational requirements. Detonation coatings have been widely used in the heavy machine industry, in nuclear, textile, paper sector, textile machines and mining, aviation and rocket sector [102], in particular for aeroplane parts subjected to highest loads, that is, blades of turbines and turbine engine compressors, gaskets and bearings, flap guides, wind joints, toothed gears, parts of hydraulic and fuel pumps, edges of attack and joints of airscrew blades, undercarriage parts and levers made of aluminium alloys and compressor blades made of titanium alloys.

Gas dynamic cold spraying (GDCS) consists of cold spraying with particles accelerated to very high velocities by means of a carrier gas passed through a converging-diverging de Laval type nozzle. After the impact, solid particles are deformed plastically with a sufficient kinetic energy and are bonded mechanically with the substrate and create a coating. A critical velocity needed to create a bond depends on the material properties, powder size and temperature. Metals, polymers, ceramics, composite materials, nanocrystalline powders and soft metals such as Cu i Al as well as W, Ta, Ti, MCrAlY, WC-Co can be deposited by the GDCS method [96, 98, 103].

Acknowledgements

The works have been implemented within the framework of the BIOLASIN project entitled 'Investigations of structure and properties of newly created porous biomimetic materials fabricated by selective laser sintering' headed by Prof. L.A. Dobrzański, funded by the Polish National Science Centre in the framework of the 'Harmony 4' competitions. The project was awarded a subsidy under the decision DEC-2013/08/M/ST8/00818.

Author details

Leszek A. Dobrzański[1*], Anna D. Dobrzańska-Danikiewicz[1], Anna Achtelik-Franczak[1], Lech B. Dobrzański[2], Eugeniusz Hajduczek[1] and Grzegorz Matula[1]

*Address all correspondence to: leszek.adam@gmail.com

1 Silesian University of Technology, Faculty of Mechanical Engineering, Gliwice, Poland

2 Centre of Medicine and Dentistry SOBIESKI, Gliwice, Poland

References

[1] Dobrzański LA, Matula G. Powder metallurgy fundamentals and sintered materials. Gliwice: International OCSCO World Press; 2012;8:1–156 (in Polish)

[2] Ruys A, Gingu O, Sima G, Maleksaeedi S. Powder processing of bulk components in manufacturing. In: Nee AYC, editor. Handbook of manufacturing engineering and technology. London: Springer-Verlag; 2015. pp. 487–566. doi: 10.1007/978-1-4471-4670-4_48

[3] Dobrzański LA. Engineering materials and materials design. Principles of materials science and physical metallurgy. Warszawa: WNT; 2006. 1600 p.

[4] Samal PK, Newkirk JW, editors. ASM handbook: volume 7: powder metallurgy. ASM International, Materials Park, OH, USA; 2015. 907 p.

[5] Jones W. Fundamental principles of powder metallurgy. London: Edward Arnold Publishers Ltd.; 1960. 1032 p.

[6] German RM. Powder metallurgy and particulate materials processing. Metal Powder Industries Federation. Princeton, New Jersey; 2005. 528 p.

[7] Dowson G, Whittaker D. Introduction to powder metallurgy. The process and its products. European Powder Metallurgy Association. Shrewsbury, UK; 1992 & 2008. 32 p.

[8] Matula G, Dobrzański LA, Dołżańska B. Influence of cobalt portion on structure and properties of FGHM. International Journal of Materials and Product Technology. 2008;33:280–290

[9] Dunkley JJ. Advances in atomisation techniques for the formation of metal powders.In: Chang I, Zhao Y, editors. Advances in powder metallurgy: properties, processing and applications. Woodhead Publishing. Cambridge, UK; 2013. pp. 3–18. doi: 10.1533/9780857098900.1.3

[10] Dobrzański LA. Descriptive physical metallurgy of iron alloys. Gliwice: Wydawnictwo Politechniki Śląskiej; 2007. 370 p. (in Polish)

[11] Dobrzański LA, Włodarczyk A, Adamiak M. The structure and properties of PM composite materials based on EN AW-2124 aluminum alloy reinforced with the BN or Al_2O_3 ceramic particles. Journal of Materials Processing Technology. 2006;175:186–191

[12] Dobrzański LA, Włodarczyk A, Adamiak M. Structure, properties and corrosion resistance of PM composite materials based on EN AW-2124 aluminum alloy reinforced with the Al_2O_3 ceramic particles. Journal of Materials Processing Technology. 2005;162–163:27–32

[13] Dobrzański LA, Dobrzańska-Danikiewicz AD. Engineering materials surface treatment. Open Access Library. 2011;5:1–480 (in Polish)

[14] Sharma AD, Sharma AK, Thakur N. Crystallographic, microstructure and mechanical characteristics of dynamically processed IN718 superalloy. Journal of Alloys and Compounds. 2014;597:175–180. doi:10.1016/j.jallcom.2014.02.011

[15] Eskandari H, Ghasemi HM. Wear behavior of Al-20vol.%SiCp composites manufactured by dynamic consolidation. Advanced Materials Research. 2013;685:40–44. doi: 10.4028/www.scientific.net/AMR.685.40

[16] Wang Z, Li X, Zhu J, Mo F, Zhao C, Wang L. Dynamic consolidation of W-Cu nanocomposites from W-CuO powder mixture. Materials Science and Engineering A. 2010;527:6098–6101. doi:10.1016/j.msea.2010.05.077

[17] Dobrzański LA, Tomiczek B, Pawlyta M, Król M. Aluminium AlMg1SiCu matrix composite materials reinforced with halloysite particles. Archives of Metallurgy and Materials. 2014;59:335–338

[18] Tomiczek B, Dobrzański LA, Macek M. Effect of milling time on microstructure and properties of AA6061/MWCNTS composite powders. Archives of Metallurgy and Materials. 2015;60:3029–3034

[19] Tomiczek B, Pawlyta M, Adamiak M, Dobrzański LA. Effect of milling time on microstructure of AA6061 composites fabricated via mechanical alloying. Archives of Metallurgy and Materials. 2015;60:789–793

[20] James WB. Powder forging. Reviews in Particulate Materials. 1994;2:173–214

[21] Park J-O, Kim K-J, Kang D-Y, Lee Y-s, Kim Y-H. An experimental study on the optimization of powder forging process parameters for an aluminum-alloy piston. Journal of Materials Processing Technology, 2001;113:486–492. doi:10.1016/S0924-0136(01)00663-X

[22] Atkinson HV, Davies S. Fundamental aspects of hot isostatic pressing: an overview. Metallurgical and Materials Transactions A. 2000;31:2981–3000. doi:10.1007/s11661-000-0078-2

[23] Froes FH, Qian M. A perspective on the future of titanium powder metallurgy. In: Qian M, Froes FH, editors. Titanium powder metallurgy: science, technology and applications. Butterworth-Heinemann. Waltham, MA, USA – Oxford, UK; 2015. pp. 602–608. doi:10.1016/B978-0-12-800054-0.00031-9

[24] Samarov V, Seliverstov D, Froes FH. Fabrication of near-net-shape cost-effective titanium components by use of prealloyed powders and hot isostatic pressing.In: Qian M, Froes FH, editors. Titanium powder metallurgy: science, technology and applications. Butterworth-Heinemann. Waltham, MA, USA – Oxford, UK; 2015. pp. 313–336. doi:10.1016/B978-0-12-800054-0.00018-6

[25] Aleksandrova EV, Ilyina AM, Grigoryev EG, Olevsky EA. Contribution of electric current into densification kinetics during spark plasma sintering of conductive powder. Journal of the American Ceramic Society. 2015;98:3509–3517. doi:10.1111/jace.13816

[26] Alaniz JE, Dupuy AD, Kodera Y, Garay JE. Effects of applied pressure on the densification rates in current-activated pressure-assisted densification (CAPAD) of nanocrystalline materials. Scripta Materialia. 2014;92:7–10. doi:10.1016/j.scriptamat.2014.07.015

[27] Yurlova MS, Demenyuk VD, Lebedeva LY, Dudina DV, Grigoryev EG, Olevsky EA. Electric pulse consolidation: an alternative to spark plasma sintering. Journal of Materials Science. 2014;49:952–985. doi:10.1007/s10853-013-7805-8

[28] Guillon O, Gonzalez-Julian J, Dargatz B, Kessel T, Schierning G, Räthel J, Herrmann M. Field-assisted sintering technology/spark plasma sintering: mechanisms, materials and technology developments. Advanced Engineering Materials. 2014;16:830–849. doi: 10.1002/adem.201300409

[29] Fais A, Actis Grande M, Forno I. Influence of processing parameters on the mechanical properties of electro-sinter-forged iron based powders. Materials and Design. 2016;93:458–466. doi:10.1016/j.matdes.2015.12.142

[30] Forno I, Actis Grande M, Fais A. On the application of electro-sinter-forging to the sintering of high-karatage gold powders. Gold Bulletin. 2015;48:127–133. doi:10.1007/s13404-015-0169-x

[31] Ding L, Xiang DP, Li YY, Zhao YW, Li JB. Phase, microstructure and properties evolution of fine-grained W–Mo–Ni–Fe alloy during spark plasma sintering. Materials & Design. 2012;37:8–12. doi:10.1016/j.matdes.2011.12.010

[32] Fong AY, Xu H, Page K, Dirmyer MR, Kodera Y, Obrey SJ, Garay JE. Synthesis and structural characterization of dense polycrystalline Mg_9Sn_5, a metastable Mg–Sn phase. Journal of Alloys and Compounds. 2014;616:333–339. doi:10.1016/j.jallcom.2014.07.122

[33] Suárez M, Fernández A, Menéndez JL, Torrecillas R, Kessel HU, Hennicke J, Kirchner R, Kessel T. Challenges and opportunities for spark plasma sintering: a key technology for a new generation of materials. In: Ertuğ B, editor. Sintering applications. InTech, Rijeka, Croatia; 2013. pp. 319–342. doi:10.5772/53706

[34] Dobrzański LA, Matula G. Powder injection molding: sinter-hardening. In: Colás R, Totten GE, editors. Encyclopedia of iron, steel and their alloys. CRC Press, Taylor & Francis Group. Abingdon, OX,USA; 2016; 14 p.

[35] Matula G, Dobrzański LA, Várez A, Levenfeld B, Torralba JM. Comparison of structure and properties of the HS12-1-5-5 type high-speed steel fabricated using the pressureless forming and PIM methods. Journal of Materials Processing Technology. 2005;162–163:230–235

[36] Dobrzański LA, Matula G, Várez A, Levenfeld B, Torralba JM. Structure and mechanical properties of HSS HS6-5-2- and HS12-1-5-5-type steel produced by modified powder injection moulding process. Journal of Materials Processing Technology. 2004;157–158:658–668

[37] Ebel T, Friederici V, Imgrund P, Hartwig T. Metal injection molding of titanium. In: Qian M, Froes FH, editors. Titanium powder metallurgy: science, technology and applications. Butterworth-Heinemann; Waltham, MA, USA – Oxford, UK; 2015. pp. 337–360. doi:10.1016/B978-0-12-800054-0.00019-8

[38] Dobrzański LA, Matula G, Herranz G, Várez A, Levenfeld B, Torralba JM. Metal injection moulding of HS12-1-5-5 high-speed steel using a PW-HDPE based binder. Journal of Materials Processing Technology. 2006;175:173–178

[39] Várez A, Levenfeld B, Torralba JM, Matula G, Dobrzański LA. Sintering in different atmospheres of T15 and M2 high speed steels produced by modified metal injection moulding process. Materials Science and Engineering A. 2004;366:318–324

[40] Nowacki J. Sintered metals and sinters with metal matrix. Warszawa: WNT; 2005 (in Polish)

[41] Suryanarayana C. Mechanical alloying and milling. Progress in Materials Science. 2001;46:1–184. doi:10.1016/S0079-6425(99)00010-9

[42] Schwarz RB, editor. Viewpoint set on mechanical alloying. Scripta Materialia. 1996;34:1–73

[43] Shingu PH, editor. Special issue on mechanical alloying. Materials Transactions of the Japan Institute of Metals. 1995;36:83–388

[44] Kaupp G. Reactive milling with metals for environmentally benign sustainable production. CrystEngComm. 2011;13:3108–3121. doi:10.1039/c1ce05085k

[45] Torralba JM, Fuentes-Pacheco L, García-Rodríguez N, Campos M. Development of high performance powder metallurgy steels by high-energy milling. Advanced Powder Technology. 2013;24:813–817. doi:10.1016/j.apt.2012.11.015

[46] Gheiratmand T, Madaah Hosseini HR, Davami P, Gjoka M, Song M. The effect of mechanical milling on the soft magnetic properties of amorphous FINEMET alloy. Journal of Magnetism and Magnetic Materials. 2015;381:322–327. doi:10.1016/j.jmmm.2015.01.016

[47] Iwata NY, Liu T, Dou P, Kasada R, Kimura A, Okuda T, Inoue M, Abe F, Ukai S, Ohnuki S, Fujisawa T. Effects of MA environment on the mechanical and microstructural properties of ODS ferritic steels. Journal of Nuclear Materials. 2011;417:162–165. doi:10.1016/j.jnucmat.2010.12.058

[48] Hsiung LL, Fluss MJ, Kimura A. Structure of oxide nanoparticles in Fe-16Cr MA/ODS ferritic steel. Materials Letters. 2010;64:1782–1785. doi:10.1016/j.matlet.2010.05.039

[49] Baker I, Iliescu B, Li J, Frost HJ. Experiments and simulations of directionally annealed ODS MA 754. Materials Science and Engineering A. 2008;492:353–363. doi:10.1016/j.msea.2008.03.032

[50] Miller MK, Hoelzer DT, Kenik EA, Russell KF. Nanometer scale precipitation in ferritic MA/ODS alloy MA957. Journal of Nuclear Materials. 2004;329–333:338–341. doi:10.1016/j.jnucmat.2004.04.085

[51] Dutta B, Froes FH. The additive manufacturing (AM) of titanium alloys. In: Qian M, Froes FH, editors. Titanium powder metallurgy: science, technology and applications.

Butterworth-Heinemann; Waltham, MA, USA – Oxford, UK; 2015. pp. 447–468. doi: 10.1016/B978-0-12-800054-0.00024-1

[52] Dobrzański LA. Overview and general ideas of the development of constructions, materials, technologies and clinical applications of scaffolds engineering for regenerative medicine. Archives of Materials Science and Engineering. 2014;69:53–80

[53] Dobrzański LA. Applications of newly developed nanostructural and microporous materials in biomedical, tissue and mechanical engineering. Archives of Materials Science and Engineering. 2015;76:53–114

[54] Dobrzański LA, Dobrzańska-Danikiewicz AD, Malara P, Gaweł TG, Dobrzański LB, Achtelik-Franczak A. Fabrication of scaffolds from Ti6Al4V powders using the computer aided laser method. Archives of Metallurgy and Materials. 2015;60:1065–1070

[55] Dobrzański LA, Dobrzańska-Danikiewicz AD, Malara P, Gaweł TG, Dobrzański LB, Achtelik A. Composite fabricated by computer-aided laser methods for craniofacial implants and its manufacturing method, Patent Application P 411689. 23.03.2015

[56] Dobrzański LA, et al. Investigations of structure and properties of newly created porous biomimetic materials fabricated by selective laser sintering, BIOLASIN. Project UMO-2013/08/M/ST8/00818. Silesian University of Technology, Gliwice; 2013–2016

[57] Sing SL, An J, Yeong WY, Wiria FE. Laser and electron-beam powder-bed additive manufacturing of metallic implants: a review on processes, materials and designs. Journal of Orthopaedic Research. 2016;34:369–385. doi:10.1002/jor.23075

[58] Dobrzański LA, Dobrzańska-Danikiewicz AD, Gaweł TG, Achtelik-Franczak A. Selective laser sintering and melting of pristine titanium and titanium Ti6Al4V alloy powders and selection of chemical environment for etching of such materials. Archives of Metallurgy and Materials. 2015;60:2039–2045

[59] Yarlagadda PKDV, Narayanan S, editors. GCMM 2004: 1st international conference on manufacturing and management. Alpha Science International; Narosa Publishing House, New Delhi, India; 2005. 714 p.

[60] Wang X, Xu S, Zhou S, Xu W, Leary M, Choong P, Qian M, Brandt M, Xie YM. Topological design and additive manufacturing of porous metals for bone scaffolds and orthopaedic implants: a review. Biomaterials. 2016;83:127–141. doi:10.1016/j.biomaterials.2016.01.012

[61] Dobrzański LA, Dobrzańska-Danikiewicz AD, Malara P, Gaweł TG, Dobrzański LB, Achtelik-Franczak A. Bone implant scaffold. Patent Application P 414424. 19.10.2015

[62] Dobrzański LA, Dobrzańska-Danikiewicz AD, Malara P, Dobrzański LB, Achtelik-Franczak A. Biological and engineering composites for regenerative medicine, Patent Application P 414723. 9.11.2015

[63] Dobrzański LA, Dobrzańska-Danikiewicz AD, Malara P, Gaweł TG, Dobrzański LB, Achtelik-Franczak A. Implant scaffold and a prosthesis of anatomical elements of a dental system and craniofacial bone, Patent Application P 414423. 19.10.2015

[64] Sahoo S, Chou K. Review on phase-field modeling of microstructure evolutions: application to electron beam additive manufacturing. In: ASME 2014 International manufacturing science and engineering conference, MSEC 2014 collocated with the JSME 2014 international conference on materials and processing and the 42nd North American manufacturing research conference; 9–13 June 2014, Detroit, Michigan. p. V002T02A020. doi:10.1115/MSEC2014-3901

[65] Arifvianto B, Zhou J. Fabrication of metallic biomedical scaffolds with the space holder method: a review. Materials. 2014;7:3588–3622. doi:10.3390/ma7053588

[66] Dobrzański LA, Dobrzańska-Danikiewicz AD, Tański T, Jonda E, Drygała A, Bonek M. Laser surface treatment in manufacturing. In: Nee AYC, editor. Handbook of manufacturing engineering and technology. London: Springer-Verlag; 2015. pp. 2677–2717. doi:10.1007/978-1-4471-4670-4_35

[67] Tański T, Pakieła W, Wiśniowski M, Dobrzański LA. Shaping of surface layer structure and mechanical properties after laser treatment of aluminium alloys. In: Öchsner A, Altenbach H, editors. Mechanical and materials engineering of modern structure and component design. Cham: Springer International Publishing; 2015. pp. 85–96

[68] Dobrzański LA, Labisz K, Piec M, Lelątko J, Klimpel A. Structure and properties of the 32CrMoV12-28 steel alloyed with WC powder using HPDL laser. Materials Science Forum. 2006;530–531:334–339

[69] Dobrzański LA, Labisz K, Klimpel A. Comparison of mechanical properties of the 32CrMoV12-28 hot work tool steels alloyed with WC, VC and TaC powder using HPDL laser. Key Engineering Materials. 2006;324–325:1233–1236

[70] Dobrzański LA, Piec M, Klimpel A, Trojanowa Z. Surface modification of hot work tool steel by high-power diode laser. International Journal of Machine Tools and Manufacture. 2007;47:773–778

[71] Dobrzański LA, Labisz K, Jonda E, Klimpel A. Comparison of the surface alloying of the 32CrMoV12-28 tool steel using TiC and WC powder. Journal of Materials Processing Technology. 2007;191:321–325

[72] Klimpel A, Dobrzański LA, Lisiecki A, Janicki D. The study of the technology of laser and plasma surfacing of engine valves face made of X40CrSiMo10-2 steel using cobalt-based powders. Journal of Materials Processing Technology. 2006;175:251–256

[73] Tański T, Jonda E, Labisz K, Dobrzański LA. Toughness of laser-treated surface layers obtained by alloying and feeding of ceramic powders. In: Zhang S, editor. Thin films and coatings. Toughening and toughness characterization. Boca Raton: CRC Press; 2015. pp. 225–314. doi:10.1201/b18729-6

[74] Dobrzański LA, Tański T, Dobrzańska-Danikiewicz AD, Jonda E, Bonek M, Drygała A. Structures, properties and development trends of laser-surface-treated hot-work steels, light metal alloys and polycrystalline silicon. In: Lawrence J, Waugh D, editors. Laser surface engineering. Processes and applications. Woodhead Publishing Series in Electronic and Optical Materials, No. 65. Amsterdam: Elsevier Ltd.; 2015. pp. 3–32. doi: 10.1016/B978-1-78242-074-3.00001-5

[75] Dobrzański LA, Bonek M, Hajduczek E, Klimpel A. Alloying the X40CrMoV5-1 steel surface layer with tungsten carbide by the use of a high power diode laser. Applied Surface Science. 2005; 247:328–332

[76] Tański T, Dobrzański LA, Pakieła W, Labisz K, Roszak M, Tomiczek B. Structure and properties of the aluminium alloy AlSi12CuNiMg after laser surface treatment. Advanced Materials Research. 2014;1036:40–45

[77] Labisz K, Tański T, Dobrzański LA, Janicki D, Korcina K. HPDL laser alloying of Al-Si-Cu alloy with Al_2O_3 powder. Archives of Materials Science and Engineering. 2013;63:36–45

[78] Dobrzański LA, Jonda E, Pakieła W, Bilewicz M. Improvement of wear resistance of the hot work tool steel by laser surface feeding with ceramic powder. Archives of Materials Science and Engineering. 2013;60:64–71

[79] Dobrzański LA, Jonda E, Labisz K. Comparison of the abrasion wear resistance of the laser alloyed hot work tool steels. Archives of Materials Science and Engineering. 2012;55:85–92

[80] Labisz K, Tański T, Dobrzański LA. HPDL laser alloying of heat treated Al-Si-Cu alloy. Archives of Materials Science and Engineering. 2012;54:13–21

[81] Bonek M, Dobrzański LA, Hajduczek E, Klimpel A. Structure and properties of laser alloyed surface layers on the hot-work tool steel. Journal of Materials Processing Technology. 2006;175:45–54

[82] Klimpel A, Dobrzański LA, Lisiecki A, Janicki D. The study of properties of Ni-W_2C and Co-W_2C powders thermal sprayed deposits. Journal of Materials Processing Technology. 2005;164–165:1068–1073

[83] Toma F-L, Potthoff A, Berger L-M, Leyens C. Demands, potentials and economic aspects of thermal spraying with suspensions: a critical review. Journal of Thermal Spray Technology. 2015;24:1143–1152. doi:10.1007/s11666-015-0274-7

[84] Gan JA, Berndt CC. Nanocomposite thermal spray review. Advanced Materials and Processes. 2015;173:40–43.

[85] Berger L-M. Application of hardmetals as thermal spray coatings. International Journal of Refractory Metals and Hard Materials. 2015;49:350–364. doi:10.1016/j.ijrmhm. 2014.09.029

[86] Fauchais P, Montavon G. Latest developments in suspension and liquid precursor thermal spraying. Journal of Thermal Spray Technology. 2010;19:226–239. doi:10.1007/s11666-009-9446-7

[87] Vo P, Goldbaum D, Wong W, Irissou E, Legoux J-G, Chromik RR, Yue S. Cold-spray processing of titanium and titanium alloys. In: Qian M, Froes FH, editors. Titanium powder metallurgy: science, technology and applications. Butterworth-Heinemann. Waltham, MA, USA – Oxford, UK; 2015. pp. 405–423. doi:10.1016/B978-0-12-800054-0.00022-8

[88] Gan JA, Berndt CC. Thermal spray forming of titanium and its alloys. In: Qian M, Froes FH, editors. Titanium powder metallurgy: science, technology and applications. Butterworth-Heinemann. Waltham, MA, USA – Oxford, UK; 2015. pp. 425–446. doi: 10.1016/B978-0-12-800054-0.00023-X

[89] Klimpel A, Dobrzański LA, Lisiecki A, Janicki D. The study of properties of Ni-WC wires surfaced deposits. Journal of Materials Processing Technology. 2005;164–165:1046–1055

[90] Klimpel A, Dobrzański LA, Janicki D, Lisiecki A. Abrasion resistance of GMA metal cored wires surfaced deposits. Journal of Materials Processing Technology. 2005;164–165:1056–1061

[91] Klimpel A, Dobrzański LA, Kik T, Rzeźnikiewicz A. Robotized GMA surfacing of cermetalic layers. Journal of Achievements in Materials and Manufacturing Engineering. 2006;17:361–364

[92] Taltavull C, Lopez AJ, Torres B, Atrens A, Rams J. Optimisation of the high velocity oxygen fuel (HVOF) parameters to produce effective corrosion control coatings on AZ91 magnesium alloy. Materials and Corrosion. 2015;66:423–433. doi:10.1002/maco.201407982

[93] García-Rodríguez S, López AJ, Torres B, Rams J. 316L stainless steel coatings on ZE41 magnesium alloy using HVOF thermal spray for corrosion protection. Surface and Coatings Technology. 2016;287:9–19. doi:10.1016/j.surfcoat.2015.12.075

[94] Nahvi SM, Jafari M. Microstructural and mechanical properties of advanced HVOF-sprayed WC-based cermet coatings. Surface and Coatings Technology. 2016;286:95–102. doi:10.1016/j.surfcoat.2015.12.016

[95] Jordan EH, Jiang C, Gell M. The solution precursor plasma spray (SPPS) process: a review with energy considerations. Journal of Thermal Spray Technology. 2015;24:1153–1165. doi:10.1007/s11666-015-0272-9

[96] Cizek J, Matejkova M, Dlouhy I, Siska F, Kay CM, Karthikeyan J, Kuroda S, Kovarik O, Siegl J, Loke K, Khor KA. Influence of cold-sprayed, warm-sprayed and plasma-sprayed layers deposition on fatigue properties of steel specimens. Journal of Thermal Spray Technology. 2015;24:758–768. doi:10.1007/s11666-015-0240-4

[97] Watanabe M, Brauns C, Komatsu M, Kuroda S, Gärtner F, Klassen T, Katanoda H. Effect of nitrogen flow rate on microstructures and mechanical properties of metallic coatings by warm spray deposition. Surface and Coatings Technology. 2013;232:587–599. doi: 10.1016/j.surfcoat.2013.06.034

[98] Kuroda S, Watanabe M, Kim K, Katanoda H. Current status and future prospects of warm spray technology. Journal of Thermal Spray Technology. 2011;20:653–676. doi: 10.1007/s11666-011-9648-7

[99] Babul T. Structures and properties of amorphous layers formed by gas detonation and other powder spraying methods. Materials and Manufacturing Processes. 1995;10:611–623

[100] Simunovic K, Saric T, Simunovic G. Different approaches to the investigation and testing of the Ni-based self-fluxing alloy coatings—a review. Part 1: general facts, wear and corrosion investigations. Tribology Transactions. 2014;57:955–979. doi: 10.1080/10402004.2014.927547

[101] Senderowski C, Bojar Z. Factors influencing abrasive wear of gas detonation sprayed FeAl-based intermetallic coatings. International Journal of Applied Mechanics and Engineering. 2004;9:65–71

[102] Kay CM. Thermal spray applications in the steel industry. Advanced Materials and Processes. 2013;171:5–6

[103] Hussain T. Cold spraying of titanium: a review of bonding mechanisms, microstructure and properties. Key Engineering Materials. 2013;533:53–90. doi:10.4028/www.scientific.net/KEM.533.53s

Chapter 3

Sintering Prealloyed Powders Fe-Ni-Cu-Mo Modified by Boron Base on Thermodynamic Investigations

Joanna Karwan-Baczewska and Bogusław Onderka

Additional information is available at the end of the chapter

http://dx.doi.org/10.5772/66875

Abstract

One of the methods to reduce porosity and increase mechanical properties of Fe-Ni-Cu-Mo powder type is applying activated sintering with the boron powder. In the experiments, a diffusion bonded prealloyed powder type Distaloy SA (Fe-1.75%, Ni-1.5%, Cu-0.5%, Mo) was used alloyed by 0.2, 0.4, and 0.6 mas.% elemental boron powder with the addition of 0.8 mas.% of zinc stearate lubricant. Powders were 15 min blended, compacted and then sintered. The sintering process was elaborated in detail based on microstructure investigations and thermodynamic analysis, which showed that the liquid phase has to be formed as a result of eutectic reaction between matrix elements (Fe, Mo, Ni) and mixed boride $(Fe, Mo, Ni)_2B$. In alloys with boron excess, the liquid phase may occur already a 1176°C in conformity with the reaction: $L \leftrightarrow \gamma\text{-}Fe + Fe_2B$. Its quantity is increased with liquid solution formed in the eutectic reaction running between boron and copper at 1027°C. If the system tends to be in equilibrium, the chemical composition of the liquid solution should be shifted toward higher Fe levels.

Keywords: prealloyed Fe-Ni-Cu-Mo powder, boron, liquid phase sintering

1. Introduction

The knowledge of thermodynamic properties of the B-Fe system was successfully applied in several branches of materials engineering, e.g., B-Fe is a subsystem in B-Fe-Nd alloys characterized with strong magnetic properties [1, 2] and in B-Fe-Ti-based composite alloys strengthened by TiB_2 [3]. In addition, boron is used as an alloying element in order to enhance steel hardenability and to produce amorphous alloys [4–6].

For interesting technological parameters, iron-based alloy systems were a subject to intensive research and theoretical investigations [7–20] and so were materials made from premelting of powders from the Fe-Mo system with max. 1.5% Mo [21–25].

With respect to the final density, alloy compositions, used quantity of boron, and other additions, the properties of Fe-Mo alloys improved [26, 27]. However, in some studies on this system [21, 28], relatively poor plastic properties (ductility) were observed.

The first papers analyzing the sintering processes occurring in Fe-2.5% Mo-B alloys—with particular emphasis laid on the microstructural evolution—were published by Sarasola and co-workers [29, 30]. According to these papers, in the sintering process of Fe-3.5% Mo 0.3% powder, some boron atoms form residues around Fe powder grains at temperatures as low as 800°C through surface diffusion in the solid state. Iron particles exhibit a polycrystalline structure (SEM investigations) formed from equiaxial ferrite grains (sized 2–50 μm). At temperatures of 1000–1100°C a more complex microstructure with vast phase deposits occurs. A gradual increase in precipitation is observed as temperature rises. Such a process starts on the surface of particles, around pores and develops on grain boundaries of ferrite crystallites. In turn, the precipitation related to the diffusion of boron from the crystallites' surface toward their lattice occurs inside the crystals. Also worth mentioning is that the process of precipitation occurs at the latest in the biggest metallic particles for the longest path of diffusion.

The described microstructure exists also at a higher temperature (i.e., 1200°C), but obtained precipitations are larger and arranged more uniformly. It should be stressed that not only all processes occurred in the solid phase, but also no traces of liquid phase were observed even at temperatures 25°C over the eutectic: $L \leftrightarrow \gamma\text{-Fe} + Fe_2B$ (1176°C).

The microstructure of material subject to sintering at 1230°C and registered by means of SEM (scanning electron microscopy) method [29, 30] exhibits a clear reduction of the number of precipitations with larger, dark areas of liquid solution of eutectic composition which is surrounded by distinct envelopes identified as the metallic matrix of an alloy with a lower Fe/Mo ratio. Such a process can continue even to 1280°C. Microphotographs of samples held at 1230 and 1280°C indicated that liquid phase areas could also exist on the surface of particles, on the boundaries of ferrite grains, nearby pores, and in Fe grain matrix viz. in places where precipitations were noticed.

While comparing the evolution of microstructure in the Fe-B and Fe 3.5% Mo-0.3% B alloys, it can be stated that the microstructure of Fe-Mo-B alloys after a heat treatment at 1000°C had revealed big quantities of clearly marked inclusions absent in the Fe-B system [29, 30]. In addition, the liquid solution in the Fe 3.5% Mo 0.3% B alloys appeared at a temperature higher than in the system Fe-B where the advanced sintering process was already observed at the eutectic temperature (1176°C) (**Figure 1**).

Moreover, the microstructure of Fe-B samples sintered at 1280°C exhibited a typical, well-developed microstructures of samples sintered with contribution from the liquid phase, whereas in the Fe 3.5% Mo-B alloys such microstructures were merely visible. An advanced

http://dx.doi.org/10.5772/66875

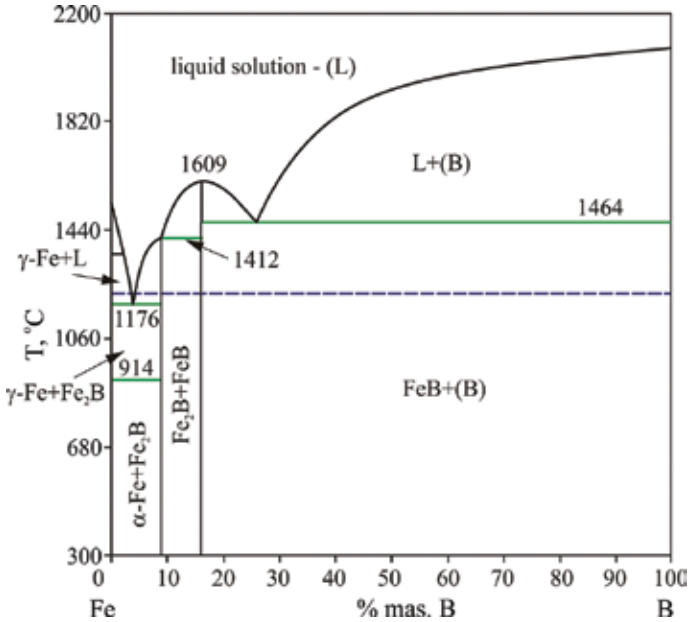

Figure 1. Phase equilibrium diagram Fe-B calculated according to the model parameters assessed by Hallemans and co-workers [31]. A dashed line in the diagram represents the temperature of sintering process (1200°C).

sintering process was observed—like in the Fe-B system—already at 1176°C in alloys with lower molybdenum contents in which the solidified liquid phase was noticed, too.

2. Experimental procedure and discussion

In the current experiments a diffusion-bonded prealloyed powder of Distaloy SA (Fe-1.75%, Ni-1.5%, Cu-0.5%, Mo) was applied. Distaloy SA powder was alloyed with the addition of 0.2, 0.4, and 0.6 mas.% of elemental boron powder with the addition of 0.8 mas.% of zinc stearate lubricant. After 15 min of blending the powder samples were compacted at 600 MPa, and then sintered for 60 min in a hydrogen gaseous envelope at 1200°C. Microstructure and the mechanical properties were investigated.

The sintering process was elaborated based on thermodynamic studies of Sarasola et al. [30]. In order to reduce the melting point of the Fe-Mo-B alloy, some quantities of Ni and Cu were also added. Copper and boron form a eutectic solution at 1027°C [32]) whose composition is strongly shifted toward Cu (97.5 mas.%) (**Figure 2**). Boron with the iron, molybdenum, and nickel (**Figures 1**, **3**, and **4a**, **b**) forms M_2B type borides.

A possibility of forecasting the effect of alloy additions is very important for understanding the sintering process in multicomponent alloys Fe-Mo-Ni-Cu-B. Small amounts of alloyed doping additions do not shift the equilibrium in a five-component alloy toward the Mo-Ni

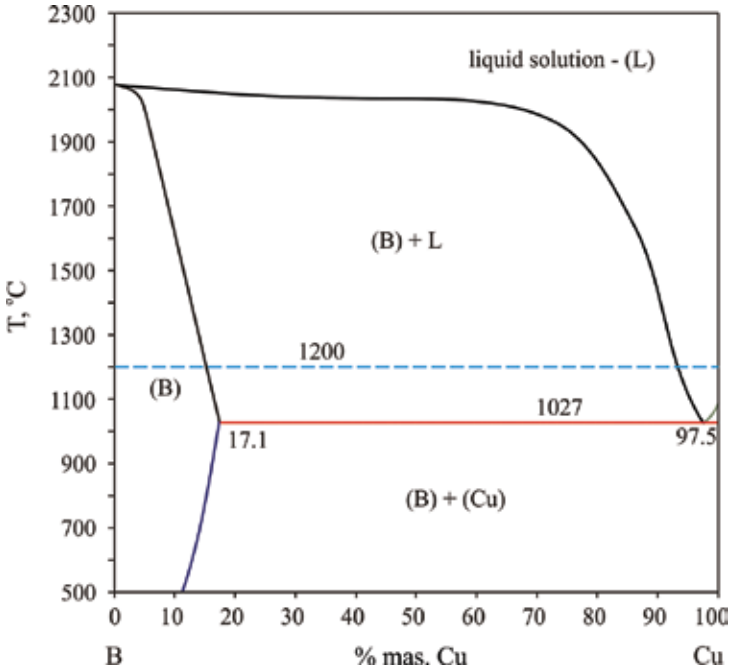

Figure 2. Phase equilibrium diagram of B-Cu system calculated from the assessed parameters of Zhang and co-workers [33]. Dashed line represents the sintering process temperature at 1200°C.

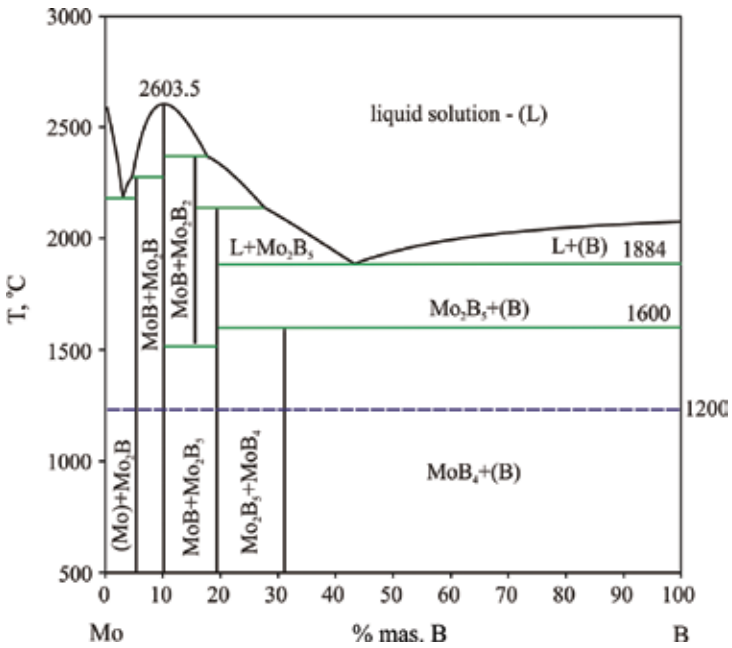

Figure 3. Phase equilibrium diagram of B-Mo system calculated from the model parameters determined by Morishita and co-workers [34]. Dashed line represents the sintering process temperature (1200°C).

http://dx.doi.org/10.5772/66875

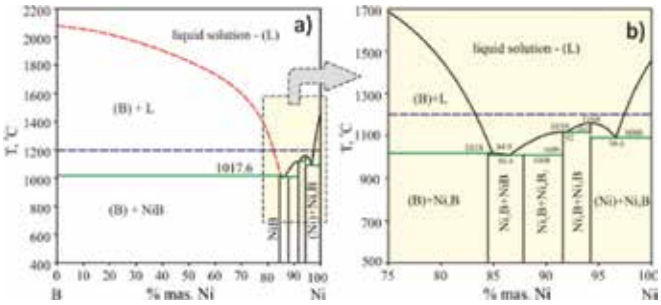

Figure 4. Equilibrium phase diagram of B-Ni system calculated according to the SGTE SSOL 5 Database - (a) and enlarged segment of the B-Ni system - (b). Dashed line - the sintering 1200°C temperature.

system, viz. there is no precipitation of brittle intermetallic compounds, formed in this system. Additionally, it should be mentioned that the sintering temperature of 1200°C is higher than the temperatures of congruent melting of nickel borides (**Figure 4**).

If samples are subject of rapid cooling, in the systems Ni-B and Fe-B, the primary crystallization is suppressed; then, the precipitations of metastable phases were found with a stable eutectic. Those phases are, respectively, $Ni_{23}B_6$ and Fe_3B whose entropy and enthalpy of formation were assessed [4]. The calculated excess specific heat of the liquid eutectic follows the trend of formation of metallic glasses.

The formation of metastable phases implies the solidification of the eutectic whose concentration is shifted toward the equilibrium eutectic, e.g., metastable eutectic between Ni and Ni_2B at 858°C and liquid concentration at 4.39 mas.% B.

The decisive effect upon the iron-rich portion of the Fe-Mo-Ni-Cu-B system is exerted by the properties of the Fe-Mo-Ni system. According to Sarasola et al. [29, 30], an appreciable portion of molybdenum which is initially in solid solution first reacts with boron and then forms a molybdenum-rich boride that is stable over 1200°C. So, the presence of molybdenum in the alloy powder leads to formation of its mixed borides, mainly $(Fe, Mo)_2B$.

Although the occurrence of $(Fe, Mo)_2B$ was not confirmed through experimental result (small XRD peaks, inaccuracy in the chemical analysis of boron with EDS and SEM), intermediate observations confirmed precipitations of this boride. First of all, over 1776°C, such precipitations were observed only when sintering powders contained 3.5 mas.% Mo [29, 30]. At lower temperatures at a constant level of boron, the quantity of such precipitations increased as molybdenum concentration rose. Secondly, the formation of a liquid phase at 1176°C was noticed during sintering of Fe-B and Fe-Mo-B powders with Mo/B atomic ratios equal 0.29 and 0.89. In opposite, no traces of liquid solution in the alloy Fe 3.5% Mo-B, with the Mo/B atomic ratio equal to 1.316 were found. Therefore, it may be concluded that when the ratio of atoms Mo to B in the alloy approaches the value of Mo_2B stoichiometry the borides produced by sintering are richer in molybdenum, and at the same time, the quantity of boron which participates in the eutectic reaction at that temperature diminishes. Additionally, Mo_2B and Fe_2B borides are iso-structural; so in consequence, the mixed boride $(Fe, Mo)_2B$ is likely to

be formed through reciprocal substitution of Fe and Mo (solid solution) in the entire range from Fe_2B to Mo_2B. In addition, it must be added that Gibbs free energy of formation of M_2B borides containing Fe and Mo is more negative than the free energy of Fe_2B, and Mo_2B cannot occur individually in thermodynamic equilibrium upon entering into contact with a Fe-based solution [30].

To understand the modifying effect of Mo, Cu, and Ni in the Fe-Mo-Ni-Cu-B system, one can compare phase diagrams calculated for the Fe-Mo-B system and a part of the five-component Fe-Mo-Ni-Cu-B phase diagram calculated at 1200°C by means of ThermoCalc software [32, 35]. Such calculations may be performed assuming that the solid solution of borides $(Fe, Mo, Ni)_2B$ can be described by means of the ideal solution model.

The lack of data for alloys containing boron in thermodynamic databases does not allow to calculate accurate isothermal sections for the Fe-Mo-B and Fe-Mo-Ni-Cu-B systems. That is why some parameters in thermodynamic models have to be assumed or assessed *a priori*.

Isothermal sections were calculated using the thermodynamic assessments of binary systems, available in the pertinent literature, i.e., B-Cu [33], B-Fe [31], B-Mo [34], Fe-Mo [36], Mo-Ni [37] and B-Ni, Fe-Ni, Cu-Fe, Cu-Ni, and Cu-Mo [32].

In the following thermodynamic description of the Fe-Mo-Ni-Cu-B system it was assumed that four types of phases are present in the iron-rich part of phase system: liquid phase—L, iron-based solid solutions (α-Fe (bcc) γ-Fe (fcc) and δ-Fe(bcc)) M_2B type boride.

Other phases occurring in the two-component systems, like FeB, MoB, and NiB borides [38] and a few phases from the Fe-Mo-Ni system were omitted because they do not occur in the temperature and composition ranges of investigation. The three-component phase B_2FeMo_2 described by Gladyshevsky and coworkers [39] was also omitted as no thermodynamic data or stability ranges are available in the literature. Neither was the phase $B_5Fe_{13}Mo_2$ taken into consideration (Haschke and others [40]) because its occurrence had not been confirmed.

Liquid solution (L) and solid terminal solutions α-Fe, γ-Fe and δ-Fe were described as substitutional solution of atoms on one sublattice. The Gibbs free energy of such a model can be written in the form:

$$\begin{aligned} G^{\theta} = {} & x_B^0 G_B^{\theta} + x_{Fe}^0 G_{Fe}^{\theta} + x_{Mo}^0 G_{Mo}^{\theta} + x_{Ni}^0 G_{Ni}^{\theta} + x_{Cu}^0 G_{Cu}^{\theta} + \\ & RT\left(x_B \ln x_B + x_{Fe} \ln x_{Fe} + x_{Mo} \ln x_{Mo} + x_{Ni} \ln x_{Ni} + x_{Cu} \ln x_{Cu}\right) + G^{ex} + G^{mo} \end{aligned} \quad (1)$$

where excess Gibbs free energy, G^{ex}, can be expressed by formula:

$$\begin{aligned} G^{ex} = {} & x_B x_{Fe} L_{B,Fe}^{\theta} + x_B x_{Mo} L_{B,Mo}^{\theta} + x_B x_{Ni} L_{B,Ni}^{\theta} + x_B x_{Cu} L_{B,Cu}^{\theta} + x_{Fe} x_{Mo} L_{B,Mo}^{\theta} + \\ & x_{Fe} x_{Ni} L_{Fe,Ni}^{\theta} + x_{Fe} x_{Cu} L_{Fe,Cu}^{\theta} + x_{Mo} x_{Ni} L_{Mo,Ni}^{\theta} + x_{Mo} x_{Cu} L_{Mo,Cu}^{\theta} + x_{Ni} x_{Cu} L_{Ni,Cu}^{\theta} \end{aligned} \quad (2)$$

The parameters for the substitutional solution L_{ij} depend on the alloy composition according to Redlich-Kister equation:

http://dx.doi.org/10.5772/66875

$$L_{i,j} = \sum_{k=0}^{n} L_{i,j}^{(k)} \left(x_i - x_j\right)^k \tag{3}$$

where parameters $L_{i,j}^{(k)}$ are the functions of temperature:

$$L_{i,j}^{(k)} = A + BT + C \cdot T \cdot \ln T + \ldots \tag{4}$$

G_i^{θ} is the Gibbs free energy of pure component (element) i in the phase θ, and term G^{mo} represents the contribution from the magnetic order as postulated by Hillert and Jarl [41].

The borides Fe_2B, Mo_2B, and Ni_2B have an identical crystal structure, so the tetragonal phase of type M_2B (mixed boride) was described as a phase consisting of two sublattices (Fe, Mo, Ni)$_{0.667}$B$_{0.333}$. The lack of interactions between Fe, Mo, and Ni on the first sublattice was assumed. In line with the chosen model, Gibbs free energy of such phase can be expressed with the following formula:

$$G^{M_2B} = y_{Fe}\,{}^0G_{Fe_2B} + y_{Mo}\,{}^0G_{Mo_2B} + y_{Ni}\,{}^0G_{Ni_2B} + RT\left(y_{Fe}\ln y_{Fe} + y_{Mo}\ \ln\ y_{Mo} + y_{Ni}\ln\ y_{Ni}\right) \tag{5}$$

where: y_{Fe} y_{Mo} and y_{Ni} are the site fraction of Fe, Mo and Ni in the first sublattice, respectively

Parameter ${}^0G_{Fe_2B}$ was taken from the work of Hallemans et al. [31], whereas ${}^0G_{Mo_2B}$ and ${}^0G_{Ni_2B}$ from the database SGTE SSOL 5 [32].

Initially, the isothermal section for 1200°C for the Fe-Mo-B system was subject to analysis. The equilibrium between liquid phase (L) and phase γ-Fe (fcc) and the iron-rich M_2B type phase (Fe, Mo)$_2$B was calculated and shown in **Figure 5**. So, at that temperature, the formation of a liquid phase is connected with the presence of such a boride. At lower Mo concentrations, that

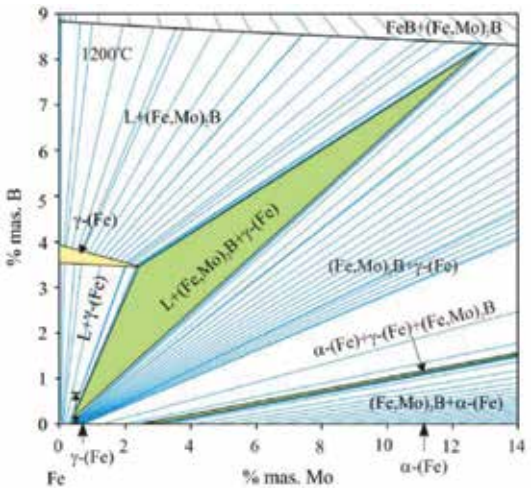

Figure 5. Iron-rich part of phase diagram of Fe-Mo-B system at 1200°C. Blue lines represent tie lines—lines of constant chemical potential of components of phases in equilibrium.

boride seems not occur in samples sintered at 1200°C, because in that area the liquid solution remains in equilibrium only with γ-Fe (fcc).

According to analysis of isothermal sections at 1200 and 1280°C presented in papers [29, 30], as temperature rises, the equilibrium between the Fe solid solution, liquid solution, and mixed boride (Fe, Mo)$_2$B shifts toward higher molybdenum contents in those three phases, which means that with increasing temperature, there will be settled an equilibrium between the liquid phase, *α*-Fe (bcc) richer in Mo, and Mo-rich (Fe, Mo)$_2$B phase (**Figure 5**).

Therefore, at each temperature within this range, a liquid phase is likely to occur at interface between the boride and the surrounding matrix under two conditions:

- the composition of the initial boride (Fe,Mo)$_2$B is such that it can enter into the eutectic reaction;
- the initially precipitated Mo-based boron becomes rich in iron.

It can be thus ascertained that in comparison with the Fe-B system, a molybdenum addition will increase the eutectic temperature because a more stable boride (Fe,Mo)$_2$B and (Fe,Mo) solution participate in the reaction. This conclusion is confirmed by the calculations on the sections of the phase diagram (**Figure 6**) where the temperature of eutectic increases in a con-

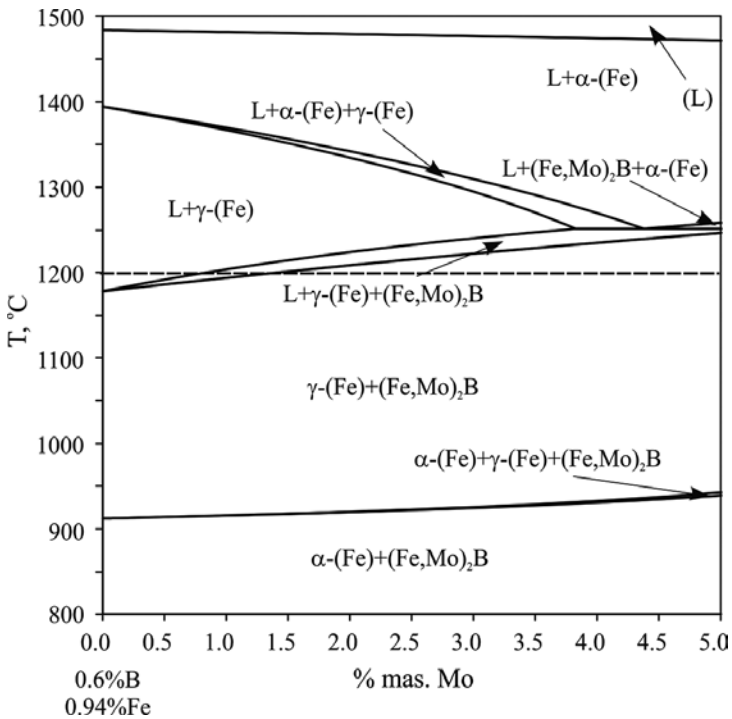

Figure 6. Section (isopleth) of phase diagram of the Fe-Mo-B system for 0.6% B. Letter L denotes liquid solution, and dashed line—sintering temperature 1200°C.

http://dx.doi.org/10.5772/66875

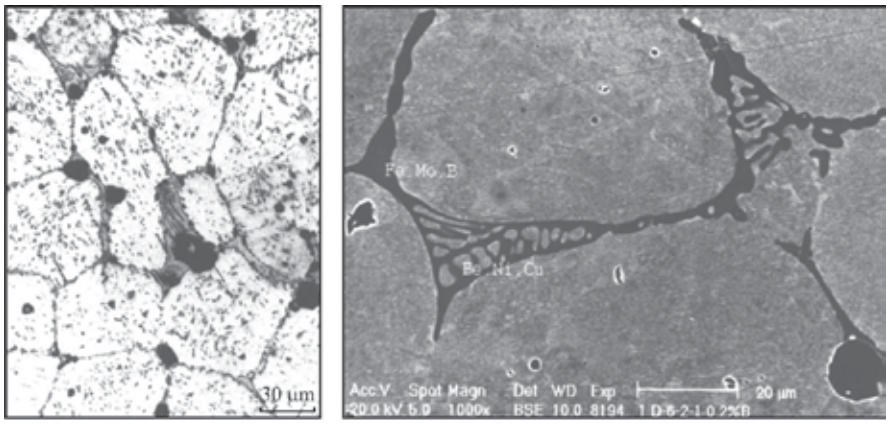

Figure 7. Microstructure of Distaloy SA sinters with 0.6 mas.% B (a) light microscope, (b) SEM/EDX.

tinuous way when the Mo/Fe ratio in $(Fe,Mo)_2B$ boride increases, and this reaction causes at the same time a reduction of the Fe/Mo ratio in the matrix surrounding the boride.

Such a conclusion is corroborated by experimental results pertinent to the areas of liquid phase occurring upon the grain boundaries in the alloy matrix with a reduced Fe/Mo ratio (**Figure 7a** and **b**).

For a given temperature above 1200°C (**Figure 8**), the system aimed from thermodynamic calculations may have a stability range of initial M_2B borides whose composition is desired (bearing in mind the inclusion of iron from the surrounding matrix (alloy) into M_2B borides,

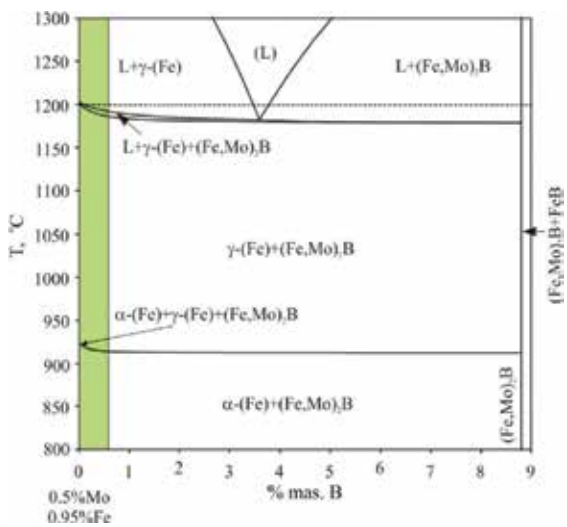

Figure 8. A part of section of the phase diagram of the Fe-Mo-B system at a constant Mo level (0.5 mas.%). Green color denotes the boron concentration range examined in this study (0–0.6 mas.%).

which will at the same time lead to an increase in the matrix Mo/Fe ratio. Such a process is thermodynamically justified and leads to the stabilization of the driving force of the Fe diffusion into boride $(Fe,Mo)_2B$. Its effect is that the areas in which the liquid solution comes to exist become poorer and poorer in Fe.

An alternative to Mo diffusion from borides to the surrounding matrix is related with a higher stability of Mo containing borides when compared to Fe-based borides. It can be assumed [30] that as iron-enriching process proceeds in the initially precipitated borides with a high Mo level, there will be settled a flow of Fe atoms moving toward those borides. In consequence, a complex concentration gradient within the grains of the matrix solid Fe-Mo will be formed solid along grain boundaries and around pores. Such an unbalanced flow of atom is simultaneously accompanied by the production of a small quantity of spheroid pores in the alloy matrix (the so-called secondary porosity) (**Figure 7**), which is caused by Kirkendall effect.

If the sintering process continues to be thermally activated, the occurrence of the liquid phase contributes to a more and more accurate determination (demarcation) of grain boundaries and the chemical gradient starts to diminish. Such microstructural changes are connected with a comprehensive trend followed by the system which moves toward an equilibrium, viz. to a phase composition resulting from the total input alloy concentration.

Analyzing a part of the section of the Fe-Mo-B system for a constant level of 0.5 mas.% Mo, it can be found out that only in the initial stage of boron addition to the Fe-0.5% Mo alloy a fall in temperature is recorded when a liquid phase comes to exist (three phase equilibrium, viz. L + γ-Fe + $(Fe, Mo)_2B$). Over 1.5 mas.% B, the temperature no longer depends on the boron concentration (**Figure 8**—plateau).

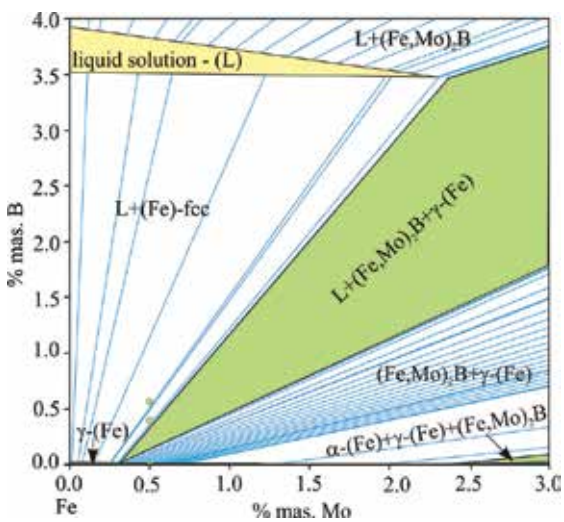

Figure 9. Enlargement of an iron-rich part of the Fe-Mo-B phase diagram at 1200°C; tie lines are marked in blue. Green points stand for compositions of samples subject to sintering.

http://dx.doi.org/10.5772/66875

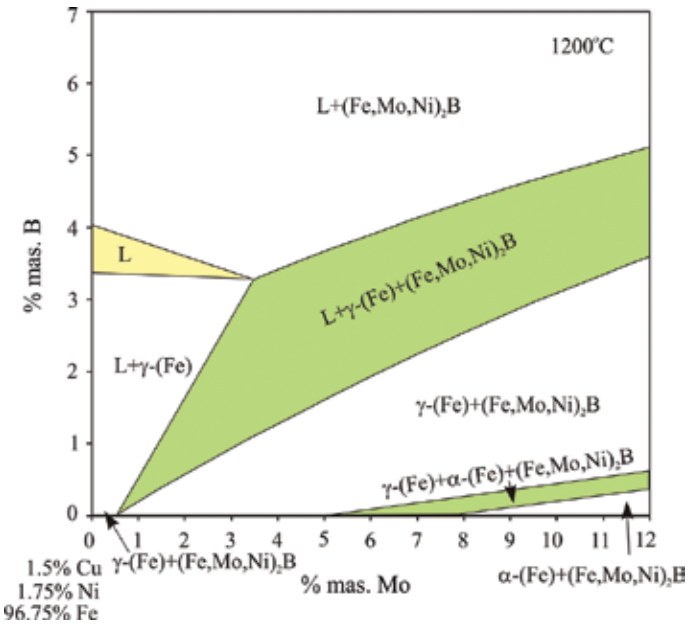

Figure 10. Phase diagram of iron-rich portion of phase diagram Fe-Mo-Ni-Cu-B calculated for 1.5 mas.% Cu, 1.75 mas.% Ni at 1200°C. Dashed line stands for the range of concentrations of samples subject to sintering.

A comparison with the iron-rich phase diagram Fe-Mo-B and Fe-Mo-Ni-Cu-B (0.5 mas.% Mo, 1.75 mas.% Ni, 1.5 mas.% Cu) performed in this work at 1200°C (**Figures 9** and **10**) can indicate that primary alloy composition remain within the two-phase field *liquid solution + solid solution* (γ-Fe) only after addition of nickel and copper into Fe-Mo-B alloy. It can be proved that when the system is to reach such an equilibrium, the chemical composition of the liquid solution shifts toward higher Fe contents. In such a situation, the liquid solution accepts iron from its surroundings, which leads to the formation of local fronts in the liquid and continuity between grain interiors precipitated from the liquid and their surface. However, it should be stressed that in the case of alloys containing the boron excess, the liquid phase may occur already over 1176°C in conformity with the reaction: $L \leftrightarrow \gamma\text{-Fe} + (Fe, Mo, Ni)_2B$.

The last stage of microstructural development takes place when the alloy is subjected to soaking at a given temperature, and shows another (extra) reduction of chemical gradient and porosity. It seems that the mobility of grain boundaries is limited not only by differences in chemical composition on both sides of those grains, but also by the dispersion of small inclusions which immobilize grain boundaries.

Such a conclusion may be formulated based upon the evaluation of formation of sintered grain boundaries at 1280°C [29, 30]. The authors of the adduced work ascertained that even after 1 h time after the process had started, the system was still away from the equilibrium, but the final density of Mo containing alloys was equal to 7.8 g/cm^3. Therefore, it can be stated that a very good characteristic of wettability of the liquid phase caused the material to be thickened.

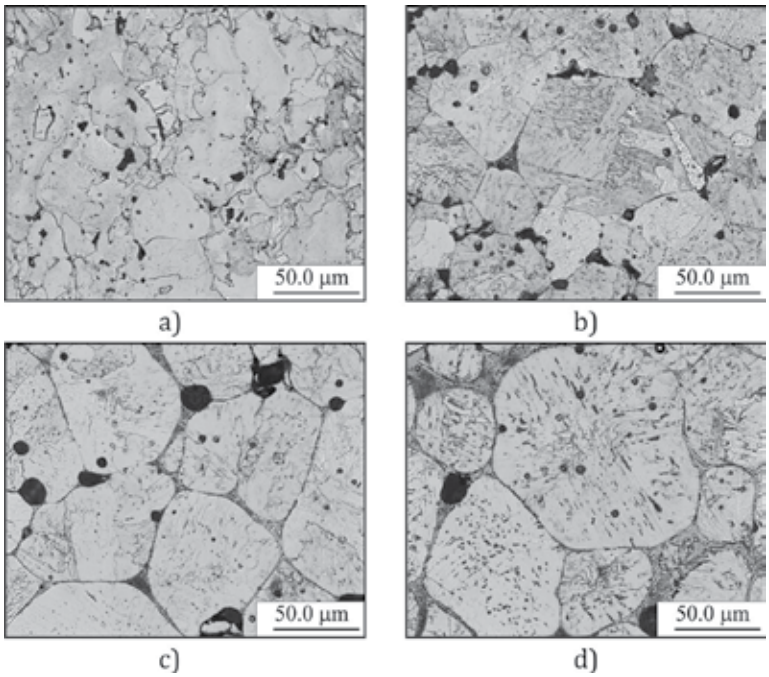

Figure 11. Microstructure of Distaloy SA sinters with boron addition (a) 0 mas.% B, (b) 0.2 mas.% B, (c) 0.4 mas.% B, (d) 0.6 mas.% B.

The thermodynamic analysis performed on the system Fe-0.5% Mo 1.75% Ni-1.5% Cu-B introduced to us the description of the sintering process for samples made from Distaloy SA powder with boron additions, respectively, 0.2, 0.4, and 0.6%, which matched the results of dilatometric tests and investigations into the microstructure of sinters. When Distaloy SA samples with boron addition are being heated up and soaked to 1200°C, before the liquid phase comes to exist at lower temperatures, some M_2B type borides occur (in line with thermodynamic analysis) (**Figure 10**). Those phases nucleate on the surface of particles and pores as well as upon the grain boundaries of ferrite and inside it (**Figures 11b–d** and **12a** and **b**).

The liquid phase is formed as a result of eutectic reaction between matrix elements (Fe, Mo, Ni) and borides $(Fe, Mo, Ni)_2B$. In alloys with boron excess, the liquid phase may occur already at 1176°C in conformity with the eutectic reaction Fe-Fe_2B (**Figure 1**). Its quantity is increased with liquid solution formed in the eutectic reaction running between boron and copper at 1013°C (**Figure 2**). Because the sinter compositions under investigation fall within the two-phase area *liquid solution + solid solution* then borides should not be in equilibrium with such phases. If the system were to attain equilibrium, the chemical composition of the liquid solution should be shifted toward higher Fe levels.

According to dilatometric tests and thermodynamic analysis, the resulting borides increase the eutectic temperature if compared with the Fe-B system where the eutectic point is 1176°C (**Figure 1**).

http://dx.doi.org/10.5772/66875

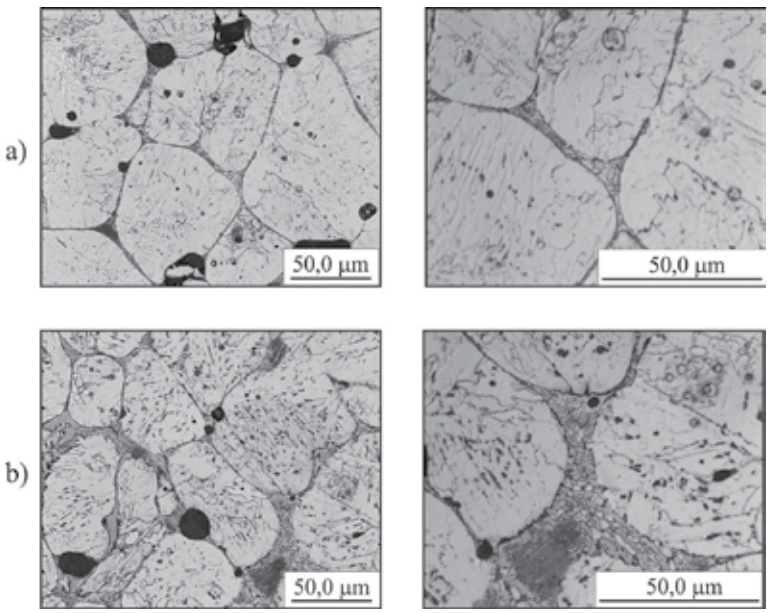

Figure 12. Microstructure of Distaloy SA sinters with boron addition (a) 0.4 mas.% B, (b) 0.6 mas.% B.

In addition, based upon the investigation into dilatometric curves for Distaloy SA samples, it can be stated that boron influences the process of linear contraction; the highest linear contraction was recorded at 1180°C in a Distaloy SA sample with boron 0.6 mas.% [41]. The recorded linear contraction in the sinters under investigation is connected with formation of borides and the liquid phase.

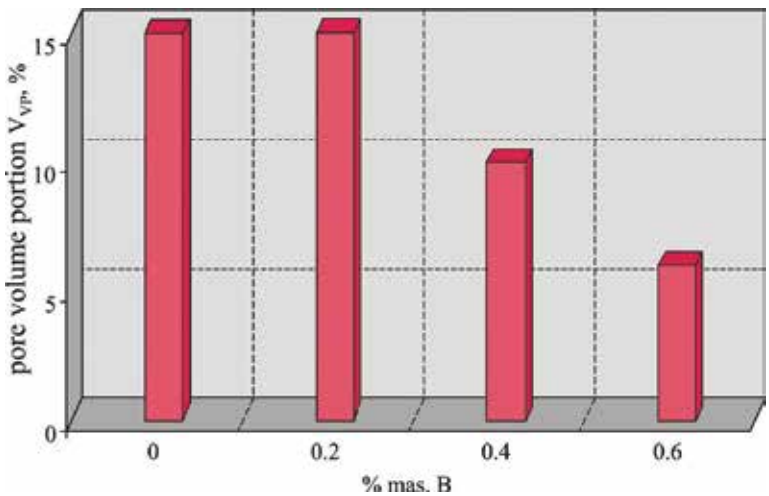

Figure 13. Effect of boron upon pore volume portion (V_{vp}) in sinters made from Distaloy SA powder. Volume portion of pores was determined through quantitative metallography. Sintering parameters: 1200°C/hydrogen/60′.

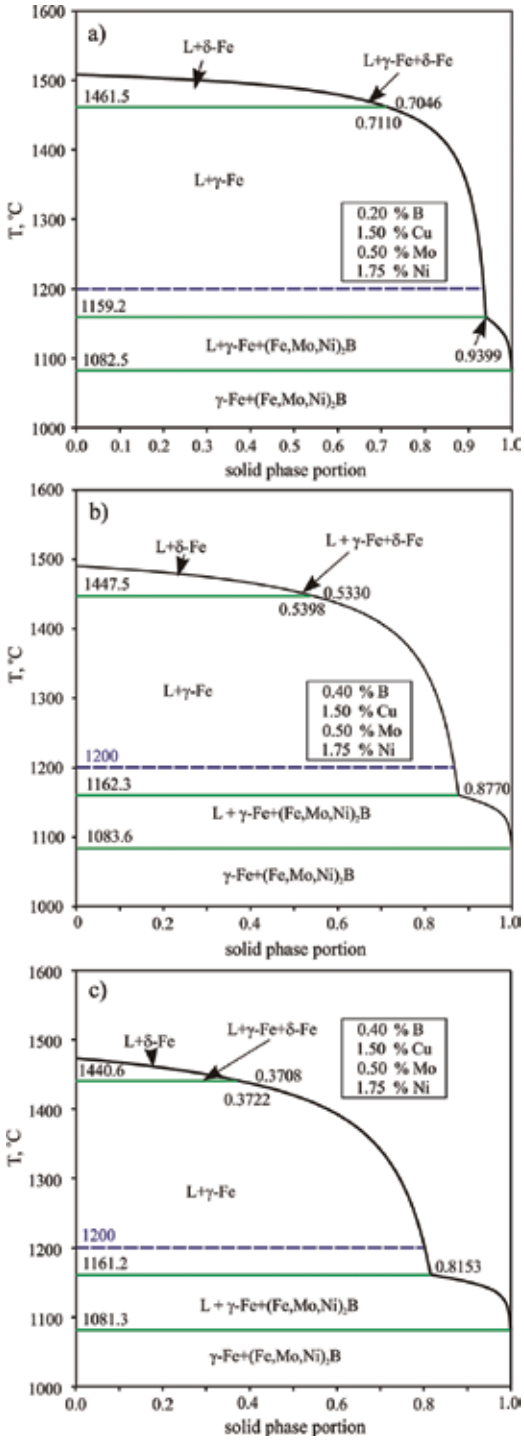

Figure 14. Comparison of crystallization paths for alloy Fe-1.5%, Cu-0.5%, Mo-1.75%, Ni with boron additions: (a) 0.2; (b) 0.4; and (c) 0.6 mas.%. An appreciably higher portion of liquid phase L at 1200°C and 0.6 mas.% B is visible.

http://dx.doi.org/10.5772/66875

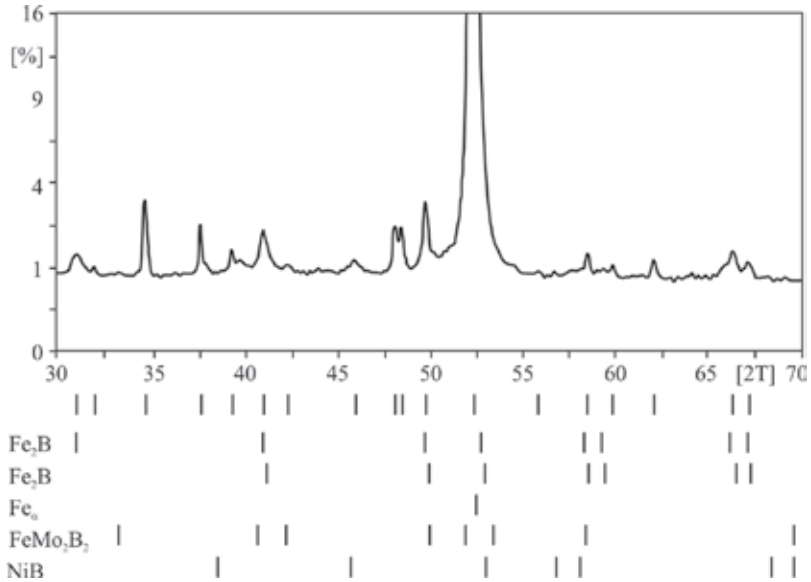

Figure 15. Diffraction pattern for Distaloy SA sinters with boron.

The results of observations of the microstructure in Distaloy SA samples with boron addition, subject to sintering at 1200°C, corroborate the sintering process postulated for that powder based upon thermodynamic data. Some changes in the porosity morphology (closing and spheroidization of pores), decrease in pore volume portion (**Figure 13**) and violent growth of grains were noticed, best seen at 0.6 mas.% B (**Figure 11**).

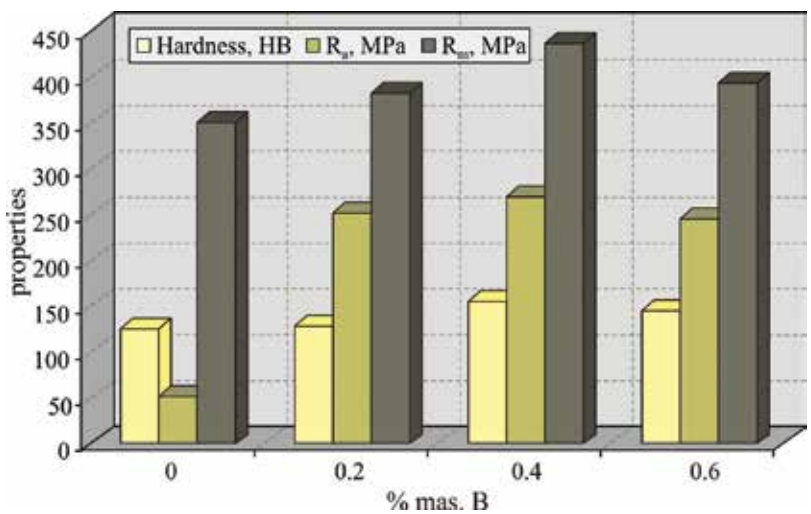

Figure 16. Mechanical properties of Distaloy SA sinters with boron.

An eutectic consisting of boride phases precipitates along grain boundaries of the γ-Fe phase. The composition of borides is different from predictions made through thermodynamic analysis, because during the experiment the system cannot reach the equilibrium state. As the boron contents in Distaloy SA sinters increase, an increase in the volume portion of eutectic was also observed, which is illustrated in **Figure 14** showing crystallization paths for alloy Fe-1.5% Cu-0.5% Mo-1.75% Ni with 0.2, 0.4, and 0.6 mas.% B. A larger portion of liquid phase is visible at 0.6% B.

The presence of borides in the Distaloy SA sinters with boron additions was identified by means of X-ray microanalysis and phase analysis. The following borides were found: Fe_2B, $FeMo_2B_2$, and NiB, and Cu (eutectic), and $FeMo_2B_2$ (matrix) (**Figure 15**) [42]. Therefore, once formed, nickel and iron borides are stable within the range of composition and temperature, subjected to investigations, and their decomposition—as the system tends toward equilibrium—is difficult to occur, which leads to a metastable state with the liquid phase of eutectic reaction, iron-based solid solution and boride phase-like $(Fe, Mo)_2B$ or $(Fe, Mo, Ni)_2B$.

The suggested sintering process in the Fe-Mo-Ni-Cu-B system favors a high degree of compaction in Distaloy SA samples.

The defined sintering process occurring in the system Fe-Mo-Ni-Cu-B is decisive for the formation of an appropriate microstructure of Distaloy SA powder with boron addition, which affects their mechanical properties. As boron contents rose in Distaloy SA samples, increases in compactness, hardness and growth of parameters R_a, R_m were noticed (**Figure 16**).

3. Conclusions

(1) Those observations imply that the liquid phase participating in the sintering process of the five-component Fe-Mo-Ni-Cu-B system is characterized by very good wettability and leads to high densities.

(2) Sintering process occurring in the system Fe-Mo-Ni-Cu-B is decisive for the formation of an appropriate microstructure of Distaloy SA powder with boron addition, which affects their mechanical properties.

(3) Sintering process of prealloyed powder with boron was explained in detail on the basis of thermodynamic analysis and microstructure investigations.

Author details

Joanna Karwan-Baczewska* and Bogusław Onderka

*Address all correspondence to: jokaba@agh.edu.pl

Faculty of Non-Ferrous Metals, AGH University of Science and Technology in Cracow, Cracow, Poland

http://dx.doi.org/10.5772/66875

References

[1] Sagawa M, Hirosawa S, Yamamoto H, Fujimura S, Matsuura Y: Nd-Fe-B permanent magnet materials. Japanese Journal of Applied Physics. 1987; **2,** (6): 785–800.

[2] Hallemans B, Wollants P, Roos J R: Thermodynamic assessment of the Fe-Nd-B phase diagram. Journal of Phase Equilibria and Diffusion. 1995; **16,** (2): 137–149.

[3] Tanaka K, Saito T: Phase equilibria in TiB_2-reinforced high modulus steel. Journal of Phase Equilibria and Diffusion. 1999; **20**: 207–214.

[4] Battezzatti L, Antonione C, Baricco M: Undercooling of Ni-B and Fe-B alloys and their metastable phase diagrams. Journal of Alloys and Compounds. 1997; **247**: 164–171.

[5] Inoue A: Stabilization of metallic supercooled liquid and bulk amorphous alloys. Acta Materialia. 2000; **48**: 279–306.

[6] Palumbo M, Cacciamani G, Bosco E, Baricco M: Driving forces for crystal nucleation in Fe-B liquid and amorphous alloys. Intermetallics. 2003; **11** (11–12): 1293–1299.

[7] Witusiewicz VT: Thermodynamics of binary and ternary melts of 3d transition metals (Cr, Mn, Fe, Co and Ni) with boron. Thermochimica Acta. 1995; **264**: 41–58.

[8] Karwan-Baczewska J: Boron influence on the liquid phase sintering and the mechanical properties of P/M Distaloy alloys. Advances in Powder Metallurgy & Particulate Materials. 1996; **3** (11–15): 11–27.

[9] Karwan-Baczewska J: Boron modified materials sintered from Distaloy SA powder. Powder Metallurgy (in Polish). 1996; **29** (3/4): 18–22.

[10] Karwan-Baczewska J: Influence of boron on the structure and mechanical properties of sintered and ion-nitrided Distaloy alloys. International Journal of Materials and Product Technology. 2000; **15** (3–5): 193–204.

[11] Karwan-Baczewska J, Pieczonka T: Sintering Process of Distaloy SA and Astaloy Mo modified by boron. In: Proceedings of the Powder Metallurgy World Congress & Exhibition (World PM1998 Congress & Exhibition); 18–22 October 1998; Granada, Spain: EPMA: 1998. vol. **3**, pp. 281–286.

[12] Karwan-Baczewska J, Rosso M: Effect of boron on microstructure and mechanical properties of PM sintered and nitride steels. Powder Metallurgy. 2001; **44** (3): 221–227.

[13] Kuroki H: A review on the effect and behavior of boron in sintered iron and steel. Japan Society of Powder and Powder Metallurgy. 2001; **48** (4): 293–304.

[14] Pieczonka T, Kazior J, Płoszczak J: Dimensional changes occurring during sintering of Astaloy CrM powder compacts with boron and carbon additions. In: Proceedings of the European Congress & Exhibition on Powder Metallurgy (EuroPM 2001 Congress & Exhibition); 22–24 October 2001; Nice, France: EPMA: 2001, vol. 1, pp. 310–315.

[15] Kazior J, Pieczonka T, Płoszczak J: The influence of boron on the mechanical properties of prealloyed Astaloy CrM powders alloys. In: Proceedings of the International Conference of Deformation and Fracture in Sintered PM Materials (DF PMM); 15–18 September 2002; Stara Lesna, Slovakia: 2002, vol. 1, pp. 125–131.

[16] Marucci M, Causton R, Lawley A, Saritas S: Effect of small additions of boron on the mechanical properties and hardenability of sintered steels. Powder Metallurgy. 2002; **46** (2): 171–174.

[17] Van Rompaey T, Hari Kumar KC, Wollants P: Thermodynamics optimization of the B-Fe system. Journals of Alloys and Compounds. 2002; **334** (1–2):173–181.

[18] Tokunaga T, Ohtani H, Hasebe M: Thermodynamic evaluation of the phase equilibria and glass-forming ability of the Fe-Si-B system. Computer Coupling of Phase Diagrams and Thermochemistry. 2004; **28** (4): 354–362.

[19] Molinari A, Kazior J, Marchetti F, Canteri R, Cristofolini I, Tiziani A: Sintering mechanisms of boron alloyed AISI 316L stainless steels. Powder Metallurgy.1994; **37** (2): 115–122.

[20] Koichu H, Mitsuru N, Hiroshi H: Effect of boron and silicon additions on liquid-phase sintering behavior and corrosion resistance of P/M ferrite type stainless steels. Journal of the Japan Society of Powder and Powder Metallurgy. 2000; **47** (10): 1091–1096.

[21] German RM, Hwang KS, Madan DS: Analysis of Fe-Mo-B sintered alloys. Powder Metallurgy International.1987; **19** (2): 15–18.

[22] Dudrova E, Selecka M, Bures R, Kabatova M: Effect of boron addition on microstructure and properties of sintered Fe-1.5 Mo Powder Materials. The Iron and Steel Institute of Japan. 1997; **37** (1): 59–64.

[23] Molinari A, Pieczonka T, Kazior J, Gialanella S, Straffelini G: Dilatometry study of the sintering behavior of boron alloyed Fe-1.5% Mo Powder. Metallurgical and Material Transactions. 2000; **31A**: 1497–1506.

[24] Liu J, German RM, Cardamone A, Potter T, Semel FJ: Boron-enhanced sintering of iron-molybdenum steels. The International Journal of Powder Metallurgy. 2001; **37** (5): 39–48.

[25] Xiu Z, Salwen A, Qin X, He F, Sun X: Sintering behavior of iron-molybdenum steels with the addition of Fe-B-C master alloy powders. Powder Metallurgy. 2003; **46** (2): 171–174.

[26] Madan DS, German RM: Enhanced sintering for ferrous components. Modern Developments in Powder Metallurgy. 1986; **15**: 441–454.

[27] Madan DS, German RM, James WB: Iron-boron enhanced sintering. Progress in Powder Metallurgy. 1986; **42**: 267–283.

[28] German RM: Diffusional activated sintering - densification microstructure and mechanical properties. The International Journal of Powder Metallurgy and Powder Technology. 1983; **19**: 277–283.

[29] Sarasola M, Tojal C, Castro F: Study of boron behavior during sintering of Fe/Mo/B/C alloys to near full density. In: Euro PM2004 Conference Proceedings (Euro PM2004 Conference); 17–21 October 2004; Vienna, Austria. 2004. **3**, pp. 319–326.

[30] Sarasola M, Gomez-Acebo T, Castro F: Liquid generation during sintering of Fe-3.5% Mo powder compacts with elemental boron additions. Acta Materialia. 2004; **52** (15): 4615–4622.

[31] Hallemans B, Wollants P, Roos JR: Thermodynamic reassessment and calculation of the Fe-B phase diagram. Zeitschrift für Metallkunde.1994; **85**: 676–682.

[32] Sundman B, Shi P: SSOL5 SGTE solution database. Stockholm, Sweden, ThermoCalc Software. 2008.

[33] Zhang W-W, Du Y, Xu H, Xiong W, Kong Y, Sun W, Pan F, Tang A: Thermodynamic assessment of the Cu-B system supported by key experiment and first-principles calculations. Journal of Phase Equilibria and Diffusion. 2009; **30** (5): 480–486

[34] Morishita M, Koyama K, Yagi S, Zhang G: Calculated phase diagram of Ni-Mo-B ternary system. Journal of Alloys Compounds. 2001; **314** (1–2): 212–218.

[35] Cao W, Chen SL, Zhang F, Wu K, Yang Y, Chang YA, Schmid-Fetzer R, Oates WA: PANDAT software with panEngine, panoptimizer and panprecipitation for multi-component phase diagram calculation and materials property simulation. Computer Coupling of Phase Diagrams and Thermochemistry. 2009; **33** (2): 328–342

[36] Guillermet AF: An assessment of the Fe-Mo system. Computer Coupling of Phase Diagrams and Thermochemistry. 1982; **6** (2): 127–140.

[37] Frisk K: Thermodynamic evaluation of the Mo-Ni system. Computer Coupling of Phase Diagrams and Thermochemistry. 1990; **14** (3): 311–320.

[38] Miettinen J, Vassilev G: Thermodynamic Description of Ternary Fe-B-X Systems. Part 2: Fe-B-Ni. Archives of Metallurgy and Materials. 2014; **59**: (2): 609–614.

[39] Gladyshevsky EI, Fedorov TF, Kuzma Yu.B, Skolozdra RV: Isothermal section of the Molybdenum-Iron-Boron system. Poroshkovaya Metallurgiya.1966; **5**: 305–310.

[40] Haschke H, Nowotny H, Benesovsky F: Untersuchungen in den dreistoffen: (Mo-W)-(Fe,Co,Ni) - B. Monatshefte Chemie. 1966; **97**: 1459–1468.

[41] Hillert M, Jarl M: A model for alloying effects in ferromagnetic metals. Computer Coupling of Phase Diagrams and Thermochemistry. 1978; **2**: 227–238.

[42] Karwan-Baczewska J: Sintered alloys based on iron powder with boron. AGH University of Science and Technology Press, Cracow, Poland, 2008. pp. 71–75 and pp. 116–117.

Chapter 4

Application of Direct Current Plasma Sintering Process in Powder Metallurgy

Silvio Francisco Brunatto,
Rodrigo Perito Cardoso and Aloísio Nelmo Klein

Additional information is available at the end of the chapter

http://dx.doi.org/10.5772/66870

Abstract

Direct current (dc) plasma-assisted sintering of metal parts is a promising and relatively new research and development field in powder metallurgy (PM). In the present entry, it is intended to introduce the reader to the main applications of the dc plasma sintering process in PM. To achieve this goal, the present entry is divided in a brief introduction and sections in which the bases of the dc plasma abnormal glow discharge regime and its influence in the sintering process are carefully treated. In this case, a clear language is purposely used to didactically introduce the reader to this "fascinating glow world", the dc plasma-assisted sintering of metal parts, aiming to put in evidence the main points on physicochemical aspects of the plasma environment, basic knowledge of the plasma heating, and surface-related phenomena during dc plasma sintering of parts. All these aspects are treated considering the main techniques of the dc plasma-assisted sintering process applied to PM. Finally, some results on DC plasma heating, sintering and surface modification are presented.

Keywords: DC plasma-assisted sintering, DC glow discharge sintering, DC hollow cathode discharge sintering, floating potential sintering

1. Introduction

New technologies tend to require more and more advanced materials and manufacturing processes. Additionally, due to environmental problems that the world is facing, especially in developed countries, the regulation concerning the environmental impact of these materials and processes are becoming increasingly restrictive. In this context, plasma-assisted processes are very competitive since they usually are low-environmental-impact processes

and they can produce high-performance materials in a very efficient way. Such aspects, allied to the possibility of producing very reductive atmospheres, motivated the development of the plasma-assisted sintering process, being that in most of research carried out in this domain, plasma is generated using direct current (dc) power supply.

In the dc plasma-assisted sintering process performed in an abnormal regime glow discharge, pressed metal parts to be sintered are subjected to a highly reactive plasma environment [1–4]. It is due to the presence of a great number of ionized and excited gas species, created by collision processes, that leads the species present in a gas mixture, usually constituted of reductive (like H_2) and neutral (like Ar) gases, to be ionized, excited, and/or dissociated. Due to the interaction of plasma and the pressed part, temperatures sufficiently high to sinter metals can be reached by the energy transfer from the plasma species to the part surface by collisions of accelerated species (this heating mode is termed "cathode heating mode"). It is also possible to heat pressed parts by an indirect way, in which the plasma energy is transferred to heating components, acting as cathode of the discharge, that heat the parts to be sintered mainly by radiation (here termed "anode and/or floating potential heating mode"). Depending on the design of the electrical discharge (electrode arrangement), different electrical configurations and heating modes are possible. In each case different potentialities of the plasma-assisted process can be explored, giving rise to different dc plasma sintering techniques [5, 6]. In addition, the very active physicochemical plasma environment, besides heating, can lead the metallic parts to present surface characteristics that are directly related to the plasma species bombardment and, so, exclusive for the plasma sintering process. The plasma environment can promote oxide-reduction reaction, cleaning, sputtering, deposition, and redeposition phenomena, all of them can be conveniently explored to tailor the sintered part surface. The abovementioned aspects suggest that during sintering, several phenomena related to the plasma will have influence in the part sintering processes, so to understand the dc plasma-assisted sintering process as a whole it is necessary to introduce some basis of plasma. In the next sections bases of dc plasma physics for the sintering purpose are presented, considering the different dc plasma sintering techniques, followed by the presentation of some results on plasma heating and surface modification. So the chapter ends by a discussion on the advantages of the plasma-assisted over the conventional sintering process and the final remarks.

2. Bases of dc plasma for sintering: the abnormal regime glow discharge

Plasmas commonly used in dc plasma sintering process characteristically present a degree of ionization of about 10^{-5} [1]. For the sintering purpose, an abnormal glow discharge can be easily obtained by applying a potential difference between two electrodes (cathode and anode) placed inside a chamber at low pressure, containing the gas mixture, which is usually constituted of 80 vol.% Ar + 20 vol.% H_2 for sintering. In the initial state, electrons are accelerated by the electric field and collide with neutral species (atoms/molecules), in much higher number density, resulting in partial ionization/excitation of the gas. When the number density of the produced ionized and excited species is great enough, a self-sustained bright-aspect glow electrical discharge is attained; thus, the plasma is formed [1–4].

http://dx.doi.org/10.5772/66870

Among the different discharge regimes which can be established from the current-voltage characteristic of a dc plasma system, namely Corona, Townsend, Subnormal, Normal, Abnormal, Transition to arc, and Arc [1, 4, 7], the abnormal regime is of special interest for dc plasma sintering process. This is mainly due to the following aspects:

- It is the discharge regime in which the cathode can be totally covered by the glow, condition necessary to perform homogeneous heating; and
- It presents the basic feature for which the electrical current monotonically increases with the applied voltage. This allows the application of high voltages resulting in increased ionization/excitation of the gas and makes possible to control the plasma reactivity and the cathode (or sintering) temperature.

The abnormal regime is sustained for current densities typically higher than 2 mA/cm^2 [1] and for pressures generally in the range of 10^{-2} to 10^2 Torr [8–10].

Figure 1 schematically presents the normal, abnormal, transition to arc, and arc regime regions in a hypothetical current-voltage characteristic of a dc discharge [1, 4, 7], being the abnormal and arc regimes typically applied for materials processing [1, 4]. It is worth to be mentioned that for certain operation conditions a specific critical voltage (V_c) for the considered dc plasma system can be attained, at least locally. In this case, the working abnormal regime discharge can abruptly change to arc (passing through the transition from abnormal regime to the arc regime), and the sintering process is interrupted by the power supply security system (arc management system). There are two main aspects that can contribute to the critical voltage of a dc plasma system to be achieved. The first one is the presence of organic constituent in the electrode surface, directly related to the dc plasma device cleanness, which is detrimental for dc plasma processes and also increases the risk of arc formation. The second one is the geometrical

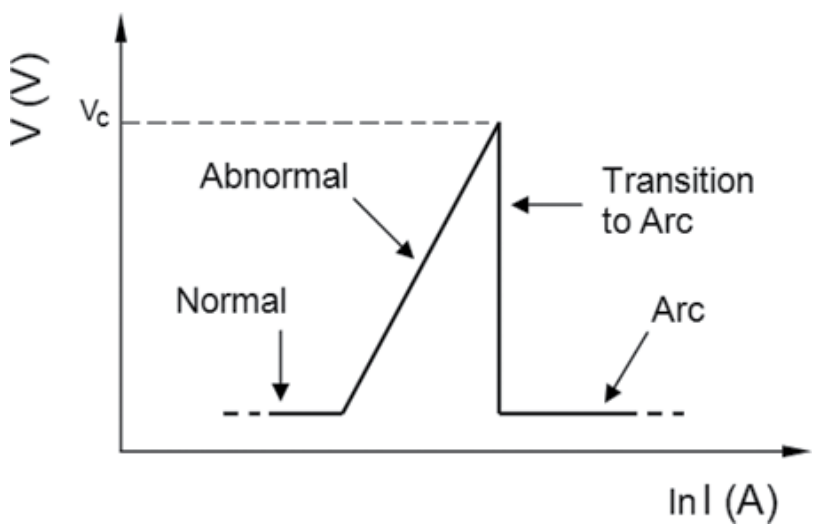

Figure 1. Schematic current-voltage characteristic of a dc discharge, showing the normal, abnormal, transition to arc, and arc regimes.

and dimensional arrangement related to the design of the electrodes and their respective insulating components.

Arc formation represents the main limitation for the use of dc plasmas in industrial applications. If the arc regime is established, high current density and high temperature (usually over 3000°C) are observed, and it can lead to surface damages in the sintering part or in the power supply system. It is to be noted that the arc formation risk in plasma processing was partially overcome in the half of the last century with the introduction of the pulsed dc plasma power supplies, and nowadays industrial plasma power supplies are additionally equipped with advanced arc managing systems to minimize such problem. In this case, for each switched-off time of the pulse (see **Figure 2a**, **b**), the system current is decreased, tending to zero, so the risk for arc formation is reduced. Despite these advances, it remains an important challenge regarding the know-how and R&D of dc plasma sintering devices.

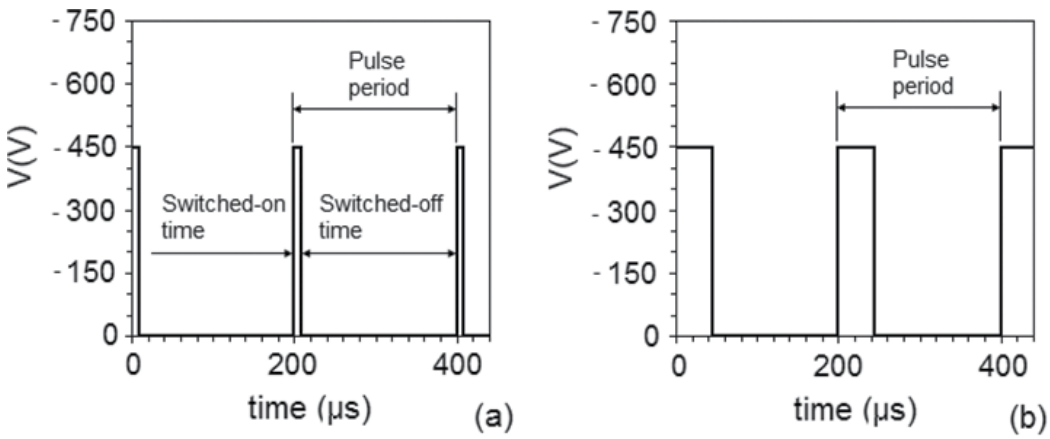

Figure 2. Scheme of square wave pulses (case of pulse voltage of −450 V and period of 200 μs) for two different switched-on times (for values of random choice): (a) 10 μs and (b) 40 μs.

By considering that the arc formation risk increases as the plasma power is increased, another strategy used in the industry to overcome this important problem is the use of hot-wall plasma chamber. In this case the power needed to reach the processing temperature is mainly provided by an auxiliary heating system, reducing the necessary plasma power to achieve the desired sintering temperature, decreasing the risk of arc formation.

To go further on the understanding of the plasma-assisted sintering, it is necessary to stress in more details how the potential distribution along the discharge is changed after breakdown (when the glow discharge or the plasma itself is obtained).

2.1. Potential distribution in the discharge

As the plasma is obtained by the gas ionization, mainly due to the collisions between high-energy electrons and neutral gas species, the potential distribution (indicated by red lines in **Figure 3a**, **b**) between the two electrodes is changed from that represented in **Figure 3(a)** to

http://dx.doi.org/10.5772/66870

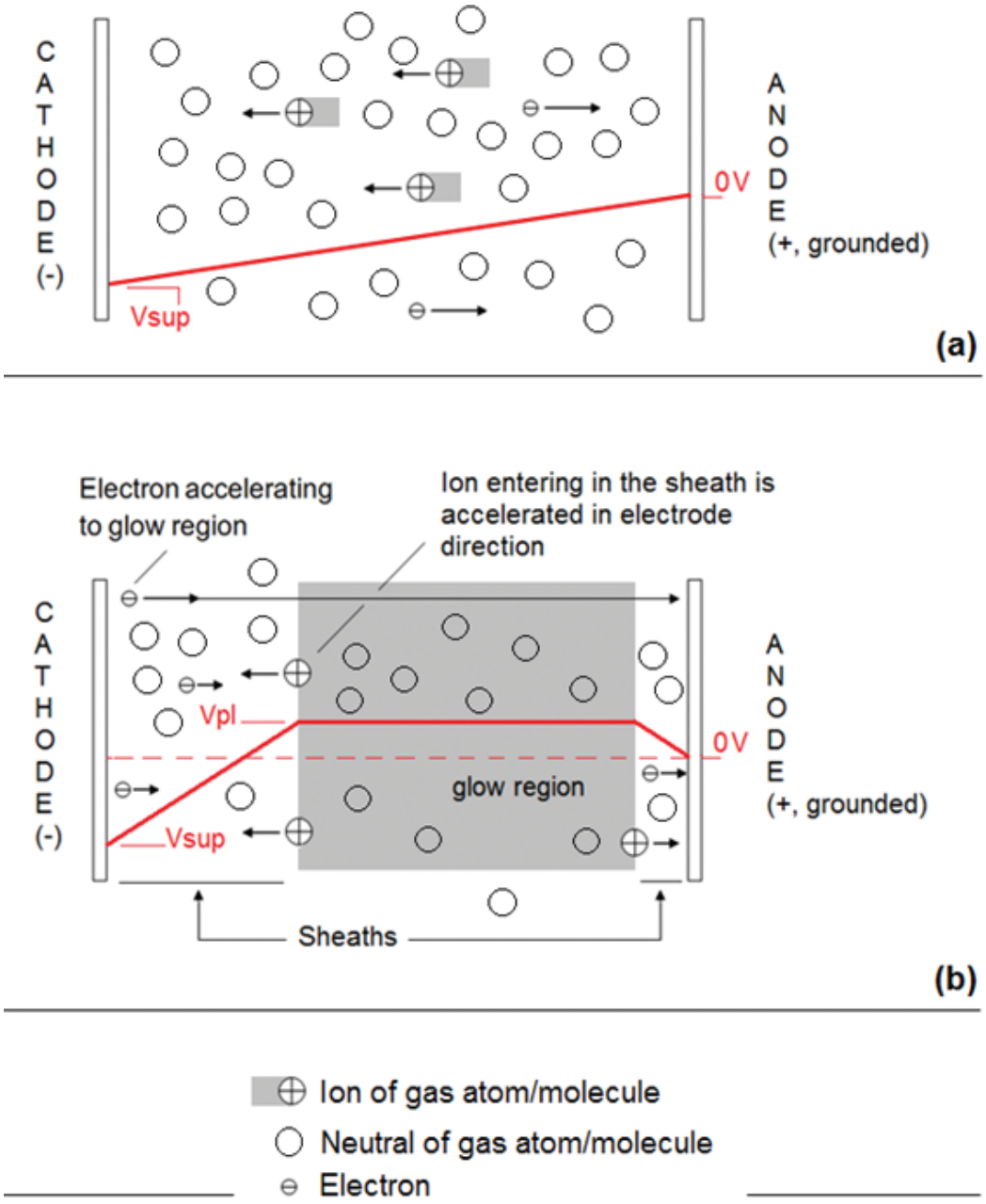

Figure 3. Discharge potential distribution between the electrodes of a typical electrical system used in dc plasma process: (a) before the glow discharge (plasma) to be established and (b) after the obtainment of plasma.

that in **Figure 3(b)**. In **Figure 3(a)**, the scheme of a gas at low pressure and the respective electrodes of a typical electrical system used in dc glow discharge chambers are shown. It is to be noted that ions and electrons of the gas, initially present at very low number density (around 10^3 cm^{-3}), are accelerated by the electrical field imposed by the power supply. For a specific

potential and sufficient low pressure, the dielectric gas breakdown is achieved, phenomena governed by Paschen's law [7], and a glow discharge (thus the plasma) is established, changing the potential distribution along the discharge to that presented in **Figure 3(b)** due to the generation of a significant number of charged species. In abnormal glow regime, the glow region is approximately equipotential (negligible electrical field), presenting a positive potential, known as plasma potential (V_{pl}), on the order of +10 V [1], and the electrical field, which before breakdown was approximately linear between the electrodes, becomes restricted next to both the cathode and anode sheaths. The ions produced by ionization collisions (with high-energy electrons) that randomly reach the glow region-sheath interfaces are accelerated to the respective electrodes and can make additional collisions with neutral species, resulting, for example, in the known charge-exchange collisions in the sheath [1]. This is an important kind of collision, since fast (high kinetic energy) neutrals driven to the electrode surfaces are produced by this mean, explaining why not only fast ions bombard such surfaces but also fast neutrals.

Figure 3(b) corresponds to the usual kind of glow discharge used in dc plasma sintering process usually termed as the cathode configuration [5, 6], where the part to be sintered acts as the cathode of the discharge. There are two distinct regions with considerable electrical fields along the discharge, the cathode fall where the potential varies from the plasma potential down to the negative potential imposed by the power supply (V_{sup}), and the anode fall where the potential varies from the plasma potential down to zero at the grounded electrode, where the part could also be placed to undergo the sintering process.

At this point it is important to introduce the reader for the different ways or techniques for which a part can be sintered under dc plasma environmental.

2.2. The different techniques of dc plasma sintering

Some different possibilities or techniques (discharge configuration) to carry out the plasma sintering process can be listed as follows:

- Case 1: Sintering of parts in the cathode configuration in cold-wall chambers (without auxiliary resistive heating);
- Case 2: Sintering of parts in the hollow cathode discharge (HCD) configuration in cold-wall chambers (without auxiliary resistive heating);
- Case 3: Sintering of parts in the anode (or floating potential) configuration in cold-wall chambers (without auxiliary resistive heating); and
- Case 4: Sintering of parts in any of the aforementioned configurations in hot-wall chambers (with auxiliary resistive heating).

For the first case, here termed as the cathode configuration in cold-wall chambers, the heating of the part at temperatures high enough for the sintering purpose (around 1100–1250°C, for iron parts) is achieved exclusively by the plasma fast species bombardment. For this case, if the gas mixture is composed of 80% Ar + 20% H_2, pressure usually varies in the range of 10–30

http://dx.doi.org/10.5772/66870

Torr (1333–3999 Pa), considering pulse voltages of 600–700 V [11–16]. This condition, i.e., for parts acting as the cathode of the plasma device, is illustrated in **Figure 3(b)**.

The second case is the hollow cathode discharge [8], as shown in **Figure 4** that is a special kind of dc abnormal glow discharge, for which the same principles of the cathode configuration (see **Figure 3b**) are also valid. But in this configuration, by considering that both the cathode walls present a same potential, the potential distribution along the discharge is changed, being comprised by two similar electrical field regions next to each cathode surface, and the

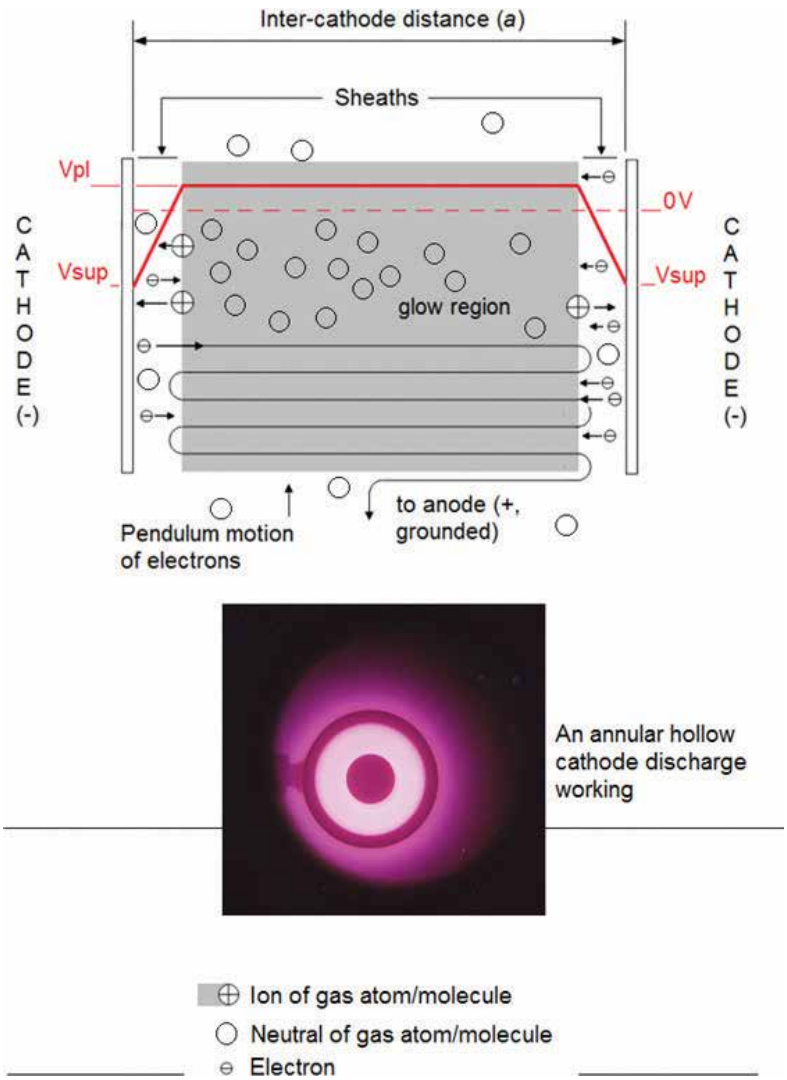

Figure 4. Discharge potential distribution at the hollow cathode discharge configuration and photo of an annular glow discharge (here, the hollow cathode effect is evidenced by the more intense light brighter than that verified outside the outer cathode (referred to the central one), which is also surrounded by plasma (in this case, presenting a less intense light bright)).

glow region that is virtually field-free. In this case, the grounded anode reference is outside from the hollow cathode region (not shown in **Figure 4**).

For the hollow cathode configuration, considering the same gas mixture, sintering temperatures can be attained by using lower gas pressures or voltage than those used in cathode configuration. In hollow cathode configuration, for a gas mixture composed of 80% Ar + 20% H_2, the pressure range usually varies from 1 (133 Pa) to 9 (1200 Pa) Torr, considering pulse voltages on the order of 450 V [5, 6, 17–23]. Here, the heating of the part to the sintering temperature is carried out by the fast plasma species bombardment, and the part to be sintered acts as one cathode of the formed hollow cathode discharge. This situation is illustrated in the bottom of **Figure 4**, in which cylindrical parts to be sintered act as the inner cathode of a typical annular hollow cathode discharge, as presented in references [17–23]. It is to be noted that, for this configuration, plasma is much more ionized than that obtained in cathode configuration. This is due to the electron pendulum motion between the cathode falls that repulse electrons, keeping most of them arrested inside the discharge, thus increasing the collision probability and the ionization rate. As a reference, in a hollow cathode discharge, the current densities can be two orders of magnitude higher than that of a conventional discharge [7].

For the third case, parts are placed in the anode or in the floating potential (electrically insulated) so that no significant heating will be produced by plasma fast species bombardment. In this case, the discharge cathode is heated, and the part is mainly heated by radiation of the "hot cathode." In addition, the very chemical-active plasma environment acts in the part surface, but the physical effects related to the fast species bombardment are strongly reduced.

Finally, all configurations presented here can be applied in a hot-wall chamber so that the heating effect can be partially supplied by an auxiliary-resistive heating system (the fourth case). For example, in sintering of parts in the cathode configuration in hot-wall chambers, the part heating can be performed by the fast plasma species bombardment as well as by the heat transferred from the auxiliary-resistive heating system. In this case, the main role of the plasma is creating a highly reactive atmosphere, as chemically as physically, by means of excited-species-enriched environment. The use of an auxiliary-resistive heating system makes possible to decrease the high risk of plasma instabilities when high power input is necessary to perform sintering. In addition, it tends to reduce the texturing effects caused by sputtering, an effect which is typical of surfaces sintered in cathode configuration, as presented in [5]. In the anode/floating potential configuration [5, 6], the heating is due to the heat transferred by radiation from the cathode walls heated by plasma species bombardment and by using an auxiliary-resistive heating system. In this case, the relatively intense fast plasma species (ions and neutrals) bombardment verified for parts acting as cathode does not occur, and the parts sintered in anode do not present significant texturing effect caused by sputtering.

Additionally, the anode configuration (with or without hot wall) also makes possible to perform simultaneous sputtering-deposition treatment with the sintering process. For this situation, atoms sputtered from the (hot) cathode wall can be deposited on the anode (and/or

floating part) surface, being that surface alloying is also expected to occur, depending on the composition of each electrode as well as the plasma parameters. This configuration has also been used to perform the debinding of powder injection molding (PIM) parts [5, 6, 24–28]. It is worth to be mentioned that the anode configuration comprises the very well-established hybrid sintering furnace (or hybrid dc plasma reactor) designed for plasma-assisted debinding and the sintering of powder injection molded parts [24–28]. This system has already been used in industrial production of PIM parts. If it is the interest, the reader can access the furnace scheme presented in reference [5].

Independently from the chosen configuration, the dc plasma sintering procedure is frequently divided into four steps. For the case of iron parts, the first step is the cleaning of the parts usually under a H_2 + Ar (or pure H_2) glow discharge at 723 K (450°C) for 30 min, using 133 Pa (1–3 Torr) pressure. The three other steps are the heating stage of the parts to be sintered at moderate heating rates up to the sintering temperature, the sintering stage, and, finally, the cooling stage under the used gas mixture flow. Such procedure is valid for all above mentioned dc plasma sintering techniques. As a general rule, cathodes are negatively biased at pulse voltage of at least 450 V, but they can be set up to about 1000 V, generally using square form pulsed power supply with frequency ranging from 1 kHz up to few hundreds of kHz. The choice of the pulse voltage and duty cycle depends on the sintering technique and on the discharge parameters like the gas mixture and pressure, besides others. In addition, for the case of hot-wall chamber, the desired power to be transferred to the plasma can be chosen by setting the auxiliary heating system parameters (keeping in mind the sintering temperature to be attained).

3. Plasma environment and chemical-potential setting in sintering

Figure 5 shows typical scheme of a sintering contact between two particles (scheme adapted from Thümmler and Oberacker [29]) but here subjected to the dc plasma environment. In that case [29], the main sintering mechanisms occurring in metals under the total absence of plasma environment, excepting the plastic flow, are presented and carefully discussed, namely, superficial diffusion (way 1), evaporation and recondensation (way 2), volume diffusion (way 3), and grain-boundary diffusion (way 4), as presented in **Figure 5**.

Under the plasma environment, for particles next to the surface, the sputtering [1, 2, 4, 8–10, 30–36] caused by the fast plasma species bombarding the cathode surface becomes important, since it leads the density of sputtered metal atoms to be increased in the plasma phase, thus acting directly on the enhancement of the evaporation and recondensation mechanism (way 2). Moreover, the superficial diffusion mechanism (way 1) tends to be strongly incremented by the fast plasma bombardment, as well as the volume diffusion mechanism (way 3) at the surface, since the vacancy density next to the surface tends to be increased, as one of the possible events of the plasma-surface (interface) interaction (see **Figure 6**). Finally, as a result of the use of high-purity hydrogen in the gas mixture, associated with the hydrogen dissociation in the plasma environment, the oxide-reduction

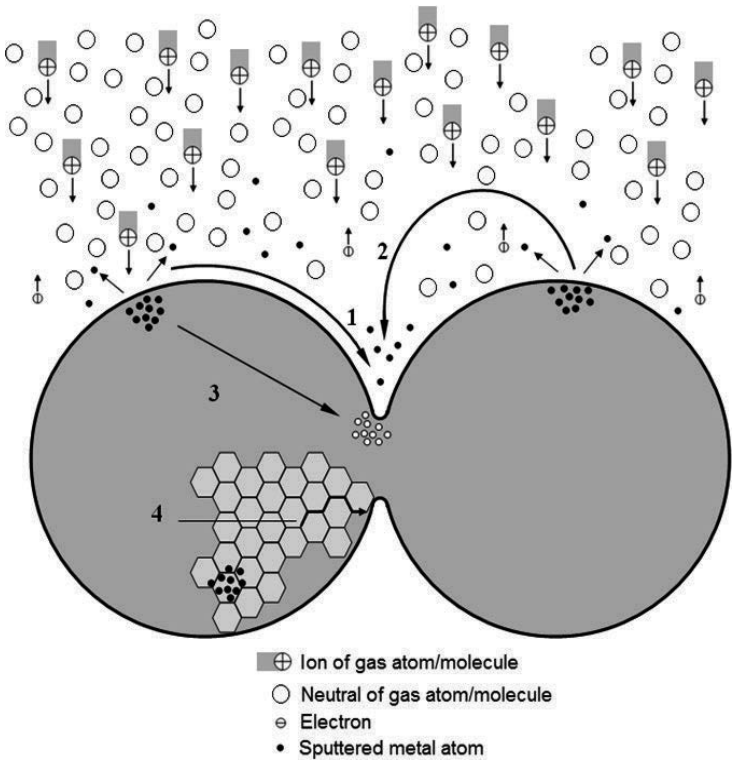

Figure 5. Scheme of a sintering contact between two particles (scheme adapted from Thümmler and Oberacker [29]), subjected to the dc plasma environment, showing the main sintering mechanisms, excepting the plastic flow: superficial diffusion (way 1), evaporation and recondensation (way 2), volume diffusion (way 3), and grain-boundary diffusion (way 4).

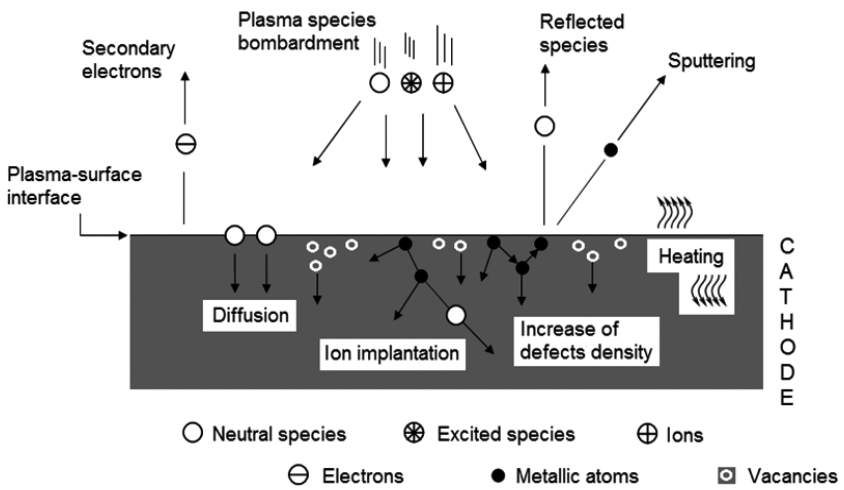

Figure 6. Typical events of the plasma-surface interface interaction (adapted from [1, 5, 6]).

http://dx.doi.org/10.5772/66870

effect is higher than in conventional processes, and the grain-boundary diffusion (way 4) tends to be also increased. It would be due to a supposed higher cleanness (based on the oxygen-free boundaries) attained in grain-boundary sites (particle contact). If the reader is interested, diffusion in solids is very well treated in [37].

Figure 6 shows the typical events of the plasma-surface interface interaction. The main events occurring more significantly in the cathode (part) surface, where the species energy is the highest, can be listed as follows [1, 5, 6]:

- Composition changes and chemical reactions as a result from the use of reactive gas species in the plasma (for all cases of dc plasma sintering techniques considered before) as well as of atoms sputtered from another cathode (it is supposed to be viable for the cases 2 and 3, only) being deposited in the part surface and diffusing into the substrate bulk;
- Ion implantation, as a result of the use of high pulse voltages, more probable in the hollow cathode discharge, due to the presence of fast species of higher energy for this particular configuration;
- Increase of the punctual defect density (like vacancies, interstitial, and/or substitutional atoms) in the first atomic layers of the substrate;
- Reflection of impingent plasma species;
- Emission of secondary electrons, which play important role in the discharge maintenance, since they are accelerated by the potential fall of the cathode sheath into the glow region, acquiring high energy;
- Sputtering, consisting of surface (metal and/or nonmetal) atoms torn off from its original surface as a result of the high-energy plasma species bombardment; and
- Heating of the cathode, as a result of the momentum transfer as the high kinetic energy species bombard its surface.

It is worth to be mentioned that in dc plasma sintering process one of the main roles of the plasma is providing a highly reductive atmosphere compared to conventional sintering furnaces. In this way, the smaller the oxygen species density in plasma, the higher is its oxide-reduction potential. Regarding the residual air pressure inside the vacuum chamber, it is to be noted that the oxygen partial pressure (P_{O2}) must be controlled and kept to low values, usually much lower than 0.27 Pa (0.21×10^{-2} Torr, the usual residual pressure of primary vacuum systems). In this case, certifying that stanch gas lines are present, by reducing leakage points all over the plasma installation, is imperative for a good sintering process. In addition, since all the dc plasma sintering techniques considered here are carried out under gas flow, gas-washing procedure of the vacuum chamber, by intercalating the evacuation/high-purity gas filling of it, makes possible to additionally decrease the P_{O2} of the referred system.

At this point, the use of the parameter gas flow regarding the plasma environment should be stressed to the good understanding of the reader. A correct gas mixture flow to the plasma

sintering treatment is important since the gas flow is responsible by changing the gas species in the vacuum chamber. As different oxygen sources can be present in the plasma sintering environment like oxygen-based species (e.g., H_2O) adsorbed in the anode walls (internal to the vacuum chamber), oxides (present as oxide film on the powder particles) in the part to be sintered, and in organic compounds (like stearates used to lubricate the metal powder particles before the compaction step of the pressed part), the use of an adequate flow can prevent a possible chemical-potential change of the atmosphere from reductive to oxidant due to impurities being incorporated to the atmosphere. In previous work [23], the influence of the gas mixture flow on the processing parameters of hollow cathode discharge iron sintering was studied, and it was shown that by using a flow of 2×10^{-6} N m^3 s^{-1}, the stainless steel external cathode was completely oxidized, but by using a flow of 5×10^{-6} N m^3 s^{-1}, a clean and bright-aspect surface was achieved after the iron part sintering in the central cathode. It is worth to be mentioned that these values are only valid for the experimental apparatus and samples used in [23].

Regarding the gas utilized in plasma sintering processes, besides hydrogen (H_2), which is a strong oxide reductor usually present in sintering gas mixtures, Ar is mainly used for the heating purpose. This is because its relatively high atomic mass makes the energy transfer for elastic collisions to the treating material more effective, resulting in heating of the metal part to be sintered. The hydrogen, since it is a strong reductive gas, is important to convert oxides into metal, considering that oxide layers are present in metal particles.

Finally, another important step to be considered in the dc plasma sintering process is the plasma cleaning stage before sintering. The cleaning stage is usually carried out using the same Ar + H_2 sintering gas mixture, or eventually in a pure H_2 predischarge at low pressure (normally at 3 Torr), before the isothermal sintering stage. It is aimed, in the cleaning stage, eliminating the undesired influence of microarcs, which can be originated from the plasma species bombarding organic molecules present in electrode surfaces, and can be responsible by leading the discharge regime change from the abnormal to arc. This step has also an important role on the degassing of the plasma chamber wall, reducing contamination by such species in the sintering step.

Now that the reader is familiar with plasma, to illustrate some important effects of plasma on the sintering process, in the next section, some results on plasma heating and surface modification during plasma sintering will be presented.

4. Plasma heating

Figure 7(a, b, c) shows different heating curves for cylindrical iron cathode (10 mm diameter × 25.4 mm height) presented in the bottom of **Figure 4** for different conditions by varying the discharge configuration (with and without hollow cathode effect) and plasma parameters. **Figure 7(a)** shows the temperatures attained by varying the switched-on time (equivalent to the duty cycle) at the hollow cathode discharge (HCD) configuration for different pressures. **Figure 7(b)** presents the temperatures attained by varying the cathode

http://dx.doi.org/10.5772/66870

pulse voltage (Vp) and the switched-on time for both the cathode and HCD (for an inter-cathode distance a = 6 mm) configurations, and the same is presented in **Figure 7(c)** but for intercathode distance a = 9 mm. The indicated temperatures in **Figure 7**(**a**, **b** and **c**) were measured in the abovementioned cathode (usually termed as the central cathode of the

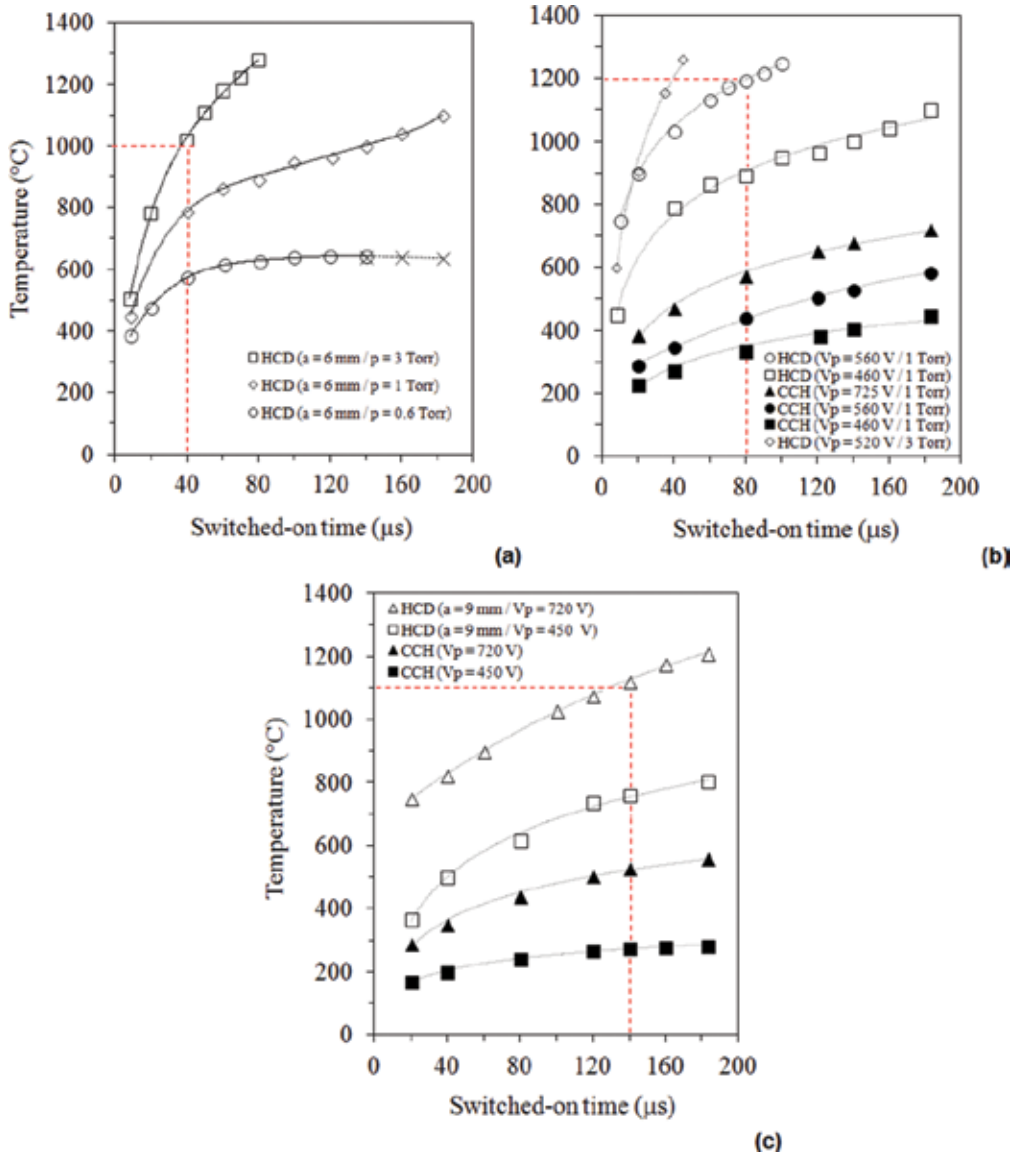

Figure 7. Different heating curves of cylindrical iron cathodes (10 mm diameter × 25.4 mm height) as functions of switched-on time (equivalent to the duty cycle) for different glow discharge configurations to dc plasma sintering purpose, for (a) hollow cathode discharge (*HCD*) (inter-cathode distance a = 6 mm) configuration as a function of the pressure, (b) both the cathode (*CCH*) and hollow cathode discharge (*HCD*) configurations at different cathode pulse voltages (Vp) and inter-cathode distance of 6 mm, and (c) the same at inter-cathode distance a = 9 mm, respectively.

hollow cathode configuration) by inserting a thermocouple inside it. For the cathode configuration, the cylindrical external (hollow) cathode was simply removed, thus leading to a heating condition where only one cathode (the central one) was present in the discharge. For more details, the reader can access the references [17–23]. In all cases, temperature increment can be expected as the switched-on time of the power supply, and thus the mean power transferred to the plasma is increased.

Considering other aspects, **Figure 7(a)** results also show the effect of the gas pressure on the cathode heating. Results indicate that the higher the pressure the higher is the ionization of the annular glow discharge, thus, the temperature achieved in the cathode. In the example shown using dashed red lines, for a specific switched-on time of 40 μs, considering square wave period of 200 μs (duty cycle of 20%), temperatures around 550, 750, and 1000°C are obtained for 0.6, 1.0, and 3.0 Torr pressures, respectively. At 0.6 Torr pressure, an annular glow discharge of instable operation is attained (indicated by the dashed black line for switched-on time ranging from 140 to 190 μs), being not adequate for the sintering purpose. This result agrees well with the expected for the product *ap* (*a* = inter-cathode distance and *p* = pressure), coming from more basic plasma studies, for which a stable hollow cathode discharge occurs for products *ap* ranging from 0.375 to 3.75 cm Torr [31]. Note that for a = 6 mm and p = 0.6 Torr, a product *ap* equal to 0.36 cm Torr is attained, which falls out of the proposed range for a stable condition. At 1 Torr, a duty cycle of 90% (maximum enabled by the power supply) has been used aiming to attain temperature high enough to perform iron sintering (~1100°C). And, for 3 Torr, the maximum temperature measurable by the K-type thermocouple was attained before the maximum duty cycle enabled by the power supply (~1250°C at 80 μs).

Figure 7(**b** and **c**) aims to put in evidence the role of the applied pulse voltage (Vp) on the cathode heating effect as well as the occurrence or not of the hollow cathode effect. It is evidenced that, as expected, the higher the voltage the higher is the temperature achieved in the cathode if considered the same configuration. On the other hand, considering the occurrence or not of hollow cathode effect, at 1 Torr pressure and *a* = 6 mm, for example, by using a 560 V pulse voltage, for a specific switched-on time of 80 μs, and considering a square wave period of 200 μs (duty cycle of 40%, see **Figure 7b**), the cathode temperature is increased from about 420°C, at the cathode configuration heating (*CCH*) to 1200°C, at the hollow cathode discharge (*HCD*). Finally, at 0.6 Torr pressure and *a* = 9 mm, for example, by using a 720 V pulse voltage, for a specific switched-on time of 140 μs, and considering a square wave period of 200 μs (duty cycle of 70%, see **Figure 7c**), the cathode temperature is increased from about 500°C, at the cathode configuration heating (*CCH*) to 1100°C, at the hollow cathode discharge (*HCD*). Being the interest, the reader can access additional details about the HCD in references [17–23].

In brief, from all results presented in **Figure 7**(**a**, **b** and **c**) as a general orientation regarding the cathode plasma heating, the use of higher pressures, pulse voltages, and duty cycles leads to higher glow discharge ionization with consequent higher current and dissipated power and thus the cathode heating to be improved, making possible to achieve tem-

http://dx.doi.org/10.5772/66870

peratures high enough to sinter several metals. If the cathode configuration is considered only, in the absence of the hollow cathode effect, the use of pressures around 10–30 Torr is necessary to attain sintering temperatures for iron components, as confirmed in [11–16], whereas pressures around 3–10 Torr are enough in the HCD, as shown in **Figure 7**(**a**, **b** and **c**).

5. Surface-related phenomena for plasma-sintered parts

Figure 8(**a**–**d**) shows, for comparison purpose, SEM micrographs of the top (subjected to *HCD*) and bottom (non-subjected to *HCD*) of a cylindrical green (pressed) iron (Ancorsteel 1000C iron powder) sample (**Figure 8a** and **c**, respectively) sintered in the central cathode of a hollow cathode discharge (HCD), using external stainless steel cathode ((**Figure 8b** and **d**, respectively). In this case, sintering was performed at 1150°C, during 2 hours, using inter-cathode distance of 6 mm, with a flow of 5×10^{-6} N m^3 s^{-1}, in 80% Ar + 20% H_2 gas mixture, and a pressure of 3 Torr. It is to be noted that in **Figure 8**(**b** and **d**), showing the surface condition after sintering, SEM micrographs were taken in the same positions of **Figure 8**(**a** and **c**), indicating the surface condition of the pressed iron sample, before sintering. The top of the sample was exposed to the plasma (as shown in **Figure 9**) aiming to put in evidence how effective the mass transport is affected by the discharge (plasma environment). Additionally to **Figure 8** (**a–d**) micrographs, **Figure 10** shows the Cr and Ni concentration profiles obtained in the originally pure iron-pressed sample surface, as a result of the deposition of metal atoms sputtered from the external cathode made of stainless steel on the pure iron sample top. All results shown in **Figures 8(a–d)** and **10** confirm the role of the sputtering, typically enhanced in *HCD*, in intensifying the mass transport in plasma phase and sample surface (as shown in **Figure 5** near the particle surfaces), thus improving the sintering mechanisms of the superficial diffusion (way 1) and the evaporation and recondensation (way 2). In this case, the role of the sputtering has supposedly increased the metal atoms density in plasma phase, which tends to recondense (or to be deposited) next to the surfaces subjected to the intense fast plasma species bombardment, preferentially in concave areas. Note that by confronting the iron sample bottom surface (non-subjected to the plasma species bombardment) in a same position in its green (before sintering) and sintered states (**Figure 8c** and **d**, respectively), apparently no additional surface densification was verified. This fact confirms that the sample bottom was sintered through the known mechanisms expected for the conventional sintering (as shown in [29]). Nevertheless, contrarily, for the top surface (subjected to the plasma species bombardment), important surface densification was achieved, which is confirmed by comparing the iron sample top surface (before plasma species bombardment) in a same position in its green and sintered states (**Figure 8a** and **b**, respectively). In this case, the sample top was sintered with increased superficial diffusion (way 1), and the evaporation and recondensation (way 2) improved by sputtering-depositing mechanism occurring in plasma (as shown in **Figure 5**) that conclude this discussion.

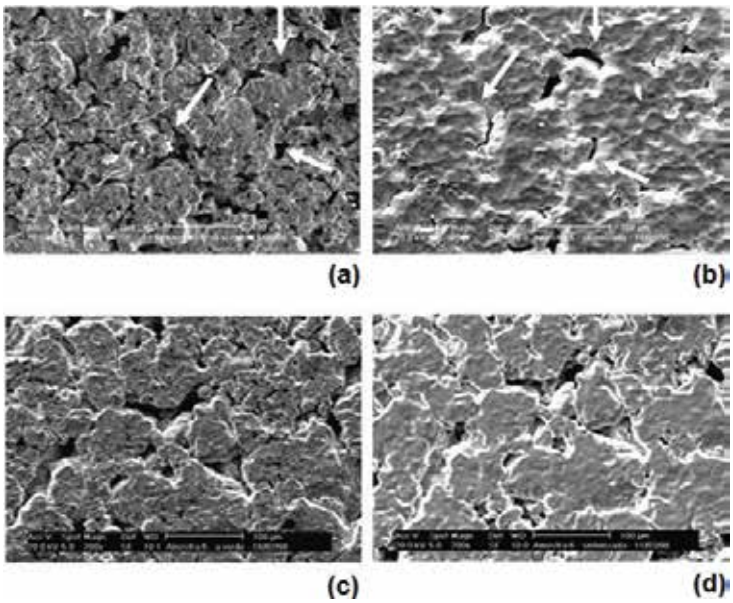

Figure 8. SEM micrographs of the (a and b) top surface (subjected to *HCD*) and (c and d) bottom (nonsubjected to *HCD*) of a cylindrical iron sample (Ancorsteel 1000C iron powder), before (a and c) and after (b and d) sintering, respectively (white arrows indicate identical positions of a same sample, before and after the sintering).

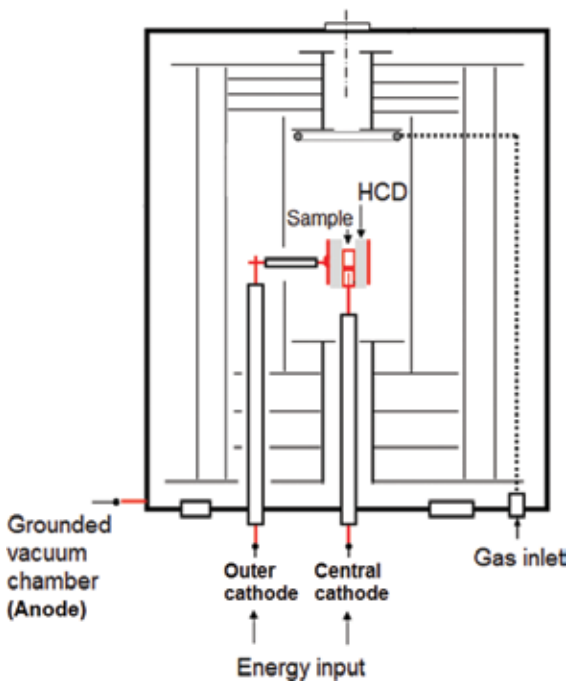

Figure 9. Scheme of *HCD* sintering experiment used to put in evidence the sintering mechanism here termed sputtering-deposition mechanism, occurring in dc plasma sintering system.

http://dx.doi.org/10.5772/66870

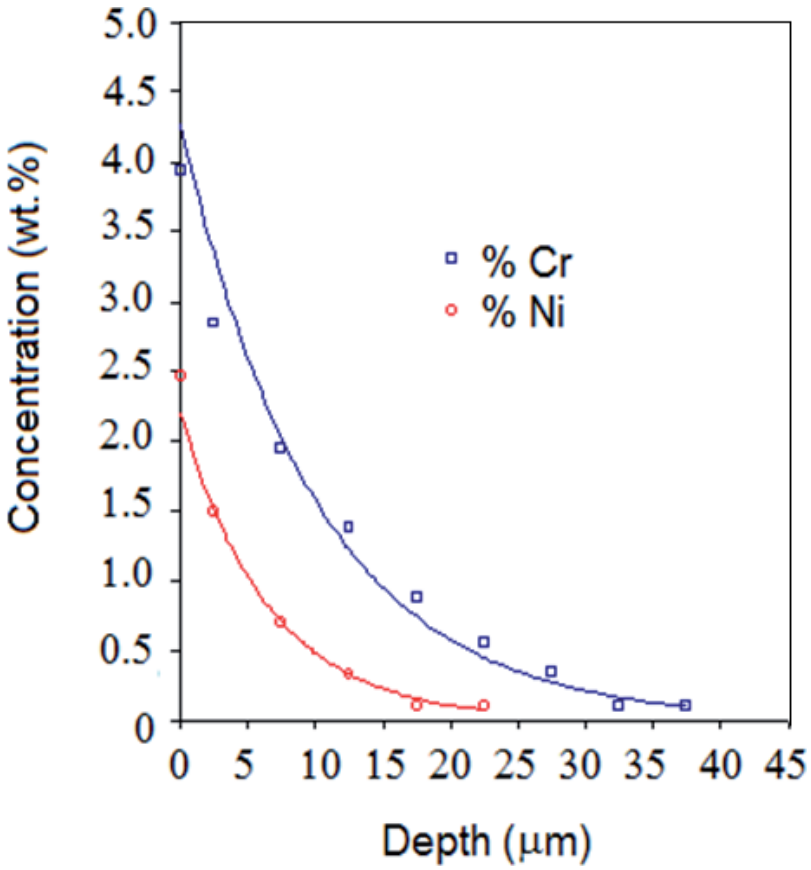

Figure 10. EDS measured Cr and Ni concentration depth profiles obtained in the sintered pure iron sample top surface, as a result of the deposition of metal atoms sputtered from the external stainless steel cathode, subjected to hollow cathode effect.

6. DC plasma sintering advantages over the conventional sintering

Considering all the presented phenomena involved in dc plasma sintering, it is expected that this process can present important technological advantage over "conventional sintering." As presented in [5, 6], some advantages of the dc plasma-assisted sintering process in respect to conventional sintering technique, as a consequence of the plasma species bombardment, besides other physicochemical phenomena, could be listed as follows:

- Possibility of surface diffusion increment;
- Possibility of surface texturing obtainment (see **Figure 8b** results) and eventual surface densification of the sintered part;
- Easy obtainment of highly reductive environment, enabling sintering of metals that tend to form very stable oxides (like Ti and stainless steels);

- Possibility of surface alloying of the sintered part carried out simultaneously to the part sintering, due to the sputtering-depositing effects (i.e., the enrichment of the part surface with alloying elements); and
- Finally, possibility of carrying out thermochemical treatments (such as nitriding, carburizing, and/or carbonitriding) that can be simultaneously performed in the sintering thermal cycle (as presented in reference [38]), or just after the sintering, in a single loading processing, by readjusting temperature and gas mixture, introducing reactive gases like nitrogen (N_2) and/or carbon (e.g., by means of the use of CH_4).

7. Final remarks

In this work, dc plasma-assisted sintering of metal parts is shown as a promising and relatively new research and development field in PM. The main aim of this work was to introduce the reader to the main applications of the dc plasma sintering process in the referred field. To achieve this goal, the present chapter was divided in a brief introduction and sections in which the bases of the abnormal glow discharge regime (dc plasma) were carefully treated, showing the main particularities of this new and "fascinating glow world" of dc plasma applied to the sintering of metal parts. Finally, the main techniques of dc plasma sintering, thermodynamic fundamentals of the plasma environment, aspects of the plasma heating, and plasma-surface-related phenomena of sintered parts were successfully treated, making possible to the reader to achieve a good understanding on the great potentialities of the dc plasma sintering process applied to the powder metallurgy.

Acknowledgements

The authors would like to acknowledge the Brazilian agency CNPq for the financial support of this work.

Author details

Silvio Francisco Brunatto[1]*, Rodrigo Perito Cardoso[1] and Aloísio Nelmo Klein[2]

*Address all correspondence to: brunatto@ufpr.br

1 Plasma Assisted Manufacturing Technology & Powder Metallurgy Group, Departamento de Engenharia Mecânica, Universidade Federal do Paraná (UFPR), Curitiba, PR, Brazil

2 Departamento de Engenharia Mecânica, Universidade Federal de Santa Catarina (UFSC), Florianópolis, SC, Brazil

http://dx.doi.org/10.5772/66870

References

[1] Chapman B. Glow Discharge Processes: Sputtering and Plasma Etching, 1st ed. John Wiley & Sons; New York: 1980. 406 p.

[2] Ricard A. Reactive Plasmas, 1st ed. Société Française du Vide; Paris, France: 1996. 180 p.

[3] Raizer Y P. Gas Discharges Physics, 1st ed. Springer-Verlag Berlin Heidelberg; Berlin, Germany: 1991 (Corrected 2nd Printing, 1997). 445 p.

[4] Roth J R. Industrial Plasma Engineering - Vol. 1 – Principles. The Institut of Physics; London, UK: 1995. 538 p.

[5] Klein A N, Cardoso R P, Pavanati H C, Binder C, Maliska A M, Hammes G, Fusão D, Seeber A, Brunatto S F, Muzart J L R. DC Plasma Technology Applied to Powder Metallurgy: an Overview. Plasma Sci. Technol. 2013; 15(1):70–81. DOI: 10.1088/1009-0630/15/1/12

[6] Brunatto S F, Cardoso R P, Klein A N, Muzart J L R. Sintering and Surface Texturing: Direct Current-Coupled Plasma-Assisted Parts Manufacturing. In: Rafael Colás; G E Totten. (Org.), Encyclopedia of Iron, Steel, and Their Alloys, Five-Volume Set (Print), 1st ed. CRC Press - Taylor & Francis Group; New York: 2016, 1–5, 3194–3207. DOI: 10.1081/E-EISA-120051668

[7] von Engel A. Ionized Gases, 2nd ed. American Institute of Physics; New York, USA: 1965 (Ed. 1994). 325 p.

[8] Mason R S, Allott R M. The Theory of Cathodic Bombardment in a Glow Discharge by Fast Neutrals. J. Phys. D Appl. Phys. 1994; 27:2372–2378.

[9] Abril I, Gras-Marti A, Valles-Abarca J A. Energy Transfer Processes in Glow Discharges. J. Vac. Sci. Technol. A 1986; 4(3):1773–1778.

[10] Mason R S, Pichilingi M. Sputtering in a Glow Discharge Ion Source - Pressure Dependence: Theory and Experiment. J. Phys. D Appl. Phys. 1994; 27:2363–2371.

[11] Maliska A M, Pavanati H C, Klein A N, Muzart J L R. The Influence of Ion Energy Bombardment on the Surface Porosity of Plasma Sintered Iron. Mater. Sci. Eng. A. 2003; 352(1–2):273–278.

[12] Pavanati H C, Straffelini G, Maliska A M, Klein A N. Dry Sliding of Plasma-Sintered Iron-the Influence of Nitriding on Wear Resistance. Wear. 2008;265(3–4):301–310. DOI: 10.1016/j.wear.2007.10.014

[13] Muzart J L R, et al. Plasma Sintering of AISI 316L Stainless Steel: The Influence of the Processing Cycle on the Sample Density. Proceedings of Advances in Powder Metallurgy & Particulate Materials 1997, Part 3:77–84, MPIF, Brazil, 1997.

[14] Batista V J, Binder R, Klein A N, Muzart J L R. Sintering Iron Using an Abnormal Glow Discharge. Int. J. Powder Metall. 1998; 34(8):55–62.

[15] Pavanati H C, Straffelini G, Maliska A M, Klein A N. Microstructural and Mechanical Characterization of Iron Samples Sintered in DC Plasma. Mater. Sci. Eng. A 2008; 474(1–2):15–23. DOI: 10.1016/j.msea.2007.04.020

[16] Marchiori R, Maliska A M, Borges P C, Klein A N, Muzart J L R. Corrosion Study of Plasma Sintered Unalloyed Iron: the Influence of Porosity Sealing and Ni Surface Enrichment. Mater. Sci. Eng. A 2007; 467(1–2):159–164. DOI:10.1016/j.msea.2007.02.090

[17] Brunatto S F, Kühn I, Muzart J L R. Sintering of Iron in Hollow Cathode Discharge: Characterization of the Heating Process. Revista Brasileira de Aplicações de Vácuo. 1998; 18:31–39. (in Portuguese)

[18] Brunatto S F, Klein A N, Muzart J L R. Hollow Cathode Discharge: Application of a Deposition Treatment in the Iron Sintering. J. Braz. Soc. Mech. Sci. Eng. 2008;30(2):145–151.

[19] Brunatto S F, Kühn I, Klein A N, Muzart J L R. Sintering Iron Using a Hollow Cathode Discharge. Mater. Sci. and Eng. A. 2003;343:163–169.

[20] Brunatto S F Plasma Assisted Parts' Manufacturing: Sintering and Surface Texturing—Part I—Influence of Sintering Time and Temperature. J. Braz. Soc. Mech. Sci. Eng. 2010;32(2):128–135.

[21] Brunatto S F. Plasma Assisted Parts' Manufacturing: Sintering and Surface Texturing—Part II—Influence of Inter-Cathode Distance and Gas Pressure. J. Braz. Soc. Mech. Sci. Eng. 2010;32(2):136–145.

[22] Brunatto S F, Kühn I, Muzart J L R. Surface Modification of Iron Sintered in Hollow Cathode Discharge Using an External Stainless Steel Cathode. J. Phys. D Appl. Phys. 2005;38:2198–2203. DOI: 10.1088/0022-3727/38/13/018

[23] Brunatto S F, Muzart J L R. Influence of the Gas Mixture Flow on the Processing Parameters of Hollow Cathode Discharge Iron Sintering. J. Phys. D Appl. Phys. 2007;40:3937–3944. DOI: 10.1088/0022-3727/40/13/005

[24] Wendhausen P A P, Fusão D, Klein A N, et al Plasma Assisted Debinding and Sintering: Process and Equipment. Powder Metallurgy World Congress & Exhibition. 2004, Viena vol 4 (European Powder Metallurgy Association, Shrewsbury, United Kingdom) p. 137.

[25] Wendhausen P A P, Muzart J L R, Souza A R, et al A New Furnace Concept Based on Plasma Technology for Processing PIM Components. Advances in Powder Metallurgy and Particulate Materials. Metal Powder Industries Federation; Princeton, New York: 2000.

[26] Klein A N, Muzart J L R, Souza A R, et al Process for Removal of Binders from Parts Produced by Powder Injection Molding (USPTO, Arlington) 2003 U.S. Patent No. 6,579,493 B1

[27] Klein A N, Muzart J L R, Souza A R, et al Plasma Process for Removing a Binder from Parts Obtained by Powder Injection Molding (EPO, Brussels) 2003 European Patent No. 1230056

[28] Machado R, Ristow Jr. W, Klein A N, et al. Industrial Plasma Reactor for Plasma Assisted thermal Debinding of Powder Injection -Molded Parts (Arlington: USPTO) 2007 U.S Patent No. 7,718,919 B2

[29] Thümmler F, Oberacker R. Introduction to Powder Metallurgy. 1st ed. The Institute of Materials; London, UK: 1993. 332 p.

[30] Benda M, Vlcek J, Cibulka V, Musil J. Plasma Nitriding Combined With a Hollow Cathode Discharge Sputtering at High Pressures. J. Vac. Sci. Technol. A. 1997;15(5):2636–2643.

[31] Koch H, Friedrich L J, et al. Hollow Cathode Discharge Sputtering Device for Uniform Large Area Thin Film Deposition. J. Vac. Sci. Technol. A. 1991;9(4):2374–2377.

[32] Dunaev V V, Zhiglinsii A G, et al. Determination of Absolute Selective Sputtering Coefficients in a Hollow—Cathode Hydrogen Plasma. Sov. Phys. Tech. Phys. 1992;32(2):134–136.

[33] Petitjean L, et al. Emission Spectroscopy Study of N2-H2 Glow Discharge for Metal Surface Nitriding. J. Phys. D Appl. Phys. 1984;17:919–929.

[34] Eltoukhy A H, Greene J E. Diffusion Enhancement Due to Low-Energy Ion Bombardment During Sputter Etching and Deposition. J. Appl. Phys. 1980;51(8):4444–4452.

[35] Dunaev V V, Zhiglinskii A G, Sukhomlinov V S, Fafurina É N. Evolution of the Density of Metallic Atoms in a Discharge with a Hollow Cathode. Sov. Phys. Tech. Phys. 1992;37(1):34–37.

[36] Jung T, et al. Gas Flow Sputtering of Oxide Coatings: Practical Aspects of the Process. Surf. Coat. Technol. 1996;86–87:218–224.

[37] Mehrer H. Diffusion in Solids. Springer-Verlag; Berlin: 2007. 651p.

[38] Brunatto S F, Meier Alisson, Henke S, Binder C, and Klein A N. Plasma Sintering-Carburizing of 410 LHC steel in Carbon Containing Atmosphere. Mater. Sci. Forum. 2014; 802:353–358. DOI:10.4028/www.scientific.net/MSF.802.353

Chapter 5

Composite Materials Infiltrated by Aluminium Alloys Based on Porous Skeletons from Alumina, Mullite and Titanium Produced by Powder Metallurgy Techniques

Leszek A. Dobrzański , Grzegorz Matula ,
Anna D. Dobrzańska-Danikiewicz , Piotr Malara ,
Marek Kremzer , Błażej Tomiczek ,
Magdalena Kujawa , Eugeniusz Hajduczek ,
Anna Achtelik-Franczak , Lech B. Dobrzański and
Jagoda Krzysteczko

Additional information is available at the end of the chapter

http://dx.doi.org/10.5772/65377

Abstract

The infiltration technology with reinforcement in the form of porous skeletons fabricated with powder metallurgy methods has been presented in relation to the general characteristics of metal alloy matrix composite materials. The results of our own investigations are presented pertaining to four alternative technologies of fabrication of porous, sintered skeletons, and their structure and their key technological properties are presented. Porous skeletons made of Al_2O_3 aluminium are sintered reactively using blowing agents or are manufactured by ceramic injection moulding (CIM) from powder. Porous skeletons made of $3Al_2O_3$ $2SiO_2$ mullite are achieved by sintering a mixture of halloysite nanotubes together with agents forming an open structure of pores. Titanium porous skeletons are achieved by selective laser sintering (SLS). The structure and properties of composite materials with an aluminium alloy matrix—mainly EN AC-AlSi12 and also EN AC-AlSi7Mg0.3 alloys—reinforced with the so manufactured skeletons are also described. A unique structure of the achieved composite materials, together with good mechanical properties and abrasive wear resistance at low density, ensured by an aluminium alloy matrix, are indicating broad application possibilities of such composites.

Keywords: composite materials, powder metallurgy, infiltration, sintering, SLS, CIM

1. General characteristics of metallic matrix composite materials

Composite materials are one of the key groups of engineering materials, and although their fabrication is often inspired by examples originating from nature, they are produced—by the rule—artificially. They consist of at least two different constituent components with the same or similar volume fraction and with a clearly marked separation boundary between them and with their properties differing from the components creating them. Such properties are principally–for strictly specified reasons—more beneficial than the properties of each of the components, which justifies the need to manufacture them [1–4].

The principal components of a composite material are a matrix and reinforcement, with each of them playing different roles. The majority of composites are manufactured by indirect methods based on the earlier and separate preparation of the matrix and reinforcement materials and then combining them into the whole. A composite material matrix is comprised of a material being the continuous phase, filling the space between the reinforcement, and thus allowing to maintain the matrix-reinforcement system in the compact form, and also ensuring the desired shape and dimensions of products made of such materials. A matrix is also transferring loads onto the reinforcement, and at the same time, it protecting against damages or negative environmental impact, and most frequently, it is also crucial for chemical and thermal properties of the composite material. A matrix material can be either metal, including ferroalloys, magnesium alloys, aluminium alloys, zinc alloys, silver alloys, nickel alloys and copper alloys. It can also be made of non-metal—a ceramic matrix (aluminium oxide, silicon carbide, aluminium nitride, graphite, cement, chamotte) and an organic matrix: polymeric (e.g. polypropylene, polycarbonate, polyesters, epoxide, polyamide) or a carbon matrix [1–5]. Another component is introduced into a matrix—reinforcement, having better properties, usually strength properties, than the matrix properties. Reinforcement can be either in the form of fibres, particles or elements with complex geometric characteristics and even such ordered spatially, for example, in the form of a skeleton, and its role in a composite is generally to ensure, among others, the required rigidity, increased yield strength and strength at room temperature, to prevent the propagation of cracks and to change matrix susceptibility to plastic deformations [1–5]. Reinforcement is a general term, however, and for this reason, for some composite materials, its role is not only, and in some cases, at all, to improve mechanical or tribological properties, but also to improve selected physiochemical properties, for example, electric, thermal or magnetic properties.

Apart from the properties of the matrix and the reinforcement, the connection between the matrix and the reinforcement, produced as a result of the technology applied, plays an important role in all composite materials. A contact zone between the matrix and the reinforcement is an organic layer in composite materials, whose thickness and physiochemical character are essential for the transfer of loads between the matrix and reinforcement, hence for the properties of the composite material produced [6–10]. Several types of matrix-reinforcement connections can be distinguished considering the character of interactions between the composite material components:

http://dx.doi.org/10.5772/65377

- chemical connections, connected with diffusive processes occurring between a matrix and reinforcement of a composite material and for this reason also often called a diffusive connection;
- mechanical connections, where reinforcement elements are mechanically 'anchored' within the matrix;
- adhesive connections, due to the bonds existing between the adjoining matrix and reinforcement surfaces, often accompanying a mechanical interaction and increasing its effectiveness.

The key factor critical to fabrication of the required connection between a matrix and reinforcement is its surface quality; for this reason, an important part of the technological process of composite material fabrication is to prepare the matrix and reinforcement correctly. A properly selected combination of all or some of the following operations has to be applied most frequently for such preparation, in relation to the matrix and reinforcement, or at least one of them, depending on the composite material manufacturing technology applied [1–4]:

- machining,
- ultrasonic treatment,
- alkaline degreasing,
- degreasing in organic solvents,
- chemical etching,
- electrochemical etching.

One of the composite material variants is a group with a metallic matrix, often called metal matrix composites (MMCs) [1, 2, 4]. Unfaltering interest has been seen in composite materials with a light metal matrix, linked to an effort to minimise the weight of parts used in the automotive, aviation, railway and ship industry to reduce the overall mass of vehicles and by means of transport in which they are incorporated, which, naturally, allows to reduce the mass and improve the coverage and bearing capacity of vehicles while lowering fuel consumption. Hence, more attention is paid to replacing steel parts with relatively high weight with light metal alloys, especially aluminium and magnesium. Unfortunately, a lower Young's modulus, lower strength, tribological properties and rigidity of light metal alloys—as compared to steel—do not always allow to use them as a conventionally manufactured alloy, even subjected to heat treatment. As a consequence, composite materials with a light metal alloy matrix having better strength properties, rigidity, wear resistance, hardness and a lower thermal expansion coefficient are often fabricated in order to improve the mentioned properties [11]. Special attention should be drawn to light metal matrix composite materials reinforced with ceramic particles or ceramic fibres, which—due to very good properties as compared to conventional alloys—such as smaller density, higher strength and creeping resistance and abrasive strength and corrosion resistance, are commonly employed in the aviation, electronic, motor and machine industry, and also in the space and arms sector, and even a sports sector. The technologies of their manufacturing processes are one of

the most sharply evolving fields of materials engineering. In order to address the expectations of the market, it is substantiated to undertake measures aimed at developing alternative methods of light metal matrix composites, mainly aluminium and magnesium alloys [12–22]. Considering a high melting point, low density and good corrosion resistance of ceramics, the fibre-reinforced or particle-reinforced composites deriving from such ceramics are of special importance here. Of special importance, here is also a quest for alternative materials for the commonly used reinforcements in the form of Al_2O_3 fibres and particles [10, 15, 23–25], SiC [6, 13], made of boron [26], whiskers of Al_2O_3 or SiC, B_4C [27], BN [12] and TiC [6, 28] particles, graphene [5] or carbon nanotubes, as well as intermetallic phases [29], and even of high-melting metals and their alloys [30, 31]. In the case of aluminium alloy matrix composites, the name of the matrix element is often provided directly in the name or abbreviation of such a composite, for example, aluminium matrix composites (AlMCs). The considerations presented further in this chapter concern such composite materials.

2. General characteristics of the infiltration technology for the fabrication of metal matrix composite materials with indirect use of powder metallurgy method

Metallic composite materials can be manufactured by various methods. The ones used most often include classical powder metallurgy methods applied directly, as well as mechanical alloying methods and hot and cold plastic consolidation described in detail in other chapters of this book. It is beneficial to fabricate composite materials with powder metallurgy methods due to the diffusive form of the matrix and reinforcement connection, as well as due to flexible choice of the reinforcement type, form and dimensions. Such methods allow to achieve composite materials through the consolidation of metal powders and ceramics, as a result of several successive operations, that is, powder and powder mixture preparation, moulding or compression, sintering or plastic consolidation and finishing. Despite many advantages of such a method, including undoubtedly a possibility to produce a series of elements with high accuracy, a possibility of automating the production and assembly of the elements produced, low power consumption and almost completely eliminated waste production, powder metallurgy requires to use specialist equipment. Moreover, powder production causes difficulties, and it is costly. The mechanical properties of the materials achieved in this way are sometimes worse than, for example, of plastically worked elements. However, owing to mechanical synthesis (mechanical milling) and the subsequent compression and hot pressing, nanostructured composite materials can be manufactured having the constant cross section, uniformly distributed reinforcement and reinforcement particles, and the resulting enhanced mechanical properties of materials [32, 33].

An alternative solution for this technology is a hybrid combination of powder metallurgy methods with a casting technology such as infiltration. In this technology, a porous skeleton with open pores is produced, usually a ceramic skeleton, but in some cases, it is also made of

http://dx.doi.org/10.5772/65377

metals or metal alloys, with powder metallurgy methods. Next, the pores are filled with liquid metal or alloy with a melting point correspondingly lower than the melting point of the metal from which the sintered skeleton was made. Melted polymeric material or special resin mixed with a hardener is also often used for filling. The task of a sintered porous skeleton, being a semi-product, is to finally reinforce, locally, the composite material produced, at the same time determining its structure and properties. The basic property of this porous skeleton, which is also representing the reinforcement of the finally produced composite material, is that it has a structure of open, linked pores forming the channels allowing the melted metal or, respectively, polymeric material to flow freely. As a result of this, a porous preform can be saturated with liquid metal or a polymeric material within the entire volume of pores. This technology can certainly be approached, as it was made in this book, as a special variant of the powder metallurgy technology, but only an indirect one although a description of this technology can also be found in works concerning the casting of metals and metal alloys. In such case, it is usually not mentioned, though, that pores can be filled with polymeric materials in the liquid state, which shows that this technology cannot be classified unequivocally as a metal casting method.

The use of infiltration as a highly profitable technology is fundamental for obtaining a wide array of composite materials and brings numerous technological benefits [23, 25, 34, 35]. This stems from the fact that a technology of fabricating metal matrix composite materials using infiltration is characterised by high efficiency, and it can be utilised in mass production and ensures a wide selection of reinforcement and matrix. Moreover, it entails a smaller risk of mechanical damage to the reinforcement, as can be the case in, for example, mechanical synthesis. Besides, parts can be produced which are reinforced within the whole volume or only locally with the near-net-shape; a structure is also produced having the type of interpenetrating crystalline networks. In view of the characteristics presented, infiltrated composite materials attract manufacturers' special attention, especially in motor industry. Nevertheless, one has to point out the obstacles for applying this technology with the requirement to prepare the internal surfaces of the reinforcement skeleton pores to improve their wettability. It is also necessary to remove the gases absorbed at the surface to avoid gas porosity. Moreover, it is not possible to ensure full reinforcement dispersion in a matrix which is dictated solely by the complex constructional characteristics of the sintered porous skeleton, most often in the form of a porous preform [15, 23, 24, 36].

The infiltration method creates relatively advantageous conditions for recycling the so produced composite materials. It is most preferable for composite materials that they can be re-used in a combined form, that is, without separation of components. Such materials are usually designed for a specifically defined use, and hence, it is difficult to find an area for reusing them. Reinforcement has to be separate from a matrix in such case. This can be done in two ways, mechanically or chemically. In mechanical separation, liquid metal is pressed from a porous skeleton under the acting pressure, or filtration of the liquid matrix is performed. In case of chemical methods of separation, it is necessary to use a material (flux) with a higher affinity from the reinforcing phase than matrix affinity. The material will infiltrate a porous sintered skeleton, by pushing away a matrix from it, which forms, together with it, a composite

material. A material with the lowest solubility in a matrix should be used as a fluxing agent. NaCl-KCl-Na_2SiF_6 used for removing oxide inclusions from a liquid alloy [11] was used for aluminium and its alloys.

A structure and properties of composite materials fabricated by the infiltration of porous sintered skeletons depend on multiple factors, including surface tension and viscosity of liquid metal and infiltration conditions, that is: pressure, addition rate, temperature of sintered skeleton, liquid metal and a moulding for infiltration [37]. The characteristics of a porous skeleton are important, including its porosity, material it is made of, shape and shape of pores, manufacturing method, and such aspect is discussed in detail in the next sub-chapter. Having in mind the multitude of the quantified factors, multi-criteria optimisation is required, and the entire technological process has to be examined thoroughly in order to achieve the required structure and properties of the composite material manufactured by the method of infiltration. For instance, if the temperature of a porous skeleton is lower than a melting point of the infiltrating alloy, it is being partly solidified during infiltration, which is leading to decreased skeleton permeability and makes it difficult to penetrate the porous skeleton by the infiltrating alloy [38, 39].

Depending on the triggering factor and on the required infiltrating pressure of liquid metal or polymeric material, infiltration methods are grouped into three main categories [40, 41]:

- assisted with external pressure;

  - pressure/squeeze infiltration, in which metal—being under the pressure of several dozen or several hundred of MPa—is flowing in and solidifies in skeleton pores under the influence of the gas situated over the metal level (gas infiltration) [6, 40, 42, 43], through a pressing piston of a mould placed in a press (squeeze casting) [13, 35, 38, 39, 44–46], by the activity of centrifugal forces or by applying an electromagnetic field inducing the Lorentz force;

  - low-pressure infiltration in which a pressure of several to several hundreds of Pa is exerted on the gas situated underneath the liquid metal level with a variant of pressureless infiltration where a skeleton is penetrated by liquid metal caused by hydrostatic pressure [27, 28, 43, 47];

- subpressure assisted;

  - vacuum infiltration where a sintered skeleton is placed in the conditions of gas pressure reduced versus atmospheric pressure, and a factor causing infiltration is a positive pressure of the liquid metal [48];

- pressureless infiltration;

  - infiltration assisted by capillary pressure or pressureless infiltration [28, 49, 50] under the activity of hydrostatic pressure.

Gas-pressure infiltration is a combination of vacuum infiltration—because a sintered porous skeleton, before being introduced into liquid metal, stays in the conditions of reduced pressure—and of pressure infiltration as pressure is exerted on the gas, inert gas by the rule, situated under the liquid metal level. This is undoubtedly most advantageous type of

http://dx.doi.org/10.5772/65377

infiltration in technological terms because, during the process, the porous skeleton being sintered as well as the alloy used for its penetration is in a protective atmosphere, that is, in vacuum during alloy melting and in an atmosphere of inert gas after introducing the skeleton into liquid metal. Moreover, vacuum-assisted infiltration allows to reduce a pressure exerted on liquid metal, as its actual pressure should be referred to the vacuum created earlier, not to atmospheric pressure, as in case of conventional pressure infiltration. This is very important due to the fact that alloy pressure cannot exceed a limit value determined by a ceramic skeleton's strength. A significant advantage of the gas-pressure method is low porosity of the final composite material. By applying external pressure, composite materials are achieved with the shape requiring no finishing; it also ensures thorough penetration of a porous skeleton by liquid metal, protecting the product against the occurrence of internal micro-shrinkages being structure discontinuities, thus impacting negatively the composite material produced and deteriorating its strength properties.

The wetting of solid bodies by liquid metal plays an important role in technological processes of composite material manufacturing with a liquid matrix [9, 51]. The following factors are predominant for the wettability of the solid body-liquid configuration [52]:

- the work of adhesion which should be performed to separate the unit surface of the contacting bodies and to create two new surfaces with the value which is a measure of molecular attraction between two different phases and
- the work of cohesion which should be performed to separate the unit surface of the same body and to create two new surfaces with the value which is a measure of molecular attraction between the particles of the same phase.

A characteristic used most often for the degree of wetting of ceramics or metals and their alloys by liquid metal is the wetting angle value θ in the range of 0° (complete wettability) to 180° (complete lack of wettability), which is an important indicator necessary to analyse the phenomena taking place at the solid body/liquid interface. Conventionally, liquid metal-ceramics systems or metals and their alloys in the solid state were grouped into wettable systems, where $\theta < 90°$, and non-wettable systems, where $\theta > 90°$. Different factors may influence the value of θ angle in case where a liquid alloy, for example, Al, is influencing a ceramic or metallic skeleton, for example, Al_2O_3. The factors are dependent upon the liquid infiltrating metal and include contact time and the presence of an oxide coating on a metal droplet. This factor—in case of aluminium—is the most important factor essential for wettability, and it is dependent, among others, on the atmosphere in which flushing takes place, being a barrier inhibiting the formation of sufficiently good contact of metal with the substrate and increasing the value of θ angle [6–9, 53]. Other factors discussed in another sub-chapter, such as surface roughness, substrate porosity, impurities, relate to a porous skeleton mainly. If the skeleton being wetted is well wetted by liquid metal, infiltration may occur by itself, without being forced externally. Low wettability of the skeleton being sintered or lack thereof is seen in the majority of liquid metal-ceramics interface or metal or metal alloy configurations, as a result of which liquid metal has to be introduced into pores under pressure. Alloy pressure must not, however, exceed the limit value dictated by a sintered skeleton's strength. For this

reason, wettability has to be very often improved before infiltration [6, 38, 42, 43], by decreasing the θ angle value by means of one of the most popular methods [47, 54], applicable to the properties of the liquid infiltrating component, by:

- increasing liquid metal or infiltrating alloy temperature,
- changing the chemical composition of the liquid metal or infiltrating alloy,
- applying a protective atmosphere preventing the oxidisation of metal droplets or infiltrating alloy.

Changes to the chemical composition of liquid metal or infiltrating alloy result from the introduction of alloy additions therein, such as Si, Ti, Mg, Ni, Cr, Ca, Li, which influence surface tension, adhesion work and wetting angle. They additionally cause chemical reactions, mainly in the area of a liquid metal-porous skeleton separation boundary, which may influence the formation of new phases [53]. For example, silicon, as an alloying element in aluminium alloys, is considerably improving the strength of connection; for this reason, an AlSi11/Al_2O_3 connection is better for each temperature as compared to an Al/Al_2O_3 connection, which confirms the suitability of using this alloy as an infiltrating material. Wettability in infiltration is also closely dependent on the properties of the sintered skeleton, which is presented in detail in the next chapter.

3. General characteristics of the structure and properties of porous skeletons manufactured by powder metallurgy methods for infiltration with metal alloys

The basis for composite materials produced by the method of infiltration is porous sintered skeletons produced by powder metallurgy methods, principally determining the structure and properties of the final product. A correctly produced sintered skeleton should be characterised by a structure of open, connected pores, enabling the easiest possible flow of liquid metal. The existence of closed pores or blind channels leads to the occurrence of areas not saturated by the infiltrating metal or alloy. The modern methods of producing porous sintered skeletons can be classified in the following way [25, 34, 35, 38, 44–46, 55, 56]:

- the sintering of ceramic or metallic powders with the addition of, or more rarely, without a binder, as the simplest and most common method in which uncompressed ceramic or metallic powders are sintered, permitting to produce skeletons with porosity of up to 50% or to sinter a mixture of powder grains with a binder added or not, initially pressed under small pressure or to represent a sponge structure;
- the fabrication of metallic or ceramic foam from an appropriately selected mixture, and the method consists of using the released gases as a result of a chemical reaction or decomposition reaction occurring at high temperature, for example:

http://dx.doi.org/10.5772/65377

$$CaCO_3 \rightarrow CaO + CO_2 \quad (1)$$

(Tab) enabling to produce skeletons with porosity of up to 90%;

- the freezing and sublimation of a solvent (usually distilled water) from ceramic or metallic powder suspensions, with a porous structure formed by the volume fraction of the solvent in a suspension, by the rate of freezing and sublimation of, for example, ice under a reduced pressure or gelling the foamed suspension [57];
- the sintering or reactive bonding of ceramic fibres or the sintering of ceramic and metallic powders with an agent added forming the structure of pores. This method is most flexible for all the methods presented here and allows to achieve infiltrated materials with a diverse structure and fraction of the material forming the foamed skeleton. The level of porosity and its character can be controlled by means of different pore-forming agents (PFA) undergoing decomposition at a high temperature, in the place of which voids are created. The most frequently used foaming substances are materials or substances with their thermal decomposition temperature much lower than sintering temperature, such as: polyethylene, wax, starch, celluloses, carbon fibres, sawdust [23, 46, 56]. The principle of this method is the same as the Powder Injection Moulding method and its variant, Ceramic Injection Moulding [58–61], however, a network of open channels has to be created in the sintered matrix after removing a binder and other foaming elements, for example, carbon fibres. This method allows to produce porous semi-products with a diverse structure and fraction of reinforcement and with open, interlinked pores supportive to the thorough penetration of liquid metal in the whole volume of material during infiltration. An agent forming the structure of pores (its fraction being dependent on the planned porosity obtained after removing it from a moulding) is added to ceramic powder (dry or in form of suspension) before pressing to undergo thermal decomposition at an elevated temperature (in a sintering operation).

A fabrication technology of porous sintered skeletons by sintering mineral nanotubes extracted from halloysite—with carbon fibres added as a foaming agent, later subjected to gas-pressure infiltration, was developed under own works [14, 16, 17, 19–22, 62, 63], and the technology is subject to patent protection [49, 50].

The own works [30, 31, 64–66] also highlight that—for this purpose—skeletons can be used of microporous metals and their alloys, also ceramic ones, with the pore size of several dozens to several hundreds of μm, made by the selecting sintering/laser melting SLS/SLM method, which are also covered by patent protection [67–70].

Permeability is the basic factor characterising the structure of open pores and porous channels of sintered skeletons. In permeability examinations, a series of measurements is carried out of the volumetric flow intensity and pressure drop of air, liquid or another factor during transition through a specimen [41]. The important factors determining this property include, in particular, diameter, grain size distribution, shape and volume fraction of the particles/reinforced fibres used [37].

Wettability in infiltration is also dependent on the properties of the sintered reinforcing skeleton. The wettability of porous sintered skeletons is dictated by the chemical composition of the reinforcing material, especially its surface roughness, although it can be assumed that if $R_a < 10$ nm, then the impact of roughness on the wetting angle is irrelevant, It is also dictated by skeleton porosity, because porosity above 5–8% of volume is reducing the wetting angle associated with the penetration of liquid metal inside the pores, and the volume of droplets, being fundamental for measuring the θ wetting angle, is reduced as a result of infiltration. Wettability can only be improved by changing technological conditions of infiltration, but especially by the surface treatment of internal pores of the sintered skeleton. A more and more widespread method of enhancing the wettability of skeletons sintered before infiltration is the deposition of thin layers, mainly metallic layers, onto an inner surface of pores. Such coatings increase a solid body's surface energy γ_c (reinforcing component) and also secure the internal surfaces of pores against damage during production, and inhibit undesired reactions with a liquid infiltrating component, which is important for skeletons made of materials susceptible to oxidisation, such as, graphite or carbon fibres [71, 72].

The special coatings fulfilling such a function are, notably, nickel alloy Ni-P layers, mainly owing to good anticorrosive properties of nickel and its resistance to high temperature, and also its simple deposition technology [10, 15, 23, 24, 48, 51]. Ni-P coatings can be used either by galvanic means, or with a commonly used electroless (chemical, catalytic) method [51, 73]. The electroless deposition method of nickel allows to metal plate practically each material after prior activation of its surface to create active centres needed to initiate the reduction of Ni^{2+} ions. Surface is activated most often using palladium chloride. The reaction is performed further autocatalytically, Ni atoms placed on active centres are becoming a catalyst. The type of the metals deposited is a constraint for this method—only metals from the copper, iron and platinum groups of the periodic table of elements. The more rarely used methods of coating deposition onto sintered skeletons before infiltration include physical and chemical vapour deposition (PVD) and (CVD) and TiO_2 deposition [9, 71–74].

The following chapters of the book present in detail, according to the results of the investigations, four examples of composite materials, infiltrated mainly with eutectic aluminium alloy EN AC-AlSi12, differing in reinforcing materials. Different skeletons with different chemical and phase composition were produced by different powder metallurgy methods.

The structures of porous skeletons Al_2O_3 were achieved in two ways: In the first method, by mixing Al_2O_3 powder with a pore-forming agent in the form of carbon fibres, the semi-products achieved are characterised by the varied porosity of 68–81% depending on the foaming agent applied. Infiltration was achieved by pressing uniaxially a porous ceramic skeleton and a liquid aluminium alloy into a closed die. In the other case, ceramic injection moulding (CIM) was used for Al_2O_3 ceramic powders by successive injection moulding, binder degradation and sintering using a binder which is a mixture of thermoplastic materials, for example, polypropylene (PP) or polyethylene (PE) with high-melting paraffin and stearic acid, by mixing ceramic powder with a binder using a screw extruding press after heating to the binder plasticisation temperature over the time allowing for the thorough homogenisation of the polymer-powder mixture, by moulding the produced powder-binder slip by injection into a

http://dx.doi.org/10.5772/65377

three-part mould and by the thermal or chemical removal of the binding component followed by sintering. Composite materials can be further fabricated as previously or by gas-pressure infiltration, as in other cases.

Another example concerns a unique technology of fabrication of porous skeletons of reinforcement by the dry mechanical milling of a mixture of halloysite nanotubes with carbon fibres, and of a slipping agent, in the form of powdered amide, micronised in a centrifugal ball mill. Next, a mixture of powders is moulded by uniaxial pressing in dies on a platen hydraulic press under the pressure of 50–100 MPa. The moulded parts are sintered in a high-temperature oven in the atmosphere of air with slow heating to degrade carbon fibres. Heating then takes place at 800°C, which is helping to degrade carbon fibres in the whole volume of specimens, with heating to a sintering temperature and sintering by cooling. Composite materials were produced by gas-pressure infiltration with an eutectic aluminium alloy EN AC-AlSi12.

A porous skeleton was made in the last of the analysed examples using pristine titanium with micropores dimensioned 100–200 μm by selective laser sintering with an additive method. A 3-D skeleton model was designed by the CAD method using unit cells with a specific structure and size and then by duplicating such a unit cell in order to design a skeleton with a repeatable structure in which the size of pores and wall thickness are fully controlled by the designer, characterised by fully open pores with the porosity of 50–80%. Next, a porous skeleton was produced from titanium powder by sintering it selectively, layer by layer, using an YFL fibre laser with an active material doped with Ytterbium and the maximum power of 200 W in the atmosphere of argon. SLS technique was employed to produce titanium skeletons, which were then used for infiltration with EN AC-AlSi12 alloy.

The following sub-chapters also describe, apart from the mentioned technology of producing porous sintered skeletons, the structure and properties of composite materials fabricated using such skeletons.

4. Structure and properties of porous Al_2O_3 skeletons sintered or manufactured by ceramic injection moulding from powder and of aluminium alloy matrix composite materials reinforced with them

An assumption is underlying the technological works presented in this sub-chapter stating that the application of infiltration allows to achieve multiple benefits while satisfying designers' specific requirements for the manufactured composite materials having a matrix of eutectic aluminium EN AC-AlSi12 alloy, and to a high extent, it is dependent on the construction and technology of a porous skeleton, ceramic Al_2O_3 in this case. It was taken into account that apart from shape selection and selection of the phase fraction, chemical wetting with nickel is influencing the formation of mechanical properties and abrasive wear resistance and corrosion of such materials fabricated by a newly developed method of pressure infiltration of porous sintered Al_2O_3 skeletons constituting a reinforcing phase.

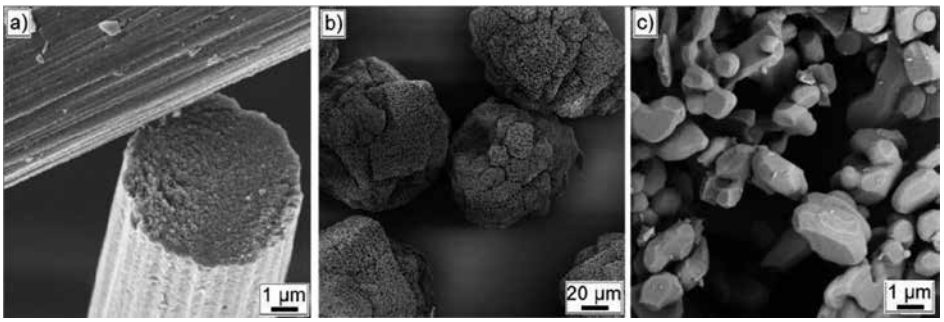

Figure 1. Structure of: (a) carbon fibres of Sigrafil C10 M250 UNS by SGL Carbon Group, (b) Al_2O_3 Alcoa CL 2500 powder as supplied, (c) Al_2O_3 Alcoa CL 2500 powder after milling.

Porous ceramic structures were fabricated by the method of sintering Al_2O_3 CL 2500 powder, by Alcoa Industrial Chemicals, with an agent added forming the structure of pores and channels in the form of carbon fibres, Sigrafil C10 M250 UNS, manufactured by SGL Carbon Group (**Figure 1**). The fabrication of porous ceramic skeletons included the preparation of powders, pressing and sintering. Al_2O_3 CL 2500 powder was milled wet in a ball mill for 5 min to disintegrate the particles concentrated in agglomerations. An agent, Dolapix CE 64, was added to the Al_2O_3 suspension preventing the formation of clusters of carbon fibres and eliminating their mutual electrostatic interactions. The added carbon fibres accounted for, respectively, 30, 40 and 50% by mass. 1% of polyvinyl alcohol, Moviol 18-8, soluble in water, was added to the mixture to facilitate subsequent pressing. The so-prepared powder was subjected to drying, consisting of freezing and sublimation of water under reduced pressure, and sifting through a screen with 0.25 mm eyes. The powders were wetted with polyvinyl alcohol for activation, packed to foil bags and left for 24 h. The powders were subjected to uniaxial pressing with a manual laboratory press, 'Nelke', equipped with a 30 mm diameter die on a platen hydraulic press, Fontune TP 400, supplied with a rectangular die sized 65 × 46 mm. The pressing pressure was, respectively, 25, 50 and 100 MPa, and its interaction time is 15 s. The moulded parts were sintered in a tubular furnace, Gero, in the atmosphere of air under a flow rate of 20 l/min. The thermal stability of carbon fibres, Sigrafil C10 M250 UNS, used as a pore-forming agent in the ceramic skeletons produced from Al_2O_3 Alcoa CL 2500 powder, was determined based on the results of a thermogravimetric (TGA) analysis. The fibres exhibit thermal stability to 390°C, and after exceeding it, their degradation takes place signified by a mass loss, and an increase in a derivative established for the mass loss. The carbon fibres are oxidised until being completely degraded by reaching the temperature of 692°C, determined with the temperature of overall technical degradation. If higher temperature is applied, up to which slow heating is seen, than the degradation temperature of carbon fibres, and when withstanding the material at such temperature, it is assured that the pore-forming agent is completely degraded and the subsequent fast increase in temperature from the rate of 300°C/h will not cause sudden reactions likely to destroy the ceramic skeleton. The tests results obtained allowed to optimise a sintering programme of ceramic porous skeletons. Sintering consists of slow heating to 800°C at a rate of 20°C/h, withstanding at that temperature

http://dx.doi.org/10.5772/65377

for 10 h for complete thermal degradation of carbon fibres, heating to 1500°C at a rate of 300°C/h, sintering for 2 h and cooling in an oven. It was not decided to apply a higher rate of heating to the thermal stability temperature of carbon fibres of 390°C due to the fact that mouldings contained are also an additive facilitating pressing, such as polyvinyl alcohol (1%) and distilled water triggering its activity (3%), the sudden evacuation of which during fast heating could cause skeleton cracks. The skeletons made by pressing a mixture of powders under the pressure of 25 and 50 MPa were characterised by insufficient strength and could crack in further treatment; hence, focus was placed solely on the sintered pressed skeletons under the pressure of 100 MPa.

Commercial semi-products produced were also used for further investigations to compare the properties of composites reinforced with skeletons made of Al_2O_3 particles with materials reinforced with skeletons consisting of fibres. Such semi-products were fabricated by sintering short, cut Al_2O_3 fibres with the diameter of 2–4 μm using a binder in form of silica. The skeletons have a 25% fraction of ceramic phase.

Economic considerations had the main influence on the use of Al_2O_3 powder, as it is about 50 times cheaper than the commonly used Al_2O_3 fibres. Carbon fibres were used as a PFA for technological benefits—their degradation product is CO_2 only, which ensures high process purity and the fact that the matrix material will assume an advantageous, in terms of mechanical properties, shape of degraded carbon fibres. Tar is exuded in case of, for example, wooden fibres or celluloses, which remains as an impurity in the material or settles on the oven walls. Two basic types of pores exist (**Figure 2**), the first of which, with larger size, are formed by degradation of carbon fibres; while the other, smaller ones occur around single ceramic particles and exist because they were not compacted deliberately. No clusters of pores formed after the degraded carbon fibres occur.

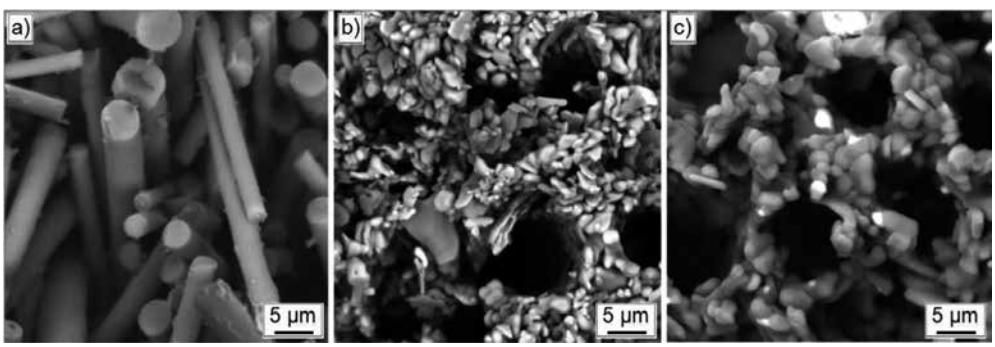

Figure 2. Structure of ceramic skeleton fracture: (a) commercial skeleton produced from Al_2O_3 fibres, (b) produced by sintering Al_2O_3 powder with 30% fraction of carbon fibres, (c) produced by sintering Al_2O_3 powder with 50% fraction of carbon fibres.

The pores and channels of ceramic skeletons were coated with nickel to improve the wettability of Al_2O_3 by a liquid aluminium alloy. Futuron technology by Atotech, used for fabrication of metallic coatings on polymer, was employed to activate the surface of ceramics. A layer of zinc

and palladium was formed on the surface after performing futuron activation. Noviganth Activator AK II solution was used to replace zinc on the surface of ceramics with metallic palladium. A layer of Ni-P alloy was deposited onto the so-prepared substrate by the electroless chemical method. The inner parts of the ceramic skeletons could be coated by using a specially constructed device for pumping solutions through them. A spiral coil, made of copper, with a stream of water flowing through it, was mounted on the apparatus to ensure the required temperature of solutions during the deposition of coatings. The skeletons, to prevent their damage during assembly in a device, were glued with a double-component 'UHU plus endfest 300' glue for aluminium rings. The nickel-coated semi-products were then cut out from rings along the glue-ceramics boundary.

The ceramic skeletons produced from Al_2O_3 Alcoa CL 2005 powder and the semi-products composed of Al_2O_3 fibres after a nickel-plating process, and those not nickel-plated, were subjected to infiltration with a liquid EN AC-AlSi12 alloy. The so-prepared ceramic skeletons were heated in an oven to the temperature of 800°C. A sintered ceramic skeleton and a liquid EN AC-AlSi12 alloy with the temperature of 800°C were put inside a mould, covered with graphite, with the temperature of 450°C. All this was covered with a die and placed on a platen hydraulic press, Fontune TP 400. The pressing rate was 17 mm/s, and the maximum press pressure was 100 MPa. The load was removed after 120 s, and the materials removed from the mould were cooled with a stream of compressed air.

Metallographic examinations of the produced composite materials reinforced with the created skeletons achieved by sintering Al_2O_3 particles allowed to confirm the uniform distribution of a reinforcing phase in the matrix (**Figure 3a**). The carbon fibres used as a pore-forming additive during uniaxial pressing of skeletons are oriented perpendicular to the direction of the load applied. In case of powder consolidation by uniaxial pressing, the foaming agent applied, whose one dimension differs largely from others (e.g. fibres, plates), may lead to the occurrence of anisotropy of the created material's properties.

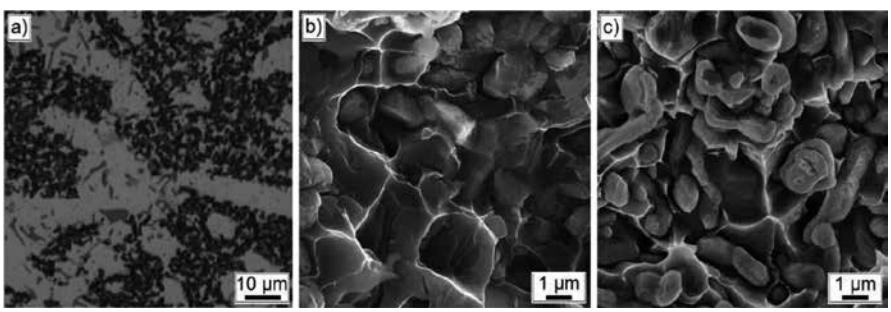

Figure 3. The structure of the created composite material with EN AC-AlSi12 matrix reinforced with porous Al_2O_3 skeleton with 30% fraction of pores: (a) microsection on the plane perpendicular to the pressing direction of porous sintered skeleton, (b) fracture, (c) fracture with pores covered with nickel.

The composite materials created are characterised by advantageous, uniform distribution of the ceramic phase in an aluminium matrix (**Figure 3a**). It was also found that infiltration

http://dx.doi.org/10.5772/65377

takes place completely, as signified by the lack of voids not saturated with metal—even the micropores created on the interface of Al_2O_3 particles are tightly filled under the pressure acting during infiltration. The fracture is of mixed nature; a plastically deformed matrix is around the reinforcing phase, whereas the fracture on the metal-ceramics interface is brittle (**Figure 3b, c**). The presence of numerous Al_2O_3 grains in the structure of such materials was confirmed diffractionally as a result of the examinations (**Figure 4**). A metal matrix, being an Al-based solid solution, and Si grains, making up an eutectic structure of EN AC-AlSi12 alloy, are situated between the regions of Al_2O_3. The presence of an Ni-based solid solution was also found in the composite materials with an Ni-P coating deposited onto Al_2O_3. Al_3Ni phase precipitates were identified in the materials with an Ni-P coating deposited onto Al_2O_3, in the area of the Al-based solid solution (**Figure 5**).

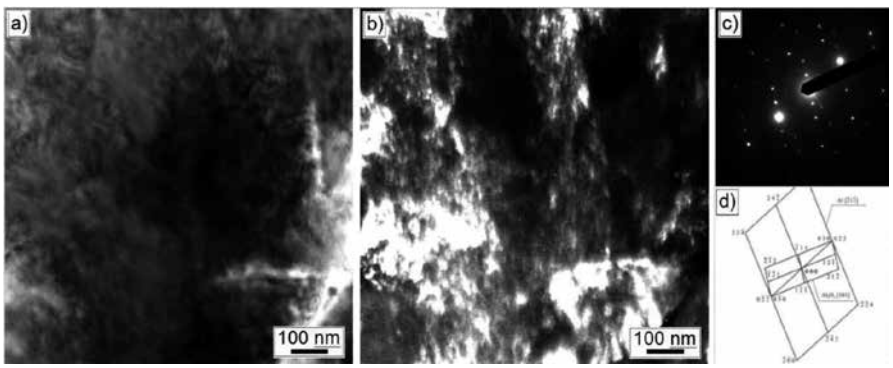

Figure 4. Structure of thin foil made from composite material with EN AC-AlSi12 matrix reinforced with porous Al_2O_3 skeleton with 50% fraction of pores in the porous skeleton: (a) image in bright field, (b) image in the dark field from reflex $1\bar{1}\bar{1}$ Al_2O_3, (c) diffraction pattern from the area as in **Figure a**, (d) diffraction pattern solution from **Figure c**.

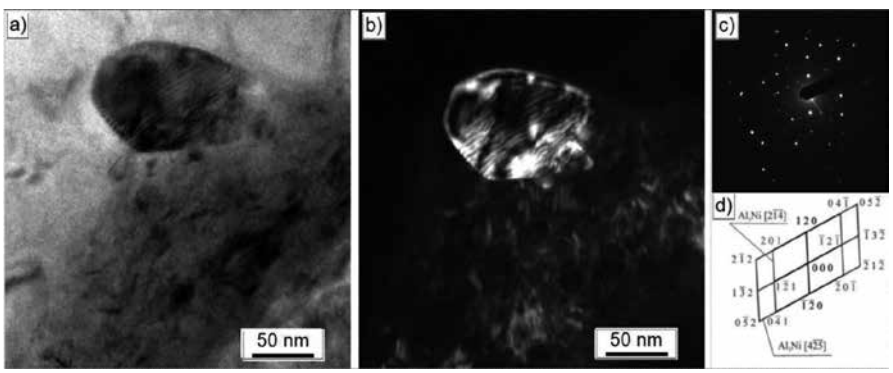

Figure 5. Structure of thin foil made from composite material with EN AC-AlSi12 matrix reinforced with porous Al_2O_3 skeleton coated with Ni with 50% fraction of pores in the porous skeleton: (a) image in bright field, (b) image in the dark field from reflex $\overline{1}20$ Al_3Ni, (c) diffraction pattern from the area as in **Figure a**, (d) diffraction pattern solution from **Figure c**.

The materials fabricated are characterised by hardness higher over two times (43–51 HRA depending on the fraction of a reinforcing phase) as compared to their matrix made up of EN AC-AlSi12 (19 HRA) alloy. The hardness of such materials is rising as the fraction of a ceramic phase is rising.

The reinforcement of an aluminium alloy with porous Al_2O_3 skeletons has a beneficial effect also on the mechanical properties of the materials created. EN AC-AlSi12 alloys have the tensile strength of up to 200 MPa, whereas the maximum tensile strength is seen for the composite materials reinforced with ceramic skeletons produced from particles with a ~25% fraction of Al_2O_3. Tensile strength is decreasing if a fraction of a ceramic phase is continued to be increased.

If hard reinforcing particles in a soft aluminium alloy matrix are added, this leads to enhanced abrasive wear resistance. The abrasive wear of composite materials is rising as the fraction of a ceramic phase is rising. It was confirmed in the tribological examinations carried out that composite materials feature much smaller wear than their matrix, and the lowest wear is exhibited by a material with the largest fraction of a ceramic phase; moreover, their wear is inversely proportional to the fraction of a ceramic phase regardless the load and the friction path.

The established method of manufacturing a composite material with a matrix made of EN AC-AlSi12 alloy reinforced with porous ceramic skeletons obtained from Al_2O_3 particles, in which they are subjected to pressure infiltration with a liquid aluminium alloy, ensures the required structure and mechanical properties, and also wear resistance much more advantageous as compared to the input aluminium alloy. Composite materials reinforced with the newly developed sintered ceramic skeletons represent, beyond doubts, a cheaper alternative for the extensively used materials reinforced with fibrous semi-products.

This sub-chapter also analysing a technology alternative with regard to the previously discussed method of the successive Al_2O_3 powder consolidations by uniaxial pressing and sintering consisting of ceramic injection moulding (CIM). As a sintered Al_2O_3 porous skeleton is obtained as a result of such activities, the same as previously, the concept of wettability inside the pores of this skeleton as well as the structure and final properties of the obtained composites infiltrated with an aluminium alloy was not analysed again in this case. It was assumed that —despite clear differences in the geometric characteristics of porous skeletons obtained with the two methods, the differences in the properties of composite materials obtained using porous skeletons by each of the methods are irrelevant. The results of examinations for the finally achieved composite materials, which are already presented in the previous sub-chapter for this type of a porous skeleton material, were not repeated, then.

The modern methods of producing porous materials which can be used, in particular, for pressure infiltration, include Powder Injection Moulding, with its variant, metal injection moulding (MIM), where a slip is basically formed with metal powders, or ceramic injection moulding (CIM), where ceramic powders are formed. This is a technique covering the fabrication of products from powders using injection moulding, binder degradation and sintering. This technique allows to obtain products with complicated shapes, with high-quality and strictly defined chemical composition. Injection moulding stands out from other technol-

http://dx.doi.org/10.5772/65377

ogies because it requires no finishing, for example, by machining or plastic working, and hence, no problems occur with production of waste such as riser heads, flashes, chips, and the material is used nearly in 100%.

The CIM technology uses ceramic powders, including aluminium oxide powder (Al_2O_3), titanium oxide powder (TiO_2), zirconium oxide powder (ZrO_2) or others. Due to unique properties of ceramic materials, that is, good mechanical properties, small own mass, high resistance and good chemical resistance, they are an interesting material with a broad range of applications in various industries.

A binder has to be used to mould elements by CIM. The main component of the binder is usually a thermoplastic polymeric material, for example, polypropylene (PP) or polyethylene (PE). The injection moulding of ceramic powders is taking place usually in four main steps by mixing ceramic powder with a binder, moulding the slip obtained by injection, by removing the binder and sintering.

Binder component	Density (g/cm^3)	Melting point (°C)	Degradation temperature (°C)
PP	0.89	163	250–450
HDPE	0.94	130	378–500
SA	0.94	73	200–350
PW	0.91	58.3	250–342

Table 1. Overview of example of multi-component binder.

In ceramic injection moulding, ceramic powder is mixed in the first place with a binder which can be a mixture of many binding agents. A technologically optimum binder should have low viscosity in moulding conditions, good wettability of the powder used, chemical or thermal degradability and should be cheap and environment friendly. A powder-to-binder ratio is linked to the powder particle shape, size, powder wettability by a binder and the properties of the binder itself as well as to the slip production conditions. The binder is usually a multi-component binding system (**Table 1**). Thermoplastic polymer materials, such as PP or PE, form a base which, when the binder is removed, is degraded as the last, and they maintain the element's shape at high temperatures. Another binding component reduces slip viscosity and is removed in the first steps of degradation, leaving the pores open, owing to which gas products formed during polymer decomposition can escape freely outside, without causing defects in the material, for example, distortion. For example, high-melting paraffin satisfies such conditions. Another element is a surfactant, for example, stearic acid, whose task is to improve ceramic powder wettability and to improve powder dispersion in a binder, and hence, a homogenous slip of powder with a binder can be produced. An additional task of stearic acid is to lower slip viscosity.

Powder is mixed with a binder using a screw extruding press, where ceramic powder with a binder is heated to the binder plasticisation temperature in time allowing for the thorough homogenisation of the polymer-powder slip. The time needed to homogenise the slip can be set by measuring the torque (**Figure 6**).

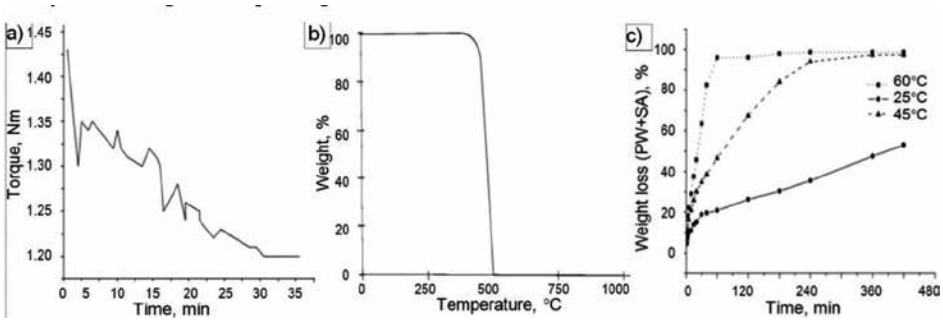

Figure 6. (a) Torque curve for powder-binder slip; (b) TGA result for polyethylene; heating rate of 7.5°C/min to temperature of 1000°C in air; (c) binder degradation by solving at different temperature, using heptane C_7H_{16}.

A difficulty in preparing the slip is to achieve the homogenous decomposition of powder in a binder. Slip is prepared in an extruder by disintegrating ceramic powder agglomerates to achieve single particles ensuring better dispersion in the slip. Single powder particles have a larger specific surface area, and hence, it is necessary to use a binder with larger fraction to improve ceramic powder wettability. **Table 2** presents the examples of composition of the powder-binder slip.

Feedstocks	Alumina		PP		HDPE		PW		SA	
%vol	%wt	%vol	%wt	%vol	%wt	%vol	%wt	%vol	%wt	%wt
A	50	81.20	22	8.11	0	0	22	8.34	6	2.35
B	50	88.37	0	0	22	9.32	22	9.07	6	2.56
C	50	84.55	11	4.32	11	4.53	22	8.68	6	2.45

Table 2. Examples of composition of powder-binder slip.

Depending on the thermal properties of the powder-binder slip, the extrusion temperature should be higher than the highest melting point of the binder component, but lower than the lowest degradation temperature of each of binder components. A thermogravimetric analysis (TGA) has to be undertaken in order to identify degradation temperature for particular binder components. TGA is a technique of examining the thermal decomposition of materials by examining changes in the mass of the given substance depending on changes in temperature or time.

Another stage in CIM technology is to mould the produced powder-binder slip by injection into a three-part mould, which allows to remove the element produced easier. Problems with extracting an item from a die are caused by low shrinkage of the material produced after injection into a die. Injection temperature and pressure, ensuring the complete filling of the die socket with the material, have to be taken into account to optimise injection. Injection temperature is selected according to the injection temperature selection principle. Insufficient injection temperature may cause problems with injecting the material into a die, whilst

http://dx.doi.org/10.5772/65377

excessive temperature may start degradation of the binder components, which leads releasing the gas created in degradation, thus to bubbles being formed in the item, which are an undesired effect.

Another stage in the process of manufacturing porous sintered skeletons for pressure infiltration is to remove thermally or chemically a binding component with the lowest degradation temperature to open the pores within the whole volume of the item, which enables to quickly remove thermally another binder component with a higher temperature of degradation. If thermal degradation is only used, it begins from the surface and goes inside the material as the temperature is rising. Channels are formed as pores are opening through which gas of the degraded binder with lower degradation temperature is escaping, and thus, pores are further opened allowing to release gas products of the binder component from the deeper and deeper parts of the material. The size of the pores formed due to degradation depends on the size of the powder grain. Thermal degradation is slow because the channels being formed make the path—covered by the gas products escaping—longer than the item thickness. If higher temperature and a higher hearing rate are applied, this may lead to specimen deformations or damages—distortion. **Table 3** shows the examples of binder degradation process conditions.

Thermal debinding (steps)	Heating rate (°C/min)	Debinding temperature (°C)	Debinding time (min)
1	3	200	60
2	1	250	30
3	1	300	30
4	1	350	60
5	1	400	60
6	1	450	60
7	1	550	30

Table 3. Binder degradation steps by thermal method.

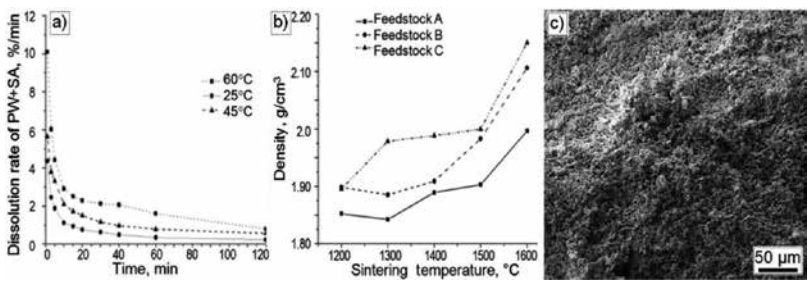

Figure 7. (a) Influence of degradation time and temperature on degradation rate of paraffin and stearic acid; (b) influence of sintering temperature on density of the item produced; (c) structure of porous ceramic skeleton of Al_2O_3 sintered at 1400°C for 1 h (SEM).

Thermal degradation is an alternative to chemical degradation, so-called solvent degradation. Its key benefit is the rate of solving, and a disadvantage is that aggressive and environment unfriendly reagents are used. The solvent method causes smaller element degradations and damages compared to thermal degradation but requires two operations connected with material transition between the initial degradation and extraction of the polymer base by thermal degradation. Chemical degradation combined with thermal degradation is becoming more and more popular. Binder degradation with a solvent is used most often in the first step of degradation of a binder component with the lowest temperature of degradation (**Figure 7**).

Sintering is the last step of a technological process in the production of ceramic porous skeletons decisive for density, porosity and mechanical properties of the ready product. A suitable degradation temperature of particular binder components, and also an oven heating rate, has to be selected based on the data acquired with a TGA analysis. An important factor during sintering is also to select the appropriate atmosphere of filling an oven chamber as it has to enable/assist the degradation process of binder components. All the factors mentioned have an effect on the quality of a ready element.

A higher sintering temperature causes better compaction and smaller porosity by diffusion and also the formation of necks between the sintered powder particles. The effect is reverse in a lower temperature, and skeleton density is decreasing, whilst the porosity is growing.

5. The structure and properties of sintered porous skeletons from mullite obtained by sintering a mixture of halloysite nanotubes with agents forming an open structure of pores and of aluminium alloy matrix composite materials reinforced with it

Considerable progress witnessed for years in the development of metallic composite materials, closely linked to the fast growth of the motor industry, is constantly necessitating a search for new, better constructional solutions, which would be lightweight, and also reliable and highly strong, as well as for new composite materials suitable for this purpose. Although pressure-infiltrated composite materials reinforced with different fibres and particles are highly popular, research works have been conducted all the time into selection of new materials for porous skeletons for the reinforcement of metal matrix composite materials. Research into the development of technologies of such materials with sintered porous ones based on halloysite nanotubes, whose potential application possibilities are still being investigated, is inscribing into the former research. Such works are becoming even more important in Poland because this is the place where, apart from the USA and New Zealand, one of the three global deposits of halloysite, that is, nitrided aluminium silicide $Al_2Si_2O_5(OH)_4 \cdot H_2O$, that is, a clay mineral of volcanic origin from the group of kaolin fossils, is located. The investigations carried out indicate that nanotubes obtained from halloysite may be an alternative reinforcement of composite materials, for instance with respect to much more costly carbon nanotubes. A reason supporting the use of halloysite nanotubes as a reinforcement of unique aluminium alloy matrix composites is that composite materials can be achieved with a structure at a nanoscale,

http://dx.doi.org/10.5772/65377

having exceptional thermal properties which, unlike composite materials reinforced with, for example, ceramic particles, are characterised by high thermal conductivity whilst maintaining low linear expansion. Thermal stability enables to use this type of material for car engine components such as engine blocks, pistons, cylinders, brake discs, with relatively better heat exchange intensity, by improving heat conductivity and the results improved machine performance. Nanostructured composites reinforced with halloysite nanotubes can, therefore, be competitive to hypereutectic silumins and Al/SiC, Al/Al_2O_3 composites used for this aim.

Halloysite is built of plates with a flat surface, partially rolled or in form of tubes, formed from rolled plates, which is related to mismatch between a tetrahedral layer and a octahedral layer making up the packet [36]. Two types of this mineral are distinguished [36]:

- hydrated halloysite-1 nm, having water in the inter-packet space, featuring low durability dependent on humidity and undergoing transformation into metahalloysite already at room temperature;
- dehydrated halloysite 0.7 nm, called metahalloysite.

If halloysite is heated at temperature above 980°C, structural transformation of halloysite into mullite is seen according to the simplified formula [75]:

$$Al_2O_3 \cdot 2SiO_2 \cdot 4H_2O \xrightarrow{\approx 600^\circ C} Al_2O_3 \cdot 2SiO_2 \xrightarrow{\approx 980^\circ C} 3Al_2O_3 \cdot 2SiO_2 + SiO_2 + H_2O$$

$$halloysite \rightarrow metahalloysite \rightarrow spinel\ Si-Al + mullite + amorphous\ SiO_2 \rightarrow mullite + cristobalite$$

$$2SiO_2 \cdot Al_2O_3 \cdot 2H_2O \xrightarrow{\approx 400-500^\circ C} 2SiO_2 \cdot Al_2O_3 + 2H_2O$$

$$halloysite \rightarrow metahalloysite$$

$$2SiO_2 \cdot Al_2O_3 \xrightarrow{\approx 980^\circ C} SiAl_2O_4 + SiO_2 \text{ or}$$

$$metahalloysite \rightarrow spinel + amorphous\ silica$$

$$2SiO_2 \cdot Al_2O_3 \xrightarrow{\approx 980^\circ C} Al_2O_3 + 2SiO_2$$

$$metahalloysite \rightarrow aluminium\ oxide-\gamma + amorphous\ silica$$

$$SiAl_2O_4 + SiO_2 \xrightarrow{\approx 1100^\circ C} \frac{1}{3}\left(3Al_2O_3 \cdot SiO_2\right) + \frac{4}{3}SiO_2\ \text{lub} \qquad (2)$$

$$spinel + amorphous\ silica \rightarrow mullite + amorphous\ silica$$

$$Al_2O_3 + 2SiO_2 \xrightarrow{>1100^\circ C} \frac{1}{3}\left(3Al_2O_3 \cdot SiO_2\right) + \frac{4}{3}SiO_2$$

$$aluminium\ oxide-\gamma + amorphous\ silica \rightarrow mullite + amorphous\ silica$$

$$3Al_2O_3 \cdot 2SiO_2 + 4SiO_2 \xrightarrow{>1200^\circ C} 3Al_2O_3 \cdot SiO_2 + 4SiO_2$$

$$mullite + amorphous\ silica \rightarrow mullite + cristobalite$$

$$3Al_2O_3 \cdot 2SiO_2 + 4SiO_2 \xrightarrow{>1500^\circ C} 3Al_2O_3 \cdot SiO_2 + 4SiO_2$$

$$mullite + cristobalite \rightarrow mullite + amorphous\ silica$$

Mullite is aluminium silicate $3Al_2O_3$ $2SiO_2$ obtained after sintering minerals containing aluminium oxide and silicon oxide in right proportions, for example, sillimanite, cyanite,

andalusite and also mixtures of kaolin and aluminium oxide. It has been used successfully as an ingredient of refractory and electro-insulating materials and as a ceramic phase reinforcing metallic composite materials, including nanostructured composite materials with an aluminium alloy matrix [12, 76]. A possibility to use mullite for this task was a reason why attempts were undertaken to apply the nanotubes obtained from halloysite, in which transformation will take place—during thermal processes—into mullite. The mullite will be acting as reinforcement in the form of a sintered porous skeleton of aluminium alloy matrix composite materials fabricated by gas-pressure infiltration methods.

Halloysite nanotubes (**Figure 8a**), as an indispensable material in this process, are multiwalled, cylindrical, hollow objects with the diameter less than 100 nm and length of about 500 nm to over 1.2 μm [11, 24]. They are sourced from fossil halloysite and have been widely employed in, for example, ceramic [77, 78], construction, fertiliser and cosmetic branch, for environment protection as universal mineral sorbents, coagula for water treatment, waste stabilisers and in biomedicine as medicine carriers [79, 80]. Halloysite nanotubes have been applied as reinforcing nanocomposites to a small degree only, and mainly for polymer matrix composites in which, when added in several to more than ten per cents, rigidity, fireproofness, strength, hardness, thermal stability, and in some cases also electrical conductivity, are improved [80, 81].

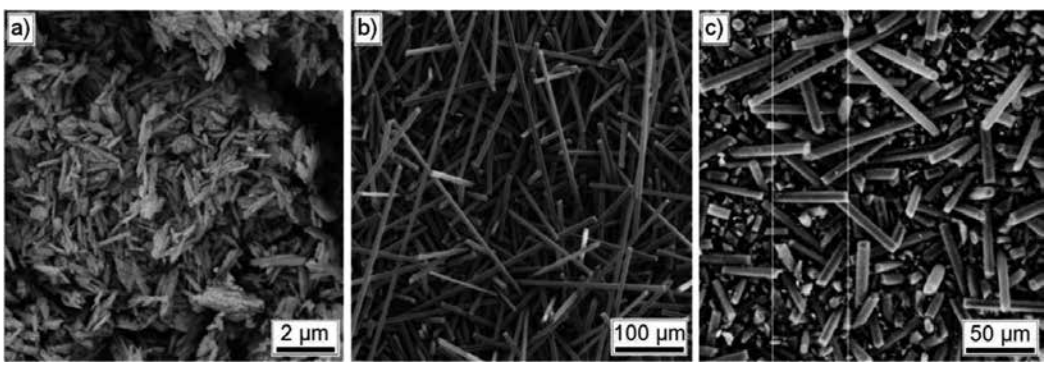

Figure 8. Morphology of base powders of: (a) halloysite nanotubes, (b) carbon fibres, (c) mixture of halloysite nanotubes made of carbon fibres with mass fraction of 50% after 5 min of mechanical milling in ball mill.

It was found as a result of own investigations that—through the pressure infiltration with a liquid aluminium alloy of porous ceramic skeletons fabricated by sintering halloysite nanotubes together with an agent forming the open structure of pores; by selecting appropriately the conditions of powder preparation, compression, sintering and pressure infiltration and a fraction of halloysite nanotubes, as a result of structural transformations taking place in sintering and pressure infiltration—it is feasible to achieve aluminium alloy matrix composite materials, reinforced with a sintered mullite porous skeleton, with enhanced mechanical properties and wear resistance, much higher than the functional properties of the matrix material. An outcome of such own works is that properties were identified and the structure was developed and created of a new generation of composite materials infiltrated by the gas-pressure method, reinforced with porous skeletons produced using the mechanical synthesis,

http://dx.doi.org/10.5772/65377

consolidation and sintering of a mixture of powders consisting of halloysite nanotubes and carbon fibres as a foaming agent, and also influence was identified by the reinforcing phase fraction on the structure and mechanical and functional properties of the so-developed engineering materials.

Porous ceramic skeletons, being the final reinforcement of composite materials with an EN AC-AlSi12 alloy matrix, were fabricated by the mechanical milling, compression and sintering of halloysite nanotubes supplied by NaturalNano (USA). Powders were prepared in order to fabricate porous ceramic skeletons, by the mechanical dry milling of a mixture of halloysite powder with an agent forming the structure and size of open and interlinked pores. Sigrafil CIO M250 UNS carbon fibres by SGL Carbon Group (Germany) were used for this purpose. The morphology of the carbon fibres used is presented in **Figure 8b**. Five sets of materials were prepared containing, respectively, a 30, 40, 50, 60 and 70% volume fraction of halloysite nanotubes (**Figure 9**). A slipping agent in the form of powdered micronised amide wax, MA7050, with a volume fraction of 1% was additionally used to change the rheological properties of the powder mixture. The task of the slipping agent is to decrease adhesion between the powder material, and a mill and grinding mediums, and also to eliminate friction between the die walls and powder particles, which is impeding pressing and production of cohesive mouldings. A centrifugal ball mill, Pulverisette 5, by Fritsch company, was used to produce a crushed and homogenous powder mixture. Milling time was selected by analysing the bulk density of the prepared powder mixtures and their morphology (**Figure 9**). As bulk density, related to milling time, was decreasing, a mixture of powders after 15 min of milling was selected for further investigations. The prepared powder mixtures were formed by cold uniaxial pressing in closed (circular and rectangular) dies on a platen hydraulic press, LabEcon 600 Fontijne Grotnes. The diameter of a die socket with round section was 30 mm, and the dimension of the rectangular die socket was 12 × 35 mm. The specimens were pressed under the pressure of 25–150 MPa with steps for every 25 MPa. The pressing time was 15 s. The influence of the applied pressing pressure was judged by the appearance of mouldings (no cracks, losses, delamination, etc.), and their strength allows to lay them on a ceramic base for subsequent sintering in a heating device. Low pressing pressure of only 25 MPa does not ensure suitable powder compression, which will have influence on cracking and chipping of the specimens' edges when removing them from the die. On the other hand, the mouldings pressed under a high pressure of 125 and 150 MPa were distinct for delamination, which was particularly visible near the front surface of the moulding, to which a working stamp was acting. It was therefore decided that the pressing pressure of 50–100 MPa will be applied. The materials pressed in such conditions are free of defects and possess suitable strength, and also porosity after sintering, as it is essential to maintain high density of open pores in the whole volume of the sinter for its infiltration. The pressing pressure was further selected by examining the shape of the pressed and sintered mouldings due to high distortion resulting from inhomogeneous shrinkage in sintering. It was initially assumed that a low pressing pressure will ensure the necessary strength of mouldings and the high porosity of the sintered specimens. Particles are more compressed due to a higher pressure applied, as a result of which the effect of shrinkage is smaller. Sinter infiltration takes place despite smaller pores; hence, it seems that such a solution is less favourable.

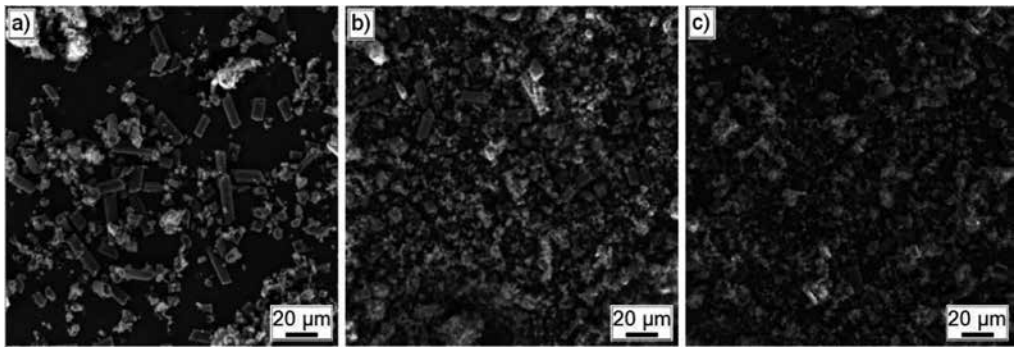

Figure 9. Morphology of mixture of halloysite nanotubes with 50% volume fraction of carbon fibres, after: (a) 30, (b) 120 and (c) 300 min of mechanical milling in ball mill.

The porous ceramic skeletons for pressure infiltration were sintered in a high-temperature oven, PRS 75W, in the atmosphere of air with a flow rate of 5 l/h, as a result of slow heating to the carbon fibre degradation temperature, heating at 800°C, selected based on a thermogravimetric curve analysis (**Figure 10a**), to degrade carbon fibres within the whole volume of the specimens, reheating to the appropriate sintering temperature, sintering and then cooling. Sintering temperature was chosen based on the results of examinations in a high-temperature microscope and derivatograph. By assuming that the melting point of the mullite formed from the applied halloysite is about 1830°C, this material should be sintered within the range of 915–1465°C, and as ion bonds and/or covalent bonds exist, it may reach even 1620°C. As mullite is not characterised by pure covalent bonds, it was thus assumed that the maximum sintering temperature will be 1500°C. Theoretically, the investigated material should be sintered at relatively low temperature at which the diffusion of atoms occurs on the surface of particles, which is the main transport mechanism of the matter. The surface of the necks connecting ceramic particles is then expanding, but the whole particles are not brought closer, and thus, an undesired effect of shrinkage does not take place (**Figure 10b**). A small rate of diffusion requires long heating times (of several dozen of hours), which is economically ungrounded. If a higher temperature of sintering is applied, diffusion certainly occurs in the examined sintered material along the grain boundaries, and volumetric diffusion occurs, which is responsible for sinter shrinkage caused by the particle centres coming closer. Halloysite nanotubes were pressed under the pressure of 100 MPa for 15 s and then heated in an oven at 100, 300, 500, 800, 1100, 1300 and 1500°C for 1 h. Shrinkage in the range of 100–1500°C could be calculated as moulding diameter dimensions changed, and the shrinkage was 22.2%. 0.07 g of halloysite nanotubes were subjected to thermogravimetric tests in the range of 20–1500°C in the atmosphere of air. It was discovered when analysing a thermogravimetric curve and its derivative that an endothermic reaction takes place while heating the halloysite nanotubes within the temperature range of 400–600°C (maximum at 516°C), and the reaction is associated with dehydroxylation and decomposition of halloysite to metahalloysite (loss mass of approx. 17%), and an endothermic reaction takes place at approx. 980°C, associated with the halloysite structure reconstruction and the creation of a spinel Si-Al phase as a transient form [36, 57, 82]. Linear changes in the function of temperature were examined with a high-temperature microscope by Leitz by the

http://dx.doi.org/10.5772/65377

microscope-photographic method within the temperature range of up to 1600°C in the atmosphere of air with a heating rate of 5 and 8°C/min In order to establish sintering temperature, pristine halloysite nanotubes and their mixtures with carbon fibres were formed manually under the pressure of 3 and 100 MPa. A series of photos presenting the behaviour of the material during heating was obtained while continuously observing and recording photographically changes in its shape and dimensions (shrinkage, expansion or local swelling) in the function of temperature, as an approximate simulation of the phenomena taking place in the examined material when producing porous ceramic skeletons. The recorded material changes were analysed with image conversion and analysis algorithms. Mouldings of mineral halloysite nanotubes pressed manually without additives (a binder in the form of water present in the structure) were examined in a high-temperature microscope in an oxidising atmosphere. The mouldings were heated at a rate of 8 and 5°C/min at 20–1600°C with recording every 100°C (**Figure 10c**). The slower heating of the material containing water in its structure does not cause abrupt volumetric changes of the moulding, and it supports its intensive shrinkage, though.

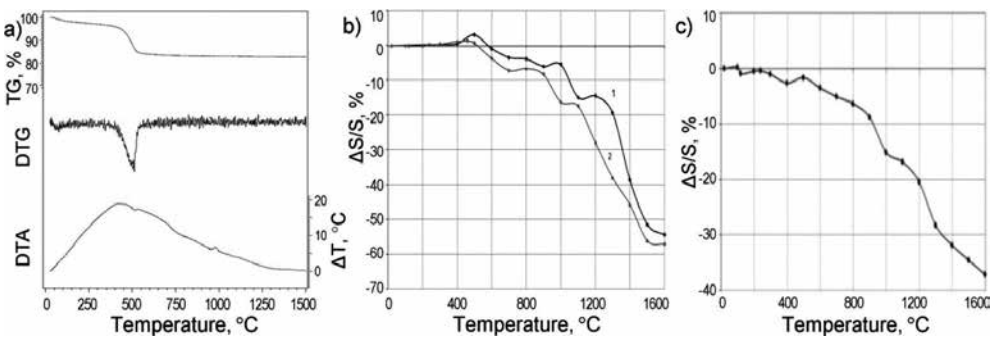

Figure 10. (a) Thermogravimetric curve (TG), differential thermogravimetry curve DTG and differential thermal analysis curve (DTA) of halloysite nanotubes (TG = 100 mg, m_o = 70 mg, 7.5°C/min, rel. 96), (b) comparison of changes in the dimensions of moulding of halloysite nanotubes ΔS/S, pressed under the pressure of 3 MPa without additives; heating rate of 1–8°C/min and 2–5°C/min, (c) changes in the dimensions ΔS/S of moulding containing halloysite nanotubes (70%) and carbon fibres (30%) pressed under the pressure of 100 MPa with Microwax slipping agent added; heating rate of 5°C/min.

No occurrence of characteristic temperature (softening, melting nor flow) of halloysite nanotubes was found for mineral halloysite due to their high melting point of approx. 1800°C. A change in the dimensions of mouldings for the temperature range of 1000–1600°C (**Figure 10b**, **c**) was found, however, due to large impact of the water contained in the structure of halloysite nanotubes. The material shows nearly linear thermal expansion to the temperature of 500°C. The first phase of shrinkage occurs above that temperature associated with halloysite dehydroxylation and the formation of the metahalloysite phase [82]. Another shrinkage occurs at 900°C, and dimensional stabilisation occurs within the range of 1000–1100°C, referred to as stability plateau, connected with crystallisation of the intermediate phase—spinel Si-Al. When halloysite is further heated, this causes the transformation of spinel $2Al_2O_3$ $3SiO_2$ into mullite $3Al_2O_3$ $2SiO_2$ with formless glazed silica SiO_2 formed at the same time, which activates sintering (**Figure 11**). A structure comprised of mullite crystals deposited in the amorphous

silica or cristobalite is produced above 1100°C (**Figures 12**, **13**). The mouldings of mixtures of halloysite nanotubes with a 50 and 30% (**Figure 10c**) fraction of carbon fibres pressed under the pressure of 100 MPa, that is, in conditions simulating the sintering of mouldings, were also examined in a high-temperature microscope in an oxidising atmosphere.

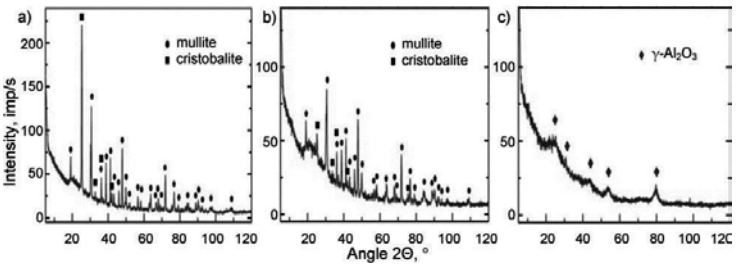

Figure 11. The results of X-ray phase analysis of porous ceramic skeletons with volume fraction of 70% of HNT, pressed under the pressure of 100 MPa and sintered in temperature of (a) 1500°C, (b) 1300°C, (c) 1100°C.

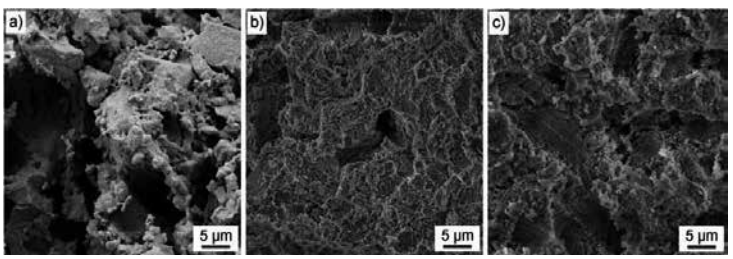

Figure 12. The morphology of porous ceramic skeletons with volume fraction of 70% of HNT, pressed under the pressure of 100 MPa and sintered in temperature of (a) 1500°C, (b) 1300°C, (c) 1100°C.

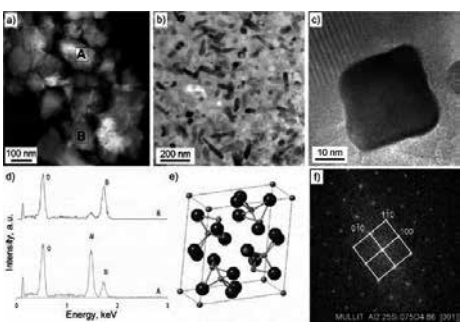

Figure 13. The structure of porous skeletons sintered at the temperature of 1500°C—mullite grains: (a) HAADF image, (b) TEM-BF image of porous skeleton, (c) high-resolution image STEM-HAADF of mullite grain in orientation [001], (d) comparison of chemical composition analysis results in two areas shown in Figure a (B—atomic percentage of atoms of: Al—28%, Si—13%, O—69%), (e) model of elementary cell of $Al_{2.25}Si_{0.75}O_{4.87}$ phase, (f) FFT piece of image shown in Figure c.

http://dx.doi.org/10.5772/65377

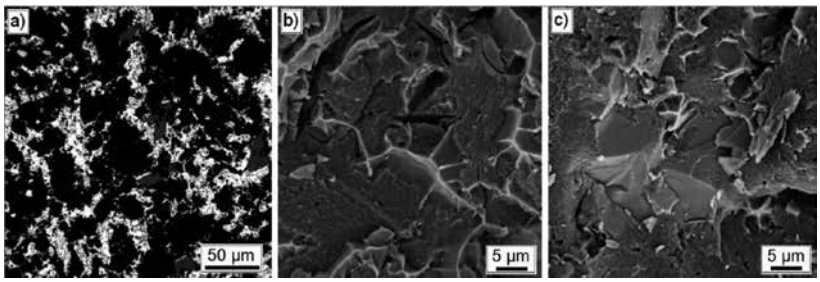

Figure 14. (a) Structure of composite materials reinforced with porous ceramic skeletons with the mass fraction of 70% HNT, pressed under the pressure of 100 MPa and sintered at the temperature of 1500°C; (b, c) structure of fractures of composite materials as in **Figure a**, with mass fraction of HNT of: (b) 50%, (c) 70%.

The presence of a solid solution of aluminium α-Al and silicon eutectics α+β, being a matrix of composite materials and a ceramic phase—mullite $3Al_2O_3$ $2SiO_2$, whose reflexes come from reinforcement in form of sintered skeletons, was found as a result of an X-ray structural analysis in the composite materials reinforced with skeletons made by the sintering of halloysite nanotubes. The structure of such composite materials is characterised by uniform distribution in the reinforcement matrix produced by sintering the halloysite nanotubes, and by the nearly full filling of pores with a liquid aluminium alloy (**Figure 14**), whereas manufacturing conditions of porous reinforcing skeletons do not exert significant impact on the structure. Significant structural differences are caused by variations in the sintering temperature of such skeletons. Numerous precipitates of coarse-grained silicon occur as a result of sintering at 1300 and 1500°C, having a tendency to crystallise on the surface of the ceramic phase, whose share increases as the fraction of reinforcement increases. The crystals of mullite $3Al_2O_3$ $2SiO_2$ (**Figure 13**) are present inside the composite material grains, along with irregularly shaped pores and those having the diameter of approx. 100 nm, whose morphology may indicate empty areas after cristobalite grains SiO_2, which were subjected to decomposition in the infiltration process. This may be evidenced by the presence of occasional precipitates with a heightened concentration of silicon and oxygen, which indicates the presence of cristobalite SiO_2. The presence of 3 main components of the composite material obtained, that is, silicon, aluminium solution and mullite $3Al_2O_3$ $2SiO_2$, was also confirmed with the EDS method in a scanning microscope (**Figure 15**). About 200 nm thick transition zone exists between aluminium solid and mullite $3Al_2O_3$ $2SiO_2$ with relatively large grains, larger than mullite grains in the external—from the side of mullite—part of the transition zone, with the presence of an aluminium solution and oxygen and a lower concentration of silicon in relation to mullite (**Figures 15**, **16**). As the SiO_2 phase is thermodynamically unstable in the presence of aluminium, it is reacting with it by creating aluminium oxide [83]. Coarse-grained precipitates of pure silicon are created as a result of aluminium acting with cristobalite SiO_2 during infiltration and diffusion, and the structure of an aluminium solution of the matrix corresponds to the structure of a hypereutectic alloy. The newly created precipitates of silicon are crystallising from an Al-Si alloy on the matrix-reinforcement boundary, and due to their higher strength in relation to matrix strength, their nucleation contributes to the reinforcement of the separation boundary. Following the infiltration and decomposition of cristobalite SiO_2,

mullite $3Al_2O_3$ $2SiO_2$ constitutes basically the only component of a ceramic skeleton which is not subject to changes. The expected interaction between liquid aluminium and mullite $3Al_2O_3$ $2SiO_2$ does not take place, therefore. This may result from infiltration conditions, that is, the flushing temperature of a liquid alloy, which is not higher than 800°C, and from a rate of infiltration and evacuation of heat directly after it, otherwise as it takes place during wettability tests or pressureless infiltration.

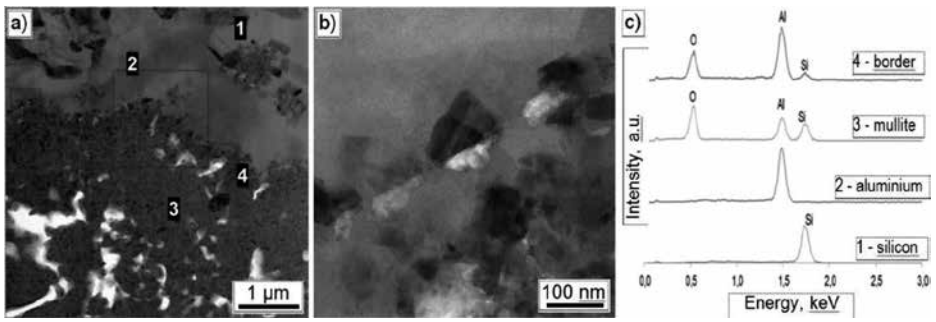

Figure 15. (a, b) Image of structure of composite material reinforced with porous skeletons, magnified pieces with transition zone between ceramics and metal, (c) results of chemical composition analysis in four areas marked in **Figure a**.

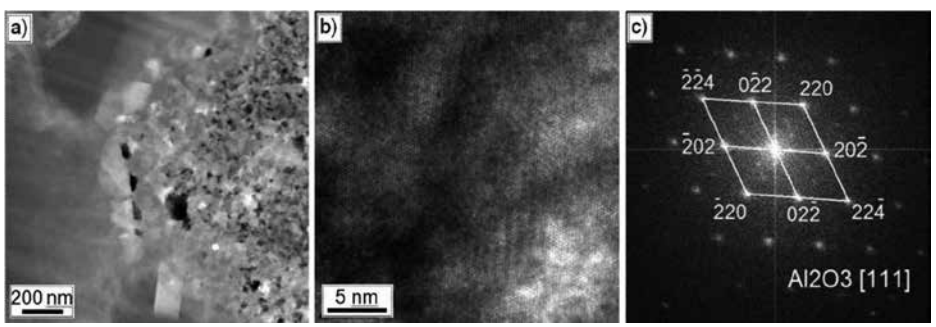

Figure 16. Transition zone between metal and ceramics: (a) STEM-BF image of area of transition zone, (b) HRTEM image, (c) Fourier transform with diffraction image solution.

As the fraction of reinforcement is increasing in the form of a porous skeleton of mullite $3Al_2O_3$ $2SiO_2$ obtained as a result of sintering the halloysite nanotubes, the hardness of the composite materials produced as a result of pressure infiltration is rising. The highest hardness of 114.6 HRF is seen for materials obtained by infiltrating sintered skeletons at 1500°C with a 70% fraction of ceramic phase, whilst the lowest, of 64.9 HRF, for materials reinforced with skeletons sintered at 1100°C. A twice higher value of hardness results from the difference in the structure of ceramic skeletons, depending on their sintering temperature. The bending strength of the analysed composite materials is increased considerably as compared to the strength of an EN AC-AlSi12 alloy forming the matrix, which is 224–276 MPa in case of reinforcing with skeletons sintered at the temperature of 1300°C with a 60% fraction of HNT,

http://dx.doi.org/10.5772/65377

and to 307 MPa after sintering porous skeletons at 1500°C with a 50% fraction of HNT. When the fraction of reinforcement is increased, the bending strength of the discussed composite materials is decreased.

6. The structure and properties of sintered titanium porous skeletons obtained by selective laser sintering and aluminium alloy matrix composite materials reinforced with them

This sub-chapter presents the possibility of manufacturing sintered porous skeletons by an additive manufacturing technology (**Figure 17**). Procedural benchmarking techniques with a dendrological matrix of technology value were used for selection of a porous material manufacturing technology [84–86]. The potential of additive technologies is much higher than of other technologies, and it is represented by opportunities ensured by 3-D design, which allows to almost fully control the materials produced in respect of their structure, dimensions and the shape of pores, and the repeatability of geometrical characteristics. The additive manufacturing technology produces no wastes and is comprised of two main stages of design and manufacture, which is also greatly improving the potential of such technologies in the aspect of porous material fabrication.

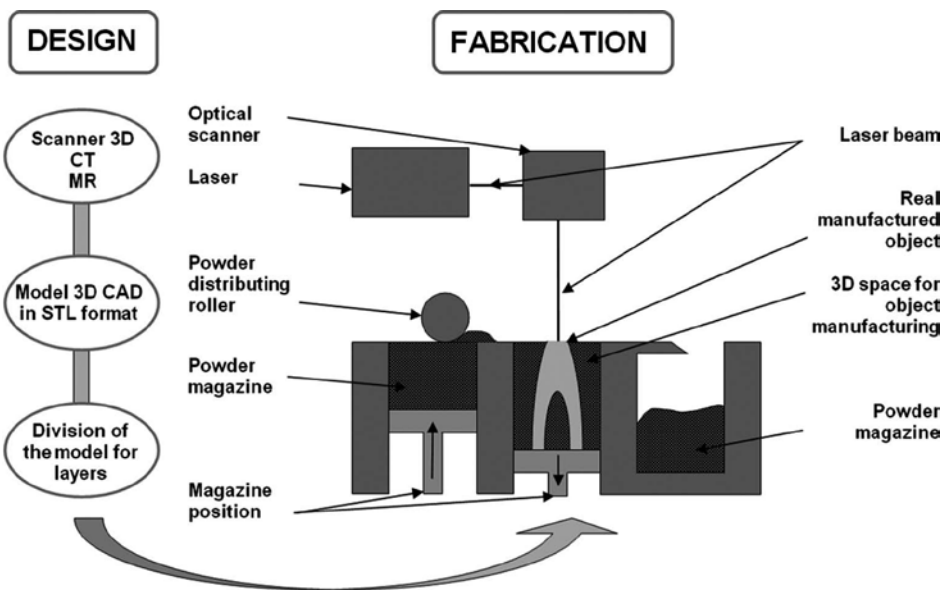

Figure 17. Selective laser sintering technology process diagram.

The attractiveness of the particular additive manufacturing technologies does not differ much. A comparative analysis result indicates SLS—selective laser sintering, and SLM—selective laser melting technologies, as having the best set of characteristics for the fabrication of metallic

porous materials. The attractiveness and potential coordinates are ranking these technologies in the wide-stretching oak quarter with the highest potential and attractiveness, thus with the best development outlooks. All the results presented below relate to pristine titanium. Titanium was chosen for its attractive properties, including anticorrosive resistance, biocompatibility, good relationship between strength and mass and due to its broad range of applications in various industries starting with the space, aviation and car industry through medicine to dentistry. For this reason, porous titanium skeletons with an adequate group of properties can find their application in different industries. The real motivations for those investigations were originally connected with the creation of biological and engineering composite materials and implant-scaffold materials planned for application in regenerative medicine and dental implantology [65–70, 74, 87–90]. The results of such investigations were next extended to develop a new group of composite materials with a metal alloy matrix, mainly aluminium, reinforced with porous skeletons made of titanium and its alloys, for example, Ti6Al4V and Ti6Al7Nb sintered by SLS/SLM, although powders of other metals such as stainless steel, cobalt and chromium alloys and others can also be used to produce reinforcement. The AM 125 system by RENISHAW with AutoFAB software was used for manufacturing porous skeletons by SLS/SLM. The YFL fibre laser with an active material doped with Ytterbium and the maximum power of 200 W was used in the AM 125 device. The AM 125 system is equipped with a vacuum chamber enabling to apply a unique device working chamber emptying method in such a manner that first all gases are pumped off from the working chamber, and then inert gas, for example, argon or nitride, is introduced. A working environment is created with such a sequence of operations, almost free of any oxygen, where such reactive materials as titanium and titanium alloys can be sintered. The level of the consumed inert gas is minimised by using a fully tight, welded working chamber. The AM 125 instrument features a powder container with automatic valves supplying additional portions of powder during the whole process, while the excess powder—when another layer is distributed in the working chamber—is diverted to a special container that is quickly and easily detachable and can be placed in a powder sieving or selecting station, and hence, the powder can be re-used in the next process. The time needed to produce the designed model depends on its size, structural complexity, as well as the number of elements which are made in a single process. The fabrication accuracy of models depends on the laser power applied: for the layer thickness of 20–50 μm, it is ±20 μm in the XY plane for low laser power and ±100 μm for high laser power.

The AM 125 instrument is also integrated with suitable software for Manufacturing Applications 3D Marcarm Engineering Autofab for computer-aided design/manufacturing CAD/CAM for rapid manufacturing technology with the SLS technique enabling to adapt the model designed to the fabrication conditions and to achieve the characterised properties. A 3-D model recorded in the stereolithography STL format permitting to produce items by a layered technique should be the outcome of such designing. Once the model reaches the appropriate size and structure, the whole model is divided into layers with specific thickness. The number of layers reflects the number of powder layers, which are sintered until a ready element is achieved. AutoFab software enables to determine optimum manufacturing conditions, among others, layer thickness, laser power, laser beam diameter, scanning rate, distance between par-

http://dx.doi.org/10.5772/65377

ticular remelting paths. More and more complicated shapes with a specific internal and external structure can be manufactured with the software available, which allows designing in three-dimensional space. Once all manufacturing conditions/characteristics are set, the model designed is transferred into the machine's software, where selective laser sintering is performed. The software allows for nearly complete control of the size, geometrical features, and also repeatability of the designed items and to fully control manufacturing conditions by steering them within their relevant applicability range.

The SLS technology is essentially an advanced powder metallurgy technology where the element constitution process begins with spreading a powder layer across the table with its position adjustable in relation to the axis *z*. The layer acts as a substrate for the item being created. A laser beam is guided across the powder surface according to the pre-entered and adequately configured information concerning the particular layers of the cross-spatial section of the part image. Next, the table with the powder is lowered by the user-defined height corresponding to the layer thickness, and another thin layer of powder is spread, where grains are again sintered/melted by remelting the particles of the new powder on the surface with the existing piece of the item being constituted. The successive layers of the cross section are intersintering/intermelting. The cycle is repeated until finishing to constitute a complex element, after which temperature is lowered, and the element produced is removed from the powder bed and subjected to finishing depending on its use, for example, sanding or polishing. Such an element has a nonuniform inner structure which allows to work it further and join with other materials, for example, a ceramic or metallic material, by infiltration.

Titanium powder Grade 2 with the grain size of up to 45 μm with spherical shape was used for selective laser sintering to produce porous skeletons (**Figure 18a**). The powder applied has a reduced concentration of oxygen to 0.14%. The concentration of oxygen in the working chamber during sintering is lowered, as appropriate, below 100 ppm.

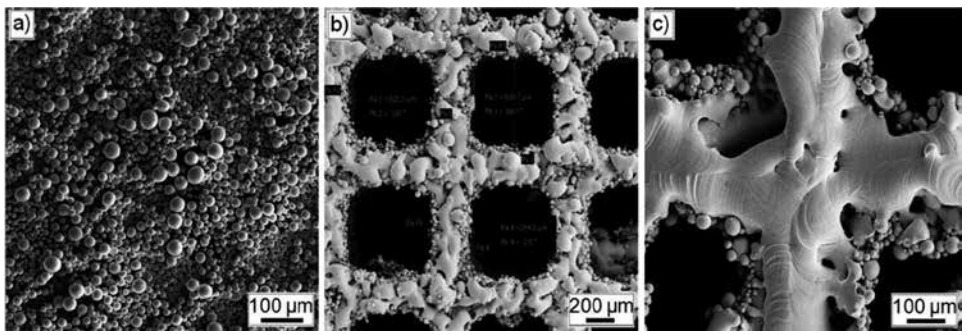

Figure 18. (a) Titanium powder with grain size of 0–45 μm; surface typography of porous titanium skeletons with different pore size: (b) 630 μm, (c) 350 μm; SEM.

A pool of base unit cells was used for designing porous titanium skeletons (**Figure 19**) which —by copying and selecting appropriate lattice values such as height, depth and width, allowed to define the structure of porous skeletons with the pore size of 250–750 μm. A hexagon cross

unit cell (**Figure 19a**), whose main advantage is a special reinforcement in a node connecting the individual skeleton fibres, was selected for producing porous titanium elements in SLS technology.

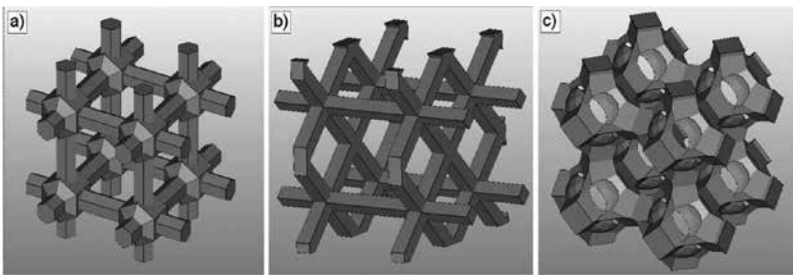

Figure 19. Examples of base unit cells with different spatial structure: (a) hexagon cross, (b) diagonal cross, (c) spherical.

Titanium skeletons were fabricated with the average pore size of ~250, ~350 i ~450 μm and a unit cell dimension of, respectively, 500, 600 and 700 μm, with a different arrangement of unit cells in the space relative to the axis of the system of coordinates (**Figure 20**) at the angle of 0° to the start of the system of coordinates, 45° relative to the axis x of the system of coordinates, 45° to the axis y, 45° to the axis x and 45° to the axis y, 45° to the axis y and 45° to the axis x.

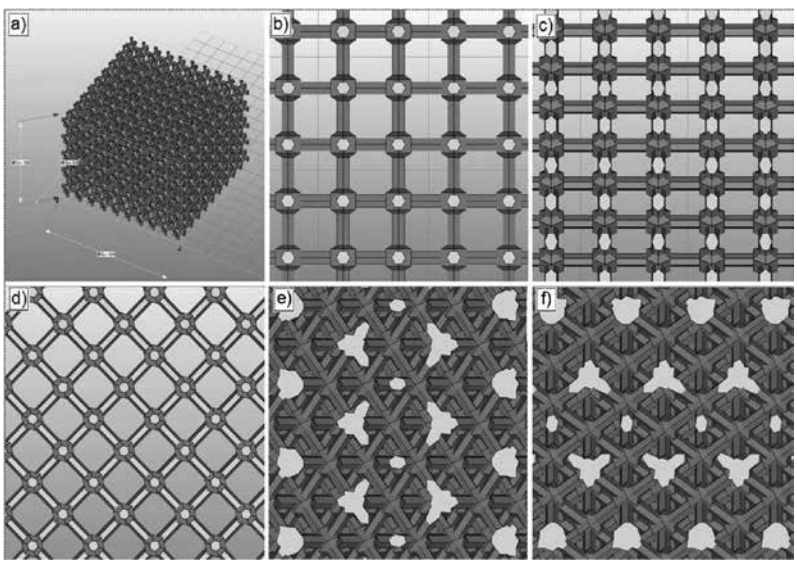

Figure 20. (a) Models of porous elements sized 10 × 10 × 5 mm; image of structure of computer models presenting the arrangement of base unit cells in the space of the system of coordinates: (b) at the angle of 0° to the start of the system of coordinates (symbol A), (c) at the angle of 45° relative to the axis x (symbol B), (d) at the angle of 45° relative to the axis y (symbol C), (e) at the angle of 45° relative to the axis x and 45° relative to the axis y (symbol D), (f) at the angle of 45° relative to the axis y and 45° relative to the axis x (symbol E).

http://dx.doi.org/10.5772/65377

The surface typography of porous titanium skeletons depends on the size of pores (**Figure 18b**, **c**), on the arrangement of unit cells relative to the system of coordinates (**Figure 21**), and also on chemical etching in an aqua regia solution (volume ratio of HCl:HNO_3 of 3:1) or in a 14% water hydrofluoric acid solution, in order to avoid partial melting on the surface and fine powder particles not bonded permanently with the previously constituted element (**Figure 22**). The roughness of porous skeletons before etching is much higher than after etching. The strength properties of the porous skeletons sintered by SLS from titanium powder depend on the size of pores and their spatial orientation (**Figure 23**).

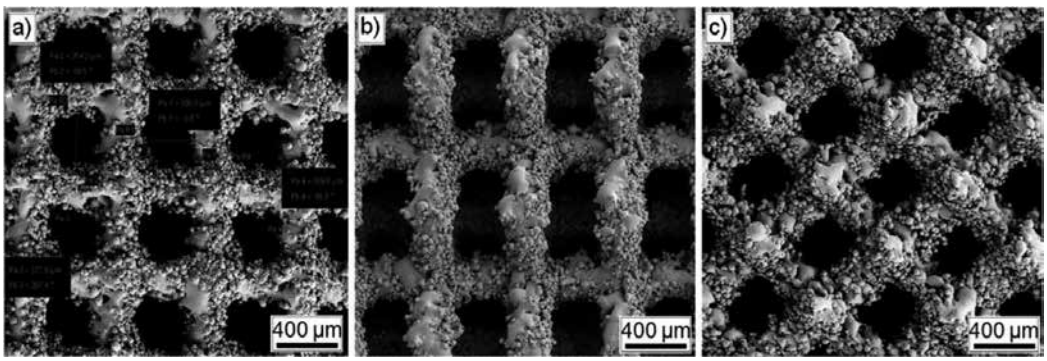

Figure 21. The surface typography of porous titanium skeletons with the pore size of 350 μm and different orientation of unit cells in relation to the system of coordinates: a) at the angle of 0° to the start of the system of coordinates, b) at the angle of 45° relative to the axis x, c) at the angle of 45° relative to the axis y; SEM.

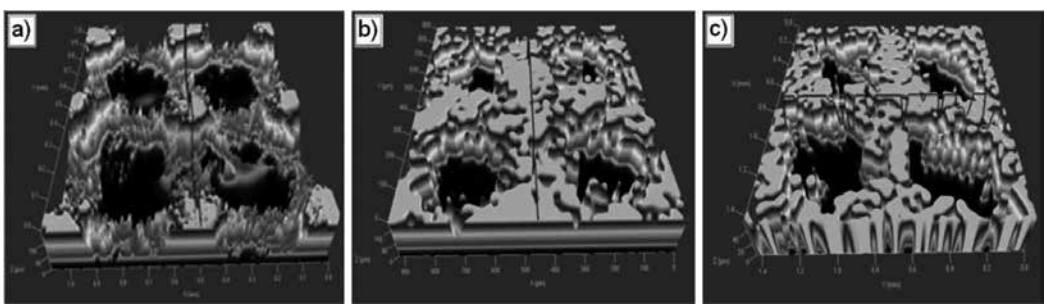

Figure 22. The surface typography of porous titanium skeletons with the pore size of: (a, b) 250 μm, (c) 450 μm; (a) without etching, (b, c) after etching in aqua regia; confocal microscope.

A lightweight titanium skeleton with the porosity of approx. 60%, distinct geometry and compressive strength of approx. 125 MPa, was produced using appropriate fabrication conditions (laser power, laser beam diameter, exposure time of powder to laser activity). Porous titanium skeletons were used for fabrication of composites by infiltration at tempera-

ture of 800°C with an EN AC-AlSi12 alloy and, respectively, EN AC-AlSi7Mg0.3 alloy, under the pressure of 2–3 MPa for 2 min; hence, composites with a new set of properties were obtained.

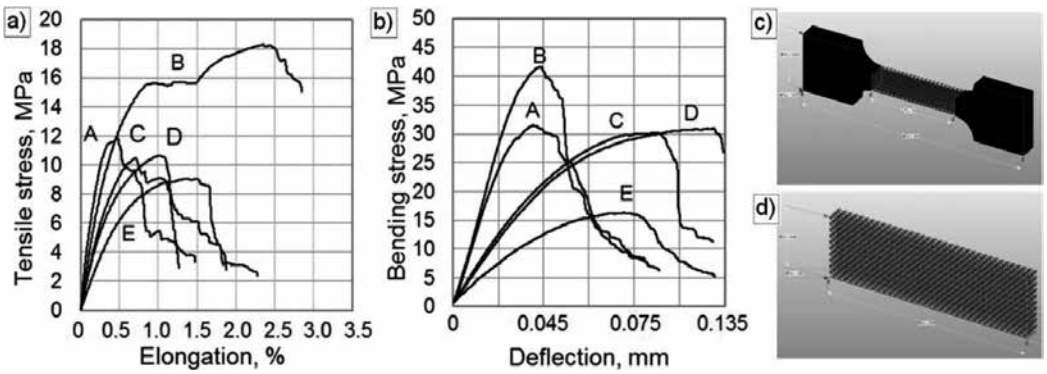

Figure 23. Progression dependency of strength curves: (a) tensile strength, (b) bending strength of skeletons with the pore size of 350 μm sintered by SLS method from titanium powder (marked as in **Figure 20**), (c, d) specimens with porous measuring part: (c) for stretching, (d) for bending.

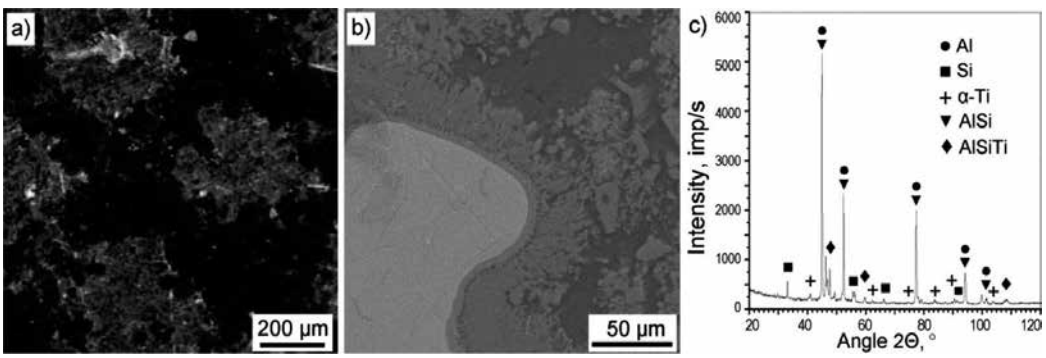

Figure 24. Structure of AlSi12/Ti composite material; (a) stereoscope microscope, (b) SEM, (c) X-ray diffraction pattern.

The structure of the sintered EN AC-AlSi12 and EN AC-AlSi7Mg0.3 aluminium alloy matrix composite material (**Figures 24**, **25**) reinforced with porous titanium skeletons manufactured by SLS methods confirms that the titanium skeleton pores are thoroughly filled as a result of infiltration. The results for X-ray structural examinations for an AlSi12/Ti composite material (**Figure 24c**) reveal that phases are created between particular composite material components during infiltration. An AlSiTi phase occurs in the composite material as a result, apart from such phases as Al, Si, Ti and AlSi. The so-achieved composite materials exhibit much higher strength properties than a matrix material and the porous skeleton itself (**Figure 25c**). This creates extensive application opportunities for such composite materials.

http://dx.doi.org/10.5772/65377

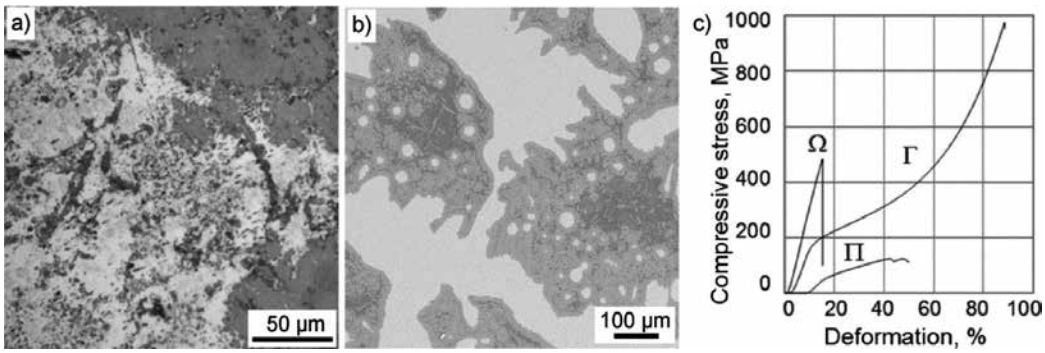

Figure 25. Structure of composite material produced by infiltration of titanium skeleton with AlSi7Mg0.3 alloy; (a) light microscope; (b) SEM; (c) compressive strength, Γ—matrix material, Π—sintered porous material, Ω—composite material.

Author details

Leszek A. Dobrzański[1*], Grzegorz Matula[1], Anna D. Dobrzańska-Danikiewicz[2], Piotr Malara[1], Marek Kremzer[1], Błażej Tomiczek[1], Magdalena Kujawa[1], Eugeniusz Hajduczek[1], Anna Achtelik-Franczak[1], Lech B. Dobrzański[3] and Jagoda Krzysteczko[1]

*Address all correspondence to: leszek.adam@gmail.com

1 Silesian University of Technology, Institute of Engineering Materials and Biomaterials, Gliwice, Poland

2 Silesian University of Technology, Institute of Engineering Processes Automation and Integrated Manufacturing Systems, Gliwice, Poland

3 Centre of Medicine and Stomatology 'SOBIESKI', Gliwice, Poland

References

[1] Kaw AK. Mechanics of composite materials. 2nd ed. Boca Raton: CRC Press, Taylor & Francis Group; 2006. 457 p.

[2] Dobrzański LA. Engineering materials and materials design. Fundamentals of materials science and physical metallurgy. 2nd ed. Warsaw: WNT; 2006. 1600 p. (in Polish) ISBN 83-204-3249-9

[3] Chawla KK. Ceramic matrix composites, 2nd ed. Boston: Kluwer Academic Publishers; 2003. 449 p.

[4] Gibson RF. Principles of composite material mechanics. 3rd ed. Boca Raton: CRC Press, Taylor & Francis Group; 2011. 683 p.

[5] Kumar HGP, Xavior MA. Graphene reinforced metal matrix composite (GRMMC): a review. Procedia Engineering. 2014;97:1033–1040. doi:10.1016/j.proeng.2014.12.381

[6] Alonso A, Pamies A, Narciso J, Garcia-Cordovilla C, Louis E. Evaluation of the wettability of liquid aluminum with ceramic particulates (SiC, TiC, Al_2O_3) by means pressure infiltration. Metallurgical Transactions: A. 1993;24:1423–1432. doi:10.1007/BF02668210

[7] Książek M, Sobczak N, Mikułowski B, Radziwiłł W, Surowiak I. Wetting and bonding strength in Al/Al_2O_3 system. Materials Science and Engineering: A. 2002;324:162–167. doi:10.1016/S0921-5093(01)01305-3

[8] Mortensen A. Interfactial phenomena in the solidification processing of metal matrix composites. Materials Science and Engineering: A. 1991;135:1–11. doi: 10.1016/0921-5093(91)90527-T

[9] Rajan TPD, Pillai RM, Pai BC. Reinforcement coatings and interfaces in aluminium metal matrix composites. Journal of Materials Science. 1998;33:3491–3503

[10] Dobrzański LA, Kremzer M, Dziekońska M. Possibility of wettability improvement of Al_2O_3 preforms infiltrated by liquid aluminium alloy by deposition Ni-P coating. Archives of Materials Science and Engineering. 2012;55:14–21

[11] Evans A, San Marchi C, Mortensen A. Metal matrix composites in industry: an introduction and a survey. New York: Springer Science+Business Media; 2003. 386 p.

[12] Li RQ, Peng F, Guan JW, Yan XZ, Liu SZ, Zhang WK, Zhou XL. Pressure infiltration of boron nitride preforms with molten aluminum for low density heat sink materials. Journal of Materials Science Materials in Electronics. 2013;24:1175–1180. doi:10.1007/s10854-012-0901-8

[13] Freitas M, Pianaro SA, Nadal FN, Tebcherani SM, Berg EAT. Preparation and characterization of SiC/kaolin/Al composite materials by squeeze-casting (in Portuguese). Cerâmica. 2009;55:271–280. doi:10.1590/S0366-69132009000300006

[14] Tomiczek B, Kujawa M, Matula G, Kremzer M, Tański T, Dobrzański LA. Aluminium AlSi12 alloy matrix composites reinforced by mullite porous preforms. Materials Science & Engineering Technology. Materialwissenschaft und Werkstofftechnik. 2015;46:368–376. doi:10.1002/mawe.201500411

[15] Dobrzański LA, Kremzer M, Gołombek K. Structure and properties of aluminum matrix composites reinforced by Al_2O_3 particles. Materials Science Forum. 2008;591–593:188–192

[16] Kremzer M, Dobrzański LA, Dziekońska M, Radziszewska A. Structure and properties of aluminium-silicon matrix composites manufactured by pressure infiltration method. Archives of Materials Science and Engineering. 2014;68:53–58

http://dx.doi.org/10.5772/65377

[17] Pawlyta M, Tomiczek B, Dobrzański LA, Kujawa M, Bierska-Piech B. Transmission electron microscopy observations on phase transformations during aluminium/mullite composites formation by gas pressure infiltration. Materials Characterization. 2016;114:9–17. doi:10.1016/j.matchar.2016.02.003

[18] Tomiczek B, Pawlyta M, Adamiak M, Dobrzański LA. Effect of milling time on microstructure of AA6061 composites fabricated via mechanical alloying. Archives of Metallurgy and Materials. 2015;60:789–793. doi:10.1515/amm-2015-0208

[19] Dobrzański LA, Tomiczek B, Matula G, Gołombek K. Role of halloysite nanoparticles and milling time on the synthesis of AA 6061 aluminium matrix composites. Advanced Materials Research. 2014;939:84–89

[20] Dobrzański LA, Tomiczek B, Pawlyta M, Król M. Aluminium AlMg1SiCu matrix composite materials reinforced with halloysite particles. Archives of Metallurgy and Materials. 2014;59:335–338. doi:10.2478/amm-2014-0055

[21] Dobrzański LA, Tomiczek B, Pawlyta M, Nuckowski P. TEM and XRD study of nanostructured composite materials reinforced with the halloysite particles. Materials Science Forum. 2014;783–786:1591–1596

[22] Dobrzański LA, Tomiczek B, Pakieła W, Tomiczek AE. Mechanical properties and wear resistance of PM composite materials reinforced with the halloysite particles. Advanced Materials Research. 2015;1127:107–112

[23] Dobrzański LA, Kremzer M, Nowak AJ, Nagel A. Aluminium matrix composites fabricated by infiltration method. Archives of Materials Science and Engineering. 2009;36:5–11

[24] Kremzer M. Structure and properties of EN AC-AlSi12 alloy matrix composites manufactured by pressure infiltration method [Ph.D. Thesis]. Gliwice, Poland: Silesian University of Technology; 2007 (in Polish)

[25] Dobrzański LA, Kremzer M, Nagel A. Structure and properties of ceramic preforms based on Al_2O_3 particles. Journal of Achievements in Materials and Manufacturing Engineering. 2009;35:7–13

[26] Mizuuchi K, Takeuchi T, Inoue K, Lee JH, Sugioka M, Itami M, Kawahara M, Yamauchi I, Asanuma H. Properties of boron fiber reinforced aluminum matrix composites fabricated by pulsed current hot pressing (PCHP). Materials Science Forum. 2007:539–543:3139–3144

[27] Luo Z, Song Y, Zhang S, Miller DJ. Interfacial microstructure in a B_4C/Al composite fabricated by pressureless infiltration. Metallurgical and Materials Transactions: A. 2012;43:281–293. doi:10. 1007/s11661-011-0817-6

[28] Lee KB, Sim HS, Kwon H. Reaction products of Al/TiC composites fabricated by the pressureless infiltration technique. Metallurgical and Materials Transactions: A. 2005;36:2517–2527. doi:10.1007/s11661-006-0052-8

[29] Adamiak M. The effect of TiAl and Ti_3Al reinforcement on microstructure changes and properties of aluminium matrix composites. Archives of Materials Science and Engineering. 2012;58:55–79

[30] Dobrzański LA, Dobrzańska-Danikiewicz AD, Gaweł TG, Achtelik-Franczak A. Selective laser sintering and melting of pristine titanium and titanium Ti6Al4V alloy powders and selection of chemical environment for etching of such materials. Archives of Metallurgy and Materials. 2015;60:2039–2045. doi:10.1515/amm-2015-0346

[31] Dobrzański LA, Dobrzańska-Danikiewicz AD, Malara P, Gaweł TG, Dobrzański LB, Achtelik-Franczak A. Fabrication of scaffolds from Ti6Al4V powders using the computer aided laser method. Archives of Metallurgy and Materials. 2015;60:1065–1070. doi:10.1515/amm-2015-0260

[32] Dobrzański LA, Tomiczek B, Adamiak M. Manufacturing of EN AW6061 matrix composites reinforced by halloysite nanotubes. Journal of Achievements in Materials and Manufacturing Engineering. 2011;49:82–89

[33] Zhang H, Maljkovic N, Mitchell BS. Structure and interfacial properties of nanocrystalline aluminum/mulite composites. Materials Science and Engineering: A. 2002;326:317–323. doi:10.1016/S0921-5093(01)01500-3

[34] Dobrzański LA, Kremzer M, Nowak AJ, Nagel A. Composite materials based on porous ceramic preform infiltrated by aluminium alloy. Journal of Achievements in Materials and Manufacturing Engineering. 2007;20:95–98

[35] Peng LM, Cao JW, Noda K, Han KS. Mechanical properties of ceramic-metal composites by pressure infiltration of metal into porous ceramics. Materials Science and Engineering A. 2004;374:1–9. doi:10.1016/j.msea.2003.12.027

[36] Yuan P, Tan D, Annabi-Bergaya F. Properties and applications of halloysite nanotubes: recent research advances and future prospects. Applied Clay Science. 2015;112–113: 75–93

[37] Garcia-Cordovilla C, Louis E, Narciso J. Pressure infiltration of packed ceramic particulates by liquid metals. Acta Materialia. 1999;47:4461–4479. doi:10.1016/S1359-6454(99)00318-3

[38] Kang CG, Seo YH. The influence of fabrication parameters on the deformation behavior of the preform of metal-matrix composites during the squeeze-casting processes. Journal of Materials Processing Technology. 1996;61:241–249. doi:10.1016/0924-0136(95)02180-9

[39] Yamauchi T, Nishida Y. Infiltration kinetics of fibrous preforms by aluminum with solidification. Acta Metallurgica et Materialia. 1995;43:1313–1321. doi:10.1016/0956-7151(94)00374-Q

[40] Eardley ES, Flower HM. Infiltration and solidification of commercial purity aluminium matrix composites. Materials Science and Engineering: A. 2003;359:303–312. doi: 10.1016/S0921-5093(03)00357-5

[41] Lianxi H, Yiwen Y, Shoujing L, Xinying X. Investigation on the kinetics of infiltration of liquid aluminium into an alumina fibrous preform. Journal of Materials Processing Technology. 1999;94:227–230. doi:10.1016/S0924-0136(99)00099-0

[42] Etter T, Papakyriacou M, Schultz P, Uggowitzer PJ. Physical properties of graphite/aluminium composites produced by gas pressure infiltration method. Carbon. 2003;41:1017–1024. doi:10.1016/S0008-6223(02)00448-7

[43] Travitzky NA. Microstructure and mechanical properties of alumina copper composites fabricated by different infiltration techniques. Materials Letters. 1998;36:114–117. doi:10.1016/S0167-577X(98)00012-3

[44] Dobrzański LA, Kremzer M, Nagel A. Aluminium EN AC-AlSi12 alloy matrix composite materials reinforced by Al_2O_3 porous performs. Archives of Material Science and Engineering. 2007;28:593–596

[45] Dobrzański LA, Kremzer M, Nagel A. Application of pressure infiltration to the manufacturing of aluminium matrix composite materials with different reinforcement shape. Journal of Achievements in Materials and Manufacturing Engineering. 2007;24:183–186

[46] Mattern A, Huchler B, Stadenecker D, Oberacker R, Nagel A, Hoffmann MJ. Preparation of interpenetrating ceramic-metal composites. Journal of European Ceramic Society. 2004;24:3399–3408. doi:10.1016/j.jeurceramsoc.2003.10.030

[47] Luo ZP, Song YG, Zhang SQ. A TEM study of the microstructure of SiC_p/Al composite prepared by pressureless infiltration method. Scripta Materialia. 2001;45:1183–1189. doi:10.1016/S1359-6462(01)01148-4

[48] Ryu YM, Yoon EP, Rhee MH. The behavior of the nickel layer in an aluminum matrix composite reinforced with nickel coated carbon fiber. Journal of Materials Science Letters. 2000;19:1103–1105. doi:10.1023/A:1006780212533

[49] Dobrzański LA, Tomiczek B, Adamiak M, Matula G, Sołtys J. Nanostructure composite material with wrought aluminum alloy and method for production thereof. Patent PL 216257. 2014

[50] Dobrzański LA, Tomiczek B, Kremzer M, Matula G, Sołtys J. Composite material with casting aluminum alloys matrix and method for producing thereof. Patent PL 217093. 2014

[51] León CA, Drew RAL. The influence of nickel coating on the wettability of aluminum on ceramics. Composites A. 2002;33:1429–1432. doi:10.1016/S1359-835X(02)00161-6

[52] Sobczak N, Asthana R, Radziwiłł W, Nowak R, Kudyba A. The role of aluminum oxidation in the wetting-bonding realtionship of Al/oxide couples. Archives of Metallurgy and Materials. 2007;52:55–65

[53] Pech-Canul MI, Katz RN, Makhlouf MM, Pickard S. The role of silicon in wetting and pressureless infiltration of SiC_p performs by aluminum alloys. Journal of Materials Science. 2000;35:2167–2173. doi:10.1016/S0924-0136(00)00664-6

[54] Hashim J, Looney L, Hashmi MSJ. The enhancement of wettability of particles in cast aluminium matrix composites. Journal of Materials Processing Technology. 2001;119:329–335. doi:10.1016/S0924-0136(01)00919-0

[55] Dobrzański LA, Kremzer M, Adamiak M. The influence of reinforcement shape on wear behaviour of aluminium matrix composite materials. Journal of Achievements in Materials and Manufacturing Engineering. 2010;42:26–32

[56] Dobrzański LA, Kremzer M, Nagel A, Huchler B. Fabrication of ceramic preforms based on Al_2O_3 CL 2500 powder. Journal of Achievements in Materials and Manufacturing Engineering 2006;18:71–74

[57] Miazga A, Konopka K, Gizowska M, Szafran M. Alumina matrix ceramic-nickel composites formed by gelcasting method. Composites Theory and Practise. 2012;12: 138–141

[58] Dobrzański LA, Matula G. Powder injection molding: sinter-hardening. In: Colás R, Totten GE, editors. Encyclopedia of iron, steel, and their alloys. Boca Raton: CRC Press, Taylor & Francis Group: 2016; 14 p. ISBN: 978-1-4665-1104-0

[59] Matula G. Gradient surface layers from tool cermets formed pressurelessly and sintered. Open Access Library. 2012;7:1–144 (in Polish)

[60] Dobrzański LA, Matula G. Powder metallurgy fundamentals and sintered materials. Open Access Library. 2012;8:1–156 (in Polish)

[61] Krzysteczko J. Structure and properties of aluminium alloy matrix composites manufactured by powder injection moulding method [Ph.D. Thesis in progress]. Gliwice, Poland: Silesian University of Technology; 2016 (in Polish)

[62] Kujawa M. Infiltrated AlSi12 alloy matrix composites reinforced with sintered halloysite nanotubes [Ph.D. Thesis]. Gliwice, Poland: Silesian University of Technology; 2015 (in Polish)

[63] Dobrzański LA, Tomiczek B, Adamiak M, Gołombek K. Mechanically milled aluminium matrix composites reinforced with halloysite nanotubes. Journal of Achievements in Materials and Manufacturing Engineering. 2012;55:654–660

[64] Dobrzański LA, et al. Investigations of structure and properties of newly created porous biomimetic materials fabricated by selective laser sintering, BIOLASIN. Project UMO-2013/08/M/ST8/00818. Silesian University of Technology, Gliwice; 2013–2016

[65] Achtelik-Franczak A. Engineering composite materials the reinforcement with the microporous titanium selective laser sintered [Ph.D. Thesis]. Gliwice, Poland: Silesian University of Technology; 2016 (in Polish)

[66] Dobrzański LB. Structure and properties of the engineering materials applied on the stomatognathic system prostheses manufactured with additive and loss-processing methods [Ph.D. Thesis in progress]. Cracow, Poland: AGH University of Science and Technology; 2016 (in Polish)

[67] Dobrzański LA, Dobrzańska-Danikiewicz AD, Malara P, Gaweł TG, Dobrzański LB, Achtelik A. Composite fabricated by computer-aided laser methods for craniofacial implants and its manufacturing method. Patent Application P 411689. 23.03.2015

[68] Dobrzański LA, Dobrzańska-Danikiewicz AD, Malara P, Gaweł TG, Dobrzański LB, Achtelik-Franczak A. Bone implant scaffold. Patent Application P 414424. 19.10.2015

[69] Dobrzański LA, Dobrzańska-Danikiewicz AD, Malara P, Dobrzański LB, Achtelik-Franczak A. Biological and engineering composites for regenerative medicine. Patent Application P 414723. 9.11.2015

[70] Dobrzański LA, Dobrzańska-Danikiewicz AD, Malara P, Gaweł TG, Dobrzański LB, Achtelik-Franczak A. Implant scaffold and a prosthesis of anatomical elements of a dental system and craniofacial bone. Patent Application P 414423. 19.10.2015

[71] Boccaccini AR, Karapappas P, Marijuan JM, Kaya C. TiO_2 coatings on silicon carbide and carbon fibre substrates by electrophoretic deposition. Journal of Materials Science. 2004;39:851–859

[72] Pipel E, Woltersdorf J, Dietrich D, Stockel S, Weise K, Marx G. CVD-coated boron nitride on continuous silicon carbide fibres: structure and nanocomposition. Journal of the European Ceramic Society. 2000;20:1837–1844

[73] Kuiry SC, Wannaparhun S, Dahotre NB, Seal S. In-situ formation of Ni-alumina nanocomposite during laser processing. Scripta Materialia. 2004;50:1237–1240. doi: 10.1016/j.scriptamat.2004.02.005

[74] Kremzer M, Dobrzański LA, Dziekońska M, Macek M. Atomic layer deposition of TiO_2 onto porous biomaterials. Archives of Materials Science and Engineering. 2015;75:63–69

[75] Saiz E, Tomsia AP, Loehman RE, Ewsuk K. Effects of composition and atmosphere on reactive metal penetration of aluminium in mulita. Journal of the European Ceramic Society. 1996;16:275–280. doi:10.1016/0955-2219(95)00156-5

[76] Kim BM, Cho YK, Yoon SY, Stevens R, Park HC. Mullite whiskers derived from kaolin. Ceramics International. 2009;35:579–583. doi:10.1016/j.ceramint.2008.01.017

[77] Rawtani D, Agrawal YK. Multifarious applications of halloysite nanotubes: a review. Reviews on Advanced Materials Science. 2012;30:282–295

[78] Kamble R, Ghag M, Gaikawad S, Panda BK. Halloysite nanotubes and applications: a review. Advanced Scientific Research. 2012;3:25–29

[79] Lvov Y, Aerov A, Fakhrullin RL. Clay nanotube encapsulation for functional biocomposites. Advances in Colloid and Interface Science. 2014;207:189–198. doi:10.1016/j.cis.2013.10.006

[80] Qia R, Guo R, Zheng F, Liu H, Yu J, Shi X. Controlled release and antibacterial activity of antibiotic-loaded electrospun halloysite/poly(lactic-co-glycolic acid) composite nanofibers. Colloids and Surfaces B: Biointerfaces. 2013;110:148–155. doi:10.1016/j.colsurfb.2013.04.036

[81] Jiang L, Zhang C, Liu M, Yang Z, Tjiu WW, Liu T. Simultaneous reinforcement and toughening of polyurethane composites with carbon nanotube/halloysite nanotube hybrids. Composites Science and Technology 2014;91:98–103. doi:10.1016/j.compscitech.2013.11.025

[82] Stoch L, Wacławska I. Dehydroxylation of kaolinite group minerals. I. Kinetics of dehydroxylation of kaolinite and halloysite. Journal of Thermal Analysis. 1981;20:291–304. doi:10.1007/BF01912877

[83] Papoulis D, Komarneni S, Panagiotaras D, Stathatos E, Christoforidis KC, Fernández-García M, Li H, Shu Y, Sato T, Katsuki H. Three-phase nanocomposites of two nanoclays and TiO_2: synthesis, characterization and photacatalytic activities. Applied Catalysis B: Environmental. 2014;147:526–533. doi:10.1016/j.apcatb.2013.09.025

[84] Dobrzańska-Danikiewicz AD. Foresight of material surface engineering as a tool building a knowledge based economy. Materials Science Forum. 2012;706–709:2511–2516. doi:10.4028/www.scientific.net/MSF.706-709.2511.

[85] Dobrzańska-Danikiewicz AD, Dobrzański LA, Sękala A. Results of Technology Foresight in the Surface Engineering Area. Applied Mechanics and Materials. 2014;657:916–920. doi:10.4028/www.scientific.net/AMM.657.916

[86] Dobrzańska-Danikiewicz AD. The acceptation of the production orders for the realisation in the manufacturing assembly systems. Journal of Materials Processing Technology 2006;175 :123–132. doi:10.1016/j.jmatprotec.2005.04.001

[87] Dobrzański LA. Applications of newly developed nanostructural and microporous materials in biomedical, tissue and mechanical engineering. Archives of Materials Science and Engineering. 2015;76:53–114

[88] Dobrzański LA. Application of the additive manufacturing by selective laser sintering for constituting implantscaffolds and hybrid multilayer biological and engineering composite materials. Keynote lecture on International Conference on Processing & Manufacturing of Advanced Materials THERMEC'2016, Processing, Fabrication, Properties, Applications. Graz, Austria; 29.05.2016–3.06.2016

http://dx.doi.org/10.5772/65377

[89] Dobrzański LA. Fabrication, structure and mechanical properties of laser sintered materials for medical applications. Invited lecture on XXV International Materials Research Congress. Cancun, Mexico; 14.08.2016–19.08.2016

[90] Dobrzański LA. Metallic implants-scaffolds for dental and orthopaedic application. Invited lecture on 9th COLAOB – Latin American Congress on Artificial Organs and Biomaterials. Foz do Iguaçu, Brazil; 24.08.2016–27.08.2016

Chapter 6

Fabrication, Composition, Properties and Application of the AlMg1SiCu Aluminium Alloy Matrix Composite Materials Reinforced with Halloysite or Carbon Nanotubes

Leszek A. Dobrzański, Błażej Tomiczek and
Magdalena Macek

Additional information is available at the end of the chapter

http://dx.doi.org/10.5772/65399

Abstract

In this chapter, the characterisation of the halloysite nanotubes (HNTs) and multiwalled carbon nanotubes (MWCNTs) as the reinforcement in the composite materials was described. The original and author technology of production of the aluminium AlMg1SiCu matrix composite materials reinforced with halloysite or carbon nanotubes using powder metallurgy techniques, including mechanical alloying and hot extrusion and the range of own research in the case to determine microstructure, as well as mechanical properties of those materials was present. It was investigated that the addition of carbon and halloysite nanotubes causes a significant improvement in mechanical properties of the obtained nanocomposites. The investigation results show that the technology used in manufacturing nanocomposite materials can find the practical application in the production of new light metal matrix nanocomposites.

Keywords: metal matrix composites, mechanical milling, carbon nanotubes, halloysite nanotubes

1. Overview of applications of halloysite and carbon nanotubes in composite materials

The diverse uses of composite materials with a matrix made of aluminium and aluminium alloys result most of all from the chemical and phase composition of reinforcing materials,

as well as from their size and fraction. Aluminium composite materials are currently one of the most dynamically developing and most intensely investigated groups of engineering materials as confirmed, in particular, by the results of research into composite materials with an aluminium alloy matrix reinforced with ceramic particles [1–4] and intermetallic phases [5, 6].

Composite materials with an aluminium matrix reinforced with ceramic particles and/or fibres are finding increasingly extensive applications in the aviation, machine, automotive and electronic industry, and the most advanced ones are adapted to the needs of the arms and space sector and for professional sports equipment. Moreover—owing to their numerous advantages—they are used for parts exposed to high temperatures (pistons, engine blocks, combustion chamber inserts) in systems undergoing intensive friction (discs, clutch and brake drums), as well as in drive systems achieving a small friction coefficient and a high vibration absorption ability. Considering the numerous manufacturing methods of metallic composite materials, powder metallurgy and pressure infiltration methods play a special role. Mechanical alloying, mechanical milling, followed by compression and hot pressing, enable to fabricate nanostructured composite materials with a permanent cross section, with a uniformly distributed reinforcing intermetallic phase and with a uniform particle size and to consequently achieve enhanced mechanical properties of the material [7, 8]. Works have been conducted all the time to employ the new phases as reinforcements in composite materials with a matrix made of aluminium alloys. The aim is, most of all, to reduce defects caused by a conventional reinforcement, and to improve the functional properties of newly developed composite materials.

The latest publications show that graphite [9, 10] and carbon nanotubes [11, 12] are used as reinforcing phases in aluminium matrix composite materials. Carbon nanotubes are characterised by good mechanical, thermal and electric properties, unlike any others, i.e., engineering materials known to date [13, 14]. Carbon nanotubes, since they have been manufactured, have become the object of extensive investigations of many research institutions around the globe. Broad interest is signified by numerous publications concerning the studies of their structure, properties and application opportunities [15–18]. Carbon nanotubes have been used mainly as reinforcements of composite materials with a polymer [19, 20] and ceramic matrix [21]; however, growing interest in carbon nanotubes has been seen in the recent years as the reinforcement of composite materials with a matrix made of light metals and their alloys [22, 23].

An alternative and cheaper solution may be to use—as reinforcing phases in metallic composite materials—mineral halloysite nanotubes (HNTs) extracted from halloysite, which is a silty material of volcanic origin present, among others, in deposits located in Poland, as in one of three places globally apart from the USA and New Zealand. Halloysite has high porosity, a large specific area, high-ion exchange capacity and is easy to work chemically and mechanically. The scarce literature reports available so far concern only polymer nanocomposites reinforced with mineral halloysite nanotubes [22–25], however, own works indicate the purposefulness of investigating and applying this type of composite materials [26, 27]. Multiple novel technologies for using halloysite for scientific and industrial purposes have been developed as a result of works lasting many years pursued by research institutions [22,

http://dx.doi.org/10.5772/65399

28, 29], among others, as a filler in polymer materials [30, 31]. The research works currently carried out, pertaining to composite materials with a polymer matrix [32, 33], point out that if several to more than 10% of mineral nanotubes are added, the strength, rigidity, hardness, thermal stability, and—in some cases—electric conductivity is enhanced. An important problem for production of such materials is difficulties in the uniform dispersion of nanotubes and the necessity to prevent aggregation, which is very disadvantageous for a composite material's strength [25]. Considering that the properties of the separation area of such phases have influence on the properties of a composite material, apart from the characteristics of its components, surface modification of halloysite becomes necessary by plasma or chemical functionalisation method, increasing surface energy and wettability [34, 35].

The second alternative reinforcement of composite materials can be carbon nanotubes which are used mainly as reinforcements of very light polymer nanocomposite materials [36, 37]. A nanocomposite material with a polyamide matrix with an addition of carbon nanotubes with the use of ultrasound mixing was produced in the work [36]. The authors have investigated the effect of the fraction of carbon nanotubes on the mechanical properties of the nanocomposite material. It was found that if a volume fraction of 0.01–0.5% of carbon nanotubes is added, the mechanical properties of the nanocomposite materials are improved. The Young's modulus of the nanocomposite material with the volume fraction of 0.05% of carbon nanotubes was increased by 110% in respect of pure polymer. In the work [38], the effect of the fraction of carbon nanotubes on electrical properties of the nanocomposite material with an epoxy resin matrix was discussed. If a volume fraction of 0.1% of carbon nanotubes is added, the electrical conductivity of the material is increased to 10^{-2} S m^{-1} compared to resin conductivity. Carbon nanotubes are also applied as reinforcements of nanocomposite materials with a ceramic matrix. A nanocomposite material with an aluminium oxide matrix reinforced with carbon nanotubes using the pressure-free moulding method was fabricated in the work [39]. A material with enhanced mechanical properties was fabricated. The bending strength of the materials went up by 25%, while crack resistance by 45% vis-à-vis aluminium oxide without a fraction of carbon nanotubes. In the publication [40], the authors focused on investigating how the structure of functionalised carbon nanotubes (length and diameter) influences the degree of dispersion of nanofibers in an aluminium oxide matrix. The material was produced by spark plasma sintering (SPS). Growing interest has been seen in the recent years in carbon nanotubes as reinforcements of composite materials with a matrix made of light metals and their alloys [41, 42], and the amount of own works is also significant here [43, 44].

Several methods of consolidation have been used to manufacture nanocomposite materials with a matrix made of aluminium and aluminium alloy reinforced with carbon nanotubes. The authors from the study [45–51] indicate that the following methods are in use: hot rolling [45], sintering [46], plasma spray forming [47], stir casting [48], semisolid powder processing (SPP) [49], spark plasma sintering (SPS) [50] and spark plasma extrusion (SPE) [51]. The methods of intensive plastic deformation, equal channel angular pressing (ECAP) [52] and friction stir processing were also employed to manufacture such nanocomposite materials [53]. Conventional hot pressing is considered to be a widely used consolidation method for producing

nanostructured composite material with an aluminium matrix and reinforced with carbon nanotubes [11, 54].

The main problem in manufacturing composite materials reinforced with halloysite and carbon nanotubes is their strong tendency to create agglomerates and difficulties in achieving their appropriate dispersion in the matrix material. The existence of reinforcement agglomerates in the case of nanocomposite material is limiting particles' ability to counteract the dislocation motion and is not effective in limiting grain growth. Both the uniform distribution of the reinforcing phase and its properties play an essential role in achieving improved material properties. One of the ways used for the uniform distribution of the reinforcing phase is to use mechanical synthesis methods, which have become one of the main ways to produce composite materials reinforced with carbon [55–57], and halloysite nanotubes [58, 59]. The manufacturing of nanostructured composite materials with a matrix of aluminium alloys reinforced with carbon and halloysite nanotubes can be divided into two phases. The first of them is the uniform distribution of nanotubes in an alloy matrix. The second is to consolidate the powders prepared in advance. This chapter presents the results of own investigations [43, 44, 60–62], although other chapter of the book discusses the possible uses of halloysite nanotubes for fabrication of a microporous skeleton acting as a preform for fabrication of aluminium matrix composites.

2. Fabrication and methodology of own research of composite materials with AlMg1SiCu alloy matrix reinforced with halloysite and carbon nanotubes

This chapter presents the method of fabrication using powder metallurgy techniques, including mechanical alloying and hot extrusion and the research methods of charge materials and the microstructure, as well as mechanical properties of aluminium alloy AlMg1SiCu matrix nanocomposites reinforced with multiwalled carbon nanotubes (MWCNTs) and halloysite nanotubes (HNTs).

The material for the investigations was prepared using, as a matrix material, a commercially available air-sputtered EN AW-AlMg1SiCu aluminium alloy powder (numerical designation EN AW-6061) manufactured by ECKA Company (Austria), whose nominal size of particles did not exceed 100 μm. The chemical composition is provided in **Table 1**. MWCNTs (supplied by Cheaptubes) and HNTs supplied by NaturalNano were used for the reinforcement of nanostructured composite materials with an EN AW-AlMg1SiCu alloy matrix (**Figure 1**).

Elements' concentration, wt.%						
Mg	**Si**	**Cu**	**Cr**	**Fe**	**Others**	**Al**
0.97	0.63	0.24	0.24	0.03	<0.3	Balance

Table 1. Chemical composition of the matrix–EN AW-AlMg1SiCu alloy powder.

http://dx.doi.org/10.5772/65399

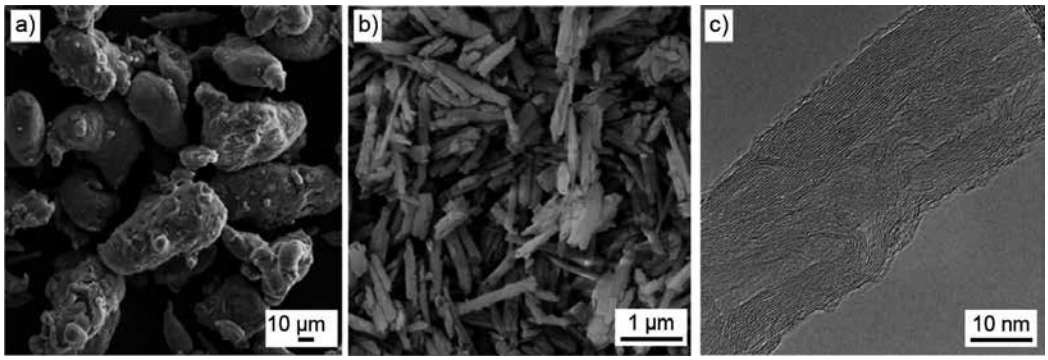

Figure 1. Morphology of the as-received (a) EN AW-AlMg1SiCu alloy powder, SEM, (b) halloysite nanotubes, SEM, (c) structure of the multiwalled carbon nanotubes, HRTEM.

A centrifugal ball mill, Pulverisette 5, by Fritsch Company, was used to produce crushed and permanently joined composite powders. The manufacturing conditions of composite powders are listed in **Table 2**. A slip additive, MA7050 (micronized ethylene-bis-stearamide-wax), reducing adhesion between the charge material and the mill material [process control agent (PCA)] with the mass fraction of 1%, was used for all the powders.

Reinforcement	**MWCNTs**	**HNTs**
Ball-to-powder weight ratio	20:01	
Ball diameter	20 mm	
Ball material	AISI 420 quenched stainless steel	
Time of milling	5; 10 h	3; 6 h
Reinforcement contents	0.5; 2; 3.5; 5 wt.%	5; 10; 15 wt.%

Table 2. Milling process parameters.

Five sets of materials were prepared containing, respectively, 5, 10 and 15% of halloysite nanotubes by mass and 2 and 5% of multiwalled carbon nanotubes by mass. The composite powders obtained in mechanical milling were cold pressed in a mould with the socket diameter of 26 mm and under the pressure of 300 MPa, and then extruded at 460–480°C using a graphite suspension in oil as a slip substance, without degassing, in a shield jacket. Direct extrusion of the cold pressed rod-shaped composite materials consisted of placing a moulding in a thick-wall sleeve closed from one side with a punch, and from the other side—with a die with a forming opening. At elevated temperature, under the influence of pressure exerted by a punch, the material was moulded through a die opening, and a rod with the desired shape and dimension was achieved and with density near the theoretical density. A die was used allowing to extrude material with the deformation degree of 10.57. The heating temperature of the charge material and the tools used was optimised; the best results were achieved for the charge

material temperature of 460–480°C (**Figure 2a**). A higher temperature led to the occurrence of the liquid phase and surface defects such as cracks and skinning (**Figure 2b** and **c**), while the lower temperature—led to the lack of appropriate connection between particular composite material grains and the related disadvantageous properties of the ready product.

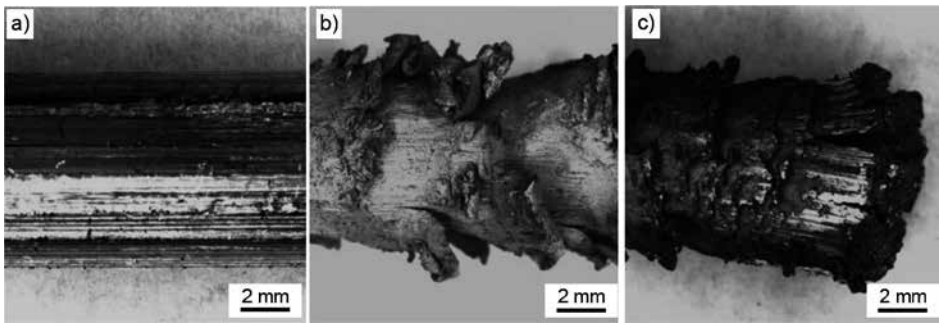

Figure 2. Macrofractography of the extruded bars at (a) 460 °C (b) and (c) 500 °C.

Complex and complementary investigations were performed to establish a dependency between the fraction of the reinforcement material in the matrix, structure and properties of the composite material produced. The morphology of EN AW-AlMg1SiCu alloy powders, halloysite and composite powders, as well as the structure of the manufactured composite materials was examined in a scanning electron microscope (SEM) SUPRA 35 by ZEISS. Secondary electron (SE) detection and back scattered electron (BSE) detection with the accelerating voltage of 7–20 kV and the maximum magnification of 50,000 times was used for obtaining the images of the examined materials. Metallographic examinations were performed for composite materials mounted in conductive phenol resin with a carbon filler. They were ground with a Tegramin-20 grinder-polisher by STRUERS with SiC sandpapers with the grain size of 120–500 μm/mm^2, and then were subjected to polishing using three suspensions of polycrystalline diamond and a colloidal silica suspension. Microsections were made in the direction perpendicular and parallel to the direction of extrusion. Metallographic observations of composite materials were carried out with a LEICA MEF4A light microscope equipped with a computer image analysis system with the magnification of 500 and 1000 times. A qualitative phase composition analysis of powders and composite materials was carried out with an X'Pert PRO X-ray diffractometer by PANalytical with an Xcelelator band detector, using filtered radiation of a copper and cobalt lamp with the voltage of 40 kV and a filament current of 30 mA. Radiation intensity measurements were made within the angle range 2θ of 5–140°. Diffraction examinations and examinations of the structure of thin foils were performed with an S/TEM TITAN 80-300 high-resolution transmission electron microscope (HRTEM) by FEI Company. The high-resolution transmission electron microscope is equipped with BF, DF and HAADF scanning transmission detectors, a Cs condenser spherical aberration corrector, an electron energy filter, electron energy-loss spectrometer EELS, energy dispersion spectrometer EDS. The distribution of grain composition of the powders used was analysed with an ANALYSETTE 22 MicroTec analyser by FRITSCH. The measurements were made at room temperature

http://dx.doi.org/10.5772/65399

for equivalent grain diameter of 80 nm to 2 mm, using water as a dispergating liquid, with a small addition of a surfactant. Powders were dispergated with ultrasounds prior to and during a measurement. The microhardness of powders and composite materials was examined on the ground microsections with a FUTURE TECH hardness tester by the Vickers method for the pressure of 0.98 ($HV_{0.1}$) and 0.49 N ($HV_{0.05}$).

3. Structure and properties of composite materials with AlMg1SiCu alloy matrix reinforced with halloysite and carbon nanotubes

This chapter presents the results of investigations determining the microstructure, as well as mechanical properties of aluminium alloy matrix nanocomposites reinforced with multiwalled carbon nanotubes (MWCNTs) and halloysite nanotubes (HNTs) fabricated using powder metallurgy techniques, including mechanical alloying and hot extrusion. AlMg1SiCu aluminium alloy powder was used as a matrix of the nanocomposites.

It was revealed with electron scanning microscopy that the primary circular particles are deformed, flattened and have a plate-like form in the initial stage of mechanical synthesis. A tendency to join the earlier deformed particles prevails when milling the powders further, leading to increasingly larger composite material components being formed (**Figure 3a**). Changes in the shape and size of the ground powders result from individual particles being welded due to collisions with grinding mediums or with the mill walls. The conglomerates of flattened particles formed as a result of welding are becoming much more reinforced, harder, and hence susceptible to cracking. As milling advances, the particles are fragmented and rejoined, and this finally contributes to the random orientation of the welded particles' boundaries. A relatively equiaxial shape of the milled powder's particles informs that the process has reached the predefined status. As opposed to the EN AW-AlMg1SiCu alloy powder being ground, it was found for the composite material powder that the deformed particles were tightly joined, thus creating a homogenous structure free of pores and discontinuities.

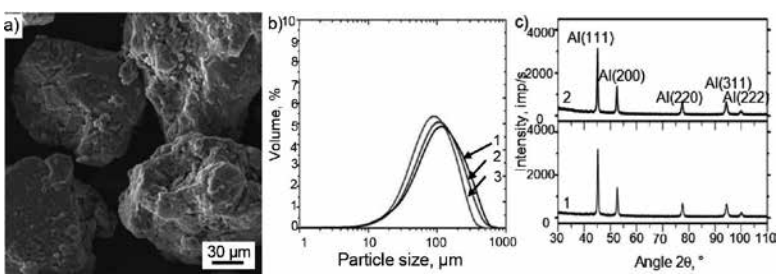

Figure 3. (a) Morphology of the composite powders AlMg1SiCu reinforced with 10% of HNTs after 6 h of mechanical milling, (b) comparison of the grain distribution of AlMg1SiCu alloy powder (1) and AlMg1SiCu alloy powder with 5% (2) and 10% (3) volume fraction of HNTs subjected to high-energy milling for 6 h and (c) X-ray diffraction pattern of AlMg1SiCu alloy powder milled with volume fraction of 10% of HNTs for 6 h (1), unmilled AlMg1SiCu (2) alloy powder.

The findings of microscopic observations are strengthened by an analysis of results of measurements carried out for the size of composite materials' powder particles (**Figure 3b**). The size distribution of the particles in the initial stage is characterised by two apexes and this is explained by the fact that the investigated powders are a mixture of particles with a largely differentiated size, but also by the measurement method itself. The thin, flat particles prevailing at the beginning of grinding may distort the measurement results depending on the angle between the laser beam and the measured irregular particle. On the other hand, it is suggested in the work [63] that—due to a larger number of the investigated particles—ultrasound mixing of the suspension during measurement and the fact that the angle between the measured particle and the measuring beam is completely accidental, the value measured indeed corresponds to the average particle diameter. As the grinding time is extending, according to the changes in morphology and structure as described earlier, a particle size distribution curve is becoming broader, thus confirming that a phenomenon exists of joining the deformed particles. The distribution curve is characterised in the next stage by an asymmetric deviation signifying a higher fraction of large particles formed as a result of multiple welding. The existing asymmetry is gradually disappearing and this is related to the cracking of large particles described earlier. It is suggested by a symmetric, relatively narrow distribution curve and a median value larger than the initial state by 50%, that the process has reached the set condition, showing the state of balance between the mechanisms of joining and fragmentation.

Mechanical synthesis, apart from the proven impact on the morphology and structure of the developed composite powders, also has an effect on their phase composition. The phase composition analysis results, shown in **Figure 3c**, depending on the milling time of a composite material reinforced with halloysite nanotubes prove that after 10 min of milling, low-angle reflections coming from mineral halloysite crystals disappear, and reflections identified as α-Al are only left on the diffraction pattern. The observed amorphisation of the halloysite reinforcing phase takes place as a result of disruptions in the packet structure, which is consistent with the observations included in the works [64–66].

The influence of a fraction of brittle reinforcement on the progress of the mechanical synthesis process can be explained in two ways [63]. Cold plastic deformation is the driving force of a welding process occurring during mechanical milling. It should be noted, though, that a deformation smaller than a critical value does not cause welding, and the presence of reinforcing particles between the matrix particles during joining them is increasing the local degree of deformation, therefore, a critical value enabling welding is exceeded. In addition, local growth in the degree of deformation caused by reinforcing particles arranged in the matrix is also causing local strain hardening which is supporting fragmentation in the next stage. The reinforcing phases accelerating the cracking mechanisms are also expediting the process of mechanical milling. The presence of fine, hard and brittle particles acting as 'micro grinding mediums' largely increasing the process energy is another phenomenon that may be decisive for an increased deformation, thus for acceleration of structural changes in mechanical milling. To summarise, the presence of reinforcing particles is supportive to a higher degree of deformation and thus accelerates milling.

http://dx.doi.org/10.5772/65399

As shown, the use of mechanical milling leads to a high degree of deformation, which–coupled with a decreased size of grain below 100 nm and the dispersion of the reinforcing refined particles—is reinforcing the material, as best illustrated by increased hardness of powders of composite materials [67, 68]. Evolution in the morphology and size of particles of milled composite powders in the initial phase does not differ between the applied types of reinforcement. Because of higher plasticity of AlMg1SiCu powder alloy and, potentially, because of dynamic recrystallisation, the cold welding mechanism is a dominant mechanism during milling in a ball mill, leading to the formation of large particles (**Figure 4a**). If MWCNTs are added, powders are more reinforced, hence particles are produced with a much smaller size. The difference in the size and shape of particles is decreased with longer milling time. **Figure 4b** compares the grain distribution of AlMg1SiCu aluminium alloy powder with a 5% volume fraction of MWCNTs subjected to high-energy milling after 10 h of milling. All the analysed distributions are unimodal. As the milling time is increasing, the range of particle size (distribution curve shape) is decreasing because the cracking of particles was the dominant mechanism during mechanical milling. The particles are smaller and smaller, the quantile value q0,9 for the ground AlMg1SiCu alloy powder decreases from 291 μm for 5 h of milling to 224 μm for 10 h of milling. Analogously, the quantile value q0,9 for the ground alloy powders with the volume fraction of 2 and 5% of MWCNTs is decreasing in the range of, respectively, 184–153 μm and 77–75 μm. The average size of particles is decreasing as the fraction of MWCNTs is increasing. Powders with the volume fraction of 5% of MWCNTs have the smallest particle size. An X-ray analysis of the milled powders of nanocomposite materials has shown the occurrence of phase α-Al only (**Figure 4c**). No visible reflections coming from carbon structures were identified despite a high maximum volume fraction of MWCNTs (5% vol.) in AlMg1SiCu alloy powders subjected to mechanical synthesis. The reflections coming from carbon structures were identified in the extruded composite materials. The Al_4C_3 phase was identified (**Figure 5a, b**).

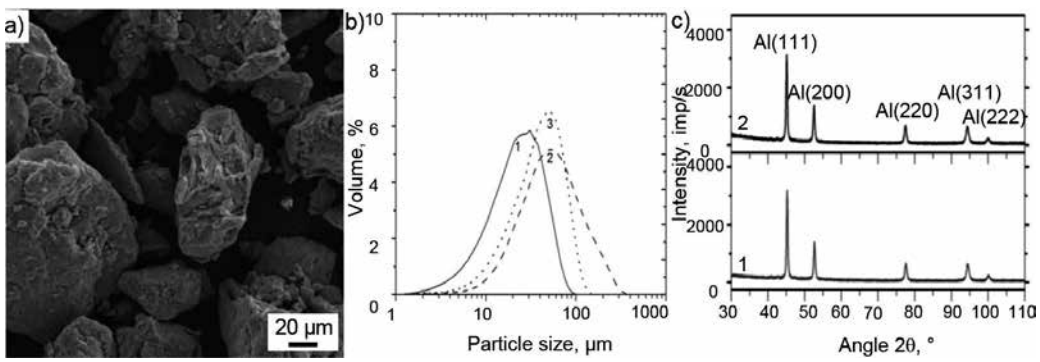

Figure 4. (a) Morphology of AlMg1SiCu alloy powder with fraction of 5% of MWCNTs by mass subject to high-energy milling for 10 h, (b) comparison of the grain distribution of AlMg1SiCu (1) alloy powder and AlMg1SiCu alloy powder with 2% (2) and 5% (3) volume fraction of MWCNTs subjected to high-energy milling for 5 and 10 h, (c) X-ray diffraction pattern of unmilled AlMg1SiCu alloy powder, milled with volume fraction of 2% (1) and 5% (2) of MWCNTs for 10 h.

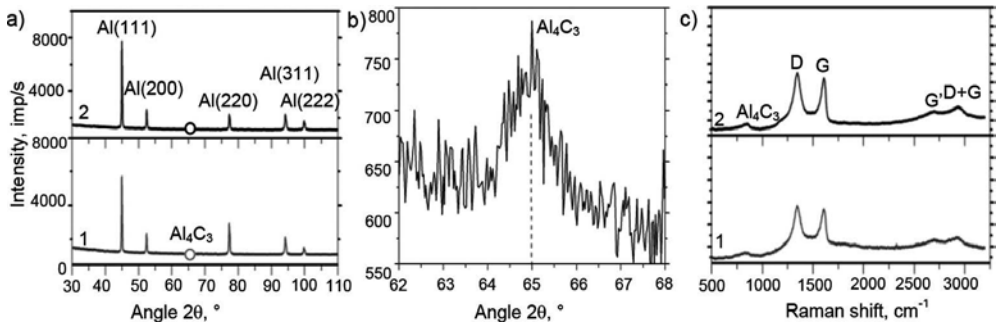

Figure 5. (a) X-ray diffraction pattern of nanocomposite material with volume fraction of 2% (1) and 5% (2) of MWCNTs for 10 h, (b) magnification of the peak of Al_4C_3 phase, (c) Raman spectrum of nanocomposite material with volume fraction of 2% (1) and 5% (2) of MWCNTs milled for 10 h.

Figure 5c shows Raman spectra of nanocomposite material powders with the volume fraction of 2 and 5% of MWCNTs subjected to high-energy milling for 10 h. The bands (D and G, G′) distinctive for MWCNTs confirm the presence of carbon nanotubes in AlMg1SiCu alloy powder. It was found as a result of a spectral analysis that the intensity of band D is higher for all powders as compared to the band existing for MWCNTs themselves, which signifies a higher number of defects, carbon impurities with sp^3 bonds and defects on the side walls as a result of breaking sp^2 bonds created in high-energy mechanical milling. The intensity of the G′ bands has decreased significantly as a result of defects. Moreover, the Raman spectra show the presence of the Al_4C_3 phase.

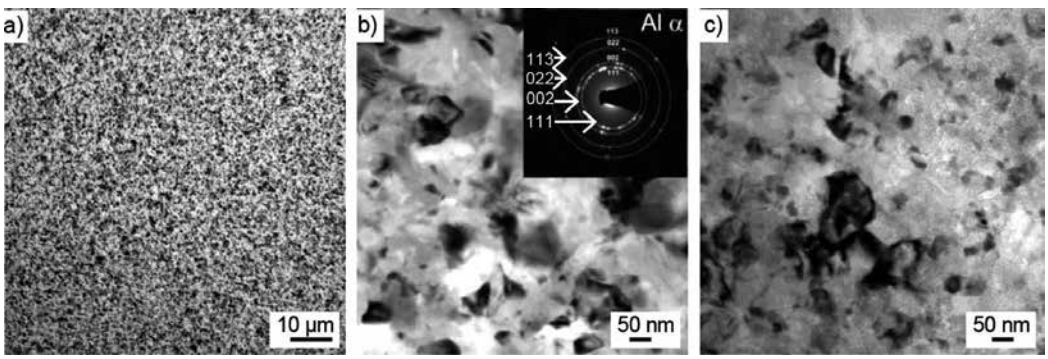

Figure 6. (a) Structure of nanocomposite material produced from AlMg1SiCu alloy powder with volume fraction of 5 and 10% of HNTs after 6 h of mechanical milling (light microscope), (b, c) structure of thin foils of materials produced by mechanical milling for 6 h and by hot pressing of (b) AlMg1SiCu alloy (c) composite material reinforced with 10% volume fraction of HNTs.

Due to the fact that the agglomeration of particles being the reinforcement of composite materials deteriorates their mechanical properties, the basic requirement posed for materials being their components is to demonstrate better properties by distributing the reinforcing

http://dx.doi.org/10.5772/65399

material uniformly in the matrix [69, 70]. Although the process of plastic consolidation by hot pressing supports the formation of a homogenous structure free of any unfavorable clusters of particles being the reinforcement of composite materials, the agglomerations of such particles are formed depending on their size, geometry, the electric charge collected on the surface, the type of material, as well as differences in their density, which are the most frequent reasons why composite materials lose their properties [63]. Halloysite reinforcing phases in the achieved composite materials are distributed very uniformly, and rarely create clusters, which only exist for composite materials reinforced with fossil halloysite. The proof that consolidation is carried out correctly is also the material achieved with a very fine structure (**Figure 6a**), deprived of any agglomerates of reinforcing particles. Slight structural fibrousness in the cross section parallel to the direction of extrusion exists in some cases only, which is associated with the extension of the original boundaries of dispersed particles of the composite material. The observations are the same as presented in the works [71, 72].

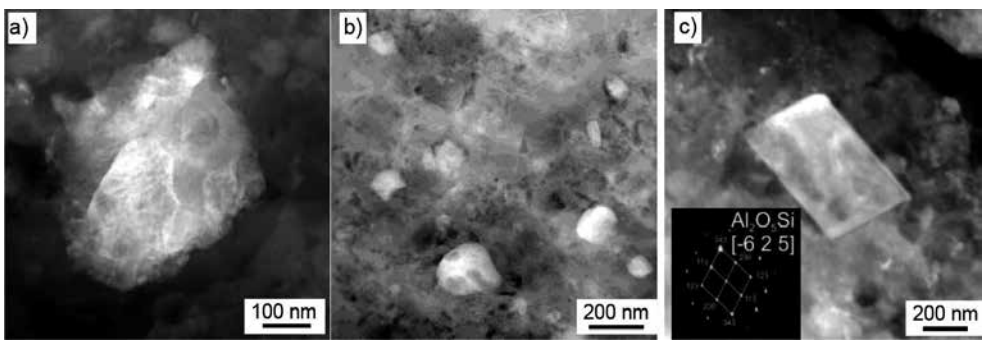

Figure 7. The structure of the aluminium alloy AlMg1SiCu composite material with reinforcement of the 15% halloysite nanotubes with the primary intermetallic phases: (a) $AlFe_3$, (b) $Al_4(Fe, Cr, Mn)Si_{0.74}$, (c) Al_2O_5Si (TEM).

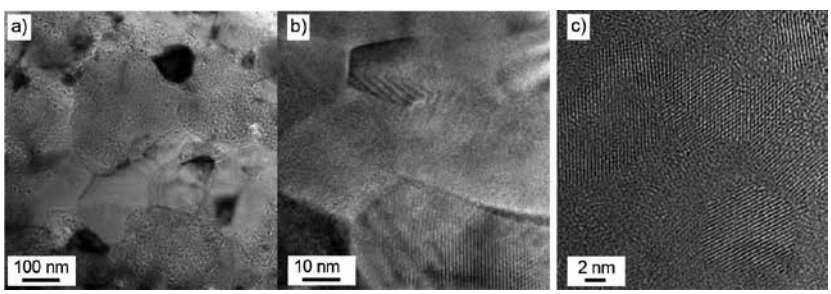

Figure 8. The structure of the aluminium alloy AlMg1SiCu composite material with reinforcement of the 15% halloysite nanotubes: (a) after mechanical alloying (STEM mode using the energy-filtered TEM microscopy technique), (b) and (c) with the occurrence of nanometric grains even 5–10 nm in the matrix (HRTEM).

The observations carried out in the scanning-transmission mode (**Figure 6b, c**) showed that —apart from a highly fine structure—the studied composite materials consist of two phases

with a contrasting structure. The lack of pores, voids and the tightly adhering phases signify that the matrix and reinforcement particles are well bonded during mechanical synthesis as well as in plastic consolidation. Examinations in the transmission mode also allowed to identify the presence of a solid aluminium solution with nanometric grains, intermetallic primary phases $AlFe_3$ and $Al_4(Fe,Cr,Mn)Si_{0.74}$ and Al_2O_5Si phase (**Figure 7**) created most probably during the mechanical milling process. Convincing evidence of diffraction signifying the existence of other primary or secondary phases was not achieved. A highly fine structure, especially the existence of grains with the size of several nanometres, was shown by means of high-resolution electron microscopy (**Figure 8**).

HNT content in Al alloy powder, vol.%	Milling time, h	Microhardness, $HV_{0.1}$
AlMg1SiCu	Unmilled	61
AlMg1SiCu/5% HNT	3	97
	6	122
AlMg1SiCu/10% HNT	3	103
	6	130

Table 3. Microhardness of the extruded composites reinforced with HNTs.

A high degree of plastic deformation, a fine structure with nanometric sizes, as well as dispersive reinforcement with particles of halloysite and oxides, all caused by mechanical milling, have an obvious effect on a nearly threefold growth of microhardness. It was found, however, that after plastic consolidation, microhardness of the created materials fell by 30% compared to the milled powders, which may be connected with recovery and partial recrystallisation caused by the effect of higher temperature in extrusion. Nevertheless, the produced composite materials are characterised by microhardness ranging between 110 and 150 $HV_{0.1}$ (**Table 3**), which clearly exceeds the values attained for a conventional EN AW-AlMg1SiCu alloy even after correct heat treatment [73, 74].

The same as for composite materials reinforced with halloysite nanotubes, the materials reinforced with MWCNTs produced in high-energy mechanical milling and hot pressing are characterised by the lack of matrix structure discontinuities (**Figure 9a**). The lack of structure discontinuities and cracks means that powder consolidation was performed correctly.

Structure examinations in a high-resolution transmission electron microscope were carried out on a nanocomposite material with the fraction volume of 5% vol. of MWCNTs fabricated from powder milled for 10 h. The examined material has a homogenous, nanocrystalline structure. This is confirmed by images obtained in the transmission mode. Grains are symmetric, nearly ball-shaped, and their size is about 50–70 nm (**Figure 9b, c**). A diffraction SAED image is characteristic for polycrystalline (nanocrystalline) materials. Two lines are present, characteristics for aluminium carbide, which do not exist in aluminium. **Figure 10** shows well-dispersed MWCNTs in the matrix of the extruded AlMg1SiCu matrix composite as well as the structure of the Al_4C_3 carbides formed as a result of the interaction between the outer shells of carbon

http://dx.doi.org/10.5772/65399

nanotubes (CNTs) and the Al matrix during mechanical alloying in the extruded AlMg1SiCu matrix composite reinforced with MWCNTs.

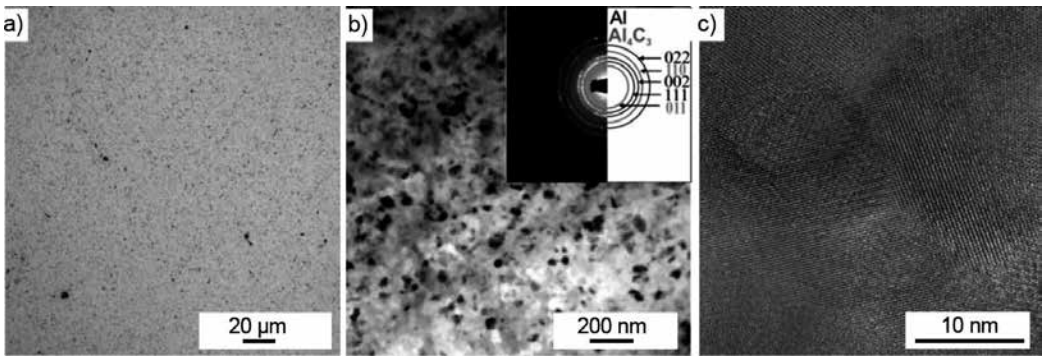

Figure 9. (a) Structure of nanocomposite material produced from AlMg1SiCu alloy powder with volume fraction of 5% of MWCNTs after 10 h of mechanical milling (light microscope), (b) structure of thin foil of nanocomposite material reinforced with 5% vol. of MWCNTs after 10 h of mechanical milling (TEM), (c) nanostructural grains in the matrix.

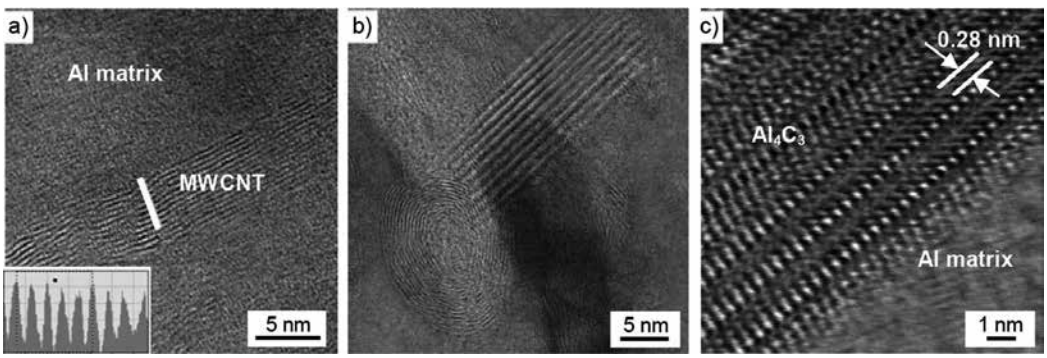

Figure 10. The structure of the extruded AlMg1SiCu matrix composite reinforced with MWCNTs, (a) well-dispersed MWCNTs in the matrix of the extruded AlMg1SiCu matrix composite, (b) and (c) the Al_4C_3 carbides formed as a result of the interaction between the outer shells of CNTs and the Al matrix during mechanical alloying in the extruded AlMg1SiCu matrix composite reinforced with MWCNTs (HRTEM).

Nanocomposite materials with a matrix made of AlMg1SiCu aluminium alloys reinforced with carbon nanotubes exhibit—in relation to a pure alloy acting as a matrix—much better mechanical properties, including compressive strength (**Figure 11**). **Table 4** shows the results of microhardness measurements of the achieved nanocomposite materials depending on the fraction of a reinforcing phase and milling time.

Nanocomposite hardness is increasing along with the growing fraction of carbon nanotubes, as well as milling time. The microhardness of nanocomposite materials reaches values higher than the microhardness of the input alloy. The hardness of nanocomposite materials is rising as the fraction of a reinforcing phase is rising. It was found that the addition of MWCNTs with

the fraction of 5% by vol. increases hardness by nearly 200% as compared to the hardness of material produced from the input, unmilled powder. The highest microhardness of 168 ± 7 HV is seen for a nanocomposite material reinforced with 5% vol. of MWCNTs, fabricated from powder milled for 10 h and is higher by 55% than the hardness of the extruded AlMg1SiCu alloy produced from powder milled over the same time.

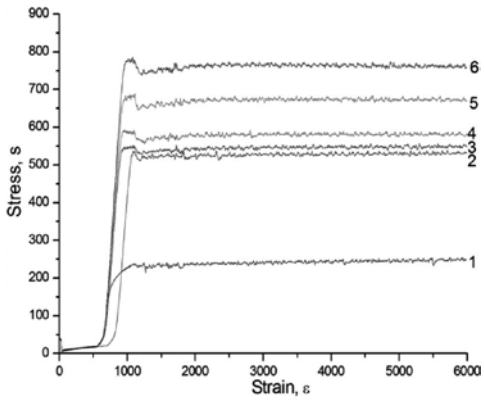

Figure 11. Compression test curves of the aluminium alloy EN AW-AlMg1SiCu composite materials with reinforcement of the different concentrations of carbon nanotubes: 1—AlMg1SiCu, 2—AlMg1SiCu/0%MWCNTs, 3–AlMg1SiCu/0.5%MWCNTs, 4–AlMg1SiCu/2%MWCNTs, 5—AlMg1SiCu/3.5%MWCNTs, 6—AlMg1SiCu/5%MWCNTs.

MWCNT content in Al alloy powder, vol.%	Milling time, h	Microhardness, $HV_{0.1}$
AlMg1SiCu	Unmilled	61
AlMg1SiCu/2% MWCNT	5	132
	10	157
AlMg1SiCu/5% MWCNT	5	158
	10	168

Table 4. Microhardness of the nanocomposites.

4. General remarks

Nanocomposite materials with a matrix made of AlMg1SiCu aluminium alloys, reinforced with carbon or halloysite nanofibers, manufactured by high-energy mechanical synthesis or low-energy mixing, cold consolidation and hot pressing, according to the developed custom original technology, exhibit much better mechanical properties in relation to the matrix alloy. Microhardness and compressive strength of the materials containing 5% of multiwalled carbon nanotubes during high-energy milling is rising nearly threefold. If 15% of halloysite nanotubes is added, this leads to a nearly threefold reduction in volume loss in abrasion tests. Strong

http://dx.doi.org/10.5772/65399

plastic deformations and a grain size reduction below 100 nm and the dispersion of reinforcing particles, all caused by mechanical milling, is substantially reinforcing the composite materials reinforced with carbon and halloysite nanotubes. A structure of nanograins, crushed even to the size of 5–10 nm, is particularly a structural cause of enhanced mechanical properties. This is explained using a high-resolution transmission electron microscope (HRTEM). In the case of carbon nanotubes, the matrix is reinforced with such nanotubes. Moreover, as a result of interactions between the external layer of carbon nanotubes and Al during mechanical alloying, the degree of defects of carbon nanotubes is increased as a result of interactions at the matrix-reinforcement boundary. Needle-like precipitates of Al_4C_3 carbide also occur, which are then crystallised during plastic consolidation at an elevated temperature. Al_4C_3 carbide is most probably not influencing positively the ductility of the composite material. Additional reinforcement with primary intermetallic phases, i.e., with $AlFe_3$ and $Al_4(Fe,Cr,Mn)Si_{0.74}$ and with the Al_2O_5Si phase, which is created most certainly during mechanical milling, is taking place in the nanocomposite materials reinforced with halloysite nanotubes. The composite materials produced in mechanical synthesis and hot pressing are characterised by a structure of uniformly arranged, fine reinforcing phase particles in a fine-grained matrix of AlMg1SiCu alloy. The examinations of the structure of the newly developed nanostructured composite materials reinforced with halloysite and carbon nanotubes prove that a mechanical milling process allows to improve the arrangement of reinforcing particles in the matrix material. A homogenous structure with uniformly arranged reinforcing particles can be achieved by applying a reinforcement with halloysite and carbon nanotubes, if short time of milling is used, thus eliminating an issue of their agglomeration; it also allows to achieve more advantageous functional properties.

5. Additional information

The investigations were made mainly in the framework of the project "NANOCOPOR—Determining the importance of the effect of the one-dimensional nanostructural materials on the structure and properties of newly developed functional nanocomposite and nanoporous materials", funded by the DEC-2012/07/B/ST8/04070 of the Polish National Science Centre in the framework of the "OPUS" competitions, headed by Prof. Leszek A. Dobrzański.

Author details

Leszek A. Dobrzański*, Błażej Tomiczek and Magdalena Macek

*Address all correspondence to: leszek.adam@gmail.com

Institute of Engineering Materials and Biomaterials, Faculty of Mechanical Engineering, Silesian University of Technology, Gliwice, Poland

References

[1] Bonollo F, Ceschini L, Garagnani GL. Mechanical and impact behaviour of $(Al_2O_3)_p$/2014 and (Al_2O_3)p/6061 Al metal matrix composites in the 25–200 °C range. Applied Composite Materials. 1998;4:173–185. DOI: 10.1007/bf02481779

[2] Dobrzański LA, Kremzer M, Nagel A. Structure and properties of ceramic preforms based on Al_2O_3 particles. Journal of Achievements in Materials and Manufacturing Engineering. 2009;35:7–13

[3] Dobrzański LA, Włodarczyk A, Adamiak M. Structure, properties and corrosion resistance of PM composite materials based on EN AW-2124 aluminum alloy reinforced with the Al_2O_3 ceramic particles. Journal of Materials Processing Technology. 2005;162:27–32. DOI: 10.1016/j.jmatprotec.2005.02.006

[4] Gómez de Salazar JM, Barrena MI. The influence of Si and Mg rich phases on the mechanical properties of 6061 Al-matrix composites reinforced with Al_2O_3. Journal of Materials Science. 2002;37:1497–1502. DOI: 10.1023/a:1014967324577

[5] Fogagnolo JB, Pallone EMJA, Martin DR, Kiminami CS, Bolfarini C, Botta WJ. Processing of Al matrix composites reinforced with Al-Ni compounds and Al_2O_3 by reactive milling and reactive sintering. Journal of Alloys and Compounds. 2009;471:448–452. DOI: 10.1016/j.jallcom.2008.03.125

[6] Fogagnolo JB, Robert MH, Ruiz-Navas EM, Torralba JM. 6061 Al reinforced with zirconium dibromide particles processed by conventional powder metallurgy and mechanical alloying. Journal of Materials Science. 2004;39:127–132. DOI: 10.1023/b:jmsc.0000007736.03608.e5

[7] Lewandowska M, Dybiec H, Kulczyk M, Latuch J, Kurzydlowski KJ. Nano-refinement, nano-consolidation: Different fabrication routes of nano-crystalline aluminium alloys. Materials Science Forum. 2011;667–669:87–90. DOI: 10.4028/www.scientific.net/msf.667-669.87

[8] Pakieła Z, Garbacz H, Lewandowska M, Drużycka-Wiencek A, Suś-Ryszkowska M, Zieliński W, Kurzydłowski KJ. Structure and properties of nanomaterials produced by severe plastic deformation. Nukleonika. 2006;51:19–25

[9] Son HT, Kim TS, Suryanarayana C, Chun BS. Homogeneous dispersion of graphite in a 6061 aluminum alloy by ball milling. Materials Science and Engineering A. 2003;348:163–169 DOI: 10.1016/s0921-5093(02)00749-9

[10] Wong SC, Sutherland EM, Uhl RM. Materials processes of graphite nanostructured composites using ball milling. Materials and Manufacturing Processes. 2006;20:159–166. DOI: 10.1081/amp-200068659

[11] Esawi AMK, Morsi K, Sayed A, Abdel Gawad A, Borah P. Fabrication and properties of dispersed carbon nanotube-aluminium composites. Materials Science and Engineering, A. 2009;508:167–173. DOI: 10.1016/j.msea.2009.01.002

[12] Morsi K, Esawi AMK, Lankaa S, Sayedb A, Taherb M. Spark plasma extrusion (SPE) of ball-milled aluminium and carbon nanotube reinforced aluminium composite powders. Composites Part A. 2010;41:322–326. DOI: 10.1016/j.compositesa.2009.09.028

[13] Peng T, Chang I. Mechanical alloying of multi-walled carbon nanotubes reinforced aluminium composite powder. Powder Technology. 2014;266:7–15. DOI: 10.1016/j.powtec.2014.05.068

[14] Dobrzańska-Danikiewicz AD, Cichocki D, Pawlyta M, et al. Synthesis conditions of carbon nanotubes with the chemical vapor deposition method. Physica Status Solidi B. 2014;251(12):2420–2425. DOI: 10.1002/pssb.201451178

[15] Bradbury CR, Gomon JK. Hardness of multi wall carbon nanotubes reinforced aluminium matrix composites. Journal of Alloys and Compounds. 2014;585:362–367. DOI: 10.1016/j.jallcom.2013.09.142

[16] Hanzel O, Sedlacek J, Sajgalik P. New approach for distribution of carbon nanotubes in alumina matrix. Journal of the European Ceramic Society. 2014;34:1845–1851. DOI: 10.1016/j.jeurceramsoc.2014.01.020

[17] Javadi AH, Mirdamadi Sh, Faghihisani MA, Shakhesi S, Soltani R. Fabrication of well-dispersed, multiwalled carbon nanotubes-reinforced aluminum matrix composites. New Carbon Materials. 2012;27:161–165. DOI: 10.1016/s1872-5805(12)60010-9

[18] Dobrzańska-Danikiewicz AD, Łukowiec D. Synthesis and characterization of Pt/MWCNTs nanocomposites. Physica Status Solidi B. 2013;250(12):2569–2574. DOI: 10.1002/pssb.201300083

[19] Opelt CV, Becker D, Lepienski CM, Coelho LAF. Reinforcement and toughening mechanism in polymer nanocomposites—carbon nanotubes and aluminum oxide. Composites Part B. 2015;75:119–126. DOI: 10.1016/j.compositesb.2015.01.019

[20] Oueiny C, Berlioz S, Perrin FX. Carbon nanotube—polyaniline composites. Progress in Polymer Science. 2014;39:707–748. DOI: 10.1016/j.progpolymsci.2013.08.009

[21] BCC Research. Ceramic Matrix Composites, Report GB-110R. Business Communications Company, Inc. Norwalk, CT [Internet]. 2000. Available from: http://www.bccresearch.com/market-research/advanced-materials/AVM014C.html [Accessed: 2016-02-20]

[22] Abdullayev E, Price R, Shchukin D, Lvov Y. Halloysite tubes as nanocontainers for anticorrosion coating with benzotriazole. Applied Materials and Interfaces. 2009;1:1437–1443. DOI: 10.1021/am9002028

[23] Deng S, Zhang J, Ye L, Wu J. Toughening epoxies with halloysite nanotubes. Polymer. 2008;49:5119–5127. DOI: 10.1016/j.polymer.2008.09.027

[24] Du M, Guo B, Jia D. Thermal stability and flame retardant effects of halloysite nanotubes on poly(propylene). European Polymer Journal. 2006;42:1362–1369. DOI: 10.1016/j.eurpolymj.2005.12.006

[25] Ismial H, Pasbakhsh P, Ahmad Fauzi MN, Abu Bakar A. Morphological, thermal and tensile properties of halloysite nanotubes filled ethylene propylene diene monomer (EPDM) nanocomposites. Polymer Testing. 2008;27:841–850. DOI: 10.1016/j.polymertesting.2008.06.007

[26] Dobrzański LA, Tomiczek B, Adamiak M, Gołombek K. Mechanically milled aluminium matrix composites reinforced with halloysite nanotubes. Journal of Achievements in Materials and Manufacturing Engineering. 2012;55:654–660

[27] Dobrzański LA, Tomiczek B, Adamiak M. Manufacturing of EN AW6061 matrix composites reinforced by halloysite nanotubes. Journal of Achievements in Materials and Manufacturing Engineering. 2011;49:82–89

[28] Marney DCO, Russell LJ, Wu DY, Nguyen T, Cramm D, Rigopoulos N, Wright N, Greaves M. The suitability of halloysite nanotubes as a fire retardant for nylon 6. Polymer Degradation and Stability. 2008;93:1971–1978. DOI: 10.1016/j.polymdegradstab.2008.06.018

[29] Sakiewicz P, Nowosielski R, Pilarczyk W, Gołombek K, Lutyński M. Selected properties of the halloysite as a component of Geosynthetic Clay Liners (GCL). Journal of Achievements in Materials and Manufacturing Engineering. 2011;48:177–191

[30] Yan L, Jiang J, Zhang Y, Liu J. Preparation and characterization of large-size halloysite nanotubes particles by a combined technique of interfacial polymerization and condensation polymerization. Journal of Nanoparticle Research. 2011;13:6555–6561. DOI: 10.1007/s11051-011-0561-2

[31] Ning N, Yin Q, Luo F, Zhang Q, Du R, Fu Q. Crystallization behavior and mechanical properties of polypropylene/halloysite composites. Polymer. 2007;48:7374–7384. DOI: 10.1016/j.polymer.2007.10.005

[32] Liu M, Guo B, Du M, Chen F, Jia D. Halloysite nanotubes as a novel β-nucleating agent for isotactic polypropylene. Polymer. 2009;50:3022–3030. DOI: 10.1016/j.polymer.2009.04.052

[33] Tang Y, Deng S, Ye L, Yang C, Yuan Q, Zhang J, Zhao C. Effects of unfolded and intercalated halloysites on mechanical properties of halloysite-epoxy nanocomposites. Composites Part A. 2011;42:345–354. DOI: 10.1016/j.compositesa.2010.12.003

[34] Yuan P, Southon PD, Liu Z, Green MER, Hook JM, Antill SJ, Kepert CJ. Functionalization of halloysite clay nanotubes by grafting with γ-aminopropyltriethoxysilane. The Journal of Physical Chemistry C. 2008;112:15742–15751. DOI: 10.1021/jp805657t

[35] Zhang L, Wang T, Liu P. Polyaniline-coated halloysite nanotubes via in-situ chemical polymerization. Applied Surface Science. 2008;255:2091–2097. DOI: 10.1016/j.apsusc.2008.06.187

[36] Chou WJ, Wang CC, Chen CY. Characteristics of polyimide-based nanocomposites containing plasma-modified multi-walled carbon nanotubes. Composite Science and Technology. 2008;68:2208–2213. DOI: 10.1016/j.compscitech.2008.04.008

[37] Hayashi T, Endo M. Carbon nanotubes as structural material and their application in composites. Composites Part B. 2011;42:2151–2157. DOI: 10.1016/j.compositesb.2011.05.011

[38] Sandler J, Shaffer MSP, Prasse T, Bauhofer W, Schulte K, Windle AH. Development of a dispersion process for carbon nanotubes in an epoxy matrix and the resulting electrical properties. Polymer. 1999;40:5967–5971. DOI: 10.1016/s0032-3861(99)00166-4

[39] Yamamot G, Shirasu K, Nozaka Y, Wang W, Hashida T. Microstructure-property relationships in pressureless-sintered carbon nanotube/alumina composites. Materials Science & Engineering A. 2014;617:179–186 DOI: 10.1016/j.msea.2014.08.068

[40] Kasperski A, Weibel A, Estournès C, Laurent Ch, Peigney A. Multi-walled carbon nanotube-Al_2O_3 composites: Covalent or non-covalent functionalization for mechanical reinforcement. Scripta Materialia. 2014;75:46–49 10.1016/j.scriptamat.2013.11.015

[41] Aung NN, Zhou W, Goh CS, Nai SML, Wei J. Effect of carbon nanotubes on corrosion of Mg-CNT composites. Corrosion Science. 2010;52:1551–1553. DOI: 10.1016/j.corsci.2010.02.025

[42] Kondoh K, Fukuda H, Umeda J, Imai H, Fugetsu B. Microstructural and mechanical analysis of carbon nanotubes reinforced magnesium alloy powder composite. Material Science and Engineering A. 2010;527:4103–4108. DOI: 10.1016/j.msea.2010.03.049

[43] Dobrzański LA, Macek M, Tomiczek B. Effect of carbon nanotubes content on morphology and properties of AlMg1SiCu matrix composite powders. Archives of Materials Science and Engineering. 2014;69:12–18

[44] Tomiczek B, Dobrzański LA, Macek M. Effect of milling time on microstructure and properties of AA6061/MWCNT composites. Archives of Metallurgy and Materials. 2015;60:3017–3022. DOI: 10.1515/amm-2015-0484

[45] Choi HJ, Shin JH, Bae DH. The effect of milling conditions on microstructures and mechanical properties of Al/MWCNT composites. Composites Part A. 2012;43:1061–1072 DOI: 10.1016/j.compositesa.2012.02.008

[46] Li H, Kang J, He C, N Zhao, Liang C, Li B. Mechanical properties and interfacial analysis of aluminum matrix composites reinforced by carbon nanotubes with diverse structures. Material Science & Engineering A. 2013;577:120–124. DOI: 10.1016/j.msea.2013.04.035

[47] Bakshi SR, Singh V, Seal S, Agarwal A. Aluminum composite reinforced with multi-walled carbon nanotubes from plasma spraying of spray dried powders. Surface & Coating Technology. 2009;203:1544–1554. DOI: 10.1016/j.surfcoat.2008.12.004

[48] Ko S, Kim B, Kim Y, Kim TY, Kim TK, McKay BJ, Shin JS. Manufacture of CNTs-Al powder precursors for casting of CNTs-Al matrix composites. Materials Science Forum. 2013;765:353–357 DOI: 10.4028/www.scientific.net/msf.765.353

[49] Wu Y, Kim GY. Carbon nanotubes reinforced aluminum composite fabricated by semi-solid powder processing. Journal of Materials Processing Technology. 2011;211:1341–1347. DOI: 10.1016/j.jmatprotec.2011.03.007

[50] Kwon H, Park DH, Silvain JF, Kawasaki A. Investigation of carbon nanotube reinforced aluminum matrix composite materials. Composites Science and Technology. 2010;70:546–550. DOI: 10.1016/j.compscitech.2009.11.025

[51] Laha T, Chen Y, Lahiri D, Agarwal A. Tensile properties of carbon nanotube reinforced aluminum nanocomposite fabricated by plasma spray forming. Composites Part A. 2009;40:589–594. DOI: 10.1016/j.compositesa.2009.02.007

[52] Han BQ, Langdon TG. Achieving enhanced tensile ductility in an Al-6061 composite processed by severe plastic deformation. Materials Science and Engineering A. 2005;410–411:430–434. DOI: 10.1016/j.msea.2005.08.045

[53] Izadi H, Gerlich AP. Distribution and stability of carbon nanotubes during multi-pass friction stir processing of carbon nanotube/aluminum composites. Carbon. 2012;50:4744–4749. DOI: 10.1016/j.carbon.2012.06.012

[54] Stein J, Lenczowski B, Fréty N, Anglaret E. Mechanical reinforcement of a high-performance aluminium alloy AA5083 with homogenously dispersed multi-walled carbon nanotubes. Carbon. 2012;50:2264–2272. DOI: 10.1016/j.carbon.2012.01.044

[55] Esawi AMK, Morsi K, Sayed A, Taher M, Lanka S. Effect of carbon nanotube (CNT) content on the mechanical properties of CNT-reinforced aluminium composites. Composites Science and Technology. 2010;70:2237–2241. DOI: 10.1016/j.compscitech.2010.05.004

[56] Singhal SK, Pasricha R, Jangra M, Chahal R, Teotia S, Mathur RB. Carbon nanotubes: Amino functionalization and its application in the fabrication of Al-matrix composites. Powder Technology. 2012;215–216:254–263. DOI: 10.1016/j.powtec.2011.10.013

[57] Macek M. Structure and properties of the aluminium matrix nanocomposites materials reinforced with multiwalled carbon nanotubes. Ph.D. Thesis, Silesian University of Technology, Gliwice, Poland; 2016 (in Polish)

[58] Tomiczek B, Pawlyta M, Adamiak M, Dobrzański LA. Effect of milling time on microstructure of AA6061 composites fabricated via mechanical alloying. Archives of Metallurgy and Materials. 2015;60:789–793. DOI: 10.1515/amm-2015-0208

[59] Dobrzański LA, Tomiczek B, Matula G, Gołombek K. Role of halloysite nanoparticles and milling time on the synthesis of AA 6061 aluminium matrix composites. Advanced Materials Research. 2014;939:84–89. DOI: 10.4028/www.scientific.net/amr.939.84

[60] Tomiczek B, Dobrzański LA. Composite materials based on EN AW-AlMg1SiCu aluminium alloy reinforced with halloysite particles. Journal of Achievements in Materials and Manufacturing Engineering. 2013;61:39–46

[61] Tomiczek B. Structure and properties of nanostructural composite materials reinforced with halloysite. Ph.D. Thesis, Silesian University of Technology, Gliwice, Poland; 2013 (in Polish)

[62] Dobrzański LA. Applications of newly developed nanostructural and microporous materials in biomedical, tissue and mechanical engineering. Archives of Materials Science and Engineering. 2015;76:53–114

[63] Fogagnolo JB, Velasco F, Robert MH, Torralba JM. Effect of mechanical alloying on the morphology, microstructure and properties of aluminium matrix composite powders. Materials Science and Engineering A. 2003;342:131–143. DOI: 10.1016/s0921-5093(02)00246-0

[64] Vizcayno C, de Gutiérrez RM, Castello R, Rodriguez E, Guerrero CE. Pozzolan obtained by mechanochemical and thermal treatments of kaolin. Applied Clay Science. 2010;49:405–413. DOI: 10.1016/j.clay.2009.09.008

[65] Valášková M, Barabaszová K, Hundáková M, Ritz M, Plevová E. Effects of brief milling and acid treatment on two ordered and disordered kaolinite structures. Applied Clay Science. 2011;54: 70–76. DOI: 10.1016/j.clay.2011.07.014

[66] Schmücker M, Schneider H, MacKenzie KJD. Mechanical amorphization of mullite and thermal recrystallization. Journal of Non-Crystalline Solids. 1998;226:99–104. DOI: 10.1016/s0022-3093(98)00366-4

[67] Suryanarayana C. Mechanical alloying and milling. Progress in Materials Science. 2001;46:1–184. DOI: 10.1016/s0079-6425(99)00010-9

[68] Tomiczek B, Dobrzański LA. Structure and selected properties of the composite materials reinforced with halloysite nanotubes. Works of the 40th School of Materials Engineering. Monograph. Cracow. 2012;293–298 (in Polish)

[69] Moon KI, Oh MS, Lee KS. Tensile properties of nitride dispersed Al-Ti alloy synthesized by reactive ball milling in N_2 gas. Journal of Alloys and Compounds. 2000;302: 227–234. DOI: 10.1016/s0925-8388(99)00785-9

[70] Son HT, Kim TS, Suryanarayana C, Chun BS. Homogeneous dispersion of graphite in a 6061 aluminum alloy by ball milling. Materials Science and Engineering A. 2003;348: 163–169. DOI: 10.1016/s0921-5093(02)00749-9

[71] Dybiec H, Kozak P. Mechanical properties of aluminium wires produced by plastic consolidation of fine grained powders. Solid State Phenomena. 2005;101–102: 131–134. DOI: 10.4028/www.scientific.net/ssp.101-102.131

[72] Dybiec H. Submicrostructure aluminium alloys. The AGH University of Science and Technology Press. Cracow. 2008. 116 p. (in Polish)

[73] Hirsch J, Skrotzki B, Gottstein G. editors. Aluminium Alloys. Their Physical and Mechanical Properties. Weinheim: Wiley-VCH Verlag GmbH &Co. KGaA; 2008

[74] Maisonnette D, Suery M, Nelias D, Chaudet P, Epicier T. Effects of heat treatments on the microstructure and mechanical properties of a 6061 aluminium alloy. Materials Science and Engineering A. 2011;528: 2718–2724. DOI: 10.1016/j.msea.2010.12.011

Chapter 7

Porous Selective Laser Melted Ti and Ti6Al4V Materials for Medical Applications

Leszek A. Dobrzański,
Anna D. Dobrzańska-Danikiewicz,
Anna Achtelik-Franczak, Lech B. Dobrzański,
Marek Szindler and Tomasz G. Gaweł

Additional information is available at the end of the chapter

http://dx.doi.org/10.5772/65375

Abstract

This chapter characterises scaffolds manufactured in line with the make-to-order concept according to individual needs of each patient. The clinical data acquired from a patient during computer tomography, nuclear magnetic resonance or using traditional plaster casts is converted by a computer into a virtual solid model of a patient's loss. The model, through the multiplication of a unit cell, is converted into a porous model on the basis of which an actual object is manufactured with the method of selective laser melting (SLM) from Ti/Ti6Al4V powders. The created scaffold is characterised by good mechanical properties, which is confirmed by the results of the performed tensile and compressive strength tests. The material is additionally subjected to surface treatment consisting of the deposition of atomic layers of titanium dioxide with nanometric thickness.

Keywords: porous materials, scaffolds, CAMD, SLM, ALD, mechanical properties

1. Introduction

Additive manufacturing technologies are proliferating and becoming increasingly popular across various industries nowadays. Owing to their benefits, they support the development of multiple disciplines in the field of engineering wherever a clear need exists to fabricate elements with a complicated shape, geometry and a distinctive structure. Such elements include individualised implants, representing living tissues, closely accommodated to a given patient based on the results of computer tomography or nuclear magnetic resonance or traditional plaster casts.

Porous structures are much desired in medicine, especially where a porous element is to replace a missing bone. In such a situation, the task of the fabricated element is to stimulate a regeneration process of the adjacent bone tissue through an osteoconductive and osteoinductive activity. Osteoconduction is a process of bone loss regeneration consisting of the in-growth of osteoblasts—which are bone-forming cells originating from the adjoining bone stock—into the porous implant. In osteoinduction, though, the differentiation of mesenchymal cells is stimulated in the environment of osteoblasts. The cells represent a connective embryonic tissue occurring only in the embryonic period, from which all types of connective tissues, bone tissue, cartilage tissue and muscle tissue are created. In order for titanium scaffolds fabricated with SLS technologies to fulfil their role well in a patient's organism, they should be characterised by the appropriate size of pores, appropriate porosity, as well as strength permitting usage in bone implants functioning as scaffolds, which become a substructure and a support for the bone growing into them. Literature data shows [1–12] that the size of pores allowing the development of the bone growth process into the created scaffold, varies between the minimum of 50–200 μm and the maximum of 500 μm and the porosity of such a scaffold should not exceed 50%. A satisfactory result of a manufacturing process of porous titanium materials is seen when an element is achieved with open pores, characterised by an appropriate level of porosity and sufficiently good strength properties, which should be similar to the corresponding properties of a living bone tissue. Bone porosity is referred to as the volume fraction of the fluid phase filling the pore space of a bone in a given bone volume unit. The bone fluid phase consists of blood vessels together with blood, nerve fibres, bone cells and extracellular bone fluid. A cortical bone has the density of 1.99 g/cm^3. It has the longitudinal compressive strength of 131–224 MPa and the longitudinal bending strength of 79–151 MPa. The transverse compressive strength of a cortical bone is 106–133 MPa and bending strength is 51–56 MPa [13, 14].

Additive manufacturing enables to create objects with the final shape while allowing to control the manufactured element in each part of its volume. An advantage of AM technologies, as compared to competitive fabrication methods of porous materials with space fillers [10–12], is also an ability to fabricate without applying costly and time-intensive casting moulds, as a result of which the product achieved does not contain external admixtures which are often present in cast products. The maximum possible reduction of wastes generated in a manufacturing process as compared to waste-generating machining is ranking AM technologies higher than traditional manufacturing processes applied until now. The entire additive manufacturing process takes place in an atmosphere of inert gas, which prevents the creation of unwanted products of the reactions occurring between a material used for fabrication of elements and air components. Selective laser melting (SLM) technology, due to its advantages, is very well suitable for manufacturing in line with the make-to-order concept of individualised craniofacial implants, including palate implants.

2. Computer-aided materials design

An additive manufacturing process carried out with the SLM technique begins at the sage of computer design of 3D models of objects planned to be manufactured in reality. The key

http://dx.doi.org/10.5772/65375

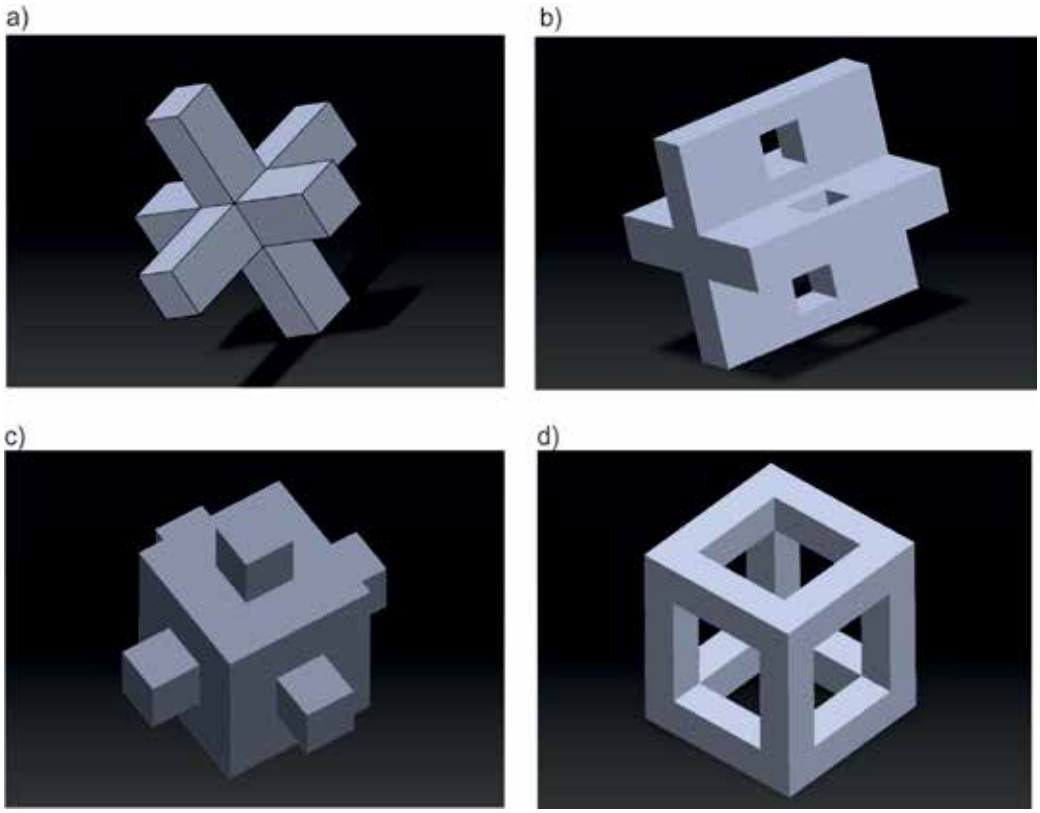

Figure 1. Unit cells according to a custom design: (a) type A: spatial cross; (b) type B: cross with openings; (c) type C: cube with tongues; (d) type D: cube skeleton.

benefit of the concept is that no constraints exist as to the shape and filling of a virtual model at the design stage; it allows representing an anatomical structure of organs, bones and human and animal tissues very accurately [15–20]. One of the specific aspects in this domain, being the subject of a series of experiments performed by the authors of this chapter, is the designing and manufacturing of porous biomimetic implants replacing a patient's palate loss. The loss may result from a genetic defect or a mechanical injury, or a neoplasm. A palate implant designed individually for each patient is a scaffold, the structure of which is made of open pores. A porous structure is to ensure appropriate growth conditions on the surface of pores for living cells by ensuring availability of nutrients. The computer-aided design of virtual models is preceded by a clinical stage at which accurate data is acquired from a patient regarding a 3D shape and dimensions of one's palate loss. The data can be acquired in the course of examinations conducted with computer tomography or nuclear magnetic resonance, or with traditional plaster casts, the shape of which is then transferred to a computer with a 3D scanner. Regardless the option chosen, the outcome of such activities is a virtual solid implant model of a palate which is further processed into a porous model.

A unit cell which, when multiplied many times, will create a porous scaffold structure, is required to create a virtual porous palate implant. A unit cell can be chosen from the avail-

able database being part of commercial software or it can be individually designed according to individual preferences. When designing a unit cell, it is significant to model it in such a way that it is symmetrical relative to all the axes of symmetry, which guarantees the correct transformation of a virtual solid model into a porous model, without errors on the created lattice. Unit cells according to a custom design are shown in **Figure 1**. All the designed unit cells inscribe themselves into a cube with the side of 500 μm. A type A cell (**Figure 1a**) has the shape of a spatial cross with arms with the dimensions of 100 × 100 μm. A type B cell (**Figure 1b**) is a cross with its arms 100 μm thick and has small quadrangle openings in such arms with the side of 100 μm. A type C cell (**Figure 1c**) is a cube with the side of 300 μm, on each wall of which tongues are arranged symmetrically in the form of smaller cubes with the side of 100 μm. A type D cell (**Figure 1d**) is a skeleton of a cube with the sides equal to 100 μm.

A solid implant model and the applied unit cell are saved in *stl* files before a virtual solid model of a piece of a palate loss is transformed into a virtual porous model. The extension is needed so that the model is transferred to a device carrying out a selective laser sintering

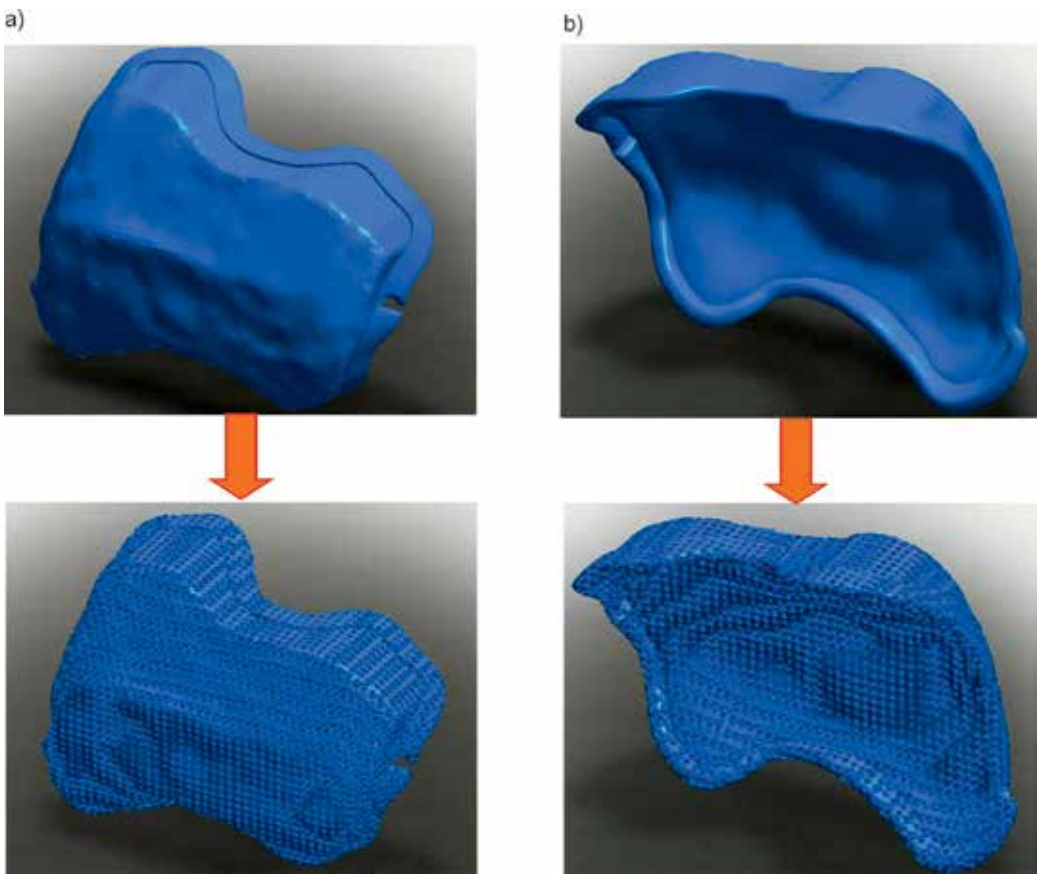

Figure 2. Virtual solid implant model and a corresponding porous model created after transformation: (a) top view; (b) bottom view.

http://dx.doi.org/10.5772/65375

(SLM) process. This ensures the automatic conversion of a virtual scaffold model into a model made of the net of triangles with the standard size of the area of a single triangle creating a net which is predefined directly by CAD software. It is possible to control the size of the area of a single triangle to densify the net, thus to control the accuracy of surface representation of an element produced having a complicated shape. If the field of a single triangle is decreased when converting the model into a net of triangles, accuracy is increased, but also the process is extended, both, at the stage of multiplication as well as at the stage of object fabrication. Highly efficient, latest generation software must therefore be used for very high accuracies. A virtual porous model created after transformation with a specifically designed structure composed of multiplied unit cells, has geometrical dimensions perfectly corresponding to the model from before the transformation (**Figure 2**).

3. Selective laser melting of scaffolds

Pristine titanium and Ti6Al4V titanium alloy, which, as per the international standard [21], is dedicated to biomedical applications, is a material used for the fabrication of actual objects which are to act as individualised palate implants. Titanium is classified as a light metal with a density of ρ = 4507 g/cm^3, a melting point of 1668°C and boiling point of 3260°C. It occurs in two allotropic variants, i.e. α and β. The α titanium variant has a hexagonal lattice (A3), which, at the temperature of 882.5°C, is converted into a high-temperature variant β crystallising in the regular system (A2). Pristine titanium occurs in the single-phase variant α and the titanium alloy Ti6Al4V in the double-phase variant α and β [22–24]. Titanium possesses high mechanical strength relative to the mass; however, its essential properties, allowing to employ it in medicine, include high biocompatibility with living tissues and pitting corrosion resistance, intercrystalline corrosion resistance and stress corrosion resistance. An input material in the form of powder must be used for the selective laser melting technology. Pristine titanium powder with the grain size of 0–45 μm and titanium Ti6Al4V alloy powder with the grain size of 15–45 μm, with the chemical composition consistent with the manufacturer's specification shown in **Table 1**, were used in the course of the experiments carried out to fabricate actual objects. The results of the qualitative chemical composition analysis performed with the EDS method (**Figure 3**) confirm the presence of the elements stated by a manufacturer in technical and commercial specifications. Powder grains in the both cases are spherically shaped, which is observable in microscopic photos (**Figure 4**).

Pristine titanium and titanium Ti6Al4V alloy powders are an input material from which porous implants for medical uses are manufactured in a selective laser sintering process. Preparatory measures are taken before the actual manufacturing process, during which, after

Powder	Al	V	C	Fe	O	N	H	Others total	Others each	Ti
Ti	–	–	0.01	0.03	0.14	0.01	. 0.004	. <0.4	. <0.01	Remainder
Ti6Al4V	6.35	4.0	0.01	0.2	0.15	0.02	0.003	≤0.4	≤0.1	

Table 1. Fraction of particular chemical elements in composition of powders subject to experiments in per cents.

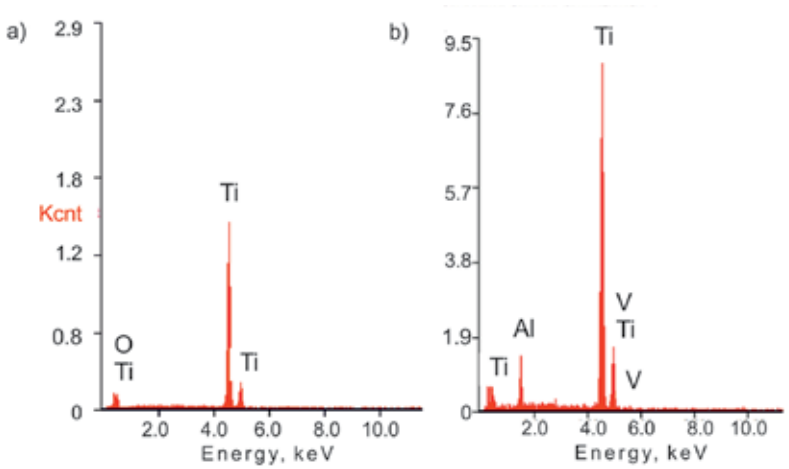

Figure 3. Results of qualitative chemical composition analysis: (a) pristine titanium; (b) TiAl6V4.

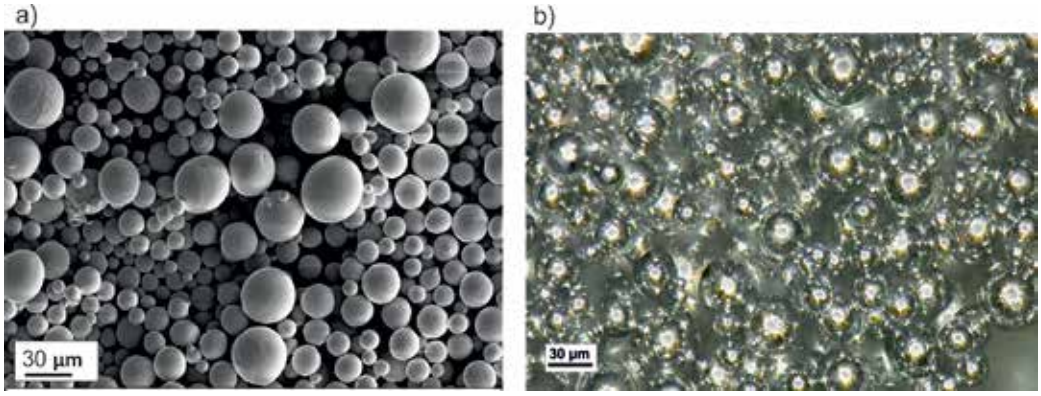

Figure 4. Powders used in laser sintering process: (a) pristine titanium; SEM image; (b) Ti6Al4V titanium alloy; image from stereoscopic microscope.

transferring a 3D virtual scaffold model to an SLM device, the virtual object is placed in a working chamber in the adequate position, i.e. on the relevant edge and under the right angle. The selection of the adequate virtual model position in a working chamber is an important aspect due to the following factors: the amount of powder needed to carry out a manufacturing process once, the mechanical properties of the scaffolds produced [25] and the number of supports needed to generate scaffolds. The purpose of the supports is to support the produced actual object and to secure it against collapse under its own weight. In the next stage, the virtual model is divided into layers parallel to the working platform surface of the device on which it is to be manufactured. The number of layers depends on the parameter set by the operator, i.e. powder layer thickness to be given before each melting. The following manufacturing conditions are also selected prior to commencing a fabrication process of an actual object: laser power, scanning rate, distance between consecutive remelting paths and the laser

http://dx.doi.org/10.5772/65375

beam diameter. Before starting the selective laser melting process, titanium powder is heated in a vacuum in the surrounding of shielding gas at an elevated temperature (160–200°C) to remove any moisture from the powder, as necessary.

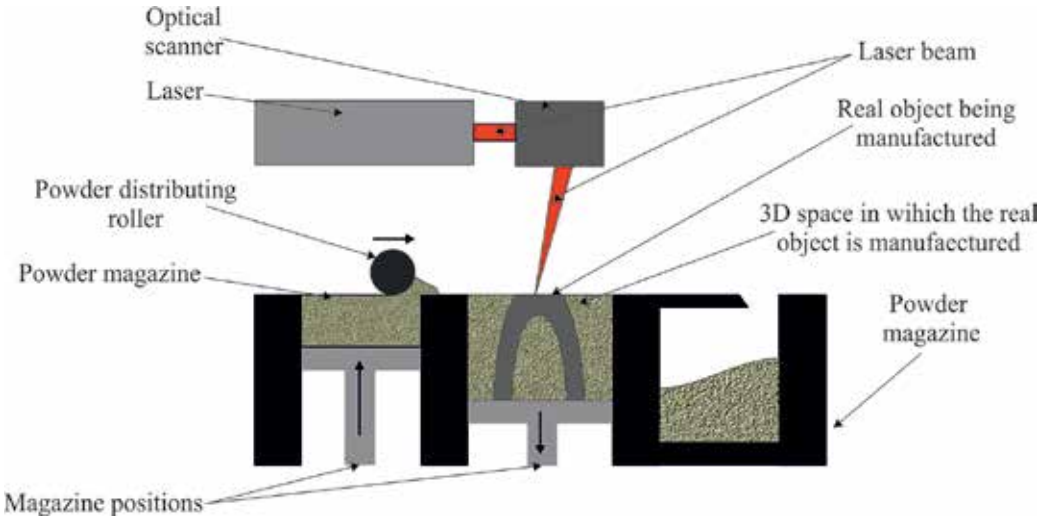

Figure 5. Schematic of the Selective Laser Melting (SLM) device; an own picture prepared on the basis of Refs. [26–28].

The actual selective laser melting process serves to produce metallic scaffolds encompasses the selective melting of powders point after point and layer after layer using a high-power laser [30–34] with a device the diagram of which is shown in **Figure 5**. A process of object manufacturing by SLM was carried out from the bottom, i.e. from the working platform side. Each layer produced is adhering to the preceding one until the process is completed [35, 36]. Powder is fed from a magazine holding loose material and is then distributed with a specific quantity with a shaft travelling across a working platform, which is descending by the exact height of the layer being sintered, whose thickness corresponds to one layer of virtual 3D model section. The excess powder is collected with a roll to a second empty magazine. A computer-controlled laser beam is melting the powder (**Figure 6**) in a specifically predefined manner and in selectively picked points. A powder layer is deposited and melted selectively in an alternate fashion, until the entire, permanently integrated real object is created. The excess powder, removed from a working platform, can be re-used, by collecting it into a separate special magazine, after being finely sifted in subsequent fabrication processes [37, 38]. An example of a scaffold observed with a bare eye, whose size matches the palate loss of one of the patients participating in clinical trials, is shown in **Figure 7**, showing, respectively, view from the top (**Figure 7a**) and from the bottom (**Figure 7b**). This scaffold, manufactured using Ti6Al4V titanium alloy powder, was removed mechanically from the working platform and supports were removed.

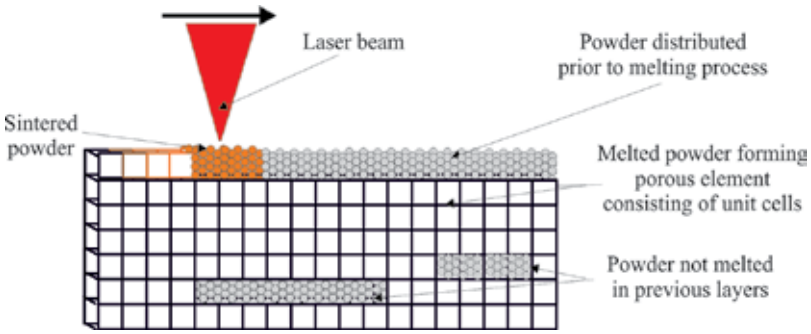

Figure 6. Sintering of individual powder layers in SLM process [29].

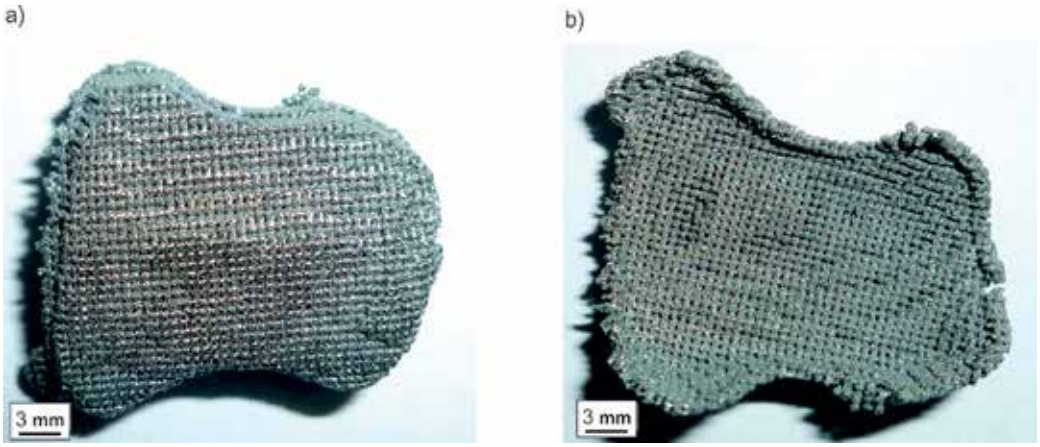

Figure 7. Example of scaffold manufactured with SLM method from Ti6Al4V powder, whose shape matches the palate loss of a patient: (a) top view; (b) bottom view.

The scaffolds created were subjected to microscopic observations using a scanning electron microscope. It was observed that the surface topography of the created scaffolds shows a porous, regular latticework-shaped structure. It was also found that the pores of the scaffolds produced are open, which was one of the designers' key assumptions due to the fact that this material, acting as an implant, is to grow through a patient's living tissue. Microscope observations of the studied material's surface topography indicate also the presence of singular, spherically shaped powder grains on its surface, which were deposited there due to adhering to the scaffold surface remelted in an SLM process. **Figure 8** shows a surface topography of the scaffolds manufactured with Ti6Al4V powder with the SLM method using the pre-produced virtual models comprised of multiplied unit cells created by the author, of, respectively, type A (**Figure 8a**), type B (**Figure 8b**), type C (**Figure 8c**) and type D (**Figure 8d**).

http://dx.doi.org/10.5772/65375

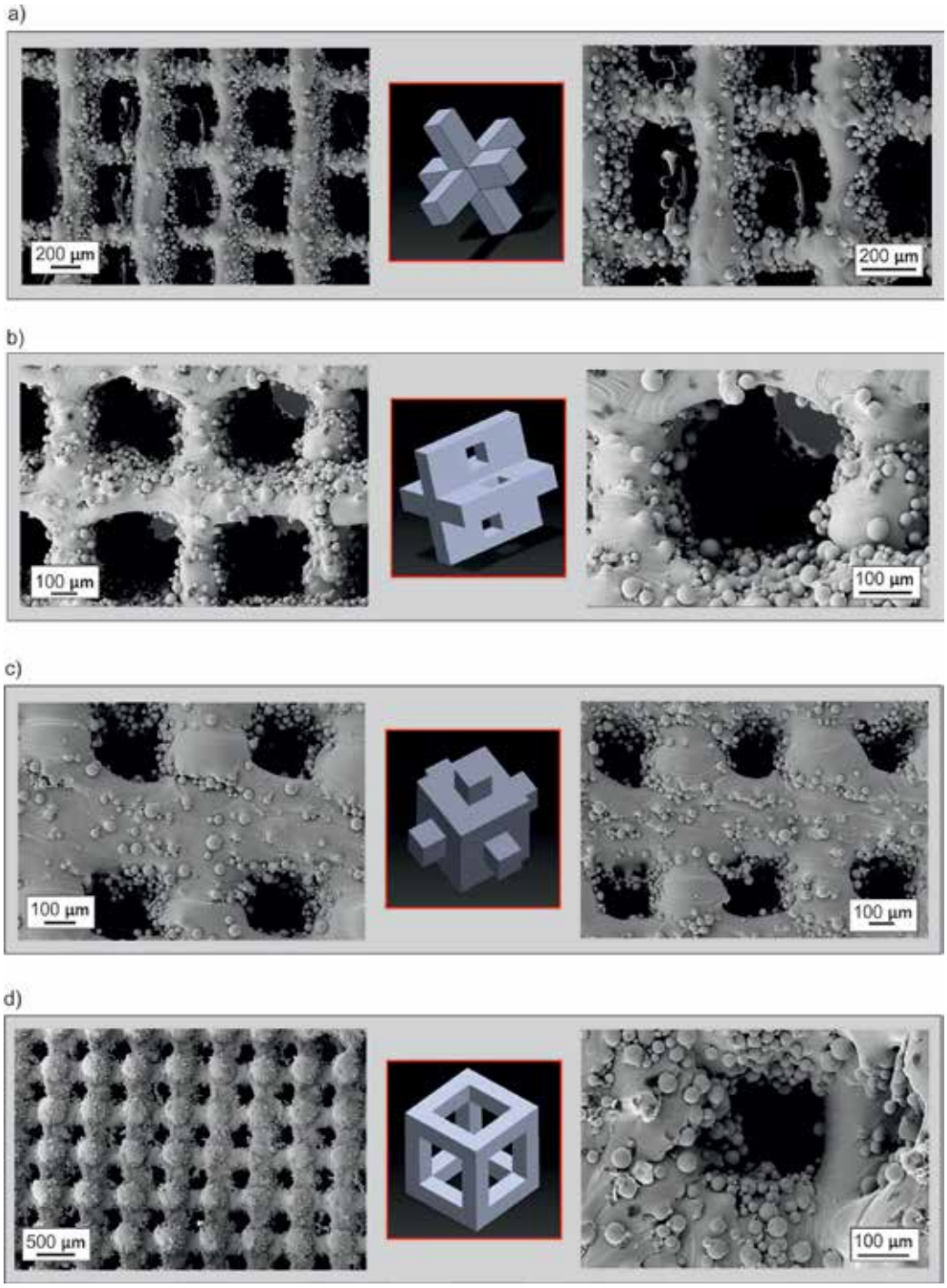

Figure 8. Surface topography of scaffolds manufactured as multiplication of units cells of type A (a), type B (b), type C (c) and type D (d).

4. Mechanical properties of scaffolds

On the one hand, scaffolds are made of robust materials such as pristine titanium and Ti6Al4V titanium alloy and on the other hand, they have a distinct structure consisting of open pores and possess interesting mechanical properties such as tensile and compressive strength. The tensile strength of material is determined according to the dependency (Eq. (1)) [39], using for calculations the results of strength tests determining the maximum tensile strength and a known field area of the sample cross section. The dependency (Eq. (2)) [39] allows to calculate the compressive strength of material using data such as the maximum compressive strength values obtained during strength tests and the sample cross section. The shape and dimensions of the samples designed to perform tensile and compressive strength tests are shown in **Figure 9**.

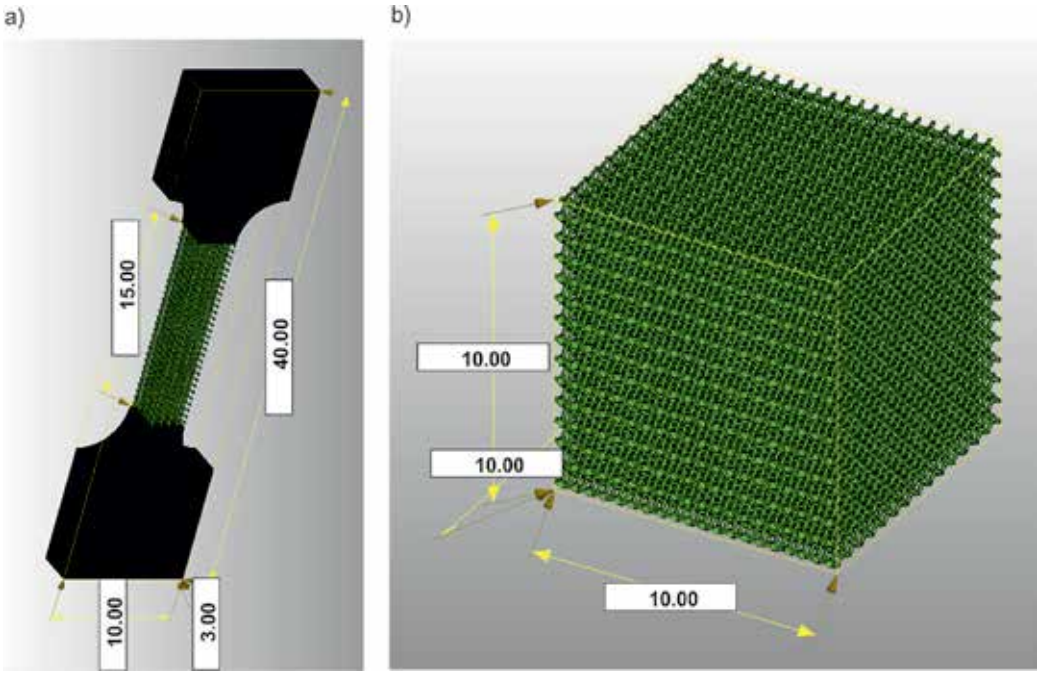

Figure 9. Samples for strength tests designed by computer: (a) for tensile strength; (b) for compressive strength.

Strength test type	Field area of sample cross section (mm²)	Material	Maximum force acting on sample (N)	Strength (MPa)	
				R_m	R_c
Tensile strength test	9	Ti	324	36	
		Ti6Al4V	423	47	
Compressive strength test	121	Ti	15 125		125
		Ti6Al4V	27 346		226

Table 2. Results of tensile and compressive strength tests made for scaffolds produced with Ti and Ti6Al4V powders (values in the table rounded to integers).

http://dx.doi.org/10.5772/65375

$$R_m = \frac{F_m}{S_0}\left[\frac{N}{m\,m^2} = MPa\right] \quad (1)$$

$$R_c = \frac{F_m}{S_0}\left[\frac{N}{m\,m^2} = MPa\right] \quad (2)$$

where:

R_m — tensile strength;

R_c — compressive strength;

F_m — maximum force acting on the sample and

S_0 — field area of cross section of sample.

The strength properties of scaffolds depend on the size of their pores, laser path curve and unit cell arrangement in the space of a system of coordinates [25]. **Table 2** shows the results of experiments made after selecting the optimum conditions of executing a manufacturing process, such as the size of scaffold pores of 250 μm, a laser path with an improved curve and unit cell arrangement at the angle of 45° relative to the axis of abscissa of the system of coordinates.

The average tensile strength value of laser-sintered scaffolds of Ti6Al4V powder is 47 MPa and is over 30% higher than the strength of scaffolds produced in the same conditions using pristine titanium powder, as presented in **Figure 10**. The characteristic of progression of tensile curves proves that both the porous titanium and porous Ti6Al4V titanium alloy are elastic-plastic materials with a clearly marked elastic strength and yield strength. Similar as in the case of tensile strength, a scaffold made of titanium alloy possesses much higher compressive strength than a titanium scaffold. The difference is much higher, though, because the compressive strength of the material made of Ti6Al4V is 225 MPa and is 80% higher than the compressive strength of a titanium sample (120 MPa). **Figure 11** shows charts presenting a dependency between compressive stress and deformation for the porous materials sintered with a laser using, respectively, Ti and Ti6Al4V powders.

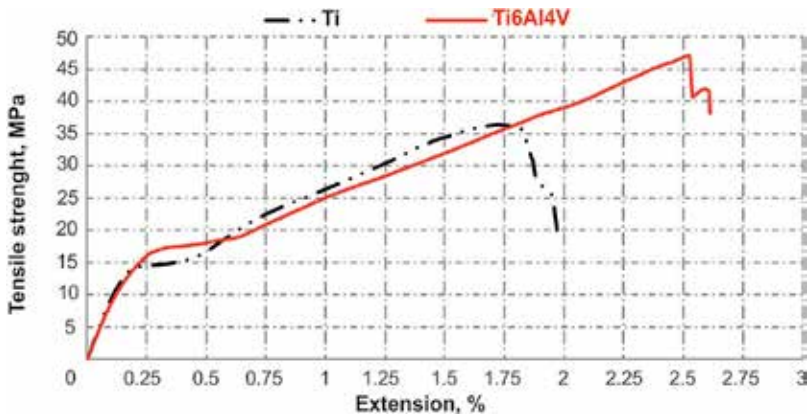

Figure 10. Dependency between tensile stress and extension recorded for porous materials sintered with laser from Ti and Ti6Al4V powders.

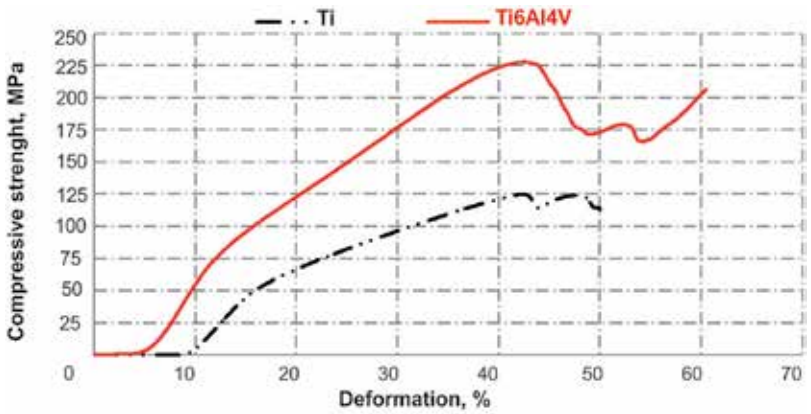

Figure 11. Dependency between compressive stress and deformation recorded for porous materials sintered with laser from Ti and Ti6Al4V powders.

5. Atomic layers of dioxide titanium deposited onto scaffolds' surface

Pristine titanium and its Ti6Al4V alloy, of which scaffolds are made which are to act as implants of palate fragments, are the materials broadly used in medicine as implants due to their low density, a beneficial strength-to-yield stress limit ratio, good corrosive resistance and biocompatibility. A further improvement in those materials' properties such as biotolerance and osteoconduction is possible by employing surface treatment. Thin layers are depos-

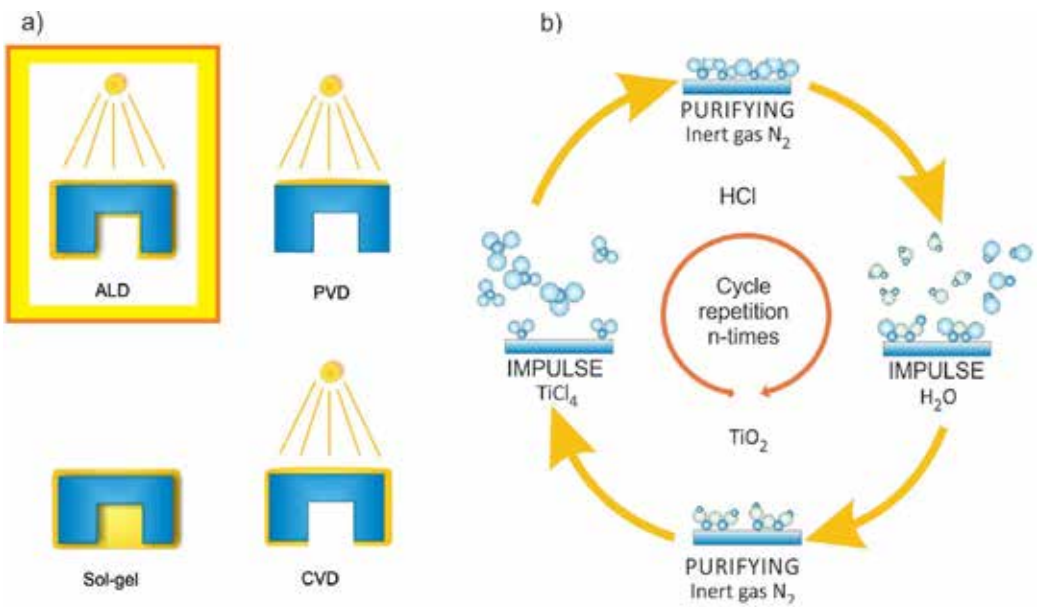

Figure 12. Atomic layer deposition: (a) ALD method versus other methods; (b) process cyclicity.

http://dx.doi.org/10.5772/65375

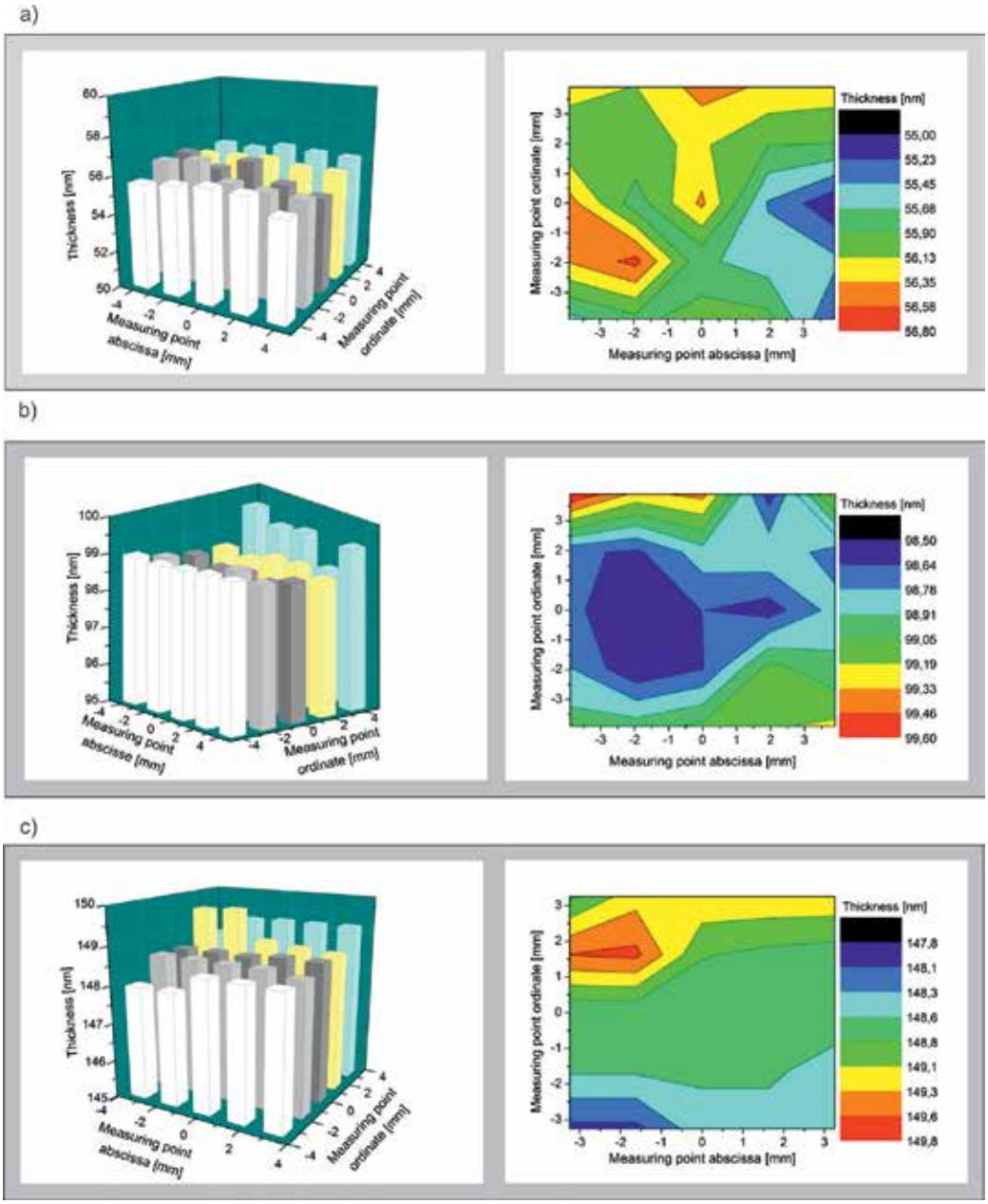

Figure 13. Layer thickness and thickness distribution map of TiO_2 layered deposited by ALD for: (a) 550 cycles; (b) 1050 cycles; (c) 1550 cycles [44].

ited permanently onto the surface of implants made of metallic biomaterials intended for long use in a human organism, most often with the following methods [40–43]: plasma sputtering, electrophoresis, physical vapour deposition (PVD) and chemical vapour deposition (CVD),

sputter coating and electrochemical deposition. Where layers are deposited onto the surface of porous biomaterials with complicated shapes, it is very important to be able to accurately control the growth mechanisms enabling to constitute a very thin layer with its thickness measured at a nanoscale, but most of all, it is essential to be able to deposit geometrically complex areas uniformly. One method, i.e. atomic layer deposition (ALD), gives such an opportunity now, as shown in **Figure 12a**, against optional methods. The ALD method is a variant of the CVD method characterised by the cyclic use of alternate precursor pulses with strong reactivity with a chamber purged with inert gas between such pulses (**Figure 12b**). By applying strongly reactive precursors, which—after supplying them into a chamber—are reacting immediately with a substrate by forming a monolayer and preventing a further reaction, each cycle increases the layer thickness by a strictly specified value within the range of 0.01–0.3 nm. The number of cycles performed preconditions the final thickness of the deposited layer. The authors of this chapter, in the course of their own works, have performed a series of experiments consisting of the deposition of atomic TiO_2 layers onto scaffolds sintered from Ti/Ti6Al4V and have carried out for this purpose, respectively, 550, 1050 and 1550 cycles.

The ALD technique enables to deposit a chosen chemical compound more uniformly across the entire surface of the part being treated, also if this part has a porous structure, as is the case with scaffolds. The thickness of the layers deposited by ALD is determined with a spectroscope ellipsometer equipped with special software. The average thickness of layers deposited by ALD technique for the said cases of 550, 1050 and 1550 cycles is 55.95, 98.90 and 148.73 nm, respectively. The difference in the thickness of the deposited TiO_2 layers on the studied area does not exceed 2 nm, which can be analysed in detail by studying layer thickness distribution maps. The best results were obtained for a layer deposited in 1050 cycles. A difference in the thickness of the deposited layer in this case does not exceed 1.1 nm across the entire area of the surface-treated item. Bar charts for each number of cycles, presenting the thickness of the deposited TiO_2 layer in the particular measuring points and the corresponding layer thickness distribution maps, are shown in **Figure 13**.

Changes in sample colour depending on the number of the executed ALD cycles, hence depending on the thickness of the deposited TiO_2 layer, is an interesting phenomenon

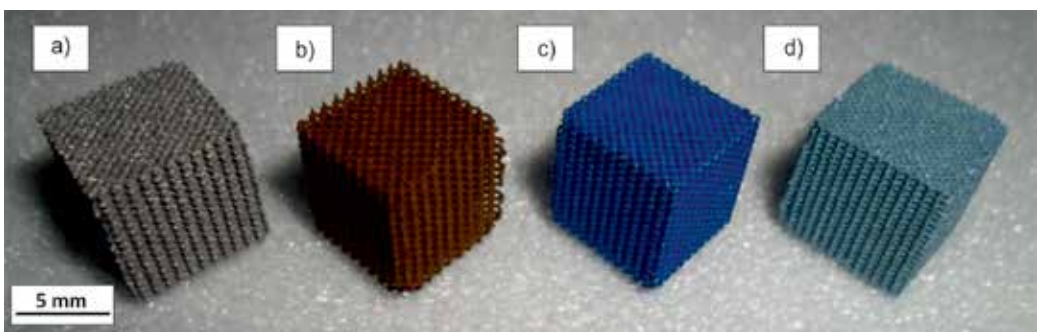

Figure 14. Cubic scaffolds viewed with a bare eye, including scaffolds without surface treatment (a) and scaffolds coated with TiO_2 layer during 550 (b), 1050 (c) and 1550 (d) cycles.

http://dx.doi.org/10.5772/65375

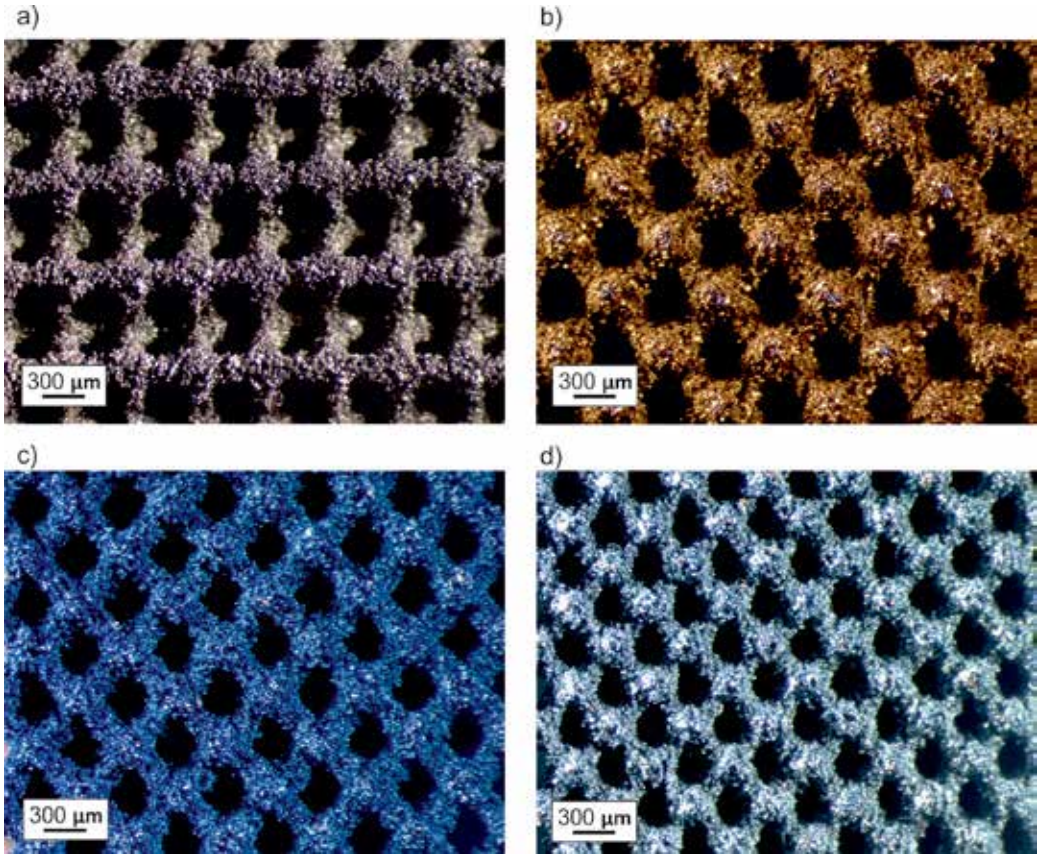

Figure 15. Stereoscopic images of scaffolds, including scaffold without surface treatment (a) and scaffolds coated with TiO_2 layer during 550 (b), 1050 (c) and 1550 (d) cycles.

observed with a bare eye (**Figure 14**) and in a light stereoscopic microscope (**Figure 15**). The uncoated element, with silver-metallic colour, undergoing surface treatment with ALD becomes, successively: brown-gold (550 cycles), dark blue (1050 cycles) and light blue with silver shade (1550 cycles).

The topography of scaffolds' surface coated with layers deposited by ALD is distinct for their irregularities measured at a nanometric scale, the number of which is rising proportionally to the number of the deposited layers. In particular, a layer deposited in 550 cycles has a rather uniform granular structure and the larger clusters of atoms are occurring on it only occasionally. In the case of a layer deposited in 1050 cycles, clusters of atoms with the diameter of about 1 µm occur every several microns. The biggest clusters of atoms, forming 'islands' with the length of up to several microns, exist in the case of a layer deposited in 1550 cycles, as shown in **Figure 16**.

The nanometric thickness of titanium dioxide layers deposited by ALD results in the fact that the layers deposited can be observed in a scanning electron microscope only for very high

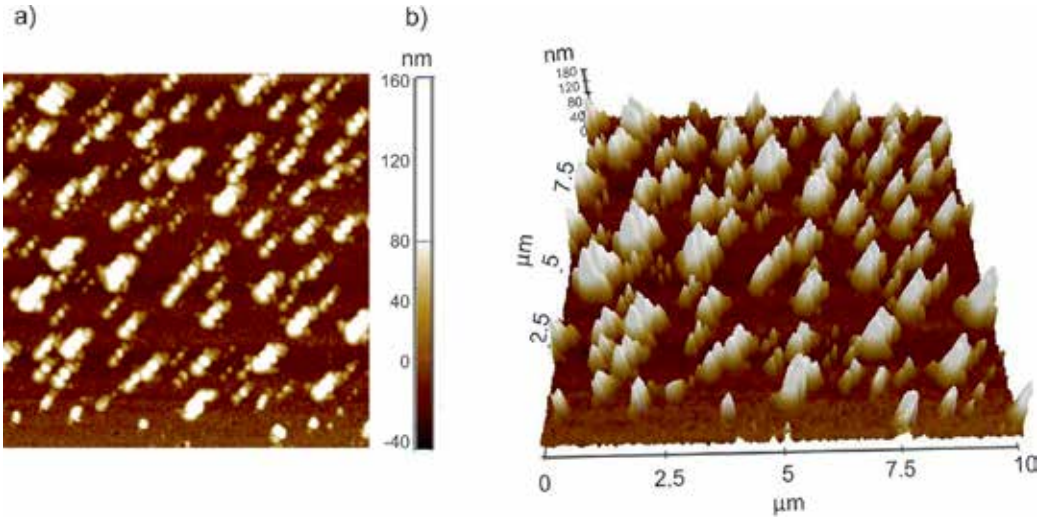

Figure 16. AFM image of surface topography of layer deposited in 1,550 cycles: (a) 2D; (b) 3D.

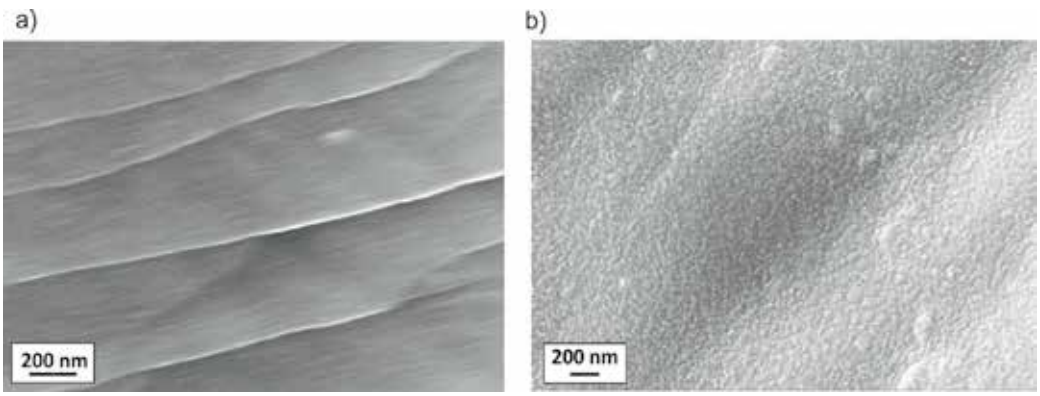

Figure 17. SEM image of scaffold surface: (a) without surface treatment; (b) with TiO_2 layer deposited in 1550 cycles.

magnifications of 150 kx. A clear difference between a scaffold surface without surface treatment (**Figure 17**) and scaffold surface covered with a TiO_2 layer in ALD (**Figure 17b**) can be observed only when such high magnifications are used. The scaffold surface, immediately following fabrication, is smooth with clear longitudinal bands arranged every several dozens of nanometres, corresponding to the laser activity direction. The deposited atomic TiO_2 layer, when magnified 150 kx, is visible as a 'sheep', i.e. a set of numerous adjacent oval granules of which only few have larger diameter.

6. Conclusions

Currently, there is a high social demand for individualised implants, which would significantly improve the quality of life of patients with partial palate losses caused by mechanical injuries, tumorous diseases or cleft palate. The methods currently in use, such as metallic or

polymeric prostheses, do not meet users' expectations as they often lack durability, convenience and aesthetics. A porous scaffold with its dimensions and shape perfectly suited to a patient plate loss made of a biocompatible material (Ti or Ti6AlV4) and additionally coated with a nanometric layer of osteoconductive titanium oxide seems to be a breakthrough solution. Modern CAMD software allows converting data acquired at a clinical stage into a 3D solid model of a palate loss piece. The model is then converted into a porous model through the multiplication of a unit cell whose dimensions and shape may be designed according to a patient's individual preferences. The pores existing in the material structure have the diameter of approx. 500 μm and should be open, because a scaffold, in its intended conditions of use, is to grow through a patient's living tissue. The experiments made confirm that the selective laser melting technology allows, following process conditions' optimisation, to produce biomimetic objects with a structure featuring open pores, as this was confirmed in microscopic (SEM) examinations. The objects have sufficiently good mechanical properties such as bending and compressive strength, which are similar to the properties of a cortical bone. The biotolerance and osteoconduction of laser-sintered scaffolds can be additionally improved through surface treatment allowing to cover a complex geometrical surface, such as a porous scaffold structure, uniformly from all sides. The treatment is carried out by the deposition of atomic layers and the deposited layer is 50–150 nm thick depending on the number of cycles.

Acknowledgements

All the results, images and detailed diagrams presented in this chapter have been developed in the framework of the BIOLASIN project entitled 'investigations of structure and properties of newly created porous biomimetic materials fabricated by selective laser sintering' headed by Prof. L.A. Dobrzański, funded by the Polish National Science Centre in the framework of the 'Harmony 4' competitions. The project was awarded a subsidy under the decision DEC-2013/08/M/ST8/00818.

Author details

Leszek A. Dobrzański[1]*, Anna D. Dobrzańska-Danikiewicz[1], Anna Achtelik-Franczak[1], Lech B. Dobrzański[2], Marek Szindler[1] and Tomasz G. Gaweł[1]

*Address all correspondence to: leszek.adam@gmail.com

1 Faculty of Mechanical Engineering, Silesian University of Technology, Gliwice, Poland

2 Centre of Medicine and Dentistry SOBIESKI, Gliwice, Poland

References

[1] A. Nouri, P.D. Hodgson, C. Wen. Biomimetic Porous Titanium Scaffolds for Orthopedic and Dental Applications. In: M. Amitava, editor. Biomimetics learning from nature. Rijeka, Croatia: InTech; 2010. pp. 415–450.

[2] S.W. Kim, H.D. Jung, M.H. Kang, H.E. Kim, Y.H. Koh, Y. Estrin. Fabrication of porous titanium scaffold with controlled porous structure and net-shape using magnesium as spacer. Materials Science and Engineering C. 2013;33(5):2808–2815. DOI: 10.1016/j.msec.2013.03.011

[3] Y. Wang, Y. Shen, Z. Wang, J. Yang, N. Liu, W. Huang. Development of highly porous titanium scaffolds by selective laser melting. Materials Letters. 2010;64(6):674–676. DOI: 10.1016/j.matlet.2009.12.035

[4] G. Ryan, A. Pandit, D.P. Apatsidis. Fabrication methods of porous metals for use in orthopaedic applications. Biomaterials. 2006;27(13):2651–2670. DOI: 10.1016/j.biomaterials.2005.12.002

[5] S.J. Simske, R.A. Ayers, T.A. Bateman. Porous materials for bone engineering. Materials Science Forum. 1997;250:151–182. DOI: 10.4028/www.scientific.net/MSF.250.151

[6] L.M.R. de Vasconcellos, M.V. de Oliveira, M.L. de Alencastro Graça. Porous titanium scaffolds produced by powder metallurgy for biomedical applications. Materials Research. 2008;11(3):275–280. DOI: 10.1590/S1516-14392008000300008

[7] Z. Esen, S. Bor. Processing of titanium foams using magnesium spacer particles. Scripta Materialia. 2007;56(5):341–344. DOI: 10.1016/j.scriptamat.2006.11.010

[8] M. Bram, H. Schiefer, D. Bogdański, M. Köller, H.P. Buchkremer, D. Stöver. Implant surgery: How bone bonds to PM titanium. Metal Powder Report. 2006;61(2):26–31. DOI: 10.1016/S00260657

[9] S. Kumar. Selective laser sintering: A qualitative and objective approach. Modeling and Characterization. 2003;55(10):43–47.

[10] W. Xue, B.V. Krishna, A. Bandyopadhyay, S. Bose. Processing and biocompatibility evaluation of laser processed porous titanium. Acta Biomaterialia. 2007;3(6):1007–1018. DOI: 10.1016/j.actbio.2007.05.009

[11] M. Bram, C. Stiller, H.P. Buchkremer, D. Stover, H. Baur. High-porosity titanium, stainless steel and superalloy parts. Advanced Engineering Materials. 2000;2(4):196–199. DOI: 10.1002/(SICI)1527-2648(200004)2:4<196::AID-ADEM196>3.0.CO;2-K

[12] B. Dąbrowski, W. Świeszkowski, D. Godliński, K.J. Kurzydlowski. Highly porous titanium scaffolds for orthopaedic applications. Journal of Biomedical Materials Research Part B: Applied Biomaterials. 2010;958(1):53–61. DOI: 10.1002/jbm.b.31682

[13] R.C. Thomson, M.C. Wake, M.J. Yaszemski, A.G. Mikos. Biodegradable polymer scaffolds to regenerate organs. Advances in Polymer Science. 2005;122:245–274.

[14] L.S. Bertol, W.K. Júnior, F.P. da Silva, C.A. Kopp. Medical design: Direct metal laser sintering of Ti-6Al-4V. Materials & Design. 2010;31(8):3982–3988. DOI: 10.1016/j.matdes.2010.02.050

[15] L. Lu, J. Fuh, Y. Wong. Laser Induseed Materials and Processes for Rapid Prototyping. In: L. Lu et al., editor. Laser-induced materials and prosesses for rapid prototyping. Dordrecht: Kluwer Publishers; 2001. pp. 89–142.

[16] L. Ciocca, M. Fantini, F. de Crescenzio, G. Corinaldesi, R. Scotti. Direct metal laser sintering (DMLS) of a customized titanium mesh for prosthetically guided bone regeneration of atrophic maxillary arches. Medical & Biological Engineering & Computing. 2011;49:1347–1352.

[17] A. Mazzoli. Selective laser sintering in biomedical engineering. Medical & Biological Engineering & Computing. 2012;51(3):245–256.

[18] A. Bandyopadhyay, F. Espana, V.K. Balla, S. Bose, Y. Ohgami, N.M. Davies. Influence of porosity on mechanical properties and in vivo responseof Ti6Al4V implants. Acta Biomaterialia. 2010;6(4):1640–1648. DOI: 10.1016/j.actbio.2009.11.011

[19] S. van Bael, Y.C. Chai, S. Truscello, M. Moesen, M. Moesen, G. Kerckhofs, H van Oosterwyck, J.P. Kruth, J. Schtooten. The effect of pore geometry on the in vitro biological behavior of human periosteum-derived cells seeded on selective laser-melted Ti6Al4V bone scaffolds. Acta Biomateralia. 2012;**8**(7):2824–2834. DOI: 10.1016/j.actbio.2012.04.001

[20] I. Shishkovsky, V. Scherbakov. Selective laser sintering of biopolymers with micro and nano. Physics Procedia. 2012;**39**:491–499. DOI: 10.1016/j.phpro.2012.10.065

[21] EN ISO 5832-3:2012. Implants for surgery – Metallic materials – Part 3: Wrought titanium 6-aluminium 4-vanadium alloy (ISO 5832-3:1996), ISC 11.040.40, European Committee for Standardization (CEN), Brussels, Belgium 2012.

[22] R. Melechow, K. Tubielewicz, W. Błaszczyk, editors. Titanium and its alloys: types, properties, applications, processing technology, degradation (in Polish). Częstochowa: PC Publishing; 2004.

[23] L.A. Dobrzański, editors. Fundamentals of materials science (in Polish). Gliwice: Publishing of Silesian University of Technology; 2012.

[24] L.A Dobrzański, Descriptive physical metallurgy of non-ferrous alloys, Silesian University of Technology Publishing, Gliwice, Poland; 2009 (in Polish).

[25] L.A. Dobrzański, A.D. Dobrzańska-Danikiewicz, A. Achtelik-Franczak, L.B. Dobrzański. Comparative analysis of mechanical properties of scaffolds sintered from Ti and Ti6Al4V powders. Archives of Materials Science and Engineering. 2015;**73**(2):69–81.

[26] G. Pyka, A. Burakowski, G. Kerckhofs, M. Moesen, S. V. Bael, J. Schrooten, M. Wevers. Surface modification of ti6al4v open porous structures produced by additive manufacturing. Advanced Engineering Materials.2012;**14**(6):363–370. DOI: 10.1002/adem.201100344

[27] L.A. Dobrzański, A. Achtelik-Franczak, M. Król. Computer aided design in Selective Laser Sintering (SLS)—application in medicine. Journal of Achievements in Materials and Manufacturing Engineering. 2013;**60**(2):66–75.

[28] M. Król, L.A. Dobrzański, Ł. Reimann, I. Czaja. Surface quality in selective laser melting of metal powders. Archives of Materials Science and Engineering.2013;**60**(2):87–92.

[29] L.A. Dobrzański, A.D. Dobrzańska-Danikiewicz, P. Malara, T.G. Gaweł, L.B. Dobrzański, A. Achtelik-Franczak. Fabrication of scaffolds from TI6AL4V powders using the computer aided laser method. Archives of Metallurgy and Materials. 2015;**60**(2):1065–1070. DOI: 10.1515/amm-2015-0260

[30] T. Węgrzyn, J. Piwnik, B. Łazarz, R. Wieszała, D. Hadryś. Parameters of welding with micro-jet cooling. Archives of Materials Science and Engineering. 2012;**54**(2):86–92.

[31] A. Sękala, G. Ćwikła, G. Kost. The role of multi-agent systems in adding functioning of manufacturing robotized cells. In: IOP Conf. Series: Materials Science and Engineering 95, editors. ModTech; Romania. Romania: IOP Publishing Ltd; 2016. p. 012097.

[32] A. Sękala, A. Gwiazda, K. Foit, W. Banaś, P. Hryniewicz, G. Kost.Agent-based models in robotized manufacturing cells designing. In: IOP Conf. Series: Materials Science and Engineering 95, editors. ModTech; Roamnia. Romania: IOP Publishing Ltd; 2015. p. 012106.

[33] A. Kaźnica, R. Joachimiak, T. Drewa, T. Rawo, J. Deszczyński. New trends in tissue engineering. Arthroscopy and Arthritis Surgery. 2007;3(3):11–16 (in Polish).

[34] N. Evans, E. Gentelman, J. Polak. Scaffolds for stem cells. Materials Today.2006;**9**(12): 26–33. DOI: 10.1016/S13697021

[35] T. Węgrzyn, R. Wieszała. Significant alloy elements in welded steel structures of car body. Archives of Metallurgy and Materials. 2012;**57**(1):45–52. DOI: 10.2478/v10172-011-0151-4

[36] L.A. Dobrzański, A.D. Dobrzańska-Danikiewicz, P. Malara, T.G. Gaweł, L.B. Dobrzański, A. Achtelik. Patent Application No. 414423. Polish Patent Office. 2015.

[37] A. Laptev, O. Vyal, M. Bram, H.P. Buchkremer, D. Stöver. Green strength of powder compacts provided for production of highly porous titanium parts. Powder Metallurgy. 2005;**48**(4):358–364. DOI: 10.1179/174329005X73838

[38] G. Budzik, D. Pająk, M. Magniszewski, W. Budzik. Rapid prototyping methods (in Polish). Steel Metals & New Technologies.2011;**1–2**:78–79.

[39] L.A. Dobrzański, R. Nowosielski, E. Hajduczek, editors. Research methods of metals and their alloys: Light and electron microscopy (in Polish). 2nd ed. Warszawa: WNT; 1987.

[40] J. Nowacki, L.A. Dobrzański, F. Gustavo, editors. Implants in the intramedullary osteosynthesis of long bones (in Polish). Gliwice: Open Access Library; 2012. 150 p.

[41] A. Mahapatro. Bio-functional nano-coatings on metallic biomaterials. Materials Science and Engineering: C. 2015;**55**:227–251. DOI: 10.1016/j.msec.2015.05.018

[42] E.O. López, A.L. Rossi, B.S. Archanjo, R.O. Ospina, A. Mello, A. M. Rossi. Crystalline nano-coatings of fluorine-substituted hydroxyapatite produced by magnetron sputtering with high plasma confinement. Surface and Coatings Technology. 2015;**264**:163–174. DOI: 10.1016/j.surfcoat.2014.12.055

[43] L A. Dobrzański, L. Reimann. Influence of Cr and Co on hardness and corrosion resistance CoCrMo alloys used on dentures. Journal of Achievement in Materials and Manufacturing Engineering. 2011;**49**(2):193–199.

[44] L.A. Dobrzański, A.D. Dobrzańska-Danikiewicz, M. Szindler, A. Achtelik-Franczak, W. Pakieła. Atomic layer deposition of TiO2 onto porous biomaterials. Archives of Materials Science and Engineering. 2015;**75**(1):5–11.

Chapter 8

Powder Application in Additive Manufacturing of Metallic Parts

Jan Džugan and Zbyšek Nový

Additional information is available at the end of the chapter

http://dx.doi.org/10.5772/66874

Abstract

This chapter is going to give up-to-date overview of development in the field of additive manufacturing (AM) of metallic components. There will be briefly mentioned input materials and specific requirement for the input materials (powders and wires). General technology process overview will be presented here, and selective laser melting (SLM) technology and beam melting technologies will be described. Advantages of 3D printing technology will be explained in terms of special designs; special properties and generally multifunctional components of production possibilities will be shown. Postprinting procedures leading to improvement of mechanical properties of printed components like thermal or thermomechanical treatment will also be mentioned here.

Keywords: additive manufacturing, 3D printing, laser sintering, beam sintering

1. Introduction

Additive manufacturing (AM), sometimes called as 3D printing, is a process that is used to manufacture complex 3D products. In additive manufacturing, an object is created by deposition of several layers over each other by computer-controlled deposition process. The objects produced can be of virtually any shape. The components are created by additive manufacturing techniques on the basis of computer 3D models. Great attention has been given to this subject recently since it offers new opportunities in factories of the future.

Additive manufacturing may be a more appropriate term to use rather than 3D printing because it includes all processes that are "additive." The term "3D printing" applies more specifically to additive manufacturing processes that use a printer-like head for deposition of the material (e.g., material jetting), and 3D printing is now only one of the processes that is

part of the additive manufacturing universe. Technical articles and standards generally use the term "additive manufacturing" to emphasize this broader meaning.

Additive manufacturing applications appear to be almost unlimited. Early use of 3D printing in the form of rapid prototyping was focused on preproduction models. However, additive manufacturing is now being used to fabricate high-tech industrial (aerospace, medical/dental, automotive, and electronic) and consumer (home, fashion, and entertainment) products, and today's materials include not only polymers but also metals and ceramics. This chapter is going to deal with powder-based additive manufacturing. In the initial part, a brief overview of powders for additive manufacturing preparation and subsequently additive manufacturing techniques is presented.

2. Preparation of input materials for additive manufacturing

There is a wide range of additive manufacturing technologies that are going to be described later in this chapter. Depending on the technology considered, an appropriate input material should be used. Generally spoken there are two basic groups of input materials: powders and wires. Wire-feed processes such as laser metal deposition (LMD) and electron beam additive manufacturing (EBAM) are typical by higher deposition rates [1] with lower shape detail accuracy in comparison to powder-bed or powder-directed energy deposition processes. Considering pricing of these two branches of the input materials, wires are significantly cheaper in comparison to powders, and also the offer of the feedstock alloys available in the form of wires is significantly wider. However, the powder-based technologies can use special materials not available in the bulk form. This fact together with higher part geometrical accuracy leads to a wide application range of powder-based processes. Further, we are going to deal mainly with powder-related additive manufacturing.

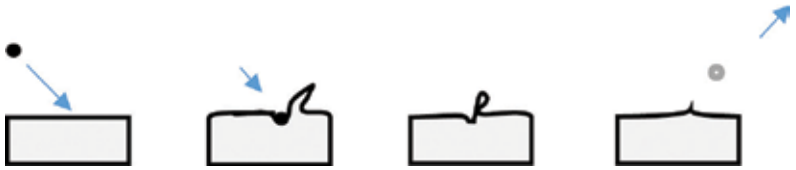

Figure 1. Water atomization principle [2].

The powders are prepared by atomization that can be done by several processes such as water atomization or gas atomization. While the water atomization, shown in **Figure 1**, leads to average particle size from 42 up to 120μm [1], the gas atomization leads to a finer particle sizes, and thus gas atomization is presently preferred for powder production and will be shown more in detail. The problem on powder productions is very wide, exceeding the scope of the current chapter, and thus a very brief overview of this field is provided here.

http://dx.doi.org/10.5772/66874

2.1. The gas atomization process

The gas atomization process is the most common process to produce spherical metal powders for additive manufacturing. In cases when highly reactive materials, such as Al, Ti, or Mg, are atomized, protective gases or vacuum shall be applied.

The initial step of the gas atomization process is molten metal pouring from a tundish through a nozzle. The liquid metal is subsequently subjected to jets of neutral gas (nitrogen or argon). The gas jets divide liquid metal into tiny droplets and contribute to droplets cooling down that continue as they fall within the atomization tower. Powders are finally accumulated on the atomization tower bottom [2].

Two main configurations of twin-fluid atomizers are distinguished within molten metal atomization. The first kind is called the confined or close-coupled atomizer, and the second kind is called the free-fall atomizer. Both concepts are illustrated in **Figure 2** [3].

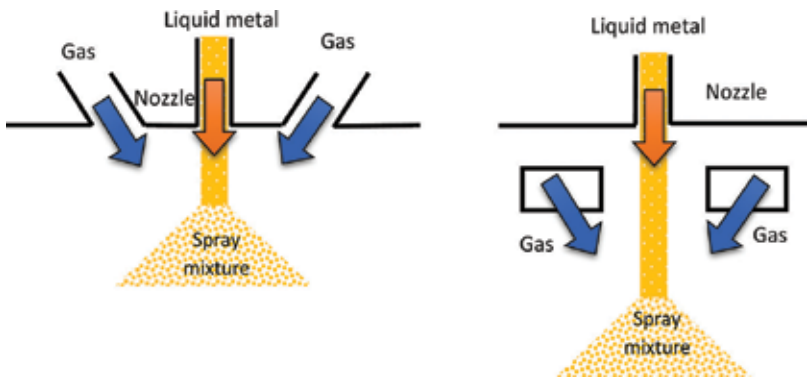

Figure 2. Principle configurations of gas atomization: left (close-coupled atomizer (confined)) and right (free-fall atomizer).

In the case of the close-coupled gas atomizer, the gas flow surrounds instantly the liquid metal pouring from the reservoir nozzle. In the case of free-fall atomizer, there is some gap between the nozzle outlet and gas jets. This fundamental difference between the atomizers leads to advantage of the higher cooling rates for the close-coupled atomizer and thus higher efficiency in comparison to the free-fall atomizer. However, the free-fall atomizer exhibits significantly lower susceptibility to freezing than the close-coupled atomizer. The freezing issue comes from very small distance between the liquid metal outlet nozzle and cooling gas that leads to very intensive cooling and thus problems with freezing at process early stage, when the nozzle is not sufficiently heated. Once the nozzle is heated up by flowing liquid metal, the problem with freezing is minimized. Additional advantage of free-fall atomizers over close-coupled ones is possibility of gas jet adjustment in the course of the process. By controlled scanning and oscillating of the gas cooling jets, running atomization process can be adjusted at any moment, and therefore desired powder size and distribution can be better

achieved. Close-coupled atomizer offers process adjustment by modification of the cooling gas pressure only that allows much lower process modification versatility in comparison to free-fall atomizer [3–5].

2.2. Special atomization processes

In the case of special material atomization, appropriate approaches shall be employed such as:

- Vacuum inert melting (VIM) where the melting takes place in a vacuum chamber. This process is recommended for super alloys in order to avoid the melt contamination by oxygen for highly reactive materials such as Ti and Al.
- Plasma atomization and spheroidization consist of in-flight heating and melting thanks to a plasma torch of feed material followed by cooling and solidification under controlled conditions. Depending on processes, the raw material can be particles as well as bar or wire feedstock. Plasma atomization can be used in particular to spheroid refractory metals such as Mo alloys, W, and WC.
- Centrifugal atomization, also known as plasma-rotating electrode process, consists in melting with a plasma torch where the end of a bar feedstock is rotating at high speed and thus ejecting centrifugally the molten droplets of metal.
- Powder blending and mechanical alloying, to produce metal matrix composites (MMCs).

2.3. Metal powder characteristics for additive manufacturing

Key metal powder characteristics for additive manufacturing are chemical composition, powder size distribution (PSD), morphology, and physical properties.

Additional points are important to consider when selecting metal powders for additive manufacturing processes such as storage and aging of powders; reusability of powder after additive manufacturing cycles; and health, safety, and environmental issues [2].

Regarding the chemical composition, it is important to take into account interstitials, such as oxygen, nitrogen, carbon, and sulfur, as they may affect significantly material properties depending on alloys. With the gas atomization process, all powder particles have the same chemical composition, but finer particles tend to have higher oxygen content due to the higher specific surface.

The chemical composition will influence in particular melting temperature, mechanical properties, weldability, and thermal properties (thermal conductivity, heat capacity, etc.). The chemical composition can also evolve slightly after multiple uses in additive manufacturing machines.

Depending on additive manufacturing technology and equipment, two main types of particle size distributions are considered:

- Powders usually below 50 μm for most powder-bed systems. In this case, finer powder particles below 10 or 20 μm shall be avoided, as they are detrimental to the powder flowability.

http://dx.doi.org/10.5772/66874

- Powder between 50 and 100–150 μm for electron beam melting (EBM) and LMD technologies.

The recommended particle morphology for additive manufacturing is spherical shape because it is beneficial for powder flowability and also to help forming uniform powder layers in powder bed systems.

The powder morphology can be observed by scanning electron microscope (SEM) (**Figure 3**). Typical defects to be controlled and minimized are:

- Irregular powder shapes such as elongated particles.
- Satellites which are small powder grains stuck on the surface of bigger grains.
- Hollow powder particles, with open or closed porosity.

Porosity content can be evaluated either by SEM observation or by helium pycnometer. The presence of excessive amounts of large pores or pores with entrapped gas can negatively affect material properties.

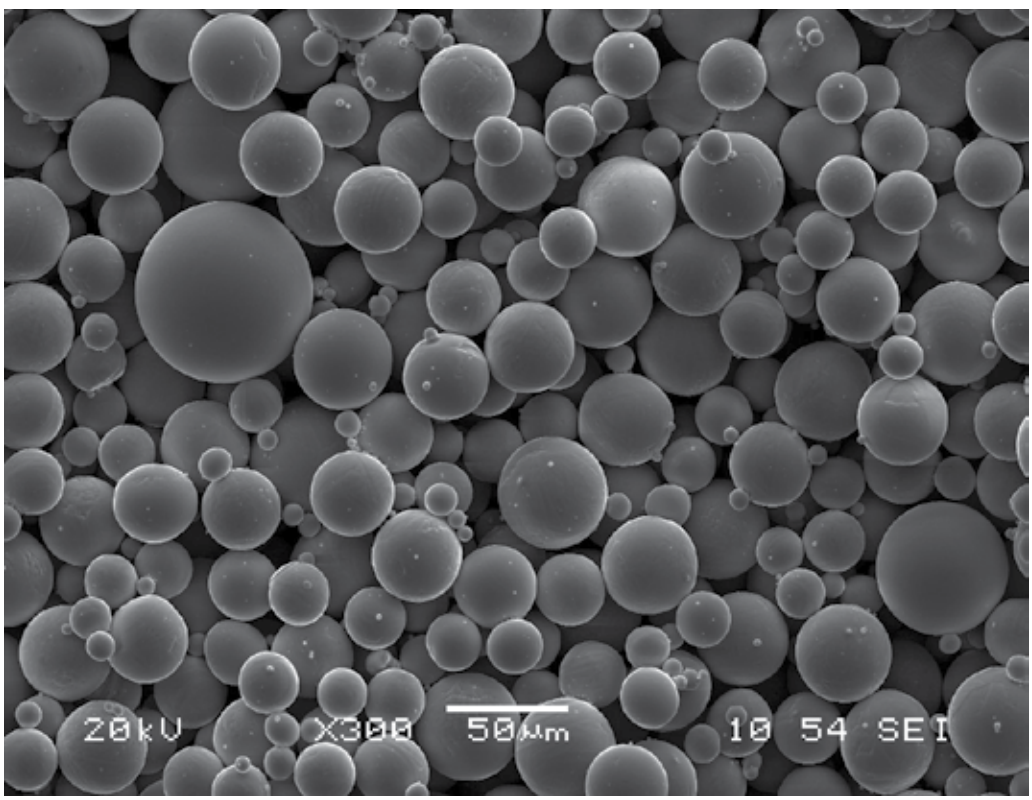

Figure 3. Example of atomized globular Ti-powder (inert gas atomizer).

3. Most common processes of metal additive manufacturing

Additive manufacturing is a very dynamic field with very wide range of new procedures being developed, so this chapter gives an overview of mostly used ones.

3.1. Powder-bed fusion processes

Powder-bed fusion (PBF) processes were among the first commercialized AM processes. Developed at the University of Texas at Austin, USA, selective laser sintering (SLS) was the first commercialized PBF process. All other PBF processes modify this basic approach in one or more ways to enhance machine productivity, to enable different materials to be processed, and/or to avoid specific patented features.

In the case of the powder-bed process, the product is created stepwise by thin powder layer sintering deposited subsequently over each other until the desired shape is achieved. The power source for powder-bed fusion processes can be laser or electron beam that melt and fuse metal particles together. Vacuum is required in the case of electron beam melting (EBM) processes or in case of highly reactive metal processing (titanium, magnesium, etc.). The input powder material is located in the container from which it is fed into processing zone where it is subsequently fused. The powder that is brought to the process zone is in the form of thin layer of thickness about 0.1 mm. There are various processes assuring even thickness of powder layers such as roller- or blade-based ones. In order to maintain constant distance between the power source and processed object, the bed is lowered with each new layer. The unfused residual powder remains on the powder bed and can be recycled for further use [6].

3.1.1. Electron beam melting (EBM)

In the EBM process, fully dense metal components are built up, layer by layer of metal powder, melted by a powerful electron beam in high vacuum. Full melting of metal powder is required in each deposited layer.

The power source of the EBM machine is high power electron beam. The beam has to have sufficient energy in order to achieve desired melting capacity and productivity. The beam is computer controlled by electromagnetic coils that can scan the beam over the process area providing desired melted layer shape [7], as can be seen in **Figure 4**. Advanced electron beam machines allow several melt pools to be maintained simultaneously—multibeam technology.

Electron beam melting is distinguished by its superior refining capacity and offers a high degree of flexibility of the heat source. Thus, it is ideal for remelting and refining of metals and alloys under high vacuum. Thanks to specific properties of this process, the main application is in the field of high-temperature resistant and reactive metals such as, e.g., titanium, zirconium, and tungsten. The EMB is widely used for ultrapure sputtering target material production and for titanium waste recycling. This solid free-form fabrication technique produces fully dense metal parts with characteristics of target material [4, 8].

http://dx.doi.org/10.5772/66874

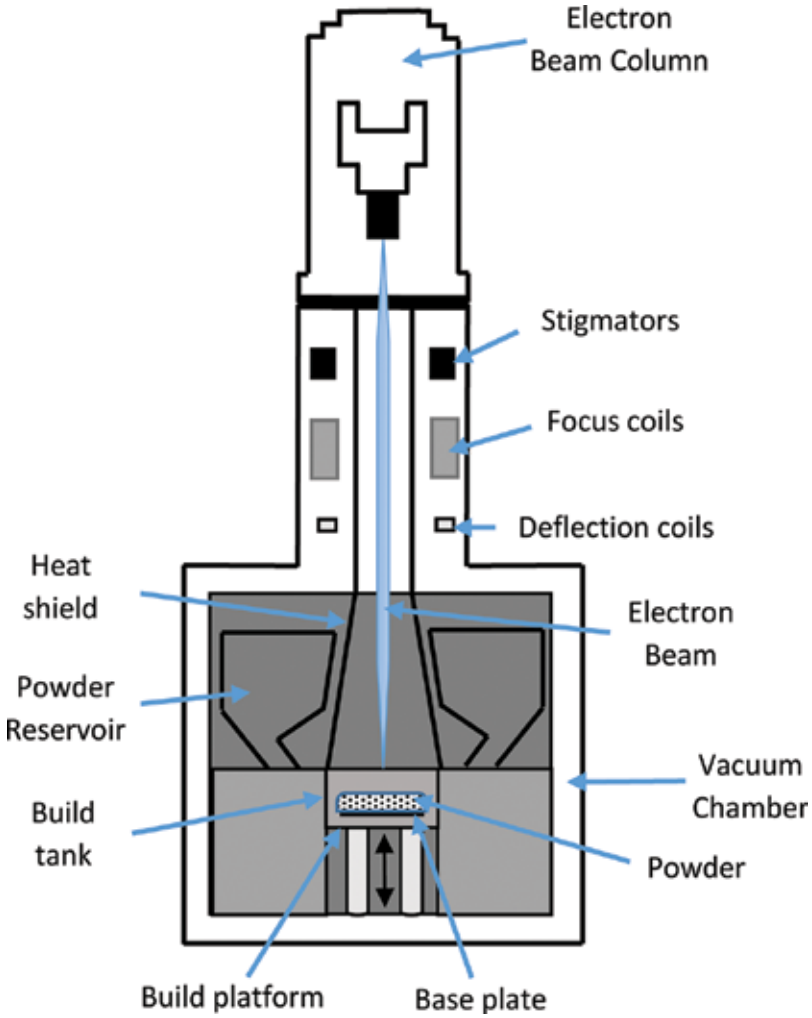

Figure 4. Electron beam additive system scheme.

The EBM process takes place in vacuum and at high temperature, resulting in stress-relieved components with material properties better than cast and comparable to wrought material. Very complex shapes can be achieved by EBM technology as can be seen in **Figure 5**.

The electron beam guns are very powerful heat sources that can achieve melting and even evaporation temperatures of most of the materials of interest. Computer control of the beam by electromagnetic coils enables fast scanning with very high accuracy. The EBM yields very good power transfer efficiency, depending on the material of interest reaching 50–80%. Thanks to high power density of the electron beam of about 100 W/cm^2, only shallow melt zone is achieved that has beneficial effect on the produced component from microstructure point of view. The process is run under high vacuum up to 0.001 Pa that leads to effective melt

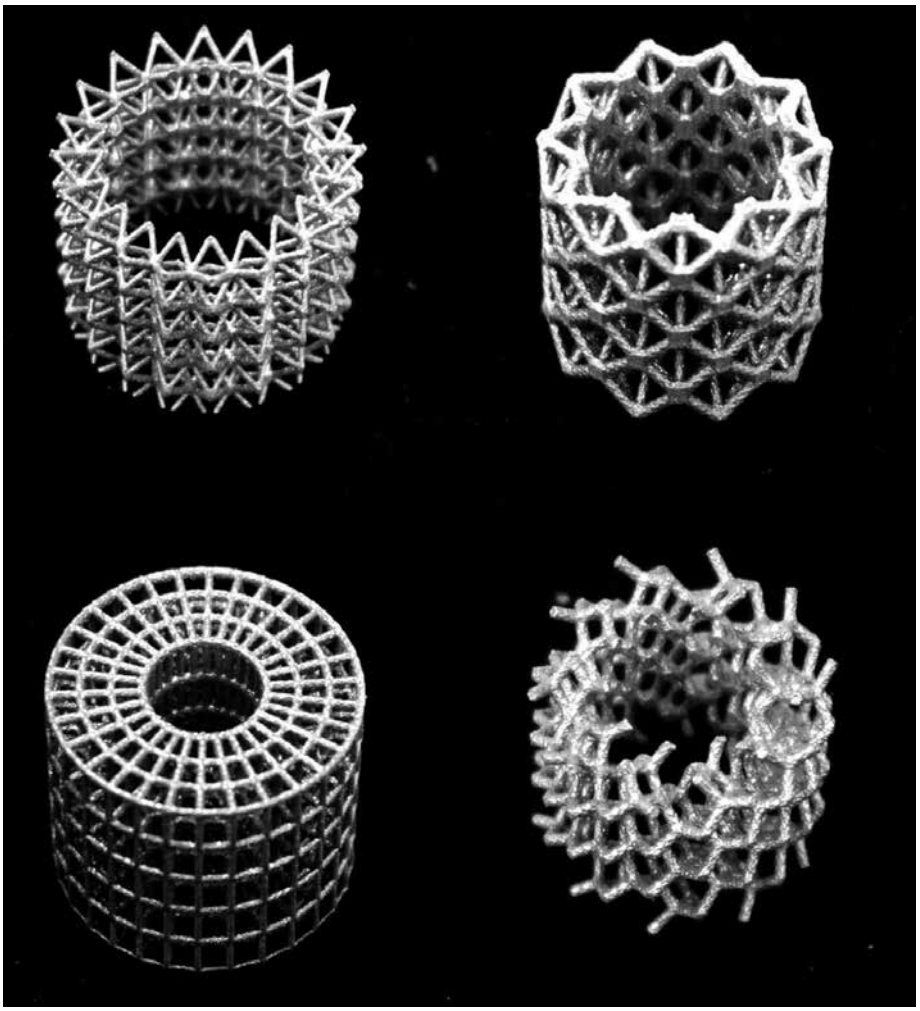

Figure 5. Examples of printed complex structures.

degassing providing high purity materials. Negative side of this effect is loss of certain alloying elements that has to be considered if special complex alloys are being processed [4, 9].

3.1.2. Direct metal laser sintering (DMLS)

Direct metal laser sintering (DMLS) is another technique from the field of additive manufacturing. The energy source here is laser beam that is computer controlled so it can scan across the applied powder layer in order to sinter shape according to CAD model into a solid component. The process is also, as in the case of EBM, incremental sintering of thin layers step by step, with typical layer thickness of 20–100μm, until full 3D object is created. Depending on the shape, complexity and component stability on the worktable, special supports might be necessary for successful component production. During the process preparation, also

http://dx.doi.org/10.5772/66874

appropriate component orientation has to be decided taking into consideration potential properties variations due to various heating conditions at different component spots and reheating of some parts more than the others. DMLS provides very complex shapes with very high accuracy, good surface, and excellent mechanical properties [10, 11]. Scheme of DMLS system is depicted in **Figure 6**.

Direct metal laser sintering (DMLS) is gradually gaining the position of a production method for rapid as well as a precise production of fully functional prototype parts or final products for various applications. Prototypes made using this technology are good for parts that cannot be easily die-casted or machined. The process produces highly durable but still fine components that are used in many industries, including aerospace, automotive, electronic or packaging industries, and medicine. A wide range of applications is gained in the production of molds and dies for plastic, ceramic, or metal products. With constantly increasing speed of devices and a permanently growing number of materials, the range of applications of this technology is higher as well. Material selection for DMLS process is very wide, from light alloys and steels to high alloyed super alloys and composites. The choice of material depends upon the end use of your application and requirements for strength, durability, sterilizability, weight, thermal properties, and corrosion resistance. DMLS is carried out for a wide range of materials among which aluminum, cobalt, chrome, nickel alloys, stainless steels, titanium alloys, and copper alloys are the most commonly offered.

The technology direct metal laser sintering has several modifications depending on the applied energy resulting either in complete local powder melting creating molten pool of metal, selective laser melting (SLM), or only local melting of single-grain parts, selective laser sintering (SLS). The SLM process yields fully dense components with mechanical properties comparable to bulk material; however, it is more difficult to control in comparison to SLS. The SLS-produced parts may require some additional treatment in order to reach better mechanical properties. Due to significantly higher energy input in the case of SLM and resulting

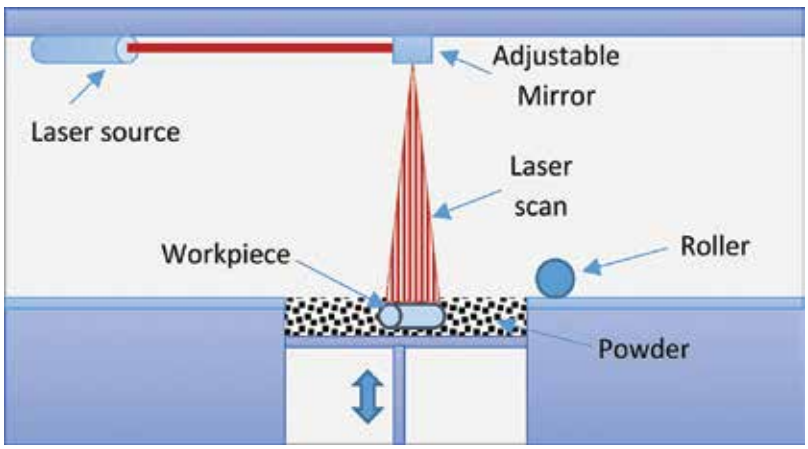

Figure 6. Schematic diagram of direct metal laser sintering process [11].

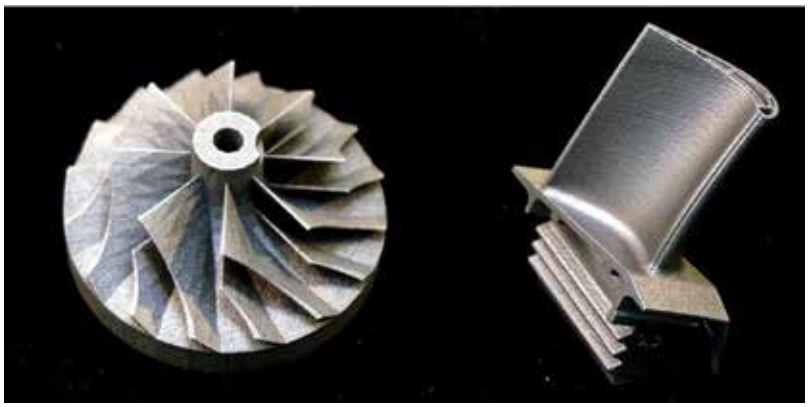

Figure 7. Examples of components produced by SLM.

complete powder melting, problems with residual stresses and geometry deformation may appear [12]. Examples of Ti alloy components produced by DMLS can be seen in **Figure 7**.

3.2. Blown powder processes

Processes using powder-bed fusion are still limited by the size of the built table and chamber. A process known as blown powder (BP) additive manufacturing can deliver some higher freedom in achieved geometry of manufactured parts. This method is available for many years. Its main difference to currently developed powder-bed methods is there is no need of powder supply in the form of layer by layer with subsequent sintering or melting. BP processes are using an additive material powder that is blown into the processing zone, where it meets with laser or plasma beam that melts the particle surface or whole particles and they are subsequently deposited on the substrate. The substrate can be present in a kind of form such as initial component layer, preprepared workpiece, or repaired serviced component. These principles were applied in many process developments [13].

3.2.1. Direct laser deposition (DLD)

The laser deposition processes are widely known under various names originating from manufactures or research institutes where they were developed. Probably, the most widely known are laser metal deposition (LMD), direct metal deposition (DMD), direct laser deposition (DLD), laser-engineered net shaping (LENS), laser cladding, laser deposition welding, and powder fusion welding [14].

In the case of laser deposition technology, the metal powder is introduced into focused beam of high power laser. The gas in the processing zone is strictly a controller to maintain repeatable stable process conditions. Molten base material is attained at localized area by focused laser beam, and additive powder is blown into this pool where it melts and subsequently solidifies creating deposition volume. Typical deposition thickness is ranging from 0.1 to 1 mm. The process is computer controlled in order to maintain constant distance between the nozzle, laser

http://dx.doi.org/10.5772/66874

beam source, and deposited surface. By movement of the laser beam with nozzle over the component/base plate movement, desired component geometry can be attained. More advanced systems offer possibility of closed-loop system for dimension control achieving very accurate geometry. Due to higher deposition, layer thickness components with lower surface variety can be attained; however, the build-up rate is significantly higher in comparison to powder-bed-based processes. These systems are quite versatile, and another possibility that is available is also the use of multimaterial deposition providing possibility to adjust local chemical composition of the component to desired properties at the specific component locations according to service loading conditions. DLD process can be used for many applications ranging from a new component production to repairs or rebuilds of broken parts, as it is explained in more details later. An example of the application is for steam turbine blade service life extension by coating of steam turbine blade edges by Stellite-6 that increases wear resistance to cavitation. Another field of applications can be reducing component costs by saving expensive special materials that can be applied on the functional surface only, while the rest of the component can be made of some low-cost material [14–17].

DLD process allows deposition of a wide range of materials such as titanium, nickel, various steels, and among others also Stellite. The microstructure of deposited material is comparable to as-welded microstructure that provide usually rather worse mechanical properties, and thus subsequent thermal processing is desirable [18]. Scheme of DLD can be seen in **Figure 8**.

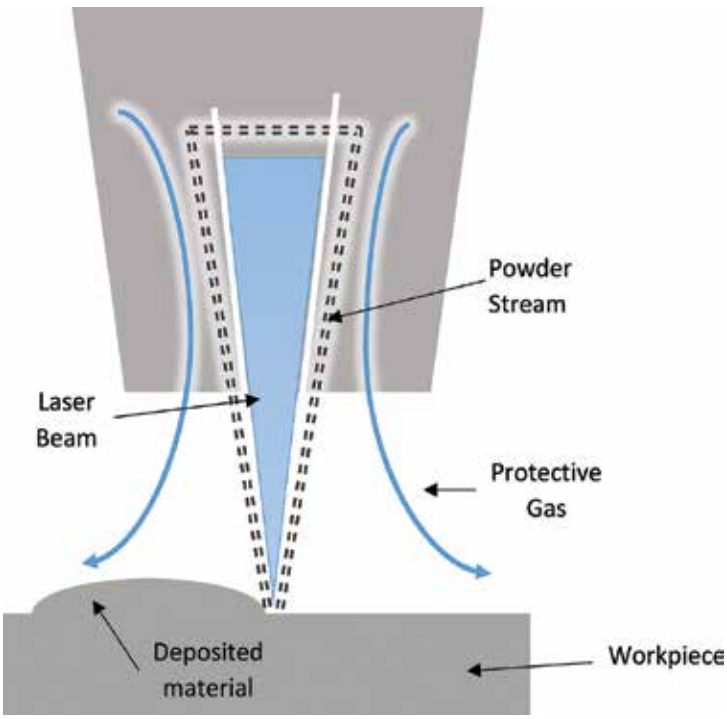

Figure 8. Laser metal deposition scheme [14].

There are basically three main applications of DLD processes [16]:

- Laser repair technology (LRT).
- Laser cladding technology (LCT).
- Laser free-form manufacturing technology (LFMT).

The laser repair technology is applied in cases when some parts of expensive constructions are worn or partly broken due to service loadings. The component replacement would be too expensive in these applications, and thus local repair can significantly increase the service life and thus safe substantial financial expenses. Typical examples of such repairs can be dies for close die forging, steam turbine rotors after smaller accidents, and mill or compressor components [16]. Examples of repaired parts by LRT are shown in **Figures 9** and **10**.

Figure 9. Laser repair technology of Titanium bearing housing [17].

Figure 10. Laser repair technology of Inconel 718 compressor seal [17].

Laser cladding technology is in contrary to LRT applying thinner layers that are mainly reconstructing worn surface, and thus smaller material volumes are deposited during this process [16]. Typical applications are bearings, seals, coupler surfaces, or shaft repairs, as shown in **Figure 11**.

http://dx.doi.org/10.5772/66874

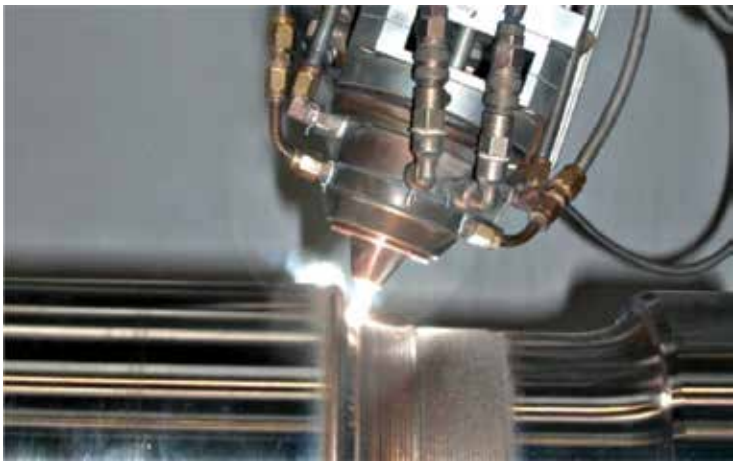

Figure 11. Laser cladding technology of wear-resistant material on shaft surface [18].

Creation of completely new components is done with the use of laser free-form manufacturing technology. This technology allows complete buildup of complex-shaped parts—free forms based on 3D computer model. This technology is applicable in prototyping or production of unique special components. The result of LFMT is almost 100% dense material with properties comparable with wrought material. Typical minimum wall thicknesses of free forms are of 1.5 mm [19]. Examples of these process products can be seen **Figure 12**.

Figure 12. Examples of parts produced by free-form technology [18].

4. Postprocessing technologies for additive manufactured parts

Although it is usually referred to additive manufactured parts, they are net shaped; some postprocessing is necessary in most cases of AM components. There are two basic reasons for subsequent processing of AM parts: geometry and properties. During AM processes there is always present partial or complete local volume melting followed by subsequent rapid cooling due to high metal conductivity of a large volume of surrounding bulk material in relation to melt size. These results in many cases in properties that are significantly lower than those achievable for bulk materials. Therefore, subsequent thermal or thermomechanical treatment provides significant improvement of mechanical properties. Additionally, it removes some residual stresses after AM.

The surface of AM components is generally uneven with visible layers or places where supporting structures were attached in the course of AM. Geometry itself can be slightly distorted by thermal stresses present during AM. Therefore, in many cases some additional processing either from dimensions or surface point of view to be applied to AM products is necessary. In cases where surface has some special function (decorative, sliding, etc.), blasting, grinding, and polishing can be applied for final-state surface achievement. In cases of high precision parts, machining is unavoidable in order to achieve desired geometrical tolerances.

The surface after AM can be uneven, and due to thermal stresses during AM, some small geometry distortions have to be expected.

Author details

Jan Džugan* and Zbyšek Nový

*Address all correspondence to: jan.dzugan@comtesfht.cz

COMTES FHT a.s., Dobřany, Czech Republic

References

[1] S. Yenwiset and collective: Effect of the Molten Metal Stream's shape on particle size distribution of water atomized metal powder, Engineering Journal, Vol. 20, No. 1 (2016), pp. 187–196. DOI: 10.4186/ej.2016.20.1.187.

[2] EPMA: Introduction to Additive Manufacturing Technology, European Powder Metallurgy Association, UK. (2012). www.epma.com/am [Accessed: 5.8.2016].

[3] U. Fritsching and V. Uhlenwinkel: Powder Metallurgy, Published by InTech, edited by Katsuyoshi Kondoh, ISBN 978-953-51-0071-3, (2012).

[4] ALD: Electron Beam Melting (EB) [Internet]. Available from: http:// http://web.ald-vt.de/cms/vakuum-technologie/technologien/vacuum-metallurgy/ [Published 2013, Accessed: 5.8.2016].

[5] InTech [Internet] (2012). Available from: http://www.cdn.intechopen.com [Accessed: 5.8.2016].

[6] Loughborough University: About Additive Manufacturing [Internet]. Available from: http://www.lboro.ac.uk/research/amrg/about/the7categoriesofadditivemanufacturing/powderbedfusion/ [Published 2014, Accessed: 5.8.2016].

[7] lay3rs: Available from: http://www.lay3rs.nl/en/ [Published 2014, Accessed: 5.8.2016].

[8] L. E. Murr and collective: Metal fabrication by additive manufacturing using laser and electron beam melting. Journal of Materials Science & Technology, Vol. 28, No. 1 (2012), pp. 1–14.

[9] S. M. Gaytan and collective: Advanced Metal Powder Based Manufacturing of Complex Components by Electron Beam Melting. Journal Materials Technology, Vol. 24, 2009 – Issue 3.

[10] T. Grünberger and collective: Direct metal laser sintering, identification of process phenomena by optical in-process monitoring. Laser Technik Journal, Vol. 12, No. 1 (2015), pp. 45–48.

[11] Available from: http://www.popular3dprinters.com/direct-metal-laser-sintering-dmls/, published 2013.

[12] J. P. Kruth and collective: Selective laser melting of iron-based powder, Journal of Materials Processing Technology, Vol. 149, No. 1–3 (2004), pp. 616–622.

[13] L. Langnau. New Dimensions in 3D Printing: Free-form Fabrication [Internet]. (2014). Available from: http://www.makepartsfast.com/new-dimensions-3D-printing-free-formfabrication/ [Accessed: 5.8.2016].

[14] LPW: Laser Metal Deposition [Internet]. Available from: http://www.lpwtechnology.com/technical-library/technical-information/laser-metal-deposition/ [Accessed: 5.8.2016].

[15] K. I. Schwendner and collective: Direct Laser Deposition of alloys from elemental powder blends. Scripta Materialia, Vol. 45 (2001), pp. 1123–1129.

[16] RPM Innovations: Laser Deposition Technology (LDT) [Internet]. Available from: http://www.rpm-innovations.com/laser_deposition_technology [Accessed: 5.8.2016].

[17] D. Gu: Laser Additive Manufacturing of High-Performance Materials. Springer. (2015). 332 p. DOI: 3662460882.

[18] Laser Cladding: Laser Cladding Process [Internet]. Available from: https://www.researchgate.net/figure/281686549_fig2_Fig-2-Blown-powder-Direct-Laser-Deposition-DLD-with-thermal-monitoring, published 2015. co.uk/Laser-Cladding-Process.aspx [Accessed: 5.8.2016].

[19] RPM Innovations: Laser Freeform Manufacturing Technology (LFMT) [Internet]. Available from: http://www.rpm-innovations.com/laser_freeform_manufacturing_technology [Published 2014, Accessed: 5.8.2016].

Chapter 9

Fabrication, Structure, Properties and Application of Gradient Sintered Carbide-Steels with HS6-5-2 Matrix

Leszek Adam Dobrzański and Anna Kloc-Ptaszna

Additional information is available at the end of the chapter

http://dx.doi.org/10.5772/65379

Abstract

This chapter presents essential information concerning sintered tool materials containing carbides, i.e. high-speed steels and metal matrix composites, including sintered carbides and carbide steels. Gradient materials, whose properties change gradually according to their volume, are characterised. The results of investigations are presented in the final part into the structure and properties of newly developed sintered graded tool materials fabricated by the conventional metallurgy method from a mixture of high-speed HS6-5-2 steel powder and WC carbides. Investigations are described for four-layer materials, where the successive transition layers with a smaller and smaller volume fraction of tungsten carbide were constituted from the surface layer side, until a substrate layer containing high-speed HS6-5-2 steel only. The outcomes are described of structural examinations in a scanning and transmission electron microscope, an X-ray microanalysis and the results of density, porosity and hardness examinations of sintered gradient materials and the results of structure and hardness examinations of heat-treated materials.

Keywords: gradient tool materials, uniaxial pressing, sintering, high-speed steel, tungsten carbide, vanadium carbide

1. General characteristics of carbide-reinforced sintered tool materials

Technical progress in tools manufacturing is manifested, most of all, by endeavours to produce tools with better properties, and powder metallurgy plays a key role in such activities. Methods permitting to improve production quality and effectiveness have been sought for continuously. The main directions of development are centred on creating new and improving the existing methods of manufacturing; on preparing and compressing powders from which sintered tool

materials are produced; on optimising the chemical composition of materials and improving the techniques of tool surface deposition with hard antiwear layers and the techniques of surface layer constitution. The fundamental direction of development should be the optimisation of chemical composition of the existing tool materials possessing good functional properties [1, 2]. The common characteristic of various materials is that, as hardness is rising, they become more brittle. Where high cracking resistance is required, material hardness is decreasing (**Figure 1a**). Efforts are hence being made to raise the ductility of materials with higher hardness.

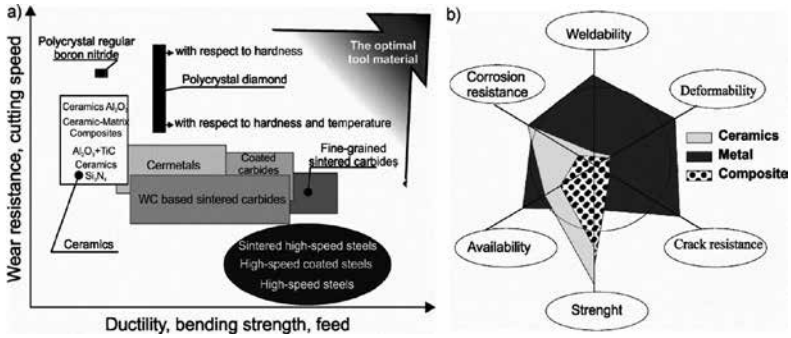

Figure 1. The schema of: (a) comparison of tool materials' properties by range and (b) selected properties of metallic, ceramic and composite materials.

Cutting tool edges are subject to various wear mechanisms in service, thus the quality of tool materials should satisfy specific requirements [1–5]. Tool materials should be characterised by:

- high hardness and possibly high ductility and high rigidity and fatigue strength to dynamic loads occurring during tool work;
- high abrasive wear;
- high resistance to the annealing activity of elevated temperature;
- good thermal fatigue resistance;
- good machining and cutting properties;
- high dimensional stability, especially important for gauges and measuring tools;
- good resistance to the harmful activity of grinding;
- good resistance to corrosive factors.

It is difficult to produce a material satisfying all the desired properties at the same time, as some of them are mutually exclusive. The application range of specific material groups has therefore been established, for which minimised wear, and consequently, service life, are the fundamental criteria for selection of the particular material type.

Tool material selection is always a compromise solution between high abrasive resistance and mechanical properties. Significant progress in production efficiency has been achieved by

http://dx.doi.org/10.5772/65379

applying advanced tool materials enabling machining with high cutting rates with the increased section of the layer being cut and with different geometrical characteristics of the edge. Their use as tool cutting parts is limited, though, due to a high price of such materials. For this reason, for example, sintered tool inserts are mounted on shanks or holders made of cheaper materials whose job is to transfer cutting forces. The best solution would be to combine the properties of metallic materials with the properties of ceramic materials, namely to produce metallic-ceramic composites (**Figure 1b**).

Hardness is the key criterion in tool material selection. It should be at least 30 HRC higher than hardness of the worked material. It is important because it is possible these days to work materials whose hardness is much higher than the hardness of many tool materials (e.g. steels hardened to 70 HRC). The hardness of tool materials can be substantially increased by changing their chemical composition. One of the directions may be an attempt to change the relative volume of hard reinforcing phases and a matrix in tool materials with a binding matrix. Furthermore, if such a change is controlled and takes place in the direction defined, a graded material is achievable with high hardness in the surface layer, while maintaining considerable continuity in its remaining part. The chemical composition, structure and properties can be freely customised in such materials using the powder metallurgy methods generally described in one of the previous chapters. High-speed steels (HSS) are an important group of sintered tool materials with a much more uniform structure as compared to conventional steel grades. The usable properties of the cutting edges manufactured from such materials have been enhanced by eliminating the basic drawbacks of conventional high-speed steels such as uneven distribution of components and carbide banding [2–5]. The technological and service properties of high-speed steels are largely dependent on the powder fabrication method and its granulation degree. It may therefore be misleading to compare the properties of steels with the same chemical composition without knowing the factors mentioned. High-speed steels are fabricated from powders obtained by sputtering liquid steel, with appropriate chemical composition, by means with water or insert gases, mainly argon, helium or nitride. Steel melting takes place usually in a medium-frequency induction furnace. Liquid metal is poured into a melting pot placed on the top of a chamber which is more than ten metres high. Afterwards, the liquid metal flows through a centric orifice into a chamber into which gas or water is supplied simultaneously, atomising the flowing metal stream into very fine droplets. The droplets, while falling onto the chamber bottom, are cooled with gas and solidify in the form of ball-like grains collecting on the chamber bottom. The so-obtained powder is sifted to remove oversized grains. The composition and size of powder grains is adjustable by selecting suitable atomisation conditions, i.e. temperature and a fraction of liquid metal and by changing the pressure and gas flow rate [2, 5, 6]. High-speed steel powders atomised with water feature a frayed shape and good compressibility. In respect of gas-atomised powders, they are more oxidised (have a 20–50 times higher concentration of O_2). Water-atomised powders are oftentimes additionally crushed mechanically (in vibration or ball mills) and powdered to the diameter of 0.001–0.002 mm. Finished mouldings can be moulded from such powders by the uniaxial cold pressing method and sintered until a moulding is fully compressed, or additional hot isostatic pressing can be applied [2, 4–7]. The shape of the sintered mouldings is similar to the shape of a ready product and have the relative density of over 65%. Approximately 10%

linear contraction in sintering has to be taken account of in designing moulding dimensions. Inert gas-atomised powders are ball-shaped with the diameter of 0.01–1 mm and a lower concentration of O_2, good liquidity, but poor compressibility. The most often used method of high-speed steel making is a Swedish ASP method, by ASEA-STORA company. Powder undergoes cold isostatic pressing in this method in a cylindrical container for pre-compression. Pressing pressure is about 400 MPa. Next, the moulded block undergoes hot isostatic pressing in the atmosphere of argon, at the temperature of 1150°C and under the pressure of 100–150 MPa in specially constructed Quintus presses. Bars are made from the so-manufactured semi-product by plastic working, the same as for conventional high-speed steels cast as ingots weighing several hundred kilos, and tools are produced from such bars in a plastic working and machining process [2, 4]. The method has been modified differently over time, including in STAMP and MICROCLEAN processes [5]. Powder injection moulding (PIM) and low-pressure moulding processes are employed more and more often to produce high-speed steels [8–11]. Metal powder in both cases is mixed with a binding agent to produce powder mass suitable for moulding. In injection moulding, a mixture of powders is additionally plasticised in a heated injection moulder cylinder and then injected into a mould via a nozzle. The moulded preforms are degraded thermally, as a result of which the binder is removed and then they are sintered. It was concluded based on the examinations of the structure and properties of HS6-5-2 high-speed steel fabricated by powder injection moulding, low-pressure moulding, pressing and sintering, that a common advantage of injection moulded and low-pressure moulded steels is a broader sintering temperature range in relation to steels produced by a conventional powder metallurgy method, for which it is approximately 5°C [8–10, 12, 13]. Injection moulded steels possess the lowest sintering temperature and the highest density as compared to pressed and sintered steels, resulting from a high concentration of carbon coming from binder degradation. Powder injection moulding also enables to produce ready-made tools, i.e. without plastic working and machining. Cutting tools made of sintered high-speed steels are heat treated to achieve an optimum structure consisting of fine matrix grains with identical size and carbides uniformly distributed in it. In the softened condition, the structure of sintered high-speed steels contains alloy ferrite with uniformly arranged MC, M_6C and $M_{23}C_6$ carbides and also contains M_2C carbides in steels with a high concentration of molybdenum and M_7C_3-type carbides in steels with a high concentration of silicon, and in steels containing $M_{23}C_6$-type carbides with a higher concentration of carbon [2, 4, 14–17]. Heating to the austenitisation temperature is usually performed in salt baths with indirect heating at the temperature of approximately 550 and 850°C, for 15 min. Austenitisation temperature for particular grades of sintered steels is lower by approximately 230–250°C compared to the austenitisation temperature of conventional steels with the analogous chemical composition. This is caused by the initial sizes of carbides. Fine carbides in sintered steels are dissolving faster than larger ones in conventional steels. With gradual heating, the time of austenitisation depends on the austenitisation temperature and is going down as the temperature is rising. Cooling from the austenitisation temperature is usually done in salt bath. Cooling in oil bath or in vacuum is also allowed [2, 4]. The same transformations take place in sintered steels as in conventional steels during cooling. The steel structure after hardening contains martensite, retained austenite (approximately 25%) and M_6C and MC carbides

http://dx.doi.org/10.5772/65379

unsolved during austenitisation, whose fraction in the structure depends on the steel grade and accounts for 20–25%. High-speed sintered steels are annealed twice or thrice, in the temperature range ensuring the maximum secondary hardness (550–560°C). The secondary hardness effect attained is caused by the precipitation of coherent M_4C_3 carbides in a martensitic matrix and by the transformation of retained austenite into martensite during cooling from the tempering temperature [4, 14–19]. The secondary hardness range in sintered steels is shifted to a slightly lower temperature than in convention steels with a similar chemical composition. The maximum hardness achieved depends on the applied austenitisation temperature [2, 4, 14–19]. The fabrication costs of sintered high-speed steels are higher than manufacturing costs of conventional steels, but the tools made of sintered steels are much more durable than those made of conventional steels. A homogenous structure of sintered steels and a sintering technology enabling to produce materials with a higher concentration of carbon and alloy elements than for conventional steels have an effect on that. Higher hardness of such materials can be attained whilst maintaining comparable ductility, and, consequently, higher abrasive resistance. Moreover, sintered high-speed steels allow for much better hot plastic forming and machining and are more susceptible to heat treatment than conventional steels. The dimensional changes taking place in such steels as a consequence of a martensitic transformation and release processes during tempering can be anticipated and considered in grinding allowances. Sintered high-speed steels are also distinct for very good grindability, whereas the steels made by isostatic hot pressing exhibit better susceptibility to grinding than those sintered in a vacuum [2, 4–6]. The tools made of sintered high-speed steels usually have better cutting properties than conventional steels with the same chemical composition. This is especially true for the treatment of steels that are hard to cut, at higher cutting rates. The indicators showing an increase in tool service life depend on the tool type and treatment conditions (including mainly the strength of the worked material) and may span between several dozen to several hundred per cents as cutting speed is rising. Additionally, it is apparent by analysing the relationship between manufacturing costs of cast and sintered high-speed steels over the last years that the manufacturing costs of sintered high-speed steels are decreasing and are approximating the manufacturing costs of conventional high-speed steels and coincide for some grades of such steels.

Tool materials with a binding matrix represent another important group of sintered tool materials. These include particulate-reinforced sintered metal matrix composites in which sintered carbides are the basic group [2, 5, 20]. Sintered carbides are also considered to be, apart from high-speed steel and carbide steels, a group of materials based on carbides of transition metals. Such classification derives from the volume fraction of carbides in the material structure [2, 4, 20]. The main components of conventional sintered steels are tungsten carbide WC and cobalt, used as a binder metal. The sinters of hard carbides of high-melting metals such as VC, TiC, TaC, NbC are also considered to be sintered carbides and nickel or iron can also be a metal matrix apart from cobalt. The carbides mentioned are distinct for their high hardness (1900–2500 HV), critical for good abrasive wear resistance of sintered carbides. However, as such carbides are highly brittle, this is limiting their application as the materials exposed to the acting dynamic external loads, e.g. in the use of cutting tools [2, 4]. As the relative volume of carbides is growing, so is growing hardness and resistance of sintered carbides to

wear in cutting, bending strength is declining, though. A higher relative volume of a metal matrix raises bending strength and reduces hardness and wear resistance in cutting [4, 5, 20]. TiC carbide improves hardness and wear resistance in cutting, but at the same time decreases the bending strength of sintered carbides. NbC and TaC carbides raise hardness at ambient and at elevated temperature, and also the bending strength of sintered carbides [2, 4]. Various aspects of fabrication and technical applications of sintered carbides are discussed in a few chapters of the book, hence only certain related aspects are touched upon in this chapter.

The manufacture of products from sintered carbides is a complex technological process. The first step in the process is to produce carbide powder by the numerous methods of: melting, carburising of powders of pristine metals, metal oxides or hydrocarbons in the solid state by sintering, carburising of powders of pristine metals, metal oxides or hydrocarbons with gases containing carbon, precipitates of gas phase, carbide precipitations from melted metals or electrolysis. Next, carbides are usually cleaned and crushed. Carbide products are manufactured by powder metallurgy methods by pressing and sintering and hot pressing [4–7, 20]. The following technologies can also be employed: pressure sintering technologies with induction heating, extrusion of bars and sleeves from powders with plasticisers added, and casting in a suspension. Such methods enable to form large-size, high-density products and such with untypical shape for sinters, e.g. rods or plates [2, 4–7, 20]. The sintered carbide grades most commonly produced are characterised by a conventional structure with carbides sized several micrometres or with carbides with their size smaller than 1 μm. The properties of sintered carbides are principally dictated by the chemical composition of carbides, by the shape and size of their grains and by the volume fraction of carbides in the structure. The most significant property of sintered carbides is their hardness in high temperature, allowing cutting at high rates.

Sintered carbides are finding their applications most of all as materials for cutting iron alloys, non-ferrous metal alloys, non-metal materials and rocks and for plastic working tools. Some grades of sintered carbides featuring a high concentration of cobalt are utilised as constructional materials of machine parts from which good abrasive resistance is required, especially at elevated temperature, e.g. slide and roller bearing parts, nozzles, guides, blades in heat machines and hydraulic plungers [2, 4–7, 20].

Carbide steels with indirect properties between tool steels and sintered carbides also belong to the group of particulate-reinforced metal matrix sintered composites. Their wear resistance versus high-speed steels is 10–20 times higher. The chemical composition of a matrix in traditional carbide steels corresponds to structural steel for quenching and tempering, stainless austenitic steel or precipitation-reinforced maraging steel. A carbide phase consists of titanium carbides TiC, which are practically insoluble in a steel matrix in heat treatment. A relative volume of a matrix in a sinter is much higher than in sintered carbides and accounts for over 50% [2, 4, 20]. Carbide steels have, therefore, higher ductility than sintered carbides, and also much higher abrasive wear resistance than tool steels. The tools made of carbide steels after sintering undergo mechanical and heat treatment (quenching and tempering). One of the chapters also describes special carbide steels with a matrix of high-speed steels with carbides of transition metals, including WC, VC, TiC, NbC and their unique manufacturing technology.

http://dx.doi.org/10.5772/65379

An advantage of carbide steels is the fact that their mechanical properties may vary over a broad range depending on the matrix material and the condition of heat treatment. The pressing and sintering of a mixture of carbide and steel powders or saturation of a pre-sintered porous carbide skeleton with steel are classified as carbide steel manufacturing methods [2, 4–7, 20]. Variations in the properties of a particulate-reinforced composite enables to combine reinforcement properties with matrix properties. The effective properties of a composite are thus dependent upon the properties and relative volume of the components forming it.

2. General concept of sintered gradient materials

Gradient materials are one of newer generations of engineering materials in which properties change gradually in the material volume as chemical composition, grain size, structure or atomic order are changing [2, 21–23]. Such materials are not a technically separate group of materials, but rather represent an engineering approach to chemical material structure and/or chemical composition formation. Such an approach is most advantageous when one material may ensure a diverse combination of properties which is hard to achieve, as in the case of the required high hardness, and also high ductility of tool materials [23]. The manufacture of such materials is hard, tough. A graded structure can be obtained by, among others, reinforcing a matrix with precipitates or particles having diverse properties, size and shape, and also by changing the function of the reinforcing phase and matrix. A material structure can then be achieved with properties changing continuously or discreetly. The examples of gradient structures are also observable in nature, for instance in plant and animal tissues, bones, teeth and shells [21]. A representative example of a graded structure is a bamboo stalk. It has a very strong outer surface and an elastic core. Fibre distribution changes on the stalk section, ensuring its high flexibility and strength.

The potential benefits resulting from the use of graded materials were considered theoretically already in 1972 [24]. It was not sooner than in 1984–1985 in Japan when a concept of functionally graded materials (FGM) was developed in aeronautics [25]. The use of graded materials as heat barriers in space shutters was considered. Systematic researches over the fabrication of such materials were initiated in 1987 under a research project [22, 26], and the Research Society for Functionally Graded Materials publishing the *FGM News* was set up a year later. An international conference on functionally graded materials, stimulating rapid advancements in materials production, has been regularly held in Sendai, Japan, since 1990 [27]. Many of the researches on graded materials are addressed to modernise and improve their manufacturing technologies already known and to search new low-input technologies with high reproducibility and performance. As growing interest in graded materials has been observed, it becomes necessary to carry out research on optimising the chemical and phase composition of such materials and their manufacturing technology.

Graded materials can be classified according to different criteria, usually in terms of structural criteria, manufacturing methods and application. With regard to their application, such materials can be divided into, notably, functionally graded materials [22, 26], tool gradient

materials (TGM) [28–36], gradient biomaterials and functionally graded piezoelectric materials (FGPM). Gradient materials, according to the type of combined materials, can be grouped into, particularly [37]: metal material-ceramic material, metal material-metal material, ceramic material-ceramic material, polymer material-ceramic material. Gradient materials are also grouped by their manufacturing methods. For example, for the powder metallurgy method, which is often used, materials can be produced with porosity gradient or porosity size, chemical composition in a single-phase material, volume fraction of phases or grain size in a material with two or many phases [22, 27]. Gradient materials can also be grouped according to gradient distribution (one-, two- or three-dimensional) or gradient range (gradient situated in a particular area, or extending in the whole section).

Different physical and chemical methods can be used for manufacturing gradient materials. It is hard to say which one of them best fulfils its task and technical requirements resulting from a complicated structure of materials. The combination of different manufacturing methods may solve problems with production of gradient materials. The combinations of such methods depend on the state of the input material and its properties. Apart from the cases where an input material is in the gaseous or liquid state and by concentrating on the solid state, the use of different powder methods should be listed, allowing easily to select the input composition of a moulding [22, 37, 38]. Several key methods of gradient material manufacturing have been developed until now, such as powder metallurgy methods, and also coating deposition methods and diffusion-based methods [1, 21, 27]. The main advantage of powder metallurgy methods is that the selection of output composition of a moulding can be controlled, which allows to obtain a sinter with variable chemical composition of phases in the material volume. Gradient materials in a conventional powder metallurgy method can be produced by filling a matrix with subsequent layers of powder mixtures differing in their chemical composition, and then the mixtures are pressed and sintered. The composition of powders depends on the required properties of the fabricated material. For instance, materials can be achieved with porosity gradient, by filling a mixture of powder with various particle size or by changing compression conditions, and with pore size gradient, by differentiating the size of powder particles. A chemical composition gradient is also attainable. If a phase balance chart indicates potential solubility above the selected range of chemical composition of a gradient material, a single phase material with a mild variation of concentration is created when sintering a mixture of powders with continuous chemical composition variation. In order to achieve a gradient material structure, a condition has to be satisfied saying that the diffusion range of the differing atoms must be higher than the average size of particles [23]. Layer thickness can to be taken into account if filling is done in successive steps. The most popular group of graded materials are those with the gradient of the volume fraction of phases or grain size in a multi-phase material. Multi-component systems of phase balance are usually distinct for the limited solubility of components. The growth of soluble phase grains in heat treatment has to be considered, especially in sintering with the presence of the liquid phase. As a result, the structure of the material obtained consists of two or more phases with a gradient in the volume of the material or grain size. Although powder moulding by filling and pressing a large number of powder layers (over 5) in a die is an uneconomical process in industrial terms, it is widespread in laboratory tests [11, 27, 36, 39].

http://dx.doi.org/10.5772/65379

Gradient materials manufactured by powder metallurgy methods are most often characterised by a gradient step of chemical composition. Automated systems of component dosing or centrifugal force are applied to avoid uneven transition between layers. The consolidation method of input materials is largely impacting the content of the structure and the character of the chemical composition change, especially in the region of layers' boundary. A liquid phase emerges very frequently when sintering multi-phase mixtures or a chemical reaction takes place [40]. Sintering with the presence of the liquid phase usually occurs at a temperature higher than the lowest melting point of one of mixture components. A sintering process is inherent to the presence of the liquid phase. A disadvantage of the process is a difficulty to maintain a concentration gradient, which sometimes tends to disappear due to component homogenisation processes [41, 42]. This can be solved by shortening the time needed to consolidate components to avoid their homogenisation. A high-temperature synthesis is used where the heat necessary for sintering comes from a chemical reaction. Self-propagating high-temperature synthesis (SHS) is a method of synthesising chemical compounds utilising mainly the heat of exothermic reactions taking place in the system. In this method, powders are heated to the adequate temperature, after exceeding which the reaction is running by itself. The method is especially effective for a synthesis of such compounds as carbides, but also oxides, nitrides and borides. The compounds are highly refractory, for this reason, to synthesise their powders, processes are necessary most often, which are occurring at measureable speed only in high temperature of 1000–2000°C. When chemical compounds are synthesised conventionally, e.g. by a mixture of constant reagents in an oven, high heat losses to the surrounding occur and heat has to be supplied constantly from external energy sources to maintain a high temperature and the reaction running. The processes are energy- and time-consuming [1, 21, 37, 43].

Different coating deposition techniques are utilised to produce graded coatings [8, 44–47]. The most widespread ones include vacuum deposition (PVD, CVD). A non-gradual change in properties occurs between the coating and the substrate, causing a concentration of stresses in the boundary region during material production and usage. Fast degradation, consisting of coating cracking and delamination, takes place in this region as a consequence. PVD and CVD methods create an opportunity to set off unfavourable phenomena and to obtain a relatively thin layer which is between several to more than ten micrometres thick. A graded coating can be produced by dosing components which are critical for the properties of the materials and by changing residual pressure or reactive gas in the deposition chamber [1, 21, 23]. Graded coatings have broad applications due to their specific properties, such as resistance to high temperature oxidisation, erosion and abrasive wear resistance. Depending on the usage, they can be grouped into, in particular, wear-resistant coatings (WRC) and thermal barrier coatings (TBC).

Nanocrystalline functionally graded materials represent a promising direction of development in modern coatings. Advanced PVD methods, in particular pulsed laser deposition (PLD), are applied to produce mono- or multilayer coatings with a nanocrystalline structure [48]. The method has been employed successfully for producing biocompatible coatings based on TiN

and hydroxyapatite, designed for use in production of bone implants and hemocompatible materials.

Own works cover numerous investigations of graded coatings deposited onto tools produced by a PM method. Graded coatings are applied in a PVD process by reactive magnetron sputtering (RMS), by Cathodic arc evaporation (CAE), Thermionic arc evaporation (TAE), Reactive ion plating (RIP) methods and by CVD method [44–46, 49–51]. The aspects of this method are detailed in one of the chapters.

The other, commonly applied graded coating manufacturing technologies include remelting, alloying and laser cladding technologies [2, 52]. They ensure good properties of a surface layer and good substrate attachment. Due to differing substrate and surface layer properties, layer cracks in the substrate heat affected zone and in the area of surface layers occur during laser production of surface layers. Cracking can be limited or totally eliminated by applying a graded fraction of hard ceramic phases or a graded fraction of an alloying component in the surface layer. If an indirect layer is used between a surface layer and a substrate, good attachment is ensured along with high corrosive resistance, wear resistance, high hardness, ductility, plasticity and fatigue strength of a coating [53, 54]. These issues are discussed in one of the first chapters of the book. Own research into laser surface engineering using a high performance diode laser [49–52, 55, 56] have shown that alloying/laser cladding technologies ensure the highest quality, 0.1–1.5 mm thick surface layers and a very high quality of the substrate attachment. The materials achieved possess enhanced abrasive wear resistance as well as good mechanical and tribological properties. Very high resistance to thermal fatigue of materials is achieved by alloying with NbC, TaC, TiC, VC and WC carbide particles.

Thermal spraying, known for many decades, offers broad opportunities to produce graded layers. Plasma spraying (PS) was patented already in 1960 and 1962. In this method, a material constituting a layer is melted in a stream of plasma and the melted particles are directed at high velocity by a stream of plasma gas onto an appropriately prepared surface [2, 57, 58]. Plasma spraying can take place in two variants. In the first of them, a coating forming the material is supplied by one burner. In the other, a system of burners with different powders is used, allowing to produce coatings easily and efficiently. Layers with specific heat parameters can be obtained with this method, e.g. thermally insulating TBC coatings [2, 47, 59, 60] and other coatings, e.g. biocompatible ones (hydroxyapatite). The methods are also generally characterised in one of the previous chapters of the book.

Materials with a graded structure can also be constituted with heat treatment processes known for thousands of years, e.g. by hardening or thermochemical treatment processes, such as carburising and nitriding [2]. Only part of the scientific environment shares a view that a material, in which surface treatment is carried out only, without combining two different materials, should be considered a gradient material. It is true, however, that a gradient of chemical composition and properties exist in the volume of such a material. Moreover, such methods, for long, were dominant as a fabrication technique of materials with a structure changing on their surface.

http://dx.doi.org/10.5772/65379

There are many gradient material manufacturing processes. Modernised or innovative manufacturing methods are often found in publications concerning gradient materials. Gradient materials offer extensive application possibilities. About 200 potential uses were proposed in 1990 in a survey made by *FGM Forum*, among others in machine, car, optic and power industry and even in nuclear physics and medicine [61]. Gradient materials are broadly used for producing parts where, in the conditions of use, a high temperature gradient exists, in particular in the space and aviation industry [1, 21, 23, 37]. They are used for producing heat barriers, shell plating or rocket engine parts most often [1, 43, 59]. Gradient materials can be used in a combustion chamber of jet turbine engines where very aggressive conditions prevail for the materials used. An innovative solution is a construction of segmented semiconductor heat sensors. The sensor is built of several modules differing in a thermal and electrical conductivity coefficient. The so-produced element has its resultant characteristic almost independent from its working temperature; any changes in electrical conductivity result only from the sensor surface layer profile being formed. It is thus easy to monitor temperature by measuring voltage on the sensor electrodes. An additional advantage is sensor construction, owing to which the sensor can have dimensions of several tenths of millimetre. It is thus possible to incorporate a sensor inside the element which is diagnosed and thus protects the sensor against an aggressive environment or mechanical damage, e.g. in a jet engine combustion chamber. Gradient materials are also used for producing solid oxide fuel cells (SOFCs), where the problem is to maintain the suitable cell durability at high working temperature of about 950°C due to various thermal expansion coefficients of its particular parts. Such a cell incorporates a cathode made of (La, Sr)MnO_3 and a cermetal Ni/ZrO_2 anode, with permanent electrolyte in between (ZrO_2 stabilised with yttrium oxide). The application of gradient materials allows to achieve cell efficiency of even 40% higher compared to a traditionally made fuel cell. Works are in progress over gradient piezoelectric excitation elements [62]. Traditional excitation elements are highly unreliable due to materials with different piezoelectric properties. At low temperature, the connecting layer, usually made of epoxy resin, is cracking and at higher temperature is excessively creeping. Hence, efforts are made to develop gradient piezoelectric excitation elements in the system of PZT (Pb(Zr, Ti)O_3)/PNN ($PbNi_{1/3}Nb_{2/3}O_3$) materials, connected diffusively [63]. Intensive studies are also held over gradient optic fibres ensuring the same light wave propagation velocity along the conductor for different modes. A core of a gradient optic fibre is made of many thousands of layers. This is aimed at simulating a smooth change of the light refractive indexes. The maximum light refractive index value is assumed on the core axis and the minimum on the boundary with the jacket. This is eliminating signal blurring to the same level as the waves propagated in larger distance from the centre are moving in the layers with a lower refractive index, hence have higher linear speed. The shape of a single mode is similar to the sinusoidal waveform. Bandwidth was consequently increased by the order of magnitude compared to a step optic fibre.

The biomedical branch is the next area of potential applications of materials with a property gradient [61, 64]. In bone surgery, ceramic materials with a porosity gradient can be used for fabrication of orthopaedic gradients, which are designed just like a living bone tissue [65–70]. The works [71, 72] describe orthopaedic implants made of hydroxyapatite and titanium. Bioactive hydroxyapatite is responsible for a strong connection with an organic tissue in such

implants, whereas titanium is used in the parts of the implant requiring high mechanical stability. Gradient and porous materials are studied in the works [66–70], applied for implants, implant-scaffolds and scaffolds manufactured by selective laser sintering, what is detailed in the respective chapters of this book.

Gradient materials may also play an important role in the machine industry, for example in a toothed gear manufacturing technology, where a body of an element should be resistant to dynamic loads, while its surface should be hard and abrasive resistant. The differing core and surface layer properties are now achieved by carburising the surface of steel toothed gears. A state-of-the-art solution can be the production of toothed gears with the inner layers made of metal, while the outer layers would consist of hard ceramics attached to metal with indirect layers. Tool gradient materials are usually designed in such a way as to ensure high abrasive resistance of tools in the working layer, while maintaining a ductile core which ensures that high dynamic loads are transferred. Sintered carbides, sintered carbide steels and sintered high-speed steels can be used as the material of a working part [1, 73–75]. An example of a tool gradient material can be a gradient sintered carbide. Such a material consists of sintered carbides WC-Co, cermetal TiCN-Ni and a thin ceramic layer made of sintered carbides [1, 74].

3. The results of own investigations into sintered gradient tool materials

Gradient material technologies have gained special importance in tool production. Cutting tool edges are subject to various wear mechanisms in service, and for this reason, special properties are required for them. The best solution would be to develop a material which, on one hand, would be characterised by high hardness, on the other, relatively high ductility. It is hard, however, to manufacture a material satisfying at the same time such contradictory properties, because as their material hardness is rising, they become more brittle. A solution to this problem may be to produce gradient materials representing a special group of composite materials. It is being endeavoured to fabricate materials with a varying fraction of hard reinforcing phases and matrix in their volume. If such a change is controlled and takes place in the direction defined (e.g. perpendicular to the surface), a graded material is achievable with high hardness in the surface layer while maintaining considerable continuity in its remaining part. A graded structure can be obtained by, among others, reinforcing a matrix with precipitates or particles having diverse properties, size and shape. The chemical composition, structure and properties of materials can be freely tailored using the powder metallurgy methods. Graded materials in the conventional powder metallurgy method can be produced by filling a matrix with the subsequent layers of powder mixtures. The mixtures differ in their chemical composition depending on the required properties of the material produced, and then the mixtures are pressed and sintered. The most popular group of graded materials are those with the gradient of the volume fraction of phases or grain size in a multi-phase material. Particulate-reinforced metal matrix composites are an important group of sintered tool materials. Reinforcement properties can be combined with matrix properties by forming the properties of composites. The effective properties of a composite are thus dependent upon the properties and relative volume of the components forming it. An example can be high-speed

http://dx.doi.org/10.5772/65379

steel having relatively high ductility applied onto a matrix material, and carbides with high hardness used onto reinforcing particles. The research now conducted by various research institutes is aimed at the fabrication of high-speed steel matrix composites with raised abrasive wear resistance. The works [1, 76–78] studied the effect of additives of WC, TiC, VC and NbC carbides on the structure and properties of high-speed steel matrix composites of HS6-5-2, HS6-5-4 and HS12-1-5-5 type. It was found that, as the relative volume of carbides is growing in the high-speed steel matrix, so is growing hardness and wear resistance of composites; their bending strength is declining, though.

Investigations were performed under own works [11, 28–36, 48, 79] to create a new group of gradient sintered carbide steels on a high-speed HS6-5-2 steel matrix, reinforced with hard WC carbide phases, to develop their manufacturing technology and identify their structure and properties.

The newly developed graded carbide steels were produced by uniaxial pressing and sintering in a vacuum furnace and in a furnace with the atmosphere of flowing nitrogen with the addition of hydrogen (N_2 + 5% H_2), at temperature of 1210–1270°C, for 30 and 60 min. The steels consisted of four layers, and the successive layers were constituted by decreasing a fraction volume of the reinforcing phase, until a substrate layer was obtained containing high-speed HS6-5-2 steel only. Its surface layer and transition layers contained, respectively, 25, 15 and 5% and 10, 7 and 4% of WC carbide. The powders were mixed for an hour, and powder mixtures were next filled successively into the matrix, thus producing layers with a gradually changing volume fraction of carbides in high-speed steel. The next transition layers containing, respectively, 15 and 5% of such carbides, were constituted—for the volume fraction in the surface layer of 25% of WC—and then they were pressed (**Figure 2**) and sintered, followed by heat treatment.

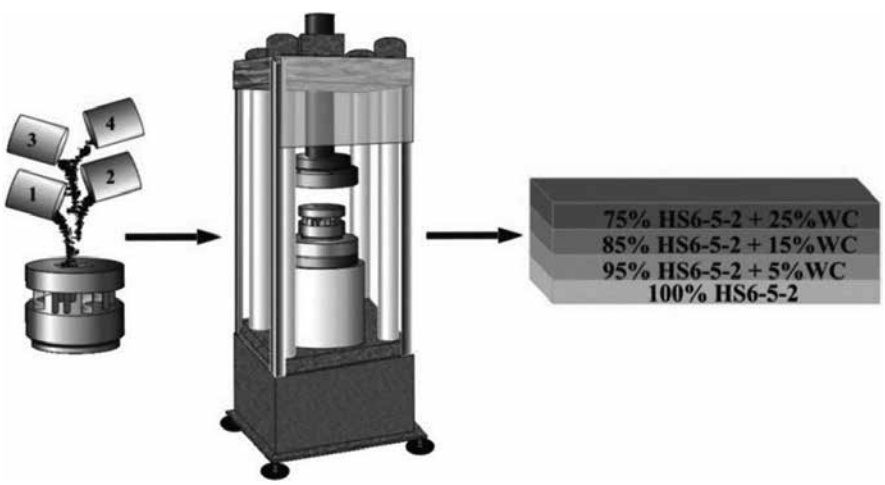

Figure 2. Moulding production scheme.

It was confirmed that a conventional powder metallurgy method—consisting of the uniaxial pressing of powder in a closed matrix and then sintering it—allows to produce graded carbide steels with the desired structure and properties. It is performed by dosing and mixing high-speed steel matrix material powders with hard carbide phases. This ensures a step-like change in the fraction of reinforcing phases in the matrix in the direction perpendicular to the surface. In addition, the newly created materials do not exhibit any cracks and delamination in the boundary zone between the layers. They are also characterised by smooth transition between the layers and show a linear variation in properties (**Figure 3**).

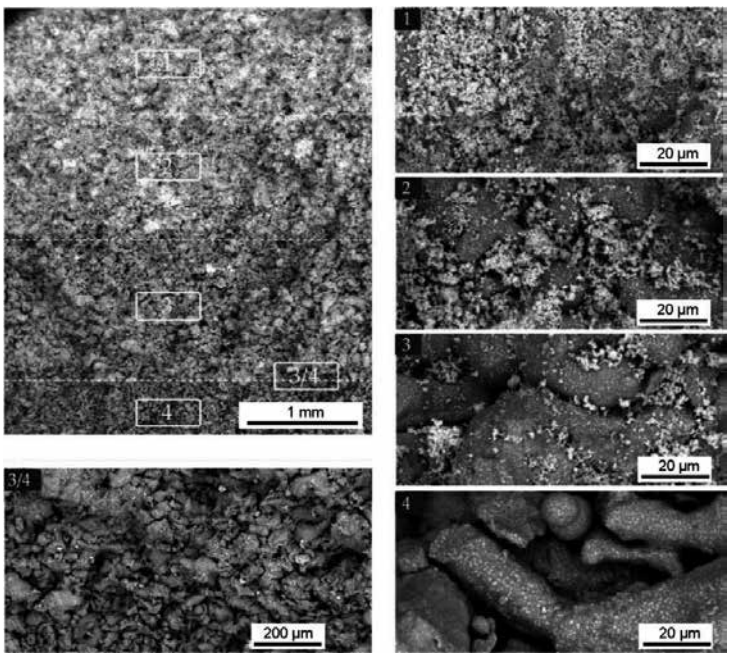

Figure 3. Moulding structure with particular layers: (1) 25%WC +75% high-speed steel, (2) 15%WC + 85% high-speed steel, (3) 5%WC + 95% high-speed steel, (4) 100% high-speed steel.

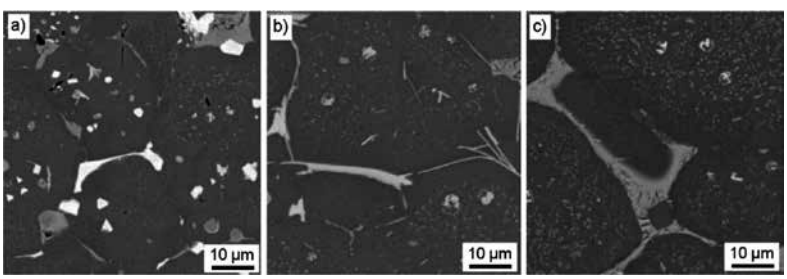

Figure 4. Structure of the high-speed steel layer of the gradient material, sintered in vacuum furnace at temperatures of: (a) 1210°C for 60 min, (b) 1230°C for 30 min, (c) 1230°C for 60 min.

http://dx.doi.org/10.5772/65379

The newly developed sintered graded carbide steels are characterised by a multi-phase structure composed of ferrite, primary high-speed steel carbides such as MC, M_2C and M_6C and WC tungsten carbide, introduced into carbide steels as powder. MC and M_6C carbides, depending on the sintering conditions, are distributed uniformly in the matrix or undergo coagulation and create large precipitates (approximately 2 μm) on the boundaries of primary austenite grains of high-speed steel (**Figures 4** and **5**).

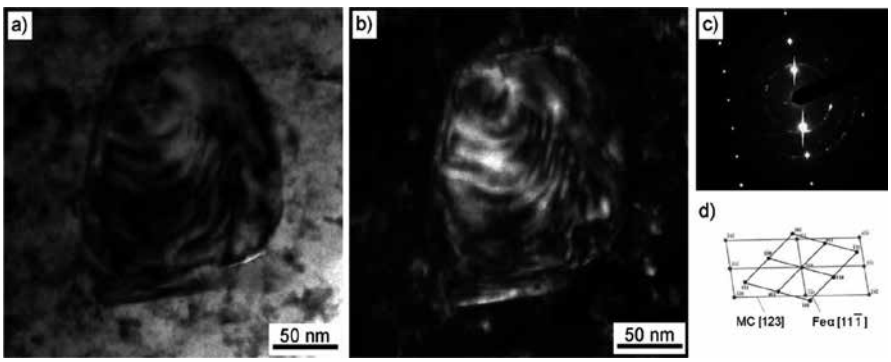

Figure 5. Structure of thin foil from the surface layer of the gradient material, sintered in vacuum furnace at temperature of 1250°C for 60 min; (a) image in the bright field, (b) image in the dark field from reflex "\11{$\bar{1}$ MC, (c) diffraction pattern from the area as in figure (a), (d) solution of the diffraction pattern from figure (c).

Gradient carbide steels should be sintered in vacuum, at 1210°C for 30 min at a heating and cooling rate to/from the sintering temperature of 5°C/min, ensuring the material density of approximately 8.6 g/cm^3 (**Figure 6a**), surface layer hardness of approximately 81 HRA (**Figure 6b**), porosity of approximately 2% (**Figure 7a**) and the substrate layer structure exhibiting no signs of remelting (**Figure 7b**).

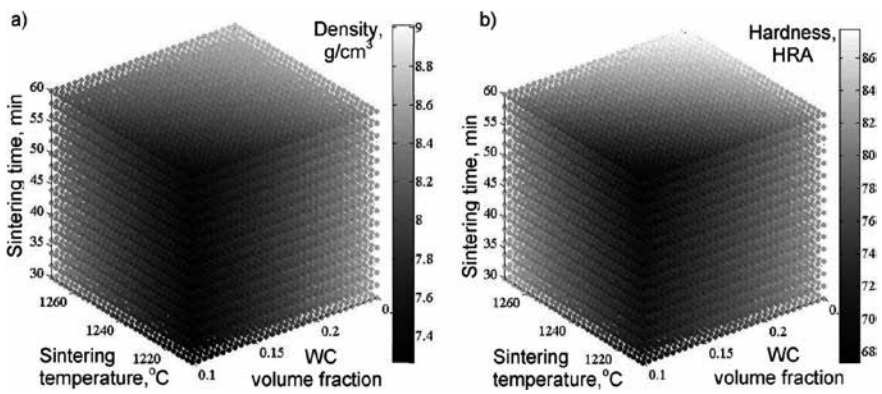

Figure 6. (a) RFP describing relationship between density and the WC volume fraction, temperature, and sintering time, for GM-HSS/WC sintered in a vacuum furnace, (b) RFP describing relationship between hardness and WC volume fraction, temperature, and sintering time, for GM-HSS/WC sintered in a vacuum furnace.

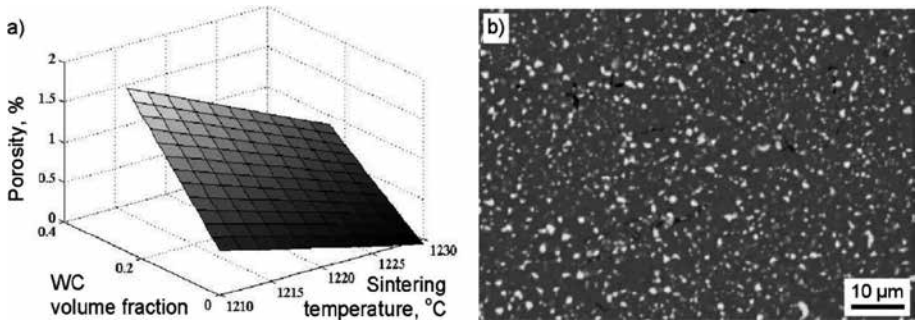

Figure 7. (a) RFP describing relationship between porosity and the volume fraction of the reinforcing phase and sintering temperature, for GM-HSS/WC sintered in a vacuum furnace for 30 min, (b) structure of the high-speed steel layer of the gradient material, sintered in vacuum furnace at temperatures of 1210°C for 30 min.

The heat treatment of the developed gradient carbide steels with a core corresponding to high-speed steel, encompassing quenching and tempering, produces a secondary hardness effect in the high-speed steel substrate layers by approximately 2–3 HRC higher than the hardness of the hardened material. The structure of graded carbide steels in the quenched condition represents martensite with residual austenite, M_6C and MC type carbides, both primary and secondary, unsolved in a solid solution during austenitising and WC carbides in the surface layer. The material austenitised at the temperature of 1120°C for 120 s, quenched and then tempered twice at the temperature of 530°C, shows the highest hardness of the surface layer of 71.2 HRC (**Figure 8**).

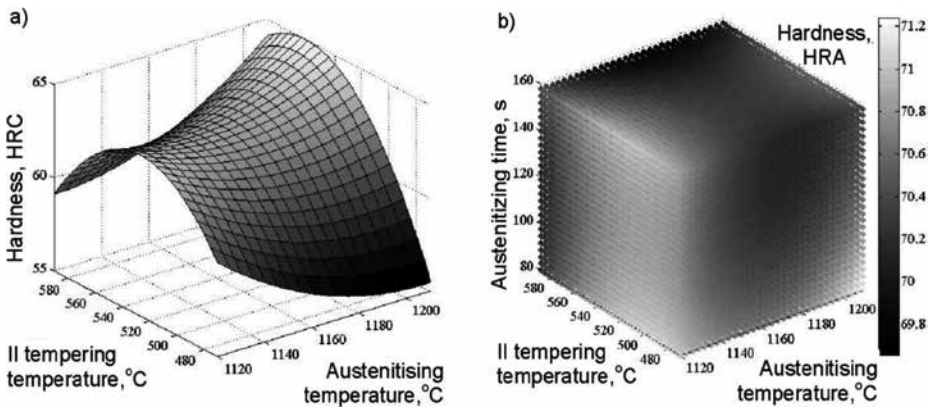

Figure 8. (a) RFP describing relationship between hardness and the second tempering temperature, and the austenitising temperature, for the high-speed steel layer of the gradient material austenitised for 120 s, (b) RFP describing relationship between hardness and the temperature, and austenitising time, and second tempering temperature for the surface layer of the gradient material.

The conventional powder metallurgy method, consisting of the uniaxial pressing of powder in a closed matrix and then sintering it, allows to produce graded carbide steels with the desired structure and properties, by dosing and mixing high-speed HS6-5-2 steel matrix material

http://dx.doi.org/10.5772/65379

powders with hard carbide phases, provided a linear change is ensured in the fraction of WC carbide reinforcing phase particles in the matrix in the direction perpendicular to the surface.

As the hardness of the surface layer of the newly developed graded HS6-5-2 high-speed steel matrix carbide steels reinforced with WC carbides can be formulated within a broad range according to their chemical composition and sintering conditions, this provides prospects for applying such materials for cutting tools.

Author details

Leszek Adam Dobrzański* and Anna Kloc-Ptaszna

*Address all correspondence to: leszek.dobrzanski@polsl.pl

Silesian University of Technology, Institute of Engineering Materials and Biomaterials, Gliwice, Poland

References

[1] Ichikawa K, editor. Functionally Graded Materials in the 21st Century: A Workshop on Trends and Forecasts. Boston: Kluwer Academic Publishers; 2001. 242 p.

[2] Dobrzański LA. Materials Engineering and Design Materials. Fundamentals of materials science and metallography. Warsaw: WNT; 2006. 1600 p. ISBN 83-204-3249-9 (in Polish)

[3] Davis JR, editor. ASM Specialty Handbook: Tool Materials. ASM International; OH; 1995. 501 p. ISBN: 978-0-87170-545-7

[4] Dobrzański LA, Hajduczek E, Marciniak J, Nowosielski R. Metallography and heat treatment of tool materials. Warsaw: WNT; 1990. 745 p. ISBN 83-204-1006-1 (in Polish)

[5] Dobrzański LA, Matula G. Powder metallurgy fundamentals and sintered materials. Open Access Library. 2012;8:1-156 (in Polish)

[6] Lee PW, editor. Metals Handbook: Volume 7: Powder Metal Technologies and Applications, 2nd ed. American Society for Metals; OH: 1998. 1151 p. ISBN13: 978-0871703873

[7] Dowson G, Whittaker D. Introduction to Powder Metallurgy. The Process and Its Products. European Powder Metallurgy Association; United Kingdom: 1992, 2008. 32 p. 26

[8] Dobrza◎ski LA, Matula G. Powder Injection Molding: Sinter-Hardening. In: Colás R, Totten GE, editors. Encyclopedia of Iron, Steel, and Their Alloys.CRC Press, Taylor & Francis Group; United Kingdom : 2016. 14 p.

[9] Dobrzański LA, Matula G, Várez A, Levenfeld B, Torralba JM. Structure and mechanical properties of HSS HS6-5-2- and HS 12-1-5-5-type steel produced by modified powder injection moulding process. Journal of Materials Processing Technology. 2004;157–158:658-668. DOI: 10.1016/j.jmatprotec.2004.07.138

[10] Várez A, Levenfeld B, Torralba JM, Matula G, Dobrzański LA. Sintering in different atmospheres of T15 and M2 high speed steels produced by a modified metal injection moulding process. Materials Science and Engineering: A. 2004;366:318-324. DOI: 10.1016/j.msea.2003.08.028

[11] Kloc A, Dobrzański LA, Matula G, Torralba JM. Effect of manufacturing methods on structure and properties of the gradient tool materials with the non-alloy steel matrix reinforced with the HS6-5-2 type high-speed steel. Materials Science Forum. 2007;539–543:2749-2754. DOI: 10.4028/www.scientific.net/MSF.539-543.2749

[12] Matula G, Dobrzański LA, Várez A, Levenfeld B, Torralba JM. Comparison of structure and properties of the HS12-1-5-5 type high-speed steel fabricated using the pressureless forming and PIM methods. Journal of Materials Processing Technology. 2005;162–163:230-235. DOI: 10.1016/j.jmatprotec.2005.02.166

[13] Matula G, Dobrzański LA, Herranz G, Várez A, Levenfeld B, Torralba JM. Influence of binders on the structure and properties of high speed-steel HS6-5-2 type fabricated using pressureless forming and PIM methods. Materials Science Forum. 2007;534–536:693-696. DOI: 10.4028/www.scientific.net/MSF.534-536.693

[14] Dobrzański LA. Effects of chemical composition and processing conditions on the structure and properties of high-speed steels. Journal of Materials Processing Technology. 1995;48:727-737. DOI: 10.1016/0924-0136(94)01715-D

[15] Dobrzański LA, Zarychta A, Ligarski M. Phase transformations during heat treatment of W-Mo-V 11-2-2 type high-speed steels with increased contents of Si and Nb or Ti. Journal of Materials Processing Technology. 1995;53:109-120. DOI: 10.1016/0924-0136(95)01967-J

[16] Dobrzański LA, Kasprzak W, Zarychta A, Ligarski M, Mazurkiewicz J. Structure and properties of W-Mo-V-Co 11-0-2-5 type and W-Mo-V 11-0-2 type high-speed steels. Journal of Materials Processing Technology. 1997;64:93-99. DOI: 10.1016/S0924-0136(96)02557-5

[17] Dobrzański LA, Ligarski M. Role of Ti in the W-Mo-V high-speed steels. Journal of Materials Processing Technology. 1997;64:101-116. DOI: 10.1016/S0924-0136(96)02558-7

[18] Dobrzański LA, Zarychta A. The structure and properties of W-Mo-V high-speed steels with increased contents of Si and Nb after heat treatment. Journal of Materials Processing Technology. 1998;77:180-193. DOI: 10.1016/S0924-0136(97)00416-0

[19] Dobrzański LA, Kasprzak W. The influence of 5% cobalt addition on structure and working properties of the 9-2-2-5, 11-2-2-5 and 11-0-2-5 high-speed steels. Journal of Materials Processing Technology. 2001;109:52-64. DOI: 10.1016/S0924-0136(00)00775-5

[20] Suresh S, Mortensen A, Needleman A, editors. Fundamentals of Metal-Matrix Composites. Boston, London, Oxford, Singapore, Sydney, Toronto, Wellington: Butterworth-Heinemann; 1993. 342 p.

[21] Miyamoto Y, Kaysser WA, Rabin BH, Kawasaki A, Ford RG, editors. Functionally Graded Materials: Design, Processing and Applications. Boston, Dordrecht, London: Kluwer Academic Publishers; 1999. 330 p. DOI: 10.1007/978-1-4615-5301-4

[22] Schwartz M, editor. New Materials, Processes, and Methods Technology. Boca Raton, London, New York: CRC Press; 2006. 686 p.

[23] Wessel JK, editor. The Handbook of Advanced Materials: Enabling New Designs. John Wiley and Sons, Incorporated; Canada: 2004. 656 p. ISBN: 978-0-471-45475-5 .

[24] Bever MB, Duwez PE. Gradients in composite materials. Materials Science and Engineering. 1972;10:1-8. DOI: 10.1016/0025-5416(72)90059-6

[25] Koizumi M. FGM activities in Japan. Composites Part B: Engineering. 1997;28:1-4. DOI: 10.1016/S1359-8368(96)00016-9

[26] Kawasaki A, Watanabe R. Concept and P/M fabrication of functionally gradient materials. Ceramics International. 1997;23:73-83. DOI: 10.1016/0272-8842(95)00143-3

[27] Kieback B, Neubrand A, Riedel H. Processing techniques for functionally graded materials. Materials Science and Engineering: A. 2003;362:81-106. DOI: 10.1016/S0921-5093(03)00578-1

[28] Dobrzański LA, Kloc-Ptaszna A, Pawlyta M, Pakieła W. Fabrication methods and heat treatment conditions effect on structure and properties of the gradient tool materials. Archives of Materials Science and Engineering. 2012;56:5-21

[29] Dobrzański LA, Kloc-Ptaszna A, Matula G. Gradient tool WC/HS6-5-2 materials produced using the powder metallurgy method. Archives of Materials Science and Engineering. 2008;31:9-12

[30] Dobrzański LA, Kloc-Ptaszna A, Matula G, Torralba JM. Structure of the gradient carbide steels of HS6-5-2 high-speed steel matrix. Archives of Materials Science and Engineering. 2007;28:589-592

[31] Dobrzański LA, Kloc-Ptaszna A, Matula G, Torralba JM. Structure and properties of the gradient tool materials of unalloyed steel matrix reinforced with HS6-5-2 high-speed steel. Archives of Materials Science and Engineering. 2007;28:197-202

[32] Dobrzański LA, Hajduczek J, Kloc-Ptaszna A. Effect of sintering parameters on structure of the gradient tool materials. Journal of Achievements in Materials and Manufacturing Engineering. 2009;36:33-40

[33] Dobrzański LA, Kloc-Ptaszna A, Matula G, Torralba JM. Structure and properties of gradient tool materials with the high-speed steel matrix. Journal of Achievements in Materials and Manufacturing Engineering. 2007;24:47-50

[34] Dobrzański LA, Kloc-Ptaszna A, Matula G, Contreras JM, Torralba JM. The impact of production methods on the properties of gradient tool materials. Journal of Achievements in Materials and Manufacturing Engineering. 2007;24:19-26

[35] Dobrzański LA, Kloc-Ptaszna A, Dybowska A, Matula G, Gordo E, Torralba JM. Effect of WC concentration on structure and properties of the gradient tool materials. Journal of Achievements in Materials and Manufacturing Engineering. 2007;20:91-94

[36] Dobrzański LA, Kloc A, Matula G, Domagała J, Torralba JM. Effect of carbon concentration on structure and properties of the gradient tool materials. Journal of Achievements in Materials and Manufacturing Engineering. 2006;17:45-48

[37] Schwartz M, editor. Encyclopedia of Smart Materials, Vol. 1–2. New York: John Wiley and Sons; 2002. 1176 p.

[38] Huang J, Li J, Kawasaki A, Watanabe R. A new method for fabrication of functionally gradient materials. Journal of Materials Science Letters. 1998;17:2033-2035. DOI: 10.1023/A:1006685328284

[39] Dobrzański LA, Kloc-Ptaszna A. Structure and properties of the gradient tool materials based on a high-speed steel HS6-5-2 reinforced with WC or VC carbides. Journal of Achievements in Materials and Manufacturing Engineering. 2009;37:213-237

[40] Panda KB, Ravi Chandran KS. Titanium-Titanium Boride (Ti-TiB) functionally graded materials through reaction sintering: synthesis, microstructure, and properties. Metallurgical and Materials Transactions: A. 2003;34:1993-2003. DOI: 10.1007/s11661-003-0164-3

[41] Chen L, Lengauer W, Ettmayer P, Dreyer K, Daub HW, Kassel D. Fundamentals of liquid phase sintering for modern cermets and functionally graded cemented carbonitrides (FGCC). International Journal of Refractory Metals and Hard Materials. 2000;18:307-322. DOI: 10.1016/S0263-4368(00)00041-X

[42] Eso O, Fang ZZ, Griffo A. Kinetics of cobalt gradient formation during the liquid phase sintering of functionally graded WC–Co. International Journal of Refractory Metals and Hard Materials. 2007;25:286-292. DOI: 10.1016/j.ijrmhm.2006.07.002

[43] Dumont A-L, Bonnet J-P, Chartier T, Ferreira JMF. $MoSi_2/Al_2O_3$ FGM: elaboration by tape casting and SHS. Journal of the European Ceramic Society. 2001;21:2353-2360. DOI: 10.1016/S0955-2219(01)00198-4

[44] Dobrzański LA, Gołombek K, Lukaszkowicz K. Physical Vapor Deposition in Manufacturing. In: Nee AYC, editor. Handbook of Manufacturing Engineering and Technology. London: Springer-Verlag; 2015. p. 2719-2754. DOI: 10.1007/978-1-4471-4670-4_29

[45] Dobrzański LA, Pakuła D, Staszuk M. Chemical Vapor Deposition in Manufacturing. In: Nee AYC, editor. Handbook of Manufacturing Engineering and Technology. London: Springer-Verlag; 2015. p. 2755-2803. DOI: 10.1007/978-1-4471-4670-4_30

[46] Dobrzański LA, Gołombek K. Structure and properties of the cutting tools made from cemented carbides and cermets with the TiN+mono-, gradient- or multi (Ti,Al,Si)N +TiN nanocrystalline coatings. Journal of Materials Processing Technology. 2005;164-165:805-815. DOI: 10.1016/j.jmatprotec.2005.02.072

[47] Wolfe D, Singh J. Functionally gradient ceramic/metallic coatings for gas turbine components by high-energy beams for high-temperature applications. Journal of Materials Science. 1998;33:3677-3692. DOI: 10.1023/A:1004675900887

[48] Eason R, editor. Pulsed Laser Deposition of Thin Films: Applications-Led Growth of Functional Materials. Hoboken: Wiley-Interscience, A John Wiley & Sons, Inc.; 2006. 682 p.

[49] Dobrzański LA, Staszuk M., Gołombek K, Śliwa A, Pancielejko M. Structure and properties PVD and CVD coatings deposited onto edges of sintered cutting tools. Archives of Metallurgy and Materials. 2010;55:187-193

[50] Dobrzański LA, Żukowska LW, Mikuła J, Gołombek K, Pakuła D, Pancielejko M. Structure and mechanical properties of gradient PVD coatings. Journal of Materials Processing Technology. 2008;201:310-314. DOI: 10.1016/j.jmatprotec.2007.11.283

[51] Dobrzański LA, Pakuła D, Kříž A, Soković M, Kopač J. Tribological properties of the PVD and CVD coatings deposited onto the nitride tool ceramics. Journal of Materials Processing Technology. 2006;175:179-185. DOI: 10.1016/j.jmatprotec.2005.04.032

[52] Dobrzański LA, Dobrzańska-Danikiewicz AD, Tański T, Jonda E, Drygała A, Bonek M. Laser Surface Treatment in Manufacturing. In: Nee AYC, editor. Handbook of Manufacturing Engineering and Technology. London: Springer-Verlag; 2015. p. 2677-2717. DOI: 10.1007/978-1-4471-4670-4_35

[53] Pei T, De Hosson JTM. Functionally graded materials produced by laser cladding. Acta Materialia. 2000;48:2617-2624. DOI: 10.1016/S1359-6454(00)00065-3

[54] Yang S, Zhong M, Liu W. TiC particulate composite coating produced in situ by laser cladding. Materials Science and Engineering: A. 2003;343:57-62. DOI: 10.1016/S0921-5093(02)00361-1

[55] Dobrzański LA, Gołombek K, Hajduczek E. Structure of the nanocrystalline coatings obtained on the CAE process on the sintered tool materials. Journal of Materials Processing Technology. 2006;175:157-162. DOI: 10.1016/j.jmatprotec.2005.04.008

[56] Dobrzański LA, Mikuła J. The structure and functional properties of PVD and CVD coated Al_2O_3 + ZrO_2 oxide tool ceramics. Journal of Materials Processing Technology. 2005;167:438-446. DOI: 10.1016/j.jmatprotec.2005.05.034

[57] Klimpel A, Dobrzański LA, Lisiecki A, Janicki D. The study of properties of Ni-W_2C and Co-W_2C powders thermal sprayed deposits. Journal of Materials Processing Technology. 2005;164-165:1068-1073. DOI: 10.1016/j.jmatprotec.2005.02.198

[58] Toma F-L, Potthoff A, Berger L-M, Leyens C. Demands, potentials, and economic aspects of thermal spraying with suspensions: a critical review. Journal of Thermal Spray Technology. 2015;24:1143-1152. DOI: 10.1007/s11666-015-0274-7

[59] Kawasaki A, Watanabe R. Thermal fracture behavior of metal/ceramic functionally graded materials. Engineering Fracture Mechanics. 2002;69:1713-1728. DOI: 10.1016/S0013-7944(02)00054-1

[60] Kobayashi A. Enhancement of TBC (thermal barrier coatings) characteristics by gas tunnel type plasma spraying. Materials Science Forum. 2007;539-543:1061-1066. DOI: 10.4028/www.scientific.net/MSF.539-543.1061

[61] Pompe W, Worch H, Epple M, Friess W, Gelinsky M, Greil P, Hempel U, Scharnweber D, Schulte K. Functionally graded materials for biomedical applications. Materials Science and Engineering: A. 2003;362:40-60. DOI: 10.1016/S0921-5093(03)00580-X

[62] Jin D, Meng Z. Functionally graded PZT/ZnO piezoelectric composites. Journal of Materials Science Letters. 2003;22:971-974. DOI: 10.1023/A:1024612929936

[63] Zhong PZ, Shang ET. Exact analysis of simply supported functionally graded piezothermoelectric plates. Journal of Intelligent Material Systems and Structures. 2005;16:643-651. DOI: 10.1177/1045389X05050530

[64] Watari F, Yokoyama A, Omori M, Hirai T, Kondo H, Uo M, Kawasaki T. Biocompatibility of materials and development to functionally graded implant for bio-medical application. Composites Science and Technology. 2004;64:893-908. DOI: 10.1016/j.compscitech.2003.09.005

[65] Thieme M, Wieters KP, Bergner F, Scharnweber D, Worch H, Ndop J, Kim TJ, Grill W. Titanium powder sintering for preparation of a porous functionally graded material destined for orthopaedic implants. Journal of Materials Science: Materials in Medicine. 2001;12:225-231 DOI: 10.1023/A:1008958914818

[66] Dobrzański LA. Overview and general ideas of the development of constructions, materials, technologies and clinical applications of scaffolds engineering for regenerative medicine. Archives of Materials Science and Engineering. 2014;69:53-80

[67] Dobrzański LA. Applications of newly developed nanostructural and microporous materials in biomedical, tissue and mechanical engineering. Archives of Materials Science and Engineering. 2015;76:53-114

[68] Dobrzański LA, Dobrzańska-Danikiewicz AD, Malara P, Gaweł TG, Dobrzański LB, Achtelik-Franczak A. Fabrication of scaffolds from Ti6Al4V powders using the computer aided laser method. Archives of Metallurgy and Materials. 2015;60:1065-1070. DOI: 10.1515/amm-2015-0260

[69] Dobrzański LA, et al. Investigations of structure and properties of newly created porous biomimetic materials fabricated by selective laser sintering, BIOLASIN. Project UMO-2013/08/M/ST8/00818. Gliwice: Silesian University of Technology; 2013-2016

[70] Dobrzański LA, Dobrzańska-Danikiewicz AD, Gaweł TG, Achtelik-Franczak A. Selective laser sintering and melting of pristine titanium and titanium Ti6Al4V alloy powders and selection of chemical environment for etching of such materials. Archives of Metallurgy and Materials. 2015;60:2039-2045. DOI: 10.1515/amm-2015-0346

[71] Abdel-Hady Gepreel M, Niinomi M. Biocompatibility of Ti-alloys for long-term implantation. Journal of the Mechanical Behavior of Biomedical Materials. 2013;20:407-415. DOI: 10.1016/j.jmbbm.2012.11.014

[72] Liao S, Wang W, Uo M, Ohkawa S, Akasaka T, Tamura K, Cui F, Watari F. A three-layered nano-carbonated hydroxyapatite/collagen/PLGA composite membrane for guided tissue regeneration. Biomaterials. 2005;26:7564-7571 DOI: 10.1016/j.biomaterials.2005.05.050

[73] Ma J, Tan GEB. Processing and characterization of metal-ceramics functionally gradient materials. Journal of Materials Processing Technology. 2001;113:446-449. DOI: 10.1016/S0924-0136(01)00613-6

[74] Nomura T, Moriguchi H, Tsuda K, Isobe K, Ikegaya A, Moriyama K. Material design method for the functionally graded cemented carbide tool. International Journal of Refractory Metals and Hard Materials. 1999;17:397-404. DOI: 10.1016/S0263-4368(99)00029-3

[75] Zhang LM, Xiong HP, Chen LD, Hirai T. Microstructures of W-Mo functionally graded material. Journal of Materials Science Letters. 2000;19:955-958. DOI: 10.1023/A:1006712104200

[76] Lengauer W, Dreyer K. Functionally graded hardmetals. Journal of Alloys and Compounds. 2002;38:194-212. DOI: 10.1016/S0925-8388(02)00232-3

[77] Matula G, Dobrzański LA, Dołżańska B. Structure and properties of TGM manufactured on the basis of cobalt. Journal of Achievements in Materials and Manufacturing Engineering. 2007;20:151-154

[78] Rosso M, Porto G, Geminiani A. Studies of graded cemented carbides components. International Journal of Refractory Metals and Hard Materials. 1999;17:187-192. DOI: 10.1016/S0263-4368(99)00006-2

[79] Kloc-Ptaszna A. Struktura i własności gradientowych węglikostali spiekanych na osnowie stali szybkotnącej HS6-5-2 [Ph.D. Thesis]. Gliwice, Poland: Silesian University of Technology; 2009.

Chapter 10

Powder Injection Moulding of Tool Materials and Materials Containing One-Dimensional Nanostructural Elements

Leszek A. Dobrzański and Grzegorz Matula

Additional information is available at the end of the chapter

http://dx.doi.org/10.5772/67353

Abstract

As modern manufacturing methods have been developing, the application methods of powders have changed, and they do not always have to be moulded prior to sintering. The powder injection moulding (PIM) method is suitable for large-lot and mass production; still, powder consumption is not too high. The metal injection moulding (MIM) is an advanced technology and not as developed as classical pressing and sintering but constantly and dynamically developing. The technology is developing towards micro-MIM, that is, production of very small parts for miniaturised devices. The chapter presents the overview of powder injection moulding as specialist powder metallurgy method and its application for fabrication of tool materials. Specially, the fabrication of high-speed steels and carbide-steels on their matrix by powder injection moulding is descripted. In last part of the chapter, the results of own investigations of the structure with nanostructural elements of high-speed steels and carbide-steels on their matrix fabricated by powder injection moulding are presented.

Keywords: powder injection moulding, debinding, sintering, tool materials nanostructural elements

1. Introduction

As modern manufacturing methods have been developing, the application methods of powders have changed, and they do not always have to be moulded prior to sintering. This depends on the technological process applied, for example, hardfacing, thermal spraying, or selective laser sintering [1, 2] exclude the need of powder forming. Powder forming itself does

not have to be connected with pressing or with shapening the item being fabricated, as seen with the example of pressure-free moulding of coatings or foils using polymer-powder slips. Classical powder metallurgy is however based on pressing and at the same time forming the powder in such a way that the item has the dimensions and shape of a ready product or semi-product after sintering, requiring only minor final treatment [3, 4].

The introduction of atomisers into mass production of metallic powders allowed to reduce the production costs of sintered materials. For instance, the manufacturing cost of high speed conventionally cast and sintered steel at the end of the last century was comparable and dependent mainly on the price of alloy additives. The automotive industry is now estimated to be the key user of elements moulded and sintered using metallic powders [5]. Powder-pressed and sintered gears intended for gearboxes are characterised by very silent work, which is associated with the suppression of vibrations in porous materials. The teeth of such gears are burnished and heat treated, which ensure their high hardness and resistance to abrasive wear. Uniaxial pressing in closed dies is still most widespread and is dedicated to symmetric elements with relatively simple shapes. Products with a highly developed surface, small dimensions, and massively produced are manufactured by the injection moulding of powders witnessing very dynamic growth in the recent years. The moulding of ignition plugs' insulators was one of the first applications of this method in 1937 [6].

The method was employed in the 1970s of the last century for producing metals and ceramics used in electronics. The earlier limitations of this method were connected with binder removal, which is technologically difficult, time-consuming and is the source of defects in the form of cracks, gas bubbles, and distortions. In the majority of cases, binder removal is based on its thermal degradation, often without access of oxygen, that is, in the process of controlled pyrolysis. The growth of the technology in the recent years has been chiefly linked to a search for alternative solutions ensuring debinding, which is fast and safe for the products manufactured and for the environment. The methods of solvent degradation under heightened pressure in a vacuum and in supercritical pressure conditions were employed as a result of such investigations. The catalytic degradation method, adopted and developed by BASF, offering at that time ready granulates and binder removal devices, turned out to be a breakthrough method [7].

Although the powder injection moulding (PIM) method is suitable for large-lot and mass production; still, powder consumption is not too high. In general, the powders of metals and powders of metal alloys produced are principally designed for moulding and sintering products, and only a small fraction of powders is used in welding processes and in other processes, for example, in chemical industry. For instance, the United States have produced about 365 thousand tonnes of iron and steel powders in 2013, of which the powders used for other purposes than powder metallurgy account for only 10%. The remaining 90% include also powders used in the metal injection moulding (MIM) process. The MIM technology represents only 1% of all the metallic powders used in Europe in powder metallurgy. This signifies that this is an advanced technology and not as developed as classical pressing and sintering, but constantly and dynamically developing, which is confirmed by numerous Refs. [8–10]. It should be noted that the comparison of consumption in tonnes of powder for the MIM technology with other manufacturing methods is not the best indicator

http://dx.doi.org/10.5772/67353

of this method's popularity, because it is employed for producing small elements. The sales of parts manufactured by this method have grown very sharply in, for example, Europe and have gone up from less than 150 to over 250 mEUR between 2003 and 2013. The technology is developing towards micro-MIM, that is, production of very small parts for miniaturised devices [8, 11, 12].

2. Overview of powder injection moulding as specialist powder metallurgy method and its application for fabrication of tool materials

Powder forming and sintering technologies offer unlimited opportunities for selection of the chemical composition of the tool materials produced. Classical powder metallurgy, based on uniaxial pressing and sintering with potential isostatic pressing at a high sintering temperature, is used for the fabrication of the most popular tool materials such as sintered carbides produced as, for example, inserts for turning tools. Frequently, the simple shapes of such inserts do not require any other powder forming technique, whereas uniaxial pressing, especially one-sided pressing, is the easiest powder forming method, with no need to use a binder or a large inclusion of slipping agents, which ensures small shrinkage of the material after sintering. An uncomplicated technological process of fabrication of sintered carbides, introduced for the first time by a German company, Krupp, in 1926, is still enjoying great popularity, and sintered carbides themselves are the most often used tool material. For example, the annual growth rate for the market of sintered and superhard tool materials in 2007–2012 was 7.5% per annum, with the projected growth for the subsequent years of 11.3% [8, 13]. It is estimated that the global market of sintered carbides and superhard materials may reach the threshold of USD 20.2 billion in 2018 owing to the development of industry and production in developing countries and due to the resulting increased demand for highly efficient machining tools [14]. This method imposes, however, substantial constraints if carbide inserts with highly complex shapes are produced. An alternative, and actually an unrivalled method in such case, is powder injection moulding. It is injection moulding's strength that we can produce a complicated geometry or products in the final or nearly final form at once. We can come close to the final goal at once, and this is the crucial reason for choosing MIM [15]. The technology is dedicated to mass production solely, due to high investment costs necessitating the use of high class equipment. Metal injection moulding (MIM) is especially significant in metallic powder forming. **Table 1** lists the key advantages of the PIM method as compared to general disadvantages and advantages of other manufacturing techniques of elements with their shapes and dimensions similar to the final shapes and dimensions.

It is assumed that the powder injection moulding technology was introduced in 1849 by pressure casting of nonferrous metal alloys [8]. Further development was associated with proficiency in the polymer processing technology and with the first piston moulders constructed in the USA and Germany. PIM's history in Europe is relatively short and dates back 30 years ago. The first elements manufactured by this method are orthodontic hooks produced in Germany in the 1980s [17].

Selected characteristics	Technology			
	PIM	**PM**	**Casting**	**Machining**
Density	98%	90%	95–99%	100%
Strength versus solid material	100%	70%	98%	100%
Complexity	High	Low	Medium	High
Part weight	Between 0.003 g and 17 kg	Between 0.1 g and 10 kg	From 1 g	From 0.1 g
Wall thickness	0.1–10 mm	2 mm	5 mm	2 mm
Surface manufacturing accuracy	0.4–0.8 μm	2 μm	2 μm	0.4 do 2 μm
Production scale	Mass	Mass	Medium/low	Medium/low

Table 1. Selected characteristics of elements manufactured by various technologies [16].

The injection moulding of a polymer-powder slip allows to produce relatively small parts with complicated shapes and developed area and requires no plastic working or machining, which is in line with the modern direction of producing ready parts, that is, "near–net-shape". Despite numerous advantages, the injection moulding process is not suitable for fabrication of large parts. The largest dimension should not exceed 100 mm. This is because subsequent debinding is required prior to sintering, as the polymer materials contained in a binder are undergoing gassing during thermal degradation, and the pressure of the gas closed in the pores is rising due to being abruptly heated to sintering temperature. The wall thickness of the parts manufactured by this method is not more than 10 mm, they have complicated shape and high manufacturing precision and low production costs [9, 18]. This method is most often applied for manufacturing parts hard to produce by other techniques, for example, elements with the smallest mass of not more than 0.5 g, in particular orthodontic hooks [16]. The technology, considering a possibility of production automation, high speed and dimensional repeatability and high costs of injection moulders and heating devices, is designed for large-lot or mass production [19, 20]. Owing to the principal advantage of this technique—where ready parts are produced without additional treatment being necessary—the technique is used more and more extensively for producing hard materials, including tool materials, which are exceptionally difficult and costly to machine [6, 9, 13, 15, 21]. The formability of metallic and ceramic powders and their mixtures enables to fabricate metal tools with relatively high ductility, ceramic tools with high hardness or metal matrix composites (MMC) and ceramic matrix composites (CMC) combining high properties distinct for metals and ceramics [22–25]. The forming of metallic or ceramic powders in a matrix of polymer binders, especially injection moulding or extrusion, has been applied for producing tool materials, including high-speed steels, carbide-steels and sintered carbides, characterised by their structure similar to commercial sintered tool materials [26–29]. It is not possible to achieve such high bending strength as for high-speed steels fabricated by hot isostatic pressing or for sintered carbides pressed

http://dx.doi.org/10.5772/67353

isostatically during sintering. The main reason for lower bending strength of the manufactured tool materials is not, however, powder forming technologies, but the process of self-sintering, which does not allow to eliminate completely the locally occurring pores being material discontinuity lowering the material's mechanical properties. It is beyond doubt a benefit of polymer-powder slip forming, mainly powder injection moulding, that plastic working and machining operations are eliminated, hence reducing the related costs, as a result of which application possibilities of the so manufactured tool materials are offered, especially where they are not subject to strong dynamic loads. Moreover, the parts produced this way do not have to act only as tool material but act as an element working in the conditions of tribological wear. An additional benefit of injection moulding of the investigated tool materials is that protective and/or reactive atmospheres can be utilised for sintering, permitting to use furnaces cheaper than vacuum furnaces and hence allowing automation. The use of modern, polymer binder-based powder forming technologies, in particular injection moulding, for preparing tool materials, offers promising perspectives for the manufacture of tool materials and is consistent with the valid development trend of this technology. The sales of products manufactured by PIM and MIM have been growing over the last 25 years and signify the industry's huge interest in such methods [30].

In powder injection moulding, an injected preform is produced, which should then undergo debinding and sintering to achieve high functional properties [16, 18, 27, 30, 31]. Classical injection moulding in moulders is the same as the moulding of thermoplastic polymers (**Figure 1**).

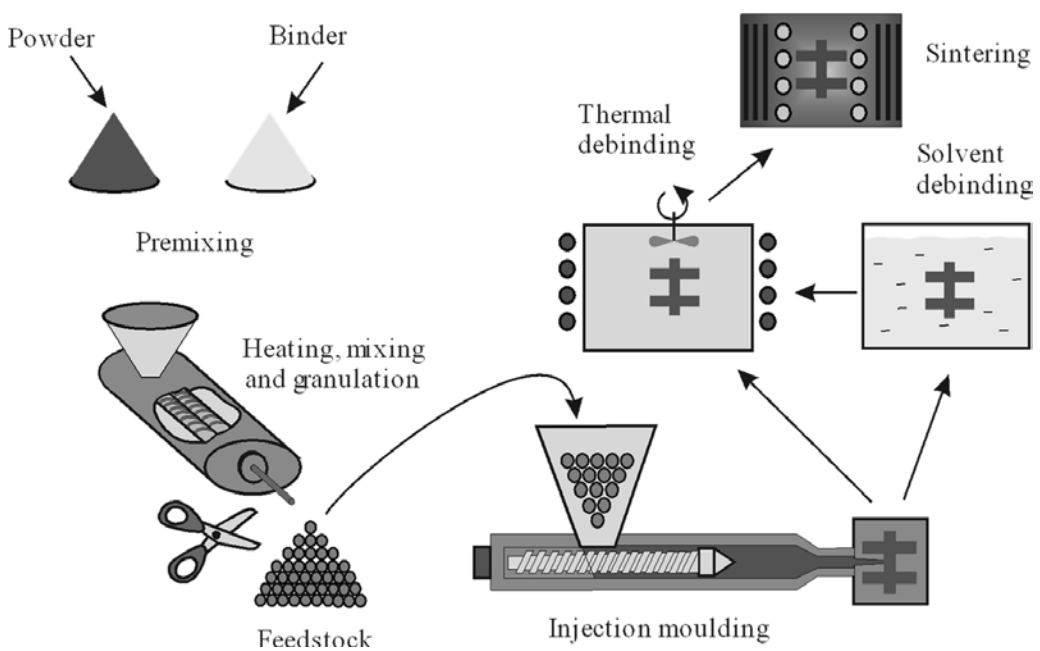

Figure 1. General chart of powder injection moulding.

Metallic or ceramic powders, and even their mixtures, are used as feedstock in powder injection moulding. The use of thermoplastic polymers as a binder, which is binding metallic or ceramic powder, enables to transport it and mould it in an injector socket. Two types of binders based on, respectively, paraffin and polymer materials and an aqueous methylcellulose solution (Wiech's or Rivers' solution), are used most often [8]. A powder-to-binder ratio is closely linked to the shape, size of powder particles, material type, powder wettability by a binder, and the properties of the binder itself and is also linked to mixture production conditions [32, 33]. By the rule, it is more difficult to mix ceramic powders with a binder and to inject them than is the case with metallic powders. A binder with larger fraction has to be used for this. **Figure 2a** shows the influence of powder fraction on viscosity curve.

Debinding must be carried out in such a way to prevent cracks, blisters, shape deformation, gas bubbles, or semi-product delamination, so it should be deformed early enough, maintaining the shape of the element produced. The most popular method of debinding used in PIM (**Figure 2b**) is thermal degradation and solvent degradation. A mixed method is linked to combined degradation techniques, for example, solvent and thermal technique.

Currently, for exceptionally small preforms formed, for example, in the μPIM process, debinding is associated with heating to a sintering temperature [8, 12]. Regardless the semi-product size, debinding is making a preform becoming very brittle. Reducing atmospheres consisting of hydrogen with a high concentration of hydrogen (85%) ensure highest strength, hence, increase carbon concentration in the preform after sintering. Preform density is about 60% of the theoretical density when the binder is completely removed. This density depends on the binder fraction, and this fraction depends on the type of the powder formed. Most often, metal powders are so selected that they are characterised by a circular shape with good wettability, which allows to reduce the binder fraction as much as possible to only 30%. The binder fraction in case of ceramic powders may reach even 55%.

Preform sintering takes place after debinding. Irrespective of the preform density, it is subjected to densification and shrinkage due to sintering. This is natural regardless the preform

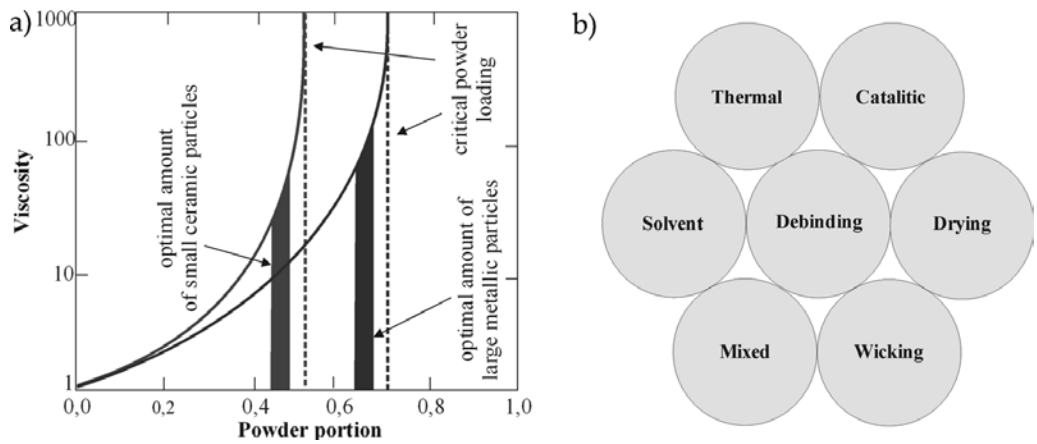

Figure 2. (a) Influence of type and amount of powder on viscosity, (b) debinding methods in PM technologies.

http://dx.doi.org/10.5772/67353

forming method; however, as a result of high porosity, shrinkage is very strong and an uncontrolled change of the sintered elements' shape may occur. Because a change in the volume of the sintered material is inversely proportional to its density after forming, growth in preform density reduces the risk of shape defects of the preform being formed. Injection pressure, powder size, and binder fraction have influence on increase in preform density. Sintering is usually the last operation of the technological process decisive for density and properties of the ready product [18]. If the ready element should have high mechanical properties, final heat treatment and often machining are used to ensure accurate dimensions of the produced sinters. The sintering of injection moulded or pressure-free moulded powders does not differ largely from the sintering of powders formed by other methods. The key properties of sinters, especially tool materials, are improved by the formation of carbonitrides as a result of the interacting atmosphere containing nitrogen during debinding and sintering [23]. Sintering is initiated by growth in the concentration of carbon resulting from debinding, however, in case of some materials such as stainless steels or high-speed steels, carbon concentration must be closely monitored due to their properties or influence on heat treatment. The type of the binder used influences the final carbon concentration [18]. Sintering is also influenced by particle size. Injection-moulded fine-grained powders with a larger specific surface area are filling the volume of the sintered preform more thoroughly and are subject to faster remelting. The powder particle size is also decisive for surface roughness and for the value of the sintered material's edge radius. In case of classical pressing, fine-grained powder is not filling the die socket so well due to low-powder liquidity. An atmosphere inside the furnace chamber is an important factor conditioning sintering [26]. Although the vacuum is not related to direct gas costs, vacuum sintering is a costly alternative considering that furnaces are equipped with vacuum systems and require maintenance. Nonetheless, vacuum is often used for sintering high-speed steels, especially those pressed in a die or pressed isostatically. The sintering of injection-moulded high-speed steels in high vacuum is quite difficult due to the gas products being released, coming from the thermal degradation of base polymer residues. Final heat treatment is required to achieve high mechanical properties for high-speed steels or sintered carbides manufactured by PIM [34–38].

3. Fabrication of high-speed steels and carbide-steels on their matrix by powder injection moulding

Two types of tool materials, that is, high-speed steels and carbide steels with the matrix of the same high-speed steels were fabricated by the powder injection moulding method. The powders of high-speed steels with the chemical composition given in **Table 2** and with the particle size determined by the laser diffraction method in the Malvern Mastersizer 2000 device shown in **Figure 3**, and with density and technological properties presented in **Table 2**, were fabricated by atomising inert gas (**Figures 3** and **4**) by Sandvik Osprey Ltd. A commercially available mixture of carbides, with the trade name of Tetra Carbides (in this chapter TetraC) by Treibacher Industrie AG containing WC, TiC, TaC, and NbC carbide powders with the volume fraction and technological properties presented in **Table 3** and other properties given in **Figure 3** and morphology given in **Figure 4** were used as hard carbide phases.

Steel grade	Mass concentration of elements (%)							
	C	W	Mo	V	Co	Cr	Mn	Si
EN HS 6-5-2	0.84	6.54	4.81	1.95	–	3.97	0.36	0.35
EN HS 12-0-5-5	1.47	11.8	0.06	4.75	4.64	4.76	0.5	0.43

Table 2. Concentration of alloy elements in high-speed steels powders used.

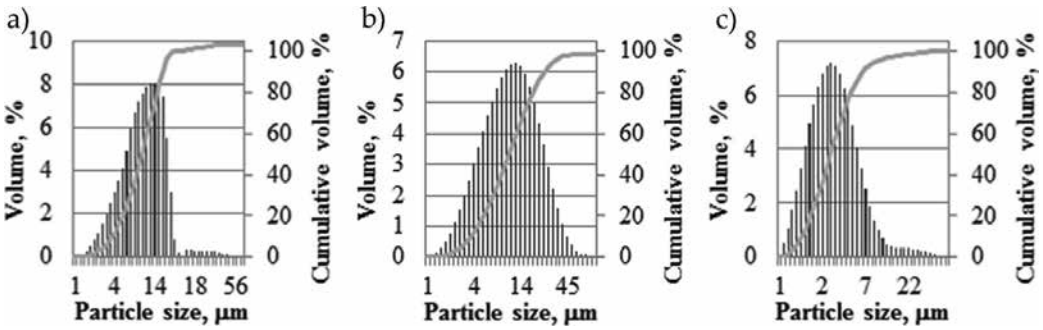

Figure 3. Particle size distribution of (a) EN HS 6-5-2, (b) EN HS 12-0-5-5 high-speed steels powder, and (c) carbides WC, TiC, TaC, NbC mixture (TetraC).

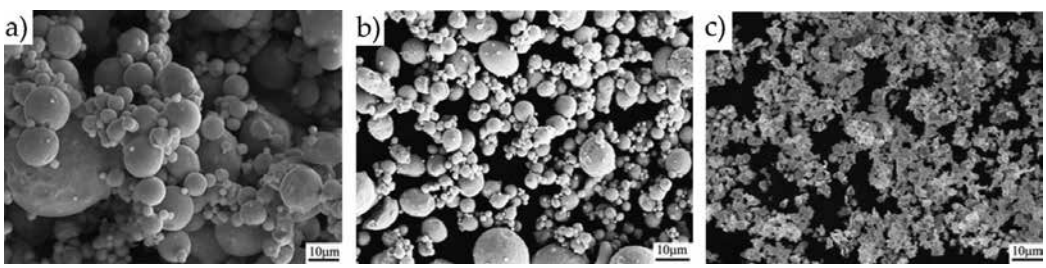

Figure 4. Morphology of (a) EN HS 6-5-2, (b) EN HS 12-0-5-5 high-speed steels, and (c) mixture of EN HS 12-0-5-5 high-speed steel and carbides WC, TiC, TaC, NbC mixture (TetraC).

Powder	Powder properties		
	Density (g/cm³)	Bulk density (g/cm³)	Tap density, (g/cm³)
EN HS 6-5-2	8.16	2.89	4.02
EN HS 12-0-5-5	8.19	3.05	4.25
Mixture 47% WC, 14% TiC, 33% TaC, 6% NbC (TetraC)	10.23	4.38	5.64

Table 3. Technological properties of used powders.

http://dx.doi.org/10.5772/67353

The applied high-speed steel powders meet the condition indicating that ball-shaped powder with the average particle size of below 20 μm is most suitable for injection moulding of powders. The ball shape is most desired due to high wettability, low slipping agent viscosity, and high-packing density of particles. The size distribution of particles is also an important factor. If particle size distribution is relatively broad, then the pores forming between large grains may be filled by small particles, as signified by the *Sw* curve inclination coefficient Eq. (1) [18].

$$Sw = \frac{2.56}{\log\frac{D_{90}}{D_{10}}}. \quad (1)$$

The powder with the *Sw* coefficient of about two is most recommended for injection moulding. It is not recommended to mould powder with the *Sw* coefficient of seven with its powder grain size distribution characteristic being very narrow. The powder particle size analysis is shown in **Table 4**. Pure steel powder, EN HS 6-5-2, has the highest *Sw* coefficient value. If a mixture of WC, TiC, TaC, and NbC carbides is introduced into the powder of high-speed steels, this is broadening the powder grain size distribution characteristic, thus advantageously reducing the *Sw* coefficient whose lowest value for the mixture of high-speed steels EN HS 12-0-5-5 with carbides is 2.69. The calculated *Sw* coefficients of the applied powders do not exceed the value 4, which signifies that they can be used for injection moulding [18]. **Table 5** presents information about the components of the formed powder and polymer-powder mixtures.

The purpose of the stearic acid used was to cover the surface of carbide powders before mixing them with high-speed steel powders. Stearic acid covering the carbides with a thin layer is increasing their wettability when mixing with other binder components and decreasing a ready feedstock's viscosity [8, 13, 31, 39]. Next, the covered carbides together with a binder and high-speed steel powder were initially agitated in a chamber of a universal Rheomex CTW100p stirrer by Haake enabling to measure torque and rotation speed of stirrers and charge temperature. The results of rheological tests for the mixtures of high-speed steel powders, carbides and binder, carried out with a capillary rheometer, Rheoflixer by ThermoHaake, at 170, 180 and 190°C, with the homogenisation speed of 10–10000 s^{-1} and with the torque depending on the phase composition of the examined polymer-powder mixtures and their homogenisation time, allowed to select a mixture with relatively low viscosity, high volume fraction of powders, good powder wettability by applying a binder and thus with the ability of fast homogenisation.

Powder	**High-speed steels**		**Carbide mixture in TetraC**	**Mixture of appropriate high-speed steels with mixture of TetraC**	
	EN HS 6-5-2	**EN HS 12-0-5-5**		**EN HS 6-5-2**	**EN HS 12-0-5-5**
Undersize D_{10} (μm)	3.5	4.68	1.45	2.8	2.8
Undersize D_{90} (μm)	16	28.5	7.3	17	25
Coefficient *Sw*	3.87	3.25	3.64	3.26	2.69

Table 4. The curve slope coefficients of the particle size distribution *Sw* calculated on the basis of undersize D_{10} and D_{90}.

Metal matrix	Carbides	Binder
EN HS 6-5-2	–	PW, PP, HDPE, SA
EN HS 12-0-5-5	–	
EN HS 6-5-2	Mixture 47% WC, 14% TiC, 33% TaC, 6% NbC (TetraC)	
EN HS 12-0-5-5		

Table 5. Components of the formed powder and polymer-powder mixtures.

The possibility of injection moulding of the applied polymer-powder mixture was initially evaluated based on the results from measuring the torque of stirrers during skip homogenisation. The maximum fraction of solid particles was thus established while maintaining relatively low viscosity of the polymer-powder mixture enabling injection moulding or extrusion. A high fraction of powder ensures minimum shrinkage in sintering, while an increase in binder fraction ensures easy forming but extends degradation time and increases sinter shrinkage which often causes the occurrence of distortions [9]. Irrespective of the polymer-powder mixture type, paraffin fraction was always equal to the fraction of the main binder component, that is, polyethylene or polypropylene.

Figure 5a shows the influence of high-density polyethylene (HDPE) and polypropylene on the torque curve during homogenisation of polymer-powder slip containing 70% of EN HS 12-0-5-5 steel powder. Regardless the homogenisation time and type of high-speed steel powder, a mixture containing a polypropylene-paraffin (PP/PW) binder is characterised by the lowest torque of stirrers in relation to a mixture containing an HDPE/PW slip. The minimum torque value for stirrers during the homogenisation of a mixture containing polyethylene for 3 h is about 2.2 Nm. In case of a feedstock containing polypropylene, torque after such long homogenisation time is 1 Nm. A curve for a mixture with polyethylene applied is not stable, which may signify inhomogeneous distribution of metallic powder in the binder matrix,

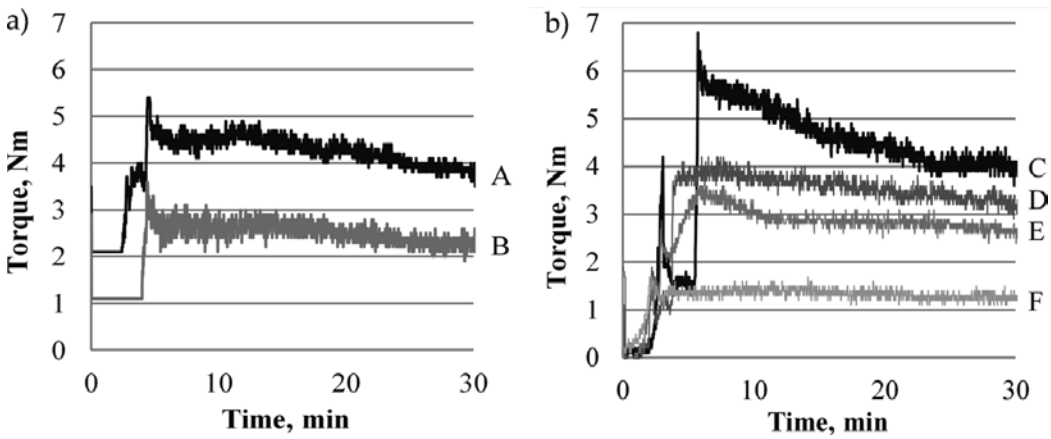

Figure 5. Torque measurements of feedstock with (a) 70% of EN HS 12-0-5-5 and two different binder compositions: A – HDPE/PW, B – PP/PW, (b) different amount of EN HS 6-5-2 powder: C – 75%, D – 70%, E – 65%, F – 60%.

http://dx.doi.org/10.5772/67353

despite long homogenisation time. Torque for a mixture with PP applied is going down over the entire homogenisation range, that is, over 3 h.

A correctly selected binder should wet the powder and reach the homogenous state within short time of about 30 min, and the torque characteristic should then stabilise. The longer time of homogenisation may lead to partial degradation of the low melting binder component, paraffin (PW) in this case, or to breaking PP and HDPE chains and to re-netting. The consequence of this would be higher torque, which is precluded by a falling tendency of the analysed curves.

Figure 5b shows torque variations depending on the fraction of high-speed steel EN HS 6-5-2 powder. If powder fraction is decreased by 5%, the torque characteristic is more uniform and the torque value after 30-min homogenisation falls from 4.0 to about 3.1 Nm. If powder fraction is again decreased by 5 and 10%, this causes the characteristic to be further equalised and torque to be reduced to the minimum value of about 1.2 Nm. The torque of the stirrers homogenising (for 1 h) a polymer and powder slip containing 60% of TetraC and a PP/PW binder is about four times higher in relation to the torque of the similar mixture containing EN HS 6-5-2 steel powder. The torque value is substantially decreased by using stearic acid (SA) covering the surface of carbides. Stearic acid was not used for covering high-speed steel powders due to its adverse impact on the high-speed steel structure after sintering, characterised by large precipitates of carbides on grain limits [31].

A low value of torque of mixtures containing polypropylene (PP) and paraffin (PW) corresponds to low viscosity. Powders of the EN HS 12-0-5-5 steel mixture with PP and PW exhibit smaller viscosity in relation to a mixture containing HDPE instead of PP, and this is independent of the homogenisation rate (**Figure 6a**). A mixture of high-speed steel with TetraC, which is accounting for 10% of the volume fraction, also has low viscosity similar to the mixture of EN HS 12-0-5-5 steel with PP and PW. Paraffin, apart from lessening the density, allows to use solvent degradation expediting the rate of thermal degradation and shortens the duration of the whole cycle.

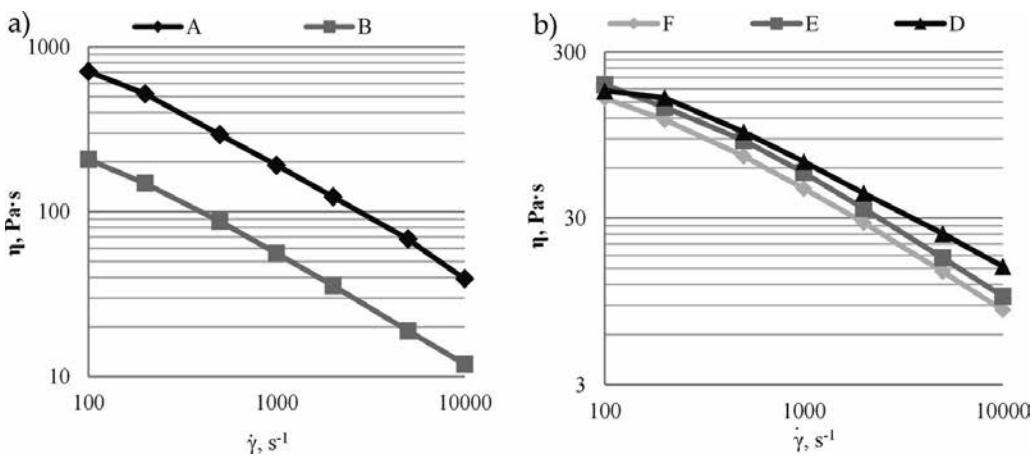

Figure 6. Viscosity curve for selected feedstock with (a) EN HS 12-0-5-5 and two different compositions: A – HDPE/PW, B – PP/PW, (b) different amount of EN HS 6-5-2 powder: D – 70%, E – 65%, F – 60%.

Metallic powder with a 60, 65 and 70% fraction containing a polypropylene-paraffin binder generally shows low viscosity regardless the fraction of powder. A mixture with the lowest content of powder exhibits the lowest viscosity (**Figure 6b**). Polypropylene and paraffin are the main binder component regardless the content of stearic acid.

Stearic acid improves wettability of metallic and ceramic powders by covering their oxidised (polar) surface that adsorbs the hydrophilic part of the chain as a result of the existing electrostatic forces between the powder and the wetting agent. The nonpolar part of the chain should be mixed without limitations with other polymers present in the binder. Apart from reducing viscosity, stearic acid is acting as a slipping agent in contact between the powder and the die surface or the surface of another particle. It also prevents powders from migrating during high-speed homogenisation. A process of migrating the powder inside the capillary or the destruction of the binder structure occur most probably during the high-speed homogenisation of a mixture not containing stearic acid. This is manifested by strongly falling viscosity together with an increased homogenisation rate. The viscosity of the mixtures containing stearic acid is not so much dependent on a homogenisation rate; hence, the growing rate of homogenisation does not have such a strong effect on the structure of a homogenous mixture. The torque is only negligibly decreased by increasing the content of stearic acid by another 4%; hence, its content did not exceed 4%.

Considering the feedstock viscosity, the maximum applicable fraction of carbides not coated with stearic acid is 50%. If stearic acid is used for a mixture containing 50% of carbides, viscosity is greatly reduced and a higher volume fraction of carbides can be obtained. The maximum volume fraction of powders which can be applied in a mixture for injection moulding was established by analysing the technological properties of polymer and powder mixtures containing binder-carbides, and hence, a mixture with only a 10% volume fraction of carbides was applied. Four different polymer-powder mixtures for injection moulding were selected and prepared. The fraction of such mixtures was presented in **Table 6**. The letter F was used in denomination to differentiate the injector's feedstock from pure powder.

The injection moulded materials were then subjected to solvent degradation, thermal degradation, sintering, and heat treatment. The specimens were sintered in a pipe furnace in the atmosphere of a flowing mixture of N_2/10%H_2 gases with the maximum sintering temperature of 1450°C. The sintering time of the moulded parts, regardless the furnace type and sintering

Injector feedstock	**Fraction volume of component (%)**						
	EN HS 6-5-2 (O)	**EN HS 12-0-5-5**	**TetraC**	**PP**	**HDPE**	**PW**	**SA**
F EN HS 6-5-2	68	–	–	–	16	16	–
F EN HS 12-0-5-5	–	68	–	–	16	16	–
F EN HS 6-5-2/TetraC	58	–	10	14	–	14	4
F EN HS 12-0-5-5/ TetraC	–	58	10	14	–	14	4

Table 6. Types of injection-moulded polymer and powder mixtures.

http://dx.doi.org/10.5772/67353

temperature, was 30 min each time. A sintering temperature was selected experimentally. The sintering temperature range was determined based on preliminary tests of 1180–1300°C with 20°C steps. Heating speed to sintering and cooling temperature was 5°C per min. Further heat treatment was performed with classical hardening from an austenitisation temperature of 1220, 1240 and 1260°C, and triple tempering in the same temperature of 540, 570, 600 or 630°C for 1 h was carried out directly after hardening in oil.

The conditions of solvent degradation were selected experimentally taking account of the element mass depending on the paraffin solving time and bath temperature. Correctly performed debinding should ensure a uniform concentration of carbon within the entire volume of the specimen. EN HS 6-5-2 steel subjected to thermal degradation at 450°C, in the atmosphere of N_2-10%H_2 and sintered at 1240–1260°C, reaches density close to theoretical density, that is, it does not exhibit any pores (**Figure 7a**). The density of EN HS 6-5-2/TetraC carbide-steel sintered within the same temperature range was shown in the **Figure 7** to compare the influence of carbon additives on the optimum sintering temperature ensuring highest density. EN HS 6-5-2/TetraC carbide-steel reaches the maximum density of 8.77 g/cm^3 after sintering at 1260°C. The density values were deliberately not referenced to the theoretical density of the material fabricated, which, based on the calculations, should be 8.69 g/cm^3. A varying chemical composition of the sinter as a result of an increased concentration of carbon, dependent upon debinding and upon the nitrogen coming from the atmosphere during sintering and forming the carbonitrides, does not allow to determine accurately what should be its maximum density. In addition, the WC, TiC, TaC and NbC carbides introduced are dissolving in a high-speed matrix during sintering at a high temperature and create M_6C and MC-type carbonitrides or MX carbonitrides in it, in case of sintering in an atmosphere containing nitrogen, identified with the diffraction methods. The density of the newly created phases differs from the carbides introduced, which is impacting the sinter's overall density. For this reason, the sinter porosity presented in **Figure 7b** is a very interesting piece of information. Regardless the sintering temperature, EN HS 6-5-2/TetraC carbide-steel is characterised by low porosity not exceeding 1%, appropriate for tool materials. The share of pores in the most

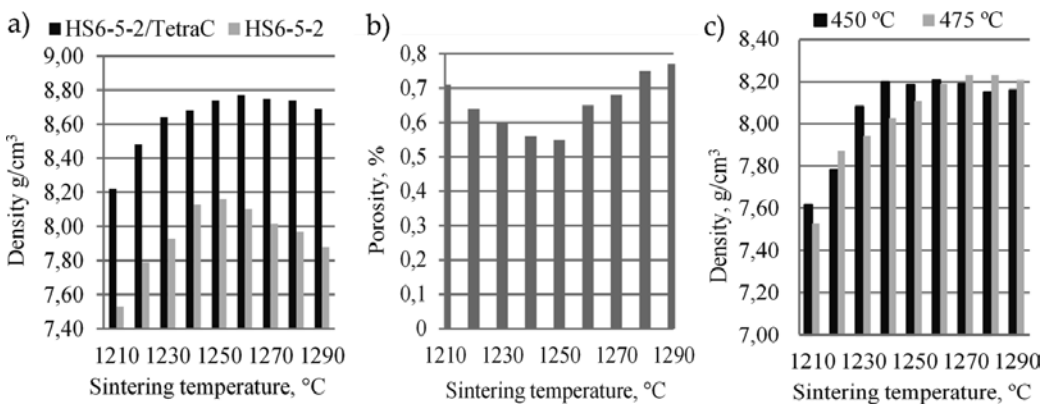

Figure 7. Influence of sintering temperature on (a) density of EN HS 6-5-2 and EN HS 6-5-2 /TetraC, (b) porosity of EN HS 6-5-2/TetraC, (c) density of EN HS 12-0-5-5 depend on debinding at 450 or 475°C and sintering temperature.

interesting range of the sintering temperature of 1240–1260°C is about 0.6%. The pores are ball shaped in the majority of cases and do not exceed the size of 2 μm; however, large pores may exist locally, which are forming most probably as a result of gas bubbles being formed during injection moulding or thermal degradation. Changes in the EN HS 12-0-5-5 steel density presented in **Figure 7c** points out that a lower degradation temperature is reducing a sintering temperature. The maximum density in the sintering temperature of 1240°C occurs after degradation at 450°C. If the degradation temperature is increased by 25°C, it becomes necessary to increase the sintering temperature by 30°C to achieve the maximum sinter density. Generally, EN HS 12-0-5-5 steel can be sintered within a broader temperature range versus EN HS 6-5-2. It was found by observing the structure of the sintered carbide-steels in which TetraC was applied covered with stearic acid that both, in EN HS 6-5-2/TetraC material and in EN HS 12-0-5-5/TetraC, the carbides surrounding the high steel grains are inhibiting their growth. The grain size of the sinter matrix is comparable to the particles of the high-speed steel powder employed. It is feasible to manufacture tool materials with high functional properties by selecting an appropriate binder, binder fraction and by controlling the technological process conditions, which enables to increase a concentration of carbon coming from thermal degradation products of the binder surrounding the nitride particles and activating a sintering process. Unfortunately, the locally occurring bubbles of the gas created during injection moulding or thermal degradation are not eliminated during free sintering, despite the presence of the liquid phase, which effectively compromises the bending strength of the sinter. Due to large gas bubbles existing in the material, further heat treatment does not influence bending strength, and the maximum value of about 1400 MPa is lower than the strength of conventional EN HS 6-5-2 cast and heat treated steel. The binder used, apart from its key task, that is, to enable injection moulding, plays an additional role as a source of carbon activating sintering. A rising concentration of carbon is dependent here upon the type of the binder and its debinding conditions.

4. Results of own investigations of the structure with nanostructural elements of high-speed steels and carbide steels on their matrix fabricated by powder injection moulding

In case of high-speed steels, dispersion carbides are released during tempering, and more rarely as pre-eutectoid precipitates when cooling from austenitisation temperature. In carbide-steels, small dispersion precipitates of the nanometric size occur extensively after quenching and tempering and after sintering. Such precipitates are surrounding large M_6C carbides and primary austenite grains blocking their growth. Moreover, they dissolve more quickly in austenitisation because of their small size, and alloy additives responsible for the secondary hardness effect are passing more easily to the matrix. The structure of EN HS 6-5-2/TetraC carbide-steel sintered at 1230°C shows small growth and coagulation of carbides in relation to the high-speed steel structure, sintered at the same temperature. Despite this, the structure of carbide-steels is still homogenous and fine-grained with carbides surrounding circular grains of high-speed steel. When comparing EN HS 6-5-2 and EN HS 6-5-2/TetraC

http://dx.doi.org/10.5772/67353

materials sintered in the same conditions at the temperature of 1300°C, one may conclude that a strong distortion occurred in the both cases, signifying an extensive liquid phase existing during sintering. A structure of carbide-steel sintered at 1300°C (**Figure 8c**) does not exhibit, however, an eutectic typical for a high-speed steel presented in **Figure 8b**. Carbides in high-speed steel with a characteristic "fishbone" shape are revealed as light phases in the image of secondary electrons and contain mainly Fe, W, Mo and a small concentration of V. The precipitates are sized up to 1 mm. If a mixture of carbides is employed, in particular interstitial phases with a regular network, stable at a high sintering and austenitisation temperature, the growth of primary austenite grains is inhibited and the hardness of carbide-steels after heat treatment is improved in relation to high-speed steel. Irrespective of the type of the binder used, which is influencing the way a polymer-powder slip is formed, and also irrespective of the sintering temperature and atmosphere, the precipitation of large, eutectic carbides typical for high-speed steels sintered freely at temperature exceeding the solidus line was completely eliminated in carbide-steels and also sometimes austenitised in such conditions, causing local remelting. Owing to such property, it is not necessary in sintering to use heating devices equipped with very accurate measuring and control systems ensuring temperature stability within a very narrow range, that is, approx. 5°C for the EN HS 6-5-2 steel applied.

The average size of carbides in carbide-steel sintered at 1300°C is rising by approx. 0.1 μm in relation to carbides existing after sintering at 1280°C. The average and maximum size of carbides and their fraction volume in EN HS 6-5-2/TetraC sintered within the entire temperature range are given in **Table 7**. The so-selected chemical composition of carbide steel sintered in the atmosphere of a flowing mixture of N_2-10% H_2 gases enables sintering within a wide temperature range ensuring a homogenous structure. If the protective atmosphere of N_2-10% H_2 is applied, surface oxidisation is prevented during thermal degradation and especially during sintering, while introducing at the same time, the desired nitrogen into the sinter forming fine nanometric carbonitride precipitates limiting the grain growth of other carbon precipitates and matrix grains, in particular carbide steels. When sintering temperature is raised from 1200 to 1300°C, the average size of carbides is increased by about 70%.

WC carbides with light colour based on secondary electrons are presented in **Figure 9**. A phase with grey colour rich in W, Fe, V, and Mo was formed from the alloy additives situated in high-speed steel or from elements coming from the solved carbides introduced into the steel. No existence of WC carbides was found at an elevated sintering temperature, which is con-

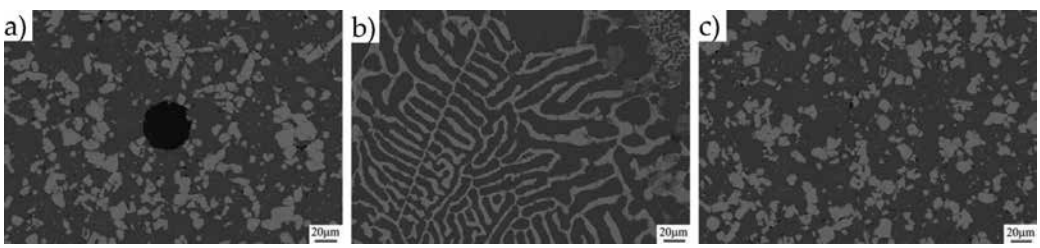

Figure 8. (a) Microstructure of metal matrix composite on the basis of EN HS 6-5-2/TetraC with large spherical pore, (b) and (c) structure of sintered at temperature 1300°C, (b) EN HS 6-5-2, (c) EN HS 6-5-2/TetraC.

Sintering temperature (°C)	1200	1220	1240	1260	1280	1300
Carbides amount (%)	36.2	35.9	33.8	33.2	34.2	34.2
Average size of carbides (μm)	1.65	2.06	2.2	2.66	2.71	2.82
Maximum size of carbides (μm)	21.57	25.68	28.54	31.58	38.17	40.58

Table 7. Average and maximum size of carbides precipitation and their amount versus sintering temperature.

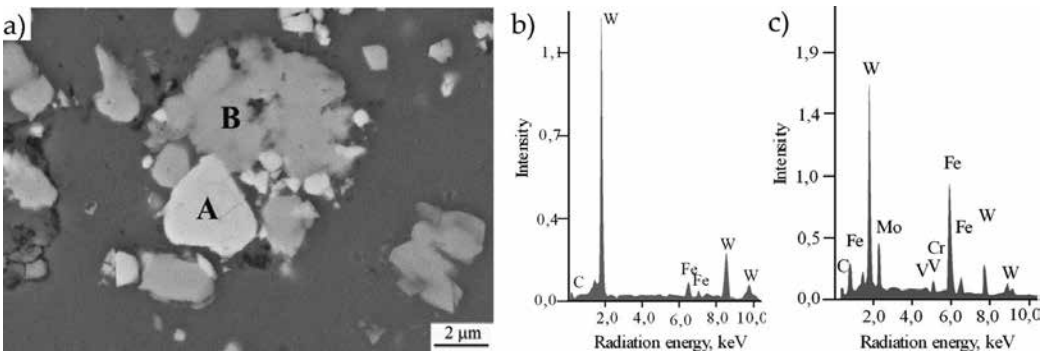

Figure 9. (a) Structure of EN HS 6-5-2/TetraC carbide-steels sintered at 1200°C and a charts of scattered X-ray radiation for the areas marked in (a) (b) A and (c) B, respectively.

firmed by the results of an X-ray phase analysis. M_6C and MC carbides typical for high-speed steel were identified, though. The growth of light carbides, shown in the image of secondary electrons, rich in W, Mo, and Fe, is limited by the surrounding grey, spherical precipitate rich in Ti and V, presented in **Figure 9a**, the size of which does not exceed mostly several dozens of nanometres, and the largest ones do not exceed 1 μm. In order to better present such nanometric precipitates, **Figure 10** shows the morphology of carbides in the form of sediment of electrolytically isolated precipitates.

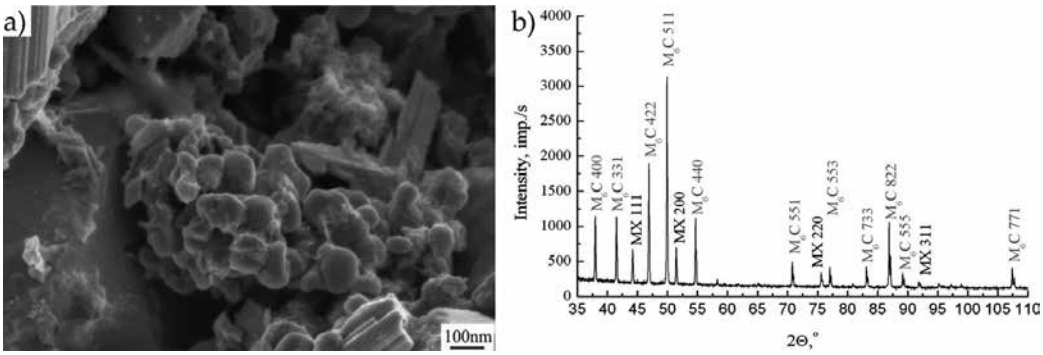

Figure 10. Structure of EN HS 6-5-2/TetraC carbide-steel sintered at 1280°C, (a) sediment of electrolytically isolated precipitates, SEM, (b) X-ray diffraction pattern of electrolytically isolated precipitates from EN HS 6-5-2/TetraC carbide-steel tempered and quenched at 540°C.

http://dx.doi.org/10.5772/67353

The existence of M_2C carbides typical for EN HS 6-5-2 high-speed steels, rich in molybdenum, in the form of long needles, precipitated at a high sintering temperature and considerably reducing mechanical properties, was not found [40]. M_6C and MX precipitates exist only in the sediment of electrolytically isolated carbides (**Figure 10**).

Nanometric precipitates in EN HS 6-5-2/TetraC carbide-steel are presented in **Figures 11a** and **12a** present results of examinations of precipitates coming from EN HS 6-5-2/TetraC carbide-steel after heat treatment in a transmission electron microscope. The diagram of the function of scattered X-ray radiation for such precipitates presented in **Figures 11b** and **12b** proves that carbides are rich in tungsten and molybdenum, which rather indicate the M_6C phase, not MC or M_2C phase released in high-speed steels during tempering. Undoubtedly, their size does not exceed 200 Nm. It should be added that typical dispersive MC or M_2C carbides, precipitating during tempering, have their size ten times smaller. A higher fraction of retained austenite in carbide-steel in relation to classical high-speed steels is caused by a higher concentration of carbon remaining after debinding. In addition, carbon is released as a result of carbonitrides being formed and the introduced carbides being dissolved. If carbon concentration is increased, the start temperature of martensite transformation is decreased; hence, a fraction volume of retained austenite after quenching in such materials is up to 62%. A higher tempering temperature of approx. 600°C has to be applied due to variations in retained austenite fraction in the matrix of the analysed carbide-steels, in relation to high-speed steel with the analogous chemical composition of the matrix. EN HS 6-5-2 high-speed steel should be quenched at below 600°C. In case of carbide-steels and a large fraction of retained austenite in such steels after hardening, it is necessary to temper at a higher temperature ensuring the transformation of retained austenite into martensite and high hardness after heat treatment. Unfortunately, M_6C carbides may precipitate at such high temperature; hence, most probably, the precipitates seen in **Figures 11** and **12** are the result of it. Precipitates with a nanometric size, formed during sintering, are rich in other elements such as V, Ti, and N.

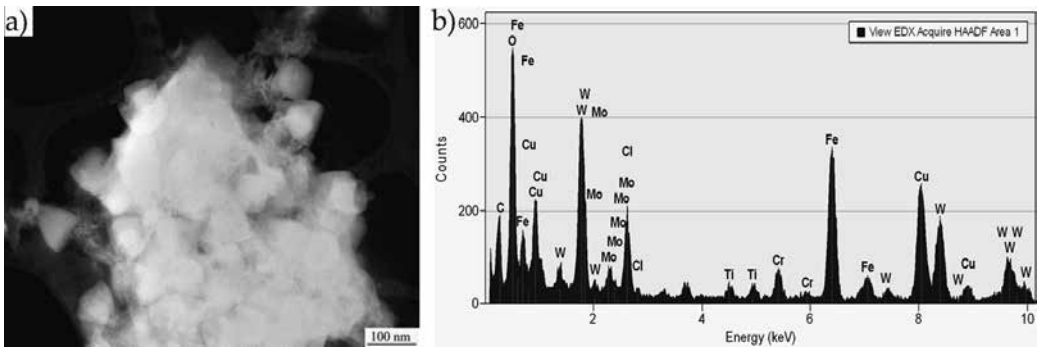

Figure 11. (a) HAADF image of precipitate in EN HS 6-5-2/TetraC carbide-steel after quenching and tempering twice at 630°C, SEM, (b) diagram of the function of scattered X-ray radiation for the carbide shown in (a).

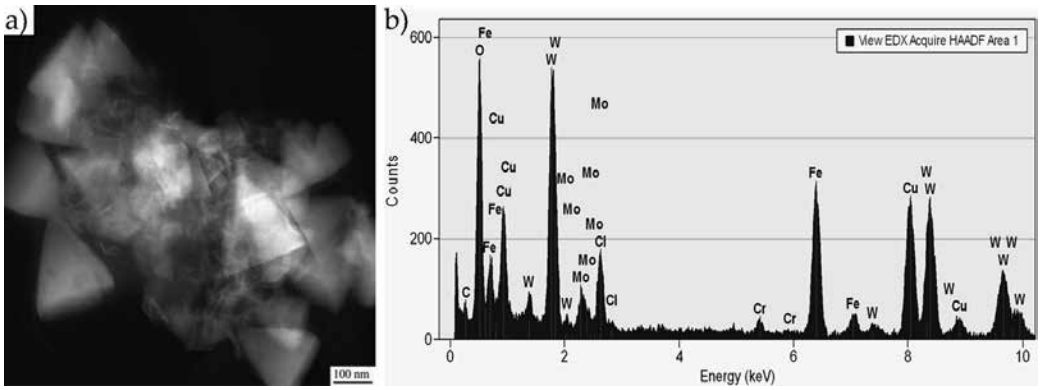

Figure 12. (a) HAADF image of precipitate in EN HS 6-5-2/TetraC carbide-steel after quenching and tempering twice at 630°C, SEM, (b) diagram of the function of scattered X-ray radiation for the carbide shown in (a).

Additional information

The results of the research carried out partially in the research Project "NANOCOPOR—Determining the importance of the effect of the one-dimensional nanostructural materials on the structure and properties of newly developed functional nanocomposite and nanoporous materials", funded by the DEC-2012/07/B/ST8/04070 of the Polish National Science Centre in the framework of the "OPUS" competitions, headed by Prof. Leszek A. Dobrzański were used in this chapter.

Author details

Leszek A. Dobrzański* and Grzegorz Matula

*Address all correspondence to: leszek.adam@gmail.com

Faculty of Mechanical Engineering, Silesian University of Technology, Gliwice, Poland

References

[1] Dobrzański LA, Dobrzańska-Danikiewicz AD, Malara P, Gaweł TG, Dobrzański LB, Achtelik-Franczak A. Fabrication of scaffolds from Ti6Al4V powders using the computer aided laser method. Archives of Metallurgy and Materials. 2015;**60**:1065–1070. doi: 10.1515/amm-2015-0260

[2] Dobrzański LA, Dobrzańska-Danikiewicz AD, Gaweł TG, Achtelik-Franczak A. Selective laser sintering and melting of pristine titanium and titanium Ti6Al4V alloy powders and selection of chemical environment for etching of such materials. Archives of Metallurgy and Materials. 2015;**60**:2039–2045. doi: 10.1515/amm-2015-0346

[3] Dobrzański LA, Matula G. Powder injection molding: Sinter-Hardening. In: Colás R, Totten GE, editors. Encyclopedia of Iron, Steel, and Their Alloys. Boca Raton: CRC Press, Taylor & Francis Group; 2016. 14 p.

[4] Dobrzański LA, Matula G. Powder metallurgy fundamentals and sintered materials. Open Access Library. 2012;**8**:1–156 (in Polish).

[5] Tański T, Dobrzańska-Danikiewicz AD, Labisz K, Matysiak W. Long-term development perspectives of selected groups of engineering materials used in the automotive industry. Archives of Metallurgy and Materials. 2014;**59**:1717–1728. doi: 10.2478/amm-2014-0290

[6] Edinsinghe MJ, Evens JRG. Review: fabrication of engineering ceramics by injection moulding. I. materials selection. International Journal of High Technology Ceramics. 1986;**2**:1–32. doi: 10.1016/0267-3762(86)90002-0

[7] Sterzel H-J, Ter Maat JHH. Thermoplastic Materials for Manufacturing Metallic Articles. European Patent 0446708 B1. 4.11.1995.

[8] Matula G. Gradient surface layers from tool cermets formed pressurelessly and sintered. Open Access Library. 2012;**7**:1–144 (in Polish).

[9] German RM. Divergences in global powder injection moulding. Powder Injection Moulding International. 2008;**2**:45–49.

[10] Dobrzańska-Danikiewicz AD. Foresight of material surface engineering as a tool building a knowledge based economy. Materials Science Forum. 2012;**706–709**:2511–2516. doi: 10.4028/www.scientific.net/MSF.706-709.2511

[11] Wiśniewska-Weinert HM. Composites with graphene-like sulfide nanoparticles. Open Access Library. 2012;**9**:1–184 (in Polish).

[12] Zauner R. Micro powder injection moulding. Microelectronic Engineering. 2006;**83**:1442–1444. doi: 10.1016/j.mee.2006.01.170

[13] Gołombek K. Structure and properties of injection moulding tool materials with nanocrystalline coatings. Open Access Library. 2013;**1**:1–136 (in Polish).

[14] Superhard Materials – Global Strategic Business Report. San Jose, CA: Global Industry Analysts Inc.; 2012. 322 p.

[15] Hultgren M. As hard as they come – new grades with metal injection moulding. The shape of things to come. Metalworking World. 2006;**2**:14–16.

[16] German RM. Powder Injection Molding – Design and Application – User's Guide. State College, PA: Innovative Material Solutions, Inc.; 2003.

[17] Petzoldt F. Metal injection moulding in Europe: ten facts that you need to know. Powder Injection Moulding International. 2007;**1**:23–28.

[18] German RM, Bose A. Injection Molding of Metals and Ceramics. Princeton: Metal Powder Industries Federation; 1997. 413 p.

[19] Dobrzańska-Danikiewicz AD. The acceptation of the production orders for the realisation in the manufacturing assembly systems. Journal of Materials Processing Technology. 2006;**175**:123–132. doi: 10.1016/j.jmatprotec.2005.04.001

[20] Krenczyk D, Dobrzańska-Danikiewicz A. The deadlock protection method used in the production systems. Journal of Materials Processing Technology. 2005;**164**:1388–1394. doi: 10.1016/j.jmatprotec.2005.02.056

[21] Hard and Superhard Materials Grow 7.5% from 2007 to 2012. New York: Dedalus Consulting; 2009.

[22] Herranz G, Matula G, Alonso R, Sánchez I, Rodríguez G. Metal Injection Moulding of Carbides Reinforced M2 HSS. Proceedings of the International Congress and Exhibition "Powder Metallurgy" Euro PM 2009, Powder Injection Moulding – Compounds and Composite Parts. Copenhagen; 2009; 99–104.

[23] Herranz G, Rodríguez GP, Alonso R, Matula G. Sintering process of M2 HSS feedstock reinforced with carbides. Powder Injection Moulding International. 2010;**4**:60–65.

[24] Ye H, Liu XY, Hong H. Fabrication of metal matrix composites by metal injection molding – a review. Journal of Materials Processing Technology. 2008;**200**:12–24. doi: 10.1016/j.jmatprotec.2007.10.066

[25] Dobrzański LA, Dołżańska B, Matula G. Structure and properties of tool gradient materials reinforced with the WC carbides. Archives of Materials Science and Engineering. 2008;**28**:35–38.

[26] Várez A, Levenfeld B, Torralba JM, Matula G, Dobrzański LA. Sintering in different atmospheres of T15 and M2 high speed steels produced by modified metal injection moulding process. Materials Science and Engineering A. 2004;**366**:318–324. doi: 10.1016/j.msea.2003.08.028

[27] Herranz G, Levenfeld B, Várez A, Torralba JM. Development of new feedstock formulation based on high density polyethylene for MIM of M2 high speed steel. Powder Metallurgy. 2005;**48**:134–138. doi: 10.1179/003258905X37828

[28] Matula G, Dobrzański LA, Várez A, Levenfeld B, Torralba JM. Comparison of structure and properties of the HS12-1-5-5 type high-speed steel fabricated using the pressureless forming and PIM methods. Journal of Materials Processing Technology. 2005;**162–163**:230–235. doi: 10.1016/j.jmatprotec.2005.02.1

[29] Matula G, Dobrzański LA, Herranz G, Várez A, Levenfeld B, Torralba JM. Structure and properties of HS6-5-2 type HSS manufactured by different P/M methods. Journal of Achievements in Materials and Manufacturing Engineering. 2007;**24**:71–74.

[30] German RM. Markets applications, and financial aspects of global metal powder injection moulding (MIM) technologies. Metal Powder Report. 2012;**1**:18–26. doi: 10.1016/S0026-0657(12)70051-6

[31] Herranz G, Nagel R, Zauner R, Levenfeld B, Várez A, Torralba JM. Influence of powder surface treatment with stearic acid on powder injection moulding of M2 HSS using a

HDPE based binder. Proceedings of the International Congress and Exhibition "Powder Metallurgy" PM 2004. Viena; 2004; 397–402.

[32] Matula G. Influence of binder composition on structure and properties of carbide alloyed composite manufactured with the PIM method. Proceedings of the 12th International Materials Symposium. Pamukkale-Denizli; 2008; 601–605.

[33] Matula G, Dobrzański LA, Várez A, Levenfeld B. Development of a feedstock formulation based on PP for MIM of carbides reinforced M2. Archives of Materials Science and Engineering. 2008;**27**:195–198.

[34] Dobrzański LA, Matula G, Várez A, Levenfeld B, Torralba JM. Fabrication methods and heat treatment conditions effect on tribological properties of high speed steels. Journal of Materials Processing Technology. 2004;**157–158**:324–330. doi: 10.1016/j.jmatprotec.2004.09.051

[35] Dobrzański LA, Matula G, Várez A, Levenfeld B, Torralba JM. Structure and mechanical properties of HSS HS6-5-2- and HS12-1-5-5-type steel produced by modified powder injection moulding process. Journal of Materials Processing Technology. 2004;**157–158**:658–668. doi: 10.1016/j.jmatprotec.2004.07.1

[36] Loh NH, Tor SB, Khor KA. Production of metal matrix composite part by powder injection molding. Journal of Materials Processing Technology. 2001;**108**:398–407. doi: 10.1016/S0924-0136(00)00855-4

[37] Liu ZY, Loh NH, Khor KA, Tor SB. Microstructure evolution during sintering of injection molded M2 high speed steel. Materials Science and Engineering A. 2000;**293**:46–55. doi: 10.1016/S0921-5093(00)01244-2

[38] Liu ZY, Loh NH, Khor KA, Tor SB. Sintering of injection molded M2 high-speed steel. Materials Letters. 2000;**45**:32–38. doi: 10.1016/S0167-577X(00)00070-7

[39] Matula G, Dobrzański LA, Herranz G, Várez A, Levenfeld B, Torralba JM. Influence of binders on the structure and properties of high speed-steel HS6-5-2 Type fabricated using pressureless forming and PIM methods. Materials Science Forum. 2007;**534–536**:693–696. doi: 10.4028/www.scientific.net/MSF.534-536.693

[40] Dobrzański LA. Effects of chemical composition and processing conditions on the structure and properties of high-speed steels. Journal of Materials Processing Technology. 1995;**48**:727–737. doi: 10.1016/0924-0136(94)01715-D

Chapter 11

Manufacturing, Composition, Properties and Application of Sintered Hard Metals

Ildiko Peter and Mario Rosso

Additional information is available at the end of the chapter

http://dx.doi.org/10.5772/66872

Abstract

Among other materials, hard metals represent an important family of functional materials. They show properties that are combinations of those of their constituents. The general idea while using hard metals is to exploit their excellent properties in terms of hardness, toughness, wear resistance, and chemical stability. These characteristics made hard metals as promising candidate for use as a cutting tool, which constitutes their main area of application. Depending on the particular use, the most important properties can be achieved: (i) by properly selecting the constituents made up the whole composition, (ii) by varying the relative composition of the phases, or (iii) by applying a suitable hard metal coating layer on the top of the cutting tool. This chapter presents a general overview of the actual scenario concerning different tool materials, including a short history and description of state-of-the-art techniques as regards their composition, their manufacturing routes and their most important properties. Some results of the own research in this field are carried out during the years will integrate this part.

Keywords: hard metals, cutting tools, improved properties

1. Introduction

Actually, different types of cutting tool materials have been employed industrially, considering their particular properties for a specific application where a well-balanced mishmash of the required features is needed. There are important differences between cutting tools and only a good knowledge of their properties can guide the designer/manufacturer for the selection of the right one for a particular application and for cutting different materials.

Generally, cutting has to be performed with a material that is harder than the material that has to be cut and at the same time it has to show a specific geometry, with clearance angles

designed in such a way that the cutting edge can appropriately interact with the piece to be cut without the rest of the tool dragging on the piece surfaces. An effective cutting tool has to hold (i) good wear resistance in order to be capable of keeping its integrity against erosion during service, (ii) an adequate toughness to be able to absorb the energy imposed by different loading/unloading forces and vibrations, and (iii) an appropriate hardness to be able to survive against the continuous alterations in shape and geometry during cutting. However, extreme hardness is not certainly a preferred property, since it is directly connected to the tool fragility and its brittleness. Hardness becomes more significant when the machining is carrying out in extreme conditions and the tool has to conserve its integrity at high temperatures.

1.1. Outline on different types of cutting tool materials

During the time, different cutting tool materials have been used and their development is still in continuous evolution. Cutting and shaping materials into different parts for particular purposes are important, especially when high cutting speed and high temperatures are involved. For these reasons, the tool material has to exhibit such properties to prevent too much wear and fracture failure during service. To withstand these harmful conditions, the cutting tool has to show an adequate (i) hardness and strength and maintain them at high temperature, (ii) toughness to absorb energy with no failure, (iii) wear resistance, (iv) chemical inertness, and (v) thermal conductivity. Generally, cutting tools have to be manufactured using a mechanically harder material with respect to the material that has to be cut. Additionally, the use of the cutting tool with a particular geometry is preferred where its clearance angle is designed in such a way so as to allow a perfect interaction between the cutting edge and the piece to be cut without that the rest of the tool slowing on the other surfaces close to the interested one. The knowledge of the differences among performances of cutting materials is essential [1–5] for their appropriate selection for cutting the materials under process.

The oldest tool materials are carbon steels (CS), but their actual use is limited. They are rarely used for metal and alloys cutting, since they are rapidly overtempered at moderately low cutting temperature. These types of steels contain about 0.6–1.5% of C and small quantities of Si, Cr, Mn, and V. In 1868, Robert Forester Mushet discovered that the hardness of steel can be enhanced by addition of W [6] and it was the starting point for the discovering of high speed steels (HSSs) [7] indispensable in case of high cutting speeds (this is the reason they are called high speed steels) and increased temperature. The addition of alloying elements to harden and strengthen the basic material and to obtain a more resistant one in extreme conditions makes the difference between CS and HSS [8]. HSS can be hardened to various depths through suitable heat treating. Generally, Mn, Cr, W, V, Mo, Co, and Nb are used as alloying elements in the composition of HSS. Co is a key element for providing higher hardness (called *cold hardness*) of HSS at high temperature than that of CS. They are used as cutting tool materials when the device geometry and mechanics of chip formation are complex or when brittle tools are not appropriate below shock loading. HSSs are appropriate for continuous cutting and they are employed for the development of tools of complex shape, like

http://dx.doi.org/10.5772/66872

drills or gear cutters. The typical cutting speeds are in the range of 10–60 m/min. Commonly used HSSs are classified into M (tool steels with Mo) and T types (tool steels with W) and they have different grades: each one works for a particular aim giving important benefits in a precise use.

During the time, the efficiency of HSSs has been enriched by modifying their properties and their surface conditions through different methods: (i) refinement of their microstructure, (ii) production with high level of Co and V to amplify their hot hardness and wear resistance too, (iii) using powder metallurgy for their production, (iv) applying by chemical vapor deposition (CVD), or physical vapor deposition (PVD) heat and wear resistant coating (especially TiC and TiN). Using these procedures it was possible to enhance their cutting speed and consequently the whole tool life of about three times [9].

In the early 1920s, a nonmagnetic, wear, and corrosion resistant Co-Cr alloy, known as Stellite [10], was introduced, which can be used at slightly higher speeds than HSS. Due to its reduced grindability and for the development of cemented/sintered carbides, the use of Stellite came to be out-of-date very soon. Currently, one of the most important tool materials, introduced in the 1930s, is cemented carbide based. For the reason that they have high hardness over a large range of temperature, high thermal conductivity, and high modulus of elasticity can be employed in many applications. Compared to HSS, they are able to reach a cutting speed of 3–5 times higher. Tungsten carbide (WC), titanium carbide (TiC), tantalum carbide (TaC_x), and niobium carbide (NbC/Nb_2C) are the most familiar hard carbides, which are embedded within a matrix of Co through sintering procedure. The performance of the carbide tools is significantly affected by the type of carbide and the Co content and based on their composition they can be used in different applications. Higher hardness can be reached with 3–6% of Co, while a higher level a Co (up to 15%) provides superior toughness, but reduces the hardness, wear resistance, and strength. As W level increases the wear resistance increases, however negatively affects the tool strength. TiC confers to the tool relatively higher wear resistance and lower toughness than WC [11–13].

The continuous industrial evolution and the need of more sophisticated performances for tool materials lead to the development of coated tools, improving the tool life, and generating higher cutting speeds. Generally, coating layer/layers were realized by PVD or CVD techniques, using TiN, TiC, TiCN, and Al_2O_3 powders and usually the thickness range of 2–10 μm is realized. For multiphase and ceramic coatings on carbide tools, the CVD technique is preferentially adopted, while the TiN layer sprayed by PVD shows some positive features, such as higher cutting-edge strength, minor friction, lower affinity to develop a built-up edge, and are smother and more constant in thickness (generally in the range of 2–4 μm). Actually, mostly for multiphase coating medium temperature chemical vapor deposition (MTCVD) can be adopted, leading to obtain superior resistance to crack propagation than CVD-coated cutting tools. In the middle of twentieth century, ceramic made sintered cutting tools have been introduced, containing Al_2O_3 (white or cold pressed ceramics), Si_3N_4 (black or of pressed ceramics), SiAlON particles [14–18].

In the 1960s, cermets [11–13] were developed, containing typically 70% Al_2O_3 and 30% TiC, with some small amounts of MoC, NbC, TaC, offering some benefits. Addition of TiC and

ZrO_2 to these compounds modifies some characteristics of ceramic tools: ZrO_2 improves the fracture toughness, but at the same time it reduces the hardness and the thermal conductivity. Compared to HSS and carbides, cermets show higher abrasion resistance, hot hardness, and chemical stability, but they have a lower tendency to form a built-up edge, have low toughness and low tensile strengths. Specific arrangements are needed during working with ceramic tools to avoid early failure of the tool. These tools are suitable for continuous operations at very high speed. Anyway, the brittleness and high cost of cermets have been problematic and their characteristics are situated between those of carbides and ceramics. The most important reason for the development of oxide-metal composite materials was to take some benefits of well-known characteristics or to realize different properties through joining different elements. The possibility to decrease the high brittleness of the pure oxide ceramics and the enhancement of the resistance at high temperature are the most important features which show the way for the development of a more complex material, like cermets.

During the time, development of cutting tools is continuously increasing. Introduction of new materials, such as cubic boron nitride (cBN), polycrystalline cBN, and polycrystalline diamond tools are on the way. They provide very high wear resistance and cutting edge strength. At high temperature, cBN is chemically inert to Fe and Ni and for these reasons they are commonly appropriate for cutting hardened ferrous and high temperature alloys. At the same time, particular attention has to be paid to equilibrate its brittleness during service. The hardest material is diamond and as a cutting tool reveals high wear resistance, it maintains a sharp cutting edge and it is often used when good surface finish and dimensional accuracy are required, particularly when soft nonferrous alloys and abrasive nonmetallic materials are machined. Due to its high chemical affinity to Fe, diamond is not appropriate for cutting steel materials [19–24].

Further improvement has been realized with the development of the whisker-reinforced nanocrystalline tool materials with improved properties, consisting of using whiskers as reinforcing fibers in composite tool materials. This solution is occasionally extended with the addition of ZrO_2 offering high fracture toughness, excellent hot hardness, excellent resistance to thermal shock, and cutting-edge strength. Evolution of nanomaterials offers excellent opportunities for the development of further enhanced tool materials [25–28].

The ideal tool is not the most costly one, but it is the one which is carefully selected to perform professionally, rapidly, and economically the planned cutting operation. Generally, as strength of the cutting tool increases, its hardness at high temperature decreases. **Figure 1** shows, in a comparative manner, that no perfect cutting tool material exists (with no information on cBN, diamond, and whiskers-reinforced tool materials). Each type of cutting materials possesses its own typical properties, which have to be understood in order to efficiently exploit them as a cutting material.

1.1.1. Hard metals: overview and some properties

Hard metals belong to the family of composite materials made of hard materials (metallic or nonmetallic types), which are joined by metallic element/s. Usually, sintering or hot pressing

http://dx.doi.org/10.5772/66872

is used for the manufacturing of components containing metallic hard metals and some of them can be employed without binder phases, as a consequence of their intrinsic fragility.

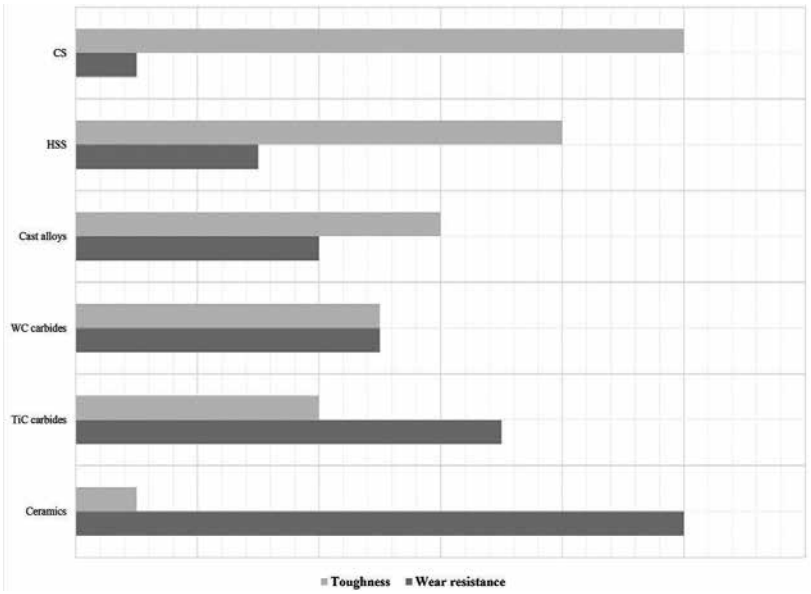

Figure 1. Qualitative indication on the evolution of the wear resistance and toughness for different tool materials.

Generally, hexagonal WC is considered as the most common carbide, and Co, because of its higher wetting properties compared to other materials, is mostly employed as a binder material [29–31]. When specific properties are required at high temperature, cubic TaC, TiC, and NbC are used with an addition of low quantity of V and Cr. Usually, the employed carbides are produced through powder metallurgy (PM) and then the components are mixed and milled together using a binder material (usually organic type), spray-dried into agglomerates and then pressed for obtaining the green forms which are sintered to remove their porosity and at the same time to enhance their mechanical strength. In the case of materials that form short machining chips, like grey cast iron, the main important types of hard metals are WC-Co, while employed in the case of materials that provide long machining chips, such as steels, WC-TiC-Co/WC-TiC-TaC-Co are employed [32–40].

The standardization of cutting tool materials is very difficult, due to the different kinds of manufacturing routes, which usually employ powder metallurgy (PM) in different alternative ways to better satisfy the requirements. ISO 513:2012 Standard provides a classification in six groups based on the materials to be machined: (1) all kinds of *steel* and *cast steel* except stainless steel with an austenitic structure, (2) *stainless steel* and *austenitic/ferritic steel* and *cast steel*, (3) *cast iron*, *cast iron with spheroidal graphite*, *malleable cast iron*, (4) nonferrous metals (Al, and other metals and nonmetallic materials), (5) *superalloys* and *Ti* (heat-resistant special alloys based on Fe, Ni, and Co, Ti, and its alloys), and (6) *hard materials* (hardened steel, hardened cast iron materials, chilled cast iron) [41].

The manufacturing of hard metals is taking place in different steps, which can be further divided into two main families: the former one is dedicated to obtain the compacted powders, while the latter one is a firing treatment, called sintering, for bonding the single particles together providing a superior strength to the obtained material. The first step is a very complex one beginning with the production of the powders, their accurate mixing using a pressing agent/binder material, crushing and it finished with the pressing procedure. As a concern, sintering starts with the elimination of the pressing agent (dewaxing) under controlled condition (in the presence of H_2 or vacuum) at about 600°C followed by the real sintering treatment in a temperature range 1350–1500°C according to the composition of the hard metal to be obtained, usually in vacuum or in a reducing atmosphere. When the powders cannot be pressed in their final shape, indirect forming is commonly used. This procedure begins from a pressed blank and after the removal of the pressing agent (at about 600°C) or after presintering (up to 1000°C) the blank has to acquire an adequate strength to assume its final shape realized by turning, crushing, and drilling. Usually, when big compacts have to be obtained, pressure-assisted process is applied, and depending on the compacts nature and composition it can be cold isostatic or hot isostatic pressing.

The microstructure, as expected, controls the most important properties and in particular, the mechanical properties are mainly affected by two aspects: the average carbide grain size and their distribution within the metallic matrix.

The raw materials employed and the binder level content, the pressure applied, the sintering time and temperature govern the growth of the grains within the structure. During sintering, enlargement of the grain size occurs as a result of coarsening. At the same time, some grains have the tendency to increase differently and to acquire unusually great dimensions, which have to be avoided, because they act as initiation sites for cracking, hence, lowering the mechanical properties of the material. To control the grain size during sintering, inhibitors can be used to restrain the grain growth and to obtain fine-grained carbides [42].

The relationship between strength, composition, and gran size of hard metals is extensively investigated in the literature [43–45]. High temperature mechanical properties of WC-Co hard metal, as a preferred material for cutting tools, are investigated, for example, in [46]. In this chapter, the influence of the Co content WC grain size on the mechanical performance of the hard metal is considered and exploited in terms of Young's Modulus, Poisson's ratio, yield strength, fatigue strength, and fracture toughness. According to this research, as temperature and Co content increase, Young's Modulus decreases. In [47], a more accentuated loss has been evidenced above 800°C and the independence of the WC grain size at room temperature. Temperature, Co content, and WC grain size do not have any effect on the Poisson' ratio. The highest the temperature and Co content the lowest the yield strength, while up to 700°C, Co level and WC gran dimensions do not influence significantly the fracture toughness of WC-Co hard metals in accordance with other studies [48–50]. Above 800°C, more than 8% of Co increases considerably these properties are in good agreement with previous studies [48, 51] because at this temperature the plastic zone is higher compared to the situation at room temperature and this changes the spreading of the fracture trajectory. Various theories are suggested for the plastic deformation of WC-Co hard metals: in line with [52–54], the deformation of the

http://dx.doi.org/10.5772/66872

material takes place inside the binder phase, while in [43, 44] the presence of a constant WC system is suggested and the carbide network is deformed at the same time with the Co binder.

As mentioned in Refs. [6, 55, 56], WC-Co hard metals, developed from an ultrafine or nanograined particles, show superior hardness compared to their coarser-grained based ones, while Lankford [57] indicates that the compressive strength of these hard metals increases when binder contents decreases. The influence of the loading rate on the compressive strength of WC-Co hard metal is illustrated in [52] as a function of Co content and the authors found that the fragments results to be finer after compressive loading with increasing strain rate and as Co content decreases, the compressive strength increases due to the increasing level of failure which is characterized by crack initiations, typical features for brittle material. Crack propagation induces a local stress release. This aspect is in a good agreement with the fineness of the fragments reported in [53–64].

For the high industrial request for titanium carbonitride (Ti(C,N))-based cutting tools with high and stable mechanical properties, the research community has paid high attention to this issue [65]. In order to increase the hardness and the mechanical properties at high temperature of such cutting tools, addition of Mo, Ni-Co, WC, TaC, HfC has been proposed in [66] and their effect has been evaluated through microstructural characterization, which is directly connected to the mechanical behavior of the system. As Ni-Co content increases the microstructure of the material become finer; more than 4% of Mo addition has a negative effect on the mechanical properties. In view of authors [67, 68] it is assumed that the hard metal obtained with a small quantity of Ni-Co and 4–8% (wt.) of Mo, the best mechanical properties can be reached. Addition of TaC increases the flexural strength, while HfC enhances the hardness of the Ti(C, N) hard metal. Additionally, some studies [65, 69, 70] reported on the beneficial effect of WC on the wettability between the interested phases producing finer microstructure and higher mechanical behavior, but at the same time due to the WC low oxidation temperature it has a negative influence on its cutting performance, particularly in high speed machining. In such cases, it is suitable to substitute, partially or completely, WC particles with TaC [71] as stated also in [69, 70–72]. Nanocrystalline cemented carbides obtained through the pulse plasma sintering process compared to the standard one produced by Hot isostatic pressing reveals higher hardness and higher relative density as illustrated in [73].

The research on the possibility to employ nanotechnology for improving the machining quality and efficiency is limited. Recently, the use of nanoparticles, including carbon nanotubes (CNT), in crushing and polishing tools, as coating materials too, has become very attractive [74–79] and the reported data [74] demonstrate that the addition of CNT tends to lower the grain size of the structural constituent of the binder determining higher strength and performance to the metallic binder.

Chemical vapor deposition and physical vapor deposition processes have been used since 1970 for deposition of different hard thin layers on cemented carbides [80–83] to amplify their life time and in particular on the active parts of the tools. Matei et al. [84] reported on the favorable effect of some coating layers (TiN, TiC, TiAlN) on the working performance of the modified WC-Co tools in a clean atmosphere considering their corrosion resistance compared

to the uncoated tools. The authors found that among the materials used for coating, TiN layer is the most promising one protecting the substrate more efficiently.

1.2. Manufacturing of cutting tool materials

The increasing use of tool materials requires high integrity and improved performances, which represent a valid support to enhancing the life of engineering components and their reliability without compromising safety issues. The economic impact and complexity of these cutting materials can justify the huge efforts, during the time, for their development and processing for different applications. Obtaining an isotropic microstructure, which is characterized by a homogeneous spreading of the elements with no segregations, is of primary importance in cutting materials application.

The use of PM route allows obtaining advanced tool materials which are able to achieve very high performance and to withstand severe service conditions without premature failure. The PM method is able to combine powders of different natures and characteristics which are difficult to compact otherwise, producing a dense final material with a hybrid or new properties. The ability of PM to perform all the processing phases in the solid state and to form the powders directly into the final or semifinal form can be considered as a main advantage of such technology. Additionally, powders, with significantly different melting temperatures with very different densities can be obtained through this technology. The possibility of making use of different constituents which have limited mutual solubility in liquid state or when the liquid metal has a high affinity for the refractory or other constituent PM is a very promising technology.

The PM process is very useful in the case of composite materials containing diamond and boron nitride and including hard metals too. After the WWII (world War II) this technology became important for the first generation of cermets production and during the time it turns to be particularly important for the second generation of cermets (containing carbides, borides, nitrides, silicides, etc.) and improving at the same time their resistance at high temperature and their wear resistance compared to the first developed cermets.

In the case of steel materials, in particular, PM leads obtaining exclusive or improved properties which cannot be realized by traditional manufacturing procedures. In particular, in a conventionally produced tool steels, the liquid metal is poured into the mold, the ingot is then forged and rolled, followed by the annealing step. Due to the conditions during the solidification stage, in conventional manufacturing methods, the ingot is affected by macrosegregation phenomena, especially as carbides. On the contrary, during the PM process, the liquid metal is transported through a small nozzle and thanks to the presence of high pressure, the liquid flow has been transformed into a spherical droplet with uniform composition; they can be collected after their fast solidification without any possibility of segregation. Rapid cooling determines the precipitation of fine carbides that maintain their feature during HIP and milling. PM technology produces an isotropic material with uniform microstructure, where the really fine distribution of the carbides contributes to amplify their wear resistance and their ductility. In the conventionally manufactured HSS,

http://dx.doi.org/10.5772/66872

high ductility can be obtained by loss of the wear resistance. Additionally, PM HSS has the tendency to quickly respond to heat treatment with superior predictability than the conventionally produced HSS.

Generally, the difference between traditionally obtained materials and those produced through PM is related not only to the production route, but shows different advantages, especially in the case of complex shape components and with high need of accuracy.

Besides the advantages, there are also some drawbacks as PM route concerns, mainly related to the relatively high costs of the metal powders and of the tools and materials used for the compaction of the powders, press capacity, etc. However, many of these difficulties can be reduced during the evolution with a correct production plan at the initial stage follow-up by a well-established and important mass production.

Generally, PM includes different technologies for manufacturing the final components, as follows:

1. Conventional PM process, with different steps, consists of mixing the elemental/alloy powders, compacting the mixture in a mold and then sintering occurs in a controlled environment in order to metallurgically bond the particles.

2. Metal injection molding (MIM) deals producing complex shapes in great quantities, using fine metal powders (typically < 20 μm) that are custom formulated with a binder (various thermoplastics, waxes, and other materials) into a feedstock, which is fed into a cavity of a traditional injection-molding device. The binder is extracted by thermal or solvent processing and the green is sintered. MIM process is very similar to high-pressure die casting but it is limited to relatively small and highly complex parts. The most important feature of this procedure is related to its ability to produce components with mechanical properties comparable to the wrought materials.

3. Isostatic pressing is a PM forming process, which applies on a powder to compact the same pressure in all directions producing a homogeneous microstructure and compared to the uniaxial pressing there are no geometrical limitations. Isostatic pressing can be realized: (i) cold when it is used to compact green at room temperatures and (ii) hot (HIP) when is used to totally combine parts at high temperatures by solid-state diffusion. HIP can also be used to eliminate residual porosity from a sintered PM part. HIP is an expensive method and actually the preference goes to alternative lower cost procedure without the use of pressure at high temperature, with positive outcome toward the environment as well.

Hot pressing combines the compacting and firing steps to obtain moderately simple symmetrical figures, which is created starting from the raw materials introduced in a high temperature mold while it is still maintained under load. As regards, hot isostatic pressing (HIP) is a constant pressure-assisted process of sintering of powders into simple or more complex forms. The difference between HIP and isostatic pressing is related to the way the pressure is applied, during sintering, being this uniform in the first case.

Actually, metal additive manufacturing (AM) has become very popular. However, it is employed for the production of some niche pieces, because of the need of more knowledge before growing to be an accurate technology for a mass-production.

Cemented carbides are, generally, sintered by liquid-phase sintering procedure in a temperature range of 1350–1650°C, obtaining more or less pore-free material. During sintering, Co becomes liquid and easily dissolves W and C coming from WC and at the same time lowering the melting temperature. Additionally, C level is of primary importance because it leads to obtain unwanted compound [42] in the sintered material.

The influence of the liquid phase on the sintering is important since it affects the sintering time: the full densification of the final product is feasible within 1 h. The ideal level of liquid combined with the high solubility of the solid in the liquid phase, as well as the complete wetting among the solid and liquid particles are the most important parameters affecting the sintering process. The main phases involved in the sintering, graphically illustrated in **Figure 2**, are:

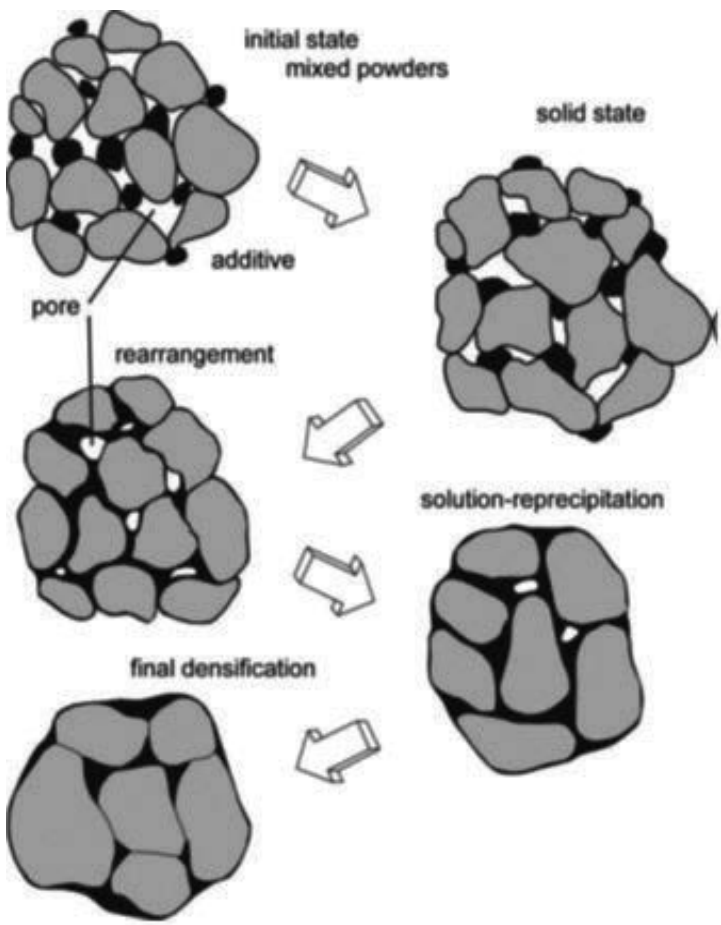

Figure 2. Layout of the most important stages in liquid-phase sintering [42].

http://dx.doi.org/10.5772/66872

- Rearrangement: development of the liquid and wetting the solid elements involved in the process with a consequent redisposition into a more compact shape;
- Solution reprecipitation: slowly the reorganization of the structure follows and coarsening of the particles take place;
- Solid-state sintering: the "compacted assembly" is "fired" into a final product [42].

Reactive sintering, as one of the innovative sintering procedures, is a sign of a continuous improvement within the different manufacturing routes aiming to obtain enhanced properties by an economically convenient route. Anyway, due to some problems concerning the control of the procedure, a widespread industrial use of such methods is still limited. The heat that is necessary for the sintering is provided by an exothermic reaction among the principal powders, and it results sufficient to transform the compacted powders into a solid material [42].

2. Experimental study results

2.1. Outline of the study

In the following, some previously obtained [85–89] experimental results on the possibility of producing Co-free metal matrixes for diamond tools and cemented carbides are illustrated. In addition to the environmental issue concerning the elimination of the toxic element (Co) from the cutting tool composition, the choice of most capable metal matrix structure to be used for hosting WC and/or diamond particles from the proposed candidates is illustrated. For the experiments, elemental powders have been used and then sintered by pressureless reactive sintering route. The use of a carbide as a metallic binder was adopted. A toxic Ti (<40 μm) powders were employed for the research as a base element, while Cu (<2.4 μm), Ni (2.2–3 μm), and Al (2.2–3 μm) powders were used to reduce the sintering temperature and at the same time to reach good mechanical properties. The composite cutting material has been prepared by addition to the metallic powders of WC powder (4 μm) or synthetic diamond grains (0.7–0.8 mm). The low elastic modulus of Ti is very important: plastic deformation and diamond pop-out can be inhibited by absorption of the energy as elastic deformation. Additionally, the low thermal expansion coefficient of Ti can be considered as benefit for pressureless sintering procedure. Furthermore, Ti does not catalyze graphitization, important feature for the sintering temperature and due to its good reactivity for diamond, chemical bonding is facilitated with the development of TiC on diamond particles and mixed TiC and WC in cemented carbides.

2.2. Alternative bonding metal matrix: preparation and characterization

For all the composite compositions, the accurately mixed powders have been uniaxially compacted at room temperature and then sintering has been achieved under high vacuum in an adequate temperature range and an isothermal step, followed by structural, microstructural, and mechanical characterization. In all cases, the sintered samples have a relative density higher than 95%. The investigated Ti-Cu and Ti-Ni-Al alloys (light grey areas on the micrographs) reveal a similar microstructural behavior with the presence of the equiaxic and lamellar intermetallic particles as shown in **Figure 3**. Development of the equilibrium alloy has been reached with

Ti-rich solid solution and the presence of the intermetallic, Ti_2Cu and Ti_2Ni, particles (**Figure 4**). **Figure 5** shows more in detail the microstructure of the Ti-Cu metal matrix with the presence of some small pores which are limited to small areas (as black points on the micrograph of **Figure 5**) and the intermetallic particles reveal two different morphologies: in some cases they are present as a larger and more irregular nature, while in other cases they are finer with a lamellar structure.

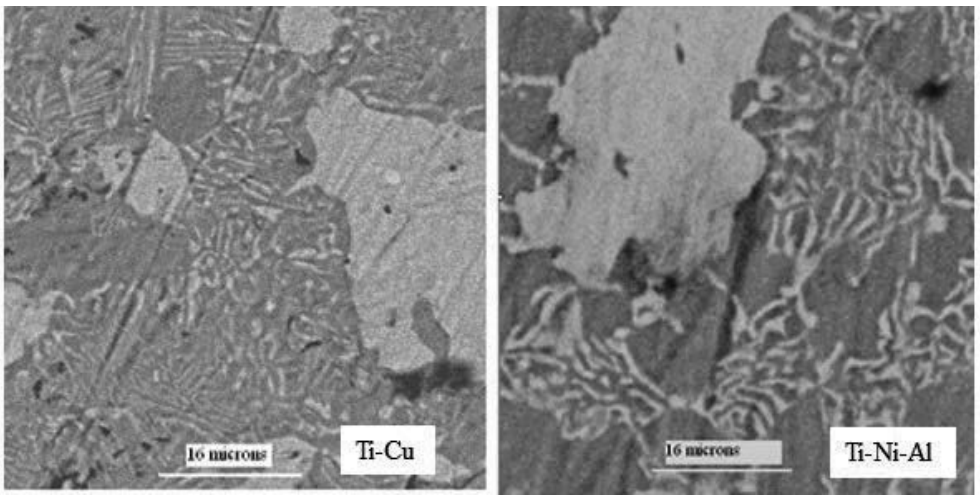

Figure 3. Optical microstructures of the investigated metallic matrices.

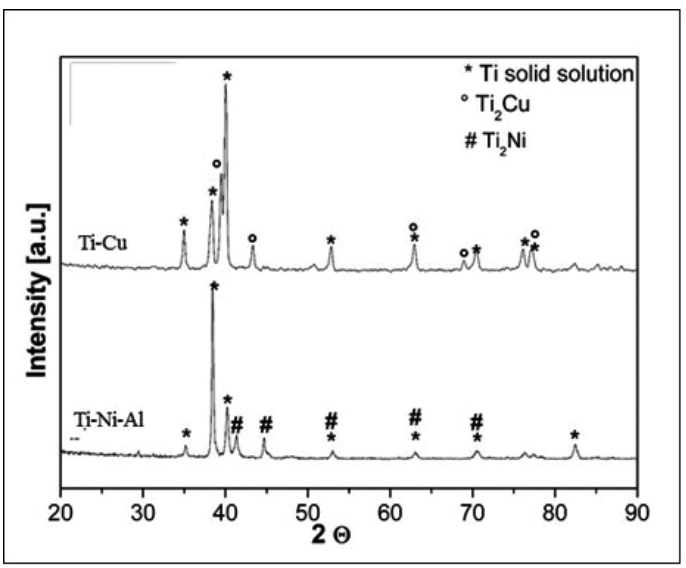

Figure 4. XRD diffraction patterns of the metallic alloys after reactive sintering.

http://dx.doi.org/10.5772/66872

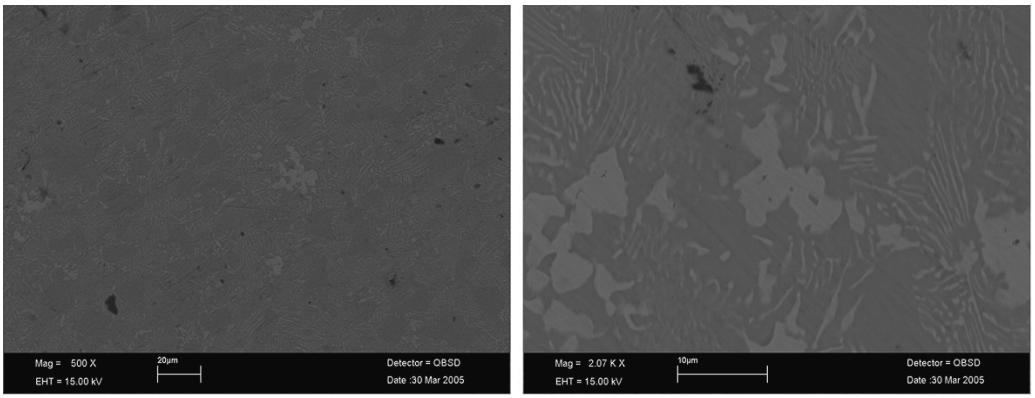

Figure 5. SEM micrographs of the Ti-Cu metal matrix showing their characteristic features in detail.

Table 1 reports the most important results obtained during mechanical characterization, where hot pressed Co was used as reference material [90]. Within the two experimentally metal matrices, Ti-Cu alloy shows a higher flexural strength and resilience compared to the Ti-Ni-Al alloy. Compared to the commercially employed hot pressed Co, Ti-Cu alloy shows a considerably lower young modulus which can be considered as a helpful element for reducing the plastic deformation at the metal matrix-diamond interface with a consequent diamond pull-out. According to Konstanty [90], the hardness of the Ti-Cu metal matrix is similar to that of the commercially employed hot pressed Co and the bending strength fulfills the condition required for the actually used Co matrixes.

	Ti-Cu	**Ti-Ni-Al**	**Reference (Co[1])**
Young modulus (GPa)	107–116	99	209
Flexural strength (MPa)	888	617	700–1100
HV40	240–315	410	318
Resilience (J/cm^2)	4	2	17

[1]Reference material [90].

Table 1. Mechanical properties of the considered metal matrices.

The resistance to the impact for both alloys is lower than that obtained in the case of Co matrices. Analyzing the fracture surface, a mixed fracture with the presence of dimples are detected on some areas of the fracture surface of the Ti-Cu alloy (**Figure 6**) evidencing the presence of shear lips, while the Ti-Ni-Al metal matrix shows a pure cleavage mechanism.

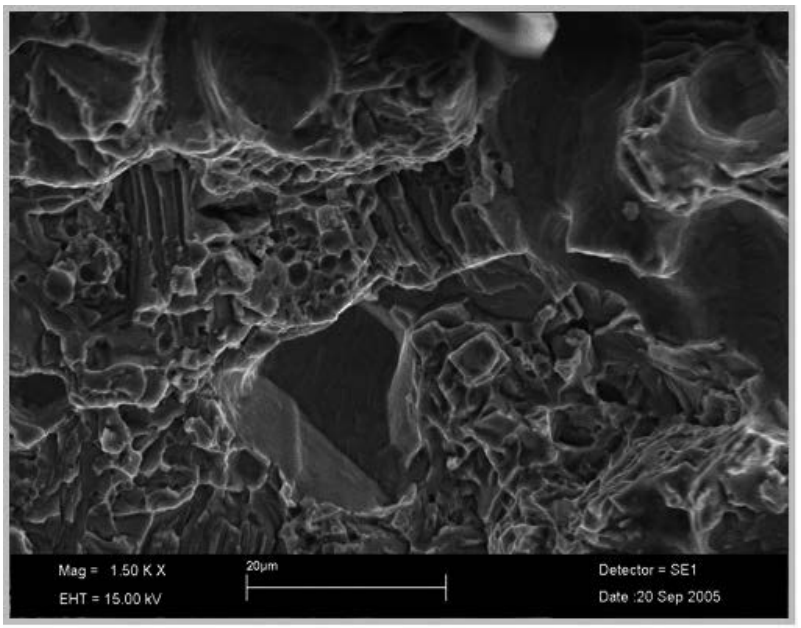

Figure 6. SEM micrograph showing the fractured surface of Ti-Cu metal matrix.

2.2.1. Measurement of the abrasivity

The abrasivity of any materials can be considered as an important element with significant impact on the wear of tool materials. There are different methods for determining these properties. One of the most employed methods is the Cerchar Abrasivity Test, which was introduced in the 1970s by the Centre d'Etudes et Recherches des Charbonages (CERCHAR) de France for abrasitiy testing in coal bearing rocks [91, 92]. The test outline is described in Cerchar [92] and in the French standard NF P94-430-1. The principle of the method is based on a steel pin with well-defined geometry and hardness scratching the surface of an irregular rock sample above a distance of 10 mm under a static load of 70 N by moving the level at a velocity of 10 mm/s. After the test, the Cerchar abrasivity index (CAI) is calculated using Eq. (1) and considering the measured diameter of the resulting wear flat on the pin, as shown in **Figure 7**. The abrasiveness of the involved material is obtained by measuring the resultant wear of the steel pin.

$$\mathrm{CAI} = 10\frac{d}{c} \tag{1}$$

where CAI = Cerchar abrasivity index; d = diameter of wear flat (mm); c = unit correction factor (c = 1 mm).

Two types of Cerchar testing tools are in use nowadays:

1. the original "Cerchar tool," in line with Cerchar [92];
2. the "West tool," according to West [93].

http://dx.doi.org/10.5772/66872

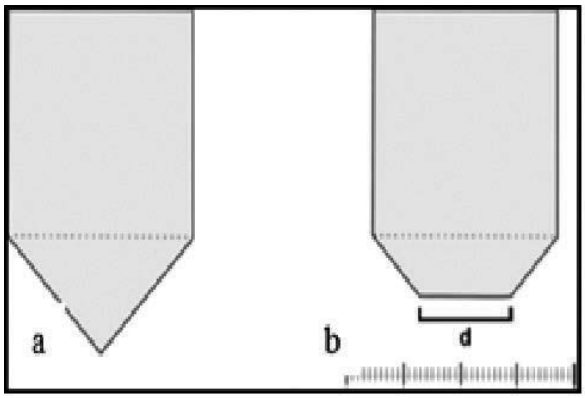

Figure 7. Outline of the pin used for the measurement before (a) and after the test (b) with the wear flat d.

In the first one (**Figure 8a**), the testing lever is directly connected to the steel pin, while in the second one (**Figure 8b**), the testing velocity is slower due to the different moving control realized by the hand crank, which moves the sample below the pin. The CAI values measured in both cases are similar.

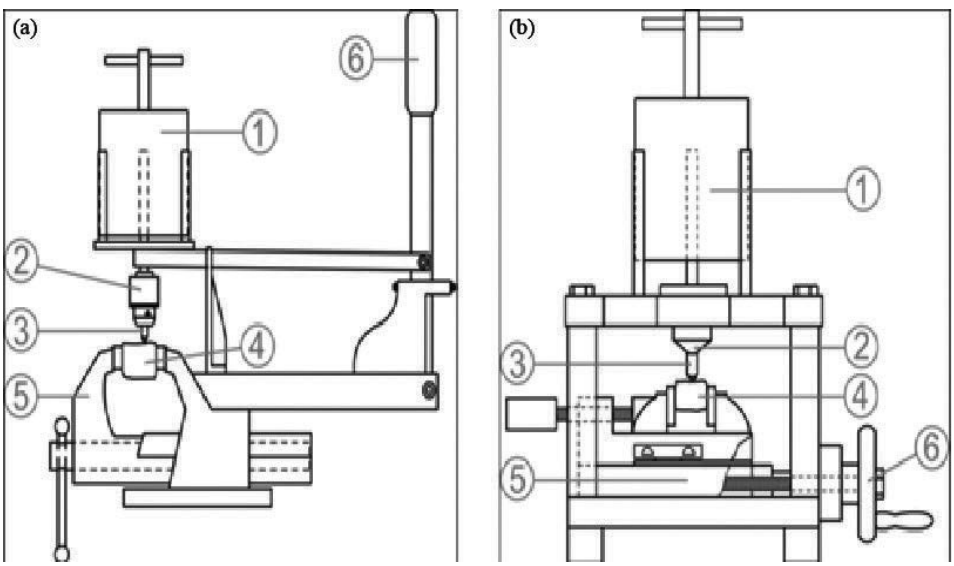

Figure 8. Setup of a modified Cerchar testing device according to Cerchar [92]. 1, weight; 2, pin chuck; 3, steel pin; 4, sample; 5, vice; 6, hand lever (a) and setup of a testing device according to West [93]. 1, weight; 2, pin guide; 3, steel pin; 4, sample; 5, vice sled; 6, hand crank (b) [92, 94].

Over the years, some modifications have been realized on these tools, considering different requirements for testing different materials and some modified versions have been developed. One important abrasivity testing device [93] (**Figure 9**), which is described in details

in the French standard P18-579, has been developed by the Laboratoire Central des Ponts et Chausées (LCPC) in France for testing rock and aggregates. This tool is built of a 750 W robust motor holding a metal impeller rotating in a cylindrical container enclosing the granular sample. The rectangular impeller is made of standardized steel with a Rockwell hardness of 60–75. The grain size of the sample has to be in a range between 4 and 6.3 mm. The LCPC abrasivity coefficient (LAC) is calculated as the mass loss of the impeller divided by the sample mass, using Eq. (2):

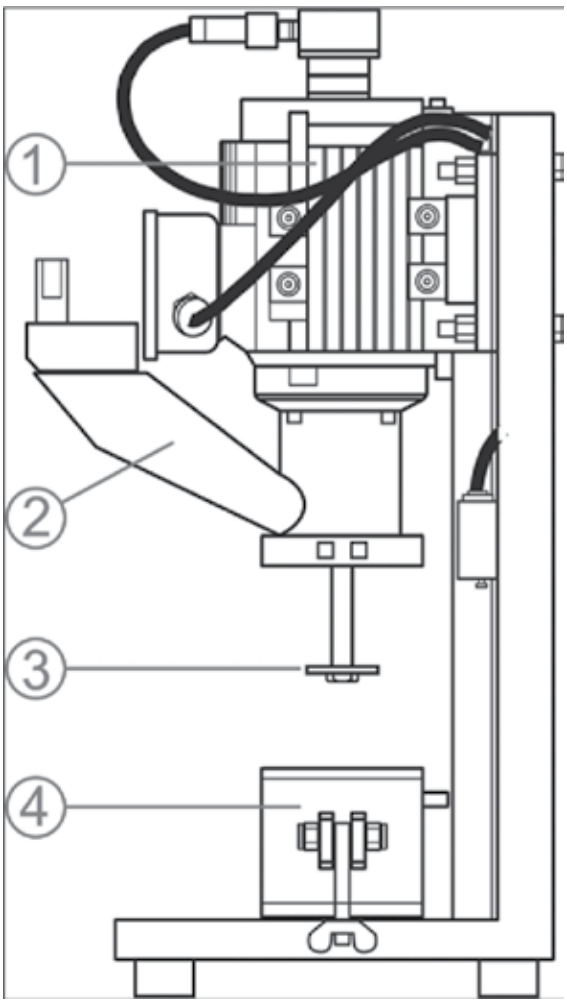

Figure 9. LCPC abrasivity testing device according the French standard P18-579 (1990). 1, motor; 2, funnel tube, 3, steel impeller; 4, sample container [94].

$$\mathrm{LAC} = \frac{m_0 - m}{M} \tag{2}$$

where LAC = LCPC (g/t); m_0 = mass of impeller before test (g); m = mass of the impeller after test (g); M = mass of the sample material (= 0.0005 t).

http://dx.doi.org/10.5772/66872

Using the proposed approach, the brittleness of the material can be calculated. The LCPC breakability coefficient (LBC) is defined as the fraction below 1.6 mm of the sample material after the test, according to Eq. (3):

$$\text{LBC} = \frac{M_{1.6} * 100}{M} \tag{3}$$

where LBC = LCPC breakability coefficient (%); $M_{1.6}$ = mass fraction < 1.6 mm after LCPC test (g); M = mass of the sample material (= 0.0005 t).

Based on the percentage of the LBC, the materials tested can be classified in four classes: low, medium, high, and very high breakability.

In this research a nonstandardized abrasion test has been performed, using a modified version of the Cerchar type tool, in line with its theory and functionality. In this case, the abrasive material is mixed with water and in particular a quartzite slurry with a grain size > 50 μm (referring on the about 58% of the total mass) has been used. Additionally, the size of the tested sample was different and in particular a rectangular profile has been used, the abrasive container has a different shape and the abrasion takes place for 10 min. At the end of the abrasion test, the volume loss has been evaluated considering the mass loss of the sample tested. The abrasion tests performed on the samples showed a linear dependence between the abraded volume of the samples and the time of the abrasion of the samples, as shown in **Figure 10**. The abrasion resistance of both experimental metal matrices is higher than that obtained for the hot pressed Co. Even if, in relation to its highest hardness, Ti-Ni-Al alloy shows the lowest abrasion rate, the microstructural investigation, as shown in **Figure 11**, reveals that the abraded sides shown a more brittle behavior compared to the Ti-Cu metal matrix. The removal of the intermetallic particles during the abrasion is more accentuated and the voids generated are more pronounced and have a bigger size in the case of Ti-Ni-Al metal matrix.

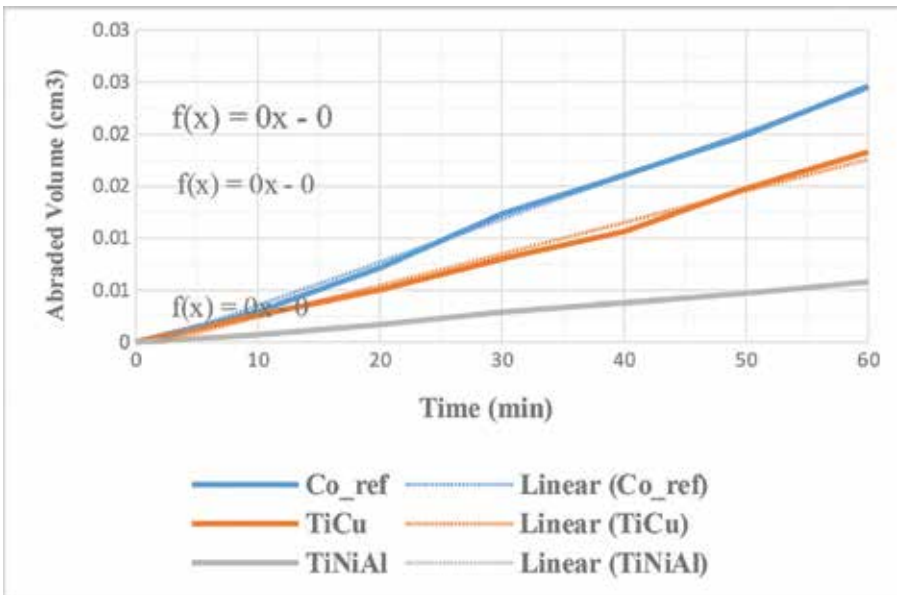

Figure 10. Abraded volume vs. time for the tested metallic matrices during abrasion test.

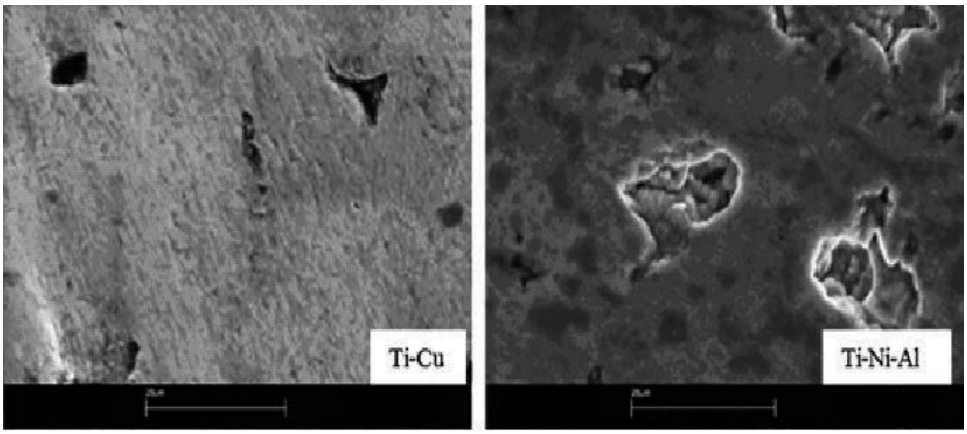

Figure 11. SEM micrographs of the metal matrices after abrasion test.

2.3. Alternative tool materials: preparation and characterization

Taking into account the results obtained in the case of the two bonding metal matrices and the more promising performance of the Ti-Cu matrix, in the present work it has been decided to include only the latter for the cemented carbide and diamond tool production. The ratio of Ti/Cu was chosen in line with some earlier research [85, 87, 94].

The investigations performed on the preparation of cemented carbides using WC particles have pointed out that the Ti matrix is relatively reactive toward the WC and the development of (W,Ti) solid solution and (W,Ti)C mixed carbides has been observed. The WC particles are well inserted into the metal matrix (**Figure 12**) and a reaction layer made of mixed carbides (WC-W_2C-(Ti+W)C) has been developed at the interface with the diffusion of the metal onto the WC (**Figure 13**). Sintering arises only in the liquid state. Different conditions have been experimentally investigated, modifying the sintering temperatures and time, the ratio of the metal matrix and WC particles, use of additives to achieve a denser sample. Density is probably the most significant parameter involved during sintering and determines the final behavior of the obtained sintered material. Higher the density, higher is the probability to obtain product with more competitive performance. Under the actual conditions, in all cases, a complete dispersion of the metal matrix, as well as an optimal infiltration of the hard particles has not been obtained, leading to a lower final density compared to the theoretical one. This aspect can compromise the mechanical properties of the material that gives rise to its lower cutting performance. The actual idea is to use some elements which can adequate the reaction between the metal matrix and the WC particles, improving the density and the overall characteristics of the sintered cemented carbide.

The following step concerning this research is dedicated to the preparation and characterization of diamond tools, starting from the Ti-Cu metal matrix and using synthetic diamond particles. The fraction of Ti/Cu was maintained in the same range that has been used for the cemented carbide preparation. High final relative density (approximately 98% of the theoretical density) has been obtained using a sintering temperature slightly higher than 900°C. The sintering temperature

http://dx.doi.org/10.5772/66872

constitutes a critical parameter because of the possible graphitization of the diamond particles. Some higher sintering temperatures have been experimentally explored, but the development of some surface porosity has been observed because of the evaporation of the metal. Additionally, from technological and environmental point of views, the use of high production temperatures is inconvenient. The sintering route is a reactive one, with the formation of an alloy close to the equilibrium, and prealloyed powders are not strictly necessary, with a relevant cost saving.

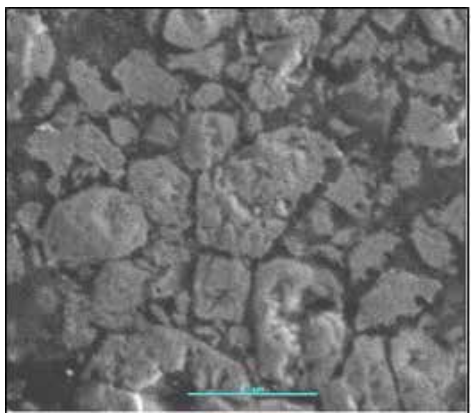

Figure 12. Optical microstructure of the sintered cemented carbide showing the presence of metal matrix (dark areas) and WC particles (lighter areas).

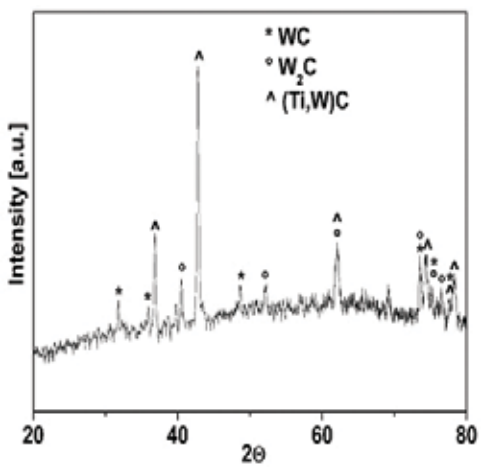

Figure 13. X-ray diffraction pattern of the interface between the metal matrix and WC particles after sintering.

Reactive sintering continues to be an encouraging mechanism, even if it is not fully employed industrially, because it produces higher densities with no use of additional hot-isostatic pressure. As an inconvenient, lower fraction of hardening particles can be arise. A detailed knowledge of the mechanisms of such reactive sintering, including how these particles influence the density and their transformation, is not yet fully understood even if in the literature it

constitutes a significant research topic [42]. As shown in **Figure 14a**, the diamond stones are well inserted in the metal matrix and no sign of any fracture at the diamond-metal matrix interface can be observed. A good diamond retention ability of the metal matrix has been evidenced with a highly protruding diamond grit and the evidence of a high adhesion force at the interface (**Figure 14b**). The chemical reaction on the diamond surfaces produces a resistant interface and in some cases, the presence of metal matrix fragments (Ti and Cu) has been identified on them as an indication of a robust and strengthened structure. The diamond grits appear with a sharp corners and tips, and no indication of any graphitization on the diamond grits was observed. This configuration guarantees avoiding the diamond pull-out during fracture.

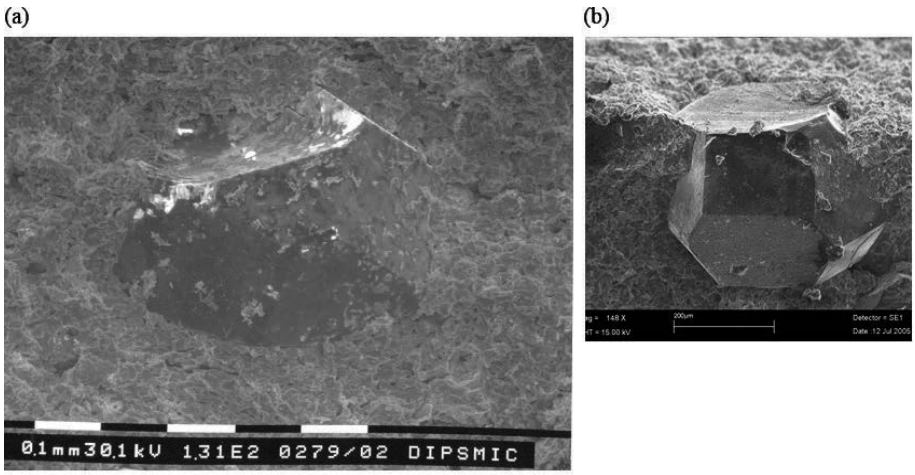

Figure 14. SEM micrograph of the fracture surface of the sintered Ti-Cu-diamond composites.

Figure 15 shows the fracture surfaces of the same sample showing its two complementary sides and evidencing the real presence of the diamond grits on the opposite face, after fracture.

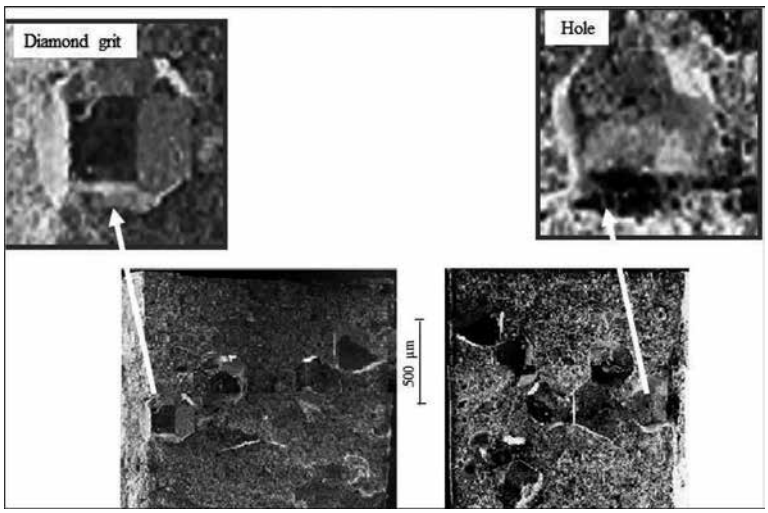

Figure 15. Two antagonistic metal-matrix-diamond fracture surfaces.

http://dx.doi.org/10.5772/66872

3. Conclusions

In this chapter, a general overview related to different tool materials has been presented, including a short history and the description concerning their composition, the most important manufacturing methods and an indication of their significant properties. Some experimentally obtained results in this field, carried out during the years, have been further added aiming to underline specific aspects of the presented analysis.

Generally, cutting has to be realized using a harder material than the material which has to be cut, the cutting edge has to correctly interact with the piece to be cut and the hardness results to be important in the case of machining in particular extreme conditions, such as high temperatures. It was pointed out that there are important differences between the various available cutting tools and only a good familiarity concerning their properties leads obtaining selection of the right one for a particular application.

One of the reasons that Co has to be substituted is related to the fact that Co is classified as a toxic material while the WC-Co mixture, according to the International Agency for Research on Cancer, is evaluated as a possibly carcinogenic material. During the experimental research, new compositions for metal matrices, for diamond tools and cemented carbides, without Co have been prepared by a low-cost sintering process at moderate temperature and without any pressure applied. Several properties of the new materials are comparable with the values requested for the currently used Co matrices.

Author details

Ildiko Peter* and Mario Rosso

*Address all correspondence to: ildiko.peter@polito.it

Department of Applied Science and Technology, Politecnico di Torino, Torino, Italy

References

[1] Shaw M.C. (2005) Metal cutting principles. 2nd edition. New York: Oxford University Press.

[2] ASM Handbook (1998) Powder metal technologies and application. ASM International Vol.7.

[3] Metal Powder Report 2016. (2016) Liz Nickels leafs through past issues of Metal Powder Report to find out what was happening in the PM industry of the past 71(1).

[4] Stoughton B. (1908) The metallurgy of iron and steel. New York: McGraw-Hill.

[5] Karbacher R.J., Merchant M.E. (1951) Basic factors in hot-machining of metals, Transactions ASME 73, 761–776.

[6] Gille G., Bredthauer J., Gries B.M.B., Heinrich W. (2000) Advanced and New Grades of WC and Binder Powder–Their Properties and Application. International Journal of Refractory Metals and Hard Materials 18, 87–102.

[7] Oberg E., Jones F.D. (1918) Iron and steel: a treatise on the smelting, refining and mechanical processes of the iron and steel industry, including the chemical and physical characteristics of wrought iron, carbon, high speed and alloy steels, cast iron, and steel casting, and the application of these materials in the machine and tool construction. New York: The Industrial Press.

[8] Machinist (2014) http://americanmachinist.com/cutting-tools/chapter-1-cutting-tool-materials.

[9] Bayer A. M., Becherer B.S., Vasco T. (1989) High speed tool steels, ASM Handbook, Volume 16: Machining, pp.51–59.

[10] Zhang S., Zhao D. (2016) Aerospace Materials Handbook. Aerospace Materials Handbook, Sam Zhang and Dongliang Zhao, CRC Press 2012 Print ISBN: 978-1-4398-7329-8, eBook ISBN: 978-1-4398-7330-4.

[11] Davim J.P. (2008) Machining: fundamentals and recent advances. London: Springer.

[12] Upadhaya G.S. (1998) Cemented tungsten carbides: production, properties and testing. USA: Noyes Publication.

[13] (2009) Springer Handbook of Mechanical Engineering, Volume 10, Grote K.H., Antonsson E.K. (Eds.).

[14] Kubaschewski O., Alcock C.B. (1979) Metallurgical thermochemistry, New York: Pergamon Press.

[15] Barin I., Knacke O (1973) Thermochemical properties of inorganic substances, Berlin, New York: Springer Verlag.

[16] Tdnshoff H.-K. et al., (1997) AIN Coatings in Dry Drilling. Wear mechanisms of Ti, .x, AIJN Coatings in Dry Drilling, Surface and Coatings Technology. 94–95, 603–609.

[17] Lugscheider E. Geiler H.D., Lake M., Zimmermann H. (1996) Investigation of thermo-physical properties of AIP coated cutting tools for dry machining, Surface and Coatings Technology. 86–87, 803–808.

[18] Koepfer C. (2006) Tooling up for hard turning. Production Machining, 10, 26.

[19] De Vries R.C. (1972) Cubic boron nitride: handbook of properties. General Electric Technical Report. 6.

[20] Heath P.J. (1986) Properties and uses of Amborite. Industrial Diamond Review. 46, 120–127.

[21] Wentorf R.H., DeVries R.C., Bundy F.P. (1980) Sintered superhard materials. Science. 208, 873–880.

[22] Tomlinson P.N., Wedlake R.J. (1983) The current status of diamond and cubic boron nitride composites. Proceedings of the International Conference on Recent Developments in Specialty Steels and Hard Materials. Oxford: Pergamon, pp. 173–184.

[23] Rong X.Z., Yano T. (2004) TEM investigation of high-pressure reaction-sintered cBN–Al composites. Journal of Material Science. 39, 4705–4710.

[24] Grzesik W. (2009) Wear development on wiper Al_2O_3-TiC mixed ceramic tools in hard machining of high strength steel. Wear 266, 1021–1028.

[25] Chu C. Y., Singh J.P., Routbort J.L. (1993) High-temperature failure mechanisms of hotpressed Si3N4 and Si3N4/Si3N 4-whisker- reinforced composites. Journal of the American Ceramic Society. 76, 1349–1353.

[26] Hu P., Wang Z. (2010) Flexural strength and fracture behavior of ZrB2–SiC ultra-high temperature ceramic composites at 1800°C. Journal of the European Ceramic Society. 30, 1021–1026.

[27] Zou B., Jin W.B., Huang C.Z., Wang J., Li S.S., Xu K.T. (2014) Effects of superfine refractory carbide additives on microstructure and mechanical properties of TiB2–TiC+Al_2O_3 composite ceramic cutting tool materials. Journal of Alloys Compound. 585, 192–202.

[28] Zou B., Huang C.Z., Jin W.B., Li S.S. (2014) Effects of Al_2O_3 and NbC additives on the microstructure and mechanical properties ofTiB2–TiC composite ceramic cutting tool materials. Ceramic International. 40, 3667–3677.

[29] German R.M. (1985) Liquid phase sintering. New York: Plenum Press.

[30] Wang Y., Heusch M., Lay S., Allibert C.H. (2002) Microstructure evolution in the cemented carbides WC-Co—I. Effect of the C/W ratio on the morphology and defects if the WC grains. Physica Status Solidi.193, 271–283.

[31] Allibert C.H. (2001) Sintering features of cemented carbides WC-Co processed from fine powders. International Journal of Refractory Metals and Hard Materials. 19, 53–61.

[32] Liu C.H., Aihua D.J., Yangyang C., Jun Z. (2012) Friction and wear properties of TiN, TiAlN, AlTiN and CrAlN PVD nitride coatings. International Journal of Refractory Metals and Hard Materials. 31, 82–88.

[33] Bemporad E., Peechio C., De Rossi S., Carassiti E. (2001) Characterization and hardness modelling of alternate TIN/TICN multilayer cathodic arc PVD coating on tool steel. Surface and Coatings Technology. 146, 363–370.

[34] Al-Bukhaiti M. A., Al-hatab K.A., Tillmann W., Hoffmann F., Sprute T. (2014) Tribological and mechanical properties of Ti/TiAlN/TiAlCN nanoscale multilayer PVD coatings deposited on AISI H11 hot work tool steel. Applied Surface Science. 318, 180–190.

[35] Lim C.Y.H., Lim S.C., Lee K.S. (1999) The performance of TiN-coated high speed steel tool inserts in turning. Tribology International. 32, 393–398.

[36] Vera M.V.E.E., Lewis R., Gallardo E.A., Laguna-Camacho J.R. (2011) A study of the wear performance of TiN, CrN and WC/C coatings on different steel substrate. Wear. 271, 2116–2124.

[37] Schneider J.M., Voevodin A., Rebholz C., Matthews A., Hogg J.H.C., Lewis D.B., Ives M. (1995) X-ray-diffraction investigations of magnetron-sputtered TiCN coatings. Surface and Coatings Technology. 74–5, 312–319.

[38] Karlsson L., Hultman L., Sundgren J.E. (2000) Influence of residual stresses on the mechanical properties of TiC_xN_{1-x} (x = 0, 0.15, 0.45) thin films deposited by arc evaporation. Thin Solid Films. 371, 167–177.

[39] Marin E., Guzman L., Lanzutti A., Fedrizzi L., Saikkonen M. (2009) Chemical and electrochemical characterization of hybrid PVD plus ALD hard coatings on tool steel. Electrochemistry Communications. 11, 2060–2063.

[40] Hosepian P.E., Reinhard C., Ehiasarian A.P. (2006) CrAlYN/CrN superlattice coatings deposited by the combined high power impulse magnetron sputtering/unbalanced magnetron sputtering technique. Surface and Coatings Technology. 201, 4105–4110.

[41] International Standard ISO 513 (2012) Classification and application of hard cutting materials for metal removal with defined cutting edges—designation of the main groups and groups of application. 4th edition. 2012-11-01.

[42] Randall M.G. (1996) Sintering theory and practice. John Wiley & Sons., Hoboken, NJ Inc. Wiley Interscience Publication.

[43] Sarin V., Johannesson T. (1975) On the Deformation of WC-Co Cemented Carbides. Metal Science. 9, 472–476.

[44] Gurland J., Bardzil P. (1955) Relation of strength, composition, and grain size of sintered WC-Co alloys. Journal of Metal. 7, 311–315.

[45] Gee M., Mingard K., Roebuck B., Nunn J., Jones H. (2011) Examination of fracture and deformation mechanisms in WC/Co hard metals. In EuroPM2011 Conference on Hard Materials, Barcelona.

[46] Bin Z., Chuanzhen H., Minga C., Meilin G., Hanlian L. (2007) High-temperature oxidation behavior and mechanism of Si_3N_4/Si_3N_4w/TiN nanocomposites ceramic cutting tool materials. Materials Science and Engineering A. 459, 86–93.

[47] Ricoult M.B., Guerin V., Huntz A.M. (2002) High-temperature oxidation behavior of high-purity α-, β-, and mixed silicon nitride ceramics. Journal of American Ceramic Society. 85 (2), 385–392.

[48] Deng J.X., Cao T.K. Liu L.L. (2005) Microstructure and evolution of (TiB2+Al2O3)/NiAl composites. Journal of the European Ceramic Society. 25, 1073.

[49] Mazerollers L., Feldhoff A., Trichet M.F., Ricoult M.B. (2005) Journal of the European Ceramic Society. 25, 1743.

[50] Beaume F.D., Cutard T., Frety N., Levaillant C. (2002) Oxidation of a Silicon Nitride-Titanium Nitride Composite: Microstructural Investigations and Phenomenological Modeling. Journal of American Ceramic Society. 85, 1860.

[51] Munoz F., Pascual L., Duran A., Rocherulle J., Marchand R. (2006) Oxidation behaviour of Li–Na–Pb–P–O–N oxynitride phosphate glasses. Journal of the European Ceramic Society. 26, 1455.

[52] Mandel K., Radajewski M., Krüger L. (2014) Strain-rate dependence of the compressive strength of WC–Co hard metals. Materials Science & Engineering A. 612, 115–122.

[53] Doi H., Fujiwara Y., Miyake K. (1969) Impact Fatigue Behavior of WC-Co Cemented Carbide. Transactions of the Metallurgical Society of AIME. 245, 1457–1470.

[54] Lee H.C., Gurland J. (1978) Hardness and deformation of cemented tungsten carbide. Materials Science & Engineering. 33, 125–133.

[55] Exner H.E. (1979) Physical and chemical nature of cemented carbides. International Metals Reviews. 4, 149–173.

[56] Ettmayer P. (1989) Hardmetals and Cermets. Annual Review of Materials Science. 19, 145–164.

[57] Exner H.E., Gurland J. (1970) A Review of Parameters Influencing some mechanical properties of Tungsten Carbide-cobalt Alloys. Powder Metallurgy. 13, 13–31.

[58] Lankford J. (1981) Mechanisms Responsible for Strain-Rate-Dependent Compressive Strength in Ceramic Materials. Journal of American Ceramic Society. 64, C-33–C-34.

[59] Evans A. (1974) Slow crack growth in brittle materials under dynamic loading conditions. International Journal of Fracture. 10, 251–259.

[60] Lankford J. (1996) High strain rate compression and plastic flow of ceramics. Journal of Materials Science Letters. 15, 745–750.

[61] Boudet J., Ciliberto S., Steinberg V. (1996) Dynamics of crack propagation in brittle materials. Journal of Physics. II6, 1493–1516.

[62] Kipp M., Grady D., Chen E. (1980) Strain-rate dependent fracture initiation. International Journal of Fracture.16, 471–478.

[63] Grady D. (1982) Local inertia effect in dynamic fragmentation. Journal of Applied Physics. 53, 322–325.

[64] Meyers M. (1994) Dynamic behavior of materials. New York: John Wiley & Sons, Inc.

[65] Zhou H.J., Huang C.Z., Zou B., Liu H.L., Zhu H.T., Yao P., et al. (2014) Effect of ball-milling time on the microstructure and mechanical properties of submicron Ti(C, N)-based cermets. Key Engineering Materials. 589–590, 584–589.

[66] Zhou H., Huang C., Zou B., Liu H., Zhu H., Yao P., Wang J. (2014) Effects of sintering processes on the mechanical properties and microstructure of Ti(C,N)-based cermet

cutting tool materials. International Journal of Refractory Metals and Hard Materials. 47, 71–79.

[67] Liu N., Xu Y.D., Li Z.H., Chen M.H., Li G.H., Zhang L.D. (2003) Ceramics International. 29, 919–925.

[68] Zhou S.Q., Zhao W., Xiong W.H., Zhou Y.N. (2008) Acta Metallurgica Sinica (English Letters). 21, 211–219.

[69] Dong G.B., Xiong J., Chen J.Z., Guo Z.X., Wan W.C., Yi C.H. (2012) Effect of WC on the microstructure and mechanical properties of nano Ti(C, N)-based cermets. International Journal of Refractory Metals and Hard Materials. 35, 159–162.

[70] Park S., Kang S. (2005) Toughened ultra-fine (Ti, W)(C, N)–Ni cermets. Scripta Materialia. 52, 129–133

[71] Park D-S., Park C., Lee Y-D. (2000) Oxidation of Ti(C, N)-based ceramics exposed at 1373 K in air. Journal of American Ceramic Society. 83, 672–674.

[72] Zou B., Zhou H., Xu K., Huang C., Wanga J., Li S. (2014) Study of a hot-pressed sintering preparation of Ti(C7N3)-based composite cermets materials and their performance as cutting tools. Journal of Alloys and Compounds. 611, 363–371.

[73] Kupczyk M.J. (2015) Cutting edges with high hardness made of nanocrystalline cemented carbides. International Journal of Refractory Metals and Hard Materials. 49, 249–255.

[74] Sidorenko D., Mishnaevsky L., Levashov E., Loginov P., Petrzhik M. (2015) Carbon nanotube reinforced metal binder for diamond cutting tools. Materials & Design. 83, 536–544.

[75] You J., Gao Y. (2009) A study of carbon nanotubes as cutting grains for nano machining. Advanced Materials Research. 502, 76–78.

[76] Suzuki T., Mitsui T., Fujino T., Kato M., Satake Y., Saito H., Kobayashi S. (2009) Development of CNT-coated diamond grains using self-assembly techniques for improving electroplated diamond tools. Key Engineering Materials. 389–390, 72–76.

[77] Suzuki T, Kato M., Saito H., Iizuka H. (2011) Effect of carbon nanotube (CNT) size on wear properties of Cu-Based CNT composite electrodes in electrical discharge machining. Journal of Solid Mechanics and Materials Engineering. 5, 348–359.

[78] Suzuki T., Konno T. (2014) Improvement in tool life of electroplated diamond tools by Ni-based carbon nanotube composite coatings. Precision Engineering. 38(3), 659–665.

[79] Jung B., Jang K., Min B., Lee S.J., Seok J. (2009) Magnetorheological finishing process for hard materials using sintered iron-CNT compound abrasives. International Journal of Machine Tools and Manufacture. 49, 407–418.

[80] Belmonte M., Oliveira F.J., Sacramento J., Fernandes A.J.S., Silvaa R.F. (2004) Cutting forces evolution with tool wear in sintered hard metal turning with CVD diamond. Diamond and Related Materials. 13, 843–847.

[81] Collier M., Cheynet J. (2002) Impact Properties of Diamond Impregnated Cobalt Metal Matrix', EURO PM 2002, European Conference on Hard Materials & Diamond Tooling, Lausanne, Switzerland October 7-9th, 2002.

[82] Vandevelde T.C.S., Vandierendonck K., Stappen M., Mong W. Du, Perremans P. (1999) Surface and Coatings Technology. 113, 80.

[83] Chen N., Shen B., Yang G., Sun F. (2013) Tribological and cutting behavior of silicon nitride tools coated with monolayerand multilayer-microcrystalline HFCVD diamond films. Applied Surface Science. 265, 850–859.

[84] Matei A.A. et al. (2015) Corrosion resistance appraisal of TiN, TiCN and TiAlN coatings deposited by CAE-PVD method on WC–Co cutting tools exposed to artificial sea water. Applied Surface Science. 358, 572–578.

[85] Spriano S., Matekovits* I., Bianchi C.L., Faga M.G., Settineri L. (2006) Structural, morphological and mechanical analysis of innovative diamond tools European powder metallurgy. In Euro PM 2006, Vol. 3, 15–20, Ghent.

[86] Corazzari I., Fenoglio I., Matekovits* I., Spriano S., Fubini B. (2006) Mechanical properties and surface reactivity in relationship to toxicity of new Ti-Cu-Co based hard metals. Proceedings of XXII Congresso Nazionale della Società Chimica Italiana, Vol. 1, 320–321, Firenze.

[87] Spriano S., Matekovits* I., Settineri L., Actis Grande M., Rosso M. (2006) Matrici metalliche prive di cobalto per utensili da taglio diamantati ed in metallo duro Materiali sinterizzati ad alte prestazioni, Padova. 14 dicembre 2006.

[88] Spriano S., Matekovits* I., Bugliosi S. (2005) Patent no.TO2005A000692/2005, Materiali compositi a matrice metallica a base di titanio e il loro impiego per la produzione di utensili di taglio.

[89] Spriano S., Matekovits* I., Bugliosi S. (2006) Patent WO/2007/039870/2006 Composite metal matrix materials based on titanium and their use for the production of cutting tools.

[90] Konstanty J. (1999) Developing a better understanding of the bonding and wear mechanism involved in using diamond impregnated tools In Proc. And International Workshop on Diamond Tool Production, Turin, Italy, November 8–10, 1999, pp 97-106.

[91] ASTM (2010) Standard test method for laboratory determination of abrasiveness of rock using the CERCHAR method. Designation: D7625-10.

[92] Cerchar—Centre d'E' tudes et des Recherches des Charbonnages de France (1986) The Cerchar abrasivity index. Verneuil.

[93] West G. (1989) Rock abrasiveness testing for tunnelling. International Journal of Rock Mechanics and Mining Sciences. 26, 151–160.

[94] Spriano S., Chen Q., Settineri L., Bugliosi S. (2005) Low content and free cobalt matrixes for diamond tools. Wear. 259, 1190–1196.

Chapter 12

Properties and Testing of Cemented Carbides

Antonín Kříž and David Bricín

Additional information is available at the end of the chapter

http://dx.doi.org/10.5772/66871

Abstract

This chapter deals with selected properties of cemented carbides and their testing. It consists of three main sub-chapters. The first one covers the degradation processes associated with grinding of cemented carbides. Among those, the focus is on the effects of thermal loads and reactions with the environment—the atmosphere. The second main sub-chapter describes the origin of residual stresses and their impact on cemented carbide properties. Finally, the third main sub-chapter explores the corrosion of cemented carbides in various environments. The choice of these topics was inspired by the impression that many users have of cemented carbides: indestructible materials in which no degradation takes place either during the production of cutting tools or during their use. As evidenced by the authors' experience described below, which has been acquired over many years in the field, damage in cemented carbides is a very frequent occurrence. Despite that it still receives very little attention, and especially the damage in cemented carbide cutting tools tends to be ascribed to various other factors, such as the applied coatings, the cutting process conditions and the material of the workpiece.

Keywords: cemented carbide, degradation, oxidation, residual stresses, mechanical properties

1. Introduction

Cemented carbides have been in use for almost a century. Over this period, they have become a common material to make cutting tools and for all applications where high hardness is required together with a certain level of toughness. As they tend to be known under various names, their users sometimes mistake them for other materials. This proves the general lack of adequate knowledge of cemented carbides. Their evolution has accelerated in recent years, spurred by the demand for greater hardness without toughness being compromised, and by requirements for a greater ability to be formed and treated by various processes: grinding, thin film deposition, along with special routes leading to the minimization of residual stresses, for instance.

The sub-chapters following the introduction outline the mechanical properties, manufacturing routes and methods of testing the characteristics of cemented carbides which are required by industry. The behaviour of these materials during grinding is explored in the next main sub-chapter. Effects of the grinding process on near-surface properties are analysed because these are decisive in industrial applications of these materials, not only in their uncoated but also in their coated variants. Such effects include thermal degradation and surface oxidation, which impact on the condition of the cobalt binder.

The second main sub-chapter deals with residual stresses. These can be induced by grinding but also by other manufacturing operations which so far have not received adequate attention, such as tumbling and polishing. Effects of thin film deposition on residual stresses are described, as well as the impact of these stresses on the properties of the resulting physical vapor deposition coatings, namely their adhesion and cohesion. All of the above dictate the ultimate life and performance of cutting tools and the quality of machined surfaces.

The topic of the last main sub-chapter is the corrosion of cemented carbides in various alkaline and acid environments. The environments described here were chosen on the basis of real-world service conditions of cemented carbides. Many users believe that—from the chemical viewpoint—cemented carbides are indestructible. Some of the environments used for testing were intended to simulate mine waters. Others included cutting fluids in which cemented carbide cutting tools operate, often as exchangeable inserts, e.g. in circular saws for cutting wood. In these applications, cemented carbides are exposed to corrosive substances released from wood which affect the life of the cutting edge.

1.1. Historical development of cemented carbides

Cemented carbides were introduced to market in the early twentieth century. Although they still comprise two fundamental constituents, the base material and the binder, they have evolved since their early days. This evolution led to alternate bonding materials, such as nickel-based and multi-component binders. One of today's multi-component binders is the Co-Ni-Cr type. Nickel-based and multi-component binders are used in applications where cobalt binders would be inadequate, e.g. in corrosive environments, or at higher temperatures. On the other hand, nickel-based binders are gradually being abandoned even in the above applications due to the health hazards associated with nickel, which causes contact dermatitis. One of the available substitutes is manganese, which is not carcinogenic and exhibits corrosion properties similar to nickel [1, 2].

Besides the binders, the base materials of cemented carbides continued to be developed. Nowadays, not only tungsten carbide (WC) but also other carbides (VC or TiC) are used as the base materials. In addition to these basic carbides, complex carbides are employed thanks to advances in their processing technology [1].

In cutting operations performed with cemented carbide tools, mechanical properties and chemical and physical processes play important roles. The temperature of the chip can rise up to 1000°C. In addition to wear resistance and an ability to sustain impact loads, one has to consider the resistance to oxidation and diffusion processes between the tool tip and the chip.

http://dx.doi.org/10.5772/66871

These improvements are mainly provided by the addition of TiC and TaC to the basic types of cemented carbides [3, 4].

As shown in **Figure 1**, a crack spreads more readily through a material with smaller grains. In such case, the resistance to crack propagation, as expressed by fracture toughness, drops. On the other hand, hardness and flexural strength increase with decreasing carbide grain size.

At the beginning of this century, efforts to achieve the highest possible hardness in cutting tools led to the use of carbide particles with sizes on the order of several hundred nanometres. Practical experience proved that such materials are only suitable for very specific applications. In some cases, the fine-grained microstructure was even revealed as the cause of extreme damage suffered by the tool. In response to this and other findings, the Ceratizit company combined multiple carbide types to improve the crack resistance of the resulting material, while maintaining high hardness thanks to fine particle size, as illustrated in **Figure 2**. Fine-grained microstructures play their role in tool grinding as well. The finer the grain, the easier it is to achieve the desired sharp edges without the risk of chipping, crumbling or cohesion failures.

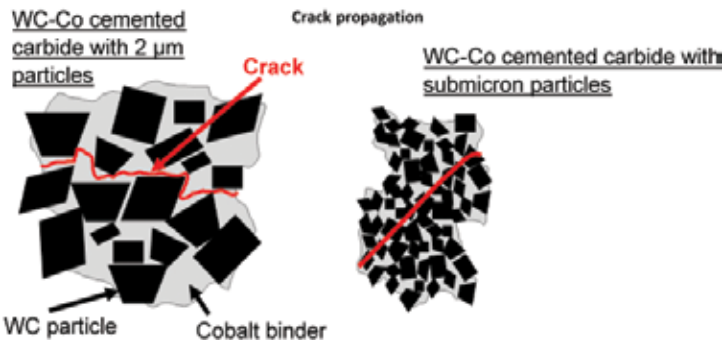

Figure 1. Structure of a cemented carbide and the formation of bonds between the hard carbide and the binder metal. The second micrograph illustrates a new trend in cemented carbides, where vanadium carbide serves to impede the propagation of cracks [5].

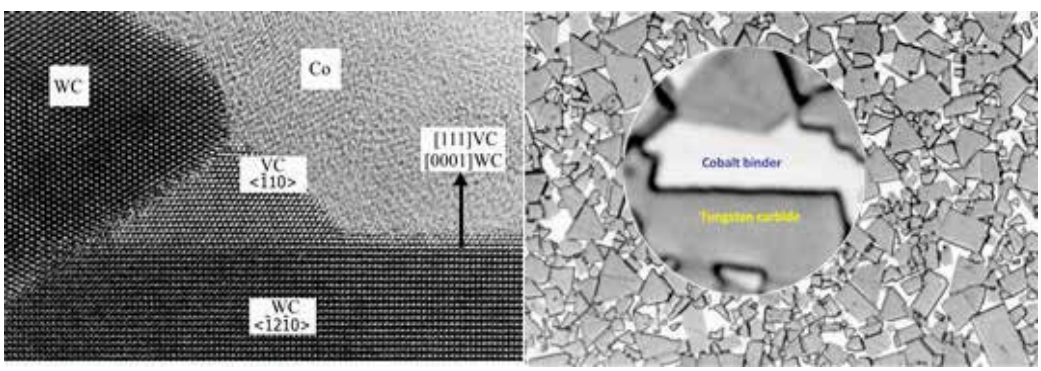

Figure 2. Crack propagation paths depending on the carbide grain size [5].

Despite the years of progress, the WC-Co grade, the oldest cemented carbide type in industrial use, remains the most widespread representative of the class. Its origin dates back to 1922, when the company Widia came up not only with the carbide itself but also with its unique name, Widia, derived from the German words "wie Diamant" or "like diamond", referring to the hardness of the material. This carbide's constant popularity is down to its internal structure. The cobalt binder is the best choice for wetting the WC particles, and therefore provides uniform pore-free products. If present, internal pores impair the mechanical properties of the material. Since cobalt has a hexagonal crystal structure that resembles the structure of the WC carbide, the bonding forces between them are very high [1].

1.2. Manufacture of cemented carbides

All properties of cemented carbides, and indeed of all powder metallurgy products, are governed by the type and purity of the primary raw materials used in their production. Primary constituents for the manufacture of WC-Co grades include, for instance, calcium tungstate $CaWO_4$ (scheelite) for the carbide powder and heterogenite for the cobalt powder. These days, powders are often manufactured from recycled cemented carbides. As a rule, the customer should be notified of the kind of raw material used, i.e. whether the product was made from pure or recycled raw materials. Although tests carried out by the authors have not revealed large differences between the properties of cemented carbides made from pure and recycled raw materials, data on machining performance reported by tool manufacturers have proved that there are such differences [1, 4, 6].

Various technologies are employed for converting carbide and binder powders into products—which therefore exhibit correspondingly varied characteristics. Powders used for this purpose are obtained by production methods which provide various particle shapes and sizes. These aspects have a bearing on the sinter activity and the chemical reactivity of the powder. The latter depends on the number of internal defects within the particles and on their surface energy. Internal defects include mainly crystallographic point defects, i.e. vacancies and interstitial atoms, and line defects, i.e. dislocations. In order to obtain sintered products of adequate density and low porosity, powders with high sinter activity and high reactivity should be used [4, 7, 8].

Once the powders have been produced, classified and mixed, they are shaped and sintered. Technologies by which the desired shapes of cemented carbide parts are achieved involve various forming operations, such as hot isostatic pressing, cold isostatic pressing and extrusion. Powder parts can also be pre-sintered during these operations. Pressing to the desired shape is followed by sintering. Sintering serves the purpose of homogenization of the cemented carbide. This is facilitated by the capillary action and good wettability of the binder with carbide particles [4, 7].

Once sintering has been completed, the product is ready for the finishing operations: grinding and, where relevant, the deposition of thin films. Thin film deposition is typically the last operation before the cemented carbide product is shipped to the customer.

In some cases, however, the sintered part is still no more than a semi-finished product whose final shape must be imparted by grinding. Nowadays, the capabilities of some other

http://dx.doi.org/10.5772/66871

cutting processes are studied to ascertain their potential for making complex-shaped tools of cemented carbides. One of the viable options is milling. Thanks to tailored milling tools and conditions, it allows machining of materials whose hardness exceeds 85 HRC.

The technologies used for producing cemented carbides have a bearing on their mechanical properties. These properties are controlled by the carbide particle size, particle distribution (gradient cemented carbides), the type and proportion of the binder, the resulting structure (brittle phase content, porosity) and impurities (oxides), which may enter or form within the cemented carbide during processing [1, 4, 7].

Cemented carbides belong to a class of brittle materials. The reason for this classification is their inability to undergo extensive plastic deformation on the macroscale. However, some plastic deformation takes place within microvolumes, namely in the cobalt binder. This is why the condition, purity and content of the binder deserve attention. There should be no admixtures with the potential for forming intermetallic phases. To enable a more effective description, the concept of mean free path (MFP) has been introduced. This criterion is used instead of grain size because the bonding material (Co) is present in the form of a network in which the tungsten carbide particles are embedded. At high bonding metal levels, or large MFP values, the binder can undergo plastic deformation and work hardening. The propagation of cracks induced by elevated stress is hindered to some extent in the tough bonding metal, depending on the mean free path (MFP). Once the ductility of cobalt is used up (due to the rising stress), macroscopic failure may set in. By contrast, decreasing cobalt content leads to expansion of the areas of contact between tungsten grains. The grains may therefore become the source of microcracks. The very thin cobalt film (between 100 and 300 nm) grows brittle, as the movement of dislocations within the film is confined, and the growth of microcracks is not arrested [9]. Mechanical properties which are evaluated in cemented carbides include flexural strength, compressive strength and fracture toughness. They are measured by destructive tests on standard specimens in special testing machines. Microstructure (carbide grain size, distribution of carbide types and microstructural homogeneity) and chemical composition are studied by means of optical and electron microscopy methods. The data gathered in this manner give an overall picture of the properties of cemented carbides. In addition to the above-mentioned techniques, non-destructive testing methods are employed. Examples include X-ray, ultrasonic and eddy current inspection. X-ray diffraction is a representative of X-ray-based methods used in this context. It is advantageous in the cases where residual stresses in the cemented carbide surface need to be quantified or when checking for the presence of the eta phase. This is a brittle phase which impairs the mechanical properties of cemented carbides. It can be identified by this method because its diffraction properties differ from those of the binder and the carbide grains. It can also be detected using eddy current inspection on account of the different magnetic properties [3, 9].

Variation in the mechanical properties of WC-Co cemented carbides (hardness and flexural strength) as a function of carbide grain size and Co binder content is illustrated in **Graph 1.**

Graph 2 shows fracture toughness and hardness levels of three WC-Co cemented carbides with carbide grain sizes in the range of 0.5–0.8 μm, and a Co binder content of 10%. These

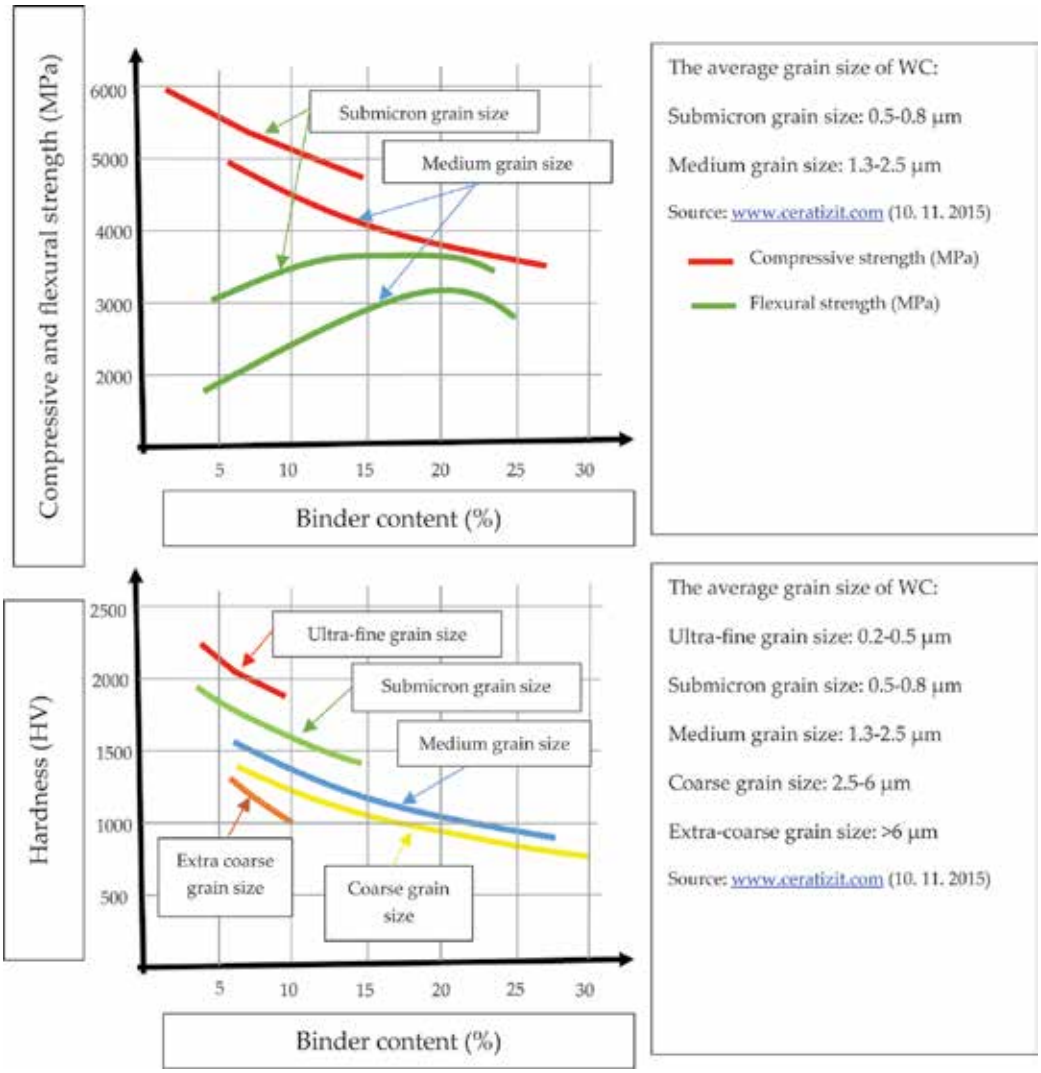

Graph 1. Effect of carbide grain size and Co binder content on hardness and flexural strength of cemented carbides [10].

specimens were provided by three different suppliers in order to compare the actual levels of mechanical properties of the materials and of those given in catalogues. The differences result from the differences between the manufacturing processes. They may arise as early as in the production of powders and their mixtures. For instance, one manufacturer may be using attritors, whereas another may be using atomization. Another source of variation is the final inspection, where one manufacturer might permit a higher fraction of coarse carbide grains of 0.8 μm than the other. The other product will therefore contain a greater amount of carbide grains of the 0.5 μm size [3].

http://dx.doi.org/10.5772/66871

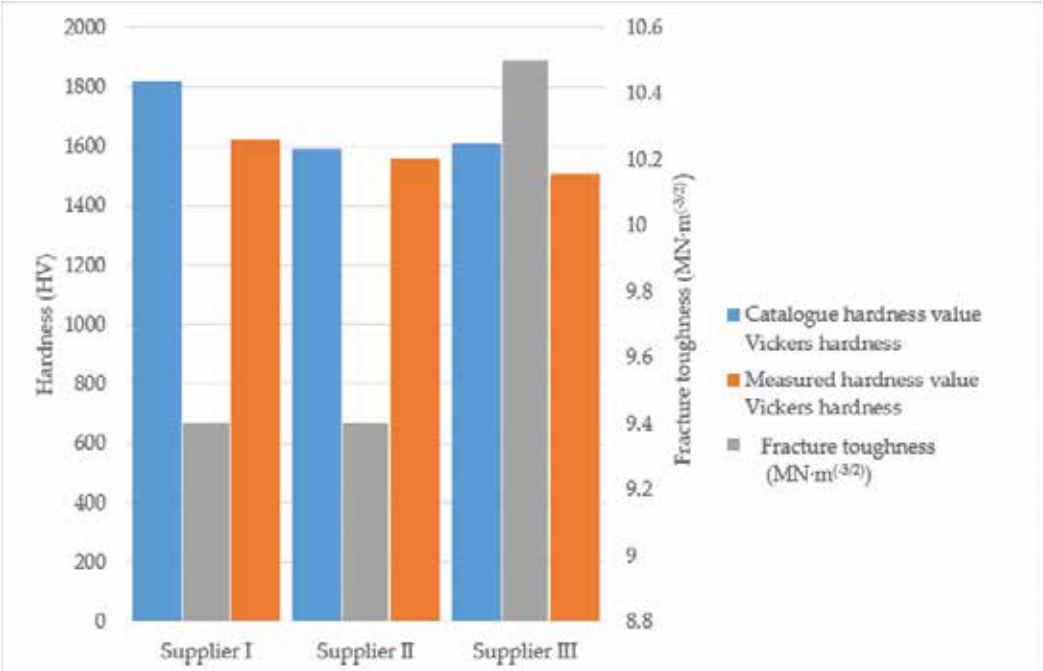

Supplier:	Catalog hardness value:	Measured hardness value:	Fracture toughness:
	Vickers hardness:	Vickers hardness:	(MN·m$^{(-3/2)}$)
Supplier I:	1820	1620	9.4
Supplier II:	1590	1558	9.4
Supplier III:	1610	1507	10.5

Graph 2. Comparison between fracture toughness and hardness levels of cemented carbides of identical composition provided by three different suppliers [3].

2. Effects of grinding on cemented carbide properties

With their hardness levels close to 85 HRC, cemented carbides belong to the class of hard materials. As a result, the main method used for shaping them after sintering is grinding. In the production of cemented carbide tools, the grinding operation provides the desired tool geometry. It can be subsequently modified in terms of microgeometry by laser processing, tumbling, blasting or brushing. A tool prepared in this way can be coated using the PVD or CVD methods.

During grinding, the surface of a cemented carbide is removed by the action of a multi-edged tool: a grinding wheel. Grinding wheels for shaping cemented carbides consist of diamond grains bonded by resin or metal (e.g. copper) [11].

The wheel is pressed against the cemented carbide surface and their movement relative to each other and the associated friction cause heating. The surface of the cemented carbide is removed by abrasion in amounts which are directly proportional to the downforce and the contact area, and inversely proportional to the ratio of the hardness of the cemented carbide surface and that of the abrasive particles of the wheel. The abrasive action scratches and gradually removes the surface layers of the cemented carbide [11, 12].

The abrasion or grinding process in fact comprises several mechanisms, occurring due to the different responses of the binder and the carbide grains to the mechanical loading imposed by the grinding wheel. One of them is brittle fracture, which occurs in carbide particles once their compressive strength is exceeded (the values reported for WC grains are up to 5000 MPa). Another operates in the binder, normally a metal, which may lose its ductility under load. As a result, a crack initiates in the binder, and an entire carbide grain may be dislodged. The stress that eventually causes a crack to form in the cemented carbide may increase suddenly or gradually, by high-cycle or low-cycle fatigue processes [11, 12].

The above mechanisms are responsible for degradation of the cemented carbide surface during grinding. Once the binder loses ductility, its bond to the carbide grains becomes weaker. The carbide grains thus become dislodged and are carried away by the cutting fluid (coolant). Depending on the grinding conditions, the loose binder and carbide particles may build up on the cemented carbide surface and form a thin work-hardened layer with a thickness of several micrometres [11] (**Figure 3**).

Along with the above-described degradation, the temperature of the cemented carbide increases during grinding. The highest temperature is in the area of contact with the grinding wheel. However, the entire volume of the cemented carbide heats up gradually. The rising temperature of the cemented carbide surface and the interaction with the environment lead to surface oxidation. The fresh oxides are stripped during grinding. Apart from grinding,

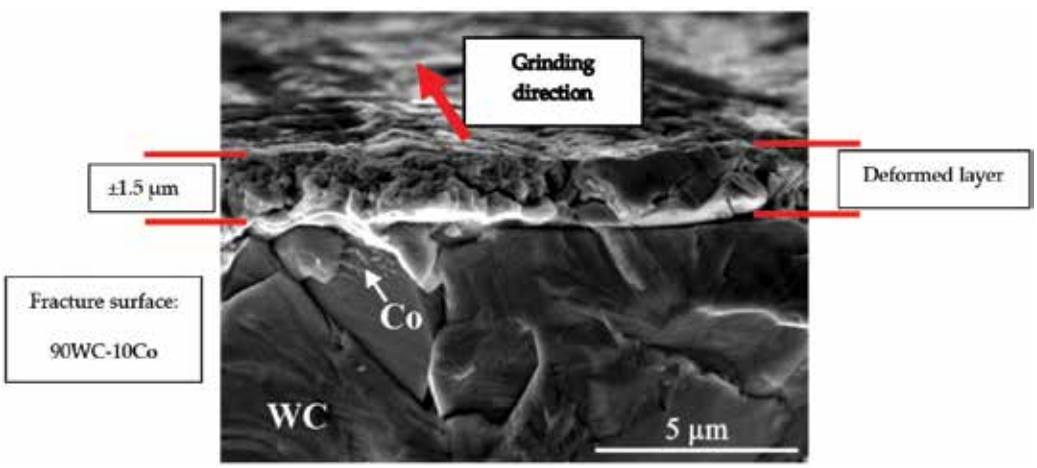

Figure 3. Deformed layer on the surface of WC-Co after grinding [13].

http://dx.doi.org/10.5772/66871

oxidation of cemented carbide may occur during other machining processes, and the new oxide layer may change the geometry of the cutting tool and impair the machining conditions.

The oxidation behaviour of cemented carbides is dictated by a range of variables. The structure-related ones include the type and content of the binder, the types and sizes of carbide particles and the content of impurities. Then there is the atmosphere, the temperature to which the cemented carbide is heated, and the rates of heating and cooling.

Finally, the oxidation behaviour of a cemented carbide depends on its surface finish. For instance, thin films applied to cutting tools prevent their oxidation during machining. Cutting tools can, however, oxidize while they are being manufactured, particularly during grinding. When a used coated tool is being reconditioned, the protective film is removed by grinding and oxidation again threatens. Consequently, the largest risk of oxidation is not associated with the actual use of a cemented carbide tool but with its production or reconditioning. Temperature, along with the chemical composition of the material, affects the progress of oxidation. Since cemented carbides are composite materials, the behaviour of their constituents, i.e. the binder and the base material, will be decisive in the progress of oxidation. In particular cases, the combined behaviour of both constituents will be the governing factor.

Cemented carbides develop a porous oxide layer on their surface consisting mainly of tungsten trioxide WO_3 in those cases where there is a low binder content. The porosity of this layer is thought to be related to gaseous CO and CO_2 being released at the interface between the cemented carbide and the atmosphere. At higher binder levels, the layer becomes less porous, more compact and consists of the complex oxide $CoWO_4$ [14–17].

In terms of thermal loads, the oxidation behaviour of cemented carbides at temperatures below approximately 720°C depends on the properties, chemical composition and content of the binder. It is because at these temperatures, the oxidation ability of the carbide phase is limited. The situation is reversed at higher temperatures: the oxidation ability of the binder is limited, and tungsten trioxide WO_3 readily forms [14–17].

Graph 3 reports data from a test which explored the oxidation behaviour of a cemented carbide. Specimens of WC-Co were heated over the range 200–800°C in an air furnace. The chemical composition of the surface layer was measured by an EDX probe in a scanning electron microscope [2].

The micrographs in **Graph 3** show that at lower temperatures (below 400°C), there is no extensive surface oxidation. Below 400°C, scratches from grinding are still visible on the surface. At higher temperatures, above 600°C, a notable oxide film forms and covers the surface. As the cemented carbide is heated to these temperatures, the scratches from grinding continue to disappear due to advancing surface oxidation. The volume of the oxides grows and they alter the surface relief.

In addition to oxidation to which cemented carbides are subjected during grinding due to the introduced heat, their surfaces also experience thermal cycles resulting from the immediate removal of this heat by the coolant. This rapid thermal cycling generates temperature gradients throughout the volume of the cemented carbide and causes thermal shocks.

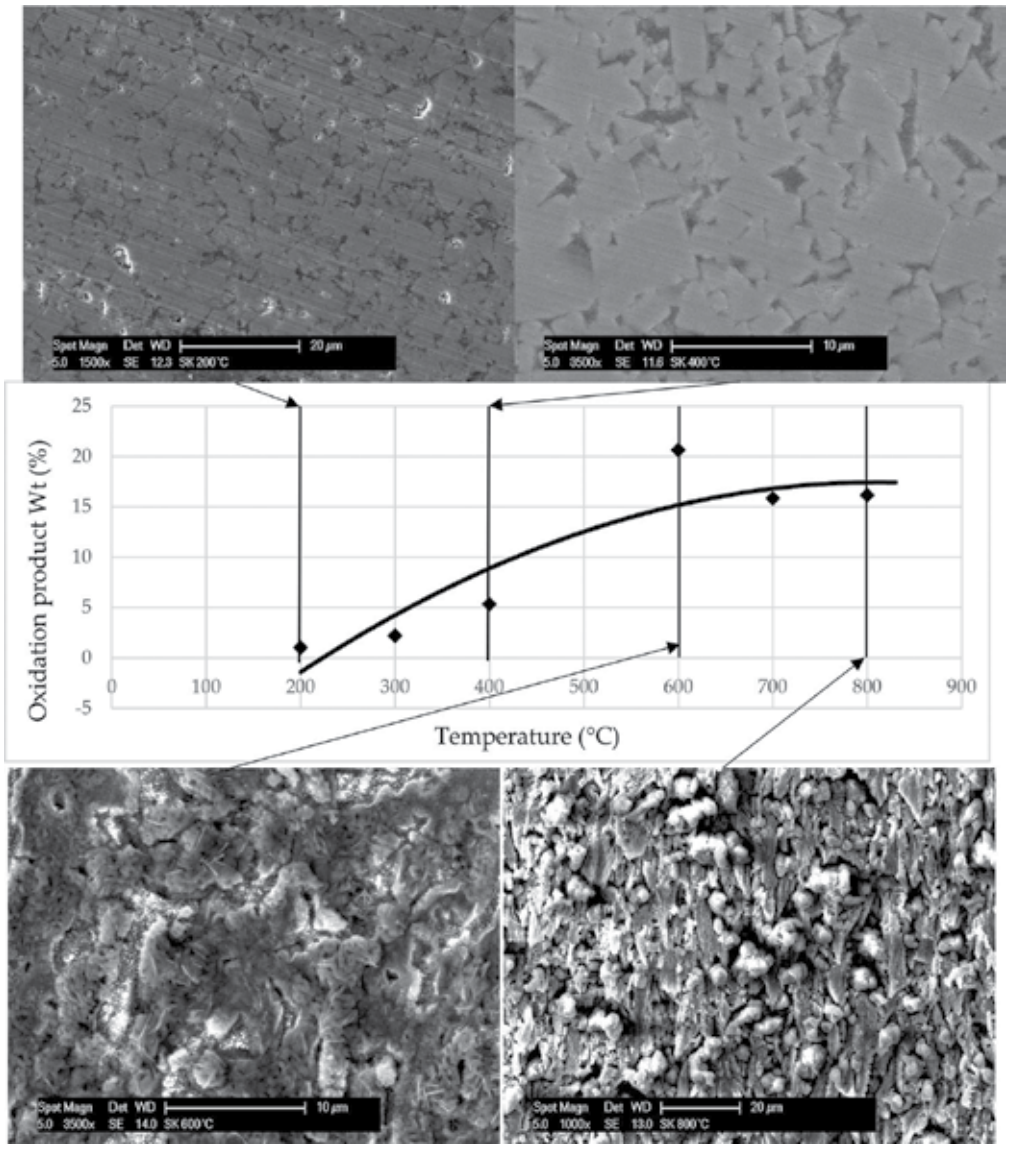

Graph 3. Cemented carbide surface at various heating temperatures [2].

Thermal cycling in the surface layer leads to dramatic variations in stress distribution, and to alternate tensile and compressive stresses. The occurrence of these stresses is associated with volume changes, where heating is accompanied by expansion, whereas cooling leads to contraction.

After a certain time, these continuously alternating stresses cause the binder to lose ductility. At that point, even moderate loads may cause the cemented carbide to develop cracks which threaten failure. Cracks may also form within carbide grains if the load exceeds their ultimate

http://dx.doi.org/10.5772/66871

strength. Microcracks frequently initiate at the interface between the carbide particle and the binder, as this location is energetically most favourable for crack formation. As such intergranular microcracks gradually propagate, carbide particles become dislodged during grinding and the cemented carbide may eventually fail through brittle fracture.

Degradation caused by cyclic thermal loading in a 90WC-10Co cemented carbide with carbide particles in the range of 0.5–0.8 μm is illustrated in **Graph 4**. The specimens were resistance heated to 450°C at a rate of 80°C/s in a thermomechanical simulator. When this temperature was achieved, they were immediately cooled at 10°C/s. Degradation was evaluated by measuring the mechanical properties of the specimens (hardness and fracture toughness) after 50 and 100 cycles. **Graph 4** shows a plot of fracture toughness after 50 and 100 cycles [3, 18].

Graph 4 shows the progress of degradation caused by cyclic thermal loading. Both specimens exhibited a decrease in fracture toughness of approximately 20%. In a real-world application of this cemented carbide, the additional mechanical load would lead to an even greater decline in mechanical properties. The difference between the initial mechanical properties of these specimens is given by their slightly different compositions. The first specimen had a larger content of coarse carbide particles. The second one contained a larger proportion of finer carbide grains, and therefore showed lower fracture toughness. The decline in fracture toughness indicated in the graph can probably be attributed to a gradual loss of ductility of the binder. Its mechanism was described above [3].

The ability of cemented carbides to withstand thermal shocks can be enhanced in various ways. One of them involves using another carbide grade with a higher binder content, or substituting a complex-grade cemented carbide, such as WC-Co-Ni-Cr, with the straight grade

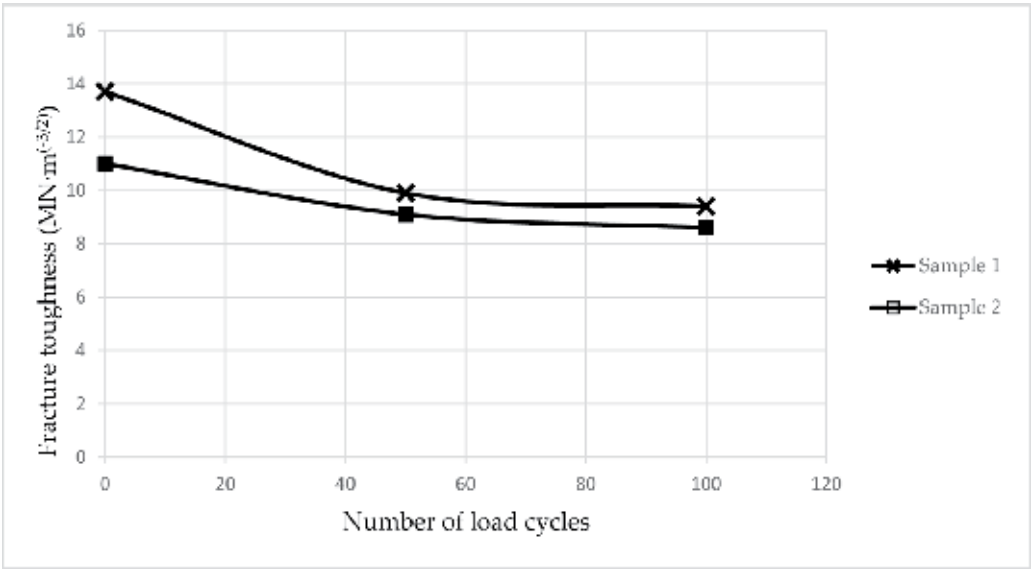

Graph 4. Degradation of cemented carbide due to cyclic thermal loading [3].

WC-Co. Another option is the deposition of a suitable thin film. Such a film can either dissipate heat, distributing it across a larger area or create a thermal barrier which prevents heat from entering the cemented carbide [3, 18].

As mentioned above, grinding causes cyclic thermal loads in the surface of a cemented carbide. As a result, temperature rises gradually throughout the carbide workpiece.

The difference can be several hundred degrees Celsius in some locations. The maximum temperature is given by the parameters of the grinding process, and by the thermal conductivities of the cemented carbide, the workpiece and the environment. When a cemented carbide is the material of a cutting tool, the temperature at the tool tip may reach 1300°C. Thermal conductivity determines the rate at which heat is transferred from a location of higher temperature to locations of lower temperatures. In cemented carbides, this physical property is affected mainly by the operating temperature and by carbide grain size. The thermal conductivity of a cemented carbide decreases with decreasing grain size and with increasing temperature. By contrast, it is not particularly sensitive to the binder content [3].

As temperature rises within cemented carbide, diffusion processes set in. Their intensity is directly proportional to the heating intensity. At temperatures near the solidus of the binder, creep occurs in cemented carbides, depending on the binder type, chemical composition and impurity content. Creep causes loss of adhesion between the binder and the carbide grains. As a result, the surface of the carbide grains becomes exposed and oxidized. All these processes lead to a failure of the cemented carbide.

Graph 5 shows the results of an experimental study of degradation of a cemented carbide. The specimens were slowly heated to 450°C and held for 10 min to allow their temperature

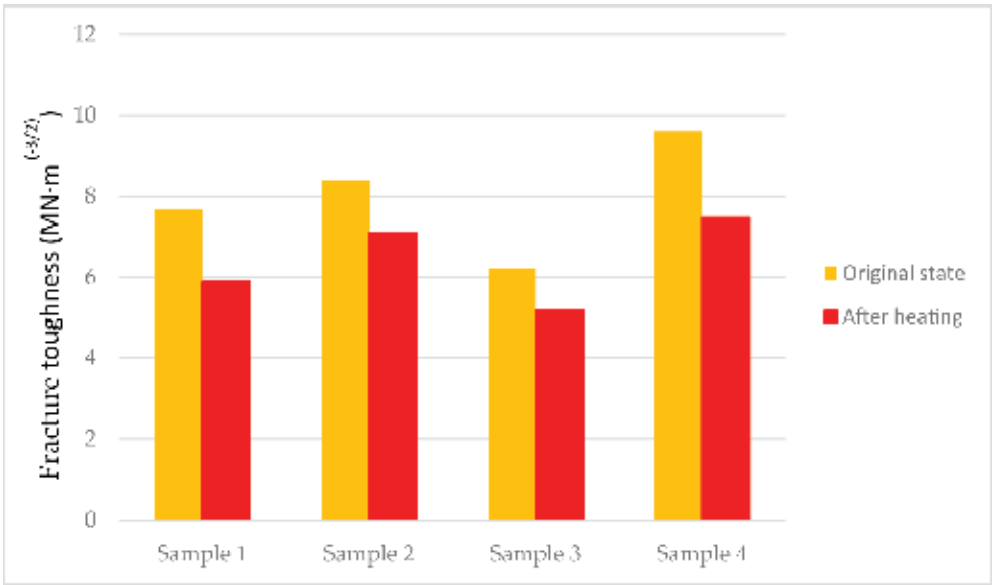

Graph 5. Degradation of cemented carbides due to heating [3].

to homogenize. Then they were cooled by water at 15°C to simulate the effect of the coolant during grinding [3].

The specimens were made of WC-Co-type cemented carbides with identical carbide grain sizes of 0.5–0.8 μm but with various binder levels.

The resistance of cemented carbides to thermal loads can be enhanced by coating them with thin films. CrAlSiN films, for instance, create an effective thermal barrier. By contrast, TiN films provide good conditions for distributing heat across a large area. Another way of controlling the thermal degradation of a cemented carbide involves altering the machining operation. When dry machining or machining with waterless cutting fluids is used, the surface of the cemented carbide is cooled less severely, and the stress gradients will be less steep [3].

Grinding and other post-sinter surface finishing operations have yet another consequence: the formation of residual stresses in the surface of cemented carbide.

3. Residual stresses and their impact on the properties of cemented carbides

Residual stresses develop within the body of a material as a result of external loads, both thermal and mechanical. In essence, they are caused by non-uniform elastic or elastic-plastic deformation of the cemented carbide surface. For residual stresses to occur, the material must experience some of the following [11]:

– Non-uniform plastic deformation, for instance, during machining;
– Non-uniform heating of the surface, which may be caused by the coolant as a cutting tool is retracted from the machining location;
– Transformational stresses related to, for instance, changes in crystal structure;
– Interaction between the surface and the atmosphere and the absorption of substances from the atmosphere by the surface of the cemented carbide.

Residual stresses induced by the above processes lead to changes in the utility properties of cemented carbides. They may also give rise to areas of high stress concentration, distort the shape or alter the product's corrosion resistance.

The magnitude of residual stresses is mainly governed by these three factors:

– Amount of absorbed heat;
– Mode of mechanical loading;
– Changes in material structure;

3.1. Magnitude and type of residual stresses

Not only the absolute value of stress but also the stress type, tensile or compressive, must be considered.

Compressive residual stresses in the cemented carbide surface are favourable for the service application. Such stresses close cracks which have formed due to thermal loads. However, if compressive stresses are to be beneficial to the cemented carbide, their magnitude must remain below a certain limit. If this limit is exceeded, which means that the compressive strength of carbide grains has been exceeded or the binder ductility has been lost, cracks will spread despite compressive stresses being present in the surface of the cemented carbide under load. One must also bear in mind that if there is compressive stress within a carbide grain, there is tensile stress in the binder (**Graph 6**). As the material is more sensitive to tensile stress, large compressive stresses within carbide grains threaten failure in the binder on account of tensile stress [11].

For instance, cracks may spread due to a compressive load applied after the cemented carbide surface has been coated with a thin film. The film imposes additional compressive stress which, after superposition on the compressive stress already present in the substrate, may exceed the ultimate strength and cause a failure of the cemented carbide.

Tensile stresses pose a greater threat to a cemented carbide surface under load than compressive stresses. The reason for this is that the former cause incipient cracks to open, which accelerates the degradation of cemented carbide properties and causes earlier failure.

When an external force acts on a cemented carbide surface, first-order residual stresses arise, causing eventual changes in the geometry of the cemented carbide product. These changes may lead to substantial distortion.

External loads, whether mechanical or thermal, cause movement, growth and decrease in the volume of individual microstructure constituents of a cemented carbide. Differences between the expansion factors of individual constituents and their relative movement lead to residual stresses between the carbide grains and the binder. This residual stress

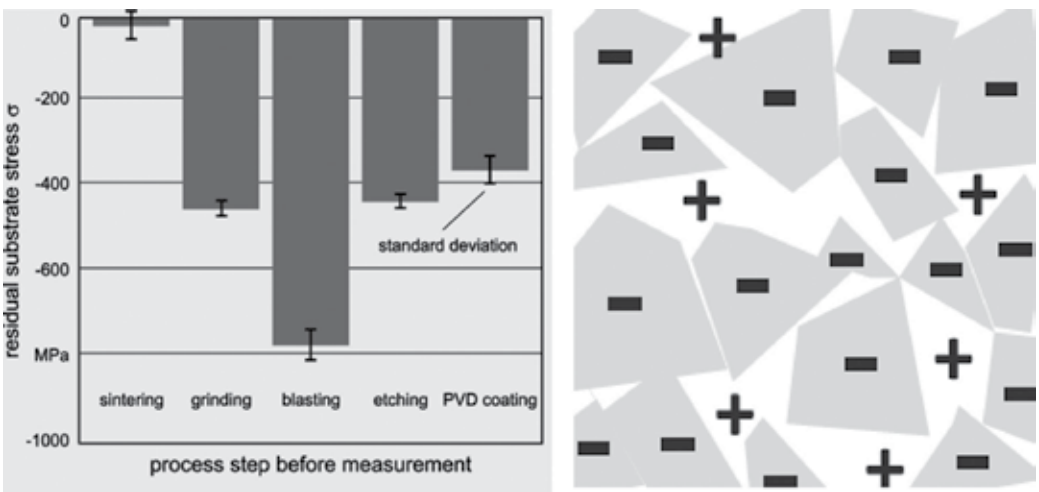

Graph 6. Effects of process steps carried out prior to measurement of residual substrate stresses in cemented carbides. The results were obtained using X-ray diffraction [19].

http://dx.doi.org/10.5772/66871

that arises at the interfaces between the grains (crystals) and the binder is referred to as second-order stress. It is also capable of causing changes in the cemented carbide geometry [11].

Furthermore, external load causes movement of dislocations, vacancies and interstitial atoms within the crystals. All these defects and their movements cause third-order residual stresses, which alone do not induce changes in the product geometry.

It follows from the above description that if external forces act on a cemented carbide, these three types of stress coexist within its volume, and the resulting residual stress is given by their superposition.

The magnitude of residual stresses can be determined by destructive and non-destructive testing methods. The former include successive etching of the cemented carbide surface or the hole-drilling method.

The latter comprise X-ray measurement of strain, where residual stresses are determined from changes in interatomic and interplanar distances, which in turn are determined from changes in the scattering angle under Bragg's law.

The microstructural aspects that affect residual stresses in cemented carbides include the type and amount of binder and the type and size of carbide grains. Cracks initiated by internal stresses may occur at the interface between the binder and the carbide particle. This is the case mainly in fine-grained cemented carbides. In coarse-grained cemented carbides, cracks may also initiate within carbide particles. Apart from the overall content of binder, the binder distribution among grains plays a role as well. It is characterized by means of the mean free path parameter. Where the amount of binder between the carbide grains is larger, the mean free path is longer and the plasticity of the cemented carbide increases. Under applied loads, new dislocations form, move and interact, which results in work hardening and deformation of the binder. If cracks developed within the binder, their propagation would require—due to the above processes—a continuous supply of energy until the ultimate strength is exceeded. Beyond that point, the substrate will suffer macroscopic failure. At low binder levels, i.e. short mean free paths, the ductility is lost sooner. The reason for this is that in such a system, the movement of dislocations is confined when compared to systems with higher binder levels. Therefore, cracks initiate and propagate faster and the cemented carbide fails more rapidly [11].

Residual stresses develop in the surface layer of cemented carbides during post-sinter operations such as grinding, polishing, tumbling, pickling or thin film deposition. These operations impose thermal and mechanical loads on the surface. Unlike in sintering, the loads are not in balance and do not cancel each other out. Therefore, they cause stresses in the surface of the sintered part.

The largest residual stresses occur in the surfaces of those cemented carbide parts which were finished by operations such as grinding or blasting (surface micro-conditioning). The depth profile of residual stress in cemented carbide starting at the surface is shown in **Graph 7.** Compressive stresses of up to 2000 MPa are introduced to the cemented carbide surface

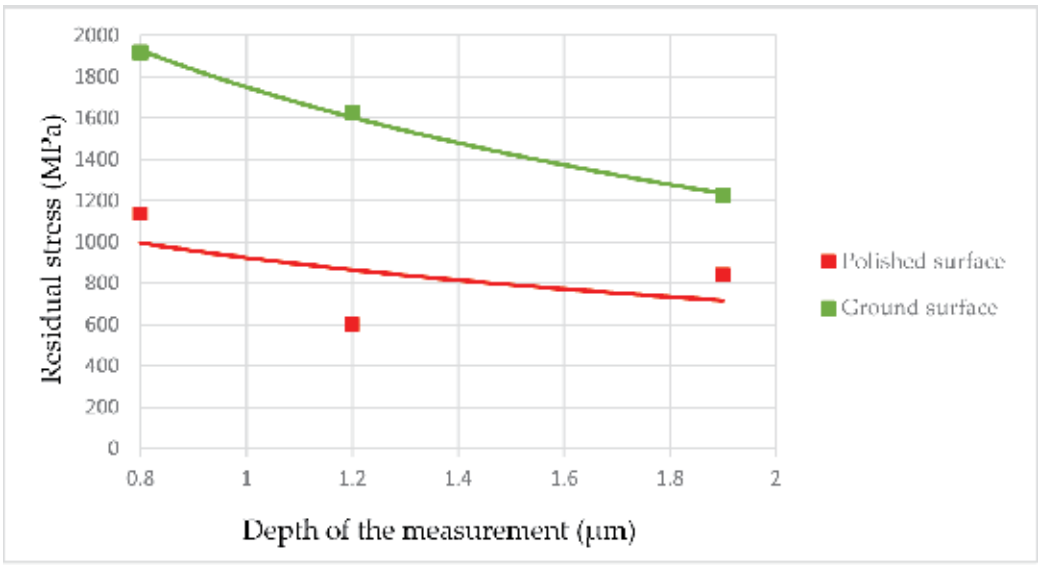

Graph 7. Depth profiles of residual stress in surfaces finished by various methods [11].

during grinding. It has been confirmed by experiments that the severity of grinding, i.e. the depth of cut, has no substantial effect on the increase in residual stress in the surface.

This high value of residual stress arises from the fact that grinding imposes predominantly mechanical load on the cemented carbide surface. Thermal loads are minimized by the use of coolant. Polishing, by contrast, is characterized by the dominance of thermal loads over mechanical ones. Polishing of cemented carbides relieves a great part of their residual stresses, as indicated by **Graph 7.** The reason for this is that polishing removes the most heavily deformed layer with the highest residual stress. Moreover, the heat that is generated in the process causes the remaining residual stress in the cemented carbide surface to relax [11].

Residual stresses in the surface upon grinding can also be reduced by annealing. Important annealing parameters include the temperature, holding time, heating and cooling method, protective atmosphere and some others. **Graph 8** illustrates the effect of annealing on the residual stress in a cemented carbide surface. The specimens were annealed in an air furnace in the range of 200–500°C. Some of them were annealed at 500°C in an ammonia atmosphere. Residual stresses were measured at 100°C intervals [11].

It is clear from the graph that at the same holding times, higher temperatures lead to better relaxation of residual stress. It is also apparent that annealing is more effective when carried out in an appropriate atmosphere. In this case, annealing in ammonia gas led to maximum stress relief. It is important to prevent oxidation of the cemented carbide surface during annealing. Any oxides on the surface impair the adhesion of thin films deposited on the cemented carbide. The surface can be protected against oxidation by using an adequate

http://dx.doi.org/10.5772/66871

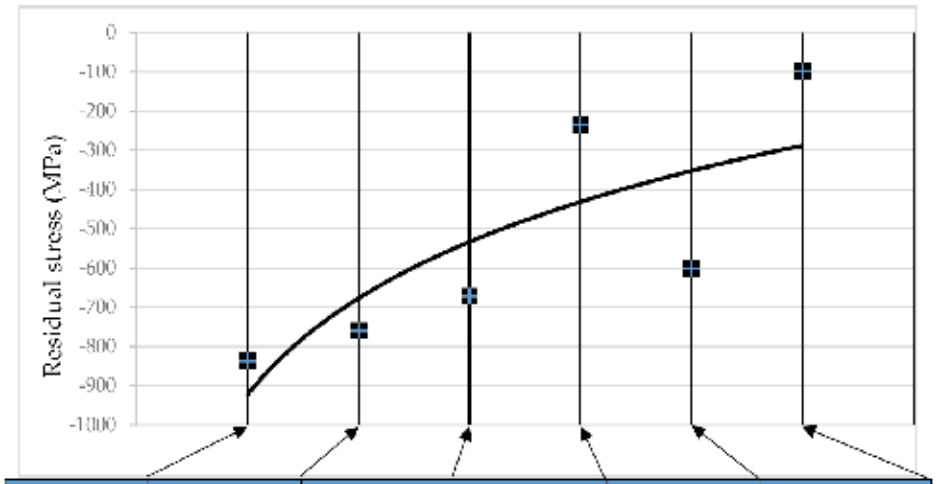

Graph 8. Effects of various annealing schedules on the relief of residual stress in a cemented carbide surface [11].

protective atmosphere, by removing the oxide layer, or by applying a protective coating, to give a few examples [11].

Thin films deposited by PVD methods on a cemented carbide surface show high compressive residual stresses ranging from 2000 to 8000 MPa. Stresses this high are beneficial to the films because they close the cracks which form in them during service. At the same time, however, they affect the substrate as well. The impact of the deposited film on residual stresses in the cemented carbide substrate is illustrated in **Table 1** [11].

A thin film deposited by the PVD method is characterized by compressive residual stress and by an inability to relax this stress. As a result, it shows high levels of residual stress. In the resulting thin film-substrate system, the residual stress levels in the film and the substrate (the cemented carbide) differ greatly. The difference is accommodated by the substrate, whose initial residual stress shifts towards tensile stress. This is illustrated in **Table 1**, where the film deposition leads to a considerable reduction in stress. This was encountered in both ground and annealed specimens. However, there is a difference in that the annealed specimens exhibit tensile residual stresses upon deposition. This is due to their prior heat treatment. Obviously, there is a thermal effect of the PVD deposition itself, but it is weaker than the force exerted by the film. The change in the stress level can be explained in terms of Newton's third law of action and reaction. The appreciable compressive stress within the film induces an opposite reaction within the substrate to establish equilibrium of forces. Hence, the value of the prior stress within the substrate changes in order to counter the stress in the

Grinded samples				
Thin film	**Thin film thickness (μm)**	**Residual stress ground samples (MPa)**	**Residual stress after annealing (MPa)**	**Residual stress after thin film deposition (MPa)**
TiN	2–3	−1657	–	−690
TiN	4–5	−1509		−403
TiCN	2–3	−1689		−346
TiCN	3–4	−1545		−501
Annealed samples				
Thin film	**Thin film thickness (μm)**	**Residual stress ground samples (MPa)**	**Residual stress after annealing (MPa)**	**Residual stress after thin film deposition (MPa)**
TiN	2–3	−1410	−266	371
TiN	4–5	−1603	−383	310
TiCN	2–3	−1380	−262	143
TiCN	3–4	−1008	−245	275

Table 1. Changes in residual stress levels induced by thin film deposition, grinding and heat treatment [11].

thin film. Another important finding is that annealing led to a decrease in stress similar to that achieved by the PVD method.

An important factor contributing to failures of coated cemented carbides is the stress state in regions of stress concentration, such as in the cutting edges of tools. In the cutting edge, residual stresses present in the thin film are superposed on other pre-existing stresses. The resulting stress has a severe impact on the cutting edge and may lead to a cohesion failure of the substrate. A schematic sketch of this phenomenon is shown in **Figure 4**. It illustrates an

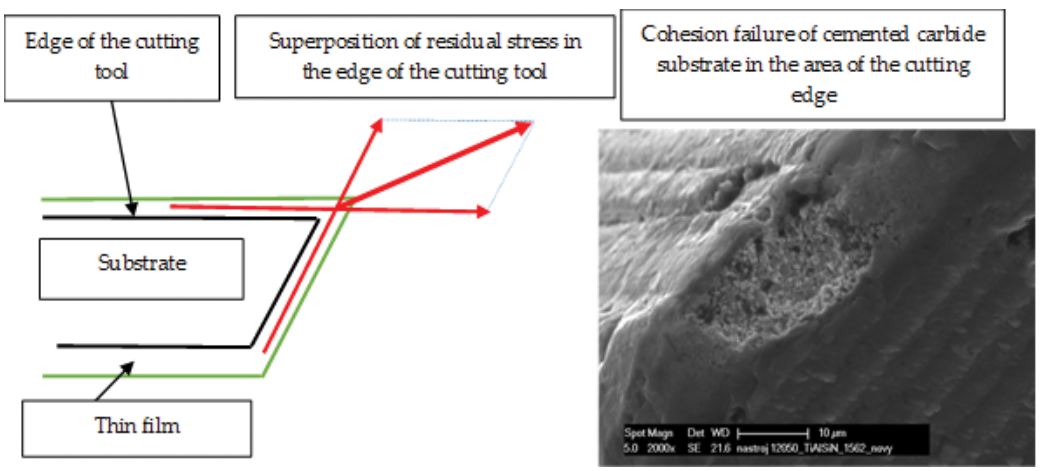

Figure 4. Cohesion failure of cemented carbide cutting edge caused by increasing residual stresses upon grinding [11].

http://dx.doi.org/10.5772/66871

available approach to dealing with this issue which, however, has not been elaborated yet by in-depth research [11].

If the stress that is concentrated in the cutting part of the tool exceeds the ultimate strength of the substrate, the cutting edge immediately fails through chipping. The stress in the cutting part of the tool can continue to rise during the cutting process owing to additional stresses which develop in the process. **Figure 4** shows the chipping of the cutting edge in a coated cemented carbide tool. Clearly, this failure was not an adhesion failure at the interface between the film and the substrate but a cohesion failure of the substrate. In terms of physics, the stress concentration will be dictated by the cutting edge geometry and the resulting superposition of stresses.

4. Corrosion of cemented carbides

Corrosion is a degradation process based on the interaction between the surface of a material and the environment. It is associated with a potential gradient which develops in the surface layer of the material [2].

Four essential components are required for electrochemical corrosion to occur: a cathode, an anode, a corrosive environment provided by an electrolyte and an electrical path between the anode and the cathode. Two chemical reactions, oxidation and reduction, occur between the anode and the cathode, forming the basis of the corrosion attack. Oxidation takes place at the anode, whereas reduction occurs at the cathode. The first involves the loss of electrons from the electron shells of atoms at the anode, whereas the latter is the gaining of electrons by atoms [2, 20].

Corrosion attacks are classified according to their fundamental principles as either chemical or electrochemical corrosion.

Cemented carbides suffer this type of degradation in wood machining processes or in the mining industry.

Cemented carbides possess a heterogeneous structure, where corrosion occurs predominantly in the binder, which has lower corrosion resistance than the base material. For instance, the most common cobalt binder has poor corrosion resistance in corrosive acids, such as sulphuric acid or formic acid. By contrast, it withstands corrosion attacks in acetone, ammonia or weak acids.

If the cobalt binder proves inadequate, other binder types are available. **Graph 9** shows a comparison between three types of cemented carbides containing different binders. The first one is the ordinary WC-Co grade. The second one is a WC-Ni type and the last one is a WC-Co-Ni-Cr cemented carbide. The grain size was identical in all specimens: 0.5–0.8 μm. The binder content was the same as well: 8%. Testing was carried out in artificial mine water with a pH of 5, and in a sodium hydroxide solution of pH = 14. **Table 2** shows the measured data [2].

These results confirm the conclusions of earlier studies on which **Table 3** is based. **Table 3** describes the corrosion resistance of cemented carbides with cobalt and nickel binders in

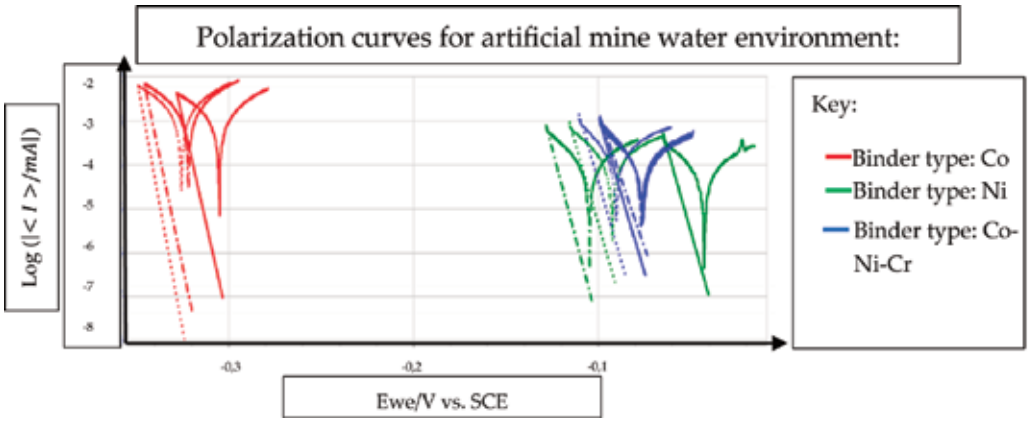

Graph 9. Polarization curves for the corrosion test in artificial mine water [2].

Environment			Type of binder								
			Co			Ni			Co-Ni-Cr		
			E_{cor} (mV/SCE)	Rp (Ω cm²)	I_{cor} (μA)	E_{cor} (mV/SCE)	Rp (Ω cm²)	I_{cor} (μA)	E_{cor} (mV/SCE)	Rp (Ω cm²)	I_{cor} (μA)
Artificial mine water	pH	5	−316	2268	6.06	−78.3	34836	0.4	−78.2	23081	5.6
NaOH	pH	14	−286	8378	1.61	−296	17570	0.79	−290	7072	2

Table 2. Corrosion behaviour of cemented carbides containing various binders. The readings were obtained using a potentiostat [2].

pH	Co binder	Ni binder
12	Very good	Very good
11		
10		
9	Good	
8		
7	Sufficient	
6	Poor	
5	Very poor or no corrosion resistance	Good
4		
3		Sufficient
2		
1		Poor
0		

Table 3. Corrosion resistance of cemented carbides with cobalt and nickel binders at various pH levels [20].

environments of various pH levels. The corrosion resistance of multi-component binders is governed by the proportions of the constituents. For instance, the presence of cobalt in the multi-component binder listed in **Table 3** impairs its corrosion resistance in these environments. By contrast, the presence of chromium improves the resistance to oxidation [2].

Other factors that play a role in the corrosion behaviour of a cemented carbide include the binder content and the size of the carbide particles. They were studied on WC-Co and WC-Ni specimens. **Table 4** lists the measured data [2].

These results confirmed experimental studies carried out by other researchers. Those showed that in acid environments, it is cemented carbides with higher cobalt binder levels which suffer more severe degradation. In alkaline environments, the corrosion rates were similar. In the case of the nickel binder, the corrosion rate increased with its content. This occurred in both acid and alkaline environments.

Carbide grain size affects the corrosion resistance of cemented carbides as well. **Table 4** confirms that fine-grained cemented carbides have better corrosion resistance in both alkaline and acid environments.

Environment	**Type of binder**						**Co**			**Amount of binder**		**(%)**	**8**
	Grain size of WC particles												
	(μm)						**(μm)**						
	3–6									**0.2–0.5**			
	E: (mV/SCE)		**Rp: (Ω cm²)**		**I: (μA)**		**E: (mV/SCE)**			**Rp: (Ω cm²)**		**I: (μA)**	
Artificial mine water pH 5	−385		802		16		−316			2273		6	
NaOH pH 14	−259		3194		4.4		−285			8380		1.6	
Environment	**Grain size of WC particles**											**(μm)**	**0.5–0.8**
	Type of binder												
	Co						**Ni**						
	Amount of binder						**Amount of binder**						
	(%)			**(%)**			**(%)**			**(%)**			
	4			**12**			**8.5**			**12**			
	E: (mV/SCE)	**Rp: (Ω cm²)**	**I: (μA)**	**E: (mV/SCE)**	**Rp: (Ω cm²)**	**I: (μA)**	**E: (mV/SCE)**	**Rp: (Ω cm²)**	**I: (μA)**	**E: (mV/SCE)**	**Rp: (Ω cm²)**	**I: (μA)**	
Artificial mine water pH 5	−350	1796	7.5	−345	1218	11	78	34836	0.4	−71	19862	0.67	
NaOH pH 14	−287	5180	2.5	−292	5631	2.4	−296	17570	0.79	−293	9319	1.7	

Table 4. Corrosion behaviour of cemented carbides with various carbide grain sizes and binder contents. The readings were obtained using a potentiostat [2].

	Type of binder			Co	Amount of binder	(%)	10
	Grain size of WC particles			(μm)	2.5–6		
Environment	Residual stress after grinding (average value) (MPa)			Residual stress after annealing (average value) (MPa)			
	−1687			−265			
	E: (mV/SCE)	Rp: (Ω cm²)	I: (μA)	E: (mV/SCE)	Rp: (Ω cm²)	I: (μA)	
Artificial mine water pH5	−458	1256	68	−579	3319	6	

Table 5. Corrosion behaviour of cemented carbide vs. residual stress levels upon grinding and heat treatment. The readings were obtained using a potentiostat [2].

The corrosion behaviour of cemented carbides is, to a certain extent, governed by residual stresses, which were dealt with in the previous sub-chapter. Data obtained from a literature review suggest that larger residual stresses will promote corrosion attack as they are linked to higher activation energy, which the material strives to lower by oxidation.

Table 5, based on the authors' own experiments, shows the effects of residual stresses on the corrosion resistance of cemented carbides. The experimental material was the 90WC-10Co grade. Grinding of the specimens introduced residual stresses to their surface layers. Some of the specimens were subsequently annealed to relax the residual stress. **Table 5** shows the average stress levels in the surface layers of the cemented carbide specimens after grinding and annealing [2].

The comparison indicates that annealing improved the corrosion resistance of the specimens. As mentioned above, the reason for this is that at lower residual stresses, more energy is required to cause the corrosion attack and, therefore, a more aggressive environment must be used. In such case, corrosion resistance will be poorer and the attack on the cemented carbide surface will accelerate.

5. Conclusion

This chapter explores the properties of cemented carbides dictated by their internal structure. It also focuses on the degradation processes associated with grinding of cemented carbides. Degradation can also be studied in processes that precede grinding: powder production, mixing, shaping and sintering, as well as in industrial applications of the resulting products, such as machining. Besides oxidation and thermal degradation, great attention was paid to residual stresses and corrosion. The latter two have a profound impact on the service life of cemented carbides, e.g. in machining and mining. Residual stresses also play a role in PVD coating of cemented carbides, where they may lead to tool failure. Such failures used

http://dx.doi.org/10.5772/66871

to be attributed to inadequate deposition processes but the present experiments showed that incorrect grinding procedures have the major impact. Therefore, these factors must be taken into account in machining applications where cemented carbides are used. Papers published by prof. B. Denkena show that it is beneficial to have as high as possible compressive stresses in the cemented carbide prior to thin film deposition. Such stresses, however, impair the corrosion resistance of the cemented carbide. The question arises whether grinding, which introduces large compressive stresses, leads to a loss of ductility of the binder. This is a plausible hazard because grinding imposes cyclic load on the surface of the cemented carbide, which may cause the loss of binder ductility and subsequent surface damage. This accelerates degradation processes such as corrosion. Besides corrosion, compressive stress can also affect the formation of tensile stress in cobalt. When combined with the added compressive stress imposed by a thin film, it may exceed the tensile strength of cobalt (binder), resulting in cohesion failure of the cemented carbide.

The ductility of the binder can be restored by annealing, a method which has been tested by the authors. Annealing relaxes the compressive residual stresses in the cemented carbide surface without changing its geometry. The disadvantages of this procedure include the risk of surface oxidation if an inadequate protective atmosphere is used, and possible degradation of the mechanical properties due to poorly chosen heating and cooling conditions. Another weakness is the risk that residual stresses in the cemented carbide may shift to the tensile stress region (as measured in the cemented carbide) during annealing or after thin film deposition on the annealed material. Tensile stress is hazardous for a tool in service, as it opens cracks that may have formed in the brittle carbide, and may initiate more cracks and impair fatigue strength under cyclic load. Such cyclic loads may include forces in machining, as well as forces resulting from rapid heating and cooling cycles. Therefore, these processes deserve adequate attention as they may lead to sudden degradation of a cutting tool. The resulting changes may then be misinterpreted and the proposed corrective measures may fail to improve the situation.

Acknowledgements

This article was made possible by the funding for the SGS-2015-016 project "Analysis of Surfaces of Structural Details and Tools by Surface Integrity Method, and Impacts on End-Use Properties".

Author details

Antonín Kříž and David Bricín*

*Address all correspondence to: bricda@kmm.zcu.cz

Department of Material Science and Technology, Faculty of Mechanical Engineering, University of West Bohemia, Pilsen, Czech Republic

References

[1] Upadhyaya G. Cemented Tungsten Carbides: Production, Properties and Testing. 1st ed. New York: William Andrew; 1999. 420 p. ISBN:0-8155-1417-4

[2] Janeček J. Corrosion properties of sintered carbides [thesis]. Pilsen: University of West Bohemia, Faculty of Mechanical Engineering; 2015. 85 p. Available from: https://portal.zcu.cz/stag?urlid=prohlizeni-prace-detail&praceIdno=63342

[3] Špirit Z. Selected properties and cutting tool applications of sintered carbides [thesis]. Pilsen: University of West Bohemia, Faculty of Mechanical Engineering; 2013. 90 p. Available from: https://portal.zcu.cz/stag?urlid=prohlizeni-prace-detail&praceIdno=52610

[4] Humár A. Materials for cutting tools. Publisher: MM Publishing VUT Brno. Brno. 2008. 235 p. ISBN: 8025422502

[5] Kathrein M. Grundlagen der Beschichtung. Kundenseminar Ceratiyit. Reutte 2002.

[6] Kurolov SA., Gusev A. Tungsten Carbides: Structure, Properties and Application in Hardmetals. New York: Springer; 2013. 242 p. DOI: 10.1007/978-3-319-00524-9

[7] Skotnicová K, Kursa M. Powder metallurgy. 1st ed. Ostrava: VŠB-Technical University of Ostrava. Ostrava; 2013. 153 p. ISBN: 978-80-248-3378-1

[8] Neikov O, Naboychenko S. Handbook of Non-Ferrous Metal Powders: Technologies and Applications. 1st ed. New York: Elsevier; 2008. 616 p. DOI: ISBN: 978-1-85617-422-0

[9] Kříž A. The effect of sintered carbide microstructures upon the life of tools and machine parts. Košice: Institute of Material Research of the Slovak Academy of Sciences; 2006. 8 p. ISBN: 80-968543-5-6

[10] Ceratizit. General Catalogue-Wear Parts [Internet]. Available from: http://www.ceratizit-j.co.jp/pdf/wear%20parts_catalogue.tif [Accessed: 10. 11. 2015]

[11] Palán J. Measuring of residual stress in relation to the technology of preparation [thesis]. Pilsen: University of West Bohemia, Faculty of Mechanical Engineering; 2015. 80 p. Available from: https://portal.zcu.cz/stag?urlid=prohlizeni-prace-detail&praceIdno=63341

[12] Suchánek J. Tribotechnika [Internet]. Available from: http://www.tribotechnika.sk/tribotechnika-12010/abrazivni-opotrebeni-kovovych-materialu.html [Accessed: 7. 12. 2015]

[13] Hegeman JBJW, De Hosson JThM, De With G. Grinding of WC-Co Hardmetals [dissertation]. Eindhoven University of Technology. Netherlands Elsevier; 2001. 10 p. Available from: http://linkinghub.elsevier.com/retrieve/pii/ S0043164800005615. DOI: 10.1016/ S0043-1648(00)00561-5

[14] Voitovich VB, Sverdel VV, Voitovich RF, Golovko EI. Oxidation of WC-Co, WC-Ni and WC-Co-Ni hard metals in the temperature range 500–800 °C. International Journal of Refractory Metals and Hard Materials; 1996 pp 289–295. DOI: 10.1016/0263-4368(96)00009-1

[15] Gu W-H, Jeong YS, Kim K, Kim J-C, Son S-H, Kim S. Thermal oxidation behavior of WC–Co hard metal machining tool tip scraps. Journal of Materials Processing Technology; 2012. pp 1250–1256. DOI: 10.1016/j.jmatprotec.2012.01.009

[16] LOFAJ F, KAGANOVSKII Yu. S. Kinetics of WC-Co oxidation accompanied by swelling. Journal of Materials Science [online]. 1995. pp 1811–1817. DOI: 10.1007/BF00351615. ISSN 0022-2461. Available from: http://link.springer.com/10.1007/BF00351615

[17] Aristizabal M, Sanchez J M, Rodriguez N, Ibarreta F, Martinez R. Comparison of the oxidation behaviour of WC–Co and WC–Ni–Co–Cr cemented carbides. Corrosion Science; 2011. pp 2754–2760. DOI: 10.1016/j.corsci.2011.05.006

[18] Kříž A, Špirit Z. Properties of cemented carbides upon thermal exposure. 25th National Conference on Heat Treatment. Čerčany: ASSOCIATION FOR HEAT TREATMENT OF METALS 2013. pp.179–186. DOI: ISBN 978-80-904462-6-7

[19] Denkena B, Köhler J, Breidenstein B, Abrão AM, Ventura CEH. Influence of the Cutting Edge Preparation Method on Characteristics and Performance of PVD Coated Carbide Inserts in Hard Turning [dissertation]. Elsevier; 2014. 8 p. Available from: http://linkinghub.elsevier.com/retrieve/pii/S0257897214005751 DOI: 10.1016/j.surfcoat.2014.07.003. ISSN 02578972

[20] Federal Carbide Company. Corrosion Resistance of Tungsten Carbide Grades [Internet]. Available from: http://www.federalcarbide.com/corrosion_resistant_tungsten_carbide_grades.html [Accessed: 16. 12. 2014]

Chapter 13

Structure and Properties of the Multicomponent and Nanostructural Coatings on the Sintered Tool Materials

Leszek A. Dobrzański, Daniel Pakuła,
Klaudiusz Gołombek,
Anna D. Dobrzańska-Danikiewicz and
Marcin Staszuk

Additional information is available at the end of the chapter

http://dx.doi.org/10.5772/65400

Abstract

This chapter presents a general characteristic of sintered tool materials, in particular sintered sialons, nitride ceramics, injection-moulded ceramic-metallic tool materials and cemented carbides and a general characteristic of their surface treatment technology and especially chemical vapour deposition (CVD) and physical vapour deposition (PVD) techniques. The results of our investigations in technology foresight methods concerning the development prospects of surface engineering of sintered tool materials are presented. In the next subsection, we discuss the outcomes of multifaceted research carried out with advanced materials engineering methods, including high-resolution transmission electron microscopy, into the structure and properties of multicomponent, graded and multilayer coatings on the investigated tool materials, including the newly developed injection moulded ceramic-metallic tool materials. Special attention was drawn to a one-dimensional structure of the studied PVD and CVD coatings and its impact on the properties of coatings.

Keywords: sintered tool materials, foresight, surface engineering, PVD, CVD, coatings, nanostructure

1. General characteristic of sintered tool materials

Powder metallurgy has found widespread applications in the manufacture of sintered tool materials. Rapidly evolving techniques and technologies necessitate higher demands for sintered tool materials in terms of mechanical properties, among others wear resistance. Advanced sintered tool materials are witnessing constant advancements connected with fast

progress in materials engineering. Advanced sintered tool materials, due to the character of their work and complex wear mechanisms to which cutting tool edges are subjected, should satisfy numerous requirements including, in particular, high hardness, high impact strength, resistance to complex wear (adhesive, diffusive, abrasive and thermal wear) and to high temperatures, high compressive strength, stretching, flexing and bending, high fatigue and thermal strength, good conductivity and thermal capacity, cutting edge stability and good ductility [1–8]. A tool material with universal applications should merge the mentioned properties as far as possible and especially the highest wear resistance and hardness with high strength and good ductility accompanied by chemical inertness towards the workpiece. Despite the intensive development of materials engineering, a tool material has still not been produced which fulfil such requirements due to a fundamental contradiction between such properties as hardness and ductility.

As mentioned in the Introduction section, in general—in the group of sintered tool materials—one can distinguish super hard sintered materials, mixed ceramic and carbide materials, ceramic materials, steels and cermetals, including sintered high speed steels, sintered carbide steels and sintered carbides as well as injection moulded ceramic-metallic tool materials. The properties and intended use of the finished products made of sintered tool materials depend on the phase composition and a content of hard phase particles in sintered tool materials (whether they are present or not) and the chemical composition of a binding material, as well as the material's thermal workability.

Sialon ceramics known as sialon (the name comes from the first letters of the elements it contains, i.e. silicon, aluminium and oxy-nitride) was developed and introduced into production and application in industrial processes by the end of the twentieth century, as a new type of machining materials combining the advantages of oxide and oxide-free materials containing Si_3N_4 [2, 3]. Sialon, with its chemical composition determined by the formula $Si_{6-z}O_zN_{8-z}$, is isomorphic with silicon nitride Si_3N_4 (**Figure 1**). The number z = 0–4, 5 corresponds to the number of Al atoms replacing Si in the lattice of β nitride. Due to isomorphicity, the mechanical and physical properties of sialon β' are similar to the corresponding properties of Si_3N_4. The chemical properties of this phase correspond to aluminium Al_2O_3, though, sialon ceramics

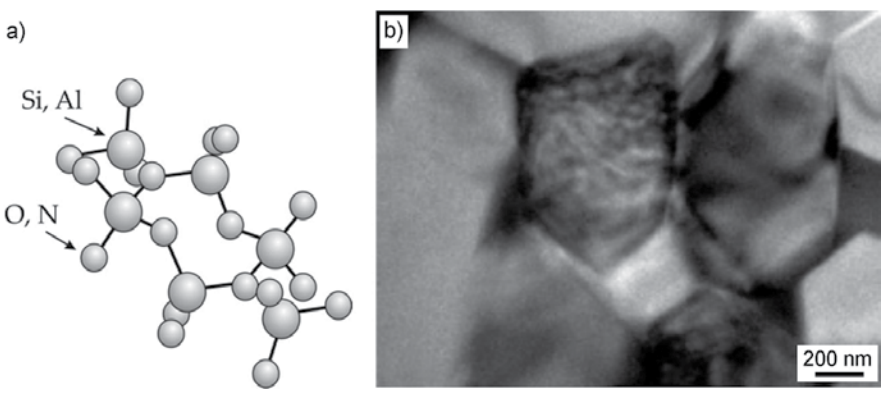

Figure 1. (a) Distribution of Si, Al, N and O atoms in crystallographic lattice of sialon β; (b) structure of thin foil parallel to the surface of sialon tool ceramics (TEM).

http://dx.doi.org/10.5772/65400

combines high physical and mechanical properties inherited from Si_3N_4 ceramics and resistance to chemical activity at a high temperature characteristic for Al_2O_3. Up to 60% of Al_2O_3 dissolves in sialon β', maintaining the hexagonal structure β-Si_3N_4. Sialons are most often produced using the method of one-stage reaction sintering of a moulded mixture of silicon nitride with an addition of oxide and aluminium nitride and a sintering additive, usually Y_2O_3, which is a source of the liquid phase during sintering. Very pure and fine-grained silicon nitride has to be utilised in this method.

Chemical composition has to be controlled very accurately during the process, as well, because even a small excess of oxygen increases the fraction of the liquid phase in sintering [3, 9]. It is favourable for technological reasons to introduce β' additives of other oxides, e.g. Y_2O_3, to a sialon sinter as this reduces vapour pressure and is essential for lowering a melting point of sialon β'. Pressure sintering instead of hot sintering is then feasible. In such case, a relatively low sintering temperature enables to maintain a fine-grained structure and thus to enhance the strength properties of the sinter. This also has an effect on a reduction in oxidisation resistance and supports accelerated decomposition of a solid solution at high temperatures. Glass is formed during cooling from a fluid created in intermolecular spaces during sialon β' densification with Y_2O_3 additive at high temperature. When heat treatment of such sinter is carried out again at 1400°C, the reaction of this glass with the β' sialon matrix takes place again:

$$\underset{\text{sialon } \beta'}{Si_5AlON_7} + \underset{\text{glass}}{Y\text{–}Si\text{–}Al\text{–}O\text{–}N} \rightarrow \underset{\text{sialon } \beta'}{Si_{5+x}Al_{1-x}N_{7+x}} + \underset{\text{YAG}}{Y_3Al_5O_{12}} \quad (1)$$

as a result of which a compound, $Y_3Al_5O_{12}$, called yttrium-aluminium-garnet (YAG), is created at the grain boundaries. The presence of this compound very effectively improves the resistance of sialon β' to oxidisation and creeping resistance.

Si_3N_4 nitride ceramics, due to its high thermomechanical properties, such as resistance to high temperature, low thermal expansion coefficient and high resistance to sudden temperature and chemical environmental changes, is regarded to be one of the most promising materials used in high-temperature processes. They exhibit high resistance to the activity of acids and reducing substances. Tools made of silicon nitride can work at the temperature of approximately 1400°C and maintain their mechanical properties. They are also resistant to corrosion and abrasion and receive thermal shocks very well. Nitride tool ceramics is manufactured by means of powder metallurgy and it is not necessary to melt the main component in a manufacturing process. This process is classical and, therefore, five main stages can be distinguished [3, 10], i.e. fabrication, preparation of powder, forming of preforms, sintering and finishing.

Si_3N_4 undergoes partial dissociation during heating above 750°C and sublimation at 2170°C. For this reason, a sintering process of silicon nitride at 1800–1900°C is conducted in glass or metallic capsules in the atmosphere of nitrogen. Sintered Si_3N_4 tool ceramics is obtained by uniaxial pressing or by hot isostatic pressing (HIP) and reactive sintering. The HIP sintering method consists of placing the sintered Si_3N_4 mass in a vacuum capsule and subjecting it to isostatic hot pressing. The simultaneous forming, sintering and compression take place; therefore, this method ensures relatively high bending strength and theoretical sinter density [11, 12].

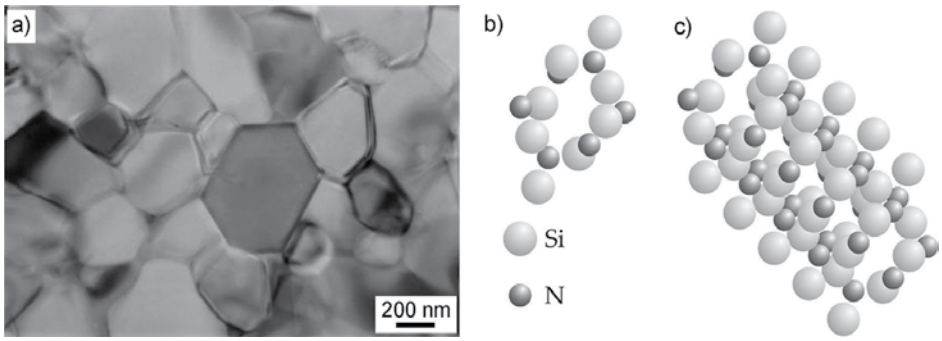

Figure 2. Structure of (a) thin foil parallel to the surface of tool layer of nitride Si_3N_4 ceramics (TEM); crystalline β-Si_3N_4 (b) single unit cell, (c) six unit cells.

Pure Si_3N_4 exhibits high strength, hardness and oxidisation resistance. After adding the necessary densifiers during sintering, i.e. MgO, Y_2O_3, Al_2O_3, HfO_2 or TiC, the very good properties deteriorate. Silicon nitride is susceptible to a chemical interaction of the treated material and to oxidisation during work at the temperature of 1000–1200°C. The properties of nitride ceramics are further improved by introducing additives in the form of zirconium oxide (ZrO_2), titanium nitride (TiN) or SiC whiskers [13]. Hardness, plasticity and wear resistance are then increased. Nitride tool ceramics exhibits a β crystalline structure after sintering (**Figure 2**) [12, 14]. Si_3N_4 nitride may be used with the addition of Y_2O_3 or TiC particles, dispersive in 30%, can be placed in a matrix containing 92% of Si_3N_4, 6% of Y_2O_3 and 2% of Al_2O_3.

The injection moulded ceramic-metallic tool materials described in this chapter were manufactured in laboratory conditions at a quarter-technical scale. Nevertheless, it was decided to incorporate them due to the expected high development prospects of this manufacturing method and of this group of ceramic-metallic materials. This technology enables to produce relatively small elements with complicated shapes and a developed surface, which in turn is a significant limitation in the application of classical powder metallurgy. The assumptions of this method are described in one of the preceding chapters. In the powder injection moulding (PIM)

	Mixture composition, %								Content of components, %		
Designation	**WC**	**TiC**	**TaC**	**NbC**	**VC**	**Co**	**Ni**	**Designation**	**Polypropylene**	**Paraffin**	**Stearic acid**
TC	33	33	25	8	–	1	–	TC60SA4	18	18	4
								WS!60SA4	18	18	4
WS1	57	20	14		–	9	–	WS157SA2	20.5	20.5	2
								WS154	23	23	0
WS2	87	5	–	–	–	8	–	WS260SA4	18	18	4
								WS260SA4	18	18	4
WS3	69	20			2	5	4	WS354SA4	21	21	4
								WS360SA4	18	18	4

Table 1. Characteristic of mixtures of powders and components of a binder of newly developed ceramic-metallic tool materials by the PIM method.

http://dx.doi.org/10.5772/65400

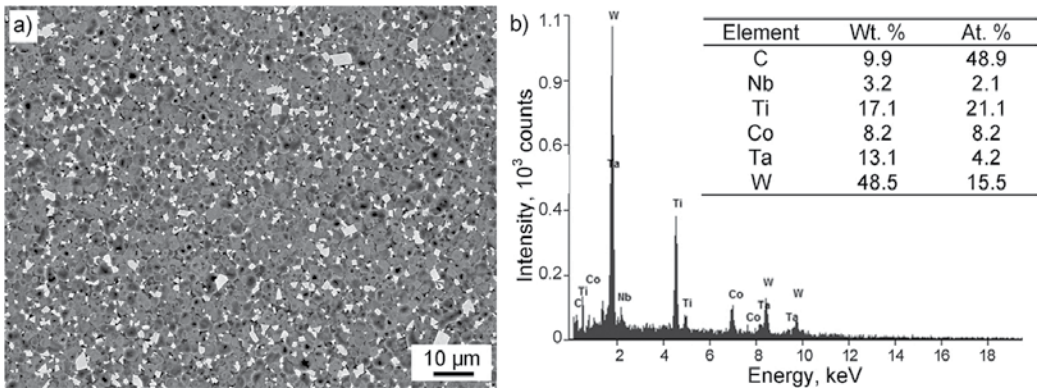

Figure 3. Substrate structure of WS1 tool material (a); EDS spectrum from area as in figure (a) and results of quantitative analysis of chemical composition (b).

method [2, 6–8, 15–25], a mixture of polymer (binder) and powders of inorganic materials is supplied to a cylinder equipped with a worm screw which, when rotating, is moving the heated mixture until the required volume of the fed material is achieved and a polymer-powder slip is sprayed into a moulding die. A brittle preform is subjected to further heating at a small rate and to long annealing for full or partial decarbonisation and then to sintering. Despite its relatively low 4% share in the global market of products manufactured with the PIM technology, the fabrication of advanced tool materials by this method has received considerable interest [2, 3, 15, 21], as it is a highly profitable technology and forms a basis for obtaining a broad group of universal tool materials that are highly complex, accurate, even considering complex geometrical features, in the form assumed, according to the requirements of the near-net-shape technology without performing finish treatment, e.g. grinding and sharpening before the deposition of coatings.

The mixtures of powders described in this work [5] were used for fabricating the newly established tool ceramic-metallic materials. Such mixtures are the key component of the charge (**Table 1**) together with slip agents (WS symbols) and were manufactured by Treibacher Industrie AG without a slipping agent (symbol: TC). A mixture of polypropylene and paraffin was used as a binder with some contents of stearic acid used as a surfactant (**Table 1**).

It was found as a result of observations in a scanning electron microscope that ceramic-metallic tool materials have a homogeneous structure with uniformly distributed hard melting carbides in a cobalt or nickel-cobalt matrix without visible precipitations of free graphite and an undesired phase η and without visible microporosity. The structure of composite tool materials of the WS1 and WS2 type is characterised by fine grains of carbides, with the size of 1–3 and 2–4 μm, respectively, arranged in a cobalt matrix. The size of carbide grains in a cobalt-nickel matrix in a WS3 tool material is 0.5–2 μm (**Figure 3**).

It was found based on the examinations of thin foils in an electron microscope that the structure of the investigated WS1 and WS2 tool materials consists of a solid solution of cobalt or cobalt and nickel γ filling the space between WC, TiC, TaC, NbC and VC carbide particles (**Figure 4**). It was also found that the average diameter of the major part of carbide particles is smaller than 2 nm, which clearly classifies the studied WS1 and WS3 carbides to the group of

fine-grained materials. It was also stated that numerous crystalline structure defects exist in the structure of hard melting carbides (**Figure 4c**).

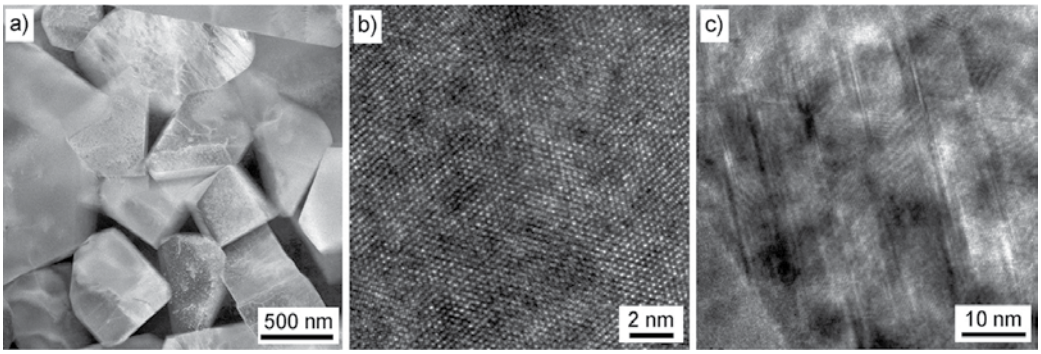

Figure 4. Structure of thin foil made from tool material (a) WS3, (b) & (c) WS1; (a) image in scanning-transmission mode, HAADF detector, (b) & (c) image in HRTEM mode.

The sintered carbides of metals are materials commonly used for cutting tools, manufactured by conventional powder metallurgy methods. Sintered carbides are materials consisting of carbides of hard melting metals, mainly W and also Ti, Ta and Nb, with a volume fraction of approximately 65–95% and a binding metal, usually cobalt. Sintered carbides can also be produced in which a binding metal is nickel, molybdenum and iron or their alloys with cobalt. The most often used types of sintered carbides include such used for the machining of materials producing a chipping, long—mainly steel and cast steel, both long and short, short—mainly cast iron, used for plastic working and for abrasion resistant device parts and also for reinforcement of mining tools. Such materials are also discussed in other chapters of the book. Carbide powders in the first stage of sintered carbides' production are usually fabricated by one of the three methods, i.e. multistage, shortened and single-stage method [2, 3, 8].

The shortened method is applied most often due to the highest efficiency and lowest costs. Sintering is usually done in induction or resistance vacuum furnaces. The single-stage method is used for special purposes—for manufacture of large products and products without pores and also for manufacture of products exposed in service to impact loads and products used for tools for plastic working. Additional densification during hot isostatic pressing at the temperature of 1350–1450°C under the argon pressure of 100–300 MPa has a decisive effect on the higher bending strength of sintered carbides and their higher density.

Sintered carbides' structure is shown in **Figure 5**. The following phases may exist in the structure of sintered carbides at room temperature [2, 3]:

- α—sintered particles initiating particles of tungsten carbide WC,
- α_1—solid secondary solution of cobalt in tungsten carbide WC, uncrystallised during sintering, existing in the form of fine-rounded grains,

http://dx.doi.org/10.5772/65400

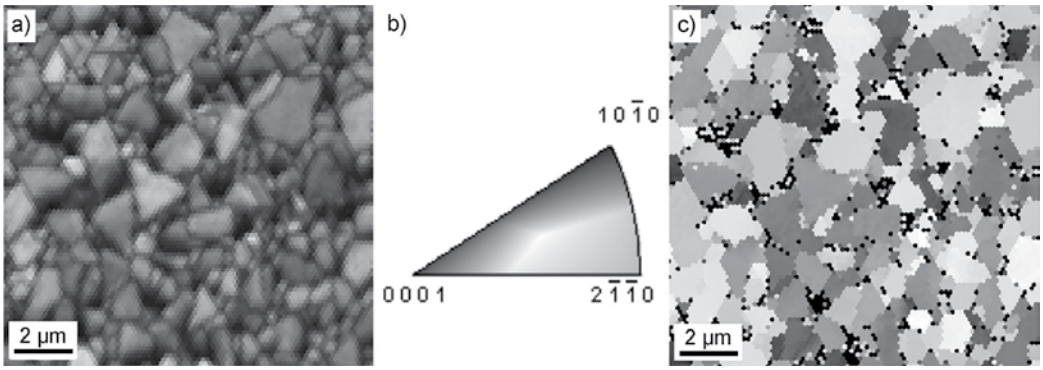

Figure 5. The results of analysis of sintered carbides WC-Co performed by diffraction of back scattered electrons (EBSD), (a) distribution map of diffraction quality, (b) reverse pole figures and (c) crystallographic orientation map of WC grains.

- α_2—solid secondary solution of cobalt in tungsten carbide WC, created as a result of crystallisation during sintering, existing as large grains with regular shapes,
- γ—solid solution of tungsten, tantalum and carbon in cobalt,
- β—(Ti,W)C, (Ta,W)C or (Ti,Ta,W)C carbides in the form of chains or ball grains,
- β'—phase β impoverished in tungsten with a higher concentration of titanium or tantalum.

The following phases can be formed in the case of insufficient carbon:

- η—a phase with a complex structure Co_3W_3C,
- Θ—a phase with a complex structure $Co_3W_6C_2$,
- χ—a phase with a complex structure $Co_3W_{10}C_4$,
- δ—Co_3W type phase.

Sintered carbides are not subjected to heat treatment as a binding metal is not subjected to phase transformations [2, 3]. Sintered carbides are not suitable for plastic and mechanical working, either, consisting of rolling and milling. They can be, however, polished or ground in or undergo surface treatment consisting of the deposition of abrasion resistance coatings.

2. General characteristic of surface treatment technologies of sintered tool materials

One of the development directions, undergoing the most intensive growth, of advanced tool materials, including sintered carbides, tool ceramics and tool cermetals, is the deposition of anti-wear coatings, usually nanostructured coatings, onto such materials, mainly in physical vapour deposition (PVD) and chemical vapour deposition (CVD). The possibilities of constituting coatings resulting from the interaction between the fabrication method, the properties

and the efficiency of the system produced allow, by matching them appropriately, to fabricate coatings possessing the expected functional properties [1–3].

The research topics concerning the fabrication of coatings with good mechanical properties and high abrasive wear resistance, including PVD and CVD, represent one of the most essential directions of surface engineering development [1–3, 26–30]. Enhanced operational properties are very frequently achieved for commonly applied materials by depositing simple monolayer, single-component coatings with PVD methods. When selecting a coating material, a constraint is encountered resulting from the fact that many properties expected from an ideal coating cannot be achieved at the same time. For instance, improved hardness and strength are reduced ductility and substrate adhesion of a coating. Coatings with different properties were bonded together for this reason, with each of them performing a relevant task aimed at achieving continuous or graded coatings with possibly most desired properties in a specific application. Graded coatings are deposited by changing gradually or continuously one or several components in the direction from the substrate to the outer surface. They represent a modern group of coatings achieved by PVD [1–3, 26, 29]. The layers or zones of the coating being produced should ensure, depending on their location, the desired properties and—by creating transition zones—guarantee transition between the properties that often vary. The layer closest to the material being coated generally ensures best adhesion to the substrate while the outer layer ensures adequate hardness, strength, tribological and anticorrosive properties. When coatings are fabricated in which chemical composition changes gradually from the substrate to the surface, it is possible to apply such coatings as anticorrosive coatings and also for structural parts, in particular for turbines and implants and surgical and dental implant-scaffolds [31–38].

A technological trend observed for many years in the field of tools production, not only cutting tools, is the deposition of anti-wear coatings onto tool materials, including those achieved by PVD and CVD and also with other advanced technologies. Numerous research studies in the recent years, including own studies [5, 26–30, 39–51], concerning deposition using coatings resistant to the wear of tool ceramics, have verified the existing stance that it is unsubstantiated to coat tool ceramics due to their high hardness. It has been demonstrated that it is clearly reasonable to coat such tools as, first of all, the life of tools' cutting edges is enhanced by decreasing the heat emitted while cutting, by reducing a friction force on the flank surface and, secondly, it was noted that coatings, by covering pores on the surface of tool ceramics, eliminate places where fractures occur and moreover, they delay the diffusion wear process. By resolving such a research problem, it is also possible to improve the efficiency and quality of machining, while reducing its energy consumption and material consumption, which is a prerequisite for ensuring competition in the conditions of free market economy. If the surface machining technology of tool materials is employed, including PVD and CVD methods, to attain graded layers with high wear resistance, also at high temperatures, the properties of such materials in machining conditions can be enhanced, among others by lowering the friction factor, ameliorating microhardness, improving conditions of tribological contact within the contact area of the tool-workpiece; adhesion and diffusion wear and oxidisation can also be prevented. If such properties are found, an optimum field of applications can identified for the ceramic materials of a substrate and for the studied multiphase and graded

http://dx.doi.org/10.5772/65400

layers. Furthermore, a correlation can be determined between the results of laboratory investigations and the wear identified as a result of technological cutting tests.

3. Own investigations of development perspectives of surface engineering of sintered tool materials

Having regard to the main development directions aimed at the improvement of sintered tool materials, apart from searching completely new materials and improving the chemical composition of the existing materials, surface treatment should be mentioned to improve their properties [52–54]. Clients expect that advanced sintered tool materials should have a wide group of properties determining their functional characteristics, as mentioned in the above subsection. The purpose of advanced technologies for the formation of the structure and properties of surface tool materials is to reach the optimum combination of the expected properties for a specific material and a product made of it.

Scientific methods were applied in the framework of the own foresight research performed—which also utilised the production process optimisation methods—in order to determine the strategic development directions of technologies, the recognition and implementation of which is to contribute towards the greatest economic and social benefits of knowledge- and innovation-based economy [55, 56]. Over 500 detailed technologies of structure and surface properties formation of engineering materials were considered in the implemented project concerning the development trends of engineering materials and biomaterials, in which approximately 500 scientists from many countries of the world participated. All the analysed technologies were grouped into 14 thematic areas (*P*1–*P*7 and *M*1–*M*7) and 10 critical technologies—considered to be a priority with the best development prospects and/or of crucial importance for the industry over the next 20 years—were chosen for each of the selected areas. The considered thematic areas encompass four areas pertaining to the treatment technologies of sintered tool materials: (1) *P*4: surface engineering of tool materials; (2) *M*2: physical vapour deposition technologies (PVD); (3) *M*3: chemical vapour deposition technologies (CVD); (4) *M*6: technologies of nanostructural surface layers [52, 53].

The best critical technologies concerning the surface treatment of sintered tool materials were presented graphically with a technology strategy matrix (**Figure 6**). A universal scale of relative states consisting of 10 scores was used to evaluate individual technologies for their value and environment influence intensity. According to the scale, which is a single-pole positive scale without zero, the lowest possible score is 1 and the highest score is 10. A 16-field matrix of strategies for technologies, indicating a long-term procedure for a given technology, derives from a four-field dendrological matrix of technology value and a four-field meteorological matrix of environment influence [52].

The dendrological matrix presents graphically expert evaluation results of the individual technologies for their potential, representing an objective value of the given technology and their attractiveness, reflecting the subjective perception of the given technology by its potential users. The best quarter of the dendrological matrix is a *wide-stretching oak* to which technologies are

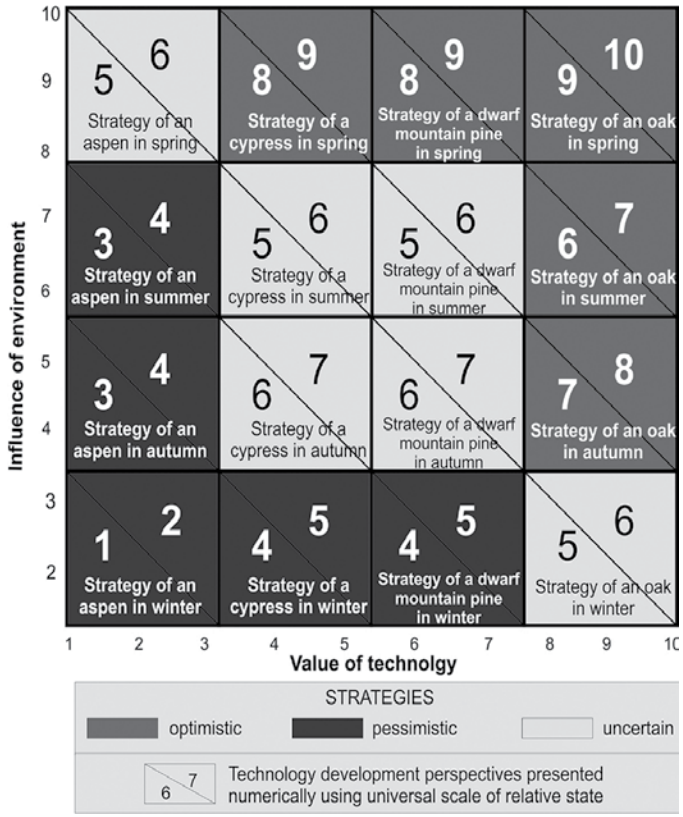

Figure 6. Matrix of strategies for technologies in general form.

assigned having high potential and attractiveness. If a technology is placed in a quarter *rooted dwarf mountain pine*, with a high potential and limited attractiveness, or in a quarter *soaring cypress*, with high attractiveness and limited potential, this means that a market success is possible in advantageous market conditions. A *quaking aspen* is a quarter with poor perspectives, though, to which technologies are assigned having a low potential and low attractiveness.

The meteorological matrix presents graphically the effect of positive and negative factors on the technologies, called opportunities and difficulties, respectively. In the best variant, called *sunny spring*, many positive stimuli come from the environment having influence on the technologies and difficulties are small. Peaceful and sustainable development of technologies is also possible as it is impacted by numerous positive and negative factors, which takes place when technologies are in the quarter *rainy autumn*. A quarter called *hot summer* corresponds to a risky environment bringing many opportunities and risks for technologies. The worst possible variant, in which many difficulties exist affecting the technologies adversely, accompanied by scarce opportunities, is called the quarter *frosty winter*.

An analysis carried out according to the results of foresight research, presented graphically using matrices called contextual matrices—due to graphical references to the commonly

http://dx.doi.org/10.5772/65400

known objects and phenomena—allowed to determine the strategic position of the critical technologies of surface engineering of sintered tool materials. The most promising technologies are presented in **Table 2**. They are characterised by high attractiveness and potential and environmental conditions are very helpful here, which is manifested by numerous opportunities and a small number of external difficulties. They are placed in the best 16 matrices of strategies for technologies called *oak in spring*, as shown in **Figure 7**. For such technologies, a

Surface engineering of tool materials *P*4	
A_{P4}	Physical vapour deposition (PVD)
B_{P4}	Chemical vapour deposition (CVD)
Physical vapour deposition technologies (PVD) *M*2	
A_{M2}	Cathodic arc deposition (CAD)
B_{M2}	Reactive magnetron sputtering (RMS)
Chemical vapour deposition technologies (CVD) *M*3	
D_{M3}	Plasma-assisted/enhanced chemical vapour deposition (PACVD/PECVD)
E_{M3}	Laser chemical vapour deposition (LCVD)
G_{M3}	Metal organic chemical vapour deposition (MOCVD)
Technologies of nanostructural surface layers *M*6	
D_{M6}	Ion beam-assisted deposition (IBAD)
E_{M6}	Electron beam physical vapour deposition (EB-PVD) of nanometric surface layer

Table 2. Key critical technologies of surface engineering of sintered tool materials.

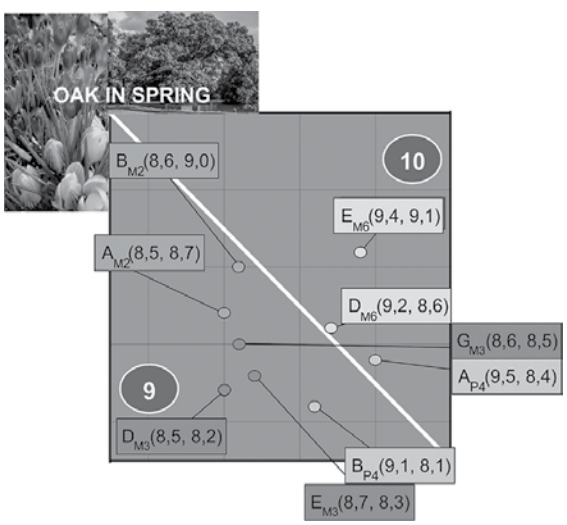

Figure 7. The best 16 matrices of strategies for technologies with points marked (top right corner), whose coordinates correspond to expert evaluation of key values of technologies and intensity of environment influence on such technologies.

winning strategy should be applied, consisting of developing, strengthening and implementing an attractive technology with a high potential in industrial practise while taking advantage of favourable environmental conditions in order to achieve a spectacular success.

The results of expert opinions presented in contextual matrices derive from the statistical surveys presented as a bar chart (**Figure 8**). As part of such heuristic research, the experts identified the forecast development trends of given technologies against the analysed thematic areas, by predicting whether the importance of particular groups of technologies in the nearest 20 years will be growing, maintaining at the same level or declining. In all the charts, grey bars correspond to, in per cents, the predicted growth of importance of a given technology group, light grey—stabilisation at the existing level and dark—a declining importance of the technology group against other technology groups of a given thematic area.

The presented results of foresight research indicate that PVD and CVD methods play a crucial role in the group of numerous surface treatment technologies applicable with respect to sintered tool materials. The most promising PVD methods include cathodic arc evaporation (CAD) and reactive magnetron sputtering (RMS). With respect to CVD methods, the best development prospects are seen for methods using plasma for assistance (PACVD/PECVD), metalorganic precursors (MOCVD) and laser (LCVD). If nanometric surface layers have to be deposited onto sintered tool materials, it is the experts' opinion that it is most advantageous to employ PVD methods with ion beam assisted deposition (IBAD) or electron beam physical vapour deposition (EB-PVD) [52–54]. The outcomes of the analyses performed may be a basis for studies aimed at the industrial implementation of the mentioned critical technologies, for

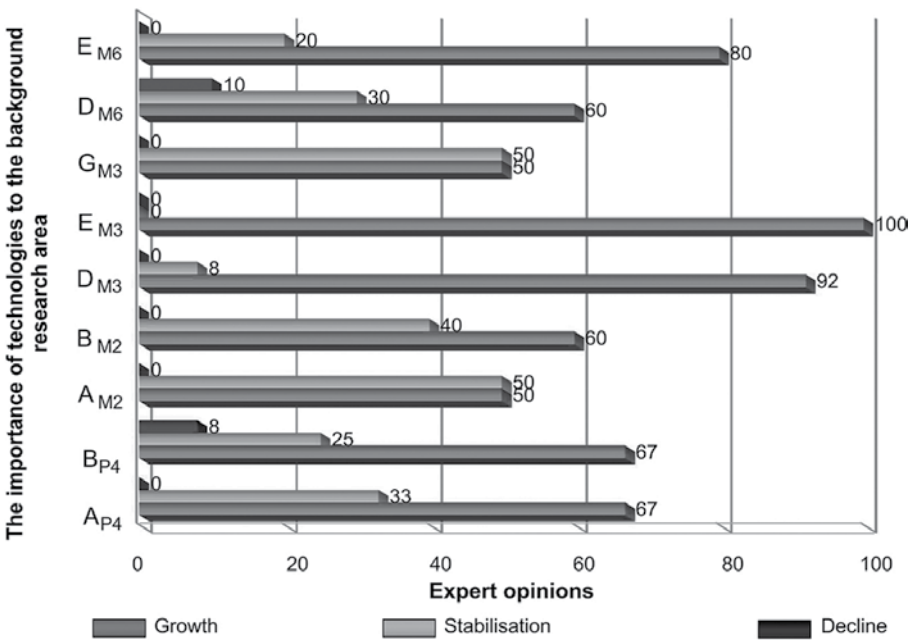

Figure 8. The predicted trends in changes of importance of key critical technologies of surface engineering of sintered tool materials.

http://dx.doi.org/10.5772/65400

example in production of cutting tools made of sintered materials, which undoubtedly provides an opportunity to improve the functional properties of the analysed group of tool materials.

4. Investigations into the structure of multicomponent coatings on the investigated sintered tool materials

The subchapter below is summarising and generalising the results of own investigations, pursued over the last decade, into the structure of sintered sialons, nitride ceramics, injection moulded ceramic-metallic tool materials and cemented carbides onto which wear resistant coatings are deposited. The methodology and detailed results of particular investigations of mechanical and functional properties of sintered tool materials with PVD and CVD coatings are presented in the own works published earlier [5, 26–30, 39–52]. The scientific aim of this paper is to present investigations into the structure and properties and to identify wear mechanisms for tools fabricated from the investigated sintered tool materials, which—to some extent—are newly created with newly developed nanocrystalline multiphase and graded coatings applied by PVD with cathodic arc evaporation techniques, as well as by a high-temperature CVD process, with the intention to improve the cutting properties of the investigated materials by considerably improving the life of the tool cutting edge. The state-of-the-art materials science research methods were employed for explaining the causes of a marked improvement in the operational properties of the tools, especially thin foils tests, including on cross sections in a high-voltage transmission electron microscope. Such coatings have not been applied to date onto any tools made of the materials mentioned. Investigations are known, however, concerning the deposition of similar coatings onto tools made of classical sintered carbides and cermetals. The deposition of coatings achieved in a CVD process onto nitride ceramics with a combination of Al_2O_3+TiN layers [28, 48, 51] is also known. The results of such research constitute a reference point for the results of the own research presented in this subchapter.

Indexable inserts made of sintered carbides and sialon and nitride tool ceramics were deposited in the process of cathodic arc evaporation (CAE-PVD) with graded coatings of the following type: Ti(B,N), (Ti,Zr)N, Ti(C,N), Ti(C,N)+(Ti,Al)N, TiN+(Ti,Al,Si)N+(Al,Si,Ti)N and the following multiphase coatings: (Al,Ti)N, (Ti,Al)N, (Al,Cr)N, (Ti,Al)N+(Al,Cr)N, (Al,Cr)N+(Ti, Al)N, TiN+multi(Ti,Al,Si)N +TiN, TiN+(Ti,Al,Si)N+TiN, as well as in a high-temperature CVD process with multilayer coatings based on Ti(C,N), Al_2O_3, TiN and TiC phases [1, 27–30, 41, 48–51]. The thickness of the investigated PVD coatings obtained in sintered carbides and tool ceramics spans between 0.7 and 5.0 μm, while the thickness of CVD coatings spans between 1.7 and 10 μm.

Note that 10 layer nanocrystalline surface coatings of the (Cr,Al,Si)N and (Al.Ti,Si)N types were applied alternatively by the modified lateral arc rotating cathodes (LARC) technique into a substrate made of the investigated ceramic-metallic tool materials [5]. CrN or TiN, respectively, were used as near-the-core layers, by placing them onto graded layers (Cr,Al)N/(Al,Cr)N and (Ti,Al)N/(Al,Ti)N, respectively. Note that eight multilayers were successively deposited

onto such layers with a variable composition in the following order: (Cr,Al,Si)N+(Al,Cr,Si)N +(Cr,Al,Si)N+(Al,Cr,Si)N+(Cr,Al,Si)N+(Al,Cr,Si)N+(Cr,Al,Si)N and, respectively, (Ti,Al,Si)N +(Al,Ti,Si)N+(Ti,Al,Si)N+(Al,Ti,Si)N+(Ti,Al,Si)N+(Al,Ti,Si)N +(Ti,Al,Si)N. The total thickness of CrAlSiN and AlTiSiN coatings is 2.5–3.0 μm. Regardless the location, all the layers forming part of the coatings tightly adhere to each other and do not show any fractures and discontinuities. In addition, fractographic tests of tool materials with the deposited (Cr,Al,Si)N and (Al,Ti,Si)N coatings do not reveal any delamination along the separation area between the coating and the substrate and show that the coatings obtained adhere strongly to the substrate.

A qualitative phase composition analysis carried out using the X-ray diffraction method confirms that coatings exist containing TiN, Ti(C,N), AlN and CrN phases and an Al_2O_3 phase in the case of CVD coatings on substrates made of sintered carbides and tool ceramics. The presence of isomorphic TiN phases was identified on the X-ray diffraction patterns obtained from Ti(B,N), (Ti,Zr)N, Ti(C,N)+(Ti,Al)N and (Ti,Al)N coatings because such phases are a secondary TiN-based solid solution. In the case of Ti(C,N) (1) and Ti(C,N) (2) coatings, the presence of titanium carbonitride was confirmed and in the case of (Al,Ti)N and (Al,Cr)N coatings, a diffraction analysis showed the presence of the AlN phase with a hexagonal lattice in the both coatings and of TiN and CrN phases, respectively. Moreover, the presence of reflexes from the substrate was determined in some cases, which is due to the fact that the thickness of the coatings is smaller than the penetration depth of X-ray beams inside the tested material.

The results of an X-ray qualitative phase analysis performed with Bragga-Brentano geometry of surface coatings of (Cr,Al,Si)N and (Al,Ti,Si)N type deposited onto ceramic-metallic tool materials (**Figure 9**) point out, as assumed, that coatings were produced on the surface of the investigated sintered carbides containing AlN and CrN phases. It is not possible to differentiate between AlN and (Al,Ti,Si)N, CrN and (Cr,Al,Si)N phases with diffraction methods because the phases are isomorphic, as, in fact, both (Al,Ti,Si)N and (Cr,Al,Si)N are secondary solid solutions based on chromium nitride CrN and aluminium nitride AlN, respectively.

It was found based on the analyses undertaken that a concentric intensity distribution of pole figures, varying along the axis of such figures, indicates the presence of a constituent axial texture

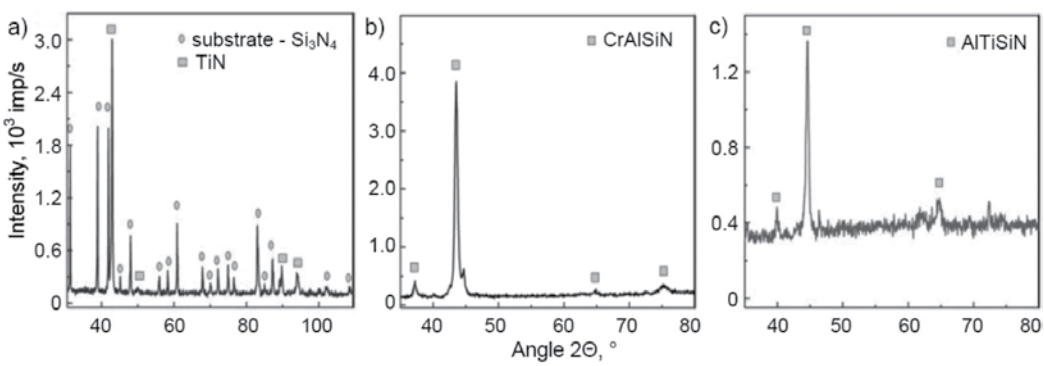

Figure 9. X-ray diffraction pattern of (a) Ti(B,N) coating deposited on the sialon ceramics, (b) CrN/(Cr,Al,Si)N coating and (c) AlN/(Al,Ti,Si)N coating deposited onto WS3 tool material, obtained by the Bragg-Brentano method.

http://dx.doi.org/10.5772/65400

of coatings produced with the cathodic arc evaporation technique on a substrate made of the investigated ceramic-metallic tool materials. Both, in the case of CrN/(Cr,Al,Si)N coatings and AlN/(Al,Ti,Si)N coatings, the intensity growth areas on the registered figures correspond to the double texture <200> and <311>, respectively, a quantitative fraction of the distinguished component <200> is 33 and 26% and of the component <311>–8.6 and 5.6% (**Figure 10**).

Variations in the atomic concentration of coating components in the direction perpendicular to the coating surface and concentration variations in the transition zone between the coating and the substrate material, depending on the number of layers deposited, were examined in a GDOS glow discharge optical spectrometer. The correct distribution of the elements forming part of the coatings and the substrate was determined. All the elements forming part of the investigated coatings occur only in the area of coatings and elements forming part of ceramics exist in the substrate area. The examinations confirm the existence of the relevant elements in the graded layers Ti(B,N), (Ti,Zr)N, Ti(C,N) (1), Ti(C,N) (2), (Al,Ti)N and in multilayer coatings Ti(C,N)+(Ti,Al)N, (Al,Cr)N+(Ti,Al)N, Ti(C,N)+Al_2O_3+TiN, Ti(C,N)+TiN (**Figure 11**). A curve of variations in a concentration of the elements forming the coatings shows their gradient structure.

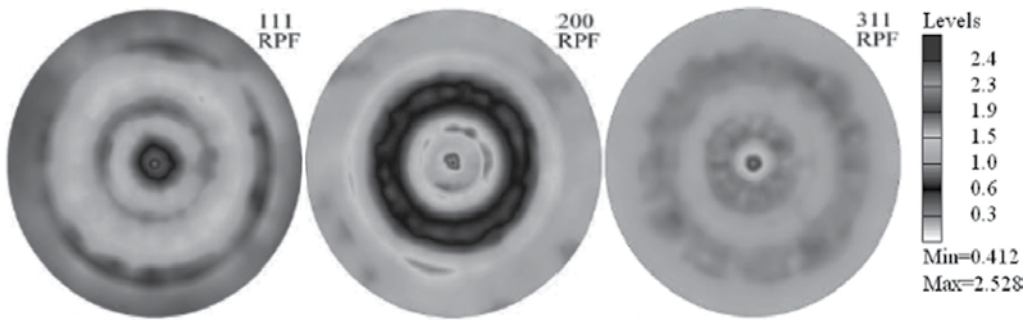

Figure 10. Pole figures (111), (200) and (311) of CrN/(Cr,Ti,Si)N coating on tool material WS1 calculated from FRO.

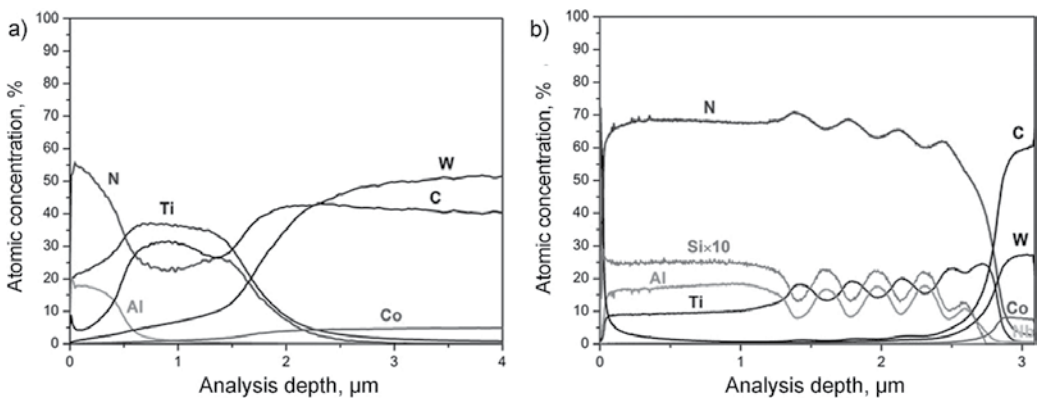

Figure 11. Changes analysed in the GDOS spectrometer of constituent concentration of (a) the Ti(C,N)+(Ti,Al)N coating on the sintered carbides substrate; (b) (Al,Ti,Si)N on WS1 ceramic-metallic tool material.

It was established through a GDOES analysis that a concentration of the elements forming part of the substrate is growing in a bonding zone from the surface of coatings with a reduction, at the same time, in a concentration of the elements forming part of the coating (**Figure 11**). This fact may be linked to the presence of a transition zone of a diffusive character between the substrate material and the coating, as suggested by the authors in earlier studies [1, 5, 57–59]. It cannot be precluded, however, that uneven evaporation of the material is possible at the same time from the surface of the specimens during an examination in a glow discharge spectrometer. The existence of a transition layer should be associated with the higher desorption of the substrate surface and with the formation of defects in a substrate as well as with the mixing of elements in a bonding zone due to the activity of high-energy ions. The existence of diffusive transition layers is supportive to the good adhesion of coatings to the substrate.

A profile analysis of chemical composition in the function of distance from the surface with the deposited (Cr,Al,Si)N and (Al,Ti,Si)N coatings on a substrate made of the investigated ceramic-metallic tool materials, as well as variations in a concentration of particular elements in a transition zone between such layers and a substrate material from the investigated ceramic-metallic tool materials were evaluated based on tests with a GDOS-850 glow discharge optical spectrometer (**Figure 12**). The character of variations in the substrate-coating bonding zone and between particular layers also confirms that transition layers exist here having the diffusive nature, as it was indicated earlier with respect to the other examined substrate materials.

An analysis of the chemical state of elements and of variations in a chemical concentration of components of (Cr,Al,Si)N and (Al,Ti,Si)N-type layers on a substrate made of the investigated ceramic-metallic tool materials was performed using the X-ray photoelectron spectroscopy (XPS) and auger electron spectroscopy (AES) technique (**Figure 12**). Photoelectric lines on an XPS spectrum obtained from a (Cr,Al,Si)N coating deposited onto a WS3 ceramic-metallic tool material, which are situated near the energy of 670.8 and 683.5 eV, derive from a 3d band of xenon atoms' electrons produced from the process of surface cleaning and are needed to create

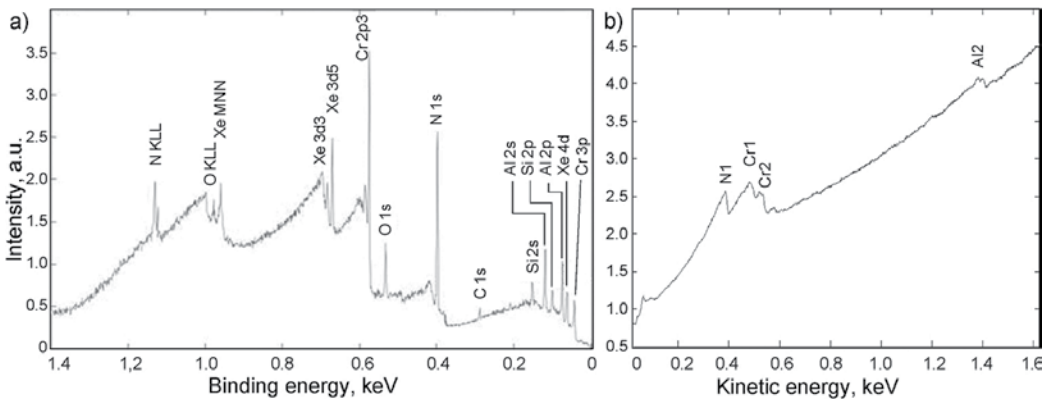

Figure 12. Spectrum of (a) XPS and (b) AES obtained from (Cr,Al,Si)N coating on tool ceramic-metallic material: (a) WS1 and (b) WS3; (a.u.)–arbitrary units.

http://dx.doi.org/10.5772/65400

a crater. The existence of the oxygen and carbon line should be associated with contamination. It was confirmed in chemical composition examinations with the AES method in areas created by etching with Xe+ ions that the chemical composition of the coatings is as assumed and a spectrum of Auger electrons obtained from the (Cr,Al,Si)N coatings has characteristic maximums corresponding to electron transitions for Cr LMM, Al KLL and N KLL.

It was also established based on fractographic tests carried out with a scanning electron microscope that the PVD and CVD coatings produced are deposited evenly and adhere tightly to the examined substrates (**Figure 13**). Particular layers in multilayer coating systems, i.e. Ti(C,N)+(Ti,Al)N, (Ti,Al)N+(Al,Cr)N, (Al,Cr)N+(Ti,Al)N, TiN+multiTiAlSiN+TiN, TiN+TiAlSiN+TiN, TiN+TiAlSiN+AlSiTiN, Ti(C,N)+Al_2O_3+TiN and Ti(C,N)+TiN, have a compact structure without delaminations and defects and tightly adhere to each other. The fractographic tests of sintered carbides and tool ceramics with coatings deposited by the PVD and CVD method do not reveal a fracture delamination along the separation area between the coating and the substrate, which also indicates good adhesion of the coatings produced to the substrate [60–62].

It was confirmed with X-ray diffraction methods and was described further in this chapter that multilayer Ti(C,N)+Al_2O_3+TiN and Ti(C,N)+TiN-type coatings fabricated with the CVD method in the coating-substrate interphase zone have a thin layer of a fine-grained TiC phase. Furthermore, a Ti(C,N) layer in CVD coatings is characterised by a structure changing in a gradient manner from a fine-grained structure near the substrate gradually transiting to a column structure. An Al_2O_3 layer exhibits a structure similar to a column structure. A top TiN layer in CVD coatings is very thin, thus preventing from determining its structure. A column structure of particular layers is also clearly visible in the case of two-layer Ti(C,N)+TiN and TiC+TiN coatings obtained on Si_3N_4 ceramics [60, 61].

It was also discovered by observing the fractures of PVD coatings that Ti(C,N) (1), (Al,Ti)N, (Ti,Al)N, Ti(C,N) (2), (Ti,Al)N+(Al,Cr)N, (Al,Cr)N+(Ti,Al)N coatings and (Al,Cr)N coatings fabricated by PVD possess a structure classified as the T zone according to Thornton's model [63]. Ti(B,N), (Ti,Zr)N coatings, though, feature a structure with thicker column grains (zone II

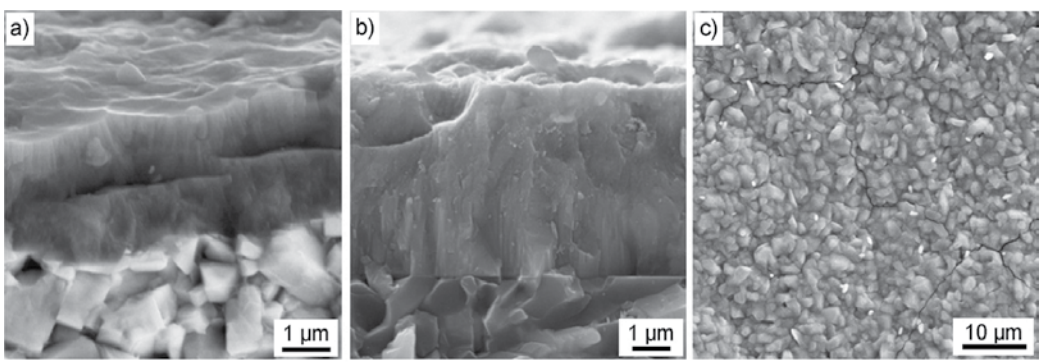

Figure 13. Fracture of the (a) Ti(C,N)+(Ti,Al)N coating deposited onto the sintered carbides substrate, (b) (Ti,Al)N+(Al,Cr)N coating deposited onto the sialon ceramics substrate and (c) surface topography of the Ti(C,N)+Al_2O_3+TiN coating deposited onto the cemented carbides substrate.

according to Thornton's model [63]). For a Ti(C,N)+(Ti,Al)N coating, the Ti(C,N) layer lying closer to the substrate and covering the two-third of the entire coating's thickness does not possess a column structure, but rather a fine-grained structure corresponding to the zone T according to Thornton's model. On the other hand, the (Ti,Al)N layer possesses a compact column structure classified as the transition zone between the zone T and zone II according to Thornton's model [63] (**Figure 13**).

The surface morphology of the coatings produced with the PVD technique is characterised by a high inhomogeneity because numerous droplet-shaped particles are present. The occurrence of such morphological defects is connected with the essence of the cathodic arc evaporation process. The size of such particles ranges between the tenths of a micrometer to a dozen or so micrometers. The presence of depressions was also discovered, which are formed, most probably, by solidified droplets being ejected after the end of the PVD process. For the coatings applied with the CVD method onto a substrate made of sintered carbides and tool ceramics, heterogeneity is seen in surface morphology related to the presence of multiple pores and networks of microcracks characteristic for such a process (**Figure 13c**). However, when an Al_2O_3 layer is situated on the substrate surface, or if this layer is in the under-the-surface zone (the top TiN layer is very thin), then the particles are needle-like or angularly shaped [60].

The observations of the surface morphology of (Cr,Al,Si)N and (Al,Ti,Si)N-type coatings on a substrate made of the investigated ceramic-metallic tool materials in a scanning electron microscope, in a microscope of atomic forces and in a confocal scanning microscope exhibit inhomogeneities connected with the occurrence of solidified microdroplets on the coating surface, characteristic for cathodic arc evaporation (**Figure 14**). Apart from droplets with a varied size of 1–5 μm, the agglomerates of particles with an elongated shape also exist, as well as depressions formed due to their ejection after finishing coating deposition. The examinations of chemical composition of microparticles, performed with an EDS spectrometer, indicate that Cr or Al prevails on their surface, which implies that these are metal droplets released from a disc, which solidify on the substrate surface.

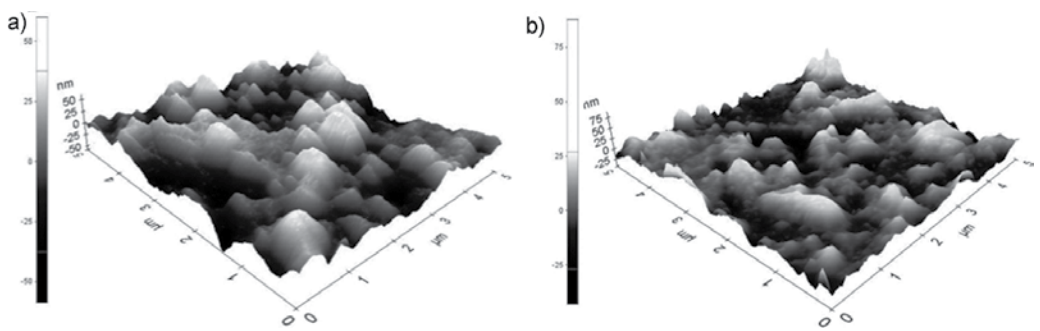

Figure 14. Surface topography of the following coatings (a) (Cr,Al,Si)N and (b) (Al,Ti,Si)N deposited onto ceramic-metallic tool material WS3; images produced using an atomic force microscope (AFM), 3D image.

http://dx.doi.org/10.5772/65400

It was found as a result of thin foils tests with an electron transmission microscope that coatings deposited in cathodic arc evaporation show a nanocrystalline structure. It was confirmed in a diffraction analysis that isomorphic phases exist with titanium nitride TiN in the case of TiN+multiTiAlSiN+TiN and Ti(B,N) coatings and the AlN phase with a hexagonal lattice in the case of an (Al,Ti)N coating. The presence of TiN and Al_2O_3 phases in TiN+Al_2O_3, TiN+Al_2O_3+TiN+Al_2O_3+TiN-type coatings was also confirmed, as assumed, in the investigations of coatings obtained by the CVD method. The Al_2O_3 layer structure with a rhombohedral lattice is characterised in its cross section by fine grains and grain size below 500 nm. A fine-crystalline structure of the TiN phase with a regular lattice is visible in the same cross section of thin foils between Al_2O_3 phase grains.

On the basis of investigations performed with an electron transmission microscope, (Cr,Al,Si)N and (Al,Ti,Si)N coatings were characterised, deposited onto a tool ceramic-metallic material, fabricated with the cathode arc evaporation (CAD) method with lateral arc rotating cathodes, composed of several layers and transition zones were investigated between the substrate as well as between the individual layers in the transmission mode and scanning-transmission mode, with BF and HAADF detectors (**Figure 15**). It was concluded based on the tests of thin foils from the cross section that they have a nanocrystalline and nanocomposite structure within the entire volume and they do not show discontinuities, cracks and porosity and have high homogeneity and a compact structure. The existence of several layers in nitride coatings was identified, both, based on Cr, Al and Si, as well as Al, Ti Si, exhibiting a varying thickness and chemical composition depending on the distance from the substrate. A layer deposited directly onto the near-the-core TiN layer shows a gradient character with a linearly decreasing concentration of Ti, accompanied by a heightening concentration of Al (**Figure 16a**) and the successive eight layers are characterised by a variable concentration of, respectively, Cr or Ti and Al (**Figure 16b**).

The HRTEM examinations of layers with a high concentration of Al prove the existence of nanograins with a differentiated orientation of planes showing the presence of long-range order typical in crystalline materials between which areas with a smaller degree of order

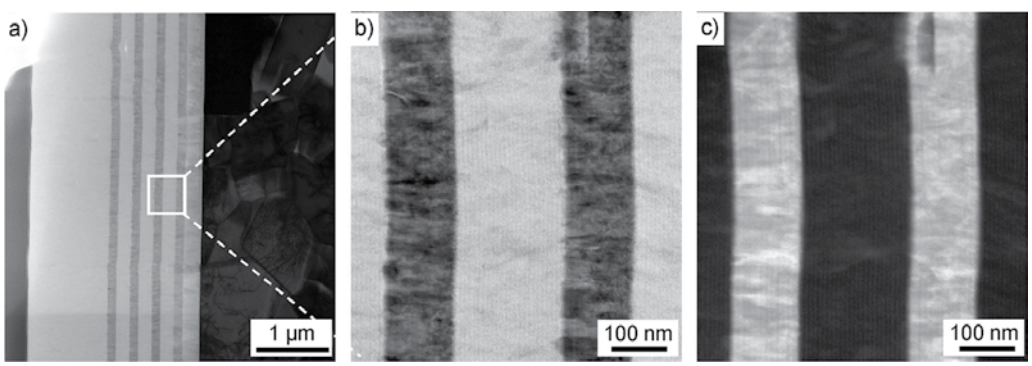

Figure 15. Structure of (Al,Ti,Si)N coatings; image in scanning-transmission mode with BF (a, b); HAADF (c) detector.

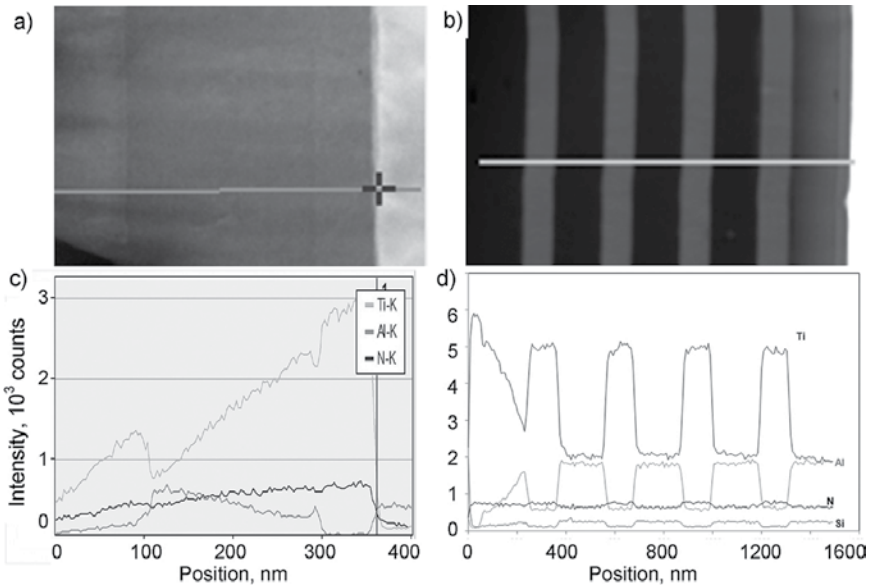

Figure 16. Profile analysis of variations in chemical composition made along the marked line using an energy dispersion spectrometer (a) and (b) of graded AlTiSiN layer (c) and (d) successive layers.

were identified. Structural observations and diffraction images using imaging in the HRTEM mode and the corresponding Fourier FFT transforms (**Figure 17**) confirm that the fabricated nitride coatings based on Al, Ti, Cr, Si exhibit a nanocrystalline and nanocomposite structure.

Profile and surface analyses of chemical composition variations performed with a high-resolution electron transmission microscope confirming the existence of transition layers between the substrate and coating and between individual layers with a varied concentration of Al and Ti may signify the existence of diffusive transition areas and thus contribute to the high adhesion of substrates produced with the cathodic arc evaporation method.

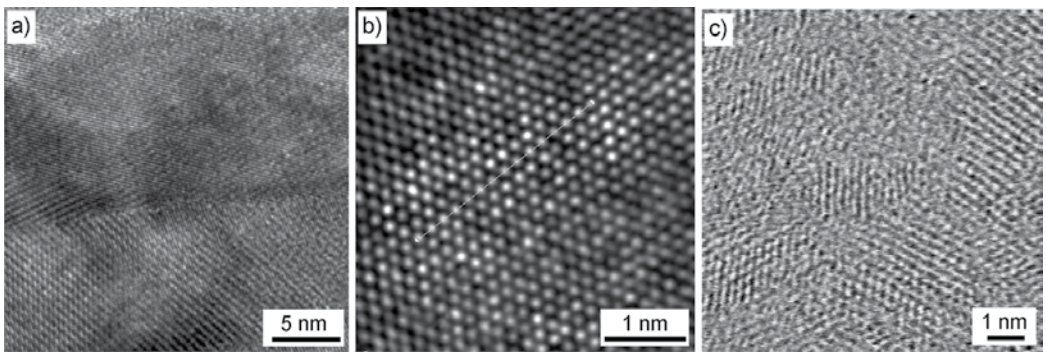

Figure 17. Coating structure (Al,Ti,Si)N (a) and (b) (3rd layer from substrate); image in HRTEM mode (c) (6th layer from substrate); image in scanning-transmission mode with BF detector.

http://dx.doi.org/10.5772/65400

5. Investigations into the properties of multicomponent coatings on the investigated sintered tool materials

The development directions of advanced tool materials, including sintered carbides, tool cermetals, tool ceramics and among others covered with anti-wear coatings, are pre-conditioning, to a high degree, improvements in the quality and efficiency of production. Enhanced operational properties are very frequently achieved for the commonly applied sintered tool materials by the deposition of coatings with PVD and CVD methods and not only simple monolayer or single-component coatings, but also complex multicomponent layers combining coatings with different properties, with each of them performing a relevant task and preferably continuous or graded coatings, with a gradual or continuous change of one or several components in the direction from the substrate to the outer surface, achieved in particular by PVD. The expected functional properties are achievable by selecting appropriately the substrate of indexable inserts and multicomponent coatings, also on sintered carbides and nitride and sialon ceramics. Their expected mechanical and operational properties can be ensured by forming the appropriate structure of coatings (presented in the previous chapter).

The thickness of the examined PVD coatings obtained on sintered carbides and nitride and sialon tool ceramics spans between 1.3 and 5.0 μm, while the thickness of CVD coatings between 2.8 and 10.0 μm. It was found as a consequence of the examinations performed that both PVD and CVD coatings on sintered carbides show a higher thickness than for substrates of the same type on a tool ceramics substrate. The exception are (Ti,Al)N and (Al,Cr)N coatings here, having a higher thickness on a sialon substrate. (Cr,Al,Si)N and (Al,Ti,Si)N coatings deposited onto ceramic-metallic tool materials are between 2.5 and 3 μm thick (**Table 3**).

The hardness of the sintered tool materials differs between 1826 HV for sintered carbides and 1850 HV for nitride ceramics and 2035 HV for sialon ceramics. The surface microhardness of the examined tool materials is greatly enhanced by depositing PVD and CVD coatings. The highest hardness is seen for multicomponent (Al,Ti)N coatings, TiN+multi(Ti,Al,Si)N+TiN multilayer coatings obtained by PVD, which accounts for nearly 100% growth in surface layer hardness in relation to the hardness of the uncoated material. The hardness of the examined coating systems is conditioning their abrasive wear, as seen most clearly for the TiN+Al_2O_3 coating—the hardest of the CVD coatings, thus contributing to the lower wear intensity of a tool cutting edge in cutting. To summarise, high abrasion resistance as well as good cutting properties of the tested tool ceramics with PVD and CVD coatings deposited are stemming from increased microhardness (**Table 3**).

It was pointed out in roughness examinations that the smallest value of the parameter R_a = 0.6 μm is seen for those surfaces of the examined sintered tool materials with no coating deposited. Following the deposition of PVD and CVD coatings onto the investigated substrates, the surface layer roughness increases and ranges R_a = 0.13–0.82 μm (**Table 3**). The increased surface roughness of the coatings deposited, in particular in the case of coatings obtained in a PVD process, should be associated with the character of the PVD cathodic arc evaporation process, as confirmed in morphological tests in a scanning electron microscope. The lowest value of the parameter R_a = 0.079 μm of ceramic-metallic tool materials is seen for the surface of the WS3

Process	Substrate	Coating	Thickness, μm	Roughness parameters R_a, μm	Microhardness, HV	Critical load Lc, N	Tool life, min
PVD	Cemented carbide	Ti(B,N)	1.8	0.29	2951	34	15
		(Ti,Zr)N	3.0	0.30	2842	40	13
		Ti(C,N) (1)	2.1	0.22	2871	49	13
		Ti(C,N)+(Ti,Al)N	2.8	0.31	3076	39	15
		Ti(C,N) (2)	2.1	0.50	3101	77	53
		(Al,Ti)N	2.5	0.18	3301	100	55
		(Ti,Al)N	3.5	0.39	3327	109	60
		(Al,Cr)N	3.8	0.28	2867	96	45
	Si_3N_4	TiN	0.8	0.34	2255	20	8
		TiN+multi(Ti,Al, Si)N+TiN	4.0	0.44	3592	22	10
		TiN+(Ti,Al,Si)N +TiN	2.0	0.45	2378	21	8
		TiN+(Ti,Al,Si)N +(Al,Si,Ti)N	2.5	0.32	2731	18	9
		Ti(B,N)	2.1	0.26	2898	12	8
		Ti(C,N)	2.1	0.34	3188	14	8
		(Ti,Zr)N	1.7	0.29	2798	30	12
		(Ti,Al)N	0.7	0.23	3408	42	14
	Sialon ceramics	(Ti,Al)N+(Al,Cr)N	4.0	0.45	3210	23	13
		(Al,Cr)N+(Ti,Al)N	3.9	0.44	2558	71	27
		Ti(C,N)+(Ti,Al)N	1.4	0.3	2786	36	6
		(Al,Ti)N	3.0	0.15	3600	112	72
		(Ti,Al)N	5.0	0.28	2961	21	9
		(Al,Cr)N	4.8	0.31	2230	53	50
		Ti(C,N) (2)	1.8	0.38	2843	26	9
		Ti(C,N) (1)	1.5	0.23	2872	25	5
		Ti(B,N)	1.3	0.25	2676	13	5
		(Ti,Zr)N	2.3	0.4	2916	21	5.5
	WS1	no coating	0	0.082	1621	–	14
	WS2		0	0.103	1497	–	11
	WS3		0	0.079	1711	–	16
	WS1	(Cr,Al,Si)N and nine layers	2.5–3	0.112	3388	116.2	78
	WS2		2.5–3	0.175	3250	100.4	59
	WS3		2.5–3	0.091	3472	124.6	82
	WS1		2.5–3	0.131	2856	104.3	62

Process	Substrate	Coating	Thickness, μm	Roughness parameters R_a, μm	Microhardness, HV	Critical load Lc, N	Tool life, min
	WS2	(Al,Ti,Si)N and nine layers	2.5–3	0.186	2252	97.2	50
	WS3		2.5–3	0.120	2908	112.3	68
	Cemented carbide	TiAlN	x	x	x	x	24
CVD	Cemented carbide	Ti(C,N) +Al_2O_3+TiN	8.4	0.63	2315	93	23
		Ti(C,N)+TiN	5.0	0.40	2443	110	27
	Si_3N_4	Ti(C,N)+TiN	4.2	0.15	2268	52	8
		Ti(C,N) +Al_2O_3+TiN	9.5	0.28	2050	27	8
		TiC+TiN	5.4	0.25	2020	67	10
		TiC+Ti(C,N) +Al_2O_3+TiN	7.8	0.27	3025	32	8
		TiN+ Al_2O_3	10.0	0.45	3320	83	16
		TiN+Al_2O_3+TiN	3.8	0.13	2487	48	15
		Al_2O_3+TiN (1)	2.6	0.25	2676	45	16
		Al_2O_3+TiN (2)	1.7	0.23	2775	27	14
		TiN+Al_2O_3+TiN+ Al_2O_3+TiN	4.5	0.6	2571	41	20
	Sialon ceramics	Ti(C,N) +Al_2O_3+TiN	7.0	0.82	2669	43	10
		Ti(C,N)+TiN	2.8	0.2	2746	72	15

x material used for comparison

Table 3. The results of the properties of sintered tool materials with the PVD and CVD coatings deposited.

material without a coating deposited. The roughness of WS1 and WS2 materials without coatings deposited is R_a = 0.082 and R_a = 0.103 μm, respectively. The results confirm that the deposition of (Cr,Al,Si)N and (Al,Ti,Si)N coatings applied onto substrates made of tool materials increases surface layer roughness and ranges R_a = 0.091–0.186 μm. The critical load value *L*c measuring the adhesion of PVD and CVD coatings to a substrate made of sintered carbides and nitride and sialon tool ceramics was determined in a scratch test. The critical load was determined as such corresponding to an increase in acoustic emission indicating the beginning of coating chipping and verification was made by measuring the friction force (F_t) of a diamond indenter and through metallographic observations in a light microscope connected to a measuring instrument. The critical load value *L*c (AE) for PVD coatings is between 13 and 131 N and for CVD coatings—between 15 and 110 N (**Table 3**). In the case of coatings deposited by the PVD method on sintered carbides, the best substrate adhesion is exhibited by (Ti,Al)N coatings, for which a critical load value *L*c = 109 N, whereas the weakest substrate adhesion is seen for the Ti (B,N) coatings, where *L*c = 34 N. The coatings deposited by the CVD method onto a substrate

made of sintered carbides show a high critical load of *Lc* = 93 N for a Ti(C,N)+Al_2O_3+TiN coating and *Lc* = 110 N for a Ti(C,N)+TiN coating [60, 61, 64]. The highest critical load of *Lc* = 112 N for the PVD coatings obtained on nitride and sialon ceramics is shown by an (Al,Ti)N coating, whilst the lowest of *Lc* = 13 N for a Ti(B,N) coating. Critical loads for the coatings obtained by CVD on nitride and sialon ceramics are between 27 and 83 N (**Table 3**). The highest critical load value of *Lc* = 124.6 N and *Lc* = 112.3 N, respectively, was identified for CrAlSiN and AlTiSiN coatings deposited onto a WS3-type substrate, as compared to WS1 and WS2 substrates. The similar dependencies were obtained for a WS1 and WS2 substrate (**Table 3**). The very good adhesion of PVD coatings, especially to a substrate made of sintered carbides and newly created ceramic-metallic tool materials and of CVD coatings to a substrate made of tool ceramics, stems from the fact that transition zones exist created at the substrate-coating boundary and at the boundary between two layers, as confirmed by tests with a transmission electron microscope and in a glow discharge spectrometer GDOES presented in the previous chapter. Coating damages formed as a result of adhesion tests with the scratch method were identified on the basis of observations in a scanning electron microscope. It was discovered subsequently to the observations that damages to PVD and CDV coatings are of the abrasive wear nature and are also characterised by a high number of single- or double-sided coating cracks at the scratch peripheries and by a delamination inside the scratch leading to coating delamination at the interface with the scratch. An increasing load during a scratch test is leading to intensified cracks at the scratch peripheries, causing a partial coating delamination. The periodical chipping of coatings also occurs (**Figure 18a**). CrAlSiN coatings deposited onto tool ceramic-metallic materials possess better substrate adhesion than AlTiSiN coatings. In the case of CrAlSiN coatings, the conformal fractures caused by stretching exist in the zone of first damages, changing into small flakings situated on the scratch bottom and peripheries and flakings and small arc chippings exist at the central zone of the scratch. Intensified conformal fractures, delamination and partial coating fragmentation take place on the scratch bottom as a load are increasing and single peripheral damages combine, thus forming local coating delamination

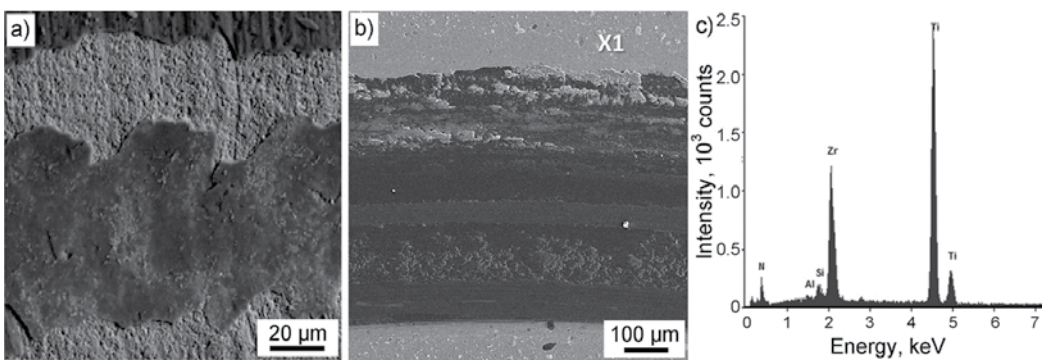

Figure 18. (a) Indenter mark for load above the critical load and the image of damages created as a result of scratch-test of Ti(B,N) coating deposited onto sintered carbides, (b) trace of tribological damage on the surface of (Ti,Zr)N coating deposited onto the substrate made of sialon ceramics and (c) diagrams of energy of backscatter X-ray radiation from the micro-area X1.

http://dx.doi.org/10.5772/65400

bands at most. The complete delamination of the CrAlSiN coating does not emerge in the final zone of the scratch with the maximum load on the penetrator.

An abrasion strength test with the pin-on-disc method was undertaken to determine fully the functional and operational characteristic of the investigated PVD and CVD coatings deposited onto a substrate of the selected sintered materials. The tests carried out show that the coatings deposited by CVD have worse tribological properties as compared to coatings deposited with the PVD technology. Coating damages to the substrate material zone occur in almost all the cases of the examined coatings. Damages to such coatings are accompanied by lost adhesion. The most frequent coating wear mechanisms are chippings and flaking as well as partial delamination (**Figure 18b** and **c**). An abrasive wear resistance test under dry slide friction conditions with the ball-on-plate method at room temperature was performed to determine the tribological properties of the examined coatings deposited on ceramic-metallic tool materials. It was stated by analysing the profiles of wear tracks formed after a tribological wear (after the distance of 500 m) that the maximum depths of wear are smaller than the thickness of a CrAlSiN, as well as an AlTiSiN layer, signifying that have not been fully worn. It can be concluded by analysing a field area of a wear track section of coatings and substrates that a CrAlSiN coating has the lowest wear index. An AlTiSiN coating has a larger field area of the wear track section and a higher wear index versus a CrAlSiN coating. The highest wear index is seen for a substrate made of WS3 tool materials.

The service life of the examined sintered tool materials was identified based on technological cutting tests. It was found as a result of cutting ability tests that the highest service life of $T = 72$ min was achieved for a cutting edge coated with an (Al,Ti)N coating, while the lowest life of $T = 5$ min on the same substrate is exhibited by Ti(B,N) and Ti(C,N) (1) coatings. The life of an uncoated cutting edge made of sialon ceramics was estimated at $T = 11$ min, which allows to confirm that (Al,Ti)N, (Al,Cr)N and Ti(C,N)+TiN coatings contribute to the enhanced life of a sialon cutting edge. A (Ti,Al)N coating has the greatest effect on the cutting edge life of $T = 60$ min for sintered carbide plates and slightly lower of $T = 55$ and 53 min, respectively, for (Al,Ti)N and Ti(C,N)(2) coatings. In the case of sintered carbides, all coatings increase the cutting edge life because the durability of an uncoated tool is $T = 2$ min, whilst the durability of plates with the lowest cutting ability with (Ti,Zr)N and Ti(C,N)(1) coatings is $T = 13$ min. A clear anti-wear impact of the presence of the combined Al_2O_3+TiN and TiN+Al_2O_3 coatings on the life of the inserts was found as a result of the grey cast iron rolling tests made with Si_3N_4 tool ceramics. A broad cutting edge durability range depending on the type of the applied coating was attained both for coated sintered carbides and coated tool nitride and sialon ceramics (**Table 3**). The hardness of ceramic-metallic tool materials as a substrate in a surface zone ranges between 1497 and 1711 HV0.1. After the deposition of CrAlSiN, AlTiSiN coatings on the examined WS1, WS2, WS3 ceramic-metallic tool materials, microhardness is growing substantially in the near-the-surface zone as compared to an uncoated substrate (**Table 3**). Dependence between substrate hardness and hardness of the deposited coating was not found. Where nanocrystalline, nanocomposite anti-wear coatings of CrAlSiN and AlTiSiN types are deposited onto tool materials, microhardness is growing substantially in the near-the-surface zone and—in connection with high substrate adhesion—contributes to lower wear intensity of cutting tools made from such materials, as was confirmed in the operational examinations. It was found as a result of metallographic observations in a scanning electron microscope for the

examined indexable inserts that the tools subjected to a cutting test indicate wear according to the abrasion and adhesion mechanism.

Additional information

The chapter was partially supported in the framework of the project 'NANOCOPOR—determining the importance of the effect of the one-dimensional nanostructural materials on the structure and properties of newly developed functional nanocomposite and nanoporous materials', funded by the DEC-2012/07/B/ST8/04070 of the Polish National Science Centre in the framework of the 'OPUS' competitions, headed by Prof. Leszek A. Dobrzański.

Author details

Leszek A. Dobrzański*, Daniel Pakuła, Klaudiusz Gołombek, Anna D. Dobrzańska-Danikiewicz and Marcin Staszuk

*Address all correspondence to: leszek.adam@gmail.com

Mechanical Engineering Faculty, Silesian University of Technology, Gliwice, Poland

References

[1] Dobrzański LA, Pakuła D, Staszuk M, Dobrzańska-Danikiewicz AD. Structure and properties of composite coatings on sintered carbide and nitride and sialon ceramics. Open Access Library. 2015;**5**:1–173 (in Polish).

[2] Dobrzański LA, Matula G. Powder metallurgy fundamentals and sintered materials. Open Access Library. 2012;**8**:1–156 (in Polish).

[3] Dobrzański LA. Engineering materials and materials design. Fundamentals of materials science and physical metallurgy. 2nd ed. Warsaw: WNT; 2006. 1600 p. (in Polish). ISBN 83-204-3249-9.

[4] Ruys A, Gingu O, Sima G, Maleksaeedi S. Powder processing of bulk components in manufacturing. In: Nee AYC, editor. Handbook of Manufacturing Engineering and Technology. London: Springer-Verlag; 2015. pp. 487–566. DOI: 10.1007/978-1-4471-4670-4_48.

[5] Gołombek K. Structure and properties of injection moulding tool materials with nanocrystalline coatings. Open Access Library. 2013;**1**:1–136 (in Polish).

[6] Dobrzański LA, Matula G. Powder injection molding: sinter-hardening. In: Colás R, Totten GE, editors. Encyclopedia of Iron, Steel and Their Alloys. Boca Raton: CRC Press, Taylor & Francis Group; 2016. 14 p. ISBN: 978-1-4665-1104-0.

[7] Matula G. Gradient surface layers from tool cermets formed pressurelessly and sintered. Open Access Library. 2012;**7**:1–144 (in Polish).

[8] German RM. Powder Metallurgy and Particulate Materials Processing. Princeton: Metal Powder Industries Federation; 2005. 528 p. ISBN 0-9762057-1-8.

[9] Kim S, Han SH, Park JK, Kim HE. Variation of WC grain shape with carbon content in the WC–Co alloys during liquid-phase sintering. Scripta Materialia. 2003;**48**:635–639. DOI: 10.1016/S1359-6462(02)00464-5.

[10] Holmberg K, Matthews A, editors. Coating Tribology. Properties, Mechanisms, Techniques and Applications in Surface Engineering. Tribology and Interface Engineering Series No. 56. Amsterdam: Elsevier; 2009. 576 p. ISBN 978-0-444-52750-9.

[11] Xiong J, Guo Z, Yang M, Wan W, Dong G. Tool life and wear of WC–TiC–Co ultrafine cemented carbide during dry cutting of AISI H13 steel. Ceramics International. 2013;**39**:337–346. DOI: 10.1016/j.ceramint.2012.06.031.

[12] Liu Y, Wang H, Long Z, Liaw PK, Yang J, Huang B. Microstructural evolution and mechanical behaviors of graded cemented carbides. Materials Science and Engineering: A. 2006;**426**:346–354. DOI: 10.1016/j.msea.2006.04.018.

[13] Zhang S. Handbook of Nanostructured Thin Films and Coatings. Boca Raton, London, New York: CRC Press, Taylor & Francis Group; 2010. 1232 p. ISBN 978-1420094350.

[14] Eriksson M, Radwan M, Shen Z. Spark plasma sintering of WC, cemented carbide and functional graded materials. International Journal of Refractory Metals and Hard Materials. 2013;**36**:31–37. DOI: 10.1016/j.ijrmhm.2012.03.007.

[15] German RM. Markets applications and financial aspects of global metal powder injection moulding (MIM) technologies. Metal Powder Report. 2012;**1**:18–26. DOI: 10.1016/S0026-0657(12)70051-6.

[16] Dobrzański LA, Matula G, Herranz G, Várez A, Levenfeld B, Torralba JM. Metal injection moulding of HS12-1-5-5 high-speed steel using a PW-HDPE based binder. Journal of Materials Processing Technology. 2006;**175**:173–178. DOI: 10.1016/j.jmatprotec.2005.04.033.

[17] Várez A, Levenfeld B, Torralba JM, Matula G, Dobrzański LA. Sintering in different atmospheres of T15 and M2 high speed steels produced by modified metal injection moulding process. Materials Science and Engineering: A. 2004;**366**:318–324. DOI: 10.1016/j.msea.2003.08.028.

[18] Matula G, Dobrzański LA, Várez A, Levenfeld B, Torralba JM. Comparison of structure and properties of the HS12-1-5-5 type high-speed steel fabricated using the pressureless forming and PIM methods. Journal of Materials Processing Technology. 2005;**162–163**:230–235. DOI: 10.1016/j.jmatprotec.2005.02.1.

[19] Dobrzański LA, Matula G, Várez A, Levenfeld B, Torralba JM. Structure and mechanical properties of HSS HS6-5-2- and HS12-1-5-5-type steel produced by modified powder

injection moulding process. Journal of Materials Processing Technology. 2004;**157–158**:658–668. DOI: 10.1016/j.jmatprotec.2004.07.1.

[20] Gołombek K, Matula G, Mikuła J, Dobrzański LA. Influence of binder composition on the properties of feedstock for cemented carbides. Archives of Materials Science and Engineering. 2011;**51**:116–124.

[21] Dobrzański LA, Matula G, Várez A, Levenfeld B, Torralba JM. Fabrication methods and heat treatment conditions effect on tribological properties of high speed steels. Journal of Materials Processing Technology. 2004;**157–158**:324–330. DOI: 10.1016/j.jmatprotec.2004.09.051

[22] Mikuła J, Matula G, Gołombek K, Dobrzański LA. Sintered composite gradient tool materials. Archives of Materials Science and Engineering. 2008;**32**:25–28.

[23] Matula G, Dobrzański LA, Ambroziak M. Simulation of powder injection moulding conditions using cadmould program. Journal of Achievements in Materials and Manufacturing Engineering. 2012;**55**:556–560.

[24] Matula G, Dobrzański LA, Várez A, Levenfeld B. Development of a feedstock formulation based on PP for MIM of carbides reinforced M2. Journal of Achievements in Materials and Manufacturing Engineering. 2008;**27**:195–198.

[25] Matula G, Dobrzański LA, Herranz G, Várez A, Levenfeld B, Torralba JM. Structure and properties of HS6-5-2 type HSS manufactured by different P/M methods. Journal of Achievements in Materials and Manufacturing Engineering. 2007;**24**:71–74.

[26] Dobrzański LA, Gołombek K, Lukaszkowicz K. Physical vapor deposition in manufacturing. In: Nee AYC, editor. Handbook of Manufacturing Engineering and Technology. London: Springer-Verlag; 2015. pp. 2719–2754. DOI: 10.1007/978-1-4471-4670-4_29.

[27] Dobrzański LA, Dobrzańska-Danikiewicz AD. Engineering materials surface treatment. Open Access Library. 2011;**5**:1–480 (in Polish).

[28] Dobrzański LA, Pakuła D, Staszuk M. Chemical vapor deposition in manufacturing. In: Nee AYC, editor. Handbook of Manufacturing Engineering and Technology. London: Springer-Verlag; 2015. pp. 2755–2803. DOI: 10.1007/978-1-4471-4670-4_30.

[29] Lukaszkowicz K, Dobrzański LA, Sondor J. Microstructure, mechanical properties and corrosion resistance of nanocomposite coatings deposited by PVD technology. In: Reddy BSR, editor. Advances in Diverse Industrial Applications of Nanocomposites. Rijeka: InTech; 2011. pp. 1–16. DOI: 10.5772/14117.

[30] Staszuk M, Dobrzański LA, Tański T, Kwaśny W, Musztyfaga-Staszuk M. The effect of PVD and CVD coating structures on the durability of sintered cutting edges. Archives of Metallurgy and Materials. 2014;**59**:269–274. DOI: 10.2478/amm-2014-0044.

[31] Dobrzański LA, et al. Investigations of Structure and Properties of Newly Created Porous Biomimetic Materials Fabricated by Selective Laser Sintering, BIOLASIN. Project UMO-2013/08/M/ST8/00818. Gliwice: Silesian University of Technology; 2013–2016.

[32] Dobrzański LA. Applications of newly developed nanostructural and microporous materials in biomedical, tissue and mechanical engineering. Archives of Materials Science and Engineering. 2015;**76**:53–114.

[33] Dobrzański LA, Dobrzańska-Danikiewicz AD, Gaweł TG, Achtelik-Franczak A. Selective laser sintering and melting of pristine titanium and titanium Ti6Al4V alloy powders and selection of chemical environment for etching of such materials. Archives of Metallurgy and Materials. 2015;**60**:2039–2045. DOI: 10.1515/amm-2015-0346.

[34] Dobrzański LA, Dobrzańska-Danikiewicz AD, Malara P, Gaweł TG, Dobrzański LB, Achtelik-Franczak A. Fabrication of scaffolds from Ti6Al4V powders using the computer aided laser method. Archives of Metallurgy and Materials. 2015;**60**:1065–1070. DOI: 10.1515/amm-2015-0260.

[35] Kremzer M, Dobrzański LA, Dziekońska M, Macek M. Atomic layer deposition of TiO_2 onto porous biomaterials. Archives of Materials Science and Engineering. 2015;**75**:63–69.

[36] Dobrzański LA, Dobrzańska-Danikiewicz AD, Szindler M, Achtelik-Franczak A, Pakieła W. Atomic layer deposition of TiO_2 onto porous biomaterials. Archives of Materials Science and Engineering. 2015;**75**:5–11.

[37] Dobrzański LA, Dobrzańska-Danikiewicz AD, Achtelik-Franczak A, Dobrzański LB. Comparative analysis of mechanical properties of scaffolds sintered from Ti and Ti6Al4V powders. Archives of Materials Science and Engineering. 2015;**73**:69–81.

[38] Dobrzański LA, Dobrzańska-Danikiewicz AD, Gaweł TG. Ti6Al4V porous elements coated by polymeric surface layer for biomedical applications. Journal of Achievements in Materials and Manufacturing Engineering. 2015;**71**:53–59.

[39] Lukaszkowicz K, Dobrzański LA, Kokot G, Ostachowski P. Characterization and properties of PVD coatings applied to extrusion dies. Vacuum. 2012;**86**:2082–2088. DOI: 10.1016/j.vacuum.2012.04.025.

[40] Dobrzański LA, Staszuk M, Gołombek K, Śliwa A, Pancielejko M. Structure and properties PVD and CVD coatings deposited onto edges of sintered cutting tools. Archives of Metallurgy and Materials. 2010;**55**:187–193.

[41] Dobrzański LA, Żukowska LW, Mikuła J, Gołombek K, Pakuła D, Pancielejko M. Structure and mechanical properties of gradient PVD coatings. Journal of Materials Processing Technology. 2008;**201**:310–314. DOI: 10.1016/j.jmatprotec.2007.11.283.

[42] Dobrzański LA, Pakuła D, Kříž A, Soković M, Kopač J. Tribological properties of the PVD and CVD coatings deposited onto the nitride tool ceramics. Journal of Materials Processing Technology. 2006;**175**:179–185. DOI: 10.1016/j.jmatprotec.2005.04.032.

[43] Dobrzański LA, Gołombek K, Hajduczek E. Structure of the nanocrystalline coatings obtained on the CAE process on the sintered tool materials. Journal of Materials Processing Technology. 2006;**175**:157–162. DOI: 10.1016/j.jmatprotec.2005.04.008.

[44] Dobrzański LA, Mikuła J. The structure and functional properties of PVD and CVD coated Al_2O_3 + ZrO_2 oxide tool ceramics. Journal of Materials Processing Technology. 2005;**167**:438–446. DOI: 10.1016/j.jmatprotec.2005.05.034.

[45] Soković M, Mikuła J, Dobrzański LA, Kopač J, Kosec L, Panjan P, Madejski J, Piech A. Cutting properties of the Al_2O_3 + $SiC_{(w)}$ based tool ceramic reinforced with the PVD and CVD wear resistant coatings. Journal of Materials Processing Technology. 2005;**164–165**:924–929. DOI: 10.1016/j.jmatprotec.2005.02.071.

[46] Dobrzański LA, Pakuła D. Comparison of the structure and properties of the PVD and CVD coatings deposited on nitride tool ceramics. Journal of Materials Processing Technology. 2005;**164–165**:832–842. DOI: 10.1016/j.jmatprotec.2005.02.094.

[47] Dobrzański LA, Mikuła J. Structure and properties of PVD and CVD coated Al_2O_3 + TiC mixed oxide tool ceramics for dry on high speed cutting processes. Journal of Materials Processing Technology. 2005;**164–165**:822–831. DOI: 10.1016/j.jmatprotec.2005.02.089.

[48] Dobrzański LA, Gołombek K. Structure and properties of the cutting tools made from cemented carbides and cermets with the TiN+mono-, gradient- or multi(Ti,Al,Si)N+TiN nanocrystalline coatings. Journal of Materials Processing Technology. 2005;**164–165**:805–815. DOI: 10.1016/j.jmatprotec.2005.02.072.

[49] Pakuła D, Dobrzański LA, Gołombek K, Pancielejko M, Kříž A. Structure and properties of the Si_3N_4 nitride ceramics with hard wear resistant coatings. Journal of Materials Processing Technology. 2004;**157–158**:388–393. DOI: 10.1016/j.jmatprotec.2004.09.060.

[50] Gołombek K, Dobrzański LA, Soković M. Properties of the wear resistant coatings deposited on the cemented carbides substrates in the cathodic arc evaporation process. Journal of Materials Processing Technology. 2004;**157–158**:341–347. DOI: 10.1016/j.jmatprotec.2004.09.053.

[51] Dobrzański LA, Pakuła D, Hajduczek E. Structure and properties of the multicomponent TiAlSiN coatings obtained in the PVD process in the nitride tool ceramics. Journal of Materials Processing Technology. 2004;**157–158**:331–340. DOI: 10.1016/j.jmatprotec.2004.09.052.

[52] Dobrzański LA, Dobrzańska-Danikiewicz AD. Foresight of the surface technology. In: Nee AYC, editor. Handbook of Manufacturing Engineering and Technology. London: Springer-Verlag; 2015. pp. 2597–2637. DOI: 10.1007/978-1-4471-4670-4_26

[53] Dobrzańska-Danikiewicz AD. Foresight of material surface engineering as a tool building a knowledge-based economy. Materials Science Forum. 2012;**706–709**:2511–2516. DOI: 10.4028/www.scientific.net/MSF.706-709.2511.

[54] Dobrzańska-Danikiewicz AD. The book of critical technologies of surface and properties formation of engineering materials. Open Access Library. 2012;**6**:1–823 (in Polish).

[55] Dobrzańska-Danikiewicz AD. The acceptation of the production orders for the realisation in the manufacturing assembly systems. Journal of Materials Processing Technology. 2006;**175:**123–132. DOI: 10.1016/j.jmatprotec.2005.04.001.

[56] Krenczyk D, Dobrzańska-Danikiewicz A. The deadlock protection method used in the production system. Journal of Materials Processing Technology 2005;**164–165**:123–132. DOI: 10.1016/j.jmatprotec.2005.02.056

[57] Gołombek K. Structure and properties of the cemented carbides and tool cermets covered of wear resistant coatings in the PVD process [Ph.D. Thesis]. Gliwice, Poland: Silesian University of Technology; 2001 (in Polish).

[58] Adamiak M. Structure and properties of the TiN and Ti(C,N) PVD coatings deposited on high speed steels [Ph.D. Thesis]. Gliwice, Poland: Silesian University of Technology; 1997 (in Polish).

[59] Lukaszkowicz K. Forming the structure and properties of hybrid coatings on reversible rotating extrusion dies. Journal of Achievements in Materials and Manufacturing Engineering. 2012;**55**:159–224.

[60] Pakuła D. Structure and properties of the multilayers PVD and CVD wear resisted coatings on the Si_3N_4 tool nitride ceramics [Ph.D. Thesis]. Gliwice, Poland: Silesian University of Technology; 2003 (in Polish).

[61] Staszuk M. Structure and properties of the gradient PVD and CVD coatings on the sialons and sintered carbides [Ph.D. Thesis]. Gliwice, Poland: Silesian University of Technology; 2009 (in Polish).

[62] Pakuła D. Forming of the surface structure and properties of tool's ceramic inserts with improved abrasion resistance. Archives of Materials Science and Engineering. 2013;**62**:55–96.

[63] Thornton JA. The microstructure of sputter-deposited coatings. Journal of Vacuum Science and Technology A. 1986;**4**:3059–3065. DOI: 10.1116/1.573628.

[64] Pakuła D, Staszuk M, Dobrzański LA. Investigations of the structure and properties of PVD coatings deposited onto sintered tool materials. Archives of Materials Science and Engineering. 2012;**58**:219–226.

Chapter 14

Powder Eutectic Materials of Fe-Mn-C-B System for Coatings of Increased Abrasive Wear

Mykhaylo Pashechko, Klaudiusz Lenik,
Joanna Szulżyk-Cieplak and Aneta Duda

Additional information is available at the end of the chapter

http://dx.doi.org/10.5772/66873

Abstract

In this chapter, selected problems of manufacturing coatings with high wear resistance obtained based on eutectic materials of the quaternary Fe-Mn-C-B system are discussed. With regard to the structural state and physico-mechanical properties of eutectic powder alloys and coatings correspond to the composite dispersion-strengthened materials. The formation of a hardened layer with the structure of eutectic on the metal surface is the creation of a new material with certain mechanical properties. The analysis of different material properties and of alloy addition enabled to work out new eutectic powder alloys based on iron of the Fe-Mn-C-B system. In particular, it enabled to determine eutectic ranges and element contents.

Keywords: powder materials, eutectic, coating, wear, quasi-ternary

1. Introduction

One of the basic possibilities for obtaining surface layers with present properties is to apply coatings of powder based on eutectic alloys of, among other systems, the quaternary Fe-Mn-C-B system to specific material. Such materials offer the possibility of selecting multi-component eutectic alloys by alloying with elements such as silicon, nickel, chromium. These components are most frequently used to obtain products with required wear resistance properties of their surfaces. It means that the research on selection of such materials relates to searching for answers concerning the possibility of producing eutectic alloys as a family of multiphase dispersion-strengthened composite alloys with a structural gradient.

2. Materials and methods

The issue discussed in this chapter relates to new materials, particularly resistant to the abrasive wear, and it has been the subject of permanent research for many years. This subject matter is of current interest due to the development and requirements for properties of various friction pairs used under increasingly new conditions. Such steel elements of some machines represent a group of items for which the research is conducted with regard, but not limited, to production of new composites with specified properties of their surface layers. The main issue for their development is the analysis of phase equilibrium systems. This also applies to the manufacture of new powder materials as eutectic alloys.

The equilibrium systems can be used as a basis for determination of phase composition, existence area and possible phase transitions in the production of eutectic alloys. The analysis of physico-chemical properties of alloying elements, considering possible phase transitions in the system, allows the possibilities of introducing elements into a specific alloy to be evaluated and the nature of their impact to be determined.

The production of solid solutions, chemical compounds, mixture of specified elements with proper predetermined structure and alloy content makes it possible to predict the properties of produced alloys based on properties of input components. In other words, there is a specific relationship between the equilibrium system and the properties of alloys. In practice, a lot of useful alloyed materials consist of more than two components, although the literature has mainly described and studied two-component systems and not many three-component ones, and there are almost no studies on systems consisting of a higher number of components [1–3]. Taking into consideration the positive impact of borides and carbides (in particular, iron and manganese ones) on physico-mechanical properties, operating characteristics of materials and surface layers as well as specific features of producing eutectic layers, the equilibrium systems with eutectic transition using specified elements (components) were analysed. The analysis shows that eutectic systems are obtained in Fe-C, Fe-B, Fe-Mn-C, Fe-Cr-C and Fe-Ni-C systems (**Table 1**) [4, 5].

For production of materials with specified properties of resistance to the abrasive wear, Fe_3C carbides as well as Fe_2B, FeB and Cr_2B borides were selected. The selection of carbides and borides as dispersion (strengthening) phases within the structure of alloy is dictated by their high hardness, wear resistance, corrosion resistance and thermal stability. Furthermore, the addition of manganese allows the ductility of Fe_3C iron carbide and produced eutectic alloy to be increased. Mn forms a solid solution with iron, extends the temperature-concentration area of the existence of Fe_3C-Mn_3C carbides and, at the same time, increases the dispersibility of their distribution [6].

In all equilibrium systems, the formation of eutectic areas is caused by the effects of elements such as Fe, Mn, C, B, Si, Ni and Cr. The discussed research is focused on increasing the yield point of surface layers while ensuring their high hardness. This can be achieved owing to formation of various eutectic layers by introducing (alloying) elements to increase the hardness and ductility. In view of the foregoing and by analysing the properties of phase components, most efficient turns out to be the Fe-B-C system followed by the Fe-Mn-C one [7]. Therefore, it is appropriate to produce powder materials and eutectic layers of the Fe-Mn-C-B system.

http://dx.doi.org/10.5772/66873

System	Alloying elements	Content of elements in eutectic alloy wt%	Phase composition of alloy	Melting point, K	
				Eutectic mixture	Alloying element
Fe-B-C	Fe	95.6	α-Fe + Fe_2B + Fe_3C	1373	1811
	B	2.9			2350
	C	1.5			4413
Fe-Mn-C	Fe	97.4–86.6	α-Fe+$(Fe, Mn)_3C$	1473	1811
	Mn	2.2–13			1518
	C	0.4			4413
Fe-Ni-B	Fe	70.2	γ-Fe + $(Fe, Ni)_2B$ + $(Fe, Ni)_3B$	–	1811
	Ni	25.0			1728
	B	4.8			2350
Fe-Cr-C	Fe	88.4	γ-Fe + F_3C + Cr_7C_3		1811
	Cr	8			2122
	C	3.6			4413
Fe-Ni-C	Fe	48	γ-$(Fe, Ni)_2B$ + Fe_3C		1811
	Ni	50			1728
	C	2			4413

Table 1. Characteristics of eutectic alloys formed based on iron and selected elements.

In the Fe-Mn-C system, there is a very durable $(Fe, Mn)_7(B, C)_3$ phase with rhombic structure. Ternary intersection of the Fe-Mn-C system [3] shows that the eutectic existence area is restricted by the carbon content only and, what is more, over a wide range of concentrations (0.2–0.8 wt%), while manganese content is not limited according to iron because of their unlimited solubility in a solid form.

In general, it can be concluded that types of elements and their specific contents in ternary systems are known. The Fe-B-C eutectic alloys contain, respectively, in wt%, 1.5% C and 2.9% B, and the Fe-Mn-C alloys contain 0.4% C and 2.2–13% Mn. As a result, the subject of development of the Fe-Mn-C-B system to identify the possibilities of producing a eutectic mixture, determine the area of its existence as well as its phase composition and content of elements is still of current interest.

Based on the X-ray structural and microstructural examinations and thermal analysis of the Fe-Mn-C-B alloys, the content of elements in the eutectic areas of Fe-Mn-C and Fe-B-C systems was determined (**Table 2**) [7].

Taking into consideration the specificity and technological details of producing eutectic alloys and surface layers as well as the obtained properties, in particular reduction in a tendency to cracking, it is advisable to adopt the same carbon and boron contents as in the Fe-Mn-C eutectic mixture. The elements of the Fe-Mn-C system offer the possibility of alloying with

components such as Ni, Cr, Ni-Cr and others. This allows manufacturing powder materials with diverse properties, i.e. provides the possibility of influencing the properties of surface layers produced.

Element	Fe-Mn-C	Fe-B-C
Fe	73.3–92.5	85.1–92.5
Mn	3.1–23.8	1.6–7.6
C	0.6–6.4	2.6–7.0
B	0.6–2.5	0.2–3.5

Table 2. Contents (wt%) of elements in eutectic areas of Fe-Mn-C and Fe-B-C systems.

Therefore, it is justified to choose iron, manganese, carbon and boron as the basic elements for manufacturing the base eutectic powder material.

Iron— the main material, included in metallic products—forms solid solutions, chemical compounds and is a carbide former. Carbon and boron in combination with iron form eutectic systems as well as iron carbides and borides with high hardness and strength. In addition, the above-mentioned elements are characterised by high diffusive permeability in the process of saturation of iron-based alloys. In combination with iron, they form chemical compounds and interstitial solid solutions. For the eutectic alloys being developed, the elements were selected based on their known interactions in iron-based alloys [1–3, 8].

Manganese is characterised by high similarity to iron, and it can exchange with it very easily in carbides, at the same time increasing their ductility and dispersion while maintaining rather high strength and thermocyclic stability. Thus, manganese is a very good carbide former. Manganese carbides Mn_3C and iron carbides Fe_3C dissolve in each other, with virtually no limitations. Manganese in combination with iron forms a solid solution. Manganese atoms may substitute iron atoms in Fe_3C carbides. When manganese content is increased in steel, its quantity also increases in carbides, while maintaining a constant ratio of 4:1. In low-carbon steels, carbon content in carbides is much higher than that in high-carbon ones. This difference can be explained by the absolute amount of carbide particles in steel and the related difference in depletion of α-solid solution of iron with manganese. The depletion grows with the increase in amount of carbide particles, and thus carbon content in steel. This is because the basic factor that determines manganese content in carbide is not its amount in steel, but the ratio of equivalent amount of manganese in solid solution to the amount of carbon particles being formed. The weight content of manganese in carbides for steels containing approx. 1% C varies from 0 to 2%, while increasing manganese content in steel from 0 to 50%, respectively (ratio of 4:1). The equivalent content of manganese carbide can only be achieved as a result of rather long steel holding of steel at high temperatures (approx. 1000 K). Manganese extends the area of the existence of γ iron. In particular, manganese increases carbon solubility in γ solid solution at high temperatures. With increasing manganese content, the carbide transition point shifts towards the area of low-carbon contents. Manganese favours shifting of the γ-α transition towards low temperatures. At the same time, the rate of ongoing diffusion processes

http://dx.doi.org/10.5772/66873

decreases, which reduces the rate of the transformation of austenite to martensite. It can be noticed that increasing manganese content in steel makes the degree of pearlite dispersion increase. However, manganese shows no visible impact on the steel hardness after quenching, tempering stability, cutability and heat resistance, which results from the absence of manganese carbides in steels.

During the formation of boride phases in surface layers, e.g. Fe_2B phase, boron atoms are transformed into Sp^2 electron configurations, which try to turn into even more energetic equivalent Sp^3 configurations. Therefore, iron tends to give some of its electrons to boron atoms and turn into a more equivalent state with formation of stable d^5 configurations. In the state of isolated atoms, boron and iron show the following configuration of valence electrons: $2s^2 2p^1$ and $3d^6 4s^2$ [2]. As a result of the electron exchange and formation of energetically stable Sp^3 and d^5 configurations, strong covalent compounds are formed between iron and boron atoms. It means that the boride phase, which shows high degree of localisation of the atomic valence electrons, is characterised by relatively high hardness, wear resistance and corrosion resistance.

With the increase in principal quantum number of valence Sp electrons, the stability of Sp^3 boron electron configuration is reduced, and thus the reliability of their occurrence is reduced too. The iron compounds containing silicon that form in the surface layer show considerably lower microhardness than iron borides.

Borides are characterised by significant resistance to abrasive wear compared to high-melting carbides and oxides. Wear resistance of boride-based surface layers decreases due to their high brittleness. In surface layers containing a slight amount of borides, wear resistance is also reduced due to the existence of a large amount of core (matrix) material. It follows that the eutectic layers containing metal borides may be characterised by high ductility, hardness, durability and significant resistance to abrasive wear.

Boron is added to practically all heat-resistant nickel-based alloys for casting in the amount of 0.01–0.10% to strengthen the grain boundaries. It shows poor solubility in nickel. First of all, it dissolves according to the grain boundaries, at contents exceeding 0.015%. Along the grain boundaries, it is precipitated as borides, thus forming the eutectic mixture. Its reinforcing effect is realised mainly by inhibiting diffusion processes at the grain boundaries. This reduces the strength of the alloys, which is connected with formation of TiB_2, CrB_2 $(Mo, W, Cr)_3B_2$ borides that practically contain no basic element—nickel.

The heat treatment being conducted has virtually no effect on the hardness of carbides and borides.

By changing the amounts of iron and ferromanganese, the eutectic degree of surface layers can be controlled. Adding B, Ni, Cr, Fe, Si, Cu, FeSi, FeB and other compounds to the base mixture makes it possible to develop a group of mixtures for forming surface layers with various properties. It allows selecting the range of mixture components to enhance the ability to saturate the surface layer while maintaining a relatively high hardness, wear resistance and ductility of produced layers. Taking into account the discussed effects, the base system of elements, i.e. Fe-Mn-C-B, as well as the area of the existence of eutectic and details of its formation were selected and defined. Based on the above-mentioned base system, the possibility of forming

materials with defined phase composition as well as properly controlled physical, chemical and mechanical properties and operating characteristics was adopted.

The developed eutectic materials were made as a powder based on iron of the Fe-Mn-C-B system for build-up welding or spraying with partial melting of the surface layer. In these processes, this may cause their insufficient deoxidation, which, in turn, may adversely affect the formation of strengthened surface layer. To prevent the potential occurrence of the above-mentioned negative effects, boron and silicon were adopted as the elements to counteract oxidation. The enhancement of diffusion properties of eutectic alloys, in particular carbon, can be achieved by addition of silicon. Silicon forms limited solid solutions with iron and manganese. In recent years, much emphasis is placed on the development of self-deoxidising iron-based alloys containing boron and silicon. These materials replace expensive toxic deoxidisers, improve working conditions, simplify technologies and increase the efficiency of surface treatment by various methods. Thus, boron and silicon can be considered together with manganese as the perspective elements for production of low-cost surface layers compared to alloys in the form of nickel-based powder [5, 6].

Silicon favours the formation of boron from B_2O_3 and production of increased amount of Fe_2B iron boride within the structure of eutectic layers. The applied silicon content in eutectic layers [9] varies between 1.2 and 9.75 wt%. Due to the impact of silicon as deoxidiser and enriching the solution with iron atoms during the partial melting of treated material, its local content in the eutectic layer varied between 0.1 and 5%. The applied silicon concentration along the layer's depth varies between 1 and 2%. At FeSi content of 13% in the mixture (0.1–5 wt% per layer), the surface layer of Fe-Mn-C-B system with increased Fe_2B content is formed. At a lower silicon content in the mixture, layers with sub-eutectic structure are produced. The use of silicon in the base system is due to the fact that it is a good deoxidiser, and together with manganese and boron it enhances self-oxidation of powder materials. Self-oxidation is necessary, particularly, while forming the surface layers by build-up welding, spraying or spraying with partial melting of the surface layer, when there is no possibility of introducing additional self-oxidising elements, like, for example, the use of B_2O_3 in build-up welding with high-frequency currents. Therefore, it is necessary to use silicon for alloying the base powder Fe-Mn-C-B system.

Iron in combination with silicon forms solid solutions (maximum silicon content is approx. 1.5%), which are characterised by good resistance to various acids and high temperatures. Steels usually contain very low amounts of silicon (0.0–1.3%). The impact of silicon on properties is slight if ignoring its effect as a deoxidiser, which is similar to that of manganese. At contents of 0.5–0.6% and above, silicon is considered as an alloying element, which increases hardness and ultimate strength of alloys at high temperatures and corrosion resistance at low temperatures and reduces ductility. When reducing silicon content within the areas of γ-solutions in alloys containing more than 3 wt% Si, there are no phase transitions up to the melting point.

In selection of elements, it is taken into consideration that silicon is the second most important component after carbon in cast irons. By reducing silicon content, the graphitisation coefficient of cast iron can be controlled. Already at Si content of 4% and more, practically all cast irons used in thin-walled casts are replaced with cast irons with grey cast iron structure. The castable cast

http://dx.doi.org/10.5772/66873

irons usually contain 1.25–4.2% Si, while the workable ones contain 0.2–2% Si, which is taken into consideration when selecting the amounts of silicon and boron in eutectic alloys.

Silicon quickly reduces the amount of carbon in eutectic mixture. At Si content of 16%, hypereutectic are even alloys containing 0.6–1.0% C. Alloys containing 14–16% Si are characterised by high-corrosion resistance, and hence they are commonly used in the chemical industry.

Silicon is an element, which significantly reduces the diffusion coefficient of carbon in the α- and γ-crystal lattice. In steel, carbides contain a small amount of silicon as its atoms are quickly moved from carbides to solid solution. Silicon is not a typical carbide former. In alloys with high silicon content (20–23% Si), SiC carbide is formed. Therefore, the limit of alloying eutectic alloys with silicon is assumed to be approx. 3–4% because the ductility of eutectic alloys decreases at its greater contents.

For examinations of the Fe-Mn-C-B phase equilibrium system, the preparation of samples from carbonyl iron (99.99%), manganese (99.5%), amorphous boron (99.3%) and synthetic graphite (99.94%) powders by alloying in an electric furnace in a purified argon atmosphere was adopted. The annealing of samples was carried out in vacuum quartz containers at 1273 K for 350 h. To determine samples with a eutectic structure, thermal and metallographic tests (Neophot-2 MIM-8, DAT, AT) were carried out and the concentration of elements ('Kamebax,' Superprobe-733) in alloys in the as-annealed (1273 K, 350 h) and standardised condition was analysed. Based on obtained data, a quasi-ternary Fe-Mn-C-B-Si system was developed (**Figure 1**). The component contents in individual intersections were changed every 10 molar parts. The area of iron concentration was 0.67–0.79 at% [6, 8].

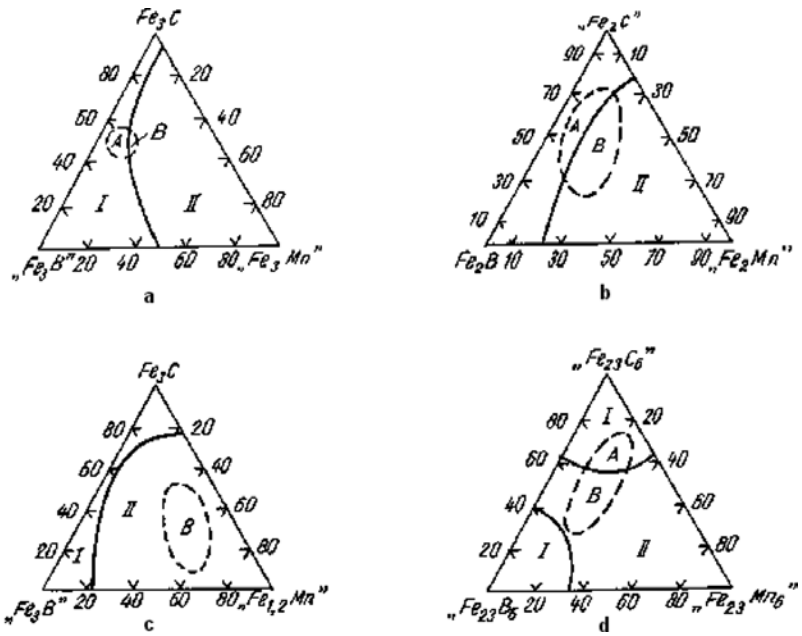

Figure 1. Phase areas (I, II, A, B) in quasi-ternary intersections: (**a**) Fe_3C-Fe_3B-'Fe_3Mn', (**b**) 'Fe_2C'-Fe_2B-'Fe_2Mn', (**c**) Fe_3C-Fe_3B-'$Fe_{1.2}Mn$', (**d**) '$Fe_{23}C_6$'-'$Fe_{23}B_6$'-'$Fe_{23}Mn_6$'.

For evaluation of the structure and phase composition of elements, the X-ray analysis of phase composition of the alloys produced and the micro-X-ray structural analysis of the content of elements was carried out.

The obtained effects of structural analyses of the alloys, in particular their phase composition and content of elements, are presented as a description of phase areas, I and II, and areas of the existence of Fe-Mn-C and Fe-B-C eutectics, A and B, in four quasi-ternary intersections (**Figure 1a–d**) [9].

3. Result and discussion

3.1. Examination and analysis of Fe_3C–Fe_3B–'Fe_3Mn' quasi-ternary intersection

In order to determine the phase areas and content of elements, the micro-X-ray and microstructural examinations of the Fe_3C–Fe_3B–'Fe_3Mn' quasi-ternary intersection were carried out. Based on the examinations performed, two phase areas were identified (**Figure 1a**; **Table 3**). Area I consists of $Fe_3(B, C)$, α-(Fe, Mn), γ-(Fe, Mn), and area II consists of α-(Fe, Mn), γ-(Fe, Mn), $(Fe, Mn)_{23}(C, B)_6$, $(Fe, Mn)_2B$.

As a result of micro-X-ray examinations, the following content of elements in hypereutectic alloys was determined (in at%): 67.8–75.0 Fe, 1.2–4.5 Mn, 8.5–14.3 B, 11.0–13.9 C [6, 10].

The quasi-ternary intersection of the equilibrium system was examined for 19 samples, annealed at 1273 K. In the analysed intersection, the $(Fe, Mn)_{23}(C, B)$ and $(Fe, Mn)_3(B, C)$ phases with $Fe_{23}C_6$ and Fe_3C structures, respectively, were established. For example, sample nos. 6 and 10 contain a phase with cementite structure the lattice of which has the following parameters: a = 0.5341, b = 0.6650, c = 4.459 nm. Parameters of the cementite structure phase lattice correspond to those of Fe_3C. Samples 1–4 and 11 contain the Fe_3C phase only with increased lattice parameters, which corresponds to those of $Fe_3(B,C)$ borocarbide. Some of the samples include the $(Fe, Mn)_{23}(B, C)_6$ phase, Fe_2B-$(Fe, Mn)_2B$-based solid solution. The peculiarity of sample nos. 1–8, 10, 11, 15, 17, 18, 19 (**Table 3**) is that they include the α-(Fe, Mn) solid solution. The obtained phase composition of hypereutectic alloy samples is presented in **Table 3**.

As it can be seen in **Table 3**, for phase area I (**Figure 1a**), the hypereutectic alloy is formed in sample no. 3 only, whereas all other samples represent solid solutions.

As it was determined from experimental metallographic and X-ray structural examinations of the alloys, sample no. 3 $Fe_{75}Mn_{3.6}B_{10}C_{12.5}$ is a hypereutectic alloy composed of $Fe_3(B, C)$ + α-(Fe, Mn) eutectic between which $Fe_{0.4}Mn_{3.6}C$ iron-manganese carbides are arranged. The second grade dendrites are arranged in the crystallographic direction [11] (**Figure 2a**). The annealing of $Fe_{75}Mn_{3.6}B_{10}C_{12.5}$ alloy at 1273 K for 350 h results in the formation of pearlitic grooves (**Figure 2b**). In carbon-enriched alloys, the $Fe_{0.4}Mn_{3.6}C$ iron-manganese carbide lamellas of 15–35 μm in length are formed (**Figure 2c**). A strip of the second eutectic phase—pearlite—is formed on the lamella surface and grows along the surface. It has the appearance of a flat den-

http://dx.doi.org/10.5772/66873

drite. The results of the examinations confirm that in the crystallisation process, the leading phase in the phase carbon-solid solution eutectics is always carbide crystals. The structure of other examined samples—α- and γ-(Fe, Mn)-based solid solutions with $Fe_3(C, B)$, $(Fe, Mn)_2B$ borocarbide or $(Fe, Mn)_{23}(C, B)_6$ carbide inclusions. The Fe-B-C eutectic exists in area A, while the Fe-Mn-C eutectic is observed in area B (**Figure 1a**).

Sample number	Component contents; molar part 10			Phase composition	Alloy type	Phase area (Figure 1a)
	Fe_3C	"Fe_3B"	"Fe_3Mn"			
3	5	4	1	$Fe_3(B, C)$ + α-(Fe, Mn) + trace amount of γ-(Fe, Mn)	Hyper-eutectic alloy	I
1	1	8	1	$Fe_3(B, C)$ + trace amount of α-(Fe, Mn)	Solid solution	
2	3	6	1			
6	2	6	2			
4	7	2	1	$Fe_3(B, C)$ + α-(Fe, Mn)	Solid solution	
10	1	6	3			
11	3	4	3			
5	8	1	1	α-(Fe, Mn)+$(Fe, Mn)_2B$+$(Fe, Mn)_{23}(C, B)_6$	Solid solution	II
8	6	2	2			
7	4	4	2	α-(Fe, Mn) + traces of transient phase +$(Fe, Mn)_{23}(C, B)_6$+ γ-(Fe, Mn) + trace amount of α-(Fe, Mn)	Solid solution	
15	2	3	5			
18	2	2	6			
17	4	1	5	$(Fe, Mn)_{23}(C, B)_6$ +γ-(Fe, Mn) + α-(Fe, Mn)	Solid solution	
19	1	2	7			
16	3	2	5	$(Fe, Mn)_{23}(C, B)_6$ + γ-(Fe, Mn)	Solid solution	

Table 3. Phase composition of Fe-Mn-C-B samples with iron content of 0.75 at%.

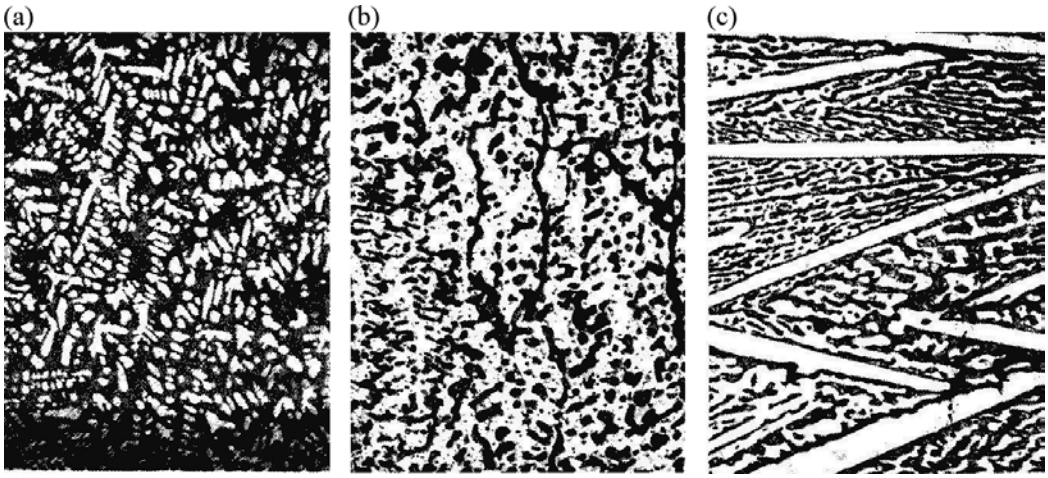

Figure 2. Microstructure (×200) of the examined samples (markings according to **Table 3**), hyper-eutectic alloy (sample no. 3, a, b) and solid solution [sample no. 5 (c)]; (a) after normalising; (b,c) after annealing (at 1273 K, 350 h).

3.2. Examination and analysis of 'Fe_2C'–Fe_2B–'Fe_2Mn' quasi-ternary intersection

To determine the phase areas and the content of elements, the examinations of 'Fe_2C'–Fe_2B–'Fe_2Mn' intersection samples (**Figure 1b**) containing the $Fe_3(B, C)$, Fe_2B, γ-(Fe, Mn) and $(Fe, Mn)_{23}(C, B)_6$ phases were carried out. Phase composition of the samples with iron content of 0.667 at% is presented in **Table 4**.

Based on the micro-X-ray and microstructural examinations performed in the 'Fe_2C'–Fe_2B–'Fe_2Mn'quasi-ternary intersection, two phase areas were identified (**Figure 1b**; **Table 4**). Area I consists of $Fe_3(C, B)$ and area II consists mainly of $(Fe, Mn)_{23}(C, B)_6$ + γ-(Fe, Mn). Hypereutectic alloys are in area II (**Figure 1b**). The Fe-B-C eutectic exists in area A, while the Fe-Mn-C eutectic is observed in area B (**Figure 1b**). Content of elements in hypereutectic alloys (at%): 66.7 Fe, 3.3–6.7 Mn, 10.0–23.3 C, 6.7–16.6 B. In hypereutectic alloys (sample Nos 3–4), the primary Fe(B, C) crystals and $(Fe, Mn)_{23}(C, B)$ iron-manganese carbide dendrites are formed, **Figure 3a** and **b**. No borocarbide inclusions were identified. In boron-enriched alloys, the primary austenite crystals are formed. In γ-(Fe, Mn)-$(Fe, Mn)_{23}(C, B)_6$ eutectic alloys, the micro-areas of γ-(Fe, Mn) solid solution and austenite dendrites were revealed. In alloys containing an increased amount of manganese, the primary dendrites $(Fe, Mn)_{23}(C, B)_6$ are formed (**Figure 3c**). Content of elements in eutectic alloys (at%): 66.6 Fe, 1.7–11.0 Mn, 7.7–25.0 C, 4.0–8.4 B [4, 9].

3.3. Examination and analysis of Fe_3C-Fe_3B-'$Fe_{1.2}Mn$' quasi-ternary intersection

In the examined quasi-ternary intersection, most of the Fe_3C-Fe_3B-"$Fe_{1.2}Mn$" samples (**Figure 1c**) comprise the $(Fe, Mn)_{23}(C, B)_6$ phase, which is in equilibrium with the $Fe_3(B, C)$ and γ-(Fe, Mn) or γ-(Fe, M) phase. According to the results of phase analysis, the $(Fe, Mn)_{23}(C, B)_6$ + γ-(Fe, Mn) + $Fe_3(C, B)$ phase area is visible very well [7, 8]. The samples contain no α-Fe-based phase. Phase composition of the samples is presented in **Table 5**. The most complex structure (number of phases) is visible in sample nos. 4, 24.

http://dx.doi.org/10.5772/66873

Sample number	Component contents; molar part 10			Phase composition	Alloy type	Phase area
	'Fe$_2$C'	Fe$_2$B	'Fe$_2$Mn'			
1	1	8	1	Fe$_3$(C, B)	Solid solution	I
2	3	6	1	„	-"-	
3	5	4	1	„	Hyper-eutectic alloy	
4	7	2	2	„	-"-	
5	7	2	2	Fe$_3$(C, B)	Solid solution	II
9	1	1	1	(Fe, Mn)$_{23}$(B, C)$_6$ + Fe$_2$B + Fe$_3$(B, C)	Solid solution	
6	3	5	2	(Fe, Mn)$_{23}$(B, C)$_6$ + Fe$_2$B + Fe$_3$(B, C)	Hyper-eutectic alloy	
7	5	3	2	(Fe, Mn)$_{23}$(B, C)$_6$+γ-(Fe, Mn)	Hyper-eutectic alloy	
10	5	2	3	(Fe, Mn)$_{23}$(C, B)$_6$+γ-(Fe, Mn)	Solid solution	
11	1	5	4	„	„	
12	3	3	4	„	„	
13	5	1	4	„	„	
15	2	2	6	„	„	
14	1	3	6	γ-(Fe, Mn)+(Fe, Mn)$_{23}$(C, B)$_6$	Solid solution	
16	3	1	6	„	„	
17	1	1	6	„	„	
8	7	1	2	γ-(Fe, Mn)	Solid solution	

Table 4. Phase composition of Fe-Mn-C-B samples with iron content of 0.667 at% ('Fe$_2$C'-Fe$_2$B-'Fe$_2$Mn' intersection (**Figure 1b**)).

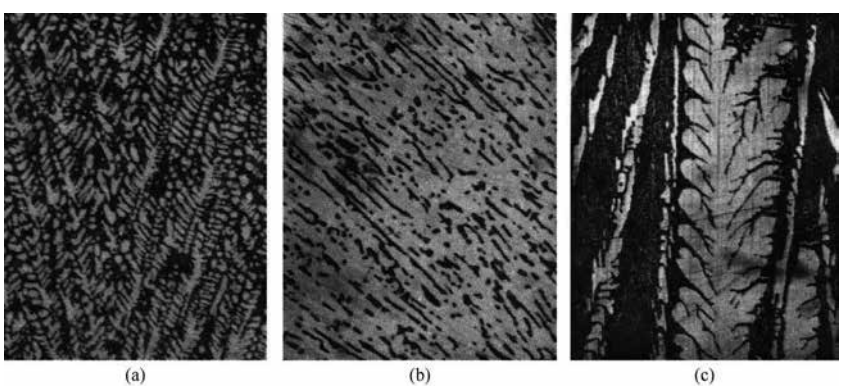

Figure 3. Microstructure (×200) of the examined 'Fe$_2$C'-Fe$_2$B-'Fe$_2$Mn' quasi-ternary intersection alloys (markings according to **Table 4**): sample no. 3 (a, b), sample no. 10 (c); (a, c) after normalisation; (b) after annealing at 1273 K, 350 h.

Sample number	Component contents; molar part 10			Phase composition	Alloy type	Phase area
	Fe_3C	Fe_3B	'$Fe_{1.2}Mn$'			
6	1	7	2	$(Fe, Mn)_{23}(C, B)_6$ + small amount of $Fe_3(B, C)$	Solid solution	I
1	1	8	1	$Fe_3(C, B)$ + γ-(Fe, Mn)	-"-	
2	2	7	1	$Fe_3(B, C)$	-"-	
5	8	1	1	-"-	-"-	
13	2	2	3	$(Fe, Mn)_{23}(B, C)_6$+γ-(Fe, Mn)	Sub-eutectic	II
20	4	1	5	-"-	Solid solution	
21	1	3	6	-"-	-"-	
3	4	5	1	-"-	-"-	
7	3	5	2	-"-	-"-	
12	3	4	3	-"-	-"-	
14	6	1	3	-"-	-"-	
16	3	3	4	-"-	-"-	
17	5	1	4	-"-	-"-	
22	2	2	6	$(Fe, Mn)_{23}(B, C)_6$+ trace amount of γ-(Fe, Mn)	-"-	
26	1	1	8	-"-	-"-	
25	2	1	7	$(Fe, Mn)_{23}(B, C)_6$+ small amount of γ-(Fe, Mn)	-"-	

Table 5. Phase composition of Fe-Mn- C-B samples, Fe_3C + Fe_3B + '$Fe_{1.2}Mn$' intersection (**Figure 1c**).

Based on the micro-X-ray and microstructural examinations performed in the Fe_3C-Fe_2B-'$Fe_{1.2}Mn$' quasi-ternary intersection, two phase areas were identified (**Figure 1c**; **Table 5**). Area I consists of $(Fe, Mn)_{23}(C, B)_6$, $Fe_3(C, B)$ and γ-(Fe, Mn) and area II consists of $(Fe, Mn)_{23}(C, B)_6$, γ-(Fe, Mn) and $Fe_3(B, C)$. Sub-eutectic alloys are in area II (**Figure 1c**). In the intersection determined, there is only the Fe-Mn-C eutectic in area B (**Figure 1c**).

In manganese-enriched sub-eutectic alloys, the primary dendrites γ-(Fe, Mn) are formed and the $(Fe, Mn)_{23}(C, B)_6$+γ-(Fe, Mn) eutectic is arranged between them (**Figure 4a**). The annealing of alloys results in homogenisation and coagulation of γ-(Fe, Mn) crystals (**Figure 4b**). Content of elements in sub-eutectic alloys (at%): 65.3–71.1 Fe, 8.7–21.5 Mn, 2.8–15.4 C, 2.9–10.4 B.

3.4. Examination and analysis of '$Fe_{23}C_6$'- '$Fe_{23}B_6$'-'$Fe_{23}Mn_6$' quasi-ternary intersection

To determine the phase areas and the content of elements, the examinations of '$Fe_{23}C_6$'-'$Fe_{23}B_6$'-'$Fe_{23}Mn_6$' intersection (**Figure 1d**) containing the phase with carbide structure $(Fe, Mn)_{23}(C,B)_6$

http://dx.doi.org/10.5772/66873

in Fe-B-C i Fe-Mn-C ternary systems, which restrict the examined intersection, were carried out. The highest number of phases in equilibrium is found in phase area II—(sample no. 7) $(Fe, Mn)_{23}(B, C)_6$ + α-(Fe, Mn) + $Fe_3(B, C)$ and in phase area I—(sample no. 10) $Fe_3(B, C)$ + traces of α-(Fe, Mn) + γ-(Fe, Mn). Samples 4, 5, 7, 10 and 19 (**Table 6**) comprise the ternary phase $Fe_3(B, C)$ [7]. Some of the samples comprise the quaternary phase $(Fe, Mn)_{23}(C, B)_6$. At the intersection of Fe-Mn-C-B system, at Fe content of 0.79 atomic parts, the phase equilibrium of $(Fe, Mn)_{23}(C, B)_6$ + $Fe_3(C, B)$ + γ-(Fe, Mn) + γ-(Fe, Mn) was identified too. In particular, the γ-(Fe, Mn) phase was observed in samples 2, 5, 7, 9, 10 and 11 (**Table 6**).

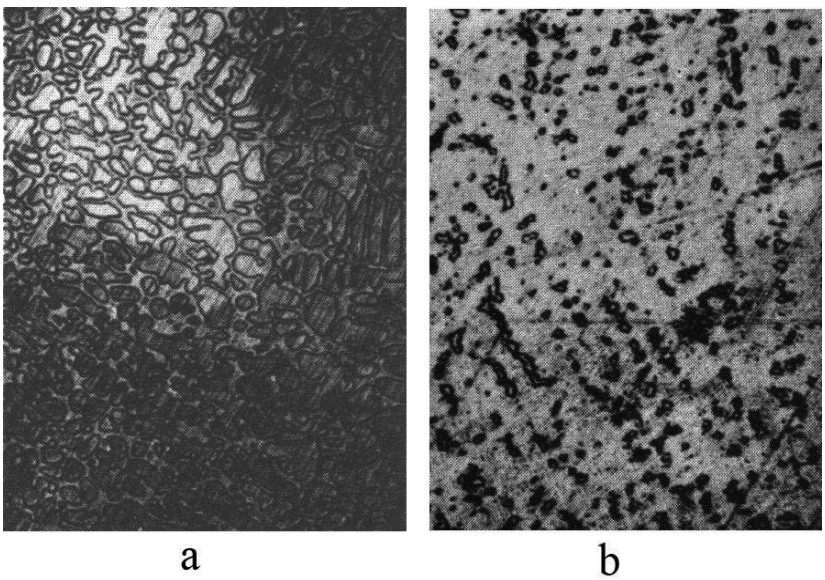

Figure 4. Microstructure (×200) of the examined Fe_3C-Fe_3B-'$Fe_{1.2}Mn$' quasi-ternary intersection alloys (markings according to **Table 5**): (a) sample no. 13, sub-eutectic alloy after normalising; (b) solid solution, sample no. 20, after annealing at 1273 K, 350 h.

Sample number	Component contents molar part 10			Phase composition	Alloy type	Phase area
	'$Fe_{23}C_6$'	'$Fe_{23}B_6$'	'$Fe_{23}Mn_6$'			
7	3	5	2	$(Fe, Mn)_{23}(B, C)_6$+ α-(Fe, Mn)+$Fe_3(B, C)$	Sub-eutectic	II
9	5	3	2	$(Fe, Mn)_{23}(B, C)_6$ + trace amount of α- Fe	-"-	
11	1	6	3	γ-(Fe, Mn)+$Fe_3(B, C)$ + $(Fe, Mn)_{23}(B, C)_6$ + α-(Fe, Mn)	-"-	
3	5	4	1	$(Fe, Mn)_{23}(B, C)_6$	-"-	
12	2	4	3	$(Fe, Mn)_{23}(B, C)_6$ + γ-(Fe, Mn)	Solid solution	
13	5	2	3	-"-	-"-	
32	2	2	6	γ-(Fe, Mn) + $(Fe, Mn)_{23}(B, C)_6$	-"-	
23	3	1	6	-"-		

Sample number	Component contents molar part 10			Phase composition	Alloy type	Phase area
	'$Fe_{23}C_6$'	'$Fe_{23}B_6$'	'$Fe_{23}Mn_6$'			
2	3	4	3	α-Fe + Fe_{23}(B, C)	-"-	I
4	7	2	1	Fe_3(B, C)	-"-	
5	8	1	1	Fe_3(B, C) + trace amount of α- Fe	-"-	
10	7	1	2	Fe_3(B, C) + trace amount of α - (Fe, Mn) +γ-(Fe, Mn)	Sub-eutectic	
19	3	2	5	γ-(Fe, Mn) + α- (Fe, Mn) + Fe_3(B, C)	-"-	

Table 6. Phase composition of Fe-Mn-C-B samples; intersection at iron content of 0.79 at%.

Based on the micro-X-ray and microstructural examinations performed in the '$Fe_{23}C$'-Fe_{23}B-'Fe_{23} Mn'quasi-ternary intersection, two phase areas were identified (**Figure 1d**; **Table 6**). Area I consists of Fe_3(C,B), α-(Fe, Mn), γ-(Fe, Mn) and α-Fe and area II consists of $(Fe, Mn)_{23}(C, B)_6$, α-(Fe, Mn), γ-(Fe, Mn) and Fe_3(B, C). Sub-eutectic alloys are in areas I and II (**Figure 1d**). The Fe-B-C eutectic exists in area A, while the Fe-Mn-C eutectic is observed in area B (**Figure 1d**).

Content of elements in sub-eutectic alloys (at%): 79.3 Fe, 2.7–6.2 Mn, 5.4–15.5 C, 1.1–10.8% B. In sub-eutectic alloys, austenite dendrites are formed at elevated carbon contents, while at lower carbon contents, pearlite dendrites are formed (**Figure 5a**). Austenite dendrites are evenly distributed throughout the alloy volume. The annealing of subeutectic alloys results in coagulation of γ-(Fe, Mn) crystals (**Figure 5b**).

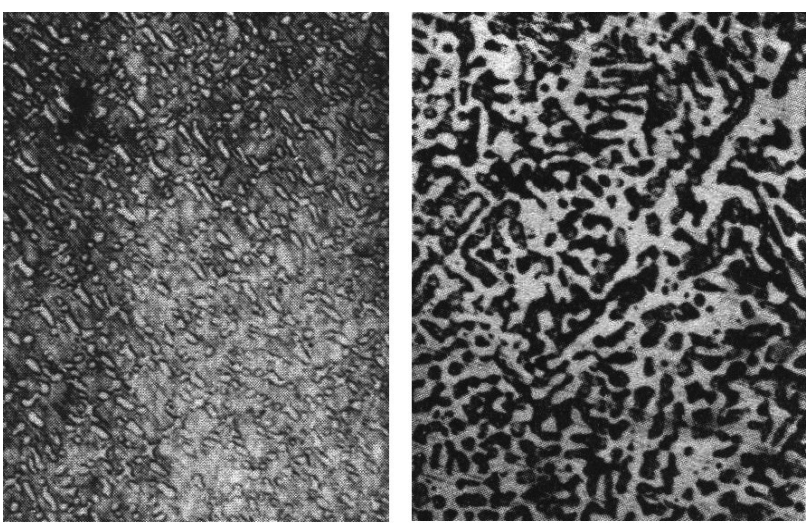

Figure 5. Microstructure (×200) of sub-eutectic alloy, sample no. 7 (markings according to **Table 6**); (a) after normalising; (b) after annealing at 1273 K, 350 h.

http://dx.doi.org/10.5772/66873

By comparing the nature of the effects of components, it can be concluded that the $(Fe, Mn)_{23}(C, B)_6$ phase was found at all intersections. As a pure phase, it exists at Fe content of 0.79 at% (molar parts°10): $5Fe_{23}C_6Fe_{23}Mn_64Fe_{23}B_6$-$4Fe_3CFe_{1.2}Mn5Fe_3B$, intersection Fe_3C-Fe_3B-$Fe_{1.2}Mn$.

The areas were identified where quaternary borocarbide is included as the basic phase: (3–4) Fe_3B(4–5)Fe_3Mn(2–3)Fe_3C-$Fe_3B8Fe_3Mn2Fe_3C$ at Fe content of 0.75 atomic parts and (1–5) Fe_2B4Fe_2Mn(1–5)Fe_2C-(2–3)Fe_2B(2–6)Fe_2Mn(2–5)Fe_2C at Fe content of 0.667 atomic parts. A relationship was observed according to which with the reduction in iron content, the area of the existence of $(Fe, Mn)_{23}(C, B)_6$ phase moves towards the area of higher manganese and boron contents and lower carbon content (**Figure1a** and **b**).

Based on theoretical assumptions and experimental verification, the areas of the existence of Fe-Mn-C-B eutectic, as a new family of dispersion-strengthened eutectic alloys with a structural gradient, were identified. The areas of the existence (**Figure 1**; **Table 7**) of hyper- and sub-eutectic alloys were identified too.

Quasi-ternary intersection		**Content of elements***			
		Fe	**Mn**	**C**	**B**
System	Fe-Mn-C-B	73.3 – 92.5 65.3-79.3	1.6–23.8 1.2-21.5	0.6–7.0 2.8-25.0	0.2–3.5 1.1-18.4
Eutectic	Fe-Mn-C	73.3–92.5 65.3-79.3	3.1–23.8 2.7-21.5	0.6–6.4 2.8-23.4	0.6–2.5 2.9-18.4
Eutectic	Fe-B-C	85.1–92.5 66.6-79.3	1.6–7.6 1,2-6,2	2.6–7.0 10,5-25,0	0.2–3.5 1,1-17,7
Intersection	Fe_2C-Fe_2B-"Fe_2Mn"	81.2–89.2 66.6	2.2–13.1 1,7-11,0	2.0–7.0 7,7-25.0	0.9–4.5 4,0-8,4
Eutectic	Fe-Mn-C	81.2–86.3 66.6	6.0–13.1 4.7-11.0	2.0–6.4 7.7-23	0.9–4.6 4.0-18.4
Eutectic	Fe-B-C	85.1–89.2 66.6	2.2–7.6 1.7-6.0	3.0–7.0 11.0-25.0	0.9–4.4 4.0-17.7
Intersection	Fe_3C-Fe_3B-"Fe_3Mn"	87.1–92.5 67.8-75.0	1.6–5.7 1.2-4.5	2.8–3.7 11.0-13.9	1.9–3.5 8.5-14.3
Eutectic	Fe-Mn-C	90.1–91.2 75.0	3.3–4.8 2.8-4.0	2.8–3.5 11.0-13.7	1.9–2.4 8.5-10.0
Eutectic	Fe-B-C	87.1–92.5 67.8-75.0	1.6–5.7 1.2-4.5	2.8–3.7 11.0-13.9	2.0–3.5 8.5-14.3
Intersection	Fe_3C-Fe_3B-$Fe_{1,2}Mn$	73.3–84.9	10.2–23.8	0.6–0.4	0.6–2.3
Eutectic	Fe-Mn-C	65.3-71.1	8.7-21.5	2.8-15.4	2.9-10.4
Intersection	"$Fe_{23}C_6$"-"$Fe_{23}B_6$"-"$Fe_{23}Mn_6$"	89.7–92.5 79.3	3.1–6.9 2.7-6.2	1.4–3.9 5.4-15.5	0.2–2.5 1.1-10.8

Quasi-ternary intersection		Content of elements*			
		Fe	Mn	C	B
Eutectic	Fe-Mn-C	89.7–92.5 79.3	3.1–6.9 2.7-6.2	1.4–2.9 5.4-10.9	0.7–2.5 3.6-10.8
Eutectic	Fe-B-C	89.7–92.5 79.3	3.1–6.7 2.7-6.1	2.8–3.9 10.7-15.5	0.2–1.5 1.1-6.8

*numerator: wt%, denominator: at%.

Table 7. Content of elements in eutectic areas of Fe_2C-Fe_2B-'Fe_2Mn', Fe_3C-Fe_3B-'Fe_3Mn', Fe_3C-Fe_3B-'$Fe_{1.2}Mn$', '$Fe_{23}C_6$'-'$Fe_{23}B_6$'-'$Fe_{23}Mn_6$' intersections of the Fe-Mn-B-C system.

Eutectic alloys are dispersion-reinforced composites with a structural gradient in which the soft matrix lamellar phase (alloying pearlite or austenite) is strengthened with hard and resistant $Fe_{0.4}Mn_{3.6}C$ phase. The structure and properties of the alloys can be controlled by changing the contents of their components. The alloying can be carried out with the majority of selected metallic elements in the periodic table over their wide concentrations. Carbon content in alloys, according to the Fe-Mn-C equilibrium diagram, can be changed in a broad range—0.6–6.4 wt%.

For the development of chemical composition of eutectic alloys, the examinations of the Fe-Mn-C-B phase equilibrium system were used to determine the eutectic areas (**Tables 3–6; Figures 1–5**). The composition of elements for the production of eutectic alloys of the Fe-Mn-C-B system is as follows (wt%):

Fe	86.6–97.4
Mn	2.2–13.0
C	0.4–1.5
B	2.9

The following content of elements in eutectic areas was identified by X-ray phase analysis after four quasi-ternary intersections (**Figure 1**; **Table 7**).

4. Conclusions

The following conclusions can be put forward based on the works performed:

(1) The analysis of the examined systems makes it possible to conclude that

(a) Fe-Mn-C eutectic exists at boron contents of 0.6–2.5 wt% and at the following contents of other elements:

Fe	73.3–92.5
Mn	1.6–23.8
C	0.6–7.0

http://dx.doi.org/10.5772/66873

(b) Fe-Mn-C-B eutectic forms at manganese contents of 1.6–7.6 wt% and at the following contents of other elements:

Fe	85.1–92.5
B	0.2–3.5
C	2.6–7.0

(2) There is a possibility of alloying the Fe-Mn-C-B system with virtually any elements in the periodic table over a wide range of their concentrations.

(3) By selection of chosen alloying elements, such as Si, Ni, Cr, it is possible to produce alloys with diverse physico-mechanical properties as a result of selection of various alloying components.

(4) Based on the examinations of the Fe-Mn-C-B system according to four quasi-ternary intersections and micro-X-ray examinations, the following content of elements in eutectic areas was identified (**Figure 1**; **Table 7**):

- Fe-B-C eutectic, at manganese content of 1.6–7.6%: 85.1–92.5 Fe; 0.2–3.5 B; 2.6–7.0 C;
- Fe-Mn-C eutectic, at boron content of 0.6–2.5%: 73.3–92.5 Fe; 3.1–23.8 Mn; 0.6–6.4 C.

In particular, the examinations of the Fe-Mn-C-B system after four quasi-ternary intersections: 'Fe_2C'-Fe_2B-'Fe_2Mn', Fe_3C-Fe_3B-'Fe_3Mn', Fe_3C-Fe_3B-'$Fe_{1.2}Mn$', '$Fe_{23}C$'-'$Fe_{23}B$'-'$Fe_{23}Mn$' and the X-ray analysis of the samples annealed at 1270 K for 350 h would make it possible to conclude as follows:

- Based on the X-ray and metallographic examinations, it has been determined that there are two phase areas at all quasi-ternary intersections, which correspond to ternary Fe-Mn-C and Fe-B-C systems (**Figure 1**): area I, Fe-B-C system: $Fe_3(C, B)$ + γ-(Fe, Mn) + α-(Fe, Mn); area II, Fe-Mn-C system: $(Fe, Mn)_{23}(C, B)_6$ + γ-(Fe, Mn) + α-(Fe, Mn).
- The alloys of the Fe_3C-Fe_3B-'$Fe_{1.2}Mn$' intersection at 0.667 at. parts of Fe contain no α-(Fe, Mn)-based phase. This phase was detected in alloys at intersections with increased iron content (0.75 atomic parts) only. It is the γ-(Fe, Mn) phase, which does not exist after quenching of samples from 1270 K.
- In eutectic alloys within the area of the highest iron content (0.79; 0.75 atomic parts), the $(Fe, Mn)_{23}(C, B)_6$ + α-(Fe, Mn) + γ-(Fe, Mn), $Fe_3(C, B)$ + α-(Fe, Mn) + γ-(Fe, Mn) phases are in equilibrium. With the reduction in iron content [0.667 atomic parts (Fe_3C-Fe_3B-'$Fe_{1.2}Mn$' intersection)], the transition from γ- into α-Fe does not occur and the $(Fe, Mn)_{23}(C, B)_6$ + γ-(Fe, Mn), $Fe_3(C, B)$ + γ-(Fe, Mn) phases are in equilibrium.
- The eutectic areas in 'Fe_2C'-Fe_2B-'Fe_2Mn', Fe_3C-*Fe_3B*'Fe_3Mn' and '$Fe_{23}C_6$-'$Fe_{23}B_6$'-'$Fe_{23}Mn_6$' quasi-ternary intersections were found in two phase areas, at the Fe_3C-Fe_3B-'$Fe_{1.2}Mn$' intersection—in area II (Fe-Mn-C eutectic). Generally, the Fe-B-C eutectic is formed in the area of increased carbon and boron contents, while the Fe-Mn-C eutectic is observed in the area of increased Mn content.

Author details

Mykhaylo Pashechko, Klaudiusz Lenik*, Joanna Szulżyk-Cieplak and Aneta Duda

*Address all correspondence to: wz.kpt@pollub.pl

Faculty of Fundamentals of Technology, Lublin University of Technology, Lublin, Poland

References

[1] Dobrzański L.A. Basics of Material Science Metal Science. Warsaw: WNT; 2002.

[2] Lenik K, Pashechko M. Development of a new family of wear-resistant eutectic alloys. In: Works of the Institute of Machine Design and Operation. No. 87. The 35th Tribology School, No. 27; Publishing House of the Wroclaw University of Technology; 2002. p. 196–201.

[3] Lenik K, editor. Anti-wear Eutectic Coatings of the Fe-Mn-C-B System. Lviv: The National Academy os Science of Ukraine, Institute on Problems of Materials Science, Euro World; 2004.

[4] Lenik K, Paszeczko M, Paszeczko L. Wear resistance eutectic composite coatings of system Fe-Mn-C-B-Si. Problems of Tribology. 2001;**3**:61–64.

[5] Jarzyna W, Augustyniak H, Bocheński H. Active Piezoelectric Structures in Control Systems. Przegląd Elektrochemiczny. 2010;**86(4):**252–255.

[6] Paszeczko M, Lenik K, Paszeczko L. Increased durability of machine parts by plasma deposition using eutectic alloys of Fe-Mn-C-B. In: II Mieżdunarodnaja N-T Konferencjja Nowyje technologii, metody obrabotki i uprocznienija dietalej energeticzeskich ustanowok; 23–28 sientiabria 2002; Zaporożje-Ałuszta, Zaporoski Państwowy Instytut 2002. p. 77–78.

[7] Paszeczko M, Lenik K, Szewczuk J. Pidwyszczennia znosostijkosti dyska kopacza korenezbyralnoji maszyny KS-6B nanesenniam ewtektycznych kompozycyjnych pokryttiw systemy Fe-Mn-C-B-Si-Cr. Problems of Tribology. 2003;**2**:154–157.

[8] Pashechko M, Gorecki T. Surface layer models and self-organisation of the surface with abrasive wear. In: Zagadnienia dydaktyczne w środowisku systemów technologicznych. Lublin: LTN. 2003. p. 157–162.

[9] Paszeczko M, Lenik K, Paszeczko L. Pidwyszczennia dowhowiczności detałej maszyn metodom płazmowogo napławlennia z wykorystanniam ewtektycznych spławiw systemy Fe-Mn-C-B. Westnik Dwigatelestrojenija. 2002;**1**:127–131.

[10] Paszeczko M, Popławskij O. Influence of surface atoms segregation on tribological properties of alloys. Problems of Tribology. 2001;**4**:115–125.

[11] Malec M, Lenik K, Pashechko M. The posibilities of increasing the lifetime of tools by using modified surface layer. In: The 7th National Conference on Tool Problems in Plastic Working. Bydgoszcz. 2001. p. 87–93.

Chapter 15

Application of Powder Metallurgy Methods for Production of a Novel Cu-Based Composite Frictional Train Brake Material

Glenn Kwabena Gyimah, Zhongning Guo,
Ping Huang and Dong Chen

Additional information is available at the end of the chapter

http://dx.doi.org/10.5772/67533

Abstract

A novel Cu-based composite frictional train brake material composed of several elements such as Al, SiO_2, Fe, graphite, Sn, Mn and SiO_2 re-enforced with other elements was treated under Powder Metallurgy (P/M) route. The materials were sintered at three different temperatures (850°C, 900°C and 950°C) at a constant pressure.

The tribological behavior of these materials was analyzed by pad-on-disk tests without lubrication and the coefficient of friction, wear rate and wear number were studied in order to identify the effects of the sintering temperature on the base materials composition. The pores in the sintered material were mainly solid lubricants such as graphite and other low melting elements. This resulted in poor hardness and mechanical properties, which were compensated by its ability to reduce seizure.

The wear mechanisms that were generated are as follows; delamination, plowing and abrasive wear. The abrasive wear were dominant and found on samples sintered at 850°C and 900°C, it is seen to be responsible for high wear rates. The friction coefficient under high pressure (3.13MPa) dry conditions had average values of 0.404, 0.343, and 0.336, at 950°C, 900°C and 850°C respectively. The investigation of worn surface was assessed by using x-ray defractory and scanned electron microscope.

Keywords: copper matrix, friction material, wear mechanism, train brake pad

1. Introduction

Railways play a major role in world transportation. Providing safety for passengers and property has always been a major concern for train manufacturers and designers. Despite this fact, accidents happen in railroad systems causing casualties and financial losses. There is an

old adage that says, "A train does not have to start, but it must stop." This presupposes that on a journey, there are changes going on within the tribological system such as the rail-wheels and brake pads/shoes. Materials are worn out and changes in structure occur due to high contact pressures. Also, temperature increase occurs which leads to an altering of mechanical properties and hardness of surface layers. Effective stopping of the train depends on the nature of the worn surface of the pads/shoes. This has been a safety issue, which always attracts additional attention, especially in a time when high-speed trains are the order of the day. The aim of engineering design of friction material is to maximize friction forces, which are the task the system is for, and to minimize wear and tear on complex technical systems. The chemical composition of pads seems to be the major controlling factor for the friction process to build up structured layers in contact zones. Yet the connection between component mixture and friction layer and rate of wear and the connection between friction layer and friction behavior and the rate of wear of the system remains unknown, which makes the entire design complex.

Wear is simply defined as "the progressive loss of substance from the operating surface of a body occurring as a result of relative motion at the surface [1]." The wear requires many changes of pads if the right materials are not used due to excessive and poor wear resistance properties. This becomes an indispensable economic issue. Wear is an applied science. Two common forms of wear are adhesive wear and abrasive wear. Adhesive wear is also known as scouring, galling, or seizing. Deformation in shear is the main mechanism in adhesive wear. During abrasive wear, the surface asperities are worn down and the contact surfaces become mated. Hard ceramic particles like as WC or SiC becoming confined between the sliding surfaces results in abrasive wear. The level of material loss is related to the relative hardness of the ceramic particles and the sliding surface. Another additional factor in wear which can lead to fretting, cavitation, and erosion is environment. Wear is also known as the system property. So variables such as the matrix, reinforcement fibers or particles, orientation of fibers with respect to the wear direction, reinforcement/matrix interface, morphology, and size, and volume fraction of the phases in the composite are all intrinsic microstructural variables and are not currently properly defined. **Figure 1** shows the basic design of the braking system. Disk

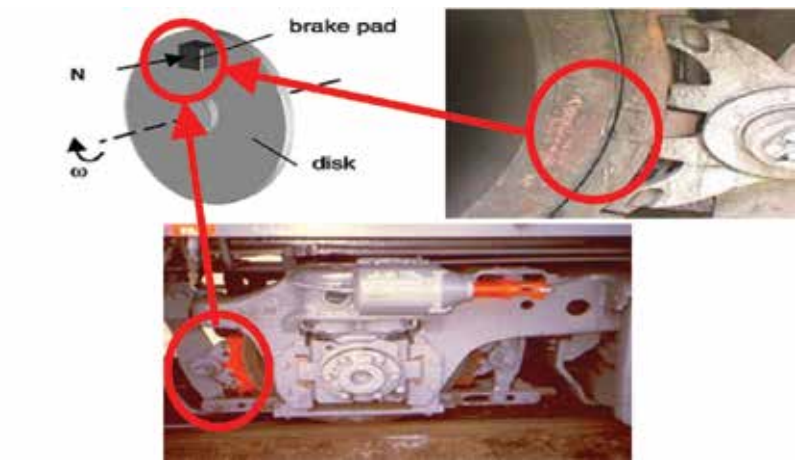

Figure 1. Basic braking system design.

http://dx.doi.org/10.5772/67533

brakes are the most common equipment used to stop vehicles such as cars and trains. This study is based on evaluating the impact of sintering conditions (sintering pressure and temperature) on the mechanical and tribological characteristics of the newly developed Cu-based frictional material for train brake pads. This study also analyzes weight reduction of the rolling stock design with the new material in contrast with old cast iron systems.

The different types of rolling stock have a form-braking device, to the extent that they decelerate and stop when required [2]. A small truck running on rails in mines was the first train car with a braking system. Apparently the mine cars employed a lever to push a wood block against a wheel. Nevertheless, these manual devices became inadequate as the mass and speed of the rolling stock increased. Braking systems using motive power were then introduced. With this in perspective, railway companies began installing braking equipment, usually using either vacuum brakes or air brakes. Only air brakes are currently still being used with the vacuum brakes in abeyance [2].

Compressed air forces piston-driven brake shoes against the wheel in an air-brake system. The composition of the brake shoes can be obtained from a number of different substances, comprising synthetic materials and cast iron. The braking force is not applied directly to the wheel in some contemporary systems. Taking in a disk brake system as an example, the force is applied by clamping brake calipers to both sides of axels-mounted or wheel-mounted disks. This normally helps to consequentially stop the wheel [2]. **Figure 2** shows the cast brake shoes with wear indicators.

Figure 2. The cast brake shoes with wear indicators.

2. Mechanical braking system

The most fundamental and elementary braking devices used by mechanical braking systems are wheel-tread brakes, axle-mounted disk brakes and wheel-mounted disk brakes. The entire mechanisms use an object such as brake shoe or lining that applies friction to the functioning disk. Whenever the applied pressure is adjusted it helps to control the braking force. When the brake shoe applies friction to the wheel threads in the wheel-tread brake, it creates a sliding effect. Since doing so would damage the wheel thread high-speed trains cannot use this type of brake.

Instead they use axle-or wheel-mounted disk brakes. Axle-mounted disks brakes are used on trailer bogies, because they have sufficient space to accommodate such a system. Wheel-mounted disks are dead weight, which are useful only during braking so operators are keen

to install light disks. Carbon/carbon-composite multidisks and aluminum composite disks offer lighter weights and are viewed with considerable interest. A frictional force that slackens the wheel or axles occurs when the carbon/carbon-composite multifiber rotor and stator rub against each other. Comparatively, the disk is lighter than conventional materials and has first-rate heat-resistant qualities. Also, aluminum-composite brake disks could be prepared much lighter than the current forged steel and cast iron brake disks in the market. Additionally, their make-up is the same for both wheel-mounted and axle disks, resulting in a much lighter disk without design alterations.

2.1. Friction materials

The main function of friction brakes is to reduce a vehicle by changing the kinetic energy of the vehicle to heat, through friction, and dissipating that heat. There are two basic types of friction brakes—pad/disk brakes and shoe/drum brakes. Heat flow, reliability, noise characteristics, and ease of maintenance are affected by the designs of the brakes. In this research, we will be looking at the later one.

According to documented historical records, the uses of diverse kinds of materials like friction materials are used for brakes. Wagon brakes used wood and leather are typical examples. A lot of the current brake materials still consist of organic-based materials, like polymers and plant fibers. Incipient railroad IT in the 1800s demanded brake materials to perform under high loads and speeds. According to Nicholson [3], Herbert Frood is credited with discovering the first brake lining material in 1897. This consisted of a cotton-based material saturated with a bitumen solution and was used for wagon wheels as well as primarily designed ancient automobiles. Herbert Frood's discovery paved the way to the initial woven brake lining materials. But in the 1920s crysotile asbestos fibers were used as a substitute. In the 1950s, the common metallic linings were resin-bonded, and the alleged semimets became established by 1960s. These comprise of a higher quantity of metal additives. Common brake materials from Nicholson can be seen in **Table 1** [3].

2.2. Additives and brake materials functionality

Shoe additives and brake pad serve differing functions. Just a slight difference of 2%of additive concentration can have adverse effect on the performance, consequently making composition control vital. The volume percent is most appropriate to list compositions of brake additives, even though many researchers do not adhere to this [3]. Brake materials and additives can be grouped according to their expected functions as shown:

- Abrasives
- Friction modifiers
- Fillers and reinforcements
- Binder materials

Some of the additives can be arranged into more than one category since they fulfill different functions to avoid ambiguity. Subsequently, overlaps of some additives are unavoidable. More so, normally, there are 5–10% of porosity present in the brake materials. The wear

http://dx.doi.org/10.5772/67533

Description of materials	Application(s)	Appro. year
Woven asbestos with brass and other wires for increased strength and performance	Automobiles and trucks	1908
Glass fibers, mineral fibers, metal fibers, carbon and synthetic fibers to provide semi-metallics with higher performance than asbestos (beginning of safety issues with asbestos)	Automotives and trucks	1960s
Dry-mix molded material to replace cast iron brake blocks that produced metallic dust that shorted electric train rails	London underground	ca. 1930
Non-asbestos (fiberglass) materials	Brake drums on original equipment cars	1980s
Cast iron on steel	Railroad car brake blocks and tires	Prior to 1870s
Use of carbon fibers	Automotive brakes	1991
Hair or cotton belting (limited by charring at about 300° F)	Wagon wheels and early automobiles	1897
Molded linings with shorter chrysotile fibers, brass particles, and low-ash bituminous coal	“““	1926
Flexible resin binders developed along with more complex formulations	Brake drum linings	1930s
Resin-bonded metallic brake linings	Industrial and aircraft applications	1950s

Table 1. The historical compositions of automotive friction brake materials.

behavior is mostly influenced by size, the form and distribution of the particle of the additive, therefore, investigation must not be limited to only the composition of additives to control friction and wear [3]. Abrasives help maintain the cleanliness of mating surfaces and control the build-up of friction films. They also increase friction, particularly when initiating a stop. These materials lubricate, raise the friction, or react with oxygen to help control interfacial films. Fillers are used to maintain the overall composition of the friction material and some have other functions as well. They can be metals, alloys, ceramics, or organic materials. Commonly known to have the capability to absorb heat generated by friction as the same time ensuring the efficiency of the brake system is cashew frictional dust. This is in a granular form. It produces a softer material at higher efficiency for wear when the brakes are relatively cold. This benefit outplays plain phenolic resin. Cardanol is the primary constituent in cashew nutshell liquid and is hydrophobic and remains liquid and flexible at very low temperatures. The popular and original binder materials are phenolic resins in the case of automotive and truck pads. In the case of aircraft, there are three basic types of aircraft friction brake materials: (1) sintered metal, (2) carbon-carbon, and (3) organic materials. But the Cu-based matrix materials tend to have a higher friction response than Fe-based metallic [4]. Asbestos is also known as hydrated magnesium silicate $Mg_3Si_2O_5$ $(OH)_4$. The content of asbestos in vehicle brakes varies between about 30–70% when it is used. The admirable properties of asbestos include accessibility at reasonable cost, insulate thermally, and stable at 500°C and above. This produces silicates, aid to regenerate the friction surface during use, flexible yet strong nature, produces harder and abrasive silicates, well processed, and wears well. It is able to maintain its fibrous property until about 1400°C, and at higher temperature, it becomes dehydroxylated [5]. The variation in cost, processing, and properties are a factor

to determine the type of asbestos to be used. Amosite and crocidolite are other asbestos minerals that are used even though chrysotile is normally available too. Actinolite, anthophyllite, and tremolite are the other types, which are not so famous and found mainly as minor impurities together with other minerals.

2.3. Typical compositions and designations of brake friction

All friction coefficients for brake material pairs have a range of 0.07–0.7, but practically, most vehicles operate within a narrower range according to Ref. [6]. Actual standards range from about 0.3 to 0.6 in friction coefficient. The frictional materials are classified into six categories, which are dependent upon operational capabilities. The operation conditions are influenced by the class number as higher class number requires severe operating conditions. Materials must be designed to withstand the energy dissipation demands of the usage. The class numbers goes with the pressure, temperature, and speeds for the operating condition [6]. Some of the most challenging issues facing the engineer are basically to understand the degradation processes known as wear, to predict the rate of wear, and to reduce it. The appreciation of wear often involves a comprehensive knowledge of mechanics, physics, chemistry, and material science, while its quantitative prediction, even to within an order of magnitude, remains in many cases a distance goal [7]. The broad definition of wear includes the loss of material, movement of material within a single surface, or transfer of material from one surface to another [8]. It is alleged that [9] the loss of substance form the operating body in a progressive order. This is as a result of the relative motion of the wear. But a comprehensive definition covering extensive range of engineering applications such as tribologist is appropriate. A damage to the body surface is a valuable account to wear, which involves progressive loss of material as a result of relative motion between the contacting bodies [10]. The mechanisms of degradation are not considered in these definitions. These may be solely mechanical, involving plastics deformation or brittle fracture, having chemical aspects. Both chemical and mechanical methods play a role in many practical cases [11].

The arrangement and grouping of wear parameters, along with descriptive terms of the wear mechanisms such as impact wear, sliding wear, rolling wear, and fretting wear are used in literature and in practice. These are used to describe the motion that occurs in wear. Nevertheless, wear mechanisms, which are mechanical, thermal, and chemical wear, are not described. Wear administered solely by the processes of deformation and fracturing are basically described by mechanical wear. For brittle materials, the deformation procedure plays a major role in its wear mechanism [12–14]. The tribochemical wear describes the wear governed by chemical and thermal. The melting is basically due to friction [15]. Other thermal wear on brittle materials are diffusive wear at elevated temperatures and fracture induced following thermal shocks [16]. These are more expressive terms for mechanical wear. The three-dimensional wear models of surface scratching by a hard asperity have already been suggested and ratified through quantitative agreements between experimental results and theoretical predictions [17, 18]. The wear volume, V, is given by the following formula:

$$V = \frac{\alpha\beta WL}{H_v} \tag{1}$$

http://dx.doi.org/10.5772/67533

where β represents the degree of wear by abrasive asperity, α the shape factor of an asperity, L the sliding distance, and W is the load. In practice, 0.1 is used for α and β, which range from 0 to 1.0, based on the depth of penetration of the abrasive particle, mechanical properties of the wearing part, and shear strength between the contact parts. If w_s is the specific wear rate as = wear volume/sliding distance × load, or K is the wear coefficient as = w_s H_v, H_v is the hardness, they are derived from Eq. (1) as follows:

$$K = \beta\alpha \tag{2}$$

$$W_s = \frac{\alpha\beta}{H_v} \tag{3}$$

These formulae are valid for only single-abrasive scratching.

As for the adhesive wear of ductile materials, no prognostic theories have been quantitatively confirmed by experimental purposes. Even though the suppositions of wear particles are removed based on unit contact, it still did not agree well with experimental data to provide a basis for a quantitative theory [19, 20]. The adhesive wear equations which are comparable to the equation are expressed as follows, Eq. (1):

$$V = w_s WL \tag{4}$$

$$V = \frac{KWL}{H_v} \tag{5}$$

Experimental results for the adhesive wear show that the wear volume increases almost linearly with the load and sliding distance. However, useful physical models were not found to explain the observed variation in values of w_s, and K, where w_s varied from 10^{-2} to 10^{-10} mm^3 N m^{-1}. Ratcheting is the flow wear, which supposes that experimental analysis agree well to the theoretical model [21, 22].

Fatigue wear estimates high-cycle fatigue, crack initiation, and propagation in a repeated contact stress cycles is dominate. The path of crack propagation decided the size of the wear asperities and its volume per unit. N_f is the critical number of rolling cycles for surface spalling caused by high-cycle fatigue fracture and is experimentally specified by the equation:

$$N_f = bW^{-n} \tag{6}$$

where b and n are constant values for the experiment and W is load. The n value is 3 for ball bearings [23]. It could be analyzed statistically by following the Weibull theory [24]. For low-cycle fatigue wear the Coffin-Manson-type relation can be employed. The theoretical wear rate model in a two-dimensional model is expressed as the plastic wave formation [25]. The K, wear coefficient, is expressed as

$$K = \frac{9 \times 3^{1/2} r\mu}{C^D \gamma_t{}^{1-D}} \tag{7}$$

where C is the monotonic effective shear strain; r, μ, and γ_t are all determined from the wave model as functions of the attack angle and the normalized shear strength of the contact

interface; and D is an experimental constant used as the power in the low-cycle fatigue law. When strain is accrued to a critical value causing fracture wear is the resulting incident.

2.4. Brake and materials

The purpose of friction brakes is to slow down a vehicle by converting the kinetic energy of the vehicle to heat, by the process of friction and then dissipating that heat. As a part of an automobile, brake materials have additional requirements such as resistance to corrosion, they need light weight, long life, low noise, stable friction, low wear rate, and tolerable cost at good performance. Shoe materials and brake pads and additives and serve a variety of functions. They help survey and improve the requirements of the pad. Even a difference of a percent or two of additive concentration can affect performance in an either negative or positive way, so composition control is crucial.

First of all, the choice of frictional brake materials used depends on several factors. Fundamentally, the properties of the materials are usually the first things to be considered but other factors, such as availability of the material, ease of manufacturing process, and cost, also play important roles. Among the properties that need to be considered are physical properties, chemical properties and mechanical properties. But in this piece of work, the properties are grouped under mechanical and tribological characteristics of the frictional material, of which the composition formation is very important. Powder metallurgy sintered metal friction materials have been used as brake disks, especially for heavy-duty applications. Because of their high performance and low wear rate under high temperatures and heavy-duty conditions, sintered friction materials have become increasingly important. Friction materials are the composites made up of sinterable metal matrixes (e.g., copper and iron), function components or modifiers (e.g., alumina, silica, and mullite), and solid lubricants (e.g., graphite and molybdenum disulfide). Comparatively, Cu-based materials are chosen above other competitors such as Fe-based and Cu-Fe-based materials because of its outstanding advantages. Cu-based materials have demonstrated better heat conductivity and friction resistance, so they are broadly used in aircrafts, trains, automobiles, and shipping brake systems.

Also, copper-based sintered composites produced by powder metallurgy processes are now widely used in industrial applications because of their high thermal conductivity, easy manufacturing, and corrosion resistance. But copper also presents limitations such as low hardness, low tensile yield strength, and poor creep resistance. But these can be overcome by integrating other elements and additives. These elements and additives improve their functions, quality, and performance in engineering applications.

2.5. Methods: powder production techniques

Using a simple powder metallurgy (P/M) route for manufacture, the material is based on the concept of combined properties of a copper-based alloy matrix for good thermal conduction and for good wear resistance performance.

http://dx.doi.org/10.5772/67533

The methodology used here is based on newly prepared sample materials listed in **Table 3** with different compositions of each material. These are subjected to a common constant sintering pressure but with three different sintering temperatures. These will then undergo various kinds of mechanical and tribological behavior tests before and after a thorough brake wear test to verify the rate of material loss which will help determine the wear ability of materials. The results will be mathematically analyzed to give a vivid conclusion about the results of the experiment. See **Figure 3** for the route.

Ingt: Cu	Matrix component (SiO_2, Fe & etc.)	Frictional component (Graphite & MoS_2)	Lubricant element (Mn, Sn & etc.)	Alloying
Wt%.	50–60	15–20	15–20	5.0

Table 2. Chemical compositions of material in mass (wt. %).

Rule of mixture (ROM)	
ρ_t (g.cm^{-3})	7.973 g.cm^{-3}
Experimental data	
Average ρ (g.cm^{-3})	6.7136 g.cm^{-3}
Average microhardness (HV)	294
Average porosity %, $P = \left(1 - \frac{\rho}{\rho_t}\right) \times 100$	15.79%

Table 3. Physical properties of cu-based composite.

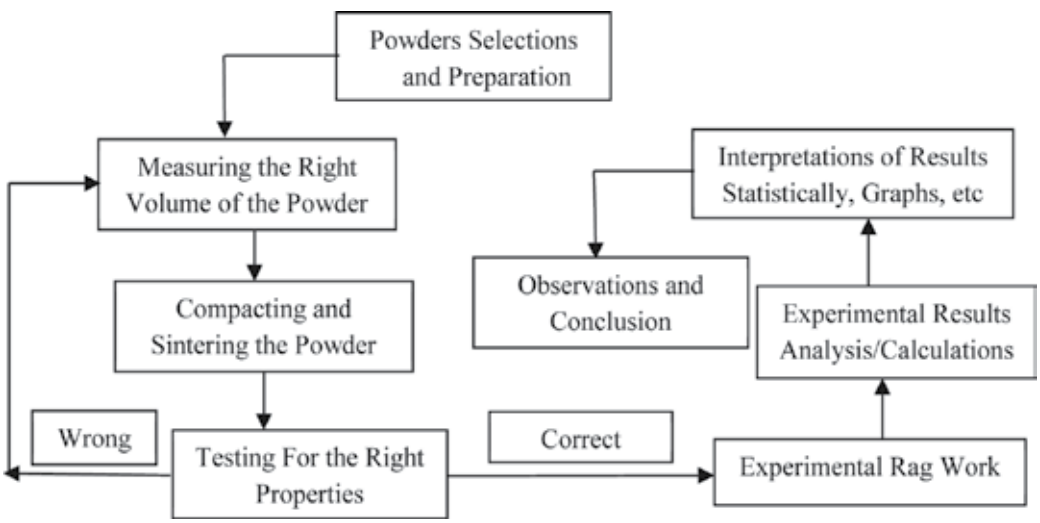

Figure 3. P/M route and experimental method schematic diagram.

2.6. Design of sample, mold, and sample holder

Design of a product is an inventive event whose primary work is to establish the multifaceted properties of objects, processes, services, and their systems in whole life cycles. This makes design a central factor of state-of-the-art humanization of technologies and a very crucial factor of cultural and economic exchange. This design is concerned about how to discover and assess elements, constituents' organization, and functional expressions at three different sintering temperatures, with the following objectives:

- Reducing wear rate of brake pad materials.
- Reducing high frequency of changing brake pads.
- Reducing heavy weight of rolling stock due to the weight of brake pad material compositions (cast iron) within braking systems.
- Improve tribological characteristics of Cu-based alloys for more functions.
- Giving Cu-based frictional products a more effective face and chance to improve upon it products.

Figures 4 and **5** show "die and two steel punches," a typical rectangular tool. This design was completed according to the ASTM B331-95. The die is made of tool steel and is a rectangular compact. The compacts are made up of the die and the punches, the die is in two layers, the inner layer and the outer layer. The inner layer is made up of high tool steel and the outer layer is made up of mild steel. The punches are also made of tool steel. The rectangular section was chosen because of the type of test rag that was used.

The rectangular blocks were obtained from this mould, which was sintered and then cut and grounded into 14 mm square of the thickness of 6.5 mm. This then gave us 196 mm^2 per piece, so that the double specimen will then be 392 mm^2. This is about 31% of the Chinese standard for 0.98 MPa constant pressure friction tester contact area of 25 mm square specimen. This was carried out since the material under consideration was meant to face higher pressure in the railway than the 0.98 MPa as the standard for automobile friction brake materials. The specimen holder was

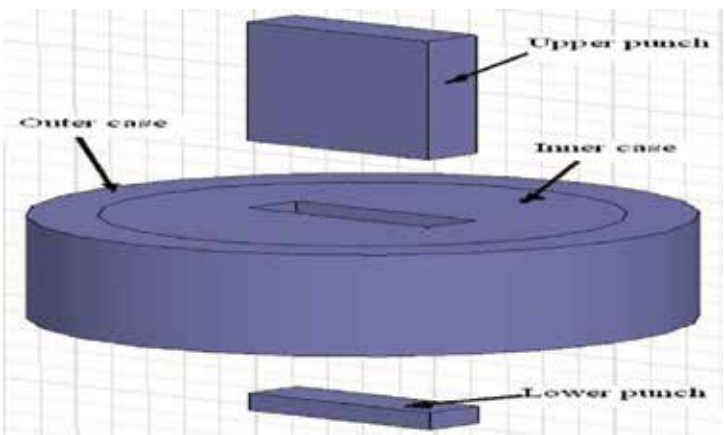

Figure 4. Die and two steel punches.

http://dx.doi.org/10.5772/67533

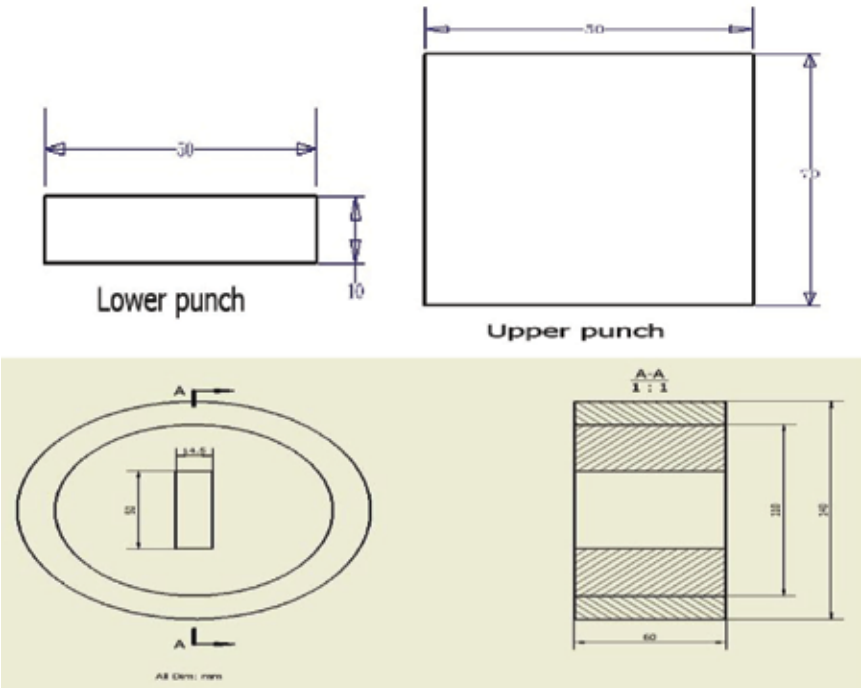

Figure 5. Cross-section of dies and punches.

originally 25 × 25 mm but due to the need for increased pressure, redesign of the holder was made. A 25 × 25 mm new holder was designed and produced. Within it was a square space of about 3.5 mm deep and was meant to accommodate a specimen of 14 × 14 mm. **Figure 6** shows a typical specimen holder. The material used to produce the specimen holder is from #45 steel.

2.7. Sample preparation

The first step was the selection of powder materials categorized under based metal on the matrix, frictional component, lubricant, and alloying element as shown in **Figure 7**. A dry, bulk solid consisting of a big number of very fine specks that may flow freely when shaken or tilted

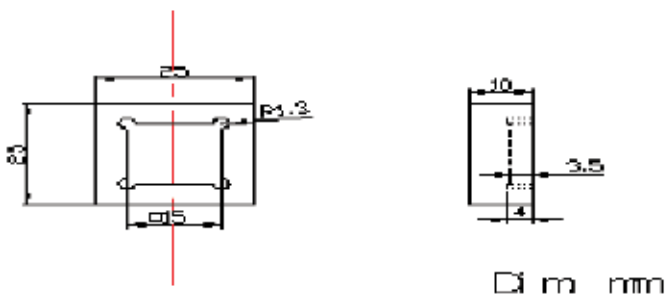

Figure 6. Elevation of the specimen holder.

Figure 7. Powders.

is termed as a powder. They are special subclass of granular materials, even though the terms powder and granular are occasionally used to differentiate separate classes of material. These were centered on the outcome of Kryachek [26] review and Yao et al. [27]. The newly developed bronze-based brake pad powder material with its chemical composition is given in **Table 2**.

The powders listed in **Table 3** were weighed in a sartorius BS224 S (Max 220g d = 0.0001 g) with their given proportion, the well-prepared powder was mixed in a V-cone mixer or double cone mixture machine (**Figure 8** is a mixing machine). The rotating speed of the double cone mixture was maintained at 150 rpm for 9 hours.

In the powder pressing process, the isostatic powder compaction press is employed with tools and dies. The die cavity that is closed on one end (vertical die, bottom end closed by a punch tool) is filled with powder that is subjected to isostatic, which is uniform in all directions, external pressure. As the pressure is isostatic, the as-pressed component is of uniform density. The powder is then in shape and then ejected from the die cavity. The compacting were done in a hardened steel die using a cold (or room-temperature) isostatic pressing hydraulic machine (SANS DCS-300 Digital hydraulic compacting machine) under the pressure of 650 MPa and is shown in **Figure 9**. The isostatic technique is only normally used for semifabricated products such as bars, billets, sheet, and roughly shaped components, all of which require considerable secondary operations to produce the final, accurately dimensioned component.

Figure 8. Mixing machine.

http://dx.doi.org/10.5772/67533

Figure 9. Isostatic compacting machine.

The process of taking metal in the form of a powder and transferring it into a mold or die is called the solid state sintering. As soon as it is compressed into the mold, the material is placed under high heat for a lengthy period of time. This heat treatment equipment is called a furnace is shown in **Figure 10**. Under heat, bonding takes place between the porous aggregate particles. When it is cooled, the powder is bonded to form a solid piece. Sintering can be considered to be made of three stages that are as follows:

1. Neck growth proceeds rapidly but powder particles remain discrete.
2. Most densification occurs, the structure recrystallizes and particles diffuse into each other.
3. The last stage, isolated pores tend to become spheroidal and densification continues at a much lower rate.

The compacts were subsequently transferred into a mesh belt continuous resistance furnace for sintering, shown in **Figure 10**. The sintering took 90 min in a controlled atmosphere furnace saturated with carbon at 850–950°C at 0.01 MPa constant pressure. In order to control the level of porosity, the component is dipped into hot oil for a few hours. The pores were then filled with oil. Finally, the resulting rectangular bar with a thickness of 5 mm was cut and grounded to a size of 14 × 14 mm test specimens. Nine pairs of specimens were prepared for the friction and wear test.

Figure 10. Mesh belt continuous resistance furnaces.

2.8. Testing procedures

The density values of the brake pad materials' were calculated by Archimedean principle, prior to sintering and after. The sample hardness was determined after the sintering process was done by a Digital Micro hardness tester HVS-1000 instrument. The values were taken under 10 N within 30 s. The sand paper grits 1200, 1000, 800, 600, 320, 240, and 180 were used to polish it after grinding. Alcohol was also used in the ultrasonic cleaner to clean all the samples. The micrograph structure investigation was done by scanning electron microscope (SEM) and the optical microscope (OM) prior to the wear test and after. The following two polishing stages of 3 and 0.05 μm, respectively, were done to enable access to the porosity, the microstructure, and the worn surfaces of the newly developed substance [28]. In addition, the energy dispersive spectroscopy (EDS) and the X-ray diffraction (XRD) were also used to observe elements composition and tribosurfaces of the worn surfaces after the wear test to determine the wear mechanism. TALYSURF CLI 1000 was also used to classify the kind of abrasive surfaces observed. **Figure 11** shows the Talysurf CLI 1000.

During the tribotests, the performance tests, which include the calculation of wear loss, frictional coefficient, friction force and a kind of wear, were executed. The parameters in this research were verified in accordance to GB5763-1998 of China National Standard. The friction material tester (X-MSM Constant Speed) of the speed 7.54 ms^{-1} at a constant pressure of 3.13 MPa used with a rotor of Brinell hardness in the range of 196, made of cast iron disk of the grade HTA5/HB. The main units of the test rig were made up of sample tool holder, disk and the control and monitoring unit. The temperatures for the friction test were 350, 300, 250, 200, and 150°C. A pair of different samples was in contact with the gray cast iron disk under a load. The total contact area was about 3.92 cm^2 and rotated at the constant speed of 7.54 ms^{-1} for 5000 revolutions [28]. **Figure 12** shows the tester and the monitor/control unit.

The initial design of the machine suits 0.98 MPa and 25 × 25 mm of contact area. The specimen holder was redesigned to cover the contact area of 14 × 14 mm, as a result of that, pressure

Figure 11. TALYSURF CLI 1000 equipment.

http://dx.doi.org/10.5772/67533

Figure 12. X-MSM constant speed friction material tester and monitor/control unit.

increased to 3.13 MPa on the tested sample. The friction coefficient data were obtained automatically from the tester. The sample pairs that were tested were five each and an average result was taken. Because there is no program to automatically obtain the wear loss directly, volume wear rate V in $mm^3\,N^{-1}m^{-1}$ was computed manually after 5000 revolutions of the disk based on pad-on-disk wear testing of ASTM G99-95a. In an unlubricated tribological application under the operating conditions of F_a load, v speed, T temperature, t operating duration, and s sliding distance, friction and wear will occur and must satisfy these standards below [25]:

$$\text{wear coefficient} = \frac{\text{wear volume}}{\text{load} \times \text{sliding distance}} \tag{8}$$

$$k = \frac{W_v}{F_a s} < 10^{-6} mm^3 N^{-1} m^{-1}$$

$$friction\ coefficient = \frac{\text{friction force}}{\text{normal load}} \tag{9}$$

$$\mu = \frac{F_F}{F_a} < 0.2$$

$$k = \frac{1}{2\pi R n} \times \frac{volume change}{average force,\ f_a},\ the\ volume\ change\ is\ A(d_1 - d_2) \tag{10}$$

where n is the number of rotations of the disk during testing (5000 rev), R is the distance from the middle of the rotating disk to the middle of the specimen (=0.15 m), A is the area of the specimen (196 mm^2), d_1 is the average thickness of the specimen before the experiment (mm), d_2 is the average thickness of specimen after the experiment (mm), and f_a is the average force of sliding friction (N). They were obtained at temperatures of 100, 150, 200, 250, 300, and 350°C, respectively. The diagrammatical illustration of the tribotester is shown in **Figure 13**.

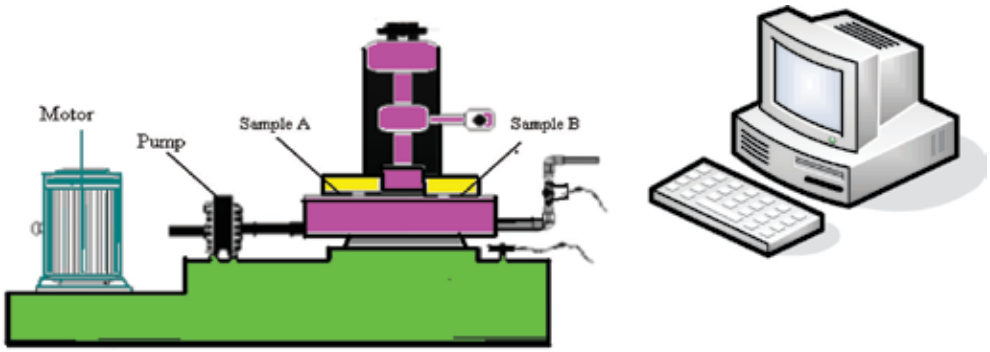

Figure 13. The diagrammatical illustration of the tribotester.

The wear numbers procedure was employed as a way of deciphering the wear resistance level of the specimen. The specimen mass was determined before and after the wear test to calculate the mass lost after 5000 revolutions, at the following temperatures; 350, 300, 250, 200, 150, and 100°C. This was done and the wear number was obtained as:

$$\text{Wear number}(W_n) = \frac{\text{Density}}{\text{Mass loss}} \tag{11}$$

where W_n in revolutions per unit volume of the sample is the wear number. The higher the wear number, the more effective the wear resistance of the material (ASTM B611). The wear numbers obtained are presented in **Table 5**.

It is necessary to examine the structural elements and defects that influence the tribological properties of the materials. Microstructure, which basically refers to the grain size and the shape and other microstructural characteristics, goes a long way in influencing the mechanical and wear behavior of a material. Optical, electron, and scanning probe microscopes are commonly used in microscopy. These instruments aid the examinations of the microstructural features of all types of materials. Microscope investigation is a very important method in the characterization and study of materials. The microstructure and tribosurfaces analysis was done with optical micrograph (OM), the scanning electronic microscope (SEM), energy dispersive spectroscopy (EDS), and X-ray diffraction (XRD). OM and the SEM help analyze the nature of microstructures and pores that are produced. This was done both before and after the wear test. The EDS and the XRD were also used to observe the tribosurfaces of the worn surfaces of the test sample after wear test. The density of friction materials is determined according to the procedure proposed in ASTM D792, which is based on Archimedes' principle. The pressure under which the powder was compacted greatly influences the density obtained. The Cu-based brake pad material was

Sintering temperature, °C	Hv	Density, ϱ(g.cm^{-3})	Porosity, p(%)
850	272	4.504	17.53
900	287	4.645	15.82
950	304	4.843	14.04

Table 4. Mechanical properties of the novel Cu-based friction material.

T_{sin}°C	Disk temperature (T_{disc})					
	100°C	**150°C**	**200°C**	**250°C**	**300°C**	**350°C**
850°C						
W_n	8.915	8.446	8.086	7.789	7.224	6.350
k*	1.428	1.520	1.540	1.560	1.580	1.600
μ	0.394	0.352	0.331	0.324	0.313	0.301
900°C						
W_n	11.16	10.02	9.305	10.62	8.757	9.605
k*	1.595	1.610	1.630	1.680	1.700	1.720
μ	0.398	0.351	0.341	0.332	0.319	0.317
950°C						
W_n	12.21	11.30	10.44	10.68	8.154	8.874
k*	0.328	0.409	0.460	0.471	0.490	0.502
μ	0.421	0.412	0.401	0.398	0.397	0.395

NB: k^*, $\times 10^{-4}mm^3N^{-1}m^{-1}$; W_n, rev/cm^3 [30].

Table 5. Properties of novel material at different T_{sin} and T_{disk}.

used on a rotor, the disk made of cast iron (grade HTA5/HB with Brinell hardness in the range 196). This fulfills the China National Standard GB5763-1998.

All tests were carried out strictly under laboratory environment and experimental standards observed. In the experiments, the speed was constantly rotating at 480 rpm (sliding velocities of 7.54 ms^{-1}); constant pressure is 3.13 MPa instead of the original 1 MPa due to the modification of the specimen holder, which eventually reduces the area of the specimen. The load used is 1226 N; the area is reduced to 196 mm^2 (14 × 14 mm). Therefore, the pressure exerted on the sample is P = F/A (MPa). The average of the experimental data of five sample pairs were taken and tested for each specimen. The volume wear rate V in mm^3 N^{-1}m^{-1} was calculated after 5000 revolutions of the disk.

3. Experimental results analysis

3.1. Temperature effect on mechanical behaviors

Strength and ductility, or brittleness, are properties affected by the temperature of operating conditions or manufacturing conditions. Manufacturing conditions affect the mechanical behavior of the material. This impacts performance, safety and economic issues. This experiment considered different heat treatment temperatures within the same composition of the material. The experiment focuses on the effect of the sintering temperature on the following: (a) density and porosity and (b) hardness of the material. To what extent does sintering temperature influence the rate of wear through density, porosity, and hardness?

The role of pores in limiting the mechanical properties of materials is very obvious. They act as areas for initiation of fracture and provide an easy path for crack propagation. The voids, serve as sites of weakness at which ductile fractures may initiate during plastic deformation. This also leads to volume change, eventually affecting the density. In contrast, the voids at certain percentages are also very needful to facilitate self-lubricating properties in dry sliding conditions. This is known in simple terms as porosity, and is defined as the total volume occupied by pores per unit volume of material and is calculated from real density and viewed density. The formula is:

$$Porosity,\ P = \left(\frac{\text{Real density} - \text{Viewed density}}{\text{Real density}}\right) \tag{12}$$

$$P = 1 - \left(\frac{\rho_v}{\rho_r}\right) \tag{13}$$

where ρ_r is the real density and ρ_v is the viewed density, in this case calculated to be 7.973 g cm^{-3} by the use of ROM. **Figure 14(a)** and **(b)** shows both the theoretical and the practical outcome of the experiment density and porosity, respectively. This shows the relationship between varied temperatures and properties (density and porosity). Measurements of the density and porosity were carried out according to the standard of the sintered samples [29] and the Archimedes principle. According to the Archimedes principle, mass density of an object is defined as:

$$\rho = m/V \tag{14}$$

where ρ is the mass density of the object, m is the mass of the object, and V is the volume of the object. The principle also asserts that, there is an upward force applied on the object by the fluid known as the buoyant force defined as:

$$F_B = g\rho_F V \tag{15}$$

where g is the acceleration due to gravity , F_B is the buoyant force on the object, V is the volume of the object immersed in a fluid, *and* ρ_F is the density of the fluid.

According to the Archimedes principle, it is possible to determine the density of an object without ever determining its volume.

$$F_B = W_A - W_F \tag{16}$$

where F_B is the buoyant force on the object, W_A is the normal weight of the object measured in air ($W_A = mg$), and W_F is the weight taken while the object is immersed in a fluid of density ρ_F.

Now, comparing Eqs. (15) and (16), the following was deduced:

$$g\rho_F V = W_A - W_F \tag{17}$$

Solving this equation for the volume of the object, the equation is as follows:

http://dx.doi.org/10.5772/67533

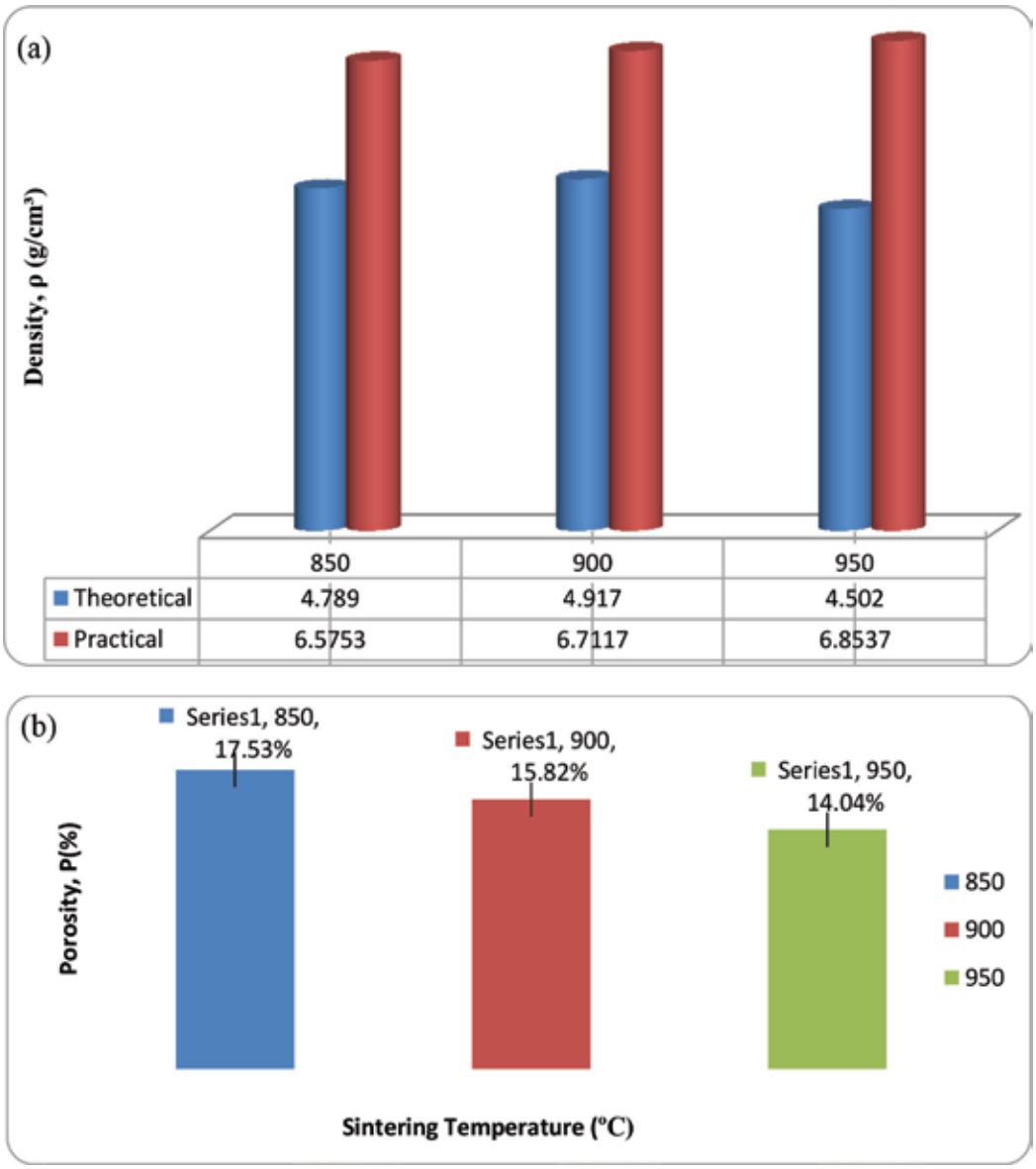

Figure 14. (a) Relationship between density and sintering temperature. (b) Relationship between porosity and sintering temperature.

$$V = (W_A - W_F)/(g\rho_F) \tag{18}$$

and substituting it into the definition of density in Eq. (14) will be (after some simplification) as shown:

$$\rho = \left(\frac{W_A}{W_A - W_F}\right)\rho_F \tag{19}$$

The rules of mixture (ROM) for composite materials were also used and the results were compared with the Archimedes principle. ROM are mathematical expressions, which give some property of the composite in terms of its properties, quantity, and arrangement of its constituents. For density, a general composite, total volume V, containing masses of constituents M_a, M_b, M_c, …, the composite density is

$$\rho = \frac{M_a + M_b + M_c + \ldots}{V} = \frac{M_a}{V} + \frac{M_b}{V} + \ldots \tag{20}$$

In terms of the densities and volumes of the constituents:

$$\rho = \frac{v_a \rho_a}{V} + \frac{v_b \rho_b}{V} + \frac{v_c \rho_c}{V} + \ldots \tag{21}$$

But $v_a/V = V_a$ is the volume fraction of the constituent a, hence:

$$\rho = V_a \rho_a + V_b \rho_b + V_c \rho_c + \ldots \tag{22}$$

For the special case of a fiber-reinforced matrix:

$$\rho = V_f \rho_f + V_m \rho_m = V_f \rho_f + (1 - V_f)\rho_m = V_f(\rho_f - \rho_m) + \rho_m \tag{23}$$

where ρ the theoretical density of the composite, V is volume fraction of the component, and the subscripts f and m refer to the fiber and matrix, respectively. It is noted that:

$$V_f + V_m = 1 \tag{24}$$

Table 3 shows the physical properties of the novel Cu-based material. The results indicate an increase of more than 5% in density and little decrease in the interconnected porosity. This all occurred at a high sintering temperature (950°C). At other subsequent temperatures (900 and 850°C), the results were not appreciating since it seemed the temperature was not sufficient for the treatment.

Hardness is not an intrinsic material property dictated by precise definitions in terms of fundamental units of mass, length and time. A hardness property value is the result of a defined measurement procedure. Hardness is an indicator of a metal's resistance to plastic deformation (e.g., a small dent or scratch) and it is an important factor that influences the rate of wear of a material. Therefore, the Vickers hardness test was performed on specimens using Digital microhardness tester HVS-1000 instrument according to the ASTM E 8-04 Standard [2]. The term "microhardness test" usually refers to static indentations made with loads not exceeding 1 kgf. The indenter is either the Vickers diamond pyramid or the Knoop elongated diamond pyramid.

The method for analysis and testing is comparable to that of the standard Vickers hardness test. The only difference is that it is accomplished on a microscopic scale with higher precision instruments. The surface being tested commonly demands a metallographic finish. The smaller the load used, the higher the surface finish demanded.

http://dx.doi.org/10.5772/67533

Precision microscopes are devices used with a magnification of around X500 and measure to an accuracy of +0.5 μm. The contact pressure used was 10N (100g) within 30 s. Prior to the test, the samples were grounded and polished with sand paper grit 180, 240, 320, 600, 800, 1000, and 1200 successively, and were finally polished on an ultrasonic cleaner. The average results of five best repeated test results out of 10 obtained from the hardness test are presented in **Table 4**. The relationship between hardness, temperature of the specimens obtained from the hardness tests, are presented in **Figure 15** (specimen heat treated at 850°C exhibited poor hardness), whereas, the materials at 900 and 950 show effective resistance to indentation.

3.2. Tribological behaviors

In many cases, lubricants are used to solve tribological problems. But in certain cases, lubrication is not possible: thus where lubrication has to be avoided (for economic or ecological reasons) or when the lubricant cannot be applied at the point at which it is needed (is inaccessible), friction and wear behavior is indispensable under critical operating conditions. Tribology is an important contribution to our prosperity, from daily life to advances in technology. Tribological research work and tribotesting achieve these important goals by:

- decreasing pollution and saving the environment
- decreasing energy losses
- preserving raw materials

Considering these in perspective, the aims of tribotesting can be specified as follows:

- To add to general tribological knowledge, with a better understanding of mechanisms as a basis for specific developments.
- The tribological characterization of improved or new materials to define their areas of application.
- The solution of real tribological problems, improvement of functionality or life by modification of materials, construction or running circumstances.

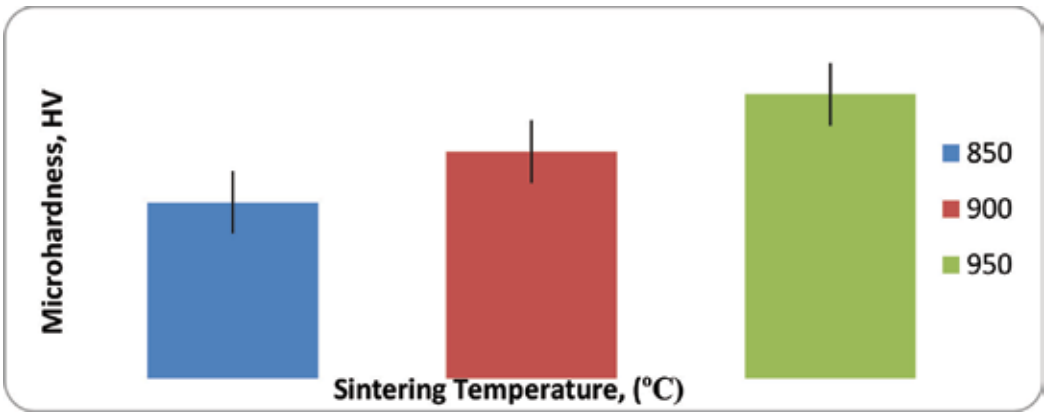

Figure 15. Relationship between hardness and sintering temperature.

Microstructure refers to the microscopic description of the individual constituents of the physical substances used as inputs to manufacturing. It is necessary to examine these individual constituents and their influence on the tribological properties of the materials. Microstructure, which basically refers to grain size and shape and other microstructural characteristics, goes a long way in influencing the mechanical and wear behavior of a material. Optical, electron, and scanning probe microscopes are commonly used in microscopy. These instruments aid the examinations of the microstructural features of all types of materials. Microscope investigation is very important tool in the study and characterization of materials. Following are some critical applications of microstructural examinations: to predict the properties of materials once these relationships have been established; to ensure that the associations between the properties and structure (and defects) are properly understood; to design alloys with new property combinations; to find whether or not a material has been correctly heat treated; and to ascertain the mode of mechanical behavior. The samples were cut and grounded to shape after sintering and oil dipping. The surfaces of the specimens were first polished with sand papers of grit 180, 240, 320, 600, 800, 1000, and 1200 successively, and then polished in two stages using 3 μm and 0.05 μm, respectively. The purpose of this study was to examine the distributions of the alloy particles in copper-based matrices and to also help evaluate the porosity and the density. The specimens were then etched with a solution 3% hydrogen peroxide (H_2O_2). Each specimen was immersed in the etchant solution, followed by immediate rinsing under running water and then alcohol rinsing, thereafter. Finally, the specimen was hand dried carefully for optical microstructure analysis. The scanning electron microscopes (SEM) were also employed to examine microstructures of the specimen before and after the tribotest. Before the SEM analysis, the samples were immersed in a cylinder containing Ethanol absolute for ultrasound cleaning in a Honda W-113 Ultrasound multi cleaner for 40 min in all however changes the ethanol absolute liquid every 10 min. The SEM equipment used was S-3700N SEM-HITACHI. The energy dispersive spectroscopy (EDS) analysis was also conducted on some particular selected zones of the samples. The QUANTAX 400-EDS was also used.

Figure 16 shows the typical SEM microstructures of compacts sintered at a constant pressure and at temperatures 850, 900, and 950°C, respectively.

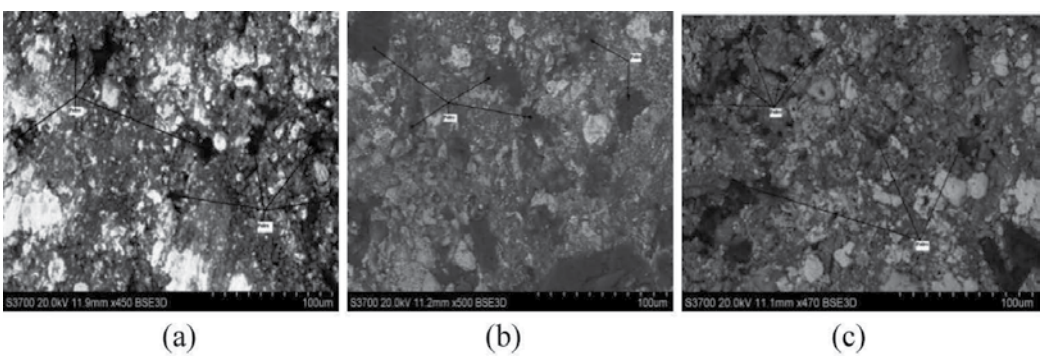

Figure 16. SEM micrograph before tribotest: (a) 850°C, (b) 900°C, and (c) 950°C.

http://dx.doi.org/10.5772/67533

The microstructure shown in **Figure 16(a)** of the test samples shows an irregular copper matrix, with fine graphite powder stored in the pores (the black spots). This could be seen almost in all the samples but the fraction is not the same therefore resulting in a different response to wear behavior.

Figure 17 shows the nature of the OM before the braking test. The dark spot found here confirms the volume of pores on the surface under examination and the influence of it on the overall performance of the novel material when subjected to braking application. Compared with the SEM, it is quite obvious that eduquate porosity can be achieved to help produce more effective material for train brake pads. These pores are as the result of graphite and other low melting alloys trapped in the voids. This eventually serves as fuel to lubricate the the dry sliding process.

The typical variation of coefficient of friction, wear coefficient, and the wear number obtained during the dry sliding tests conducted on the X-MSM Constant Speed Friction Material Tester at the applied constant pressure of 3.13 MPa is shown in **Table 5** for the materials investigated.

Figure 18(a) shows the relationship of the coefficient of friction and the sintering temperature. The coefficient and the disk operating temperature graphs are also shown in **Figure 18(b)**, which shows that, at the start of the test, the coefficient was high for all the samples, but exhibited a little reduction as it kept increasing in revolution. The average rate of reduction was recorded at 0.0186, 0.0162, and 0.0052 for all the materials investigated at a temperature of 850, 900, and 950°C, respectively.

The wear behavior phenomenon of the material at different sintering temperatures was critically surveyed. The volume loss during the tribotest at various disk operating temperatures was compared to the mathematical evaluations of the volume loss and the results are shown in **Table 6**. The pin-on-disk tribotester method was used, to relate the volume loss with the porosity of the material at different sintering temperatures bearing in mind the operating conditions. **Figure 19(a)** shows the varied relationship between the wear number and the wear coefficient at the same sintering temperatures. **Figure 19(b)** shows the relationship developed between the wear number and the porosity at sintering temperatures. The relationship between the wear number and the wear coefficient at disk operating temperatures is also shown in **Figure 19(c)**. The behavior of the coefficient of friction and the hardness at sintering temperature is shown in

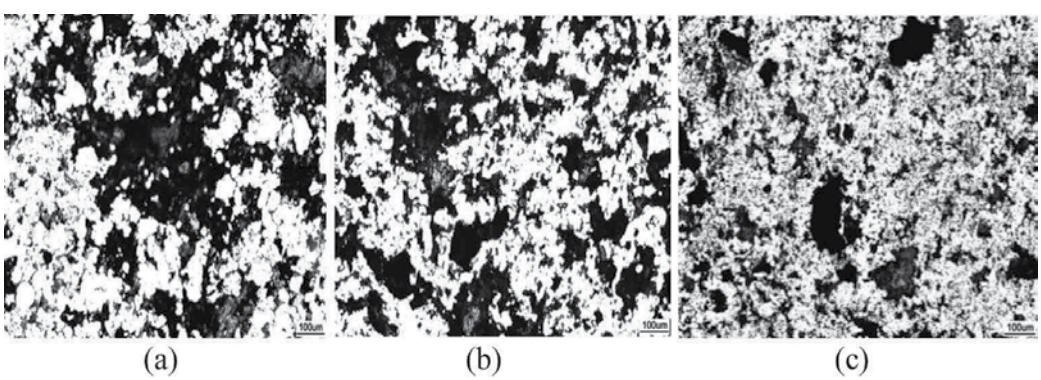

Figure 17. OM micrograph before tribotest: (a) 850°C, (b) 900°C, and (c) 950°C.

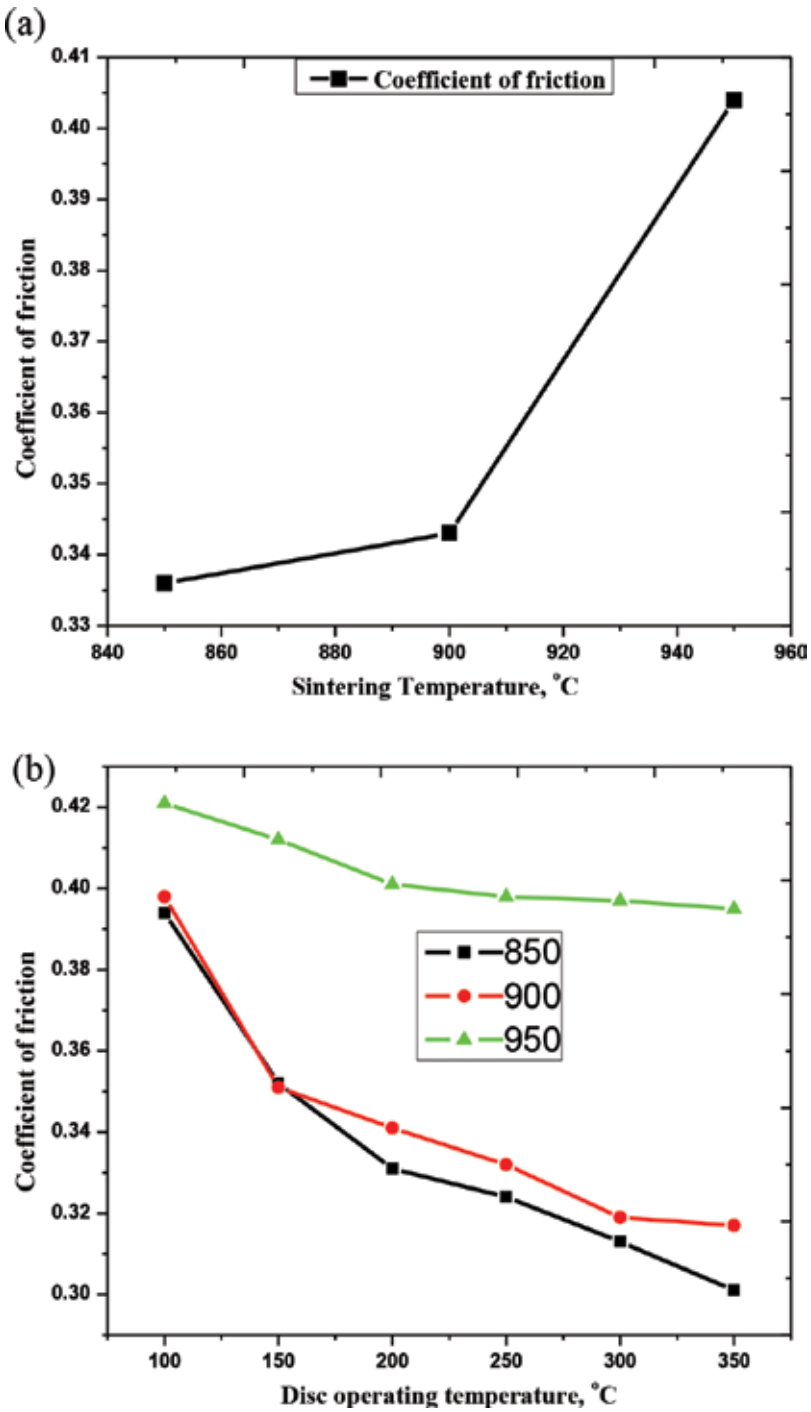

Figure 18. Coefficient of friction as a function of (a) the sintering temperatures and (b) disk operating temperatures.

http://dx.doi.org/10.5772/67533

T_{sin}°C	Disk temperature (T_{disk})						
	Volume	**100°C**	**150°C**	**200°C**	**250°C**	**300°C**	**350°C**
850°C	V_p	0.512	0.515	0.517	0.519	0.521	0.522
	V_t	0.737	0.742	0.745	0.748	0.751	0.752
900°C	V_p	0.679	0.681	0.685	0.687	0.689	0.691
	V_t	0.927	0.930	0.936	0.938	0.941	0.943
950°C	V_p	0.213	0.257	0.287	0.291	0.301	0.308
	V_t	0.275	0.331	0.370	0.375	0.388	0.397

NB: V_p and V_t are all in mm^3.

Table 6. Comparing the volume loss (theoretical and practical).

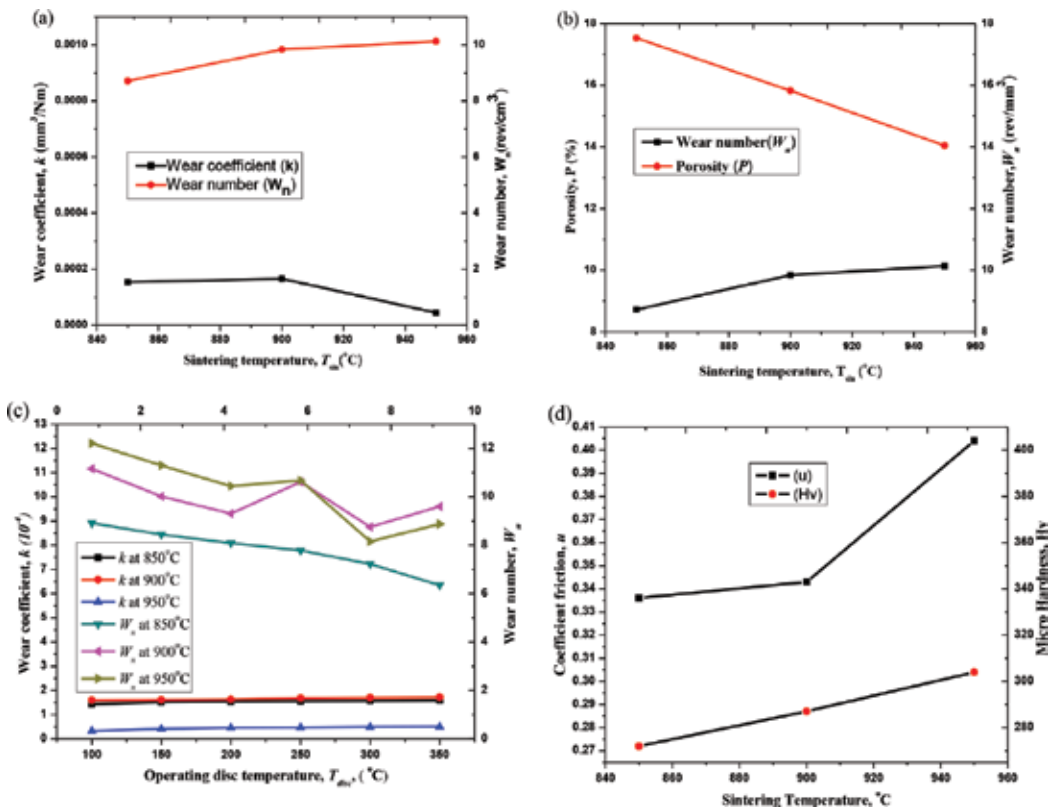

Figure 19. Tribological behaviors varying with temperatures. (a) Variation of wear number and wear coefficient as a function of sintering temperatures; (b) variation of wear number and the porosity as a function of sintering temperatures; (c) the wear number, the wear coefficient as a function of the disk operating temperature; (d) the μ, and Hv as a function of sintering temperatures; (e) the Hv and Wn as a function of sintering temperatures.

Figure 19(d). Finally, the variation of the wear coefficient and the microhardness at sintering temperatures is also shown in (e).

The mathematical expression of the volume loss used to compare with the derived one from the experiment is shown as follows;

$$V = \frac{kPL}{H} \tag{25}$$

where ***H*** is the hardness of specimen, ***V*** is the volume loss, P the applied load, L the sliding distance, and k the wear coefficient. The equation shows that the volume loss of a material is inversely proportional to its hardness. Therefore, the higher the reinforcement elements in content, the better wear resistance and reduction rate of volume loss.

The wear mechanisms of the sintered Cu-based composite rubbing against a rotor, the disk made of cast iron (grade HTA5/HB with Brinell hardness in the range 196), the worn surfaces of the composite specimen and wear debris were examined by SEM. The typical SEM micro-photograph of the worn surface for novel Cu-based composite containing 17.53% porosity and sintered at 850°C is shown in **Figure 20(a)**. The exerted braking pressure is 3.13 MPa and the constant sliding speed of 7.4 m s^{-1}.

The use of X-rays are electromagnetic radiation of wavelength about 1 Å (10–10 m), which is about the same size as an atom. They occur in that portion of the electromagnetic spectrum between gamma-rays and the ultraviolet rays. X-ray diffraction is one of the most important characterization tools used in solid state chemistry and materials science, therefore it is used here to determine the size and the shape of the unit constituents in the composition of the material.

Figure 21(a–c) shows the XRD pattern of the worn surface of material at sintered temperatures of 850, 900, and 950°C, respectively.

The electrons interact with the atoms that make up the sample producing signals that contain information about the sample's surface topography, composition and other properties.

The typical SEM microphotographs of the worn surface for novel Cu-based composite after undergoing a successful braking process are shown in **Figure 22**. These micrographs are

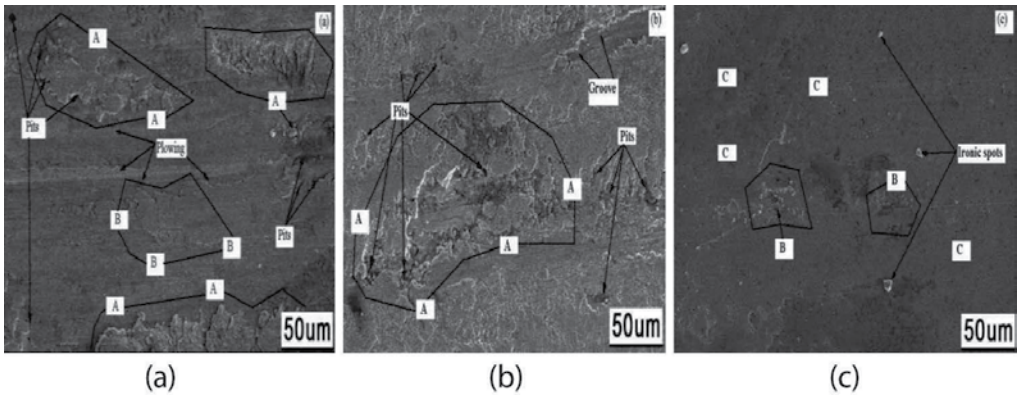

Figure 20. SEM micrograph of friction surfaces at: (a) 850°C, (b) 900°C, and (c) 950°C.

http://dx.doi.org/10.5772/67533

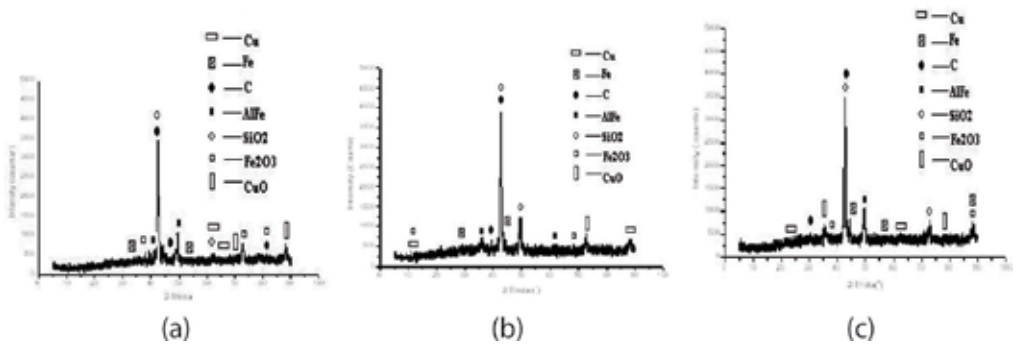

Figure 21. XRD of worn surface at sintering temperatures at: (a) 850°C, (b) 900°C, and (c) 950°C.

typically the nature of the novel material under the SEM microscopy. Sample (a) sintered at 850°C; (b) sintered at 900°C; (c) sintered at 950°C shows worn surfaces of various degrees after successful braking application.

The image processing and computer-based world have generated an automated tribological surface. These generated surfaces are quality control during manufacturing, wear failure analysis of engineering components, and wear particles monitoring in machine condition. **Figure 23** shows 3D Talysurf shaped images of the hybrid fractal-wavelet; they are of three classes of abrasive surfaces as indicated by reference [31].

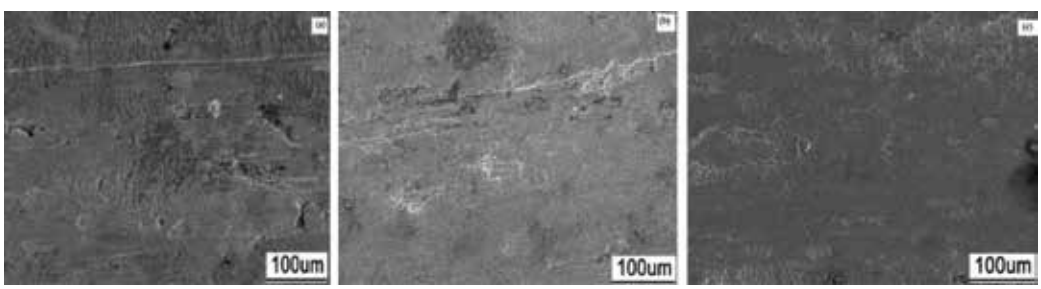

Figure 22. SEM micrographs of the worn surface for Cu-based composite.

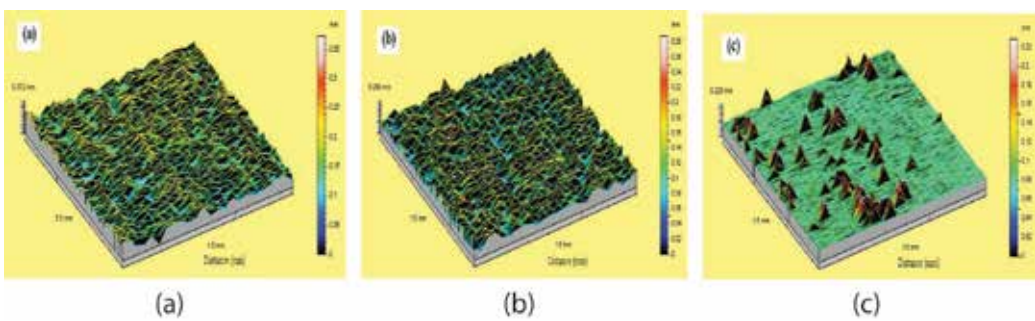

Figure 23. 3D Talysurf images of the surface at: (a) 850°C, (b) 900°C, and (c) 950°C.

4. Results analysis

4.1. Mechanical behaviors

The average apparent density for the novel composite material was 6.7136 g/cm^3. The ROM calculated density value of the same material was 7.973 g/cm^3 as shown in **Table 3**. The apparent density for the novel material was lower than the theoretical, therefore reducing brake weight and lowering total material usage and improving brake surface. The results generated an average porosity of 15.79% in the composite as the discrepancy between the experimental data and the calculated result, which is within the acceptable range (10–35%) of porosity in PM materials. This is illustrated in **Figure 14(a)** and **(b)**. The sintering temperature of 950°C of the specimen produced a remarkable porosity reduction and a better densification. These were as a result of the reduction and elimination of pores in Fe particles primarily bring about the densification of the composite. It can further be ascertained that a high sintering temperature promotes the sintering driving force and self-diffusion and interdiffusion of atoms.

At higher sintering temperatures, better mechanical properties of the material were achieved. A favorable porosity of 14.4% of the novel composite material was within the acceptable porosity of 15% of a composite PM material for dry sliding friction required to serve as self-lubrication property of the novel material which helps prevent seizure. Also, adequate internal porosity enhances brake formulations by reducing brake weight and lowering total material usage as well as improving brake surface. **Figure 14(a)** and **(b)** shows that the novel material has the potential of being able to maintain effective friction material for high speed train brake pads, particularly the sample sintered at 950°C. Therefore, sintering temperature in this case influences the porosity and improves the density of the material.

In this investigation, the material's ability to withstand wear and indentation or scratches is well associated with the degree of hardness (hardenability). In **Figure 15**, the results show that the highest hardness of the novel material was achieved at the maximum sintering temperature (950°C). Within the same sintered material, a good wear resistance of the material is also observed in **Figure 19(c)**. This result evidenced decreases in the wear rate and high wear number of the novel material indicating high resistance to wear of the sliding pair (ASTM B611). It can also be observed in **Figure 18(a)** that there is a relationship between the coefficient of friction and the hardness since the highest sintered novel material also exhibits the highest coefficient of friction.

The graph in **Figure 15** also indicates that the hardness is proportional to the sintering temperature. This can be attributed to the fact that high sintering temperature promotes complete diffusion of both self and inter of the atoms. Information can also be observed in **Tables 3** and **4**, which contains some of the physical and mechanical properties of the novel material.

4.2. Tribological behavior

The phenomenon here is very simple when you look at both surfaces of the SEM and OM shown in **Figures 16** and **17** before the braking process. The surface characteristic shows dark spots on both micrographs, therefore, indicating that the degree of porosity could be high. This

http://dx.doi.org/10.5772/67533

enables the needed pores for effective dry sliding operation except when novel materials with incomplete diffusion particularly 850°C and 900°C are not able to demonstrate better resistance to wear as shown in **Figure 19(a–e)**.

At high porosity, the self-lubrication property becomes high and reduces seizure. Many large pores are exposed in the frictional process. These pores may collect the debris, usually oxides. The collected oxides not only increase the real contact area between the pin and disk but also act as a solid lubricant source when the nonporous areas have metallic contacts with the disk. In this case, the high porosity sintered specimens have relatively low frictional-coefficients because oxides always exist on the contact area even in the case of metal-metal contact. These oxides and the wear debris plow or cut the specimen surface as abrasives or the disk surface when found inserted in the surface pores. When these specimens are in dry sliding operation, the main contact areas become smaller for high mass loss samples, and the high contact pressure makes thin contact areas between pores easily worn off. However, the sintered specimen with high porosity yielded high volume loss and those with low porosity yielded low volume loss.

It can be seen in **Figure 18(a)** that the entire sintered specimen saw a decline from the highest to the lowest frictional coefficient at the increase of the disk operating temperature. The specimen with the highest porosity was observed at a low sintered temperature, which contains an extremely low frictional coefficient. This indicates that the sintering treatment temperature influenced the frictional coefficient under the given wear test condition. In this case, it was observed that, the higher the sintering temperature gives a better coefficient friction, which confirms the fact that, the minimum porosity expected to reduce the rate of wear was obtained at a high sintering temperature. When porosity was formed in the material, a low coefficient of friction was observed, mostly at the lower sintering temperatures.

The wear number and the wear coefficient variation with operating disk temperatures for sintered specimen at 850, 900, and 950°C with different porosity are plotted in **Figure 19(c)**. The sintered specimens with high porosity (850 and 900°C) have a high volume loss. This is confirmed by the values obtained as the wear coefficient and the wear number, which contain low and high values for the one with low porosity (950°C) and also contain low volume loss at constant pressure and sliding speed (3.13 MPa and 7.5 ms^{-1}) under which the machine was operating. This indicates that during the entire sliding wear testing, the volume loss of the sintered specimen decreases with a decrease of porosity, which is observed as a result of the sintering temperature.

The specimens with higher porosity have higher volume loss and the one with the lower porosity has lower volume loss. The specimens with the higher porosity also are those sintered at low sintering temperature and those with lower porosity were sintered at high sintering temperature. From the above experimental results, it can be concluded that the volume loss and wear coefficient of sintered Cu-based composite increase with the increase of sintering temperature, thereby increasing the porosity of the composite.

The influence of the sintering temperature on porosity affects the volume loss and can be linked to the wear number and the wear coefficient, which is illustrated in **Table 5** and can be

seen in **Figure 19(c)**. The samples with high wear numbers were noted to be those with low porosity and therefore have low volume loss. On the other hand, those with low porosity have low wear numbers and high volume loss. The low wear coefficient was seen to also have low porosity and high wear coefficient contains high porosity, therefore resulting in high volume loss and low volume loss, respectively. The wear mechanisms of the sintered Cu-based composite rubbing against a rotor, the disk made of cast iron (grade HTA5/HB with Brinell hardness in the range 196), the worn surfaces of the composite specimen and wear debris were examined by SEM. The typical SEM microphotograph of the worn surface of the novel Cu-based composite that contained 17.53% porosity and was sintered at 850°C is shown in **Figure 20(a)**. The exerted pressure was 3.13 MPa and the sliding speed was 7.4 m/s. The worn surface appears to contain some small fine grooves of wear tracks and break-away abrasive kinds of wear.

Figure 20(b) shows the SEM microphotograph of the worn surface for the novel Cu-based composite containing 15.82% porosity, sintered at 900°C resulting from dry sliding against the same cast iron rotor at constant pressure and sliding speed as mentioned above. The presence of high pores in both micrographs before wear test have led to some portions of the specimen to appear with flake-like fragments containing initiation and propagation of subsurface cracks. The intensity of the pressure was also observed as part of the problem. In addition, some pits or cavities could be observed on the specimen's surface due to stress induced by high pressure. The delamination wear was observed. This can be attributed to insufficient heat causing the necessary diffusion. In this case, the porosity becomes affected, which eventually affects the densification as well.

Figure 20(c) shows material containing 14.04% porosity tested under the same conditions as the previous two samples. There are a few iron particles feasible on the surface. The micrograph shows a very smooth surface with these iron spots that turn to reduce the area of contact between the disk and the specimen, therefore reducing the rate of wear. Generally, the friction's firm destruction observed are grouped into three sections; namely, intense wear very rough surface, medium wear-relatively smooth surface and smooth surface-mirror like surface. The A sections on the photograph indicate intense wear sections. B sections show relatively rough wear and section C representing a mirror-like surface, a better wear resistance surface. Here, the samples were assumed to have had sufficient heating during the sintering operation, therefore, showing less destruction of the tested surface.

The groove (in **Figure 20a**) reveals plowing that occurred during sliding. The novel Cu-based composites are composed of several elements with different wear resistance properties. The elements with hard particles have better wear resistance than the soft elements. Therefore, hard particles projected on the friction surface; whereby the relative motion between composite and counterpart is prevented, turn to produce a higher coefficient of friction than the soft ones. At the same time, the hard particles projected turn to reduce the area of contact between the friction surfaces in contact thereby reducing the rate of wear. These high porosity specimens are known to have fewer hard particles than low porosity specimens. The high porosity sintered composites have more interconnected pores and fewer hard particles. These exhibit lower strength, are much easier to deform and are easily torn off, especially at the start of the

http://dx.doi.org/10.5772/67533

wear process. Therefore, high porosity samples have a low coefficient of friction, low wear number and high wear coefficient resulting in high volume loss as shown in **Table 5**. There were shallow and deep pits on the surface of high porosity Cu-based composites (a and b). This is a result of inherent pores, which are on the surface of sintered specimens or were discovered when the material above was worn away during the tribo test. At lower porosity, the size and number of pits is minimized. This is caused mainly by the surface fatigue (**Figure 20a**), i.e., where delamination wear occurred. Also abrasive wear occurred as the result of using wear debris as an abrasive for plowing both the oxide layer and metallic area. From the discussions above, the wear mechanisms of Cu-based train brake composites underwent plowing wear, delamination wear and abrasive wear. Any of these can lead to severe destruction of the worn surface and result in excessive wear, rough braking, and even failure in braking.

Figure 21(a–c) shows the XRD pattern of the worn surface at sintering temperatures of 850, 900, and 950°C, respectively. The worn surface depicts the pattern that the main components of the worn surface are graphite, SO_2, Fe, Cu, and oxides of Fe and Cu (Fe_2O_3 and CuO) and AlFe. Graphite has a layer structure with wider interlayer spacing, which tends to cleave along the layers. So it is widely used as lubricant to eliminate seizure and make the brake process stable. Consequently, the tribological properties of brake materials are improved [32]. The resistance and hardness of SiO_2 and CuO particles are much higher than those of the Cu and Fe matrix due to particulate hardening. Therefore, the friction coefficient is improved remarkably as a result of friction of SiO_2 against counterpart and this is intense during sliding, which hinders the relative movement of friction pairs yielding a high friction coefficient.

The typical SEM microphotographs of the worn surface for Cu-based composites are shown in **Figure 22**. The (a) sintered at 850°C shows that the worn surface appears to contain some small fine grooves and break-away abrasive kind of wear. The groove in **Figure 22(a)** reveals that plowing occurred during sliding. The (b) sintered at 900°C shows flake-like fragment, initiation, and propagation of subsurface cracks. Some pits or cavities can be observed at the specimen's surface due to stress caused by high pressure or load during operation. Delamination wear was exhibited which was attributed to insufficient heat to cause necessary diffusion. In c, sintered at 950°C, there are a few iron particles feasible on the surface. The micrograph shows a very smooth surface with these iron spots that turn to reduce the area of contact between the disk and the specimen, therefore reducing the rate of wear. Generally, the worn surfaces observed are grouped into three sections, namely destructive wear section (found mostly on (a) and (b)), medium wear section (mostly on (a) and very small area on (c)), and low wear section (only on (c)).

The Cu-based composites are composed of several elements with different wear resistance properties. The elements with hard particles have more substantial wear resistance than the softer elements. Therefore, the hard particles projected on the friction surface; whereby the relative motion between composite and counterpart is prevented, turn to produce a higher coefficient of friction than the soft ones. At the same time, the hard particles projected turn to reduce the area of contact between the friction surfaces in contact thereby reducing the rate of wear.

In **Figure 23**, our investigation generated abrasive surfaces classified into the following sections: smooth surface due to minimal wear rate and better wear resistance property, rough surface because of moderate wear rate, and highly rough surface due to excessive wear. The 3D Talysurf images of the surfaces are shown in **Figure 23**. **Figure 23(a)** shows a highly rough abrasive surface; it has fewer peaks that are ironic to withstand pressure from the braking system. **Figure 23(b)** represents the rough abrasive surface with moderate peaks withstanding the exerted pressure of the braking system. The (c) is the one that was observed as having enough ironic peaks to withstand the exerted pressure and therefore given a smooth abrasive surface.

5. Conclusions

According to this research, the following conclusions were made on the mechanical and tribological characteristics during the sliding wear behavior of novel Cu-based composite material against a cast iron (grade HTA5/HB with Brinell hardness in the range of 196).

- Generally, tribological behavior of all the sample material is temperature sensitive such that the transition from severe wear which initiates at lower temperatures (850 and 900°C) reduces as the temperature increases during high sintering temperature (950°C). This means the samples sintered at low temperatures suffer severe wear but at high temperatures low wear was calculated and practically recorded as well.
- As porosity was reduced, densification of the material was also improved indicating the reduction and elimination of pores in Fe particles to improve densification of the composite. Furthermore, high sintering temperature promotes the sintering impetus, the self-diffusion, and interdiffusion of atoms that are improved to accelerate the densification. Also graphite entrapped in the pores then leads to strengthening the densification of the composites to a certain degree.
- The dominant wear mechanisms observed were plowing, delamination, and abrasive wear. High porosity samples were affected by delamination and plowing wear. Many pits and grooves were observed. Large flakes were also observed due to the intense nature of the delamination wear. Abrasive wear and delamination wear were the main cause of high wear coefficient, low wear number and low coefficient of friction. This was dominant in high porosity samples. Intense wear and mild wear were feasible in the high porosity samples. Low porosity samples endured less mild wear and showed a mirror-like surface, glassy luster, and integrated friction film. This gives evidence that this section has better wear resistance property.
- The friction coefficient at high sintering temperature with high values indicating firm gripping at stopping at the same time demonstrated low rate of wear. This can be improved further and considered for manufacturing commercial brake pads. The main components of worn surfaces are graphite, SO_2, Fe, Cu, and oxides of Fe and Cu (Fe_2O_3 and CuO) and AlFe. The worn surfaces were divided into three sections: destructive wear section, medium wear section and low wear section. This is due to the level of destruction of friction firm during dry sliding.

- The characteristics of abrasive surfaces generated were into three categories, namely smooth surface, which shows minimal wear rate; the rough surface, which depicts temperate wear rate; and the highly rough surface showing extreme wear with a high degree of surface destruction.
- The volumetric and wear coefficient progresses greatly with the increase in sintering temperature. The wear coefficient (k) and the coefficient of friction were generated mathematically as shown in Ref. [28].

Sintering temperature affects the porosity and advances the density of the material. This eventually affects the hardness of the material which decreases the volumetric wear rate and yields a high wear number of the novel material, indicating high resistance to wear of the sliding pair. Further increase of sintering temperature greatly affects microstructures and tribological characteristics of Cu-based friction materials. It is clear that further studies of this material can improve the manufacturing of commercial brake pads [28].

Acknowledgements

This work was supported by the National Natural Science Foundation of China (Grant Nos.: 51575190, 51675105 and 51575113) and China Post-Doctoral Fund (Grant No: 2015M582357).

Author details

Glenn Kwabena Gyimah[1]*, Zhongning Guo[1], Ping Huang[2] and Dong Chen[2]

*Address all correspondence to: gk.gyimah@yahoo.com

1 Faculty of Electromechanical Engineering, Guangdong University of Technology, Guangzhou, China

2 School of Mechanical and Automotive Engineering, South China University of Technology, Guangzhou, China

References

[1] Savage, G., Applications of Carbon-Carbon composites. Carbon-Carbon Composites, first ed., Chapman & Hall, London, 1993, pp. 323–346.

[2] Hasegawa, I., Uchida, S, "Braking Systems," - Japan Railway Technology Today (Edited by Kanji Wako), Japan, June, 1999.

[3] Nicholson, G., (1995) Facts About Friction, P &W Price Enterprises, Inc., Croydon, PA.

[4] Tatarzicki, Y.T. and Webb, R. T., Friction and Wear of Aircraft Brakes, ASM Handbook, Vol. 18ASM International, Materials Park, Ohio, 1992, pp. 582–587.

[5] Spurr R. T., (1972) "Fillers in Friction Materials" Wear, 22, pp. 367-409.

[6] Anderson A. E., "Wear of Brake Materials" in Wear Control Handbook (edited by M.B. Peterson and W.O. Winer), ASME, New York, USA, 1980, pp. 843–857.

[7] Hutchings, I. M., Wear – Materials, Mechanisms and Practice (Edited by Gwidon W. Stachowiak), November, 2005, John Willey & Sons, Ltd, Chichester.

[8] Almen, J. O., in Mechanical Wear (ed. J. T. Burwell) Ameracan Society of Metals, 1950, pp. 229–288.

[9] Glossary of terms and definition in the field of friction, wear and lubrication, research group on wear of Engineering Materials, organization for Economic co-operation and development, 1969, reprinted in wear control Handbook (edited by M. B. Peterson and W. O. Winner), American society of mechanical engineers, New York, 1980, pp. 1143–1303.

[10] Standard terminology relating to wear and erosion, standard G-40-01, American Society for Testing and Materials, 2001.

[11] Kato, K., Classification of wear mechanisms in wear—mechanisms, materials and practice (ed. G.W. Stachowiak). John Wiley & Sons Ltd, Chichester, 2006 pp. 9–20.

[12] Fischer, T. E. and Sexton, M. D. The tribochemistry of oxidative wear in physical chemistry of the solid state. Applications of metals and their compounds (ed. P. Lacombe) Elsevier, Amsterdem, 1984. pp. 97–107.

[13] Fischer, T. E. and Mullins, W. M. Chemical aspects of ceramic tribology, The Journal of Physical Chemistry, 96, 1992, 5690–5701.

[14] Gates, R. S., Hsu, S. M. and Klaus, E. E. The tribochemistry mechanism of alumina with water, tribology transactions, STLE 32(3) 1989, 357–363.

[15] Lim, S. C. and Ashby, M. F., Wear Mechanism map, Acta Metallurgica, 35, 1987, 1–25.

[16] Adachi, K., Kato, K. and Chen, N., Wear Map of ceramics, Wear 203–204, 1997, 291–301.

[17] Zum Gahr, K. H. Microstructure and Wear of Materials Tribology Series, Elsevier, Amsterdam, 1987, pp. 132–148.

[18] Hokkirigawa, K. and Kato, K., Theoretical Estimation of Abrasive Wear Resistance Based on Microscopic Wear Mechanisms Wear of Materials (ed. K. C. Ludema), ASME, New York, 1989, pp. 1–8.

[19] Archard, J. F., Contact and robbing of flat surfaces, Journal of Applied Physics, 24, 1953, 981 – 988.

[20] Rabinowiez, E., Friction and Wear of Materials, 2nd edn. Wiley-Interscience, New York, 1995.

http://dx.doi.org/10.5772/67533

[21] Kapoor, A. and Johnson, K. L. Plastic ratcheting as a mechanism of metallic wear, Proceedings of the Royal Society of London, 445, 1994, 367–381.

[22] Kapoor, A., Johnson, K. L and William, J. A. A model for the mild Ratcheting Wear of Metals; Wear, 200, 1996, 38–44.

[23] Lundkey, G. and Palongrev, A. Dynamic Capacity of Rolling Bearings, Ingeniorsveten – S Kapsademicns, no. 96, 1947.

[24] Weibull, W. A statistical theory of the strength of materials, Royal Swedish Academy of Engineering Science Proceedings, 151, 1930, 5–45.

[25] Challen, J. M., Oxley, P. L. B. and Hockenhull, B. S. Prediction of Archard's wear coefficient of metallic sliding friction assuming a low cycle fatigue wear mechanism, Wear, 3, 1986, 275–288.

[26] Kryachek, V. M. "Sintered Metals and Alloys Friction Composites: Traditions and New Solutions(Review). Powder Materials" Powder Metallurgy and Metal Ceramics, Vol. 43, Nos. 11–12, 2004 Spring Science + Business Media, Inc.

[27] Yao, P., Sheng, H., Xiong, X., Huang, B. Worn surface characteristics of Cu-based powder metallurgy brake for aircraft, Transactions of Nonferrous Metals Society of China, 17, 2007, 99–103.

[28] Gyimah, G. K., Chen, D., and Huang, P. Dry Sliding Wear Studies of Cu-Based Powder Metallurgy Brake Materials, Volume 3. Design Materials and Manufacturing Parts A B and C, 2012.

[29] Xiong, X., Sheng, H., Chen, J., and Yao, P. Effects of sintering pressure and temperature on microstructure and tribological characteristic of Cu-based aircraft brake material, Transactions of Nonferrous Metals Society of China, 17, 2007, 669–675.

[30] Gyimah, G. K., Huang, P., and Chen, D. "*Dry sliding wear studies of copper-based powder metallurgy brake materials*", ASME Journal of Tribology, *J. Tribol*. Volume 136, Issue 4, pp. 041601-041606 (May 19, 2014).

[31] Stachowaik, G. W., Stachowiak, G. B., De Pellegrin, D., Posiadlo, P. Characterization and Classification of Abrasive Particles and Surfaces, Wear–materials, mechanisms and practice. Edited by G. Stachowiak, 2005, pp. 339–368.

[32] Stachowiak, G. W., Podsiadlo, P. Surface characterization of wear particles, Wear, 1999, 2251229: 1171–1185.

Edited by Leszek A. Dobrzanski

The book presents the fundamentals and the role of powder metallurgy in contemporary technologies and the state of the art of classical powder metallurgy technologies and a general description of new variants and special and hybrid technologies used in powder metallurgy. The next part includes over a dozen case studies provided in the following chapters, comprehensively describing authors' accomplishments of numerous teams from different countries across the world in advanced research areas relating to powder metallurgy and to special and hybrid technologies. The detailed information, largely deriving from own and original research and R&D works pursued by the authors, will be beneficial for the readers to develop their knowledge and harmonise specific information concerning these topics and will convince the manufacturers about the advantages of using the powder metallurgy technology in many branches of industry.

ISBN 978-953-51-4892-0

Photo by v_alex / iStock

IntechOpen